AN $^{18}O/^{16}O$ STUDY OF MESOZOIC AND EARLY TERTIARY GRANITIC BATHOLITHS OF THE SOUTHWESTERN NORTH AMERICAN CORDILLERA

Thesis by

G. Cleve Solomon

In Partial Fullfillment of the Requirements

for the Degree of

Doctor of Philosophy

California Institute of Technology

Pasadena, California

1989

(Submitted on April 7, 1989)

ACKNOWLEDGEMENTS

I have a long list of individuals and institutions in whose debt I stand, and without whose help I wouldn't have begun this project, executed, or drawn it to conclusion. I gratefully acknowledge financial support from CONOCO Fellowships, and NSF Grants EAR 83-13106 and 88-16413. I also thank the Geological Society of America for a Penrose Grant.

Hugh Taylor is the top person on my list; he suggested that I follow, into the rest of the Cordillera of the SW United States, the trail of the $^{18}O/^{16}O$ zones that he and Lee Silver discovered in the Peninsular Ranges Batholith (PRB). At the time, we were going to characterize the eastward extension into SE California of the low- to intermediate-^{18}O zone, which they found in the extreme northeastern parts of the PRB, and I don't think either of us realized that we would find the high-^{18}O eastern PRB in western Nevada. Through the years, Hugh generously provided me with financial and moral support in the pursuit of my $^{18}O/^{16}O$ mapping, and he has helped me conquer my writer's block (!) with his critical and insightful reviews of thesis drafts. Hugh also suggested another avenue of research, which I have pursued, namely infrared spectroscopic studies of ^{18}O-exchanged feldspars.

George Rossman is another major contributor to my research efforts at Caltech. George guided me through my IR studies of feldspars (providing some financial support along the way with NSF Grants EAR 77-23147, 83-13098 and 86-18200), and although the results of this work do not appear in this formal rendition of my thesis, this work occupied a large amount of my time at Caltech. Some of this work is published and the rest is in the process of being written up. I feel extremely fortunate

to have been associated with George as one of my mentors, and as co-author on a number of papers dealing with feldspars.

My wife Bette has enriched my life immensely, and has been wonderfully patient in spite of our son Bodie's antics, during the many hours I have devoted to thesis work. She has also aided me considerably to develop my writing skills, and not least of all, has helped with several thesis chores such as compiling the bibliography. Thank you, love.

The list has not gotten much shorter after mentioning the above three people, and I am going to have to be brief with the rest. I will say that, beyond this point, my briefness is, more often than not, inversely proportional to my gratitude. R.E. Criss, J.H. Dilles, S. Epstein, G.L. Farmer, R.T. Gregory, G. Haxel, R.I. Hill, K.A. Howard, E. James, P.B. Larson, K.E. Meisling, C.F. Miller, R.E. Powell, L.T. Silver, S.M. Wickham, J.A. Whitney, and J.E. Wright have all contributed much in the way of ideas and help in my attempt to understand granite genesis; in particular, Bob Criss taught me much of what I needed to know about $^{18}O/^{16}O$ silicate extractions and mass spectrometry, and Lee Silver shared his knowledge of the geology of southern California and southern Arizona. I am also indebted to Dilles, Farmer, Haxel, Howard, Miller, and Powell for providing samples, geological information, and, in some cases, isotopic and geochemical analyses from their own studies (mentioned in Chapter 2, or by referring to publications). To Gordon Haxel, I want to especially say thanks for the helicopter rides and for helping in the sample collecting; Gordon was the one who got me started with the often overwhelming task of collecting rock samples in remote areas of southern Arizona. I also particularly thank John Dilles, and note that it sure was a lot of fun camping out in the 10°F weather outside of Yerington,

Nevada. Also, L. Marnoch and J. Mayne have been very helpful with their respective typing and drafting skills. T. Weber kindly provided his Apple Macintosh SE and software for some of the graphic work. I praise the Lord for giving me the opportunity to share time and collaborate with these people.

ABSTRACT

Abundant evidence from previous studies indicates that, as long as samples are collected well away from pluton margins, the whole-rock $\delta^{18}O$ value of an unaltered granitic pluton is not likely to vary by more than ±0.5 per mil from the original $^{18}O/^{16}O$ composition of its source rocks. Therefore, granitic plutons may be viewed as "remote-sensing probes" which sample deep portions of the continental crust or upper mantle, and $^{18}O/^{16}O$ studies of such plutons can provide detailed information on lithologic boundaries at depth. This thesis presents approximately 350 new $^{18}O/^{16}O$ analyses of whole-rock and quartz powders from Mesozoic and Cenozoic granitic plutons in the Northern Great Basin (NGB) and Southern Basin and Range (SBR) provinces of the western United States. The samples were collected along two broad, regional traverses eastward from the Sierra Nevada Batholith (SNB) and the Peninsular Ranges Batholith (PRB) in California: (1) the NGB traverse from western Nevada, near Carson City, eastward to the area around Salt Lake City, Utah; (2) the SBR traverse in southeastern California (SECA), eastward from the Central and Eastern Transverse Ranges across the Mojave Desert to the Colorado River, and then southeastward into southern Arizona. Where available, whole-rock major-element geochemistry, ϵ_{Nd}, and $(^{87}Sr/^{86}Sr)_i$ analyses of the same samples by other workers are integrated with these $^{18}O/^{16}O$ analyses. In addition, several hundred whole-rock $^{18}O/^{16}O$ analyses and, where available, Nd and Sr isotopic data, have been taken from the literature and combined with the new results to compile a data base that provides virtually complete reconnaissance coverage of the batholithic terranes in the Cordillera of southwestern North America.

Samples in the southern Arizona part of the SBR traverse were collected from Jurassic, late Cretaceous, and early Tertiary granitic plutons emplaced well within mapped boundaries of the >1.5 Ga craton. The Jurassic plutons are metaluminous, alkali-calcic, epizonal syenites, monzodiorites and granodiorites (avg. whole-rock $\delta^{18}O$: +6.7 to +7.4). The late Cretaceous plutons are metaluminous hornblende-bearing monzogranites and granodiorites ($+7.4 < \delta^{18}O < +9.9$). The early Tertiary (Laramide) plutons are all peraluminous, leucocratic, two-mica granites ($+8.2 < \delta^{18}O < +9.0$), which exhibit synkinematic and post-kinematic features. The Cretaceous suite is <u>slightly</u> more ^{18}O-enriched and less oxidized than the Jurassic suite. The peraluminous two-mica granites, which are mineralogically closest to typical S-type plutons (as defined in SE Australia), have distinctly lower $\delta^{18}O$ values than most S-type granitic rocks throughout the world. We therefore classify all of these Arizona granites as basically I-type; there is no isotopic evidence for a major, pelitic, S-type source in southern Arizona. The two-mica granites probably represent highly fractionated "first-melts" of cratonal basement, while the epizonal Jurassic and Cretaceous plutons probably formed from "drier" melts that originated deeper in the crust.

The samples in the Transverse Ranges and the SECA part of the SBR traverse were obtained from Triassic monzonites and syenogranites, Jurassic granodiorites and monzogranites, and late Cretaceous granodiorites, monzogranites, and two-mica granites. Most of these plutons are alkali-calcic to alkalic and were intruded upward through Precambrian basement rocks, with the exception of Cretaceous calc-alkaline monzogranites and rare two-mica granites emplaced west of cratonal basement rocks in the San Bernardino Mountains (SBM) and San Gabriel Mountains (SGM). The

Triassic plutons (e.g. Mt. Lowe pluton) have uniformly low $\delta^{18}O$ values (+6.7 to +8.0). The Jurassic and Cretaceous magmas had $\delta^{18}O$ values between +6.7 and +9.3, including the two-mica granites of the Old Woman Mountains (+7.2 to +9.3), Cadiz Valley Batholith (+7.7 to +9), Chemehuevi Mountains (+7.8), and eastern SBM (+8.8 to +8.9). As in southern Arizona, these "cratonal" two-mica granites have lower $\delta^{18}O$ values than typical S-type plutons. In contrast, the Cretaceous plutons emplaced west of mapped cratonal basement in the SBM and SGM have high $\delta^{18}O$ values, between +8.5 and +10.8. This east-west change in primary whole-rock $\delta^{18}O$ marks a fundamental, regional $^{18}O/^{16}O$ boundary, which we believe can be used to map the western edge of the craton in the Cordillera of the southwestern USA. The whole-rock $\delta^{18}O$ values of the plutons in the fault-reconstructed SGM terrane, the SBM terrane, and in the Little San Bernardino Mountains (LSB) can be contoured in a systematic fashion, and these contours are subparallel to the aforementioned regional $^{18}O/^{16}O$ boundary.

Nearly all of the Jurassic plutons in the SBR traverse were emplaced into shallow volcanic centers, and they show characteristics related to calderas, including hydrothermal alteration by heated low-^{18}O meteoric waters. The altered plutons have $\delta^{18}O$ values ranging from -3.4 to +5.7, and where sampling density permits, contouring of $\delta^{18}O$ values reveals map patterns similar to those found at other meteoric-hydrothermal centers throughout the world. The best-studied of these Jurassic centers in this work is the Rodman-Ord Mountains (ROM) area, where the distinctive $^{18}O/^{16}O$ map patterns produced by the Jurassic hydrothermal events have been used to estimate approximately 3 to 4 km of left-lateral strike-slip displacement along the late Cenozoic Camp Rock Fault. These SBR calderas

are apparently part of a major Jurassic rift-system that extends from southeastern Arizona to the California-Nevada border. The low $\delta^{18}O$ values of the altered Jurassic plutons in SECA indicate that the paleoclimate in that portion of the rift was typical of mountainous regions today.

The Oligocene to Jurassic plutons in the NGB traverse in Nevada and Utah are the same samples analyzed by Farmer and DePaolo (1983) in their Nd-Sr isotopic study of NGB plutonism: (1) calc-alkaline, metaluminous granodiorites and monzogranites intrude eugeoclinal Paleozoic allochthonous terranes between the SNB and the Roberts Mountain Thrust; (2) calc-alkaline, metaluminous to peraluminous granodiorites, monzogranites and two-mica granites intrude miogeoclinal terranes between the Roberts Mountain Thrust and the first outcrops of >1.5 Ga cratonal basement going east; (3) alkali-calcic monzodiorites, granodiorites, and monzogranites intrude cratonal shelf sediments deposited on >1.5 Ga craton in northeastern Nevada and western Utah. The primary, whole-rock $\delta^{18}O$ values in the first of the above groups exhibit the same geographic systematics discovered by Taylor and Silver (1978) for the PRB in southern and Baja California. There is a sharp, north-trending $^{18}O/^{16}O$ boundary in western Nevada, analogous to the longitudinal "^{18}O-step" down the center of the PRB. West of this boundary, the NGB plutons have $\delta^{18}O$ values that are uniformly lower than +8.5, and east of this boundary the plutons have $\delta^{18}O > +8.5$, ranging up to +13.2. The highest $^{18}O/^{16}O$ areas coincide with the second of the above groups, particulary where two-mica granite plutons occur. Just east of the Utah border, the third group of plutons exhibits $\delta^{18}O$ values < +9, and farther inland, $\delta^{18}O$ decreases to values as low as +6.7. This eastern boundary is inferred to be the same one we observe in the eastern Transverse Ranges in SECA.

We use the $^{18}O/^{16}O$ data from the NGB and SBR traverses, combined and augmented with literature-derived data on the PRB, SNB, and Idaho Batholith to provide a framework for viewing the subcrustal distribution of petrotectonic assemblages in much of the western United States. In conjunction with the Nd-, Pb- and Sr-isotopic signatures, the $^{18}O/^{16}O$ data are used to map isotopic variations in the source regions of these plutons. This method yields a well-constrained model for the continental crust (especially when compared with earlier models that do not take into account the $^{18}O/^{16}O$ values). Such studies are particularly helpful in constraining rock-types in these source regions, because $^{18}O/^{16}O$ variations in rocks arise in a totally different manner than do the radiogenic isotope variations, which are mostly dependent upon age and upon various trace element concentrations.

As discovered in the PRB by Taylor and Silver (1978), the $\delta^{18}O$ values of granitic rocks in the western United States define a series of sharp isotopic boundaries, independent of pluton lithologies, between different geographic groupings of granitic plutons. These are extremely well defined for the Cretaceous magmatic arc, for which three north-trending belts of plutons exist: (1) a Western Zone (WZ) of low-^{18}O plutons with $+5.5 < \delta^{18}O < +8.5$; (2) a Central Zone (CZ) of high-^{18}O plutons with $\delta^{18}O$ between +8.5 and +13.2; and (3) an Eastern Zone (EZ) with variable $\delta^{18}O$, typically lower than +9.0, but locally exhibiting plutonic centers with $\delta^{18}O > +9.0$ (commonly associated with metamorphic core complexes). When $(^{87}Sr/^{86}Sr)_i$ values are taken into account, the Central Zone in the NGB must be divided into two geographic and geochemical entities; one lying west of a north-trending $(^{87}Sr/^{86}Sr)_i$ "step" (<0.7080 to the west and > 0.7100 to the east), and one between

this $^{87}Sr/^{86}Sr$ "step" and the CZ-EZ boundary. The westernmost part is here termed the Central V-type subzone (CZ-V), and the eastern part is termed the Central S-type subzone (CZ-S). The CZ-S subzone is not present (except on a very small, local scale) south of approximately latitude 37°N, but it makes up approximately half of the Central Zone in the NGB, and dominates the CZ in the Idaho Batholith, north of the NGB. In contrast, the CZ-V subzone extends along the entire length of the Cordillera in the western USA, although it is very narrow north of 40°N latitude in the western portions of the Idaho Batholith.

The three geographic $^{18}O/^{16}O$ zones have boundaries coincident with several fundamental geologic features. The WZ occurs west of the quartz diorite line of Moore (1959) while the CZ is centered on the thickest portions of the late Precambrian-early Phanerozoic (0.3 to 1.5 Ga) Cordilleran geosyncline. The CZ in general lies east of the quartz diorite line, and west of the western limits of >1.5 Ga Precambrian crystalline basement. The CZ-V subzone lies within the area of the geosyncline characterized by accreted terranes and dominated by eugeoclinal lithologies, whereas the CZ-S subzone appears to be associated with late Proterozoic miogeoclinal metasedimentary rocks. The EZ is located east of the western limit of older (>1.5 Ga) crystalline basement and east of the thick geosynclinal sedimentary section. The EZ hosts most of the major porphyry copper deposits of the region, whereas the CZ hosts the known tungsten-skarn deposits.

The isotopic data suggest that the Cordilleran granitic plutons are derived from varying proportions of the following major end-member components (largely by simple two-component mixing): (1) upper mantle and/or subducted oceanic crust, either an Oceanic Island Arc (OIA), or

MORB-type source, with $\delta^{18}O$ = +6 to +7, $(^{87}Sr/^{86}Sr)_i$ ~ 0.702 to 0.704, and ε_{Nd} ~ +2 to +7; (2) "eugeosynclinal" sediments and altered volcanic rocks (SAV-type sources) with $\delta^{18}O$ = +10 to +13.5, $(^{87}Sr/^{86}Sr)_i$ ~ 0.705 to 0.710, and ε_{Nd} = -2 to -9; (3) "miogeosynclinal" continental margin sediments (MCM), with $\delta^{18}O$ > +10, $(^{87}Sr/^{86}Sr)_i$ > 0.715, and ε_{Nd} < -9; (4) some type of "model lithospheric component" in the lower continental crust (LCC, >1.5 Ga) and/or upper mantle (SCL), having evolved, crustal characteristics and $(^{87}Sr/^{86}Sr)_i$ of about 0.705 to 0.710, with $\delta^{18}O$ values of +6.0 to +8.0 in the SBR and +7.5 to +9 in the NGB, and ε_{Nd} = -6 and -12 in the NGB and -4 and -10 in the SBR; and (5) mid-level continental crust of the craton (MCC) with $\delta^{18}O$ = +8 to +10, $(^{87}Sr/^{86}Sr)_i$ > 0.715, and ε_{Nd} < -12 to as low as -20. The latter values depend on the age of the crust.

The simplest way to characterize each geographic $^{18}O/^{16}O$ zone is by simple two-component melt-solid or solid-solid mixing of source-region materials, although the lack of specific isotopic data on the actual end-members precludes a rigorous evaluation of the relative importance of assimilation-fractional crystallization (AFC) processes. Western Zone: OIA-SAV with OIA dominant. Central V-type subzone: OIA-SAV with SAV dominant. Central S-type subzone: dominantly MCM with minor SAV, LCC, and OIA(?). Eastern Zone: dominantly LCC/SCL with widely varying proportions of some other end-members, such as MCC and/or a modified OIA mantle component (i.e., one that is older and more LIL-enriched than Cretaceous OIA or MORB, and thus one with a relatively high Sr content and high $^{87}Sr/^{86}Sr$ ratio).

Previous workers place the "edge of the craton" beneath the ~0.706 (Kistler and Peterman, 1978) or ~0.708 (Farmer and DePaolo, 1983)

$(^{87}Sr/^{86}Sr)_i$ boundaries. However, we suggest that, in the NGB the $(^{87}Sr/^{86}Sr)_i$ "step" (0.708) is not the edge of the craton, but instead is probably a structural discontinuity that has juxtaposed an accreted terrane of eugeosynclinal volcanic and volcanogenic sedimentary rocks on the west against a late Precambrian sedimentary terrane on the east. The sharpness of this boundary implies that it is either the edge of an ancient rift-zone (Kistler and Peterman, 1978), a strike-slip fault, or a suture zone. The hypothetical late Precambrian metasedimentary basin that we infer east of the $^{87}Sr/^{86}Sr$ "step" could represent an in-filled pull-apart basin, which opened during southward transport of the "Mojavia" terrane of Bennett and DePaolo (1987), thus explaining the east-trending boundary between the CZ and EZ that extends all the way across south-central Nevada.

The isotopic differences inferred for the deep continental crustal sources (LCC/SCL) in the NGB ($\delta^{18}O$ = +7 to +9) and SBR ($\delta^{18}O$ = +6 to +8) bear on the structure of the craton. The $\delta^{18}O$ of the LCC/SCL component in SECA is similar to that in southern Arizona, implying that the $^{18}O/^{16}O$ composition of LCC/SCL in the SBR was acquired after any of the hypothetical tectonic movements that shifted "Mojavia" from the NGB southward into southeastern California (Bennett and DePaolo, 1987). This means that: (1) a relatively low-^{18}O source could have underplated the SBR (including Mojavia) after tectonic emplacement of "Mojavia" athwart the southern Arizona region; or (2) previous fusion events at 1.4 Ga and 1.1 Ga could have modified the SBR deep sources, such that the $\delta^{18}O$ of the LCC/SCL underneath the SBR was lowered relative to the equivalent zone in the NGB.

TABLE OF CONTENTS

CHAPTER 4. CONTINUED

CHAPTER 7. CONTINUED

List of Figures

List of Figures, cont'd.

List of Figures, cont'd.

List of Figures, cont'd.

List of Figures, cont'd.

List of Figures, cont'd.

List of Figures, cont'd.

LIST OF TABLES

Appendix

CHAPTER 1. INTRODUCTION

1.1 Purpose of Study

The origin of granites has held a fascination for geologists, and has been the subject of scrutiny for many years (Bowen, 1928; Tuttle and Bowen, 1958; Chappell and White, 1974; Wyllie, 1977, 1978, 1981a). Granitic plutonism bears a relationship to the timing of tectonic events such as subduction and continental collision (Taylor and Silver, 1978; Pitcher, 1979), to the intensity of metamorphism both on a regional and local scale (Buddington, 1959), and to the general tectonic framework in the surrounding country rocks. The chemical compositions of the granitic plutons are directly related to their level of emplacement and their potential for hosting ore deposits (Strong, 1980; Lowell, 1974; Burnham, 1979; Michard-Vitrac et al. 1980; Newberry and Einaudi, 1981). As such, an understanding of the origin of granitic rocks continues to be crucial to many aspects of geology.

One important facet of the study of granites is the determination of the characteristics of the magmatic source regions (Chappell and White, 1974; Lee, et al., 1982). This question may be addressed by comparing the chemical "signatures" or "fingerprints" of plutons with those of their hypothetical source regions, in order to see if a "match" can be established. In this regard, stable isotopes, especially those of oxygen, provide one of the most useful tools for the "fingerprinting" (O'Neil and Chappell, 1977; O'Neil et al., 1977; Taylor, 1968, 1978; Taylor and Silver, 1978).

The principal purpose of this thesis is to try to establish the relative importance of various kinds of protoliths or source regions in

the generation of Mesozoic and early Tertiary granitic melts in the southern part of the Cordilleran orogenic belt of North America. The major impetus behind the thesis is an earlier $^{18}O/^{16}O$ study of the Peninsular Ranges batholith (PRB) of southern and Baja California, where Taylor and Silver (1978) discovered striking geographic regularities and transverse asymmetries in $\delta^{18}O$ along this north-northwest trending Cretaceous plutonic arc. The present study was undertaken to see whether the batholithic rocks to the east of the PRB also display systematic $\delta^{18}O$ patterns.

Except for the Idaho batholith (Criss and Taylor, 1983; Fleck and Criss, 1985; Criss and Fleck, 1987), most other $\delta^{18}O$ studies of batholiths in the North American Cordillera (Masi et al., 1981; Lee et al., 1981a; Saleeby et al., 1987) have not shown the clear patterns established for the PRB. However, as will be indicated below, the results of the present study show that the broad zone of granitic batholiths in the southwestern United States exhibits $^{18}O/^{16}O$ regularities grossly similar to those of the PRB. It was only by filling in the gaps in our $^{18}O/^{16}O$ sampling of these other Cordilleran batholiths that we were finally able to discern the overall $\delta^{18}O$ systematics for the entire region.

This thesis also attempts to answer the following specific questions:

1. What is the distribution and range of $\delta^{18}O$ values in Mesozoic and early Tertiary plutons in the southern Cordillera, and is it possible to delineate regularities with sufficient accuracy that these can be used to monitor offsets along major Cenozoic structural discontinuities such as strike-slip faults?
2. What is the significance of the $\delta^{18}O$ variation between dif-

ferent types and ages of plutons, especially between two-mica ± garnet-bearing granites and the more common quartz monzonites and granodiorites?

3. What is the relationship, if any, between mineral deposits and the primary $\delta^{18}O$ values of the associated granitic plutons? Also, is there any evidence for the kinds of low-^{18}O meteoric-hydrothermal alteration effects that are so common in the northern Cordillera and along the extreme western edge of the PRB?

4. How do the $\delta^{18}O$ data and the models derived therefrom fit into earlier models of the origin of these granitic batholiths based on petrography, chemical compositions, and strontium, neodymium, and lead isotopic compositions of such rocks?

5. How closely can we characterize the source regions or protoliths from which the granitic magmas were derived, particularly with regard to their lithology, age, bulk chemistry, and distribution within the crust or mantle?

The data in this thesis were mainly obtained on whole-rock samples of Mesozoic and early Cenozoic plutonic rocks in southeastern California, southern Arizona, and the Basin and Range Province in Nevada and Utah (shown in Figure 1.1). The detailed $\delta^{18}O$ maps of these areas presented in this thesis have importance for petrogenetic studies because the primary magmatic oxygen isotopic composition of a pluton reflects the $^{18}O/^{16}O$ ratio of its source region. The detailed maps, then, provide a powerful tool for studying relationships between batholithic terranes, their mineral deposits, and the tectonic frameworks in which they occur.

Figure 1.1 Map of the southwestern United States and northwestern Mexico showing the Mesozoic and early Tertiary batholithic terranes discussed in this thesis: (1) The Basin and Range Province of central Nevada, western Utah, and southern Arizona, subdivided by latitude 38°N into the Northern Great Basin (NGB) and the Southern Basin and Range (SBR); (2) The Sierra Nevada Batholith (SNB) of central California; (3) The Southeastern California Area (SECA), subdivided into the Mojave Desert and the Central and Eastern Transverse Ranges; from west to southeast these mountain ranges include the San Gabriel Mountains (SGM), the San Bernardino Mountains (SBM), and the Little San Bernardino Mountains (LSB); and (4) The Peninsular Ranges Batholith (PRB) of southern California and Baja California, Mexico. The Coast Ranges batholithic terrane is not considered in any detail in this thesis; however, parts of the Coast Ranges would belong to terrane (3) after restoration of late Cenozoic movement along the San Andreas fault.

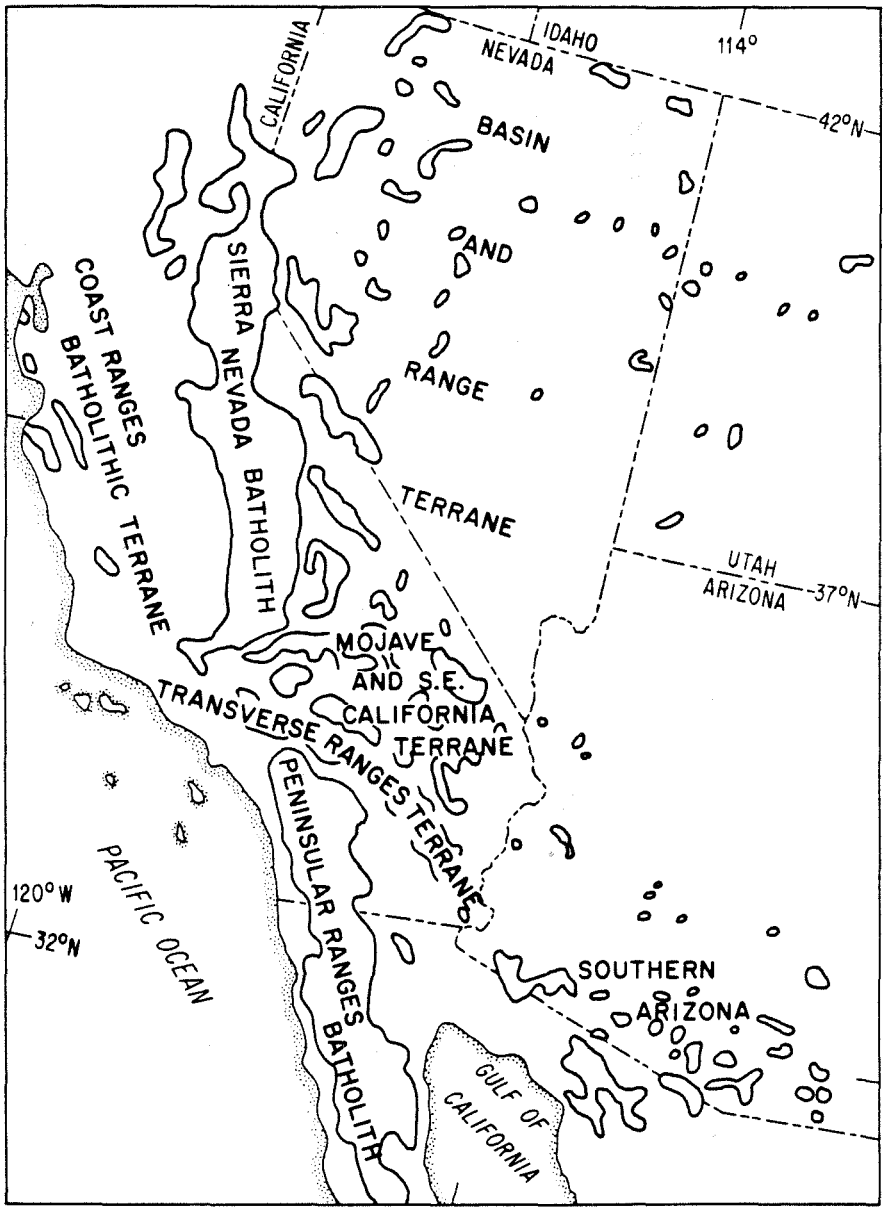
CALIFORNIA
NEVADA
IDAHO
114°
42°N
BASIN
AND
RANGE
TERRANE
SIERRA NEVADA BATHOLITH
COAST RANGES BATHOLITHIC TERRANE
UTAH
ARIZONA
37°N
MOJAVE AND S.E. CALIFORNIA TERRANE
TRANSVERSE RANGES TERRANE
PENINSULAR RANGES BATHOLITH
PACIFIC OCEAN
120° W
32°N
SOUTHERN ARIZONA
GULF OF CALIFORNIA

1.2 Brief Review of Previous Studies

1.2.1 $^{18}O/^{16}O$ Studies of Granitic Rocks

In order to evaluate the link between batholithic source regions and the $\delta^{18}O$ patterns obtained for the granitic plutons, it is first necessary to understand how various igneous, metamorphic, and hydrothermal processes can affect the $\delta^{18}O$ systematics of a granitic body in ways other than the straightforward and simplistic "fingerprinting" of its source. A detailed analysis of these problems is taken up in Chapter 3. Of primary importance as background to this objective are the works of Silverman (1951), Taylor and Epstein (1962a; 1962b), and Taylor (1968), as well as reviews by Taylor (1974; 1977; 1978) and Taylor and Sheppard (1986).

Silverman (1951) showed that there was a measureable range of $^{18}O/^{16}O$ ratios in igneous, metamorphic, and sedimentary rocks, from about +5 to +35 per mil. He found that mafic igneous rocks had low-^{18}O contents, with $\delta^{18}O$ values generally no greater than +7.0, and generally not less than +6.0. He also found that in any single granitic rock, quartz tends to be more ^{18}O-rich than coexisting alkali feldspar, and that the $^{18}O/^{16}O$ fractionation or difference in $\delta^{18}O$ values between these two minerals ($\Delta^{18}O$ value) was generally around 1.2 per mil. As shown by much subsequent work, this $\Delta^{18}O$ value of about 1.0 to 1.5 per mil provides an excellent constraint to test whether the coexisting quartz and alkali feldspar in a granite have preserved the original $\delta^{18}O$ values established by equilibration at near-magmatic temperatures.

Modern consideration of the oxygen isotopic variations in igneous rocks began with the works of Taylor and Epstein (1962a; 1962b). Using the fluorine extraction technique described by Baertschi and Silverman

(1951), they showed that $^{18}O/^{16}O$ analyses could be performed fairly routinely. They confirmed the observation of Silverman (1951) that mafic igneous rocks are generally lower in $\delta^{18}O$ than granitic rocks, and they established that the mineral phases present in most granites display a unique and systematic sequence of fractionation of oxygen isotopes: quartz, alkali feldspar, plagioclase, muscovite or hornblende, biotite, ilmenite, and magnetite, going from highest $\delta^{18}O$ to lowest $\delta^{18}O$. In later studies, it was discovered that this sequence varies only if a disequilibrium, subsolidus event (such as hydrothermal alteration) subsequently disturbed the primary igneous $^{18}O/^{16}O$ compositions of the minerals (Taylor, 1968).

In addition to observing detailed $^{18}O/^{16}O$ fractionation data for plutonic minerals, Taylor and Epstein (1962b) were the first to calculate the effects of fractional crystallization upon the $\delta^{18}O$ composition of a melt. They modelled a silicate melt-crystal system as a simple binary system, which fractionated oxygen according to the Rayleigh equation:

$$R/R_o = f^{(\alpha - 1)} \qquad (1.1)$$

where f = the fraction of melt remaining at any time, α = the fractionation factor between the bulk crystals and the melt (assumed to be constant), R_o = the isotopic ratio in the original melt, and R = the isotopic ratio of the melt at any time. Inherent in their calculation is the Rayleigh fractionation constraint, whereby melt is instantly removed from equilibrium contact with the crystals as soon as the crystals form. These calculations showed that, even with values of α close to 1, significant $^{18}O/^{16}O$ changes might be observed in the late differentiates formed at the very end stages of fractional crystallization. In this respect, knowledge of the exact value of α is crucial in deciding whether any appreciable $^{18}O/^{16}O$ changes will occur during magmatic differentiation.

More recently, Taylor (1974; 1977; 1978; 1986) discussed the oxygen isotopic systematics of granites in the North American Cordillera, and elsewhere. A main emphasis of these studies was to establish the importance of subsolidus exchange between heated meteoric waters and the granitic plutons. However, these studies also touched on several items of fundamental importance to the present study.

Taylor (1968; 1977; 1978) divided plutonic granitic rocks into three broad groups based upon their whole-rock $\delta^{18}O$ values: low-^{18}O rocks with $\delta^{18}O < +6$ per mil; normal-^{18}O rocks with $+6 < \delta^{18}O < +10$; and high-^{18}O rocks with $\delta^{18}O > +10$ per mil. He noted that the plutons in the high-^{18}O group could not be derived by simple fractional crystallization from the lower-^{18}O magmas, because of the small melt-crystal $^{18}O/^{16}O$ fractionations at magmatic temperatures and because there is a cancelling effect among the various mineral-melt α values. For example, in granitic magmas the quartz-melt $^{18}O/^{16}O$ fractionation (Δ value) is positive, while the other mineral-melt $\Delta^{18}O$ values are negative; these factors are practically equal and opposite in their overall material-balance effects on the $\delta^{18}O$ of the crystallizing magma (e.g., see Garlick, 1966; Taylor, 1968). Therefore, the high-^{18}O granitic plutons must have attained their heavy isotopic composition by anatexis of high-^{18}O source rocks, or by exchange with or assimilation of high-^{18}O rocks by the magma during its development and evolution.

Support for the above conclusions came from a variety of experimentally and empirically determined melt-solid $^{18}O/^{16}O$ fractionation factors in high-temperature silicate-melt systems; these were all shown to be very small, and thus fractional crystallization would have little effect on determining the isotopic composition of the final melts that comprise

plutons. This assertion has been discussed in detail by Taylor and Sheppard (1986), and it is reviewed in more detail in Chapter 3.

An important point discussed by Taylor (1977; 1978) is that subsolidus exchange of oxygen isotopes between heated meteoric waters and plutons is locally common in batholithic rocks of the Cordillera. This phenomenon is widespread in epizonal plutons throughout the world, especially where they are emplaced into rift zones, or into jointed, permeable volcanic cover, as in the Hebrides Islands of Scotland; at the Skaergaard intrusion, Greenland; and in the San Juan volcanic field, western United States (Forester and Taylor, 1972, 1977; Taylor and Forester, 1971, 1979; Taylor, 1974; Larson and Taylor, 1986). Inasmuch as this exchange process often produces drastic depletions of ^{18}O in the affected plutons, it may obscure the primary, magmatic $\delta^{18}O$ that a pluton inherits from its source; thus it becomes necessary to find some means to "see through" these effects. As explained in Chapter 3, even in the case of heavily altered rocks, it is usually possible to "correct" the whole-rock $\delta^{18}O$ values back to their original primary values by analyzing the $\delta^{18}O$ of the quartz.

Taylor (1968, 1978) noted that the values of $\Delta^{18}O$ (approximately equal to $1000 \ln \alpha$) for coexisting quartz and alkali feldspar in undisturbed plutonic rocks are typically about +1.0 to +1.5 per mil, while the fractionations between quartz and more calcic plagioclase are higher at +1.5 to +2.5 per mil. Any appreciable deviation from these values constitutes evidence that sub-solidus hydrothermal exchange has affected the rock in question. Taylor and Magaritz (1978) studied the above-described effects in the batholithic terranes of the Cordillera in Alaska and Canada, and found them to be common in rocks that were emplaced within about

5 km of the surface, particularly in the vicinity of major fracture zones in the crust. These effects are especially easy to see in plutons located in northern latitudes where the local meteoric waters were very low in ^{18}O during Mesozoic and Cenozoic times.

1.2.2 General $^{18}O/^{16}O$ and $^{87}Sr/^{86}Sr$ Relationships in Cordilleran Batholiths

Although this thesis itself is the principal source of $^{18}O/^{16}O$ data gathered from granitic plutons in southeastern California and southern Arizona, and to a lesser extent in Nevada and Utah as well, we also rely heavily on published analyses from several other major $^{18}O/^{16}O$ studies of Cordilleran batholiths. These terranes are: (1) the Sierra Nevada batholith (SNB) (Masi et al., 1981; Saleeby et al., 1987); (2) the PRB (Turi and Taylor, 1971a; Taylor and Silver, 1978; Hill et al., 1986); and (3) plutons in Nevada and Utah (Lee et al., 1981a). The first and second terranes also have available a substantial number of $^{87}Sr/^{86}Sr$ analyses. These are discussed in relation to corresponding $^{18}O/^{16}O$ analyses in Section 1.2.6.

We also include $^{18}O/^{16}O$ data from a number of studies of individual granitic stocks throughout the area, including Sheppard et al. (1971, Ajo, Arizona; Bingham, Utah; Santa Rita, New Mexico); Taylor (1968, Alta Stock, Utah); Taylor and O'Neil (1977, Osgood Mountains, Nevada); Batchelder (1977, Copper Canyon, Nevada); Turi and Taylor (1971b, Texas Canyon, Arizona); Shieh and Taylor (1969a,b, Birch Creek Pluton, California; Santa Rosa Range, Nevada; Eldora Stock, Caribou Stock, Colorado); Hall et al. (1974, Climax, Colorado); and Larson and Taylor (1986, western San Juan Mountains, Colorado). These studies and others, when combined with the present thesis study, provide a fairly complete reconnaissance

sampling of Mesozoic and early Cenozoic plutons south of latitude 43°N, and north of approximately latitude 31°N between longitudes 121°W and 108°W.

In addition, for areas farther north, major portions of the Coast Plutonic Complex in British Columbia and Alaska, and from the Idaho and Boulder batholiths can be included from the works of Magaritz and Taylor (1976a, 1976b, 1986), Criss and Taylor (1983), Criss and Fleck (1987), and Sheppard and Taylor (1974).

1.2.3 Sierra Nevada Batholith (SNB)

Masi et al. (1981) measured whole rock $\delta^{18}O$ values for tonalites, granodiorites, and quartz monzonites in the Sierra Nevada batholith and the western Mojave Desert of California. They also presented previously determined (Kistler and Peterman, 1973, 1978; and other unpublished data of R.W. Kistler) initial $^{87}Sr/^{86}Sr$ values for the same samples. Saleeby et al. (1987) analyzed $\delta^{18}O$ and initial $^{87}Sr/^{86}Sr$ in a number of tonalites, granodiorites and gabbros from the extreme southern part of the SNB, just north of the Garlock fault. Figure 1.2 is a map of the batholithic rocks, showing the sample localities where isotopic compositions were determined. Table 1.1 lists these $\delta^{18}O$ values and initial $^{87}Sr/^{86}Sr$ ratios. The $\delta^{18}O$ values range from +5.9 to +12.4, with the bulk of samples lying between +7.0 and +10.0 (Figure 1.3). This figure indicates that the majority of Sierra Nevada rocks lie in the range considered "normal" according to the classification of Taylor (1968, 1978). However, rocks in the Mojave Desert and southern SNB contain a higher percentage of high-^{18}O plutons.

Assuming that all of the analyses indeed represent primary magmatic $\delta^{18}O$ values, it is plain to see that certain geographic localities stud-

Figure 1.2 Map of the Sierra Nevada Batholith (SNB) and western Mojave Desert, showing sample localities from studies by Masi et al. (1981) and Saleeby et al. (1987). Sample numbers shown next to symbols correspond with information on rock type, whole-rock $\delta^{18}O$, initial $^{87}Sr/^{86}Sr$, and ε_{Nd} listed in Table 1.1. Triangles indicate samples from plutons older than 145 Ma and circles indicate samples from plutons younger than 135 Ma (ages estimated from data of Chen and Moore, 1982; Kistler and Peterman, 1973, 1978; and map of Saleeby, 1981). Heavy dashed lines indicate boundaries of $\delta^{18}O$ geographic zones discussed in Chapters 9 and 10. The westernmost dashed line is the boundary between the Western Low-^{18}O Zone and the Central High-^{18}O Zone, and the easternmost dashed line defines the boundary between the Central Zone and the Eastern Intermediate-^{18}O Zone. Those boundaries are poorly defined south of Garlock fault because of Cenozoic tectonic disruptions (see Chapter 10). Each sample is classified according to its $\delta^{18}O$ zone in Table 1.1. The arrows divide the SNB into a north half and a south half; the $\delta^{18}O$ values of all of the samples from the north half of the SNB are projected onto the cross section shown in Figure 9.2 in Chapter 9.

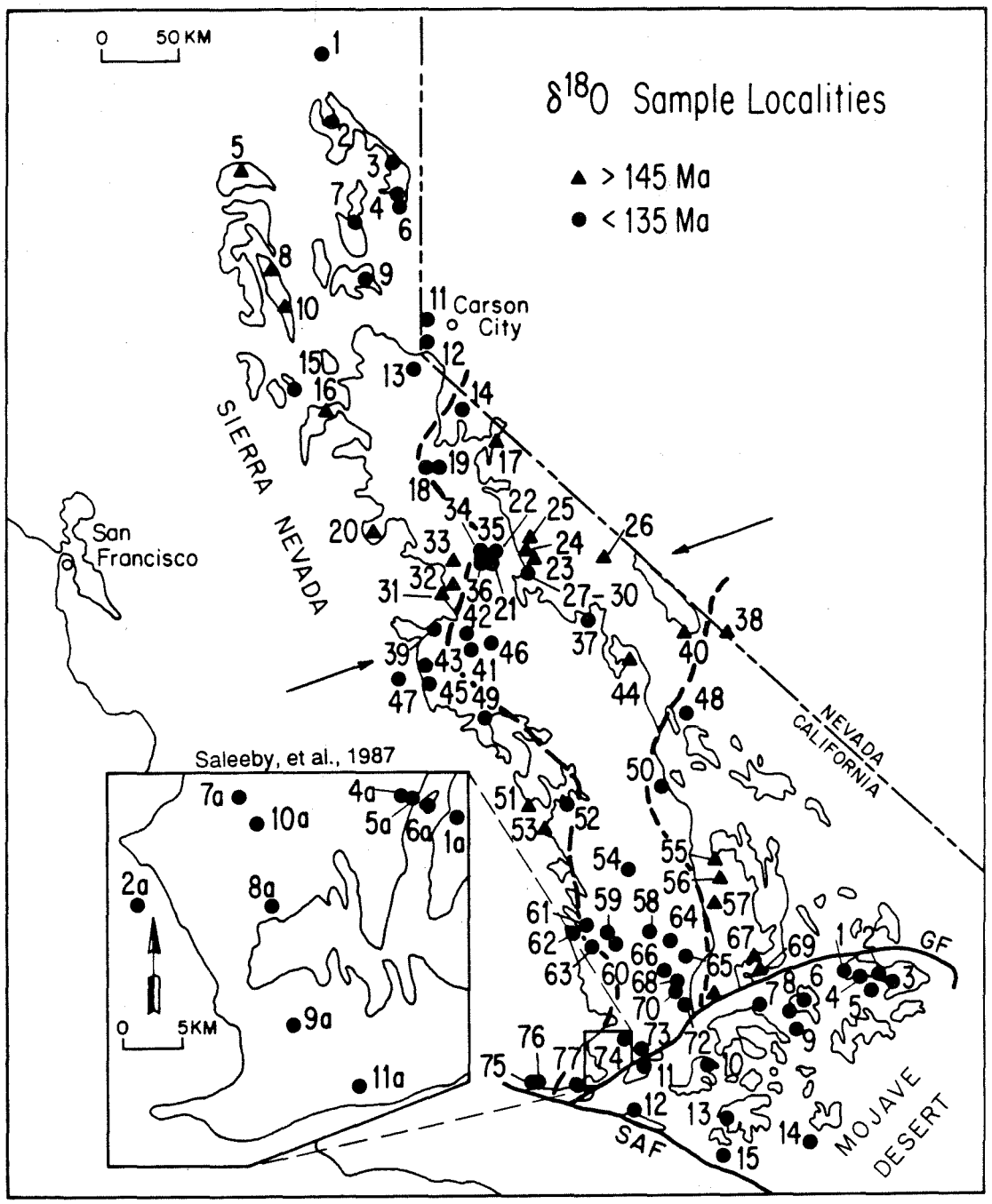
0 50 KM
δ18O Sample Localities
▲ > 145 Ma
● < 135 Ma
Carson City
SIERRA NEVADA
San Francisco
NEVADA
CALIFORNIA
GF
SAF
MOJAVE DESERT
Saleeby, et al., 1987
0 5KM

Table 1.1 Whole-rock $\delta^{18}O$, initial $^{87}Sr/^{86}Sr$ and ε_{Nd} for the Sierra Nevada batholith and western Mojave Desert.[a]

Sample No.	Rock Type	Whole rock $\delta^{18}O$	Initial $^{87}Sr/^{86}Sr$	ε_{Nd}
	Sierra Nevada batholith			
1	Granite	+7.5	0.7037	+5.1
1A	Granite	+11.3	0.7073	--
2	Granite	+7.6	0.7041	--
2A	Granite	+10.0	0.7078	--
3	Granite	+6.6	0.7039	--
4	Granite	+6.8	0.7043	--
4A	Tonalite	+10.1	0.7058	--
5	Tonalite	+7.7	0.7037	--
5A	Tonalite	+9.1	0.7057	--
6	Granite	+8.2	0.7048	+1.2
6A	Tonalite	+10.1	0.7070	--
7	Tonalite	+6.3	0.7048	--
7A	Tonalite	+8.6	0.7059	--
8	Tonalite	+7.4	0.7041	--
8A	Tonalite	+9.6	0.7064	--
9	Granite	+7.5	0.7061	--
9A	Tonalite	+9.1	0.7068	--
10	Tonalite	+8.3	0.7043	--
10A	Diorite	+7.8	0.7060	--
11	Granite	+9.4	0.7045	--
11A	Tonalite	+5.7	0.7050	--
12	Granite	+7.0	0.7045	--
13	Granite	+6.3	0.7067	--
14	Quartz Monzonite	+8.6	0.7058	--
15	Tonalite	+6.9	0.7037	--
16	Granite	+7.9	0.7047	--
17	Quartz Monzonite	+7.1	--	--
18	Granite	+8.7	0.7067	--
19	Granite	+8.9	0.7056	--
20	Quartz Monzonite	+9.9	0.7046	--
21	Quartz Monzonite	+8.0	0.7060	--
22	Quartz Monzonite	+9.5	0.7065	--
23	Quartz Monzonite	+7.0	0.7062	--
24	Quartz Monzonite	+7.0	0.7062	--
25	Quartz Monzonite	+7.3	0.7062	--

Table 1.1, cont'd.

Sample No.	Rock Type	Whole rock $\delta^{18}O$	Initial $^{87}Sr/^{86}Sr$	ε_{Nd}
	Sierra Nevada batholith, cont'd.			
26	Granite	+8.2	0.7052	-3.5
27	Quartz Monzonite	+8.2	0.7048	-6.3
28	Quartz Monzonite	+8.1	0.7048	--
29	Quartz Monzonite	+8.2	0.7048	--
30	Granite	+7.5	0.7048	--
31	Granite	+8.6	0.7065	--
32	Granite	+8.3	0.7065	-3.9
33	Granite	+8.5	0.7065	--
34	Granite	+8.9	0.7065	--
35	Granite	+8.5	0.7065	--
36	Granite	+7.8	0.7065	--
37	Quartz Monzonite	+7.9	--	--
38	Granite	+8.3	0.7068	--
39	Tonalite	+8.4	0.7047	--
40	Quartz Monzonite	+8.1	--	--
41	Granite	+9.7	--	--
42	Granite	+10.3	0.7045	--
43	Granite	+8.1	0.7045	--
44	Granite	+7.0	--	--
45	Granite	+9.0	0.7048	--
46	Granite	+8.7	0.7075	--
47	Tonalite	+9.2	0.7032	+6.5
48	Quartz Monzonite	+8.4	0.7066	--
49	Tonalite	+7.6	0.7042	+3.3
50	Granite	+7.9	0.7068	--
51	Tonalite	+6.6	0.7038	--
52	Quartz Monzonite	+8.3	--	--
53	Quartz Monzonite	+5.9	--	--
54	Tonalite	+9.6	0.7064	--
55	Granite	+7.5	0.7041	--
56	Tonalite	+5.6	0.7060	--
57	Tonalite	+7.2	0.7060	--
58	Granite	+9.4	0.7081	--
59	Granite	+9.4	0.7061	-2.4
60	Granite	+9.9	0.7053	--

Table 1.1, cont'd.

Sample No.	Rock Type	Whole rock $\delta^{18}O$	Initial $^{87}Sr/^{86}Sr$	ε_{Nd}
	Sierra Nevada batholith, cont'd.			
61	Quartz Monzonite	+9.1	0.7043	--
62	Tonalite	+8.3	0.7038	--
63	Tonalite	+7.3	0.7032	+6.0
64	Quartz Monzonite	+11.0	0.7082	-7.6
65	Granodiorite	+7.8	0.7049	+0.6
66	Quartz Monzonite	+10.4	0.7058	--
67	Granodiorite	+7.9	0.7041	--
68	Quartz Monzonite	+10.9	0.7075	--
69	Quartz Monzonite	+7.9	0.7081	--
70	Quartz Monzonite	+10.6	0.7080	--
71	Quartz Monzonite	+8.5	0.7042	--
72	Granodiorite	+9.7	0.7070	--
73	Granodiorite	+8.5	0.7055	--
74	Granodiorite	+11.7	0.7050	--
75	Gabbro	+7.1	0.7038	--
76	Gabbro	+6.2	0.7031	--
77	Granodiorite	+12.4	0.7078	--
	Western Mojave Desert			
1	Granite	+7.7	0.7070	--
2	Quartz Monzonite	+7.3	0.7070	--
3	Quartz Monzonite	+5.0	--	--
4	Quartz Monzonite	+8.3	0.7070	--
5	Quartz Monzonite	+9.0	0.7070	--
6	Quartz Monzonite	+8.3	0.7041	--
7	Granite	+10.2	0.7066	--
8	Quartz Monzonite	+10.3	0.7064	-6.3
9	Quartz Monzonite	+10.1	--	--
10	Quartz Monzonite	+10.0	0.7077	--
11	Tonalite	+8.2	0.7058	--
12	Tonalite	+10.0	0.7083	--
13	Granite	+9.1	0.7081	--
14	Granite	+7.5	0.7095	--
15	Granite	+9.0	0.7083	--

[a] Whole-rock ε_{Nd} and initial $^{87}Sr/^{86}Sr$ from Masi et al., 1981 and Saleeby et al., 1987; ε_{Nd} from DePaolo, 1981a; Sample locations are shown on Figure 1.2, "A" indicates data from Saleeby et al., 1987.

Figure 1.3 Histogram showing the range and frequency of occurrence of primary whole-rock $\delta^{18}O$ values for Mesozoic plutonic samples from the Sierra Nevada Batholith (SNB). Data are from Masi et al. (1981) and Saleeby et al. (1987), as listed in Table 1.1. Sample localities are shown on the map in Figure 1.2.

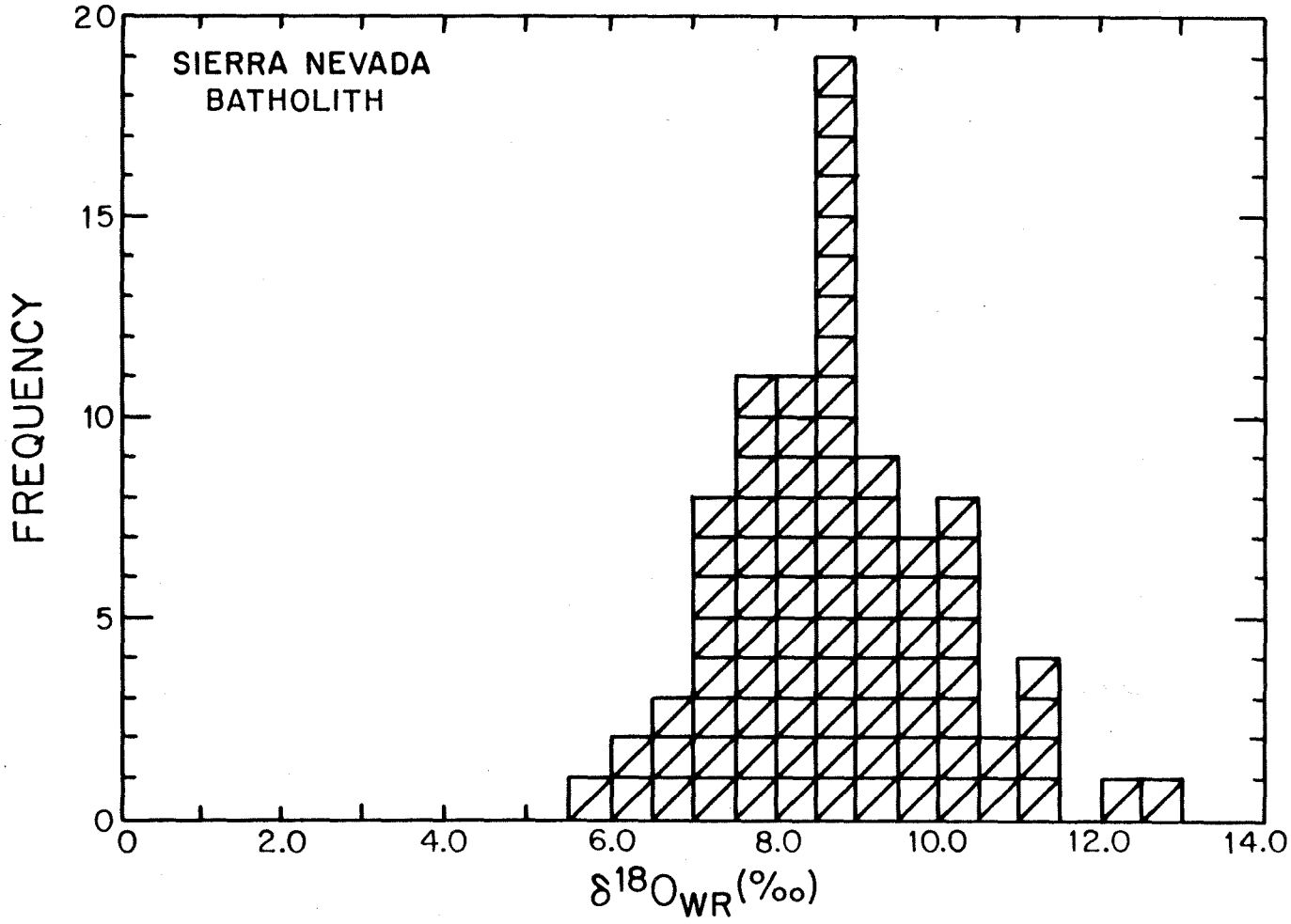
SIERRA NEVADA
BATHOLITH
FREQUENCY
0
5
10
15
20
0
2.0
4.0
6.0
8.0
10.0
12.0
14.0
δ18OWR(‰)

ied by Masi et al. (1981) are relatively homogeneous in, and thus may be characterized by, their $\delta^{18}O$ values. The five quartz analyses presented by Masi et al. (1981) yielded quartz-whole rock fractionations between +0.7 and +2.0 per mil, thus providing some evidence that this set of samples has not been seriously hydrothermally altered.

1.2.4 Basin and Range Province

Lee et al. (1981a) determined a large number of $\delta^{18}O$ values of plutons in the Basin and Range province of Nevada, western Utah, southeastern California and southern Arizona. Figure 1.4 shows a map of their $\delta^{18}O$ sample localities; the data are tabulated in Table 1.2 and shown on a histogram in Figure 1.5.

The U.S.G.S. laboratory in Denver reports a $\delta^{18}O$ for the NBS-28 standard of +9.7 per mil relative to Standard Mean Ocean Water or SMOW (Friedman et al., 1974), whereas the Caltech laboratory, and many others including the U.S.G.S. laboratory in Menlo Park (Masi et al., 1981), recognize a value of +9.60 per mil for this quartz standard. Hence, all $\delta^{18}O$ values listed in Table 1.2 were normalized to the +9.6 value by subtracting +0.1 per mil from the values given by Lee et al. (1981a).

No geographic pattern in $\delta^{18}O$ was recognized by Lee et al. (1981a); they attribute this lack of pattern to the complex magmatic and tectonic history of the area. However, we note that $\delta^{18}O$ values greater than +9.0 per mil are characteristic of a broad zone in the northern Basin and Range in central Nevada (Figure 1.4; Table 1.2), with a lobe extending just across the border into west-central Utah. Values less than +9.0 are common outside these areas, and surround this high-^{18}O central zone on the west, south, and east.

Figure 1.4 Map showing localities of samples from Mesozoic and Tertiary plutons studied by Lee et al. (1981a) and Lee (1984) in the Northern Great Basin (NGB) of Nevada and western Utah, and in the southern Basin and Range (SBR) of southern Nevada, southeastern California and southern Arizona. Sample numbers correspond with whole-rock $\delta^{18}O$ values and major-element geochemistry listed in Table 1.2. Samples are classified in Table 1.2 according to the $\delta^{18}O$ geographic zones discussed in Chapters 9 and 10. The Sierra Nevada Batholith (SNB), Mojave Desert, and Peninsular Ranges Batholith (PRB) terranes (discussed in this chapter; see Figures 1.2 and 1.6) are outlined by heavy solid lines. This thesis describes new $\delta^{18}O$ analyses of whole-rock powders (and in some cases quartz) from samples of granitic plutons from the diagonally-striped areas: (1) South-Central Arizona (Chapter 5); (2) Southern California (SECA, Chapters 6 through 8); and (3) Northern Great Basin (NGB, Chapter 9); Table 1 in the appendix contains all of the new $\delta^{18}O$ analyses, and Tables 5.1, 7.1 and 9.1 present the major-element and isotopic geochemistry, where available. Some ϵ_{Nd} and initial $^{87}Sr/^{86}Sr$ data are also available; in some cases these data are on the same samples analyzed for $\delta^{18}O$. Chapter 10 summarizes $\delta^{18}O$, initial $^{87}Sr/^{86}Sr$, ϵ_{Nd} and major-element relations for this entire area.

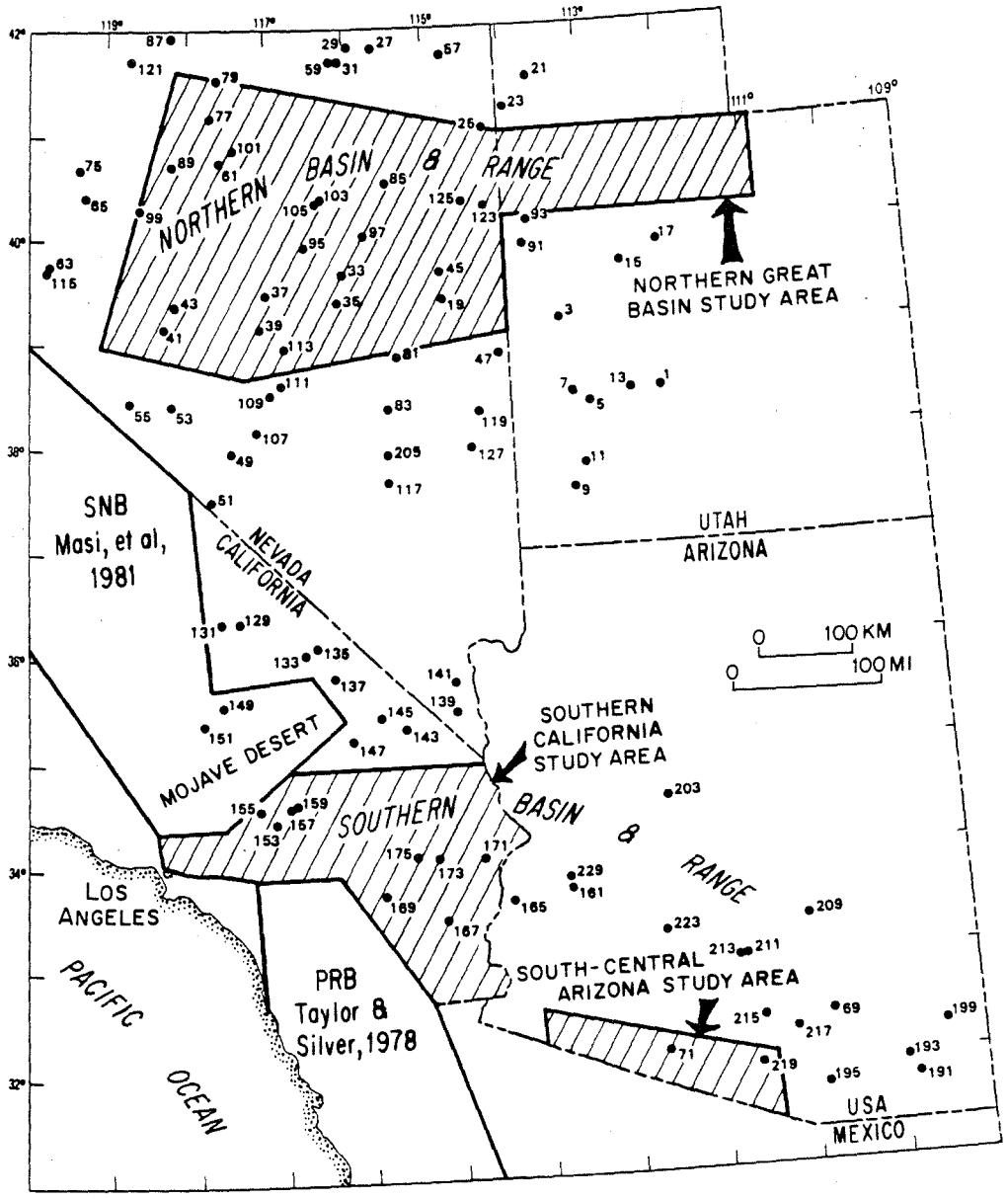
NORTHERN BASIN & RANGE
NORTHERN GREAT BASIN STUDY AREA
SNB
Masi, et al, 1981
NEVADA
CALIFORNIA
UTAH
ARIZONA
0 100 KM
0 100 MI
SOUTHERN CALIFORNIA STUDY AREA
MOJAVE DESERT
SOUTHERN BASIN & RANGE
LOS ANGELES
PACIFIC OCEAN
PRB
Taylor & Silver, 1978
SOUTH-CENTRAL ARIZONA STUDY AREA
USA
MEXICO

Table 1.2 Whole-rock $\delta^{18}O$ and selected geochemical parameters for plutons in the northern and southern Basin and Range, USA.[a]

Sample No.	Whole rock $\delta^{18}O$	Weight per cent SiO_2	CaO	Na_2O	K_2O	Fe^{3+}/ total Fe[b]	Al_2O_3/ Na_2O+K_2O+CaO[b]
		Northern Basin and Range - western Utah					
1	+4.4	58.30	5.00	3.80	4.70	0.53	0.76
3	+9.2	71.70	1.70	4.00	3.60	0.63	1.02
5	+4.4	64.20	4.10	3.60	3.30	0.49	0.88
7	+6.9	60.20	5.00	3.60	3.40	0.54	0.80
9	+7.3	63.50	4.00	3.30	3.60	0.56	0.90
11	+8.1	62.30	3.80	3.30	3.80	0.80	0.91
13	+2.3	57.40	5.20	3.50	4.00	0.42	0.80
15	+7.9	69.80	2.30	3.80	4.30	0.52	0.97
17	+0.5	60.60	4.20	3.70	3.70	0.62	0.85
21	+7.5	70.40	2.10	3.90	3.50	0.42	1.01
23	+7.8	70.30	2.40	3.90	4.00	0.44	0.97
91	+9.5	71.20	2.10	3.40	4.40	0.29	1.00
93	+6.6	61.00	5.00	3.40	3.90	0.40	0.78
		Northern Basin and Range - Nevada					
19	+9.3	70.80	2.80	3.20	3.90	0.44	1.00
25	+8.5	74.00	0.89	4.00	4.20	0.77	1.11
27	+8.8	68.10	3.30	3.70	3.40	0.52	0.98
29	+9.5	68.50	3.40	3.30	3.60	0.47	0.96
31	+7.7	58.60	5.90	3.90	1.60	0.07	0.85
33	+10.1	73.60	0.65	3.80	4.30	0.80	1.17
35	+10.0	70.80	2.40	2.80	4.70	0.35	1.00
37	+10.3	67.20	3.30	3.60	3.80	0.37	0.93
39	+3.8	68.30	3.50	3.50	3.10	0.55	1.01
41	+8.6	70.70	2.60	4.90	2.80	0.53	0.94
43	+11.5	64.00	4.00	3.60	3.80	0.53	0.88
45	+8.5	76.40	0.80	3.80	4.50	0.70	0.99
47	+10.5	74.10	2.10	3.40	3.10	0.82	1.02
49	+9.7	77.80	0.75	3.50	4.60	0.73	1.00
51	+8.8	67.70	2.50	3.70	4.30	0.50	0.96
53	+12.0	74.60	0.17	3.60	5.40	0.83	1.08
55	+7.7	72.80	1.30	4.40	3.80	0.59	0.98
57	+8.5	65.30	4.30	3.80	3.50	0.41	0.84
59	+10.7	65.50	4.30	4.00	2.50	0.20	0.92
61	+10.3	69.40	2.40	3.30	4.60	0.23	0.95

Table 1.2, cont'd.

Sample No.	Whole rock $\delta^{18}O$	Weight per cent SiO_2	CaO	Na_2O	K_2O	Fe^{3+}/ total Fe[b]	Al_2O_3/ Na_2O+K_2O+CaO[b]
		Northern Basin and Range - Nevada, cont'd.					
63	+6.7	62.20	5.10	3.90	2.50	0.48	0.88
65	+7.7	61.00	5.60	3.80	2.30	0.41	0.88
75	+8.4	66.10	3.90	4.40	2.60	0.47	0.93
77	+9.6	65.70	4.60	3.90	2.60	0.50	0.90
79	+8.6	66.50	3.40	4.60	2.40	0.42	0.94
81	+10.7	69.50	3.60	3.00	3.60	0.39	0.96
83	+11.0	72.80	2.20	3.70	3.10	0.44	1.11
85	+9.7	69.80	3.00	3.20	3.50	0.31	1.01
87	+7.6	65.10	3.80	4.60	2.60	0.59	0.93
89	+10.1	67.00	3.30	3.60	3.50	0.46	0.96
95	+4.7	66.80	3.20	3.20	3.90	0.42	0.99
97	+10.7	67.50	3.50	3.60	3.20	0.28	1.00
99	+11.0	69.00	3.50	3.60	3.70	0.33	0.92
101	+9.8	64.30	3.80	3.90	3.00	0.37	0.96
103	+9.3	70.30	1.50	3.40	4.50	0.37	1.08
105	+9.8	64.20	5.10	4.10	4.00	0.33	0.73
107	+3.6	62.80	4.70	3.30	3.70	0.48	0.88
109	+10.0	71.70	1.40	4.70	4.40	0.64	0.98
111	+10.9	71.50	1.40	4.50	3.70	0.38	1.10
113	+10.3	64.90	4.00	4.20	2.20	0.19	0.98
115	+9.0	68.40	2.70	4.20	3.60	0.55	1.01
117	+10.7	70.10	2.00	3.80	4.60	0.71	1.04
119	+6.0	66.50	3.70	2.90	3.80	0.66	0.92
121	+9.5	70.00	2.50	4.90	2.90	0.61	0.99
123	+10.3	70.10	2.30	3.70	4.00	0.45	0.96
125	+9.0	60.10	2.80	4.50	6.30	0.60	0.92
128	+8.1	--	--	--	--	--	--
		Southern Basin and Range - Nevada					
139	+3.3	65.30	2.70	4.20	4.40	0.64	0.90
141	+8.6	73.70	0.56	4.60	5.00	0.77	0.99

Table 1.2, cont'd.

Sample No.	Whole rock $\delta^{18}O$	Weight per cent SiO_2	CaO	Na_2O	K_2O	Fe^{3+}/ total Fe[b]	Al_2O_3/ Na_2O+K_2O+CaO[b]
Southern Basin and Range - southeastern California							
129	+8.5	53.40	7.20	3.70	3.00	0.47	0.80
131	+9.0	72.10	1.20	3.60	5.10	0.84	1.02
133	+8.4	67.50	2.70	4.80	3.70	0.52	0.95
135	+7.5	69.10	1.40	4.90	4.00	0.67	0.98
137	+4.5	72.20	0.75	4.60	5.10	0.79	0.99
143	+6.9	69.80	2.20	4.10	4.00	0.67	1.01
145	+12.9	72.90	1.00	4.00	4.40	0.59	1.03
147	+8.0	76.70	0.37	4.30	4.40	0.86	0.98
149	+7.6	68.70	2.60	3.00	4.60	0.54	1.01
151	+8.2	65.60	5.00	4.10	1.80	0.53	0.92
153	+8.1	61.40	4.20	4.70	4.90	0.57	0.92
155	+10.8	70.70	2.40	3.80	3.80	0.58	0.99
157	+7.4	74.20	1.70	3.40	4.60	0.57	1.00
159	+5.4	68.80	2.90	3.70	3.80	0.51	0.95
167	+8.6	62.00	4.70	3.70	3.00	0.38	0.90
169	+7.3	64.60	2.40	4.50	5.20	0.44	0.92
171	+9.2	65.00	4.50	3.50	2.90	0.45	0.91
173	+8.2	73.20	1.80	4.10	4.00	0.54	1.01
175[c]	+9.9	74.30	1.60	4.00	4.40	0.63	1.00
Southern Basin and Range - southern Arizona							
69	+9.2	71.90	1.20	4.30	3.80	0.71	1.11
71	+7.8	66.00	3.30	4.30	3.40	0.52	0.94
161	+9.3	66.70	3.50	3.70	3.50	0.45	0.95
165	+7.6	68.00	3.10	3.30	4.40	0.56	0.95
191	+6.0	76.10	0.25	3.70	4.60	0.92	1.11
193	+8.4	75.40	0.43	3.90	5.00	0.59	1.02
195	+6.9	65.00	4.00	3.90	3.80	0.49	0.89
199	+8.0	71.60	2.30	4.10	3.40	0.43	1.01
203	+8.8	68.70	2.40	5.10	2.30	0.44	1.02
205	+8.2	72.70	0.97	3.60	4.90	0.83	1.03
209	+8.4	70.00	2.20	4.60	3.60	0.62	0.99
211	+9.0	72.20	2.80	4.30	2.80	0.49	0.99
213	+9.5	69.30	3.30	3.60	3.20	0.59	1.01
215	+6.5	72.80	0.96	3.70	4.50	0.54	1.08
217	+6.7	56.90	5.80	3.80	3.00	0.47	0.81

Table 1.2, cont'd.

Sample No.	Whole rock $\delta^{18}O$	Weight per cent SiO_2	CaO	Na_2O	K_2O	Fe^{3+}/ total Fe[b]	Al_2O_3/ Na_2O+K_2O+CaO[b]
Southern Basin and Range - Arizona, cont'd.							
219	+7.6	63.20	4.10	4.20	3.30	0.38	0.93
223	+4.9	74.10	1.20	3.50	4.50	0.47	1.05
229	+7.9	75.50	0.85	4.70	4.00	0.87	1.01

[a] Sample locations plotted on Figure 1.4. Whole-rock $\delta^{18}O$ from Lee et al., 1981a; major-element geochemistry from Lee, 1984.
[b] Calculated using molar ratios.
[c] Sample GR-175 has ε_{Sr}=+84 and Sr=323 ppm (data of R.W. Kistler reported by Calzia et al., 1986).

Figure 1.5 Histogram showing the range and frequency of occurrence of whole-rock $\delta^{18}O$ values for Mesozoic and Tertiary plutonic samples from the Basin and Range Province of Nevada, western Utah, southeastern California and southern Arizona. Data are from Lee et al. (1981a), as listed in Table 1.2. Sample localities are shown on the map in Figure 1.4. Samples with $\delta^{18}O < +6$ per mil are all assumed to have been hydrothermally altered by low-^{18}O meteoric waters. Most of the whole-rock $\delta^{18}O$ values > +6 per mil probably represent primary values; however, no quartz $\delta^{18}O$ values are presented by Lee et al. (1981a) to confirm this assumption. In general, however, our new quartz and whole-rock $\delta^{18}O$ data from the NGB, and SBR areas (see Figure 1.4, Table 1 in the appendix, and Table 9.1) do confirm that the whole-rock $\delta^{18}O$ values of +6 to +13 are primary igneous values.

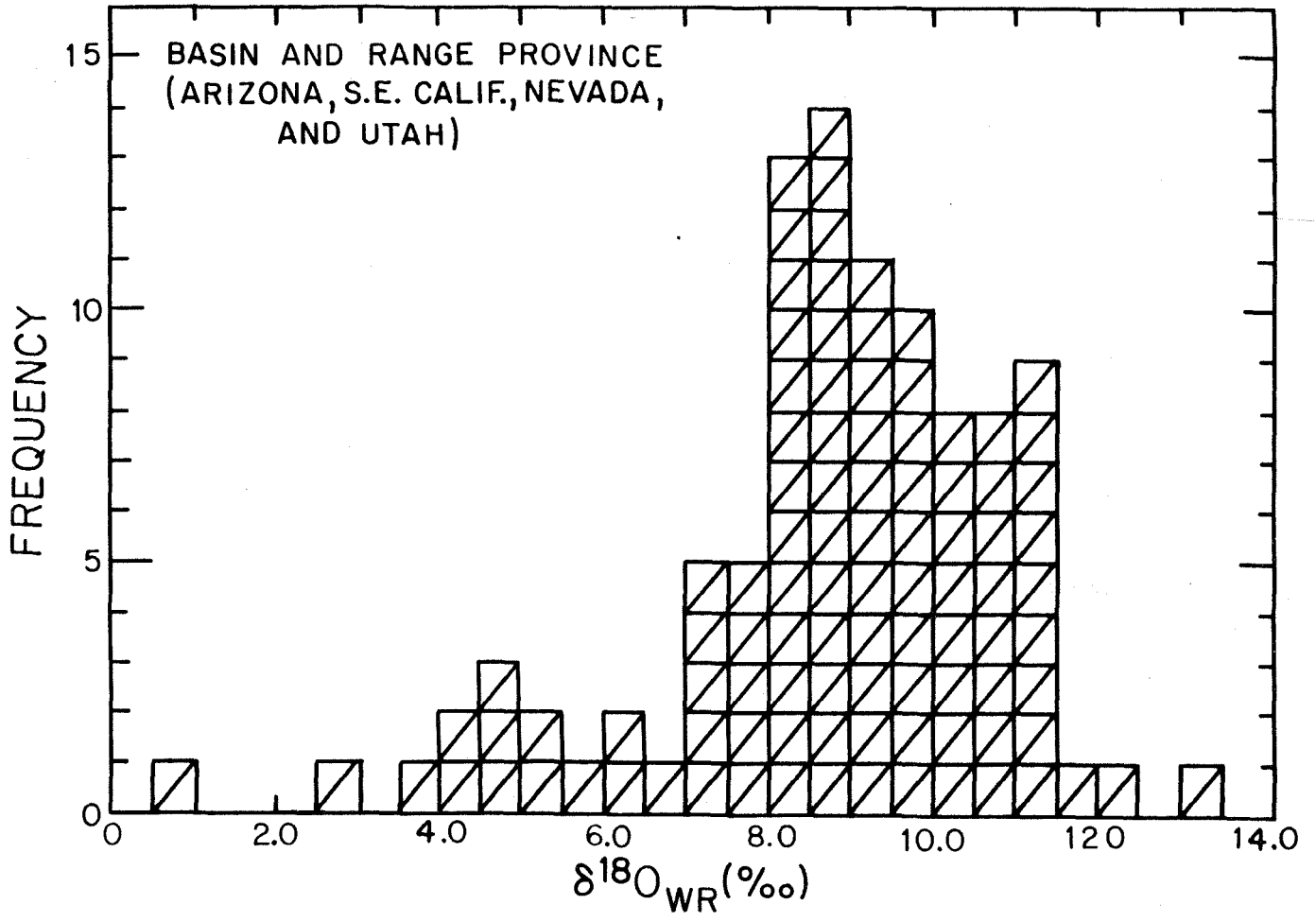
BASIN AND RANGE PROVINCE
(ARIZONA, S.E. CALIF., NEVADA,
AND UTAH)
FREQUENCY
0
5
10
15
0
2.0
4.0
6.0
8.0
10.0
12.0
14.0
δ18OWR(‰)

Samples with $\delta^{18}O$ values less than +6.5 per mil are observed locally throughout the Basin and Range area, but most of these low-^{18}O samples are clearly attributable to the type of meteoric-hydrothermal exchange discussed by Taylor (1977). Unfortunately, no quartz analyses are included in the data of Lee et al. (1981a), and therefore their low-^{18}O samples cannot be corrected to their primary, unaltered values. In spite of these problems, one thing that is clear from the work of Lee et al. (1981a) is that the northern Basin and Range of Nevada and western Utah contains a much higher percentage of high-^{18}O granitic plutons than does the SNB (compare Table 1.2 with Table 1.1). Only the data from the southern SNB and western Mojave are at all comparable to the northern Basin and Range data set.

1.2.5 Peninsular Ranges Batholith (PRB)

Taylor and Silver (1978) discovered remarkably systematic $\delta^{18}O$ relationships in the PRB of southern and Baja California. These data are also discussed by Silver et al. (1979) and by Taylor (1986). The $\delta^{18}O$ values of the PRB display geographic regularities and transverse asymmetries related to the north-northwest trend of the batholith. Figure 1.6 is a $\delta^{18}O$ contour map constructed for the PRB by Taylor and Silver (1978). This map shows that the whole-rock $\delta^{18}O$ values of the plutons increase systematically from west to east across the strike of the batholith, along almost its entire 600 km length. This isotopic distribution is essentially independent of rock type, with all of the analyzed samples from a given area in the batholith having uniform $\delta^{18}O$, from quartz gabbros and mafic tonalites with SiO_2 between 53 and 58 weight per cent, all the way to granodiorites and quartz monzonites with SiO_2 contents as high as 76 weight per cent. Essentially, the $^{18}O/^{16}O$ distribution is only a

Figure 1.6 Map of Southern and Baja California showing whole-rock $\delta^{18}O$ contours and locations of samples in the Peninsular Ranges Batholith (PRB). Solid circles indicate granitic rocks (predominantly tonalites, and granodiorites), open circles indicate gabbros. The light dashed line indicates the boundary of the PRB. The dot-dash line is the international boundary between USA and Mexico. Modified after Taylor and Silver (1978), taken from Taylor (1986). The main body of the PRB extends from just north of Riverside (USA) southeast along the length of Baja California. The San Jacinto-Santa Rosa (SJ-SR) block referred to in the text is located northeast of the +10 per mil contour immediately southwest of the city of Indio (USA).

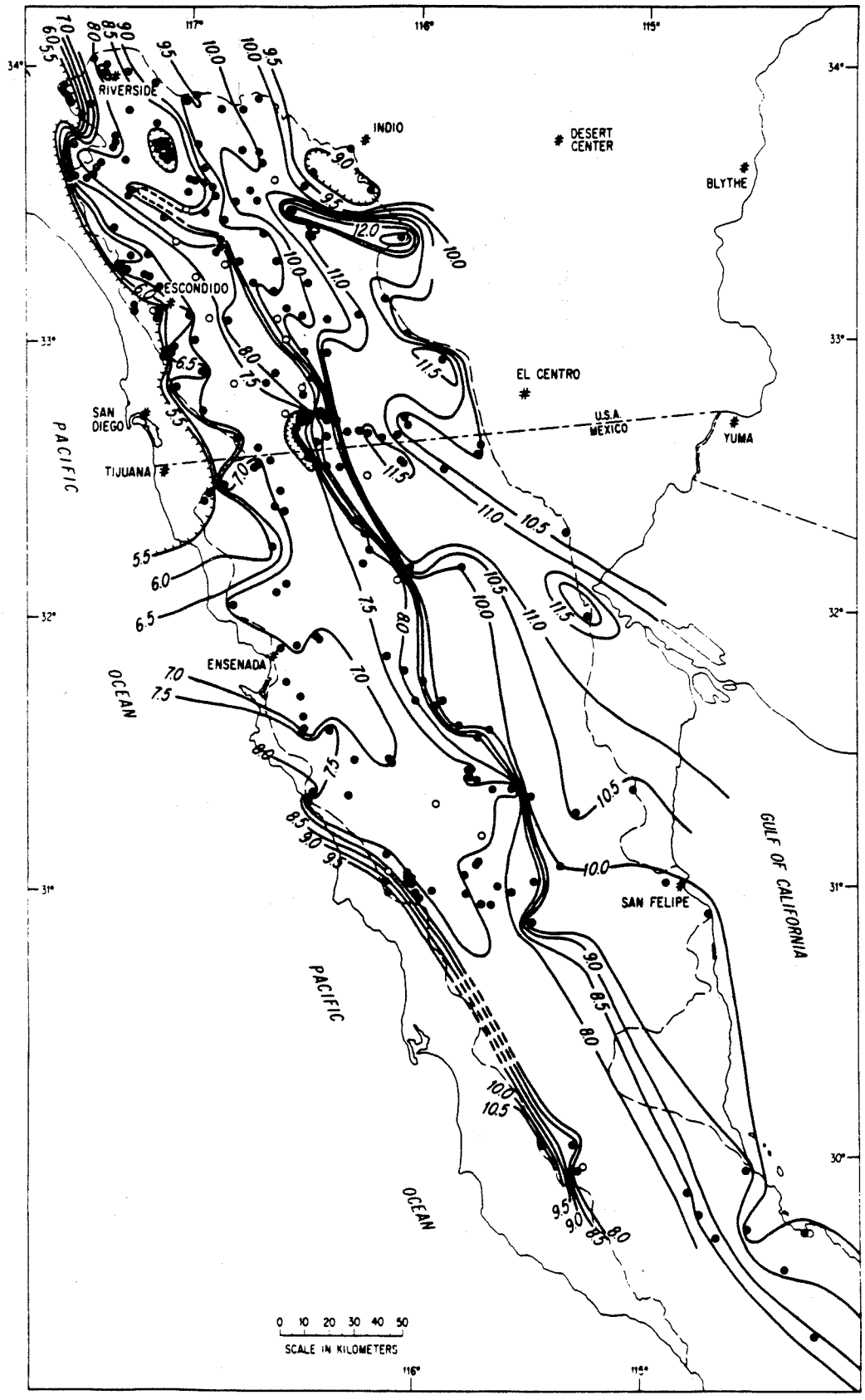
RIVERSIDE
INDIO
DESERT CENTER
BLYTHE
ESCONDIDO
EL CENTRO
SAN DIEGO
U.S.A.
MEXICO
YUMA
TIJUANA
PACIFIC
OCEAN
ENSENADA
SAN FELIPE
GULF OF CALIFORNIA
0 10 20 30 40 50
SCALE IN KILOMETERS

function of geography. The $\delta^{18}O$ values range from +6.0 in the west to as high as +13.0 in the east, before they start back down to lower values as one proceeds further east.

A significant $\delta^{18}O$ "step" separates the western half of the PRB from the eastern portion, and is manifested by the close spacing of the +8.5 and +9.0 contours (also see the histogram of $\delta^{18}O$ values presented in Figure 1.7). This is significant because, as discussed below, +8.5 per mil is precisely the value separating the bimodal distribution of $\delta^{18}O$ compiled for both the PRB itself and for all the batholithic rocks discussed in this thesis. This boundary in the PRB roughly coincides with an age boundary between plutons having 130 to 105 Ma ages on the west, and those having 105 to 85 Ma ages on the east (Taylor and Silver, 1978; Silver et al., 1979). The $\delta^{18}O$ "step" is also very close to the geographic transition from epizonal and mesozonal plutons on the west side, to deeper-seated plutons on the east side (Silver et al., 1979). In other words, the higher-^{18}O plutons on the eastern side of the PRB were emplaced at deeper levels in the crust than the lower-^{18}O plutons of the western side of the PRB. As shown below in later chapters, this relationship also seems to pertain to much of the the Cordillera elsewhere in North America.

1.2.6 $^{87}Sr/^{86}Sr$ - $^{18}O/^{16}O$ Correlations

The $^{18}O/^{16}O$ systematics discussed for the PRB in section 1.2.5 correlate closely with the west-to-east $^{87}Sr/^{86}Sr$ patterns described by Early and Silver (1973). Figure 1.8 shows the correlation between these two isotopic systems. The +8.5 to +9.0 per mil $\delta^{18}O$ "step" shows up as a "gap" in the data set on Figure 1.8. In general, where subsolidus hydrothermal events have not interfered with oxygen and strontium isotopic

Figure 1.7 Histogram showing the range and frequency of occurrence of whole-rock $\delta^{18}O$ values for samples from the Cretaceous Peninsular Ranges Batholith (PRB) of southern California (USA) and Baja California (Mexico), based on data from Taylor and Silver (1978) and Silver *et al.* (1979). Note the distinct bimodal distribution of the analyses; the $\delta^{18}O$ = +8.5 to +8.9 group clearly divides the PRB into two populations, basically a western half with primary $\delta^{18}O$ of +6 to +8.5, and an eastern half with $\delta^{18}O$ = +9 to +13. Samples with $\delta^{18}O$ < +5.5 are confined to the extreme west side (roof) of the PRB (see Figure 1.6), and all have been hydrothermally altered by low-^{18}O meteoric waters.

Figure 1.8 Plot of initial $^{87}Sr/^{86}Sr$ versus whole-rock $\delta^{18}O$ for the PRB. Data are grouped according to geographic location, either west of, or east of the +8.5 to +9 "$\delta^{18}O$-step" discussed in the text and shown in Figure 1.6. In addition, those samples located within the San Jacinto-Santa Rosa block (see Figure 1.6) are grouped separately. Modified after Taylor and Silver (1978).

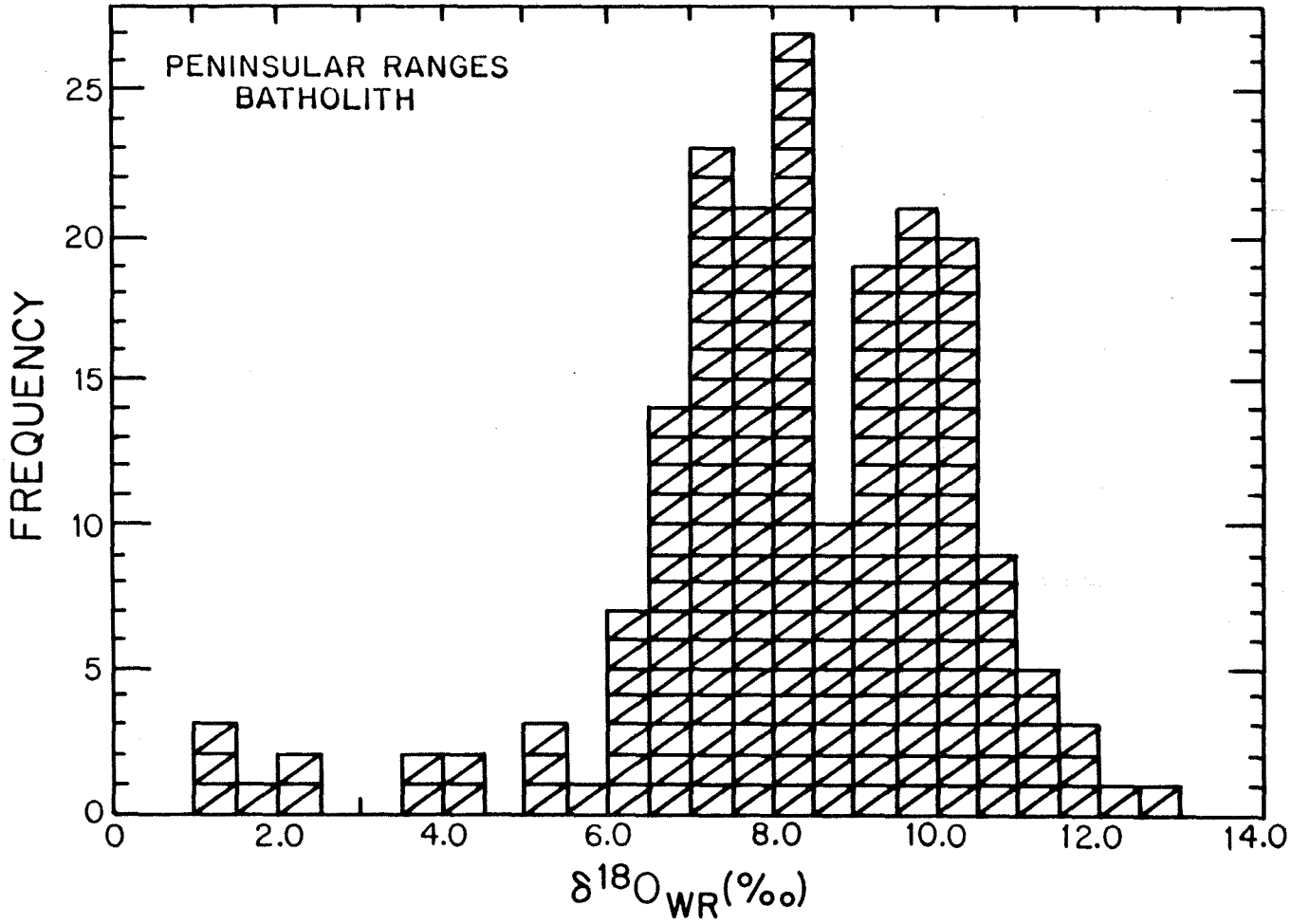
PENINSULAR RANGES
BATHOLITH
FREQUENCY
0
5
10
15
20
25
0
2.0
4.0
6.0
8.0
10.0
12.0
14.0
δ18OWR(‰)

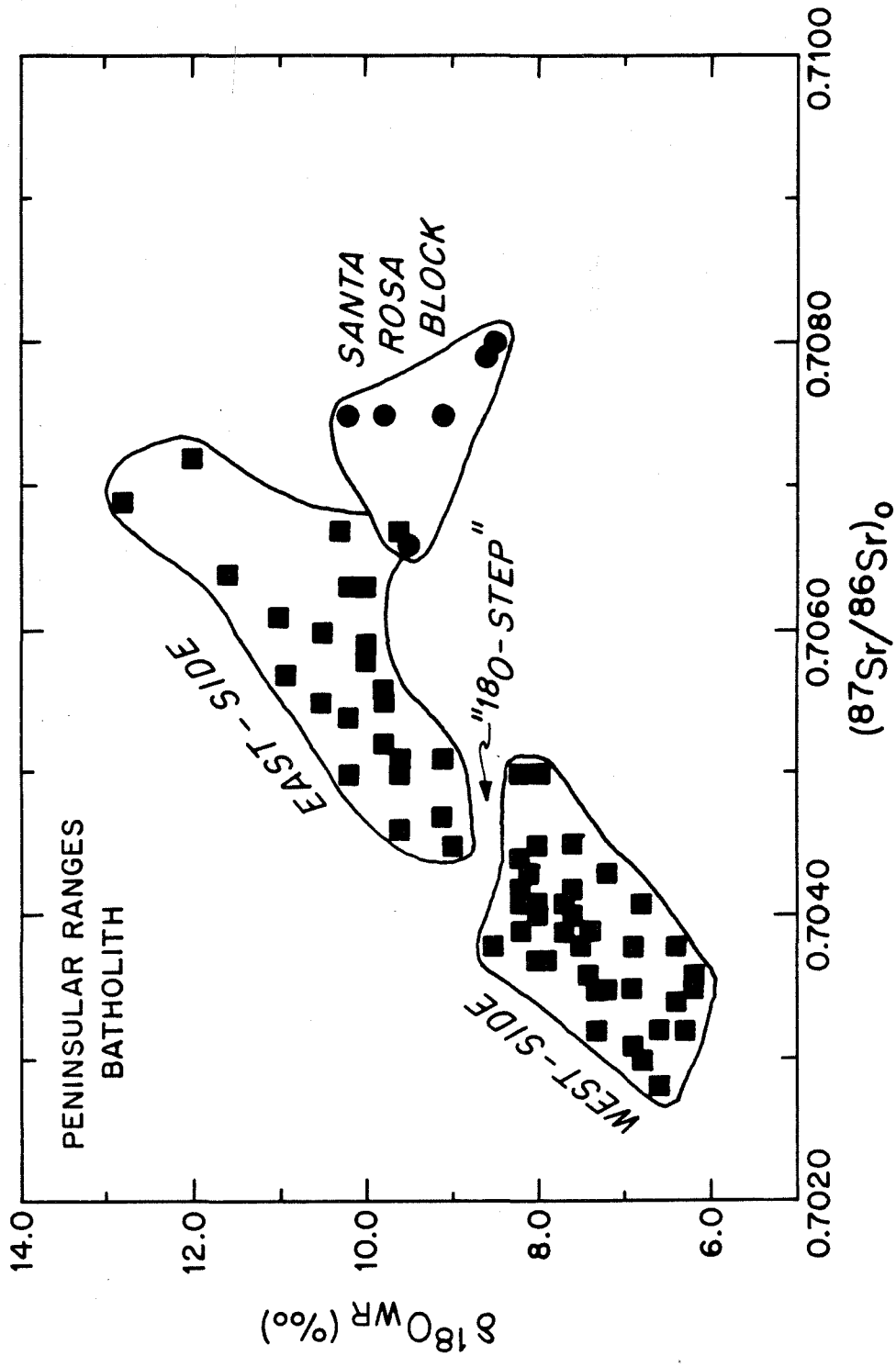
PENINSULAR RANGES
BATHOLITH
SANTA
ROSA
BLOCK
EAST-SIDE
WEST-SIDE
"18O-STEP"
14.0
12.0
10.0
8.0
6.0
δ18OWR (‰)
0.7020
0.7040
0.7060
0.7080
0.7100
(87Sr/86Sr)o

compositions, the initial $^{87}Sr/^{86}Sr$ ratios steadily increase eastward, in harmony with the increase in ^{18}O-content of the rocks. Because of this, Taylor and Silver (1978) believe that the same basic process is responsible for the systematics observed in each isotope system. Plutonic rocks of the San Jacinto-Santa Rosa Mountains (SJ-SR) block, however, have anomalously low $\delta^{18}O$ and high $^{87}Sr/^{86}Sr$ compared with the overall trend for the PRB (Figure 1.8).

Figure 1.9 shows a comparison between the strontium and oxygen isotope data for the SNB (Masi et al., 1981; Saleeby et al., 1987) and the PRB (Taylor and Silver, 1978). The comparison highlights regional similarities between these two terranes. First, rocks of the Klamath Mountains show a trend that is similar to hydrothermally altered rocks from the extreme west side (roof zone) of the PRB. Both these terranes have uniform initial $^{87}Sr/^{86}Sr$ (0.704) with widely varying $\delta^{18}O$ values (+4.0 to +12.2). Unfortunately, no $\delta^{18}O$ analyses of quartz are available from the Klamath Mountains to substantiate hydrothermal exchange in that area. In addition, plutons from the Mojave Desert region and eastern parts of the SNB show atypically low $\delta^{18}O$ values in comparison with their relatively high initial $^{87}Sr/^{86}Sr$ values. This suggests a genetic link between these rocks and the SJ-SR block of the PRB (Hill et al., 1986). The majority of the rest of the SNB samples plot in the same positions as most samples from the PRB; they display increasing initial $^{87}Sr/^{86}Sr$ in conjunction with increasing $\delta^{18}O$ values.

1.3 Source Regions and Isotopic Compositions

In an attempt to explain some of the "anomalies" described above (e.g., relatively low $\delta^{18}O$ combined with high $^{87}Sr/^{86}Sr$) in the Mojave Desert-eastern SNB and the SJ-SR terrane, more detailed studies were

Figure 1.9 Plot of whole-rock $\delta^{18}O$ versus initial $^{87}Sr/^{86}Sr$ showing generalized data fields for geographic groupings from the Sierra Nevada Batholith (SNB) and the western Mojave Desert. Shaded region indicates the trend defined by samples from the main part of the Peninsular Ranges Batholith (PRB), excluding the SJ-SR block (see Figure 1.8). Note that samples from the Sierran Foothills of the northern and southern SNB plot within the main PRB data envelope. The western Mojave Desert samples lie along a trajectory similar to the one defined for the San Jacinto-Santa Rosa block. The star indicates the Model Lower Crust (MLC) composition proposed by Hill et al. (1986) for an upper mantle - lower continental crustal source region for the Mojave and SJ-SR block plutons. Modified after similar diagram in Hill et al. (1986) as used by Taylor (1986).

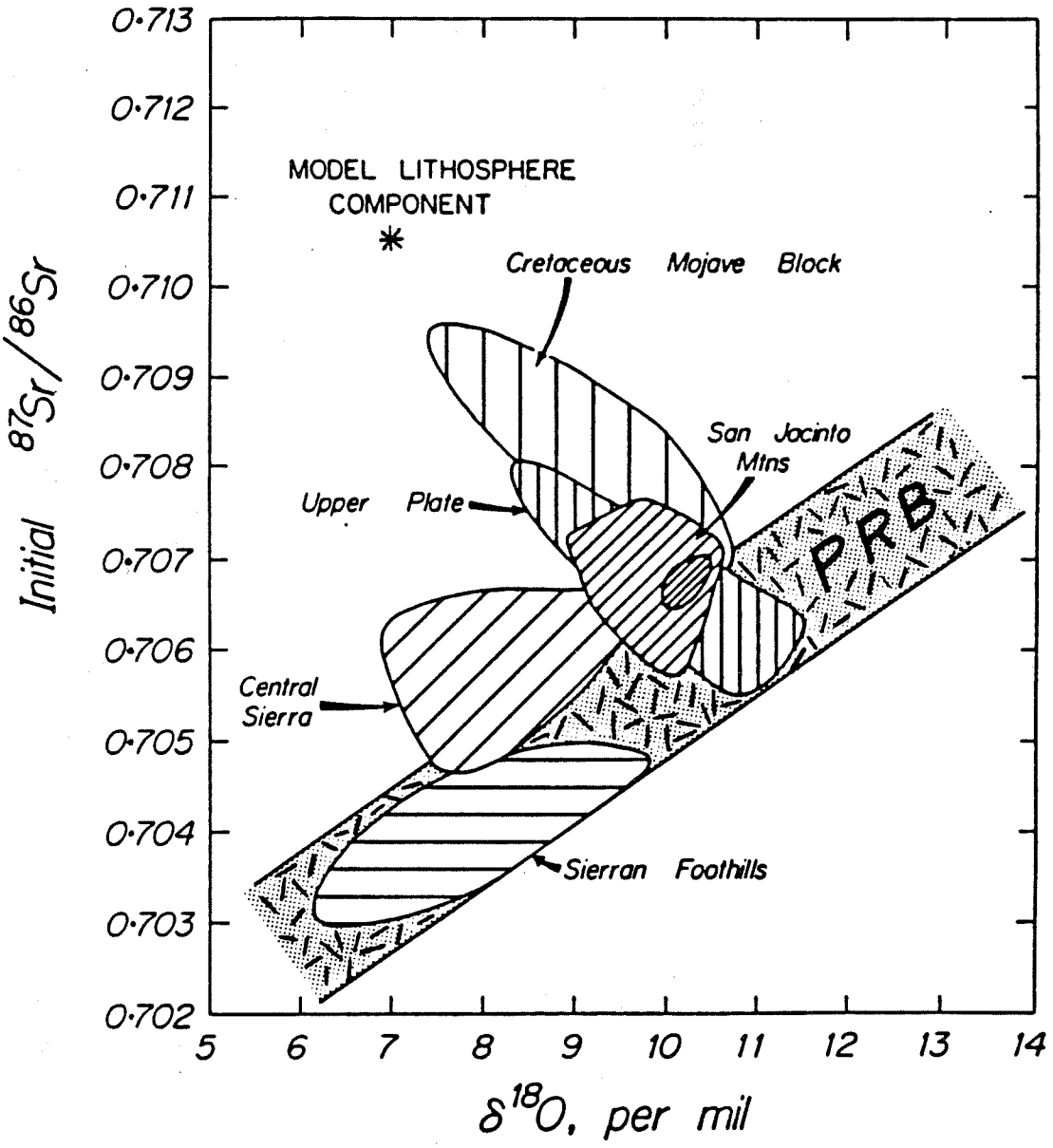
0·713
0·712
0·711
0·710
0·709
0·708
0·707
0·706
0·705
0·704
0·703
0·702
Initial $^{87}Sr/^{86}Sr$
MODEL LITHOSPHERE COMPONENT
Cretaceous Mojave Block
San Jocinto Mtns
Upper Plate
PRB
Central Sierra
Sierran Foothills
5
6
7
8
9
10
11
12
13
14
$\delta^{18}O$, per mil

carried out by Hill (1984) and Hill et al. (1986). They concluded that these so-called "anomalies" probably indicate a downturn in $\delta^{18}O$ from west to east, as a result of impingement of the Cordilleran batholithic arc upon a fundamental boundary between the plutonic source regions at depth. Taylor and Silver (1978) proposed that this "reversal" in the $^{18}O/^{16}O$ trend could be attributed to involvement of the extreme southwestern edge of crystalline basement of the North American craton in the magmas that formed the SJ-SR terrane at the northeastern tip of the PRB.

In contrast, the high-^{18}O plutonic rocks of the eastern zone of the main part of the PRB must have been derived from rocks that once resided at, or near, the Earth's surface. Suitable candidates for that source region could be a thick section of metasedimentary rocks or altered high-^{18}O volcanic rocks, perhaps similar to the eugeosyclinal rocks observed in the Jurassic Franciscan formation of the California Coast Ranges (Magaritz and Taylor, 1976c). To test these ideas, we felt it was important in the present study to determine the $\delta^{18}O$ values of plutons from radically different kinds of environments, for example from well within the confines of the crystalline basement (southern Basin and Range of southern Arizona and southeastern California), as well as from the thickest portion of the great miogeosyncline of North America (northern Basin and Range of Nevada and Utah). It is important in this regard to construct a $\delta^{18}O$ map of the Cordilleran plutons throughout the entire southwestern United States.

From the results of the present study, together with those by Criss and Fleck (1987), Hill et al. (1986), and Farmer and DePaolo (1983, 1984) we now know that the initial $^{18}O/^{16}O$ investigation of the PRB by Taylor

and Silver (1978) probably identified the three most fundamental source regions for the Cordilleran plutonic arc. Although several sub-units can be characterized, and there is appreciable "fine structure" superimposed upon the broad regional variations, the major geographic regularities in $^{18}O/^{16}O$ found by Taylor and Silver (1978) will be shown below to grossly apply to the entire southern Cordillera taken as a unit.

CHAPTER 2. ANALYTICAL METHODS AND DATA

2.1 $^{18}O/^{16}O$ Analytical Procedures for Silicate Samples

The method used for the analysis of $\delta^{18}O$ in all samples analyzed in this thesis follows that outlined by Taylor and Epstein (1962a), with the exception that HF is no longer employed. Samples were prepared for oxygen extraction by crushing a representative portion of the rock, 4 to 5 cm diameter, down to <2 mm-sized material, being careful not to lose any of the crushed rock. Most of the analyzed samples are fine- to medium-grained plutonic rocks, and grain size was not a problem in obtaining a representative sample of these rocks. Coarser-grained samples were handled in a special way, utilizing a significantly larger initial rock specimen. After crushing, the sample was then mixed into a homogeneous mass and this material was then split into four equal fractions. One fraction was ground with a tungsten carbide mortar and pestle into less than 200 mesh powder, again being careful not to lose any of the powder.

If a quartz sample was desired, quartz was handpicked from one of the remaining coarse fractions, and this quartz separate was then ground to less than 200 mesh powder. Purity of the quartz separate was always greater than 96% as determined both by inspection under a binocular microscope, and by the oxygen yield upon extraction.

In each extraction procedure, five whole-rock powders and/or quartz separates were weighed to between 20 and 30 mg, and together with a sample of the Caltech Rose Quartz standard material, were each placed into a separate nickel reaction vessel. The loading was carried out after drying for at least 24 hours in a dry-box with zero humidity, maintained by dry P_2O_5. The reaction vessels were then attached to the metal portion

of a vacuum system, similar to the one described in Taylor and Epstein (1962a).

Before evacuating the reaction vessels, about 1/6 of an atmosphere of F_2 gas was introduced into the metal sections outside the vessels, and heated by torch to react any possible contaminating atmospheric H_2O introduced during the previous procedures. This reacted fluorine was then expelled from the system by reacting it with hot (about 120°C) KBr pellets, and trapping the resultant Br gas in cold traps. Following this, the system was evacuated to a vacuum of about 10 microns (including the reaction vessels).

Approximately 5/6 of an atmosphere of fresh F_2 was then introduced and sealed into the reaction vessels, and the vessels were heated for at least 12 hours at about 525°C by external furnaces. During the 12-hour period, F_2 reacted with each silicate sample to liberate 100% of its oxygen as O_2. Following reaction, the gases in a single reaction vessel were allowed to expand through several liquid N_2 traps and a heated KBr trap in the metal portion of the vacuum system. This removed the excess F_2 and all condensable gases, leaving only O_2 (and a negligible amount of N_2 contaminant from the original F_2). The resultant O_2 gas was then combusted with a spectrographic-grade, resistance-heated carbon rod to produce CO_2, which was simultaneously frozen away from the rod by a liquid N_2 trap. To insure that no CO was inadvertently formed during this procedure, an aliquot of fresh O_2 was always introduced into the carbon-rod chamber at the end of the first combustion; this procedure is known to result in complete conversion to CO_2 (Taylor and Epstein, 1962a). After measuring the amount of CO_2 produced in a calibrated Hg manometer, the gas was further purified by reacting it with hot Hg vapor

before trapping it in a glass sample container for transport to the mass spectrometer.

Mass spectrometer analyses were performed on a McKinney-Nier, 60° sector double-collecting mass spectrometer. Data from the mass spectrometric analyses are presented in standard form following Taylor and Epstein (1962a) and Friedman and O'Neil (1977), where:

$$\delta^{18}O_x = [(R_x - R_{std})/R_{std}]\ 1000 \qquad (2.1)$$

with:

$$R_x = (^{18}O/^{16}O)_x \qquad (2.2)$$

$$R_{std} = (^{18}O/^{16}O)_{std} \qquad (2.3)$$

where std = an arbitrary standard, in this case Standard Mean Ocean Water (SMOW) as defined by Craig (1961). In this way, the oxygen isotopic ratio of the sample (x) is reported as a per mil difference in the ^{18}O content of the sample relative to the oxygen isotopic ratio of ocean water.

For practical purposes, the CO_2 samples were analyzed relative to the Harding Iceland Spar (HIS) carbon dioxide reference gas instead of carbon dioxide prepared directly from SMOW. The analyses were corrected to $\delta^{18}O$ (SMOW) values by the following equation:

$$\delta^{18}O(SMOW)_x = [\delta^{18}O(HIS)_x - [\delta^{18}O(HIS)_{rs}]\ [A] + B \qquad (2.4)$$

where rs = Rose Quartz standard CO_2 relative to the standard in parentheses, and the parameters A and B are:

$$A = (1.02162)(1 + \text{Background}/2520) \qquad (2.5)$$

$$B = +8.45 \text{ per mil.} \qquad (2.6)$$

The first multiplicative factor in the A parameter is the fractionation factor between the HIS standard and the SMOW standard, and is essentially equal to $\delta^{18}O(SMOW)_{HIS}/1000$. We have not applied the ^{17}O correction of

Craig (1957) because it is negligible for all of our analyses. The second factor takes into account the background CO_2 signal in the source system of the mass spectrometer, as well as the communication leakage across the sample and reference gas inlet valves; this factor was usually around 1.025. A precision of better than 0.2 per mil was typically obtained for the average sample, whose $\delta^{18}O$ was usually very close to that of the Rose Quartz reference standard, typically about +6 to +12 per mil on the SMOW scale.

Parameter B is the accepted $\delta^{18}O$ (SMOW) of the Caltech Rose Quartz standard CO_2. Many comparisons indicate that $\delta^{18}O$ = +9.60 per mil for the NBS-28 standard on this scale where the Rose Quartz standard $\delta^{18}O$ = +8.45. A Rose Quartz standard was run along with virtually every batch of 5 samples. Analyses prior to May, 1981 use $\delta^{18}O(HIS)_{rs}$ = -13.2 per mil, whereas those performed during and after May 1981 use $\delta^{18}O(HIS)_{rs}$ = -13.3 per mil. This slight discrepancy in the standard value is attributed to a major maintenance that refurbished many of the interior components in the extraction apparatus in April 1981.

All records of analyses were kept in a laboratory book, which has now been deposited with Dr. Hugh P. Taylor, Jr. of the Division of Geological and Planetary Sciences, California Institute of Technology. These records are keyed to the mass spectrometric records kept by the Caltech laboratory in the basement of North Mudd building.

2.2 Sample Localities and $^{18}O/^{16}O$ Data Tables

Sample localities are listed along with the $^{18}O/^{16}O$ analyses for the samples in Table 1 in the appendix. Also, latitude and longitude positions of each locality are given in degrees and minutes (to the nearest hundredth of a minute). The data are organized into geographic popula-

tions so that the entries in Table 1 can be easily compared with the $\delta^{18}O$ maps presented in Chapters 5 through 10.

Most of the analyzed samples were collected from outcrops by the author; the other samples were obtained from geologists involved in field studies in the areas of interest. The samples collected by the author are all accurately located, either on 15-minute quadrangle topographic maps (southern Arizona and portions of southeastern California), or 7-minute quadrangle topographic maps (San Bernardino Mountain region, southern California), or on California 2° x 2° state geologic sheets.

Prior to sampling, geologic reports and maps were consulted to determine the best sampling locations for Mesozoic and younger plutons. The geologic maps were field checked in a reconnaissance fashion by the author during sampling. The geochronologic relationships of these plutons are discussed below in Section 2.3, as well as in Chapters 5, 6, 7, and 9. Localities were chosen well away from pluton contacts with wall rocks, in most cases at least 300 to 500 meters from major contacts. This constraint is necessary because Shieh and Taylor (1969a,b), Turi and Taylor (1971a,b), and Hill et al. (1986) showed that the $\delta^{18}O$ values of samples near the margins of plutons usually have been modified by exchange with the local country rocks. Rock types were determined by examination of thin sections or hand specimens, and classified using the nomenclature of Streckeisen (1976) (see listings in Table 1 in the appendix).

Care was taken to choose samples with a minimum amount of chemical weathering, as arbitrarily determined using a hand lens and the "hammer ring" technique, where ringing samples are preferentially chosen over those displaying a dull, thudding sound. In most areas, samples meeting

the above criteria could be obtained, most often from blasted roadcuts. Outcrops not meeting the above criteria were simply avoided.

Samples listed in Table 1 (appendix) that are associated with the studies of another geologist show his or her name in parentheses. Samples shown with another geologist's name, following the abbreviation "Coll.," indicate that the sample was actually collected by, and documented by, that geologist (however, in some instances field assistants working with that geologist may have collected the sample). Those samples without the "Coll.," but with another geologist's name in parentheses, indicate that although the sample was collected by the author, it was collected with that particular geologist's direct or indirect help. Usually such samples have corresponding sample numbers in the collection of the particular geologist, and these corresponding samples were collected for related studies carried out by these other workers.

The related studies in the sample areas are as follows:

1. Geologic study of the Papago Indian Reservation and Ajo 2° map, Arizona by the U.S. Geological Survey, with Dr. Gordon Haxel as project chief (Haxel et al., 1981; Haxel et al., 1978; Briskey et al., 1978; Rytuba et al., 1978; Wright and Haxel, 1983; Haxel et al., 1980a,b).

2. Geologic study of the Needles 2° map, California by the U.S. Geological Survey, with Dr. Keith Howard as project chief (John, 1981, 1982, 1989; Calzia et al., 1986; Miller et al., 1982, 1989; Howard et al., 1982).

3. A samarium/neodymium isotopic study of plutons in the Great Basin region of Nevada and Utah (Farmer and DePaolo, 1983).

4. Geologic study of the Cottonwood Mountains, and surrounding areas, California (Powell, 1981, 1982).

2.3 Geochronology

Age assignments for the samples listed in Table 1 (appendix) are taken from a variety of sources, and represent several different types of radiometric age determination, or field correlation with other units that have been dated radiometrically. The methods include Rb-Sr isochrons, K-Ar dating on biotites and hornblendes, and U-Pb dating of zircons.

Each technique records information characteristic for the isotopic systematics for that technique, and care must be taken when interpreting the age data. For instance, K-Ar dating of hornblende and biotite records the date, in millions of years, when the sample mineral cooled to its "blocking temperature," and retained Ar. For biotite this temperature is in the neighborhood of 300°C, and for hornblende it is near 450 to 500°C (Criss et al., 1982). So, in effect, these K-Ar "ages" do not represent emplacement ages, but cooling ages.

Rb-Sr methods and U-Pb methods more closely represent the actual ages of emplacement of plutons. However, U-Pb (zircon) and Rb-Sr ages are only available on some of the samples analyzed for $\delta^{18}O$; these are noted as such in Table 1 (appendix).

Except in the cases of GCS001-79 and GCS360-81 through GCS386-81, the age assignments are based on samples other than the ones actually collected for $\delta^{18}O$ analyses (although often they are from the same outcrop). GCS001-79 was designated by G. Haxel as his sample number PUP14, which was dated using the U-Pb method on zircons (see Wright and Haxel, 1983). Samples GCS360-81 through GCS386-81 were dated by the Rb-Sr isochron method by Farmer and DePaolo (1983).

The other age dates in Table 1 (appendix) are taken from analyses reported in the literature for the specific pluton from which the $^{18}O/^{16}O$ sample was collected. In all cases, the ages listed represent samples located in the closest possible proximity to the sample collected for $\delta^{18}O$ analysis, often from the same outcrop or the same series of outcrops.

In some cases, only an approximate age is reported for a particular sample, and in such cases the sample might be designated simply as either greater than 145 Ma, or less than 135 Ma. These represent samples either (1) where no age date is reported in the literature, but field relations suggest an association with the designated age category; or (2) where the field relations are utilized in preference to a reported K-Ar cooling age(s) that appears to be drastically younger than the actual emplacment age. The reference list for the geochronology data is reported in Table 2 in the appendix.

2.4 Strontium and Neodymium Isotope Data Sources

Initial strontium isotopic ratios and ε_{Nd} values have been determined by Farmer and DePaolo (1983, 1984) for some of the samples collected from plutons in the Basin and Range of Nevada, western Utah, southeastern California and southern Arizona. In addition, Bennett and DePaolo (1987) and Miller et al. (1981, 1989) report neodymium and strontium isotope analyses from the Old Woman batholith in southeastern California. DePaolo (1981a) reported ε_{Nd} data for samples from the Sierra Nevada batholith that had been analyzed for initial $^{87}Sr/^{86}Sr$ by Kistler and Peterman (1973, 1978). As discussed in Chapter 1, we include many of these samples in our $\delta^{18}O$ study because of the availability of $^{18}O/^{16}O$ data (Masi et al., 1981). Other plutons located throughout southeastern California

have been analyzed for initial strontium isotope ratios by M.A. Lanphere (unpublished data) and R.W. Kistler (Calzia et al., 1986) in conjunction with the studies of Keith Howard (Howard et al., 1982). Many of these samples analyzed by other investigators were also analyzed for $\delta^{18}O$ in this thesis.

The initial strontium isotope ratios, and where applicable, the ε_{Nd} values, are listed in Tables 1.1, 1.2, 5.1, 7.1, 9.1 and 10.1, along with the corresponding $\delta^{18}O$ values and references to the data sources. All samples listed as being analyzed for $(^{87}Sr/^{86}Sr)_o$, ε_{Nd}, and $\delta^{18}O$ are either from exactly the same rock specimens, or they were collected from precisely the same sampling locality, except as noted in the various tables. Relationships between the $\delta^{18}O$ values and these various isotopic ratios are discussed in Chapters 8, 9, and 10.

CHAPTER 3. SOURCE-EXCLUDED $^{18}O/^{16}O$ VARIATIONS IN GRANITES

3.1 Equilibrium $^{18}O/^{16}O$ Fractionations Among Coexisting Quartz and Feldspars

In order to understand the link between the measured whole-rock $\delta^{18}O$ of a pluton and the $\delta^{18}O$ of its source region, it is necessary to evaluate the kinds of $\delta^{18}O$ variations that can be brought about by factors other than source-region isotopic composition. These factors include hydrothermal exchange, magmatic differentiation, fractionation during fusion, weathering, exchange with country rocks during ascent or emplacement of the magmas, and assimilation processes. In evaluating the $\delta^{18}O$ variations attributable to these effects, it is important to consider what constitutes a reasonable $^{18}O/^{16}O$ equilibrium fractionation factor for coexisting quartz and feldspar under magmatic conditions.

Based mainly on experimental work by O'Neil and Clayton (1964) and O'Neil and Taylor (1967), Bottinga and Javoy (1975) in a review article report equilibrium fractionations for quartz and plagioclase (An_{60}) at 1000°C and 650°C to be +1 to +2 per mil, respectively. Similarly, Bottinga and Javoy (1973) report equilibrium quartz-alkali feldspar Δ values of +0.6 to +1.2 per mil, respectively, for the same temperatures. More recently, Matsuhisa *et al.* (1979) and Matthews *et al.* (1983) have determined fractionations for quartz-albite and quartz-anorthite at H_2O-pressures between 1 and 24 kb, and for temperatures from 400°C to 800°C. For these conditions they found $1000 \ln \alpha = (A)(10^6 T^{-2})$ where (A) is 0.5 and 1.59 for quartz-albite and quartz-anorthite, respectively. Using this equation, the fractionations at 800°C and 650°C for quartz-albite and quartz-anorthite are +0.4 to +0.6, and +1.4 to +1.9 per mil, respective-

ly. However, recent work (R. N. Clayton, pers. comm.) suggests that the Matsuhisa-Matthews quartz-feldspar values are too small, and that the original O'Neil-Clayton-Taylor results reported in the 1960's are more accurate; thus, in the present study we shall utilize the latter values. In any case, the small discrepancies in the various calibrations do not in any way affect the following discussion.

The $^{18}O/^{16}O$ "fractionation" between quartz and its coexisting whole-rock mineral assemblage (conveniently analyzed as readily obtained whole-rock powder) is roughly equivalent to the fractionation between quartz and feldspar. Although this is only an approximation (Taylor, 1968, 1971), it is usually a very good one for granitic rocks because the $\delta^{18}O$ values of intermediate plagioclases and alkali feldspars in such rocks are ordinarily very close to the values of the whole-rock powders. This is because the bulk of the granite is composed of quartz and either one or two feldspars, and all the other minerals such as biotite, magnetite, and muscovite are lower in $\delta^{18}O$ than the feldspars; thus, these other minerals balance out the $\delta^{18}O$ value of the quartz, which is, of course, a major constituent of the whole-rock powder. This approximation clearly fails for a rock with little or no mafic minerals, such as leucogranite; in such cases the whole-rock $\delta^{18}O$ will usually be 0.1 to 0.5 per mil higher than the $\delta^{18}O$ of the feldspar. A reverse discrepancy would be observed for a very mafic-rich granitoid, such as a biotite-rich or hornblende-rich tonalite, and in such cases the whole-rock $\delta^{18}O$ might be as much as 0.5 per mil lower than that of the plagioclase.

3.2 $^{18}O/^{16}O$ Exchange with Hydrothermal Fluids

The upper portions of granitic batholiths commonly intrude to within 5 km of the Earth's surface. These zones often exhibit profound $^{18}O/^{16}O$

exchange effects related to deeply circulating hydrothermal waters (Taylor, 1968, 1974, 1977; Taylor and Magaritz, 1978; Forester and Taylor, 1977; Criss and Taylor, 1983). Interaction between granitic minerals and heated water results in isotopic exchange reactions that can change the whole-rock $\delta^{18}O$ of a pluton to values drastically different from the original primary values. Fortunately, quartz behaves in a refractory manner during such hydrothermal exchange (Taylor, 1968, 1977), so it is usually possible to calculate the original whole-rock $\delta^{18}O$ value by assuming an equilibrium $^{18}O/^{16}O$ fractionation between quartz and wholerock. Although the $\delta^{18}O$ of quartz also changes slightly during hydrothermal alteration (Criss and Taylor, 1983, 1986; Magaritz and Taylor, 1986; Taylor and Sheppard, 1986), this is usually a very small effect (< 0.4 per mil) except in cases where the $\delta^{18}O$ of the whole-rock has changed by more than 8 to 10 per mil.

In this work we shall use +1.2 per mil as a reasonable primary $^{18}O/^{16}O$ fractionation for quartz and whole-rock in granites; this is a characteristic value that would be attained under near-magmatic conditions during sub-solidus cooling down to about 550 to 600°C. This is also the average of the range in equilibrium values discussed in Section 3.1 above, and it is very similar to the values actually calculated for a large number of quartz and whole-rock determinations in the present study, as well (see Figure 3.1). For example, in his discussion of $\delta^{18}O$ in the hydrothermally altered portions of the granites from the Cornubian batholith (England), Sheppard (1977) also utilized a value of +1.2 per mil.

Therefore, in the present study, whenever whole-rock $\delta^{18}O$ values are significantly lower than the appropriate "equilibrium" range, based on

Figure 3.1 Plot of $\delta^{18}O$ quartz versus $\delta^{18}O$ whole-rock for Mesozoic and early Tertiary granitic plutons in the southwestern USA. Data taken from Table 1 (Appendix) for plutons located in the Northern Great Basin (NGB) of Nevada, the Central and Eastern Transverse Ranges of southern California, and the southern Basin and Range (SBR) of Arizona (see study areas shown in Figure 1.4.). Diagonal lines indicate trends of constant quartz-whole-rock $^{18}O/^{16}O$ fractionation (values shown on figure).

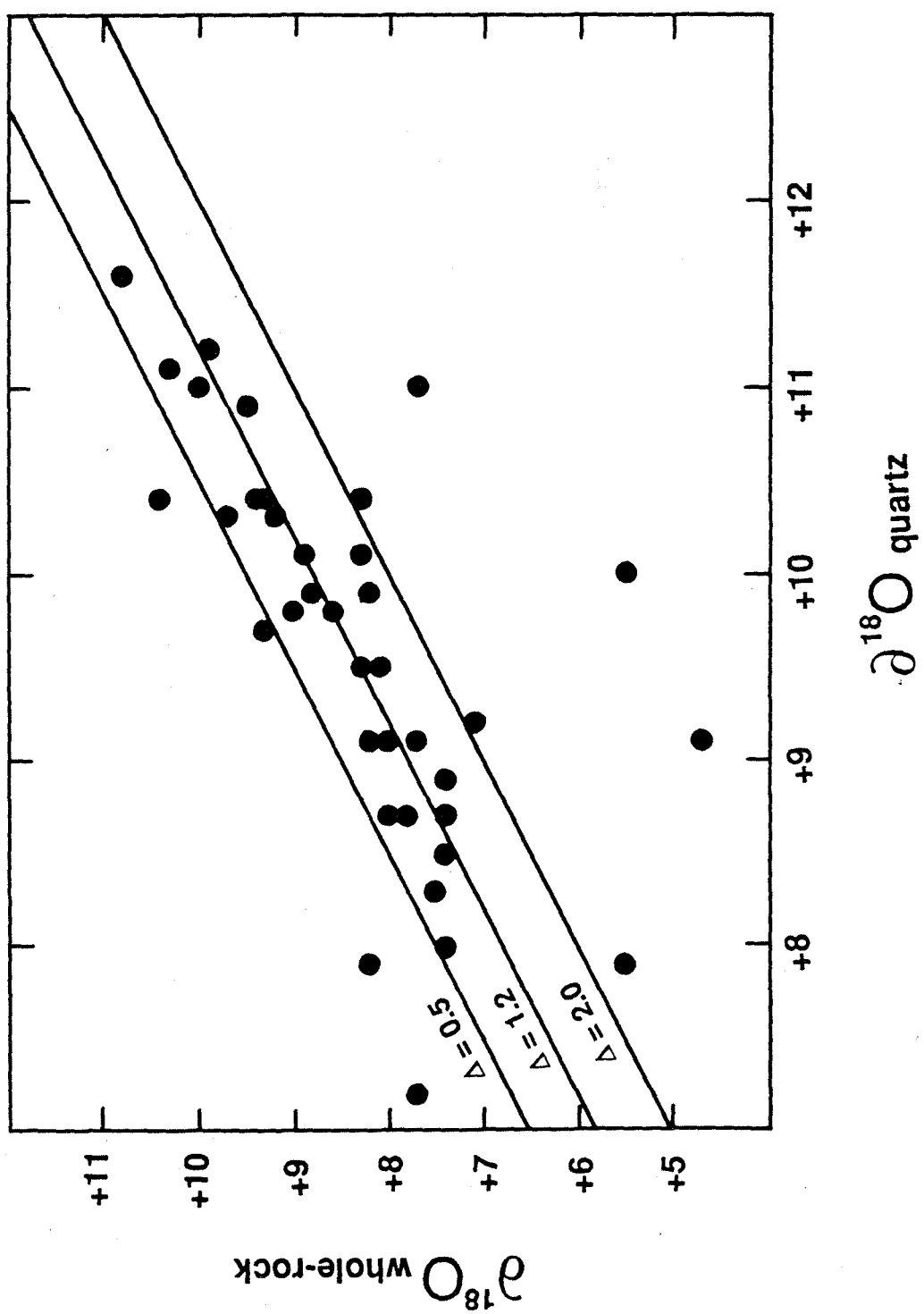
$\partial^{18}O$ whole-rock
$\partial^{18}O$ quartz
+5
+6
+7
+8
+9
+10
+11
+12
Δ = 0.5
Δ = 1.2
Δ = 2.0

analyses of the coexisting quartz, the whole-rock $\delta^{18}O$ is assumed to have been lowered by hydrothermal alteration, and the quartz $\delta^{18}O$ is considered to be essentially "undisturbed." The primary $\delta^{18}O$ of the rock is then calculated by subtracting 1.2 per mil from the quartz $\delta^{18}O$ value, giving a more accurate $\delta^{18}O$ value for the original magma than can be obtained by direct $^{18}O/^{16}O$ analysis of the altered rock itself. This adjustment was made in a few cases, and only when necessary, to fill out the primary $\delta^{18}O$ patterns shown in the $^{18}O/^{16}O$ maps presented in Chapters 5 to 10.

3.3 Magmatic Differentiation

The degree to which the $\delta^{18}O$ of a magma is changed during differentiation will depend on the mechanism of crystal fractionation and upon the $^{18}O/^{16}O$ fractionation factors between the minerals and the silicate melt (Taylor and Epstein, 1962b). To date, only a small amount of experimental information is available concerning these fractionation factors. Thus, most of our information regarding these parameters has been gleaned from study of natural assemblages.

Some large layered gabbroic intrusions, such as the Skaergaard intrusion in Greenland and the Kiglapait intrusion in Labrador appear to approximate closed-system behavior during differentiation (Wager and Deer, 1939; McBirney and Noyes, 1979; Morse, 1969). This type of intrusion often has a chilled border zone that corresponds to a "frozen" sample of the original undifferentiated magma; these chilled "rinds" typically enclose the main mass of layered, differentiated gabbroic units.

$^{18}O/^{16}O$ measurements of mineral phases in both the Kiglapait and the Skaergaard intrusions (Taylor, 1968; Taylor and Forester, 1979; Kalamarides, 1984) prove that these gabbro magmas did not change by any more

than 0.2 per mil during at least the first 95% of their crystallization history, based on a comparison of the original $\delta^{18}O$ of the magma body with the $\delta^{18}O$ variations in the entire series of later differentiates. This conclusion could be reached even in the case of the Skaergaard intrusion, which has undergone major ^{18}O-depletions as a result of interactions with an Eocene hydrothermal system that has partially obliterated the primary magmatic $^{18}O/^{16}O$ values for plagioclase and other minerals throughout the Skaergaard layered series.

As another example, volcanic rocks can provide a sample of quenched melt (for instance, the glassy groundmass can often be considered to represent "frozen" magma) that coexisted with its phenocrysts at the temperature of eruption. Such rocks are typically free of the effects of retrograde cooling that are invariably present in more slowly cooled plutons (Taylor, 1968). Thus, most of our direct knowledge of melt-mineral fractionation factors comes from $^{18}O/^{16}O$ fractionations measured for volcanic glass and its coexisting mineral phases.

Garlick (1966) noted that phenocryst-groundmass $^{18}O/^{16}O$ fractionations in mafic volcanic rocks were very small, around 0.2 to 0.4 per mil, not much larger than analytical error. Anderson et al. (1971) measured $^{18}O/^{16}O$ in basalts from several oceanic islands, and found that the $\delta^{18}O$ differences between groundmass and phenocrysts were generally less than 0.2 per mil, and almost never greater than 0.4 per mil. In a similar study dealing with intermediate volcanic rocks in Japan, Matsuhisa et al. (1973) estimated that the α values for coexisting silicate melt and crystals were between 0.9997 and 0.9995 for tholeiitic basalts and basaltic andesites ($1000 \ln \alpha = +0.3$ to $+0.5$). From these data it seems that liquid-crystal $^{18}O/^{16}O$ fractionations for most magmas are negligibly

small, at least at temperatures above 900° to 1000°C. Therefore, as also recently reviewed by Taylor and Sheppard (1986), large variations (more than 1.0 per mil) in $^{18}O/^{16}O$ in a suite of "cogenetic" igneous rocks can only be due to open-system effects, or to extreme effects of fractional crystallization.

Magmatic $^{18}O/^{16}O$ variations have been investigated in several open and closed-system differentiation environments. Matsuhisa et al. (1973) plotted $\delta^{18}O$ versus a differentiation parameter defined as:

$$SI = [MgO/(MgO+FeO+Fe_2O_3+Na_2O+K_2O)]100,$$

for several cogenetic sequences of lava flows in the Japanese Islands. In these volcanic rock series, Matsuhisa et al. (1973) observed that $\delta^{18}O$ increased with increasing differentiation in every case; however, for a range in SiO_2 content from < 50 wt % to > 70 wt %, the $^{18}O/^{16}O$ change was found to be only about +0.5 to +0.8 per mil for the Izu-Hakone series, which was thought to be a good example of closed-system differentiation (see Figure 3.2). In fact, Taylor and Sheppard (1986) believe that even this small $^{18}O/^{16}O$ change in the Izu-Hakone rocks may in part be attributable to open-system addition of ^{18}O-enriched material.

An igneous-rock series that is known from $^{87}Sr/^{86}Sr$ data to represent an open-system is the Tuolumne Intrusive Series of the Sierra Nevada batholith (Kistler and Swanson, 1981). This is a differentiation sequence of plutons ranging in composition from mafic tonalite and diorite to a very late-stage felsic granite porphyry (Bateman and Chappell, 1979). The intrusive series is made up of several pulses of fractionated magma originating from an apparent equilibrium fusion event at depth (Presnall and Bateman, 1973). An $^{18}O/^{16}O$ study of the successive intrusive phases of the series showed that the ^{18}O-enrichment from mafic to felsic rocks

Figure 3.2 Plots of differentiation index (SI)[a] versus whole-rock $\delta^{18}O$ for andesitic volcanoes from the East Japan Island Arc. Modified after similar graphs in Matsuhisa et al. (1973). The data from Izu-Hakone are a good example showing that strongly differentiated lavas in an island arc setting generally exhibit $\delta^{18}O$ variations of less than +1 per mil. As discussed in Taylor (1986) and Section 4.5 of this thesis, lavas from this particular volcano may have experienced open-system contamination, indicating that the $\delta^{18}O$ variation due to differentiation should be even less than 1 per mil.

[a] $SI = MgO/(MgO+FeO+Fe_2O_3+Na_2O+K_2O)]100$,

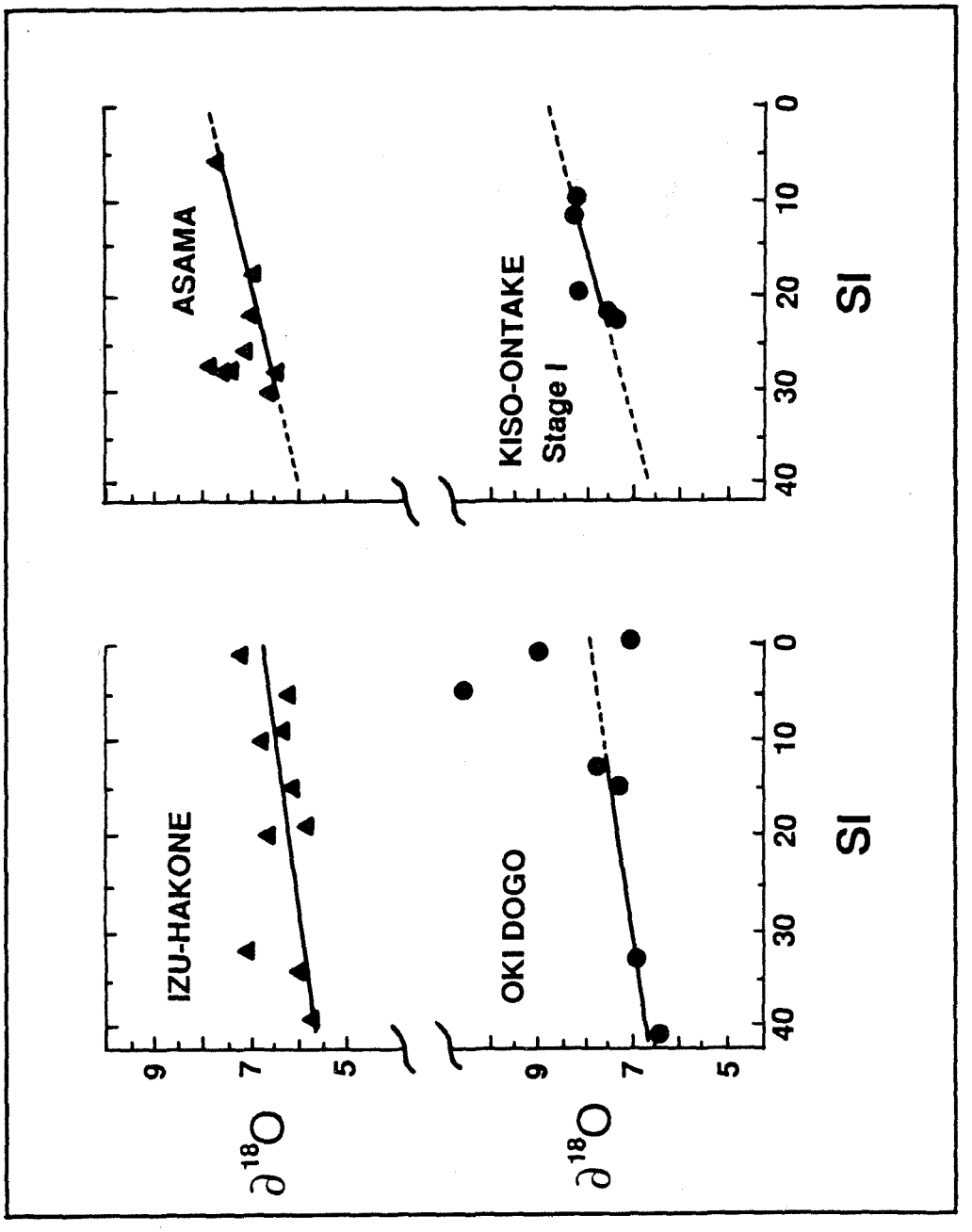
IZU-HAKONE
OKI DOGO
ASAMA
KISO-ONTAKE
Stage I
$\partial^{18}O$
SI
9
7
5
40
30
20
10
0

was not more than +0.8 per mil, even in the last 1% of the differentiation sequence (J.R. O'Neil, pers. comm.). Thus even in this case, where we know from the $^{87}Sr/^{86}Sr$ effects that there has been some open-system addition of material during differentiation, the measured $^{18}O/^{16}O$ changes are very small. Following Taylor and Sheppard (1986), we shall therefore assume that large (i.e., > 0.5 to 1.0 per mil) $^{18}O/^{16}O$ changes in a suite of plutonic igneous rocks cannot be attributed to a magmatic differentiation process; such effects must reflect either source variations or additions of foreign material to the magma system.

3.4 Assimilation

Detailed considerations of the $^{18}O/^{16}O$ effects of assimilation may be found in Taylor et al. (1979), Taylor (1980), Taylor and Sheppard (1986), and DePaolo (1981b). Taylor (1980) has modeled the predicted variations that assimilation would produce upon the $^{18}O/^{16}O$ - $^{87}Sr/^{86}Sr_o$ systematics of a crystallizing magma.

In general, magmatic systems or suites of cogenetic igneous rocks tend to show a positive correlation between $\delta^{18}O$ and $^{87}Sr/^{86}Sr$ (Figure 3.3). This is an important observation because the variations in these two isotopic systems are a result of two totally independent mechanisms; ^{87}Sr is enriched in rocks through the time-dependent decay of ^{87}Rb. On the other hand, $\delta^{18}O$ can only be markedly enriched in rocks if there is some type of interaction with surface waters at low temperatures (weathering or hydrothermal alteration). Thus, any major portions of the Earth's crust that have high $\delta^{18}O$ values must ultimately be derived from material that at one time resided either at, or very close to the Earth's surface. The observed correlations between $\delta^{18}O$ and $^{87}Sr/^{86}Sr$ (Figure 3.3) indicate that the reservoirs involved in magmatism in general

Figure 3.3 Plot of initial $^{87}Sr/^{86}Sr$ versus whole-rock $\delta^{18}O$ showing generalized data fields for igneous rocks from various orogenic regions around the world. Modified after Taylor (1980). Data fields generally: (1) trend towards the idealized mantle composition indicated by the box, and (2) exhibit a positive linear correlation between initial $^{87}Sr/^{86}Sr$ and $\delta^{18}O$. As discussed in the text (this chapter and Chapter 9), these linear trends generally indicate bulk mixing phenomena, not AFC processes (the plotted data exclude contaminated samples collected from the margins of plutons).

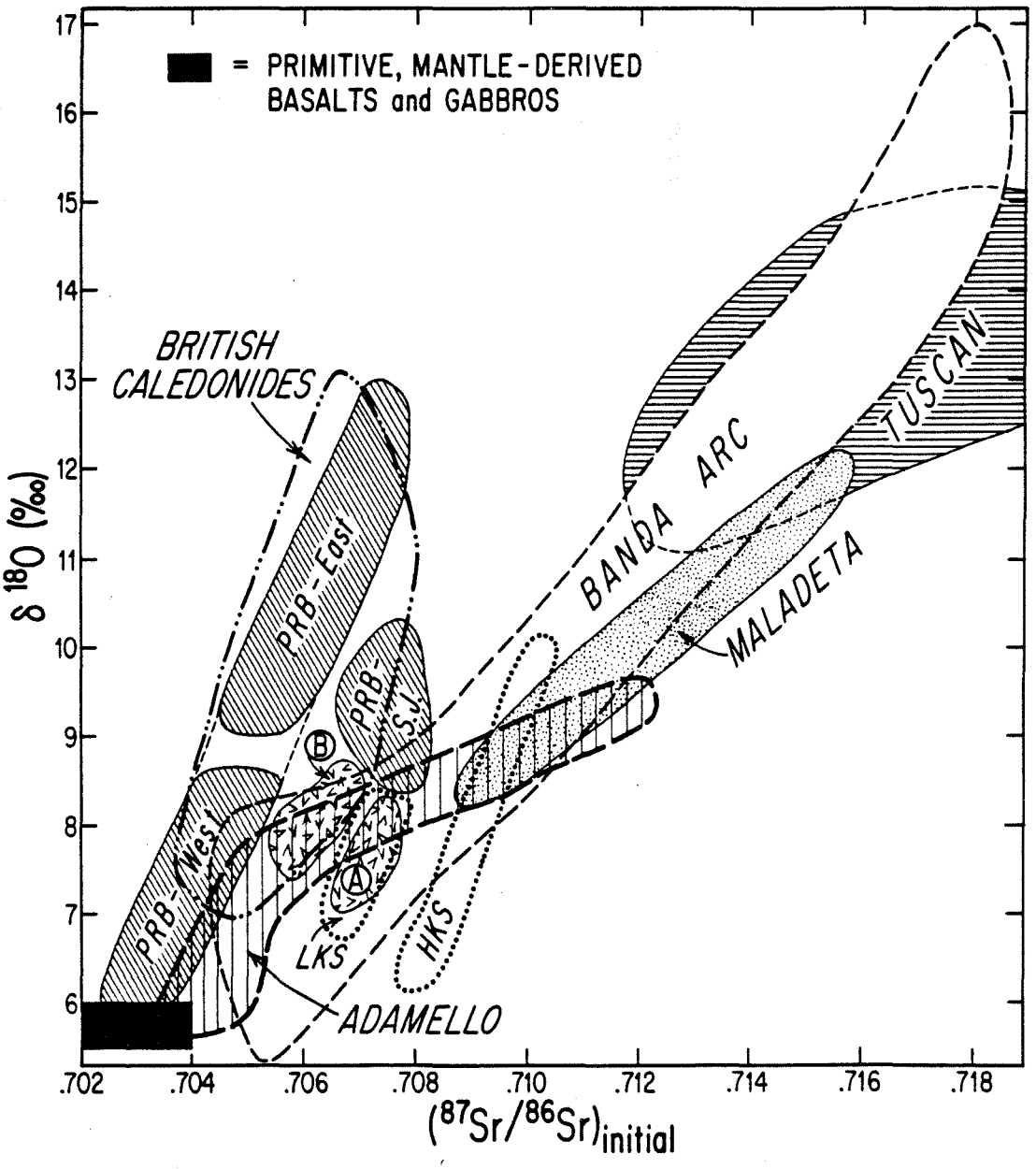
= PRIMITIVE, MANTLE-DERIVED BASALTS and GABBROS
BRITISH CALEDONIDES
PRB-East
PRB-S.J.
PRB-West
BANDA ARC
TUSCAN
MALADETA
ADAMELLO
LKS
HKS
A
B
δ 18O (‰)
(87Sr/86Sr)initial
17
16
15
14
13
12
11
10
9
8
7
6
.702
.704
.706
.708
.710
.712
.714
.716
.718

include both an older continental crustal component and a component that at one time "saw" the Earth's surface. These ^{18}O-rich and ^{87}Sr-rich components were either added to the system at the time of partial melting of the source, or through assimilation of country rocks as the magma ascended upward through the crust.

As pointed out by Taylor (1980), mixing models for igneous suites that have undergone assimilation-fractional crystallization (AFC) processes must incorporate at least three constituents: the magma, the country rocks, and the igneous cumulates. It is necessary to consider cumulate material because the heat of crystallization released by this component must be present for melting of country rock to occur, barring unlikely extreme geothermal gradients (McBirney and Noyes, 1979; Tuttle and Bowen, 1958).

The $\delta^{18}O$-$^{87}Sr/^{86}Sr$ correlations thus far published in the literature for granitic batholiths cannot be easily explained by assimilation of adjacent country rocks. The data typically display either straight-line behavior, or a hyperbolic configuration (see, for example, Figure 10.9a in Chapter 10). Either of these relations could result from simple two-component mixing in the source regions of the magmas. On the other hand, if assimilation were generally important in accounting for high-^{18}O granitic rocks, the late-stage, SiO_2-rich differentiates of such magmatic suites ought to be appreciably enriched in ^{18}O relative to the early, SiO_2-poor differentiates, and this is typically not the case. For example, the Peninsular Ranges batholith provides very clear-cut support for this statement; even though very large $^{18}O/^{16}O$ and $^{87}Sr/^{86}Sr$ variations exist in this batholith, the fact is that the <u>entire</u> series of plutonic rocks lying in a north-trending belt along the west side of the PRB, from

San Marcos gabbro (45-50 wt% SiO_2) to Bonsall tonalite (58-64 wt% SiO_2) to Woodson Mountain leucogranodiorite (73-76 wt% SiO_2), has very uniform $\delta^{18}O$ values of +6.5 to +7.5 per mil and uniform $^{87}Sr/^{86}Sr$ of 0.7030 to 0.7040 (Taylor and Silver, 1978). Thus, except for (1) the possibility of appreciable assimilation in the very high temperature zones either near to, or within, the actual zone of melting, or (2) very limited effects in local regions of the uppermost portions of magma chambers, assimilation of country rocks is almost certainly not the principal mechanism responsible for the variations of $^{18}O/^{16}O$ observed in most of the calc-alkaline batholithic rocks on Earth. However, these types of effects can indeed become important right at the edges of such plutons, as discussed in the next section. Further on, in Section 9.4.4 of Chapter 9, we analyze the relative importance of AFC processes in the emplacement of plutons in the northern Basin and Range of Nevada and western Utah, where a fairly complete data set ($\delta^{18}O$, ε_{Nd}, ε_{Sr}) now exists for Mesozoic and younger plutons.

3.5 Local Exchange with Country Rocks

Field evidence (for example, gradational contacts, presence of xenoliths, and presence of a common penetrative deformation in both country rock and pluton) indicates that deeply emplaced plutons (greater than about 5 km) generally interact to a greater degree with their surrounding country rocks than do shallow, epizonal plutons (Buddington, 1959). Thus, one of the more likely processes that can influence the $\delta^{18}O$ of a pluton during ascent and emplacement (especially for a deeply emplaced pluton) is exchange of $\delta^{18}O$ between the magma and its country rocks. This process occurs at relatively high temperatures where the $^{18}O/^{16}O$ equilibrium fractionations among mineral phases and silicate melt reflect

near-magmatic temperatures. Thus, unlike the epizonal meteoric-hydrothermal effects, mineral-pair $^{18}O/^{16}O$ fractionations do not monitor the effects of this type of fluid-rock exchange process.

To test the effects of such exchanges, Turi and Taylor (1971a) studied $\delta^{18}O$ distribution within and around the Domenigoni Valley granodiorite, a moderately deeply emplaced mesozonal pluton in the western side of the PRB (Larsen, 1948). The core of the Domenigoni pluton (50% of the outcrop area) is homogeneous with respect to $\delta^{18}O$ (+7.24 ± 0.11 per mil). The surrounding country rocks are composed chiefly of phyllites and schists with $\delta^{18}O$ equal to +18 to +20, and minor meta-arkose of +13 to +15. The results from several $\delta^{18}O$ traverses from within the pluton outward across the contact and into the country rocks show that the outermost 200 meters of the pluton are enriched in $\delta^{18}O$ by as much as +1.0 to +4.0 per mil, whereas the remaining outcrop outside the homogeneous core shows ^{18}O-enrichments of only 0.4 to 0.5 per mil, or less, compared with the unexchanged core (Figure 3.4). It is evident that in order to be certain of measuring the primary $\delta^{18}O$ of a pluton, samples ought to be collected at least 500 meters from the nearest contact, especially in the presence of high-^{18}O country rocks. Effects similar to those in the Domenigoni pluton are also found in plutons from the Santa Rosa Range in Nevada and in the White Mountains, California (Shieh and Taylor, 1969a,b), as well as in the San Jacinto-Santa Rosa Mountains block of the PRB (Hill et al., 1986).

As plutons approach shallower levels of emplacement, the effects of country rock exchange diminish, especially if water/rock values are low. The late Cretaceous Texas Canyon quartz monzonite in southeast Arizona is an epizonal pluton, which intruded moderately high-^{18}O country

Figure 3.4 Plot of distance from pluton-country rock contacts (in feet) versus $\delta^{18}O$ for two traverses across the Domenigoni granodiorite pluton in the Peninsular Ranges Batholith (PRB) of southern California. Modified after diagrams presented in Turi and Taylor (1971a). The Domenigoni pluton has outcrop dimensions of about 6 km x 10 km; and in both traverses, $^{18}O/^{16}O$-exchange effects in the pluton are limited to zones within 100 to 500 meters (approximately 300 to 1,500 feet) of contacts. The Winchester traverse (top diagram) shows how a small septum of granodiorite (approximately 200 feet across and surrounded by schist) near the contact has acquired very high $\delta^{18}O$ of +13.41 (qtz) through $^{18}O/^{16}O$ exchange with the quartz-biotite schist (whole-rock $\delta^{18}O$ = +19.29 to +20.18). The Homeland traverse (bottom diagram) shows a sharp decrease in $\delta^{18}O$ of the granodiorite from +13.23 (qtz) at the contact to +9.99 (qtz) 3 feet from the contact. Within 200 to 300 feet of the contact, $\delta^{18}O$ (qtz) in the granodiorite shows a negligible $\delta^{18}O$ gradient with values near +9 per mil.

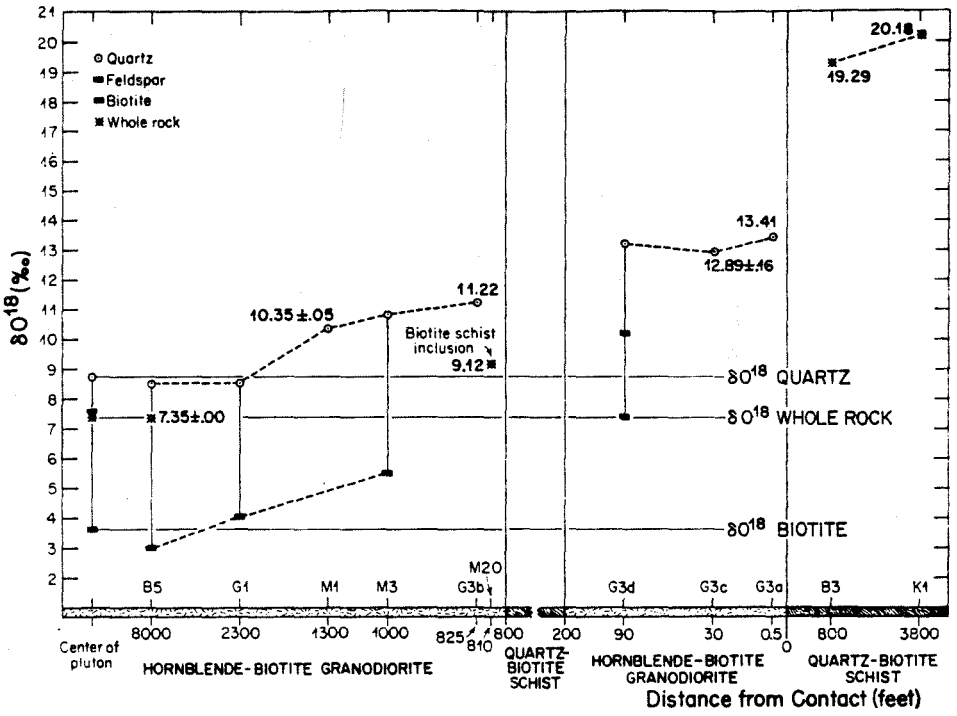
Quartz
Feldspar
Biotite
Whole rock
20.18
19.29
13.41
12.89±.16
11.22
10.35±.05
Biotite schist inclusion
9.12
7.35±.00
δO18 QUARTZ
δO18 WHOLE ROCK
δO18 BIOTITE
δO18(‰)
B5 G1 M1 M3 M20 G3b G3d G3c G3a B3 K1
8000 2300 1300 1000 825 810 800 200 90 30 0.5 0 800 3800
Center of pluton
HORNBLENDE-BIOTITE GRANODIORITE
QUARTZ-BIOTITE SCHIST
HORNBLENDE-BIOTITE GRANODIORITE
QUARTZ-BIOTITE SCHIST
Distance from Contact (feet)

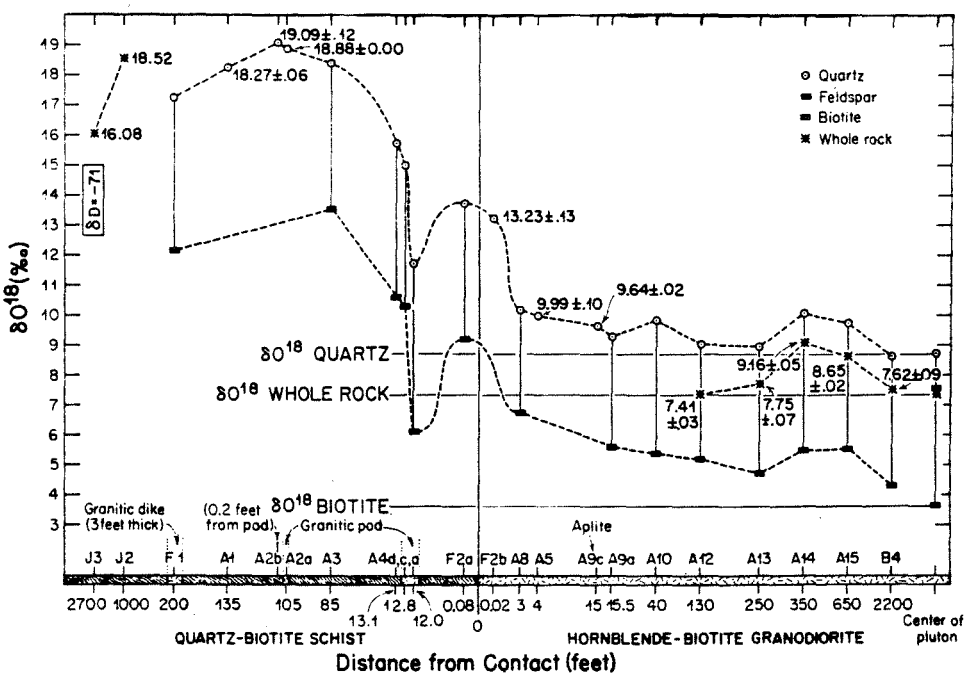
δO18(‰)
δD=-71
18.52
16.08
19.09±.12
18.88±0.00
18.27±.06
13.23±.13
9.99±.10
9.64±.02
9.16±.05
8.65 ±.02
7.62±.09
7.41 ±.03
7.75 ±.07
δO18 QUARTZ
δO18 WHOLE ROCK
δO18 BIOTITE
Quartz
Feldspar
Biotite
Whole rock
Granitic dike (3 feet thick)
(0.2 feet from pad)
Granitic pod
Aplite
J3 J2 F1 A1 A2b A2a A3 A4d,c,a F2a F2b A8 A5 A9c A9a A10 A12 A13 A14 A15 B4
2700 1000 200 135 105 85 13.1 12.8 12.0 0.08 0 0.02 3 4 15 15.5 40 130 250 350 650 2200
QUARTZ-BIOTITE SCHIST
HORNBLENDE-BIOTITE GRANODIORITE
Center of pluton
Distance from Contact (feet)

rocks that are only slightly higher in ^{18}O than the pluton; the exchange effects in this pluton are limited to a tiny, 15 cm contact zone (Turi and Taylor, 1971b). The $\delta^{18}O$ of quartz in these narrow border zones is as high as +10.4 per mil, but throughout the rest of the pluton, the quartz is extremely homogeneous, with $\delta^{18}O = +9.4 \pm 0.1$ per mil. Analogous effects have also been observed for the epizonal Caribou and Eldora stocks of the Front Range in Colorado (Shieh and Taylor, 1969b).

3.6 Weathering

Weathering of granitic outcrops in dry, arid regions yields grus in place of resistant outcrop. This particular type of weathering is characteristic in much of the field area in this study. Inasmuch as a good deal of the sampling in this study involved outcrop, instead of fresh road cut, we briefly review the effects of weathering on $^{18}O/^{16}O$ in granites.

Lawrence and Taylor (1972) measured $\delta^{18}O$ in weathering profiles developed on granitic rocks in climates that ranged from semi-arid (quartz diorite, Big Sur, California) to subtropical (quartz monzonite, Elberton, Georgia). Igneous quartz and biotite were found to have uniform "normal" igneous $\delta^{18}O$ values, as well as "normal" quartz-biotite $\Delta^{18}O$ values of approximately +6.0 per mil throughout the profiles, even though these minerals were in intimate contact with abundant kaolinite and other clays. These clay minerals had drastically different $\delta^{18}O$ values of around +20 to +22 per mil, indicating low-temperature genesis (Savin and Epstein, 1970).

It is apparent from the above studies that the whole-rock $\delta^{18}O$ values of granites that have simply undergone physical weathering, and have low clay-material contents, should be essentially identical to their

primary, igneous values (assuming there has been no hydrothermal alteration). Significant reversals in the "normal" igneous quartz-whole rock $^{18}O/^{16}O$ fractionation would be indicative of chemical weathering. However, even in rocks that contain abundant clay material produced by weathering, we can still obtain fairly accurate estimates of the primary igneous $^{18}O/^{16}O$ ratios, because the primary quartz phenocrysts are essentially inert in the weathering environment. In this manner, Sheppard (1977) determined the primary $^{18}O/^{16}O$ ratios of granitic batholiths even in the extremely heavily kaolinized ceramic-clay quarries in Cornwall, England. In conclusion, based on the very limited weathering suffered by the samples analyzed in this thesis, weathering cannot have affected any of the measured $\delta^{18}O$ values, and this problem is not referred to again.

3.7 Fusion-Related Fractionation

The remaining source-excluded factor that could affect $^{18}O/^{16}O$ in a granitic melt is the process of fusion. Fractional and equilibrium fusion of crustal rocks, with or without subsequent fractional crystallization, have been considered by Presnall (1969), and Presnall and Bateman (1973) to explain major element chemistry of plutons in the Sierra Nevada batholith, and in other magmatic systems.

Equilibrium fusion occurs when the melt remains in equilibrium with the crystal residue at the site of melting, after which it is assumed to undergo upward mobilization without further chemical exchange. Fractional fusion consists of an "infinite" number of equilibrium fusion events, each followed by immediate melt separation (in this case, the extracted melt does not interact with the crystal residue). Perfect equilibrium fusion would be attained when the number of extractions is decreased to one. These two processes have profoundly different effects on the way

major elements evolve in a magmatic system similar to the Sierra Nevada batholith, because liquid compositions evolve differently for the two types of fusion.

Similarly, each particular fusion process could have a different effect on $^{18}O/^{16}O$ systematics. During fractional fusion, $^{18}O/^{16}O$ equilibrates between the melt and the source residue, but the source and the small amount of melt are physically separated immediately following equilibration. Kyser et al. (1981, 1982) discuss the $^{18}O/^{16}O$ effects due to fusion in basaltic systems. They also use a Rayleigh melting model to define the limits of $^{18}O/^{16}O$ variation during fractional fusion. They show that at 1300°C, and for liquids in equilibrium with pyroxene, olivine, or plagioclase, melting of less than 40% of the source region is accompanied by less than a +0.3 per mil $\delta^{18}O$ increase in the melt. Because melt-plagioclase $^{18}O/^{16}O$ fractionations are very small at all temperatures from 700°C through 1200°C (Figure 3.5), it is likely that granitic melts effectively mirror their source-region $\delta^{18}O$ values during fractional fusion.

The variation in $\delta^{18}O$ of the liquid derived from equilibrium fusion is strictly a function of temperature, not degree of melting, because melts are extracted in one batch without numerous separations from the residue. We do not know the fractionation factors between plagioclase and silicate melt well enough to discuss this process in any detail. However, in general, we can expect the $\delta^{18}O$ of the residue (or "restite" in the terminology of White and Chappell, 1977) that is left behind in the source region to be slightly lower in ^{18}O than the magma that was extracted from it, simply because it would be made up of a more mafic-rich assemblage (more hornblende and/or biotite), and such minerals at

Figure 3.5 Plot of temperature (°C) versus $^{18}O/^{16}O$ fractionation factor for equilibrium between liquid basalt and plagioclase ($\sim An_{60-70}$) at temperatures between 1,050°C and 1,500°C. Modified after diagram presented by Kyser et al. (1982). Error bars indicate magnitude of 2σ uncertainty for data points.

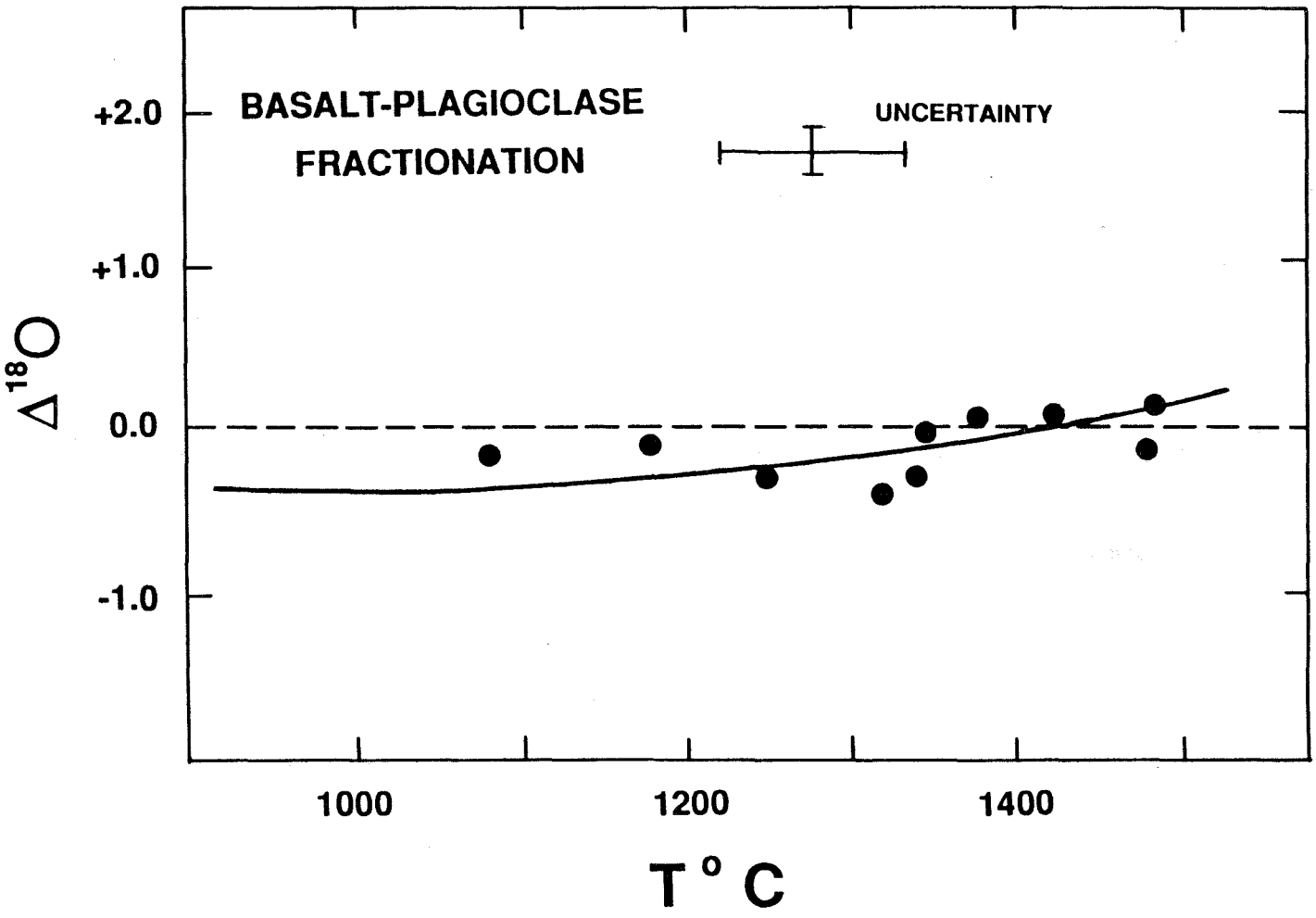
BASALT-PLAGIOCLASE
FRACTIONATION
UNCERTAINTY
+2.0
+1.0
0.0
-1.0
Δ 18O
1000
1200
1400
T ° C

equilibrium are lower in ^{18}O than the coexisting (more felsic) melt. Given the expected mineral assemblages and temperatures of melt extraction (~ 750° to 1000°C), this effect would be expected to exceed 1.0 per mil only rarely. Note also that such restite material would be lower in ^{18}O than the original source rock from which it was derived, and thus, by material-balance, the extracted melt would be richer in ^{18}O than the original source rock. Therefore, the $\delta^{18}O$ of the extracted magma will always be closer to the $\delta^{18}O$ of the original source rock than to the $\delta^{18}O$ of the restite. Obviously, as the per cent of melting increases, again by material-balance, the magma must get closer and closer to the whole-rock $\delta^{18}O$ of the source material. At values nearing 80 to 100% melting, the $\delta^{18}O$ of the melt and that of the source rock will become identical, regardless of the value of the melt-crystal $^{18}O/^{16}O$ fractionation.

3.8 Summary

From the above discussion it should be apparent that the most important "unknowns" affecting our ability to determine the exact $\delta^{18}O$ values of the source regions from the measured $\delta^{18}O$ values of the plutons are (1) a lack of detailed knowledge of the $^{18}O/^{16}O$ fractionations between minerals and magmas, and (2) the $^{18}O/^{16}O$ effects of fractional and equilibrium fusion and fractional and equilibrium crystallization. However, we know the above parameters well enough to demonstrate that, even taking into account the various unknown effects of fusion and fractional crystallization, there ought to be no more than about a +0.5 to +1.0 per mil change in granitic magma relative to the source-region $\delta^{18}O$ value. The effect is most likely closer to 0.1-0.4 per mil, decreasing to zero per mil as the per cent of melting increases to 100% (if it in fact ever does reach such high values). It thus seems clear that neither of the two

extremes in fusion mechanism would affect the $\delta^{18}O$ of resultant silicate melts in any dramatic way (also see Taylor and Sheppard, 1986). All other effects can be dealt with either by careful sample selection, or by calculating "corrected" whole-rock $\delta^{18}O$ compositions from analyses of the quartz.

It is therefore possible to construct a reasonable model for the $\delta^{18}O$ values of possible source regions, and to utilize the $\delta^{18}O$ map of the granitic batholiths of the Cordillera to infer the characteristics of such source regions. Within the 0.5-1.0 per mil uncertainty, we should be able to see how source $\delta^{18}O$ is distributed throughout the southern Cordillera, and evaluate possible lithologies for a possible "match" of their isotopic "fingerprints" with those of the plutons. This is particularly true when the $\delta^{18}O$ data are utilized in conjunction with $(^{87}Sr/^{86}Sr)_o$ and ε_{Nd} isotopic data.

CHAPTER 4. OXYGEN ISOTOPIC COMPOSITIONS OF POSSIBLE SOURCE REGIONS

4.1 General Statement

The purpose of this chapter is to discuss the $^{18}O/^{16}O$ compositions of possible source regions for the Mesozoic and early Tertiary plutons of southeastern California, southern Arizona, and the Great Basin of Nevada and Utah. The $\delta^{18}O$ values in the magmas that crystallized to form these plutons should be very closely equivalent to the corresponding $\delta^{18}O$ values in their sources (as discussed in Chapter 3). Therefore, using models for the $^{18}O/^{16}O$ distribution in crustal and subcrustal environments, we can attempt to connect plutons to specific source regions. Then, given the geographic variations in $\delta^{18}O$ for the plutons, we can attempt to model the distribution of sources in the southwestern United States, as discussed below in Chapters 5, 6, and 7. Finally, in Chapters 8, 9, and 10, the distribution of the radiogenic daughter isotopes Nd, Pb, and Sr will be discussed in relation to the $^{18}O/^{16}O$ source-model.

The source region model presented in this chapter depicts the generalized distribution of major rock-types beneath southwestern North America during Mesozoic and early Tertiary times. The model source region is divided into two major zones, the crust and the upper mantle. From east to west (see Figure 4.1), the crust is divided laterally into 3 parts: the craton, the continental margin, and the oceanic crust, with the continental margin being subdivided into the mio- and eugeoclines. The craton is subdivided vertically into lower and middle continental crust. The mantle is subdivided into asthenospheric mantle and into subcontinental- and suboceanic-lithospheric mantle. In this chapter we shall not discuss north-south variations in the $^{18}O/^{16}O$ model, although

Figure 4.1 Schematic east-west geologic cross-section through the area of the Northern Great Basin (NGB), showing the source-region model for the granitic plutons discussed in the text. Geology of the upper 10 to 15 km of the crust is taken from the synthesis of regional studies found in Miller et al. (1988) and Miller and Gans (1989). Geological relations in the lower crust are based on discussions by Hamilton (1981), Silver et al. (1977), Stewart (1972), King (1977), Gromet and Silver (1987), Hill et al. (1986), and McGetchin and Silver (1972). Calc-alkaline to alkali-calcic Mesozoic and Cenozoic plutons are indicated by solid black blebs; peraluminous granitic plutons are indicated by white blebs with small crosses on their interiors. Source-regions are abbreviated following the conventions listed in Table 4.1 and discussed in the text: OIA - oceanic island arc; MORB - mid-ocean ridge basalt; SAV - sedimentary and altered volcanic rocks; MCM - miogeosynclinal continental margin sediments, dominantly Paleozoic and late Proterozoic in age; SCL - subcontinental lithospheric mantle; LCC - lower continental crust; MCC - mid-level continental crust. The range in isotopic compositions for each source type is taken from discussions in this chapter and in Chapters 8, 9, and 10 (see Figures 8.7, 9.5, and 10.9). The "wavy" boundary between SAV and MCM indicates a sharp lithologic break in pluton geochemistry observed in Sr and Nd-isotopic studies (see Farmer and DePaolo, 1983, and Chapter 9). The model for the Southern Basin and Range (SBR) Province is similar, except that the "absent" MCM zone is inferred to be much narrower and thinner, generally younger (early Paleozoic) in age, and largely confined to the region labeled "cratonal platform sediments." The SBR model has more or less the same isotopic compositions, as the NGB model, except that the LCC-SCL component appears to have different $\delta^{18}O$ and ε_{Nd} values.

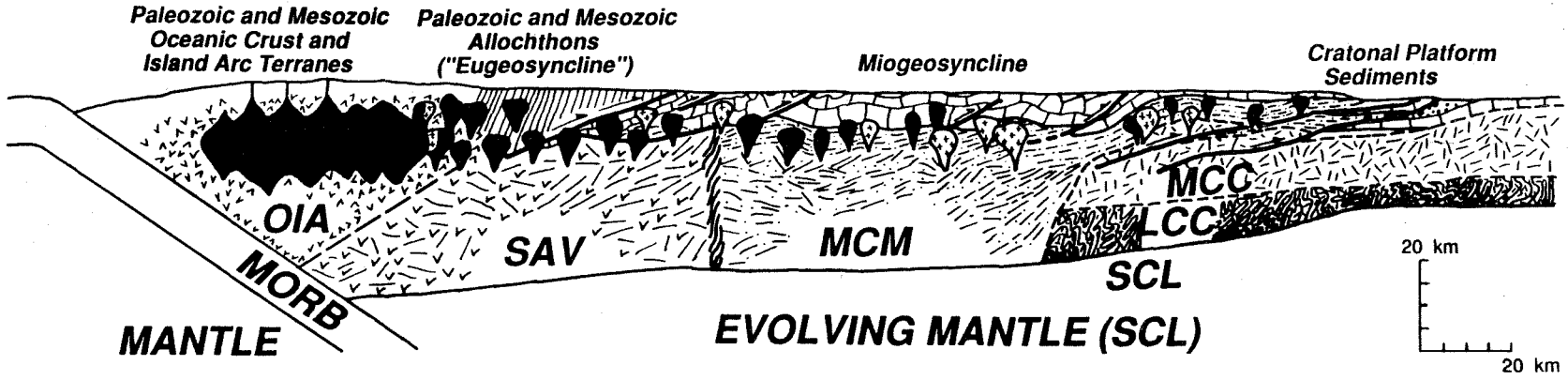

ISOTOPIC COMPOSITIONS (O; Sr; Nd)

	NGB			SBR
OIA-MORB	+6 to +7 ;	.702 to .704;	+2 to +7	Same
SAV	+10 to +13.5;	.703 to .710;	-2 to -9	Same
MCM	>+10;	>.715;	-9 to -20	Absent
MCC	+7.5 to +10;	>.715;	-12 to -20	Same
LCC-SCL	+7 to +9;	.705 to .710;	-6 to -12	+6 to +8; .705 to .710; -4 to -10

they are alluded to on Figure 4.1, in preparation for a more complete discussion of this model in Chapter 10. The Pb isotope data of Zartman (1974) and Nd isotope data of Farmer and DePaolo (1983, 1984) show that there is, in fact, a clear distinction between the northern and southern parts of the craton in the western U.S.A.

We also do not discuss or distinguish the various mechanisms whereby fusion of the source regions might be brought about. It is known, however, that during Mesozoic and early Tertiary times, oceanic crust was being subducted beneath the western North American continent (Atwater, 1970; King, 1977; Taylor and Silver, 1978; Davis et al., 1978; Ernst, 1970; Blake and Jones, 1981; Coleman and Lanphere, 1971). It is also known that in addition to the magmatism that produces a calc-alkaline volcanic-plutonic arc directly above a Benioff Zone, rifting and back-arc volcanism are also commonly associated with such tectonic events. Extensional volcanism was in fact widespread in the Cordillera during the Tertiary. Any or all of these events may have provided the energy input necessary for fusion to take place, by underplating large amounts of basaltic magma beneath the continent or by introducing such magmas into the lower continental crust. It is also possible, however, that rapid uplift of large packages of rocks could have brought superheated rock upward from depth into a low-pressure zone where melting could occur (Tuttle and Bowen, 1958; Hyndman, 1981).

Regardless of the mechanisms required to generate fusion, any rocks in the composite E-W section shown in Figure 4.1 that have bulk major oxide compositions plotting within the Ab-Or-An-Qtz tetrahedron are plausible protoliths for the types of granitic plutons now exposed as the Mesozoic and early Tertiary batholiths (Tuttle and Bowen, 1958; Presnall

and Bateman, 1978; Bateman and Dodge, 1970; Taylor and Silver, 1978; Whitney, 1975; Baird et al., 1979). In fact, for granitic plutons of tonalitic composition, basalt itself is also a plausible, or even a likely, protolith (e.g., Wyllie, 1981; Gromet and Silver, 1987).

4.2 The Craton

Hamilton (1981) reviews possible geologic configurations for the lower and middle continental crust in the western United States, based on observed geological relations in surface outcrops. Rocks characteristic of the Proterozoic middle continental crust (MCC) are well exposed in several 1.5 to 1.8 Ga basement complexes in Idaho (Salmon River Arch; Armstrong, 1975), Nevada (Ruby Mountains; Kistler et al., 1981), southern Arizona-southeastern California (Old Woman Mountains; Miller et al., 1982; the San Gabriel Mountains and adjacent areas; Ehlig, 1981; Powell, 1981), and areas in Arizona (1.6 to 1.8 Ga Yavapai and Pinal schist with associated intrusions, typically including "Oracle" type 1.4 to 1.5 Ga anorogenic granites; Anderson and Silver, 1971; Silver et al., 1977a,b). In general, these Proterozoic rocks are made up of complex, intermingled older metasediments, metavolcanics, gneisses and granitoids associated with various proportions of migmatite. Metamorphism up to grades of amphibolite facies or higher is common.

The lower continental crust (LCC) is difficult to characterize in the western United States because there are very few outcrops of rocks that at one time resided at such great depths. Hamilton (1981) and Fyfe et al. (1979) discuss once-deep crustal sections now exposed in the Canadian Shield and elsewhere on Earth, and Hamilton (1981) extrapolates this information to the western United States. Metasediments, which record metamorphic events typical for depths of 25 to 40 km, are

intercalated with igneous rocks such as gabbros, anorthosites, and granitic rocks containing abundant pyroxene and mesoperthitic feldspar. The metasediments include refractory assemblages such as quartzite, marble, and aluminous metapelites, and many of these rocks appear to have been depleted of their granitic components. MCC-type rocks (migmatites, granites, and associated metasediments) become less hydrated downward in the crust as they experience the transition from upper amphibolite facies to lower granulite facies.

These granulitic assemblages (anorthosite and associated mafic rocks, charnockitic granite, and high-grade metasediments) can be observed in regions of extreme uplift along the San Andreas Fault Zone in the San Gabriel and Orocopia Mountains (Carter and Silver, 1971, 1972; Ehlig, 1981). A similar assemblage is described by McGetchin and Silver (1972) in xenolith populations within a kimberlite dike in the Colorado Plateau region. According to McGetchin and Silver (1972), the upper 20 km of the continental crust is characterized by diorite, gabbro, metavolcanics, granite, and gneissic granite, with mafic igneous rocks comprising approximately 80% of the bulk volume. The LCC thus appears to be dominated by mafic granulitic gneisses. Hamilton (1981) believes that anorthosite, charnockite and garnet-sillimanite granulite may be fairly common as the lower crustal assemblage in the Cordilleran region.

Few detailed $^{18}O/^{16}O$ studies have been made in terranes that may be characteristic of the lower continental crust of the craton. Anorthosite massifs generally have a restricted range of $\delta^{18}O$ around $+7.0 \pm 0.5$, except in the Adirondack Mountains of New York, where fluid-rock interaction resulted in anorthosites with high $\delta^{18}O$ around +9.0 per mil (Taylor, 1970). Feldspar $\delta^{18}O$ values for granulite-facies felsic and mafic meta-

sediments and metaintrusives from the Musgrave Ranges, Australia, range from +6.6 to +8.0 (Wilson et al., 1970), while values range from +5.5 to +7.8 for granulite-facies rocks from the In Ouzzal area of the Saharan Desert (Fourcade and Javoy, 1973). In the Pyrenees Mountains in France, Wickham and Taylor (1987) describe a series of granulite-facies metasediments that range in $\delta^{18}O$ from +6 (in mafic gneisses) to +16 in calc-silicates and marbles, with the bulk of the samples lying between +8 and +12. These numbers are not surprising for igneous-type protoliths, but are anomalously low for metasediments. Apparently, high-grade metamorphic and magmatic processes involving aqueous fluid-rock and silicate melt-rock interactions in the lower crust tend to homogenize and lower the $\delta^{18}O$ values of originally high-$\delta^{18}O$ sedimentary rocks. Rocks with $\delta^{18}O$ > 10.0 per mil may be rare in the lower continental crust, although more detailed studies are needed to establish this. Granulite-facies rocks with $\delta^{18}O$ > 10.0 per mil for the most part are refractory, high-alumina calc-silicates, diopsidic gneisses, quartzites, and marbles (Taylor, 1970; Wickham and Taylor, 1987).

The $^{18}O/^{16}O$ composition of middle continental crustal material is much more definitely characterized, based on numerous analyses obtained throughout the Cordillera and the stable cratonic portions of the Canadian Shield. Early Proterozoic and older crystalline basement of various metamorphic grades up to upper amphibolite facies in the Canadian Shield, Colorado, New Mexico, and Arizona, exhibit $\delta^{18}O$ values that average between +8.0 to +10.0 per mil, although numerous samples of metasedimentary rocks are known with values between +9.0 to +15.0. Granitic rocks in the MCC display a $\delta^{18}O$ range of +6.5 to +9.0 (Shieh and Schwarcz, 1977; Longstaffe and Schwarcz, 1977; Barker et al., 1976; Turi and Taylor,

1971b). Shieh and Schwarcz (1977) calculated the average $\delta^{18}O$ of various parts of the exposed regions of the Canadian Shield, with the following results: granitic rocks, +7.6 to +8.6; basic intrusive rocks, +7.2; metasedimentary rocks, +9.2; and volcanic rocks, +7.6.

4.3 Continental Margin

Thick sections (up to 8 to 10 km) of sedimentary rocks are located along the "paleo" western continental margin that formed the border of the North American craton during late Precambrian and early Paleozoic times (Stewart, 1972; Burchfiel and Davis, 1981a; Hill, 1984). The eastern portion of this zone contains thick sections of sediments derived from the craton, and is here termed the miogeoclinal continental margin (MCM), following the usage of Blake and Jones (1981). The western portion is comprised of immature graywackes, flysch-type strata, basaltic and andesitic volcanic rocks, and metavolcanic sediments, and was termed the eugeoclinal continental margin by Blake and Jones (1981); in this thesis we emphasize the weathered and hydrothermally altered character of this type of material (as these are the factors that determine its high-$\delta^{18}O$ values), and we shall refer to it as a mixture of sediments and altered volcanics (SAV).

A number of workers have recently re-interpreted the eugeoclinal portions of the continental margin as being tectonically accreted terranes (Irwin, 1981; Blake and Jones, 1981; Schweikert and Snyder, 1981) that are allochthonous to the North American craton. However, the main tectonism responsible for this accretion event is pre-batholithic in age, and in many cases it simply involves a lateral transport of similar packages of eugeoclinal and miogeoclinal rocks northward parallel to the Mesozoic coastline of North America. Thus, except for local effects,

such accretionary tectonics may not drastically affect the nature of the source regions of the Mesozoic granitic melts.

The Franciscan Formation of west-Central and Northern California is typical of "eugeosynclinal" or SAV-type sedimentation. It is divided into three main belts named the Coastal belt, Central belt, and Yolla Bolly belt. The Coastal belt is mostly arkosic with less lithic volcanic material in it than the other belts (Bailey et al., 1964). The Central belt is mostly a melange of graywacke and metagreywacke mixed with greenstone, chert, and serpentinite. The melange matrix is interbedded mudstone and graywacke. The Yolla Bolly belt includes metachert, metagreenstone, pelitic schist, and quartzofeldsparthic schist. The characteristic SAV lithologies are pillow lavas and immature volcaniclastic sediments.

Metamorphism can be characterized as low-temperature, high-pressure type with pumpellyite-chlorite and jadeitic pyroxene assemblages present in graywackes. The Yolla Bolly belt is a discontinuous group of metaclastic rocks including metachert, metagreenstone, pelitic schist, and quartzofeldspathic schist. The age of these belts is not clear, but metamorphism in the Yolla Bolly belt was dated by Suppe and Armstrong (1972), and Maxwell (1974) to be between 77 and 143 Ma. Lanphere et al. (1978) suggest that the best age is around 120 Ma. The other two belts contain fossils indicating ages from the late Jurassic through to the late Cretaceous (Blake and Jones, 1974).

Magaritz and Taylor (1976c) and Taylor and Coleman (1968) made a detailed $^{18}O/^{16}O$ study of the SAV-type rocks of the Franciscan and Great Valley Formation in California. They found that the very abundant graywackes had very uniform $\delta^{18}O$ values of +13.0 to +14.5. Other components

of the Franciscan assemblage were as follows: serpentinites (+8.0 to +10.0); metabasalts (+9.0 to +15.0); pelagic metasediments (+16.0 to +30.0); blueschists (+10.0 to +15.0); and eclogites (+8.0 to +10.0).

Other eugeoclinal SAV assemblages in the western Cordillera include the Shoo Fly and Calaveras Complexes of the western Sierra Nevada; the Duzel Formation and Central metamorphic belt of the Klamath Mountains; and the Roberts Mountain and Golconda allochthons of central Nevada (Schweikert and Snyder, 1981). These units all are characterized by volcaniclastic-type sedimentation, and although folding no doubt repeats stratigraphy, they appear to reach thicknesses exceeding 20 km (King, 1977).

Miogeoclinal rocks in southwestern North America form a broad belt extending from Montana and Idaho as far south as the San Bernardino Mountains in southern California (Stewart and Poole, 1975; King, 1977). Hill (1984) describes miogeoclinal sections of possible early Paleozoic age in the Peninsular Ranges of southern California. Highly metamorphosed rocks of uncertain age in the Sur Series in the Coast Ranges of central California may be equivalent to the miogeoclinal sections (King, 1979).

In the northern part of the Cordillera, these MCM rocks are represented by the middle and late Proterozoic Belt Series and Windemere Group, overlain by Paleozoic rocks. Farther south, the miogeoclinal sections are represented by rocks equivalent to late Proterozoic Pahrump and Unkar Groups overlain by Paleozoic sections. All of these units are characterized by varying proportions of limestone and dolomite, quartzite, fine-grained clastic rocks (shale, siltstone, and sandstone) and red-bed sandstone. The combined thickness of the Proterozoic through Permian sections in the northern and southern portions of the Cordillera is more

than 15 km in the western-most exposures (Stewart, 1972; Stewart and Poole, 1974; King, 1977).

Supracrustal rocks younger than 1.5 Ga, including the Ruby Mountain complex in eastern Nevada, the Belt Supergroup of Montana, and younger geosynclinal sediments tend to have relatively high $\delta^{18}O$, usually +10.0 to +18.0 per mil (Kistler et al., 1981; Eslinger and Savin, 1973; Magaritz and Taylor, 1976c).

4.4 Oceanic Crust

Studies of ophiolites (Coleman, 1977) probably provide the best available descriptions of the geological components of Paleozoic and Mesozoic oceanic crust (OC). Ophiolites can be subdivided from top to bottom into minor pelagic sediments, basaltic pillow lavas, sheeted-dike swarms, plagiogranites and hornblende gabbros, layered gabbros, and ultramafic cumulates. Below this sequence is suboceanic mantle, represented by metamorphosed peridotite (typically, depleted harzburgite). The thickness from the top to the mantle-crust boundary is generally close to 10 km.

The rocks that immediately overlie the metamorphosed peridotite are cumulate sequences ranging in composition from peridotite through gabbro, with some plagiogranite near the top of the sequence. The lower rocks are characterized by olivine-rich cumulates grading into clinopyroxene and plagioclase-rich gabbro. Small-volumes (< 2%) of plagiogranite are probably the end product of differentiation of the cumulate gabbro magmas (Coleman and Peterman, 1975).

Diabasic sheeted dikes occur within the upper parts of ophiolite sections. Above these are spilitized pillow basalts. The sheeted dikes are unusual in that they are nearly 100% dike-rock without older country-

rock screens. These rocks are fine- to medium-grained diabase made up of plagioclase, clinopyroxene, and Fe-Ti oxides. Plagioclase composition is zoned between An_{55-60} and An_{20-30}. The pillow basalts contain plagioclase (An_{40-60}) and clinopyroxene with rare grains of olivine, and they invariably show evidence for hydrothermal alteration, with glassy portions transformed to smectite and chlorite (Bischoff and Dickson, 1975). Overlying the pillow basalts are volumetrically insignificant amounts of pelitic sediments characteristic of deep water sedimentation.

Based on studies of ophiolites, Gregory and Taylor (1981) and Stakes and Taylor (1984) showed that although oceanic crust in general appears to have a fairly uniform <u>average</u> $\delta^{18}O$ of +5.7, it exhibits pronounced gradients in $\delta^{18}O$ as a function of depth, as well as laterally as a function of permeability (e.g., the $^{18}O/^{16}O$ alteration effects are much larger near fracture zones such as transform faults). These isotopic heterogeneities are a result of hydrothermal ^{18}O exchange between seawater and the rocks of the oceanic crust; this takes place well down into the lower cumulate gabbros, and even has been observed in fractures within the upper mantle peridotites. The lower sections from cumulate gabbros through high-level gabbros are depleted in $\delta^{18}O$ down to values as low as +2.5 by high-temperature (>350°C) seawater-derived fluids. ^{18}O-enrichments relative to the bulk average have occurred in the upper levels. Spilitized pillow basalts typically have $\delta^{18}O$ values from +11 to +14 per mil, and the sheeted diabase dike swarm typically ranges from +5 to +11. These $\delta^{18}O$-enriched rocks comprise the upper ~2.7 km of the ~10 km-thick ophiolite section (similar in thickness to present-day oceanic crust), and are volumetrically < 30% of the section. The basaltic oceanic crust, as a possible source region for granitic (i.e., tonalitic)

melts, thus conceivably could provide an oxygen isotopic signature ranging from about +3 to about +14 per mil. However, on a km-sized scale the bulk samples would be closer to the average value of the section, probably between +5 and +7.

4.5 Oceanic Island Arc

Oceanic island arcs (OIA), such as the Marianas Arc, the southernmost portion of the East Japan Island Arc, the Aleutian Arc and other intra-oceanic volcanic chains (Ito and Stern, 1986; Matsuhisa, 1979) form from magmas generated in the vicinity of a Benioff Zone above a downgoing oceanic slab. These erupt as arcuate chains of volcanoes in-board of a deep ocean trench, and, in the above-mentioned cases, are thought to be built up largely on oceanic crust, with little or no continental material present. The magmas erupted are characteristically tholeiitic basalt, high-Al basalt, boninite and basaltic andesite. Magmas in this type of setting provide us with insight into subduction-related igneous rocks that are uncontaminated with continental crustal material. This is obviously an important potential source region to consider in our general isotopic model, and it will be referred to by the designation OIA.

The southern portion of the Marianas-East Japan Arc represents a good example of an oceanic island arc system. Ito and Stern (1986) have determined whole-rock $\delta^{18}O$ values for these volcanic rocks, and Taylor (1986) has summarized their results. It is remarkable that, in spite of the known $\delta^{18}O$ heterogeneity in subducted oceanic crust (e.g, +2.5 to +15.0; see above), the magmas produced above the Benioff Zone in the Marianas Arc are extremely uniform, with $\delta^{18}O$ between +5.5 and +6.2. Ito and Stern (1986) concluded that no more than 1% bulk mixing of high-^{18}O pelagic sedimentary material could be included with the melts from the

Benioff Zone to produce the $^{18}O/^{16}O$ compositions of these lavas. Also, because there is such a large variation of $\delta^{18}O$ in older, hydrated oceanic crust carried down into the mantle along a subduction zone, the above isotopic studies demonstrate either that: (1) essentially the entire basaltic crust must melt and be homogenized (producing magmas with a uniform $\delta^{18}O$ of about +5.7 ±0.3, identical to the average MORB $\delta^{18}O$ value of +5.7); or (2) a large proportion of the overlying, upper mantle must melt (fluxed by dehydration H_2O derived from the subduction zone?), thereby overshadowing ^{18}O-heterogeneities introduced by the contribution from subducted oceanic crust. As noted by Taylor (1986), this uniformity of $\delta^{18}O$ along the 500 km-length of the Marianas Arc implies either a very carefully balanced mixing process, or an extremely uniform $^{18}O/^{16}O$ composition of source material in the mantle.

Where a set of pristine, OIA volcanic islands are traced along strike into a continental crustal environment, we might expect to observe higher $\delta^{18}O$ values. In this connection, note that the Izu Arc (see Figure 3.2, page 57) forms the northward extension of the Marianas Arc, and although the Izu lavas also have relatively low whole-rock $\delta^{18}O$, they are distinctly higher than in the Marianas Arc ($\delta^{18}O$ typically between +6.1 and +7.2 with only a few samples lower than +6.1; Matsuhisa, 1979). Even in Japan proper, these island arc magmas typically do not attain $\delta^{18}O$ values any higher than about +8.5 per mil (Matsuhisa, 1979). We conclude that the OIA source region has $\delta^{18}O$ between +5.5 and +7.5 per mil, with the lower-end of this range occupied by magmas generated in a pristine OIA environment where there is little or no involvement of continental material.

4.6 Suboceanic and Subcontinental Lithospheric Mantle

Suboceanic lithosphere (SOL) is well studied in ophiolites (Coleman, 1977) where it occurs as tectonized, metamorphosed peridotite underlying the cumulate section. Subcontinental lithosphere (SCL) is less well characterized, but has been described from xenoliths in kimberlites and basalt flows (e.g., McGetchin and Silver, 1972), and in high-temperature (Alpine-type) ultramafic intrusions exposed in tectonically active regions (e.g., Loomis, 1972; Thayer, 1963).

The metamorphosed peridotites that occupy the basal portions of ophiolites are composed of minor dunite and predominant harzburgite. The harzburgite contains olivine, orthopyroxene, and chromian spinel as the major phases, with minor amounts of chromium diopside. The dunites are dominantly olivine with accessory orthopyroxene, clinopyroxene, and chromian spinel. No systematic variations have been noted in modal compositions for these rocks worldwide (Coleman, 1977).

Subcontinental lithosphere, in comparison, is much more diverse in composition than suboceanic lithosphere. One such "SCL-type" lithology is peridotite, which occurs in association with deep fundamental faults in the Earth's crust. These rocks show mineralogical and compositional zoning, and contact metamorphic aureoles (Loomis, 1972) indicating magmatic diapirism. Such peridotites (lherzolitic sub-type) have more clinopyroxene and plagioclase than do the oceanic peridotites, and are notably more alkalic with slightly higher amounts of SiO_2.

McGetchin and Silver (1972), along with their descriptions of lithologies representative for the LCC, describe xenoliths of deeper origin from the kimberlites. These xenoliths provide a "window" to view subcontinental lithospheric compositions. The host kimberlites were in part

derived from disaggregated spinel- and garnet-lherzolite, and contain clinopyroxenes derived from between 50 and 200 km depth in the mantle. Eclogite, jadeitic clinopyroxenite, and websterite occur as xenoliths in the lherzolitic kimberlite, and are probably representative of kimberlitic vent walls. However, their xenolithic population is so small that no reliable estimate can be made of the SCL abundance.

Lunar basalts and fresh, unweathered, and unaltered terrestrial basalts uncontaminated by the continental lithosphere or the hydrosphere display a very narrow range of $\delta^{18}O$ values between +5.0 and +7.0 per mil (Taylor and Epstein, 1970; Taylor, 1968, 1978). Values outside these limits are virtually nonexistent, indicating a remarkably uniform asthenospheric upper mantle composition for the Earth, particularly in those areas where continental masses do not overlie the upper mantle. An even narrower range of $\delta^{18}O$ is observed in the MORB source region, probably within the limits +5.5 to +5.9 (Taylor, 1968; Muehlenbachs and Clayton, 1972; Ito and Clayton, 1983; Ito et al., 1987).

The story is somewhat different for basaltic rocks and ultramafic nodules that originate in areas overlain by continents, or in areas where deep hydrothermal convection systems operate (e.g., Iceland, Yellowstone Park). However, even in these areas, $\delta^{18}O$ values outside the above range of +5 to +7 are relatively rare. Continental basanites from diverse localities such as Nevada, Arizona, and Baja California have $\delta^{18}O$ = +6.1 ± 0.3, with one or two samples as high as +7.6. Continental tholeiites have $\delta^{18}O$ = +5.3 to +7.0, but generally cluster near +6.7. Ultramafic nodules from basalt flows in continental areas (Massif Central, France; San Quentin, Baja California; Dish Hill, California; San Carlos, Arizona; Kilbourne Hole, New Mexico) show a whole-rock $\delta^{18}O$ range from +5.2 to +7.0 (Kyser et al., 1981).

Eclogitic nodules in kimberlite pipes and alpine thrust belts (Garlick et al., 1971; Vogel and Garlick, 1970) show a considerably greater spread in $\delta^{18}O$, from about +2 to +11. This range is very similar to the range observed in ophiolitic oceanic crust. Gregory and Taylor (1981, 1986) conclude that most such eclogite samples are indeed probably fragments of ancient oceanic crust subducted down into the upper mantle and then returned to the surface.

4.6 Summary

The results of this brief review of the probable oxygen isotopic compositions of possible source regions of granitic magmas are summarized in Figure 4.1 and Table 4.1. More detailed discussions of $^{18}O/^{16}O$ variations within possible source regions are given in Chapters 5 through 10.

The radiogenic isotope systems are also very important in constraining possible source materials of granitic magmas. The neodymium, lead, and strontium isotope variations in these potential source regions are discussed in DePaolo and Wasserburg (1979), Zartman (1974), DePaolo (1981a), Farmer and DePaolo (1983, 1984), Bennett and DePaolo (1987) and Taylor and Sheppard (1986), as well as in portions of the text of Chapters 8, 9, and 10.

Table 4.1 Approximate $\delta^{18}O$ compositions of potential source regions for Cordilleran granitic plutons from the southwestern United States.[a]

	Source Region	Whole-rock $\delta^{18}O$ (per mil) Average	Range
MORB	Sub-oceanic asthenospheric mantle	+5.7	+5.5 to +6.0
OC	Oceanic crust (rocks above MOHO)	+5.5 to +6.0	+2.5 to +15.0[b]
SOL	Sub-oceanic lithospheric upper mantle	+5.5 to +6.0	+5.0 to +6.5
OIA	Oceanic island-arc magma source (Benioff Zone?)	+6.0 to +7.0	+5.5 to +7.5
SCL	Sub-continental lithospheric upper mantle	+6.0 to +7.0	+2.5 to +11.0
LCC	Lower continental crust of the craton	+6.5 to +8.0	+5.0 to +11.0[c]
MCC	Middle continental crust of the craton	+7.5 to +9.0	+5.0 to +18.0[d]
	Older plutons and gneisses (outcrop in Archean shields)	+7.5 to +9.0	+5.0 to +16.0
	Older supracrustal metasediments/ metavolcanics	+8.5 to +10.0	+6.0 to +18.0[d]
SAV	Eugeoclinal sediments/volcanics	+10.0 to +13.5	+6.0 to +33.0[e]
MCM	Late Precambrian/early Phanerozoic miogeoclinal sediments	+10.0 to +18.0	+8.0 to +27.0[f]

[a] Generalized from data sources listed in the text.
[b] Variations in $\delta^{18}O$ mainly attributable to seawater-hydrothermal metamorphism; upper 3-4 km (pillow lavas and dikes) between +7.0 and +15.0 per mil; lower 5-8 km (gabbros and cumulates) between +2.5 and +8.0.
[c] Except for refractory metasedimentary material with $\delta^{18}O$=+10.0 to +16.0 per mil.
[d] Depending upon rock type, age, and metamorphic grade.
[e] Data available only for Mesozoic rocks (Franciscan Formation, CA), and includes pelagic sediments and cherts with $\delta^{18}O$=+20 to +33.
[f] Higher $\delta^{18}O$ range (+22 to +27) includes only limestones and dolomites, which can be only indirectly involved in the production of granitic magmas.

CHAPTER 5. $^{18}O/^{16}O$ COMPOSITIONS OF MESOZOIC AND EARLY TERTIARY PLUTONS IN SOUTH-CENTRAL ARIZONA

5.1 Introduction

The purpose of this chapter is to present the $^{18}O/^{16}O$ compositions of some Mesozoic and early Tertiary plutons in south-central Arizona within the context of their geology, geochronology, and major-element geochemistry. This chapter provides part of the basis for a synthesis of plutonic source regions for Mesozoic magmatism across the entire Cordillera of the southwestern United States (described in Chapter 10).

The $^{18}O/^{16}O$ and major-element geochemistry of the plutons, together with a literature-derived description of the geological relations between plutons and country rocks, are presented for three adjacent geographic areas lying just north of the Arizona-Sonora border (see Fig. 5.1 for the location of each area):

1) the Presumido Peak - Coyote Mountains (PPCM) Area,
2) the Gunsight Hills - Sierra Blanca (GHSB) Area, and
3) the Western Area

Because of the remoteness of many of the localities it was not possible to obtain the same detail of sampling density that was carried out for southern California (described in Chapters 6 and 7). However, the sample population provides useful reconnaissance information on the primary $\delta^{18}O$ compositions of the plutons in southern Arizona.

5.2 Regional Geologic Setting

Fig. 5.2 shows south-central Arizona in relation to some major geologic features of the western United States and Mexico. The Rocky Mountain uplift and Colorado Plateau are bounded on the west and south by the

Figure 5.1 Map of the southwestern United States and northwestern Mexico showing the locations of sampling areas (shown by diagonal shading within heavy boundaries) in the southern Basin and Range Province (SBR) of Arizona. From west to east these areas are: (1) the Western Area; (2) the Gunsight Hills - Sierra Blanca (GHSB) Area; and (3) the Presumido Peak - Coyote Mountains (PPCM) Area. Also shown are outlines of Mesozoic and early Tertiary batholithic rocks from the Cordillera of the southwestern United States.

Figure 5.2 Map of the southwestern United States and northwestern Mexico showing regional geologic features discussed in text, modified after similar map in Haxel et al. (1984). Mesozoic and early Tertiary batholithic rocks are shown by solid outlines (location of Jurassic Arc indicated by diagonally-shaded zone within dashed boundaries); solid black areas comprise the eastern metamorphic belt (Haxel et al., 1984); heavy dashed lines indicate the proposed trace of the Mojave-Sonora megashear (Silver and Anderson, 1974); generalized faults of the frontal fold and thrust belt shown by thrust-fault symbols (hatchered on the upper-plate of the thrust).

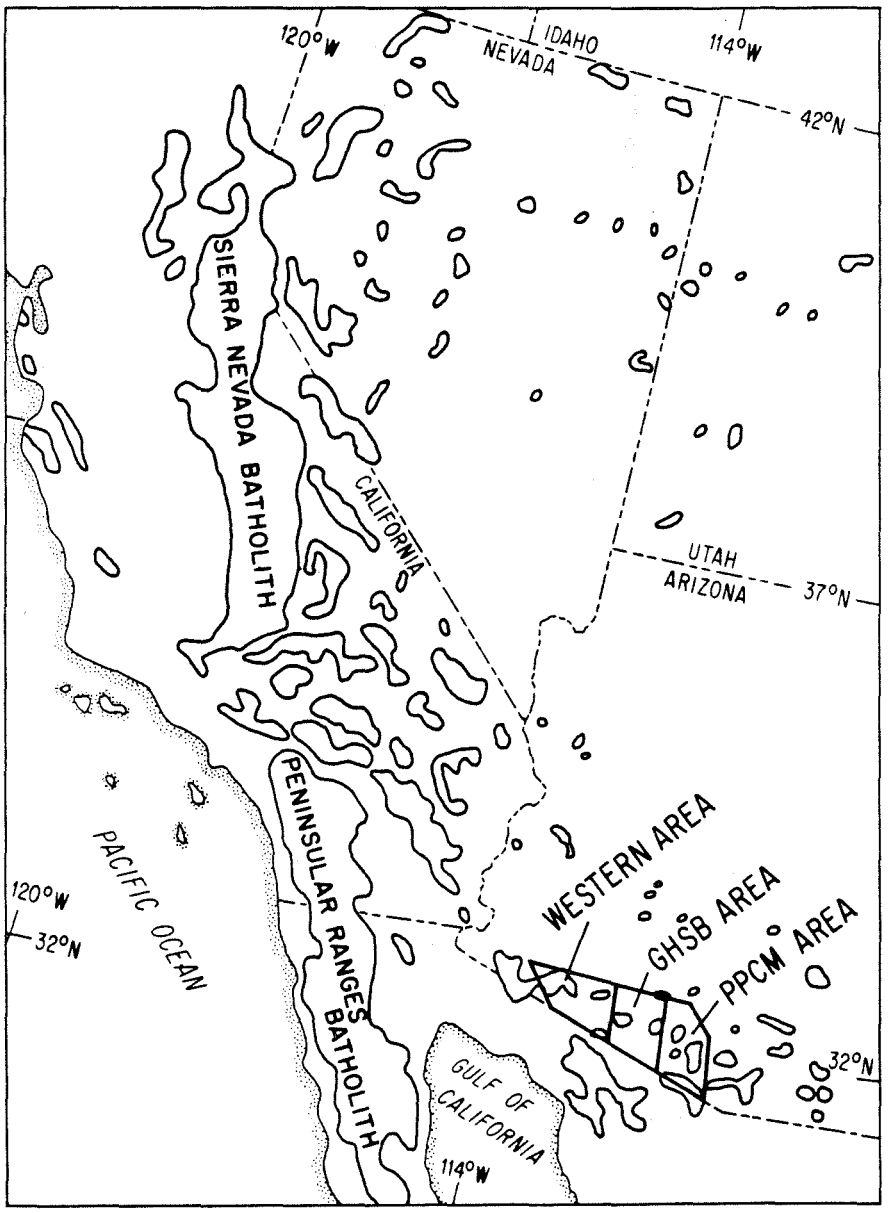
120°W
IDAHO
NEVADA
114°W
42°N
SIERRA NEVADA BATHOLITH
CALIFORNIA
UTAH
ARIZONA
37°N
PACIFIC OCEAN
PENINSULAR RANGES BATHOLITH
WESTERN AREA
GHSB AREA
PPCM AREA
120°W
32°N
GULF OF CALIFORNIA
32°N
114°W

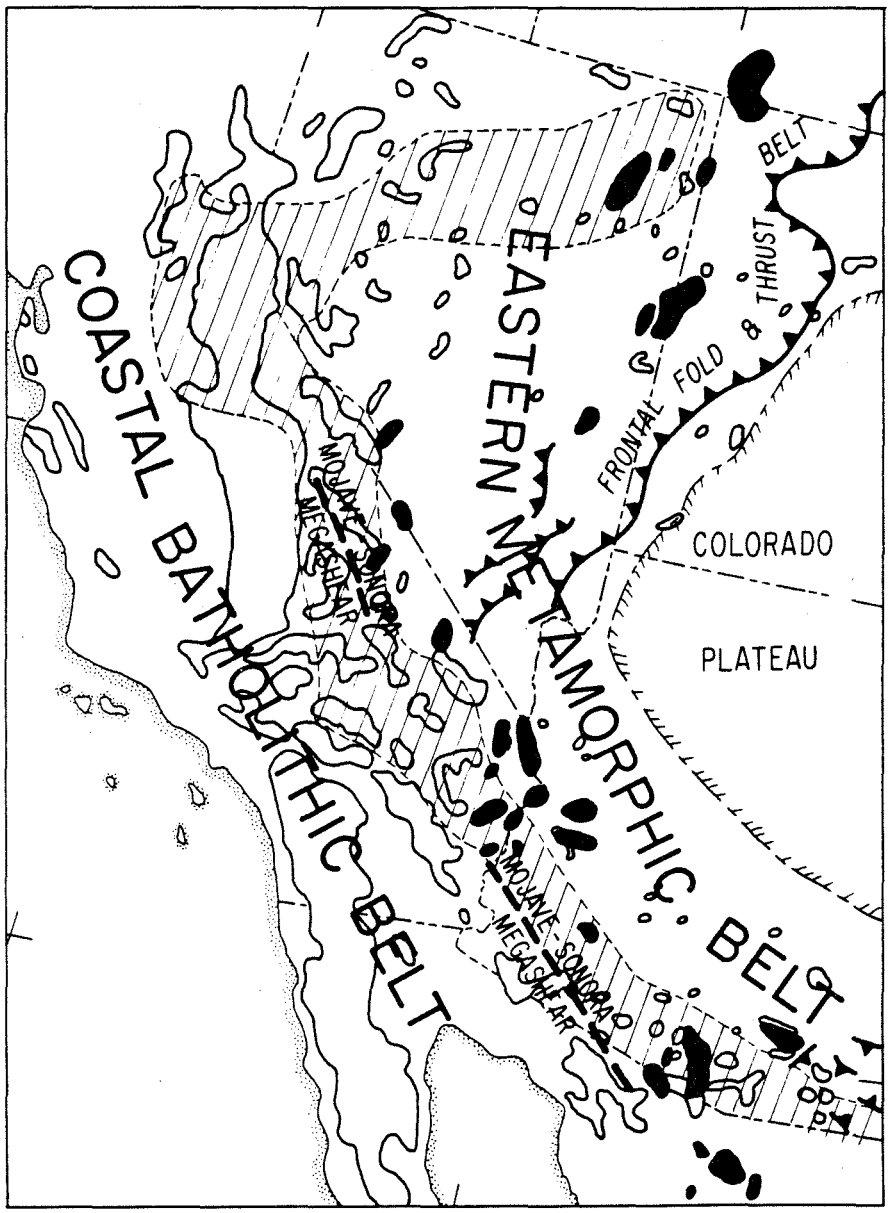
COASTAL BATHOLITHIC BELT
EASTERN METAMORPHIC BELT
FRONTAL FOLD & THRUST BELT
COLORADO PLATEAU
MOJAVE MEGASHEAR
MOJAVE-SONORA MEGASHEAR

more or less continuous Frontal Thrust and Fold Belt. The latter is made up of structurally disrupted, relatively unmetamorphosed, sedimentary rocks that lie unconformably upon Precambrian crystalline basement of varying lithology (the "craton").

To the west and southwest of the zone of thrusting, there exists a discontinuously exposed zone of late Mesozoic to early Cenozoic plutonism, and an area of ductile deformation and metamorphism known as the "eastern metamorphic belt" (Haxel et al., 1984; Miller and Bradfish, 1980; Best et al., 1974). The rocks of the "eastern metamorphic belt" are offset along thrust faults that displace crystalline Precambrian basement rocks or Mesozoic plutonic rocks (Howard et al., 1982; John, 1982; Haxel et al., 1984), and this is locally accompanied by metamorphism up to and including sillimanite grade (Miller et al., 1982). This area represents the northern part of a larger region that extends southward into north-central Sonora, Mexico. This part of Mexico was not sampled during this study, and because there are no available $\delta^{18}O$ data on this region, it is not part of this thesis.

Precambrian gneisses crop out southwest of a major structural discontinuity proposed by Silver and Anderson (1974), the Mojave-Sonora Megashear. This feature is discussed by Dickinson (1981a), and its probable trace is indicated in Fig. 5.2. However, in the main portions of the study area, Precambrian rocks are not recognized, and the oldest autochthonous rocks of regional extent are the volcanic and plutonic rocks of Jurassic age.

The region shown in Fig. 5.2 by diagonal-shading is a part of the Jurassic continental magmatic arc that extends across southern Arizona and northern Sonora, into southeastern California, and up through the

Sierra Nevada of California (Coney, 1978; Anderson and Silver, 1978; John, 1981; Haxel et al., 1980b; Saleeby, 1981; Chen and Moore, 1982; Busby-Spera, 1988). A second major episode of plutonism is locally superimposed upon this arc and is composed of latest Cretaceous granodiorites and early Tertiary two-mica (± garnet) granites (Haxel et al., 1984; Wright and Haxel, 1983); these plutons locally intrude deformed and metamorphosed Jurassic arc rocks.

5.3 The Presumido Peak - Coyote Mountains (PPCM) Area

5.3.1 Geology and Geochronology

The easternmost, or Presumido Peak - Coyote Mountains (PPCM) Area (Fig. 5.1) contains two large mountain ranges (the Baboquivari Mountains and the Comobabi Mountains). Several smaller ranges occur to the southwest, and include the Alvarez Mountains, Morena Mountain, Las Animas Mountain, and the Artesa Mountains. The Quinlan Mountains and Coyote Mountains are located north of the main Baboquivari range, and the Haivana Nakya Hills and Sil Nakya Hills flank the Comobabi range on the east and north, respectively. May and Haxel (1980), Haxel et al. (1978), Haxel et al. (1980a) and Haxel et al. (1981) have performed reconnaissance geological mapping in the Comobabi, Presumido Peak, Baboquivari Peak and Sells 15-minute quadrangles. Figure 5.3 summarizes the geologic relations determined by these workers in the PPCM area, with locations and corresponding $\delta^{18}O$ values of the analyzed samples (also see Table 1 in the appendix).

Lower Jurassic quartzofeldspathic schist, quartzite, metarhyolite, and calc-silicate schists and granofels crop out in the northwestern and southern Baboquivari Mountains (Haxel et al., 1984). Similar rocks crop out in the Haivana Nakya Hills and form the lower plate of the north-

Figure 5.3 Geologic map, $^{18}O/^{16}O$ sample localities and isotopic data for the region surrounding the Baboquivari, Comobabi, Coyote and Presumido Mountains (PPCM Area) in south-central Arizona. Sample localities indicated by solid circles; whole-rock $\delta^{18}O$ values shown alongside (Q after number indicates quartz $\delta^{18}O$); where available, ε_{Nd} values are shown enveloped in rectangles (data from Farmer and DePaolo, 1984). Dashed line is international border between Sonora, Mexico and Arizona, USA. Geology modified after Haxel et al. (1984) and Wilson et al. (1969): Tv - Tertiary volcanic rocks; cross-hatched areas - early Tertiary two-mica granites; Jg - Jurassic granitic plutons (outlined by cross pattern along margins of plutons); Jp - upper-plate Jurassic supracrustal rocks; Jb - lower-plate Jurassic supracrustal rocks; gn - gneissic rocks of uncertain age in the Alvarez Mountains. Thrust-fault symbol indicates boundary between upper- and lower-plates discussed in text. Road through the town of Sells is Arizona State Highway 86.

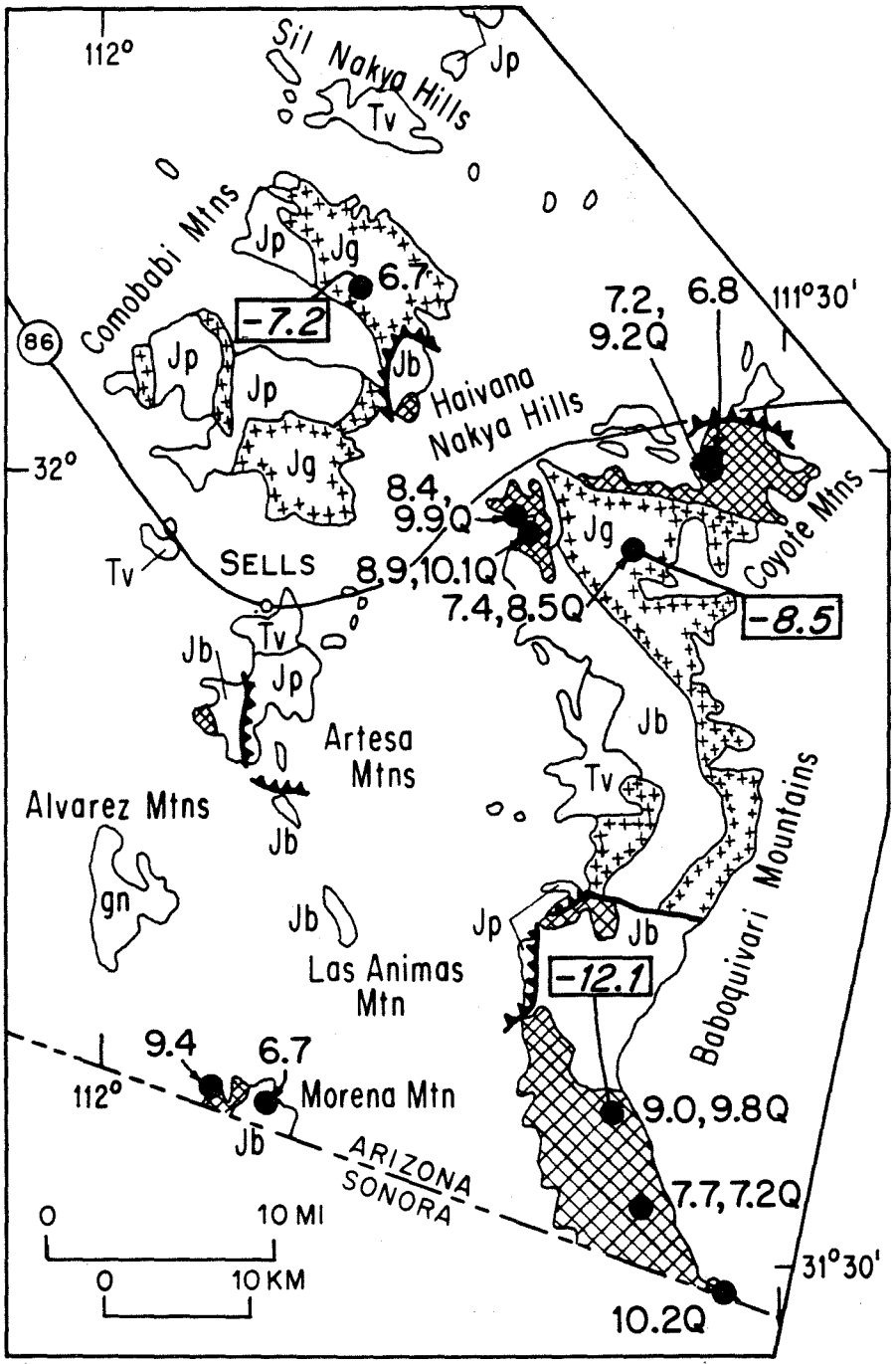
112°
Sil Nakya Hills
Jp
Tv
Comobabi Mtns
Jp
Jg
6.7
-7.2
Jb
Haivana Nakya Hills
Jp
Jp
Jg
86
32°
7.2, 9.2Q
6.8
111°30'
8.4, 9.9Q
Coyote Mtns
Jg
Tv
SELLS
8.9,10.1Q
7.4,8.5Q
-8.5
Jb
Tv
Jp
Artesa Mtns
Jb
Jb
Tv
Alvarez Mtns
gn
Jb
Jp
Jb
Las Animas Mtn
-12.1
Baboquivari Mountains
9.4
6.7
112°
Morena Mtn
Jb
ARIZONA
SONORA
9.0,9.8Q
7.7,7.2Q
31°30'
10.2Q
0
10 MI
0
10 KM

and west-dipping Baboquivari thrust fault. The schists contain the mineral assemblages quartz-muscovite-biotite and quartz-muscovite with or without chlorite and (or) epidote. The main mass of the Comobabi Mountains forms the upper plate of this fault.

The upper plate, which most likely also includes most of the exposures in the Artesa Mountains, consists mainly of Jurassic granitic and volcanic rocks unconformably overlain by Cretaceous sedimentary and volcanic rocks. The foliations in blastomylonites at the base of the upper plate are parallel to the foliation in the schists of the lower plate, suggesting that thrusting was synmetamorphic. Haxel et al. (1984) have proposed that the Baboquivari thrust fault extends southward along the western flank of the Baboquivari Mountains, where rocks similar to the main mass of the Comobabi Mountains are separated from typical "lower plate" rocks of the Baboquivari Mountains.

Jurassic plutonic rocks crop out in both the Comobabi and Baboquivari Mountains, but the lower plate granitoids are not associated with coeval volcanic units. Typical of the lower plate is the Kitt Peak granodiorite, which crops out in the northern Baboquivari range. This is a sphene-bearing, medium-grained, hornblende-biotite to biotite granodiorite. Also included in the lower plate plutonic rocks are biotite-hornblende quartz diorite, tonalite, hornblende diorite and lesser amounts of syenogranite.

The upper plate Jurassic igneous rocks that crop out in the Comobabi Mountains represent a subvolcanic environment near the interface between a large, near-surface plutonic complex and its overlying derivative volcanic pile (Haxel et al., 1978). The igneous complex contains porphyritic to equigranular quartz monzonite, granodiorite, diorite, and quartz

syenite, together with porphyritic hypabyssal intrusions and flows, flow breccias, and welded tuffs of both andesitic and more silicic compositions. Wright and Haxel (1983) report Upper Jurassic (~ 145 Ma) U-Pb isotopic ages for single fractions of zircon from two plutonic units in the lower plate near Kitt Peak. Wright et al. (1981) also report early Jurassic U-Pb ages for zircons from the supracrustal portions of the igneous complexes.

The lower plate rocks of the Baboquivari thrust are intruded by early Tertiary garnet-two-mica granites in the southern and northern Baboquivari Mountains, in the Coyote Mountains, in the Haivana Hakya Hills, in the Artesa Mountains and at Morena Mountain. The Pan Tak granite, which crops out in the Coyote Mountains, is a representative example of this type of pluton. This is a biotite- and muscovite-biotite granite that is locally intruded by garnet-muscovite and garnet-biotite granite with associated pegmatites. Wright and Haxel (1983) report that U-Pb isotope ratios of five size fractions of discordant zircons in the Pan Tak granite define a chord with a lower concordia intercept age of approximately 58 Ma, and a late Precambrian upper intercept.

In the Haivana Nakya Hills and northwest Baboquivari Mountains, where two-mica granite intrudes schist, the foliation in the schist is parallel with granitic contacts, and locally, portions of the main body of the granite have foliations oriented parallel to the country rock fabric (Haxel et al., 1984). Farther south and east, in the southern Baboquivaris, this parallelism dies out, schist adjacent to granite has been reoriented, and the granites sharply crosscut country rocks. However, locally there has been folding of the pegmatitic dikes that cut the schist adjacent to the two-mica plutons. These textural and struct-

ural relations indicate that intrusion of the two-mica granites was at least partially synkinematic, with the deformation associated with metamorphism and thrusting.

5.3.2 $^{18}O/^{16}O$ Data

Whole-rock $\delta^{18}O$ values of 3 samples from Jurassic plutons within the PPCM area (Fig. 5.3, Table 1 in the appendix) range from +6.7 per mil in quartz syenite of the Comobabi Mountains and in granodiorite from Morena Mountain to +7.4 per mil in the Kitt Peak granodiorite in the Northern Baboquivaris. A quartz separate from the ~ 165 Ma Kitt Peak pluton has $\delta^{18}O$ equal to +8.5, which falls within the reasonable range for "magmatic" fractionation between whole-rock and quartz (Taylor, 1978). Thus, this whole-rock $\delta^{18}O$ value of +7.4 certainly represents a good, primary value. The somewhat lower $^{18}O/^{16}O$ ratios in the Comobabi Mountains and at Morena Mountain are also probably primary, although we cannot exclude the possibility that those particular plutons locally interacted with low-^{18}O meteoric-hydrothermal fluids. The existence of minor meteoric-hydrothermal effects would not be surprising in light of the epizonal characteristics of some of the Jurassic plutons in the upper plate rocks. Verification of this will have to await a more detailed $^{18}O/^{16}O$ study of the area.

A single sample from a < 135 Ma (early Tertiary?) pluton west of Morena Mountain has $\delta^{18}O$ = +9.4. This is distinctly higher than any of the Jurassic samples. The early Tertiary plutons (~ 60 Ma) were sampled more extensively than the Jurassic plutons, and these have whole-rock $\delta^{18}O$ values that range from +6.8 to +9.0 per mil. However, the two lowest-^{18}O samples (+6.8 and +7.2) are suspect because they were both collected within 20 m of one another from the two-mica Pan Tak granite, and

one of the samples displays a non-equilibrium $\Delta^{18}O$ quartz-whole-rock value of 2.0 per mil. One other low-^{18}O sample (+7.7) is also clearly "disturbed" in that it has a reversed quartz-whole-rock $\Delta^{18}O$ value. Except for the latter sample, which has a much lower whole-rock $\delta^{18}O$ than another specimen collected from the same pluton (+9.0), the quartz separates from the Tertiary plutons yielded uniform $\delta^{18}O$ values between +9.2 and +10.2, with all but one of the analyses between +9.8 and +10.2. For the particular samples on which whole-rock analyses were made, the quartz-whole-rock $\Delta^{18}O$ values were very uniform at 1.2, 1.5 and 0.8, excluding the "disturbed" 2.0 value from the aforementioned Pan Tak granite. The other analyses are all indicative of essentially "normal magmatic" isotopic fractionations.

If we "correct" the $\delta^{18}O$ value of the Pan Tak granite by assuming that the $\delta^{18}O$ of its quartz is close to the primary value, we obtain a $\delta^{18}O \sim +8.2$ for this rock. With this correction, the range of primary, whole-rock $\delta^{18}O$ values for the single Cretaceous(?) sample and all of the early Tertiary (~ 60 Ma) granites of the PPCM area becomes +8.2 to +9.4. These are similar to $\delta^{18}O$ values found in a similar-age pluton located much farther to the east, about 100 km east of Tucson, the Texas Canyon quartz monzonite (Turi and Taylor, 1971b). Based on analyses of plutons associated with porphyry copper deposits (Sheppard et al., 1969, 1971), it is likely that the primary $\delta^{18}O$ values of the post-Jurassic plutons may extend down to values as low as those of the Jurassic PPCM plutons; however, we have no direct evidence of this in the PPCM sample population.

An important feature of these results is that primary, unaltered, two-mica granites in the PPCM area (even taking into account the "correc-

ted" $\delta^{18}O$ of the Pan Tak granite) all have moderately low whole-rock $\delta^{18}O$ values less than +9.2, as compared with most other two-mica plutons throughout the world (e.g., Taylor, 1968; Taylor and Turi, 1976; O'Neil and Chappell, 1977; O'Neil et al., 1977; Michard-Vitrac et al., 1980; Kistler et al., 1981; Lee et al., 1981b; Sheppard, 1977; Wickham and Taylor, 1985, 1987). Such two-mica plutons elsewhere commonly have $\delta^{18}O$ > 10.0 per mil, and are probably derived from sedimentary source rocks. Such an origin clearly does not apply to the southwest Arizona two-mica granites, which basically have $\delta^{18}O$ values very similar to the other Cretaceous and early Tertiary granites in this area.

5.4 The Gunsight Hills - Sierra Blanca (GHSB) Area

5.4.1 Geology and Geochronology

The Gunsight Hills-Sierra Blanca (GHSB) Area encompasses from northeast to southwest: the Cimar and Sheridan Mountains; the Brownell Mountains, Quijotoa Mountains, and the Sierra Blanca; and the Gunsight Hills (see Figure 5.4). Reconnaissance geologic mapping has been completed in these and surrounding areas by Briskey et al. (1978), Blacet et al. (1978), Berquist et al. (1978), Rytuba et al. (1978), and Tosdal et al. (1986). Figure 5.4 summarizes the geology of the GHSB area.

The Sheridan Mountains contain latest Jurassic and Cretaceous conglomerate and sandstone with subordinant volcanic and hypabyssal rocks. These units increase in metamorphic grade to the southwest, where sedimentary bedding becomes progressively obscured and folded, and where foliation is increasingly more pervasively developed. The greatest degree of recrystallization results in rocks that have been transformed to quartz-mica and quartzofeldspathic schists and greenschists.

Figure 5.4 Geologic map, $^{18}O/^{16}O$ sample localities and isotopic data for the region surrounding the Gunsight Hills and Sierra Blanca (GHSB Area) in south-central Arizona. Sample localities indicated by solid circles; whole-rock $\delta^{18}O$ values shown alongside (Q after number indicates quartz $\delta^{18}O$); where available, ε_{Nd} values are shown enveloped in rectangles (data from Farmer and DePaolo, 1984). Dashed line is international border between Sonora, Mexico and Arizona, USA. Geology modified after Haxel et al. (1984) and Wilson et al. (1969): Tv - Tertiary volcanic rocks; cross-hatched area - early Tertiary two-mica granite of Sierra Blanca; Kqm - late Cretaceous biotite hornblende monzogranites of Gunsight Hills and Cimar Mountains (stippled pattern along inside of pluton margins); Jg - Jurassic granite of Brownell Mountains (outlined by cross pattern along pluton margins); Jp - upper-plate Jurassic supracrustal rocks; Jb - lower-plate Jurassic supracrustal rocks; gn - gneissic rocks of uncertain age in the Kupk Hills and Cimar Mountains. Thrust-fault symbol indicates boundary between upper- and lower-plates discussed in text. Road through the village of Wahak-Hotrontk is Ajo Highway; road through village of Gu Achi is Arizona State Highway 86.

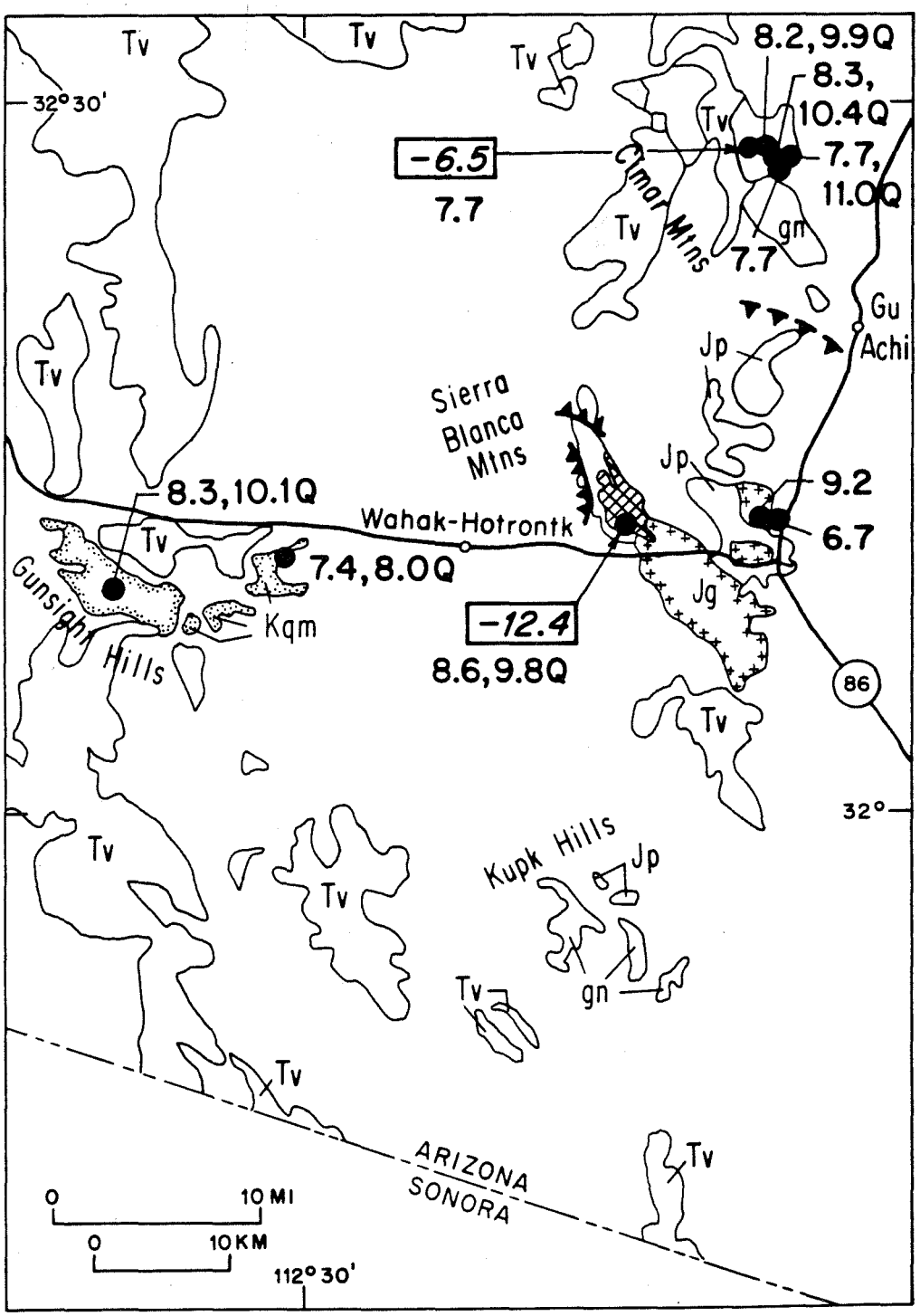
Tv
Tv
Tv
8.2,9.9Q
8.3,
10.4Q
32°30'
-6.5
7.7
Tv
7.7,
11.0Q
Cmar Mtns
Tv
gn
7.7
Gu
Achi
Jp
Tv
Sierra
Blanca
Mtns
Jp
9.2
8.3,10.1Q
Wahak-Hotrontk
6.7
Tv
7.4,8.0Q
Gunsight Hills
Kqm
-12.4
8.6,9.8Q
Jg
86
Tv
32°
Tv
Kupk Hills
Jp
Tv
gn
Tv
ARIZONA
SONORA
Tv
0
10 MI
0
10 KM
112°30'

Haxel et al. (1984) have proposed that this metamorphism is a result of proximity to a thrust fault buried in the alluvium to the southwest. These authors believe that rocks farther to the southwest in the Brownell Mountains (Jurassic plutonic-volcanic complex) are part of the upper plate of the proposed thrust. K-Ar dates determined on phyllites and schists in the adjacent Santa Rosa Range are 70 and 72 Ma; thus the metamorphic pulse cooled through the K-Ar blocking temperatures during latest Cretaceous time (Haxel et al., 1984).

The Brownell and Quijotoa Mountains are underlain for the most part by Jurassic igneous rocks similar to the upper plate rocks of the Comobabi Mountains in the PPCM area. The most prominent intrusive rock is a quartz monzonite, which is locally altered to epidote and chlorite, and which grades into a porphyritic roof facies consisting of medium- to coarse-grained quartz latite porphyry with 40 per cent finely crystalline groundmass. Associated with these rocks are andesitic flows with calcite- and epidote-filled amygdules, and a hornblende diorite that has been partially chloritized. The plutonic-volcanic complex of the Brownell and Quijotoa Mountains is in fault contact with crystalline rocks of the Sierra Blanca.

In the Sierra Blanca, at its northwest portion, quartzofeldspathic and epidote-quartz schist and schistose conglomerate are overlain along the synmetamorphic Window Mountain Well thrust fault by Precambrian (?) augen orthogneiss. Haxel et al. (1984) have assumed that the upper plate plutonic-volcanic complex of the Quijotoa and Brownell Mountains comprise part of this thrust system, although there is no mappable connection between these rocks and the Precambrian rocks. The lower plate schists of Sierra Blanca are equivalent to rocks of the lower plate in the PPCM area.

A garnet-muscovite granite, termed the granite of Sierra Blanca by Haxel et al. (1984), intrudes the schists of the lower plate, and, in the southeastern Sierra Blanca, this unit contains small schistose pendants. The contact between country rock and the granite consists of a swarm of granite and pegmatitic dikes and sills that are unfoliated, and there is no single discrete contact with the wall rocks.

Sierra Blanca upper- and lower-plate rocks occur within the granite as inclusions, which suggests a post-Jurassic age for the granite. As with the early Tertiary peraluminous intrusives in the PPCM area, textural relations indicate a synkinematic emplacement style for the Sierra Blanca muscovite granite, although the xenolith population demands that its emplacement be in part postkinematic. Because of its synkinematic nature (similar to the Pan Tak granite), its emplacement is probably time-equivalent with that of the Pan Tak granite (at around 58 Ma).

The two remaining localities, the Gunsight Hills and the Cimar Mountains, are underlain by hornblende-biotite granodiorite and quartz monzonite of early Tertiary to latest Cretaceous age. Most of the time-equivalent plutons in the PPCM and GHSB areas are peraluminous in nature; thus there is a strong contrast in plutonic style between the Gunsight Hills plutonic rocks and the remainder of the GHSB area.

Haxel et al. (1984) have reported K-Ar and U-Pb ages of 68 to 69 Ma (unpublished data of R.M. Tosdal and J.E. Wright) for hornblende-bearing plutons in the Cimar Mountains, and they also have reported revised K-Ar dates of 64 to 65 Ma for the plutons of the Gunsight Hills (based upon the data of McDowell, 1971). These dates agree fairly well with a U-Pb age of 74 Ma for a similar pluton in north-central Sonora, Mexico (Anderson et al., 1980).

The rocks in the Cimar Mountains are relatively undeformed, although they locally exhibit epizonal-style hydrothermal alteration associated with epidote and quartz veining. Unfoliated granitic rocks in the northwestern and central Gunsight Hills grade southeastward into crystalloblastic amphibolite-facies hornblende biotite and biotite orthogneiss and orthoschist. The northeastern Gunsight Hills contain relatively undeformed hornblende-biotite granodiorite that is intruded by leucocratic biotite granite.

Based upon the distribution of fissure veins and textures in the granites, as well as the spatial variation of K-Ar ages, Tosdal et al. (1986) propose that the entire sequence of plutonic rocks of the Gunsight Hills is tilted on its side, and that it now represents a > 4-km vertical section through a pluton that grades at depth into a ductile shear zone. Haxel et al. (1984) infer that this shear zone could be an early-Tertiary or latest-Cretaceous thrust fault.

5.4.2 $^{18}O/^{16}O$ Data

The $^{18}O/^{16}O$ sample population for the GHSB area is comprised of two specimens of quartz monzonite from the Jurassic plutonic-volcanic complex in the Brownell Mountains, a sample from the early Tertiary muscovite granite of Sierra Blanca, and several samples from the latest Cretaceous granodiorites and quartz monzonites of the Gunsight Hills and Cimar Mountains (Fig. 5.4, Table 1 in the appendix).

The Jurassic whole-rock $\delta^{18}O$ values are +6.7 for a very Fe-rich, alkali-rich, quartz gabbro and +9.2 for a granite. The lower value corresponds well with values determined for Jurassic plutons in the PPCM area, but the +9.2 value is 2 per mil higher than average PPCM Jurassic values, and is by far the highest-^{18}O Jurassic sample yet analyzed from

southern Arizona. No quartz $^{18}O/^{16}O$ analyses were performed for these samples, so we cannot be absolutely certain whether they represent "magmatic" equilibrium values. Nevertheless, the +6.7 value is very reasonable for a rock with such a low-SiO_2 content (50.9 wt. %), and meteoric-hydrothermal alteration in general would not be expected to increase the $\delta^{18}O$ value of a pluton, so the +9.2 value is also probably primary.

The measured whole-rock $\delta^{18}O$ values of the early Tertiary to latest Cretaceous plutons in the GHSB area range from +7.4 to +8.6, and their corresponding quartz $\delta^{18}O$ values range from +8.0 to +11.0. The two samples from the Gunsight Hills plutonic complex have quartz-whole-rock fractionations of 0.6 to 1.8 per mil; the 0.6 value clearly reflects a near-equilibrium $^{18}O/^{16}O$ fractionation, so the +7.4 whole-rock $\delta^{18}O$ of this sample should represent a valid primary value. The other sample, with a $\Delta^{18}O$ value of 1.8 per mil, appears to be slightly "disturbed", although we note that there are no obvious hydrothermal alteration effects in the Gunsight Hills samples, as these are located away from the upper levels of this "tilted," vertically-exposed pluton, and they are also not located in the zone of shear deformation.

The quartz-whole-rock $\Delta^{18}O$ values of the other GHSB samples are 1.2, 1.7, 2.1, and 3.3, and several of these are too large to represent equilibrium at magmatic temperatures. The two samples with the greatest quartz-whole rock fractionations are in fact both from the hydrothermally altered Cimar Mountains area, and it is obvious that the $\delta^{18}O$ values of these two rocks were markedly lowered during the hydrothermal events. If we make the plausible assumption that the quartz $\delta^{18}O$ values for the Cimar Mountains pluton are essentially unaffected by the hydrothermal activity, we can estimate the whole-rock $\delta^{18}O$ values of the three samples

with $\Delta^{18}O$ quartz-whole rock $\geq$ 1.7 to be about +8.8 to +9.9, assuming an average quartz-whole-rock $\Delta^{18}O$ = 1.1 per mil for these quartz monzonites (see Chapter 3). Thus, the primary whole-rock $\delta^{18}O$ range in the GHSB post-Jurassic plutons would be +7.4 to +9.9, markedly wider than in the PPCM area. However, excluding the isotopically most "disturbed" sample, which also has an anomalously high $\delta^{18}O$ quartz = +11.0, the overall $\delta^{18}O$ range of this age grouping in the GHSB area becomes only +7.4 to +9.4.

The early Tertiary muscovite granite of Sierra Blanca has a whole-rock $\delta^{18}O$ = +8.6, and a quartz $\delta^{18}O$ = +9.8. Thus, this whole-rock $\delta^{18}O$ value of +8.6 is certainly an "undisturbed" primary, magmatic value, and like the two-mica plutons of the PPCM area, the Sierra Blanca pluton is much lower in ^{18}O than typical S-type two-mica granites throughout the world. Haxel et al. (1984) believe that the Sierra Blanca pluton shows more evidence for postkinematic emplacement than the somewhat similar Pan Tak granite from the PPCP area, whose emplacement occurred during regional deformation in the Baboquivari Mountains. Thus, the slight $^{18}O/^{16}O$ "disequilibrium" effects observed between quartz and whole-rock in the Pan Tak granite conceivably could reflect alteration by fluids during waning stages of synkinematic deformation, whereas the Sierra Blanca intrusive event clearly could not have involved any significant quantities of circulating fluids.

5.5 The Western Area

5.5.1 Geology and Geochronology

The geology and locations of $^{18}O/^{16}O$ samples in the Western Area are shown in Figure 5.5. Plutonic rocks that were sampled for this study were located adjacent to the town of Ajo, Arizona, in the vicinity of the Quitobaquito Hills to the south, and in the western mountain ranges be-

Figure 5.5 Geologic map, $^{18}O/^{16}O$ sample localities and isotopic data for the eastern portion of the Gunnery Range batholith, and the terrane between Ajo and the Quitobaquito Hills (Western Area) in south-central Arizona. Sample localities indicated by solid circles; whole-rock $\delta^{18}O$ values shown alongside (Q after number indicates quartz $\delta^{18}O$); where available, ε_{Nd} values are shown enveloped in rectangles (data from Farmer and DePaolo, 1984). Dashed line is international border between Sonora, Mexico and Arizona, USA. Geology modified after Haxel et al. (1984); Shafiqullah et al. (1980); Wilson et al. (1969); and personal communication with L.T. Silver (1988): Tv - Tertiary volcanic rocks; cross-hatched area - early Tertiary two-mica granite; stippled pattern on inside of pluton margins - late Cretaceous biotite monzogranites and muscovite granite of Gunnery Range batholith (boundary indicated by heavy dashed line); monzogranites of Quitobaquito Hills and biotite hornblende monzogranite of Little Ajo Mountains; Kv - Cretaceous volcanic rocks (Concentrator Volcanics of Gilluly, 1946); small crosses on pluton margins - Jurassic granite of Puerto Blanco Mountains; Jb - lower-plate Jurassic supracrustal rocks; PGgn - Precambrian gneissic rocks discussed in text (L.T. Silver, pers. comm., 1988) Thrust-fault symbol indicates boundary between upper- and lower-plates discussed in text. Road through the town of Ajo is Arizona State Highway 85.

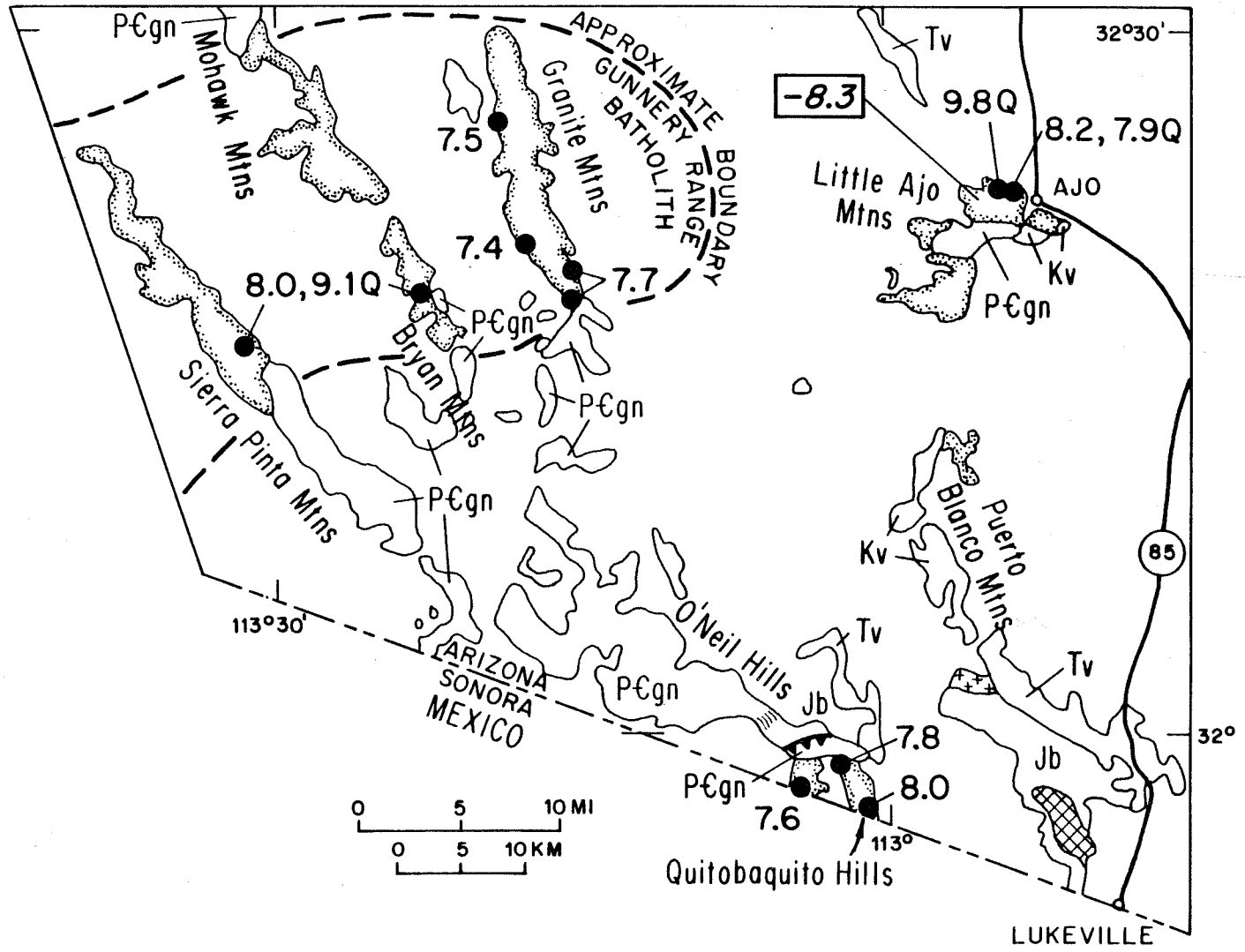
P€gn
Mohawk Mtns
APPROXIMATE GUNNERY BATHOLITH BOUNDARY RANGE
Granite Mtns
7.5
7.4
7.7
8.0,9.1Q
P€gn
Bryan Mtns
P€gn
P€gn
Sierra Pinta Mtns
113°30'
ARIZONA
SONORA
MEXICO
P€gn
O'Neil Hills
Jb
7.8
8.0
7.6
P€gn
113°
Quitobaquito Hills
0 5 10 MI
0 5 10 KM
Tv
-8.3
9.8Q
8.2, 7.9Q
32°30'
Little Ajo Mtns
AJO
Kv
P€gn
Kv
Puerto Blanco Mtns
Tv
Tv
85
32°
Jb
LUKEVILLE

tween Ajo and Yuma, California. These western ranges include, from east to west, the Granite, Mohawk, and Sierra Pinta Mountains.

Most of the Western Area is especially inaccessible compared with the PPCM and GHSB areas, because much of it is in the Yuma Gunnery Range, or is included in the Cabeza Prieta National Wildlife Refuge where travel is restricted. Sampling restrictions are also in effect in the Organ Pipe National Monument, south of Ajo. The author collected the specimens near Ajo, but all of the other samples from the Western Area were collected by G. Haxel and R.M. Tosdal during their reconnaissance studies of these restricted areas. Samples were not obtained from the Tinajas Altas and Cabeza Prieta Mountains in extreme southwestern Arizona, because of the remoteness of these areas.

Because of the remoteness of most of the region, much of the geology of the Western Area has not been substantially modified since the initial reconnaissance mapping in the 1920's and 1930's by Eldred Wilson (Shafiqullah et al., 1980). Wilson's work appears on the Arizona State Geologic Map (Wilson et al., 1969). More recently, descriptions of the geology near Ajo and around the Quitobaquito Hills have been published by Gilluly (1946), Haxel et al. (1984), and May (1981).

In the Ajo region, the Cornelia quartz monzonite intrudes rhyolitic and andesitic pyroclastic rocks that have been albitized. Farther to the west, this body intrudes the Cardigan gneiss of possible Precambrian (?) age. The proposed Mojave-Sonora megashear separates the Precambrian (?) rocks around Ajo from those farther south and west, so the geochronologic framework established for the Precambrian of northern Sonora by Anderson and Silver (1970, 1971, 1979) may not apply to the Ajo rocks.

The volcanic rocks around Ajo are termed the Concentrator Volcanics; these were considered to be of Cretaceous age by Gilluly (1946). McDowell (1971) reports K-Ar ages of 64 and 65 Ma for the Cornelia quartz monzonite, similar to the ages of the hornblende-bearing, latest Cretaceous to earliest Tertiary plutons discussed by Haxel et al. (1984) for the Papago Indian Reservation. The Cornelia quartz monzonite hosts a major porphyry copper deposit, and exhibits widespread epizonal-style hydrothermal effects such as potassic, phyllic, and propylitic alteration (for $\delta^{18}O$ analyses of these rocks see Sheppard et al., 1969; 1971). Post-emplacement normal faults have displaced portions of the Cornelia pluton in the northeastern portion of the Little Ajo Mountains, but no synkinematic deformational events have been described.

The western portion of the Western Area contains numerous Precambrian (?) outcrops that may be time-correlative to those studied by Anderson and Silver (1970, 1971) in northern Sonora. These authors dated the Bamori schist in the Caborca region at 1660 Ma; this has been corroborated by K-Ar dating on hornblende in the schist by Shafiqullah et al. (1980). Anderson and Silver (1979) report U-Pb ages for metamorphic rocks near the Pinacate volcanic field (1670 to 1650 Ma), and these rocks are intruded by 1450 Ma gneissic granites.

The most abundantly exposed rocks in the western portion of the Western area are from a single granitic batholith; Shafiqullah et al. (1980) proposed the name "Gunnery Range Batholith" for this latest Cretaceous to earliest Tertiary plutonic mass, which underlies most of the Granite, Mohawk, and Sierra Pinta Mountains. The Gunnery Range Batholith is mainly composed of leucocratic biotite granite with some two-mica variants. Aerial photography shows that contacts with surrounding "Pre-

cambrian" gneisses are sharp. K-Ar ages on biotites (Shafiqullah et al., 1980) range from 52.5 to 53.1 Ma, but it is likely that these represent only minimum ages because Precambrian wall rocks record "reset" K-Ar ages around 59 Ma (Eberly and Stanley, 1978). This implies a true age greater than 59 Ma because the closure temperature for Ar in biotite is between 250°C to 300°C (Criss et al., 1982). Thus, some period of time elapsed between magmatic conditions in the batholith and the time at which its biotite cooled below 300°C.

The Quitobaquito Hills are underlain by metamorphosed Precambrian (?) gneiss and schist that lie allochthonously on top of Jurassic supracrustal and plutonic rocks along the complex, imbricate Quitobaquito thrust fault. The lower plate rocks (Haxel et al., 1984) bear a close resemblance to isotopically-dated Jurassic units in the PPCM and GHSB areas (Wright et al., 1981; Haxel et al., 1980b), and in northern Sonora (Anderson and Silver, 1978, 1979). Above the Quitobaquito thrust fault, a ductile shear zone has placed latest Cretaceous biotite granite (the Aquajita Spring granite) structurally above the Precambrian gneiss unit (Haxel et al., 1984). The biotite granite locally intrudes the gneiss on both sides of this shear zone.

Haxel et al. (1984) report that muscovites from rocks along the Quitobaquito thrust zone have K-Ar ages between 54 and 60 Ma, and these authors have correlated this deformational event with the latest Cretaceous and early Tertiary thrusting found elsewhere in the study area. These data would indicate that the Aquajita Spring granite was emplaced prior to the formation of the Quitobaquito thrust fault.

5.5.2 $^{18}O/^{16}O$ Data

Our $^{18}O/^{16}O$ sample population does not include any Jurassic plutons, although such rocks do crop out within the Western Area. The population is comprised of (1) a broad traverse across the eastern portion of the Gunnery Range batholith (latest Cretaceous to earliest Tertiary in age), (2) samples from the latest Cretaceous biotite granite in the Quitobaquito Hills, and (3) samples from the Cornelia pluton at Ajo. The $^{18}O/^{16}O$ data are listed in Table 1 in the appendix and shown on the map in Figure 5.5.

Six widely spaced samples from the eastern half of the 60 km x 20 km Gunnery Range batholith display a narrow range of whole-rock $\delta^{18}O$ = +7.4 to +8.0. The analyzed quartz separates in two of these samples yielded uniform $\delta^{18}O$ values = +9.1 and $\Delta^{18}O$ quartz-whole-rock = +1.1. These data indicate that these whole-rock $\delta^{18}O$ values are primary magmatic values. The latest Cretaceous biotite granite from the Quitobaquito Hills has $\delta^{18}O$ whole-rock = +7.6 to +8.0. No $\delta^{18}O$ analyses of quartz were made from these rocks.

As might be expected in a mining district, the $^{18}O/^{16}O$ data from the Cornelia pluton near Ajo show the effects of subsolidus interaction with hydrothermal fluids. The two hand specimens taken from the pluton both exhibit strong chloritization of mafic minerals, and a whitening of the feldspars that is most likely due to albitization. The samples were collected within fifty feet of one another from the main mass of the Cornelia pluton, on the northwest side of the Gibson Fault in a zone of propylitic alteration (see Gilluly, 1946).

One Ajo sample has a whole-rock $\delta^{18}O$ = +8.2, while the coexisting extremely fine-grained (< 1 mm) quartz phenocrysts have $\delta^{18}O$ = +7.9 per

mil. Although most igneous quartz grains affected by meteoric-hydrothermal systems have been shown to be relatively unexchanged, we know that very fine-grained quartz in such environments is typically slightly depleted in ^{18}O. It is thus likely that these $\delta^{18}O$ values do not exactly reflect magmatic $^{18}O/^{16}O$ compositions. Coarser-grained quartz (> 2 mm) from the other sample was also analyzed, and it has $\delta^{18}O$ = +9.8 per mil. This is probably close to the primary magmatic value, and if so, the corresponding calculated whole-rock $\delta^{18}O$ value becomes +8.8, which is more in line with whole-rock values for most of the early Tertiary to latest Cretaceous rocks farther east in the PPCM and GHSB areas.

5.6 Comparison of the $^{18}O/^{16}O$ and Major-Element Geochemistry

Summing up the "corrected" and measured whole-rock $^{18}O/^{16}O$ relationships in southern Arizona, we note that the Cretaceous to early Tertiary plutons have $\delta^{18}O$ = +7.4 to +9.9, while the Jurassic plutons are distinctly lower at +6.7 to +7.4 (excluding a single Jurassic sample from the GHSB area with $\delta^{18}O$ = +9.2). The post-Jurassic plutons show some geographic systematics: Whole-rock $\delta^{18}O$ values are +8.2 to +9.4 in the eastern (PPCM) area and +7.4 to +8.0 in the western part of the Western Area. The central (GHSB) area and the northeast corner of the Western Area (Ajo) are transitional in the sense that they contain some samples as low as +7.4 to +7.7 and some as high as +9.4 to +9.9. Thus, there is a very slight west-to-east ^{18}O-enrichment observed in the Cretaceous and early Tertiary plutons across southern Arizona. The two-mica granites do not differ appreciably in whole-rock $\delta^{18}O$ compared to other plutons of similar age.

Many different petrological and geochemical classification schemes have been proposed for granitic rocks throughout the years. In particul-

ar, much interest has been generated recently by classification schemes applied to Australian granitoids (e.g., Chappell, 1978; Hine et al., 1978). These workers propose that in southeastern Australia, the chemical compositions of Upper Paleozoic plutons directly reflect the nature of their source regions, either dominantly sedimentary ("S-types") or dominantly igneous ("I-types").

Many other workers have also become interested in such genetic classifications of granites, and it has been found that modern geochemical studies of granites are the best way to attack this problem. It is now generally accepted that in the absence of secondary alteration, the most powerful approach to a study of the nature of magmatic source regions is to combine stable and radiogenic isotopic information with studies of the major- and trace-element geochemistry.

With the above approach in mind, the major-element geochemistry of the Arizona plutons is discussed in combination with the $\delta^{18}O$ data. The data are presented in the form of Ab-An-Or C.I.P.W. normative graphs, Peacock Indices, and the Chappell-White "I-" and "S-type" classifications.

Figure 5.6 shows a ternary plot of the C.I.P.W. normative values for An, Ab, and Or (normalized to 100 per cent) from the data in Table 5.1. Also shown is the "Sierra Nevada batholith trend line" of Presnall and Bateman (1973). The data from southern Arizona are divided into a Jurassic suite and a late Cretaceous - early Tertiary suite. Both trends plot close to the Sierra Nevada trend.

Presnall and Bateman (1973) proposed that the general shape of the Sierra Nevada trend is a result of equilibrium fusion of a calcic quartzofeldspathic source material (indicated by region A in Fig. 5.6), comb-

Figure 5.6 Ternary diagram plotting calculated percentages of An-Ab-Or end-members (C.I.P.W. normative mineralogy; normalized to 100%) of granitic plutons from south-central Arizona study areas. Data from Table 5.1 were used to calculate normative values. Solid circles indicate late Cretaceous and early Tertiary samples; open circles - Jurassic samples. Line M-N is the Sierra Nevada Batholith trend of Presnell and Bateman (1973). Dashed outline labeled "A" is a hypothetical source region composition for Sierra Nevada-type plutons; dashed outline "B" represents minimum-melt compositions.

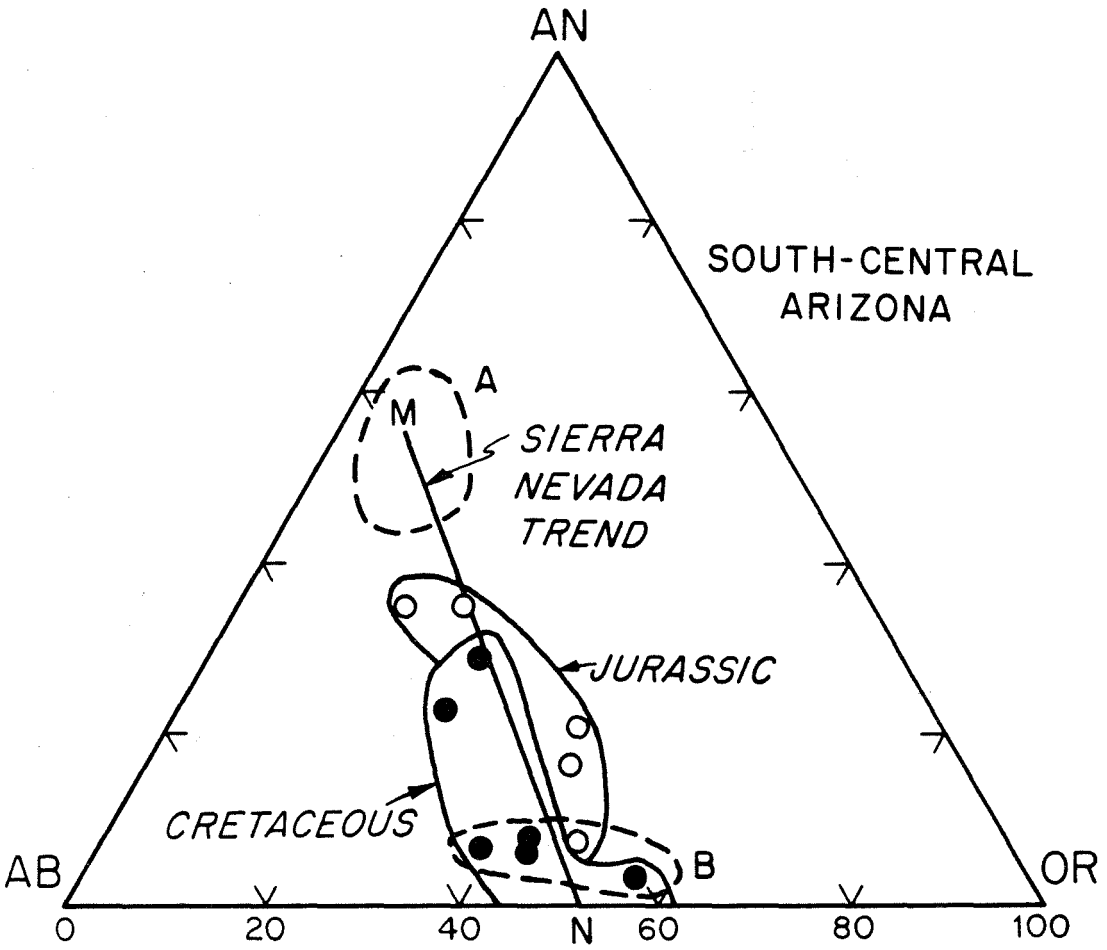
AN
SOUTH-CENTRAL
ARIZONA
A
M
SIERRA
NEVADA
TREND
JURASSIC
CRETACEOUS
AB
B
OR
0
20
40
N
60
80
100

Table 5.1 Major-element geochemistry, C.I.P.W normative mineralogy and isotopic data (whole-rock $\delta^{18}O$, ε_{Sr}, ε_{Nd}) for selected plutons in the southern Basin and Range of south-central Arizona.

	Sample Identifier[a]										
	B33	B48	PUP4	PUP6	PUP9	PUP11	PUP14	PUP32	PUP50	PUP51	SP701
Major-Element Geochemistry[b]											
SiO_2	50.90	66.20	66.70	74.90	58.60	65.70	74.70	74.20	67.10	73.50	57.80
TiO_2	1.53	0.69	0.64	0.02	0.87	0.46	0.07	0.04	0.54	0.20	0.78
Al_2O_3	15.80	15.30	15.00	14.40	15.70	16.20	14.00	14.40	15.90	13.90	18.40
Fe_2O_3	11.60	3.26	3.30	0.48	2.50	3.52	0.28	0.30	1.51	0.40	3.28
FeO	6.38	1.27	0.91	0.16	3.90	1.81	0.90	0.57	3.46	1.67	6.55
MgO	4.06	1.46	1.49	0.14	3.60	1.24	0.20	0.16	1.37	0.40	2.33
CaO	6.99	2.34	1.15	0.80	4.50	3.02	0.97	0.86	3.18	0.40	5.69
Na_2O	3.10	3.34	3.85	3.54	3.30	3.17	3.61	4.08	4.02	2.81	4.13
K_2O	2.48	5.18	6.13	4.51	3.10	5.10	4.62	4.24	3.18	5.73	2.13
Tot	102.84	99.04	99.17	98.95	96.07	100.22	99.35	98.85	100.26	99.01	101.09
Trace Element and Isotopic Data[c]											
$\delta^{18}O$	+6.7	+9.2	+6.7	+8.6	+7.7	+7.4	+7.2	+9.0	+7.8	N.D.	+6.7
Age,Ma	165	165	150	58	68	165	58	58	Kt	Kt	Jr
I(Sr)[d]	--	--	0.7071	0.7158	0.7096	0.7071	--	0.7208	--	--	--
ε_{Sr}	--	--	+40	+162	+74	+40	--	+232	--	--	--
Sr,ppm	--	--	218	66	628	381	--	163	--	--	--
ε_{Nd}	--	--	-7.2	-12.4	-6.5	-8.5	--	-12.1	--	--	--
C.I.P.W. Normative Mineralogy[e]											
Qtz	4.97	19.98	16.33	35.50	12.09	19.40	33.86	32.53	22.63	34.11	10.46
Cor	--	--	2.26	--	--	1.31	1.55	0.06	2.37	--	--
Or	14.25	30.91	36.53	26.93	19.07	30.07	27.48	25.35	18.74	34.20	12.45
Ab	25.51	28.54	32.85	30.27	29.07	26.76	30.75	34.93	33.93	24.02	34.60
An	21.27	11.57	5.59	4.01	19.64	14.88	4.84	4.32	15.73	2.00	25.10

[a] Sample Identifier linked to "GCS" Sample Number in Table 1 (appendix).
[b] Unpublished data of G. Haxel (pers. comm., 1984).
[c] GCS-015-79 (Cornelia Stock, Ajo) has $\delta^{18}O$ = +8.2, nearby sample has I(Sr) = 0.7076, ε_{Nd} = -8.3; ε_{Sr} and ε_{Nd} data from Farmer and DePaolo (1984).
[d] Calculated using equation in Farmer and DePaolo (1983).
[e] Calculated using Ed Stolper's computer program (1984).

ined with subsequent fractional crystallization of the melts. The similar trend exhibited by the Arizona plutons might also fit such a scheme. Whitney (1975) has shown in laboratory melting experiments that partial melts of calcic quartzofeldspathic material would follow such a trend; the position occupied by the two-mica granites (indicated by region B in Fig. 5.6) would correspond either to minimum melts, or to extremely differentiated melts in the Qtz-Ab-An-Or system at $P_{water} < 15$ Kbars.

Figure 5.7 shows a Peacock diagram plotting the variation of CaO and ($Na_2O + K_2O$) versus SiO_2 for the two south-central Arizona plutonic suites. Although the data are sparse, and the Jurassic suite appears to be somewhat more alkali-rich, both of the trends converge to a more or less common alkali-lime index of approximately 55 to 57 weight per cent SiO_2. According to the classification scheme of Peacock (1931), these southern Arizona plutonic suites would thus be "alkali-calcic," verging upon "calc-alkaline." For comparison, the Sierra Nevada batholith is calc-alkaline (Bateman et al., 1963; Kistler, 1974; Lockwood, 1975; Bateman and Lockwood, 1976), and the western Idaho batholith and the Peninsular Ranges batholith are both calcic (Larsen and Schmidt, 1958; Silver et al., 1979; Criss and Fleck, 1987). Plutons in the Great Basin region of Nevada occupy a geologic and geographic position similar to those in southern Arizona (relative to the "eastern metamorphic zone" shown in Fig. 5.2), but they have an alkali-lime index of approximately 60 wt. % SiO_2 (Lee, 1984), which makes them "calc-alkaline." The geographic distribution of the Peacock alkali-lime index in the Cordilleran plutons of western North America is further examined in Chapters 9 and 10.

Dickinson (1975) has related the potassium content of plutons in orogenic zones to the so-called "depth of the Benioff Zone," with relati-

Figure 5.7 Plot of SiO_2 (wt.%) versus Na_2O+K_2O and CaO (wt.%) (Peacock Diagram; see Peacock, 1931) for Mesozoic and early Tertiary granitic plutons from south-central Arizona study areas, based on data listed in Table 5.1. Open circles indicate Jurassic samples; circles with cross - Cretaceous samples; solid circles - early Tertiary two-mica granites.

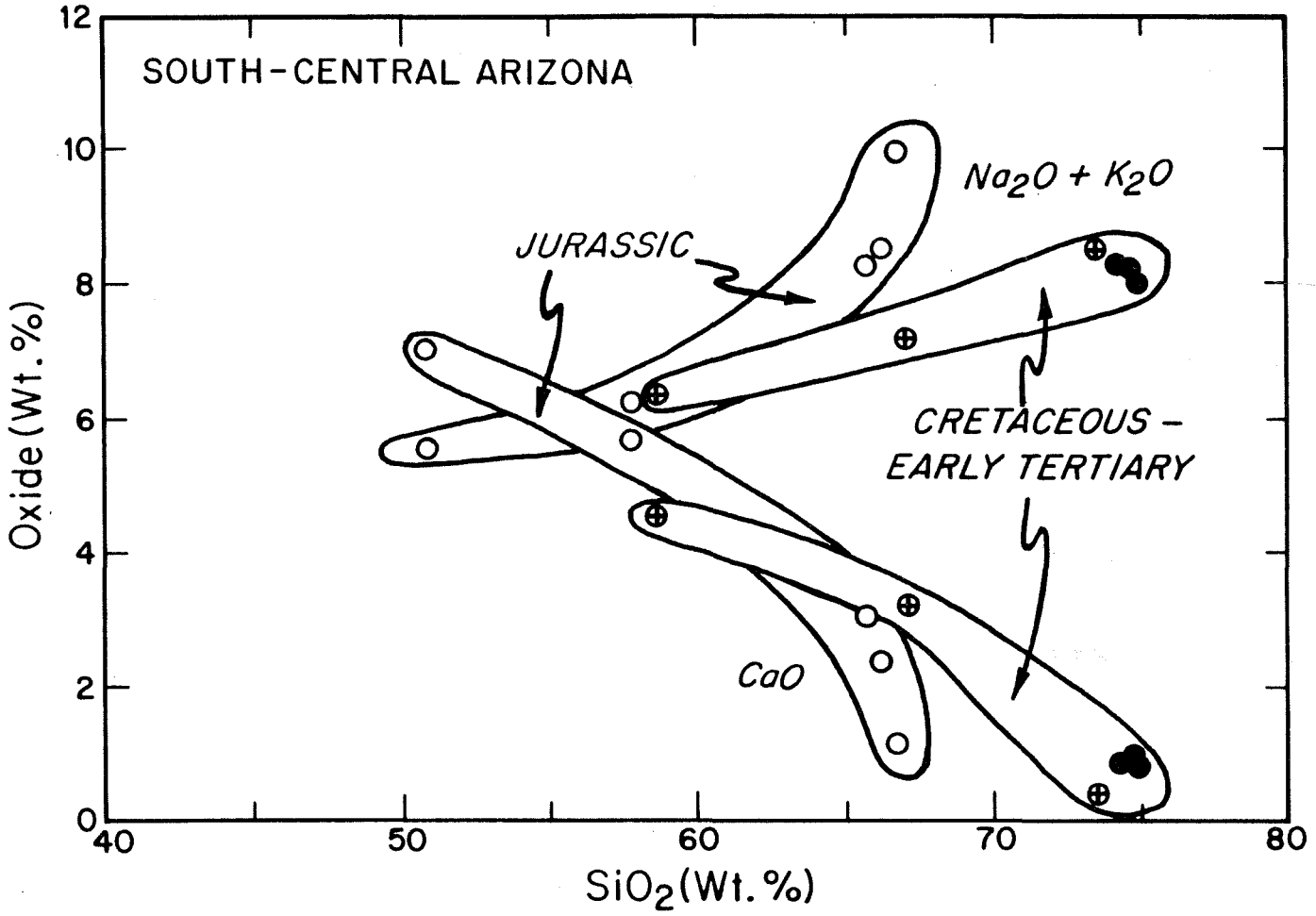
SOUTH-CENTRAL ARIZONA
$Na_2O + K_2O$
JURASSIC
CRETACEOUS – EARLY TERTIARY
CaO
Oxide (Wt.%)
SiO_2 (Wt.%)
0
2
4
6
8
10
12
40
50
60
70
80

vely higher K_2O contents correlating with deeper zones of magma generation. It seems unlikely, however, that "depth to a Benioff Zone" would be sufficiently constant over the long period of magmatism from the Jurassic to the Tertiary to produce the consistent major-element patterns observed in plutons generated beneath the eastern metamorphic belt as compared with those farther to the west. It is more likely that variations in the major-element geochemistry of the source regions are responsible for the geographic variations in the alkali-lime index of the SW USA Cordilleran batholiths. Cordillera-wide lateral variations in the bulk composition of source-region "A" in Figure 5.6 could account for the differences in alkali-lime index for the batholiths (see Chapters 9 and 10).

According to the Chappell-White classification scheme, plutons derived from pelitic metasedimentary sources (S-type) have mole ratios: $Al/(Na + K + Ca/2) > 1.1$ and $Fe^{3+}/(Fe^{3+} + Fe^{2+}) < 0.2$. Also, the S-types generally do not contain hornblende, and they often have abundant biotite and (or) muscovite as primary phases. Plutons derived from igneous-type (I-type) sources often do have hornblende as a primary phase, and are metaluminous and have $Fe^{3+}/(Fe^{3+} + Fe^{2+}) > 0.2$.

Major-element trends combined with $\delta^{18}O$ values provide a powerful tool for source discrimination. O'Neil and Chappell (1977) and O'Neil et al. (1977) found that, in eastern Australian Paleozoic plutons, the I-type plutons (as classified with major-element data) have $\delta^{18}O < 10.0$ per mil, and the S-type plutons have $\delta^{18}O > 10.0$ per mil. The discussion in Chapter 3 showed that primary $\delta^{18}O$ values in plutons typically should reflect source compositions to within about 0.5 to 1.0 per mil. Therefore, a fairly good characterization of sources is possible from a consi-

deration of the geochemical classification together with isotopic constraints.

Figure 5.8 is a plot of the variations in Fe_2O_3 and FeO for the south-central Arizona plutons. Also shown for comparison are the values that the Australian I- and S-type plutons display. The Jurassic suite from Arizona contains relatively high amounts of both ferric and ferrous iron whereas the Cretaceous suite generally has lower iron contents. The Jurassic samples that plot with $Fe_2O_3 > 4.0$ wt. % also have anomalously high iron contents relative to most average granitoids (Nockolds and Allen, 1953). The southern Arizona samples overlap the I-type field, but plot with distinctly higher ferric iron values than do typical S-type plutons. Note also that the two-mica granites from Arizona are extremely deficient in FeO compared to the Australian S-type plutons. In fact, Chappell and White (1974) point out that neither the simple presence of muscovite, nor the existence of peraluminous characteristics, are sufficient to indicate an S-type origin in the case of such leucocratic granitic rocks. This is borne out in the Arizona samples, where the low $\delta^{18}O$ values of the two-mica granites (< +9) clearly indicate that these magmas were <u>not</u> directly derived from a pelitic source rock.

Graphs of whole-rock $\delta^{18}O$ against mole per cent Fe^{3+} (Fig. 5.9), and against the ratio of alumina to combined alkalies and calcium (Fig. 5.10), are both crucial to the I-type and S-type classification scheme. Except for one sample, the ferric/total iron ratios for both the Cretaceous and the Jurassic suites in Arizona are narrowly bracketed between 0.6 and 0.8 for the entire $\delta^{18}O$ range between +6.7 and +9.2 per mil. There is no overlap whatsoever with the Australian S-type field, both because $\delta^{18}O$ is less than +10.0 per mil for all of the Arizona samples,

Figure 5.8 Plot of FeO (wt.%) versus Fe_2O_3 (wt.%) for granitic plutons from south-central Arizona study areas, based on data listed in Table 5.1. Open circles indicate Jurassic samples; circles with cross - Cretaceous samples; solid circles - early Tertiary two-mica granites. Fields labeled "S.E. Australian I- and S-type" indicate the generalized data fields for plutons studied by Hine et al. (1978) in the Lachlan Fold Belt of southeastern Australia.

Figure 5.9 Plot of whole-rock $\delta^{18}O$ versus the mole ratio of Fe^{3+} to total Fe for granitic plutons from south-central Arizona study areas, based on data listed in Table 5.1. Open circles indicate Jurassic samples; circles with cross - Cretaceous samples; solid circles - early Tertiary two-mica granites. Note that sample PUP14 (GCS001 in Table 1, appendix) has "corrected" whole-rock $\delta^{18}O$ = +8.2 per mil based on assumed +1.0 per mil fractionation with quartz $\delta^{18}O$ of +9.2. In this case, we use +1.0 instead of +1.2 per mil for the correction because this two-mica granite is leucocratic, and thus would have a smaller equilibrium fractionation factor than a granite containing abundant mafic minerals such as biotite or hornblende. The generalized data field for Australian I-type plutons is shown for comparison (data from McCullough and Chappell, 1982 and Chappell, 1984).

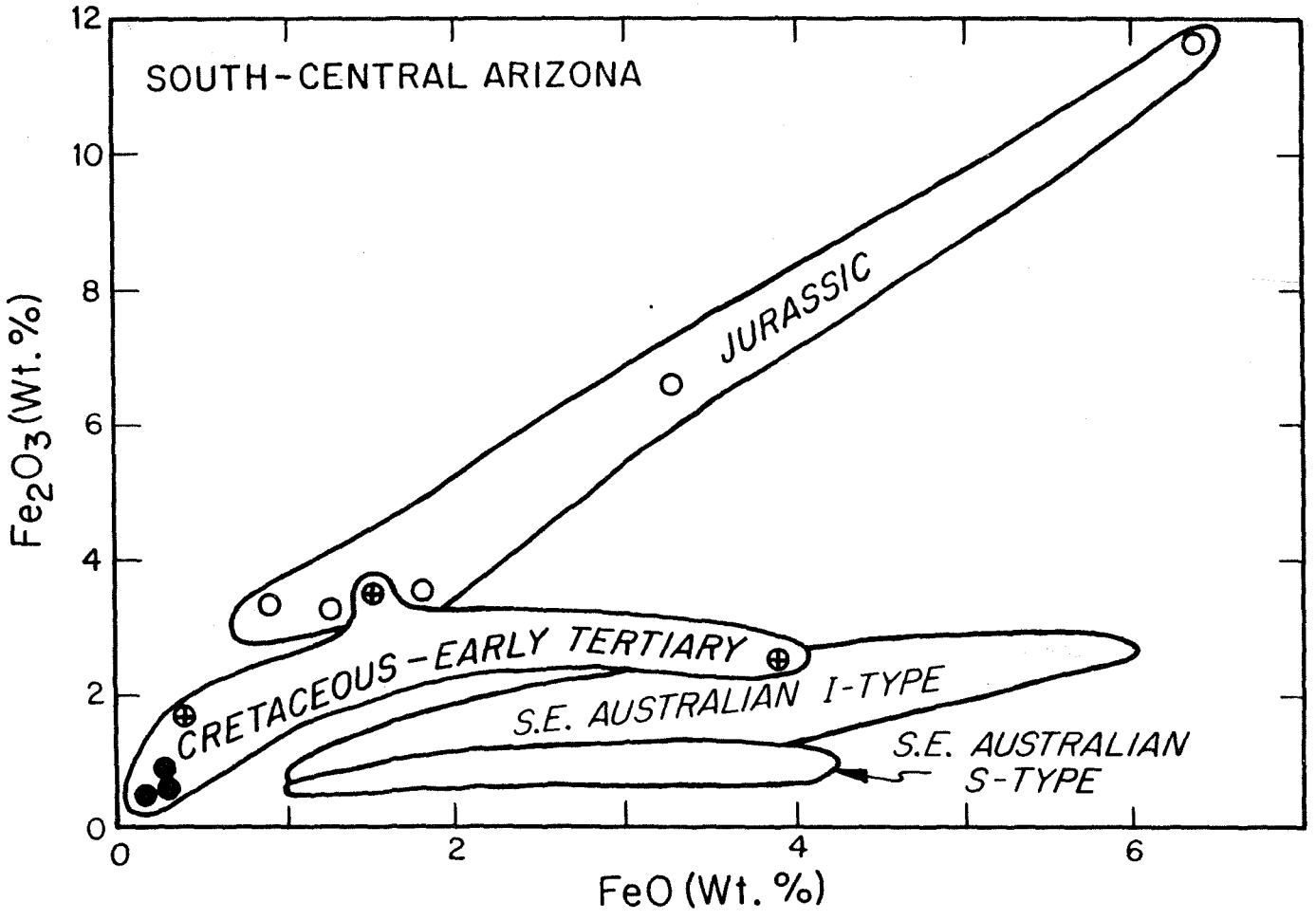
SOUTH-CENTRAL ARIZONA
JURASSIC
CRETACEOUS-EARLY TERTIARY
S.E. AUSTRALIAN I-TYPE
S.E. AUSTRALIAN S-TYPE
Fe2O3 (Wt. %)
FeO (Wt. %)
0
2
4
6
8
10
12

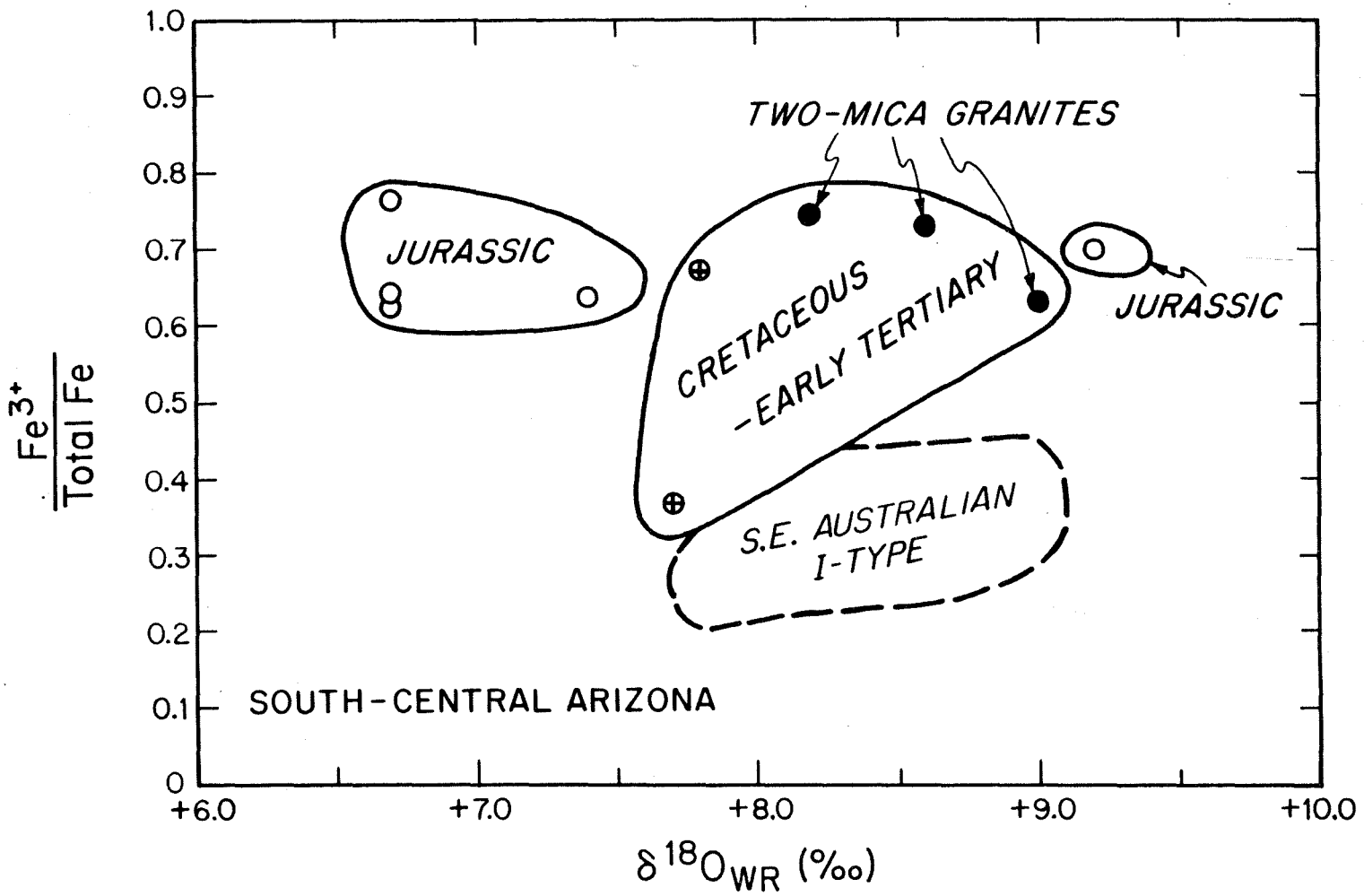
TWO-MICA GRANITES
JURASSIC
CRETACEOUS
-EARLY TERTIARY
JURASSIC
S.E. AUSTRALIAN
I-TYPE
SOUTH-CENTRAL ARIZONA
1.0
0.9
0.8
0.7
0.6
0.5
0.4
0.3
0.2
0.1
0
+6.0
+7.0
+8.0
+9.0
+10.0
$\frac{Fe^{3+}}{Total\ Fe}$
$\delta^{18}O_{WR}$ (‰)

and because all of the Arizona samples have much higher ferric iron contents than the typical Australian S-type plutons. Although the $\delta^{18}O$ values of the Arizona plutons are identical to those of the Australian I-types, the latter are readily distinguished from the Arizona samples by their less-oxidized characteristics (Fig. 5.9).

The Jurassic samples are metaluminous with $Al/(Na + K + Ca/2) < 1.05$ throughout the $\delta^{18}O$ range, and overlap the I-type field on Figure 5.10. The two latest Cretaceous samples also display these characteristics. The early Tertiary "two-mica" granites, however, show peraluminous values (> 1.05, and as high as 1.2) similar to the Australian S-types. Thus, on a plot like Figure 5.10 these Arizona samples can only be distinguished from the S-types by their much lower $\delta^{18}O$ values.

Figure 5.11 is a plot of the variation in SiO_2 content versus $\delta^{18}O$ for the Arizona samples. SiO_2 ranges from around 50 weight percent to as high as nearly 75 weight percent, but the Jurassic samples have distinctly lower SiO_2. With the exception of a single high-^{18}O sample, the Jurassic plutons display a variation of only 0.8 per mil in $\delta^{18}O$, even though they cover a very wide range in SiO_2 from 50 to 67 weight percent.

The latest Cretaceous and early Tertiary samples shown on Figure 5.11 also display a relatively narrow range of only 1.3 per mil between 58 and 75 percent silica, but this range would go up to about 2.5 per mil if we include samples not analyzed for SiO_2 (Table 1 in the appendix). It is evident from the discussion in Chapter 3 that the 0.8 per mil variation in the Jurassic samples could be due to differentiation, but the variations in the younger plutons cannot be, because of the large spread in $\delta^{18}O$. In addition, the age difference between the ~67 Ma old

Figure 5.10 Plot of whole-rock $\delta^{18}O$ versus the mole ratio of Al_2O_3 to Na_2O+K_2O+CaO for granitic plutons from south-central Arizona study areas, based on data listed in Table 5.1. Open circles indicate Jurassic samples, circles with cross - Cretaceous; solid circles - early Tertiary two-mica granites. The $\delta^{18}O$ value for PUP14 has been corrected to +8.2 (see Figure 5.9 caption for explanation). Generalized data field for Australian I-type plutons shown for comparison (data from McCullough and Chappell, 1982; Chappell, 1984).

Figure 5.11 Plot of whole-rock $\delta^{18}O$ versus SiO_2 (wt.%) for granitic plutons from south-central Arizona study areas, based on data listed in Table 5.1. Open circles indicate Jurassic samples; circles with cross - Cretaceous samples; solid circles - early Tertiary two-mica granites. Sample PUP14 has corrected whole-rock $\delta^{18}O$ value as explained for Figure 5.9. Generalized data field for Australian I-type plutons shown for comparison (data from McCullough and Chappell, 1982; Chappell, 1984).

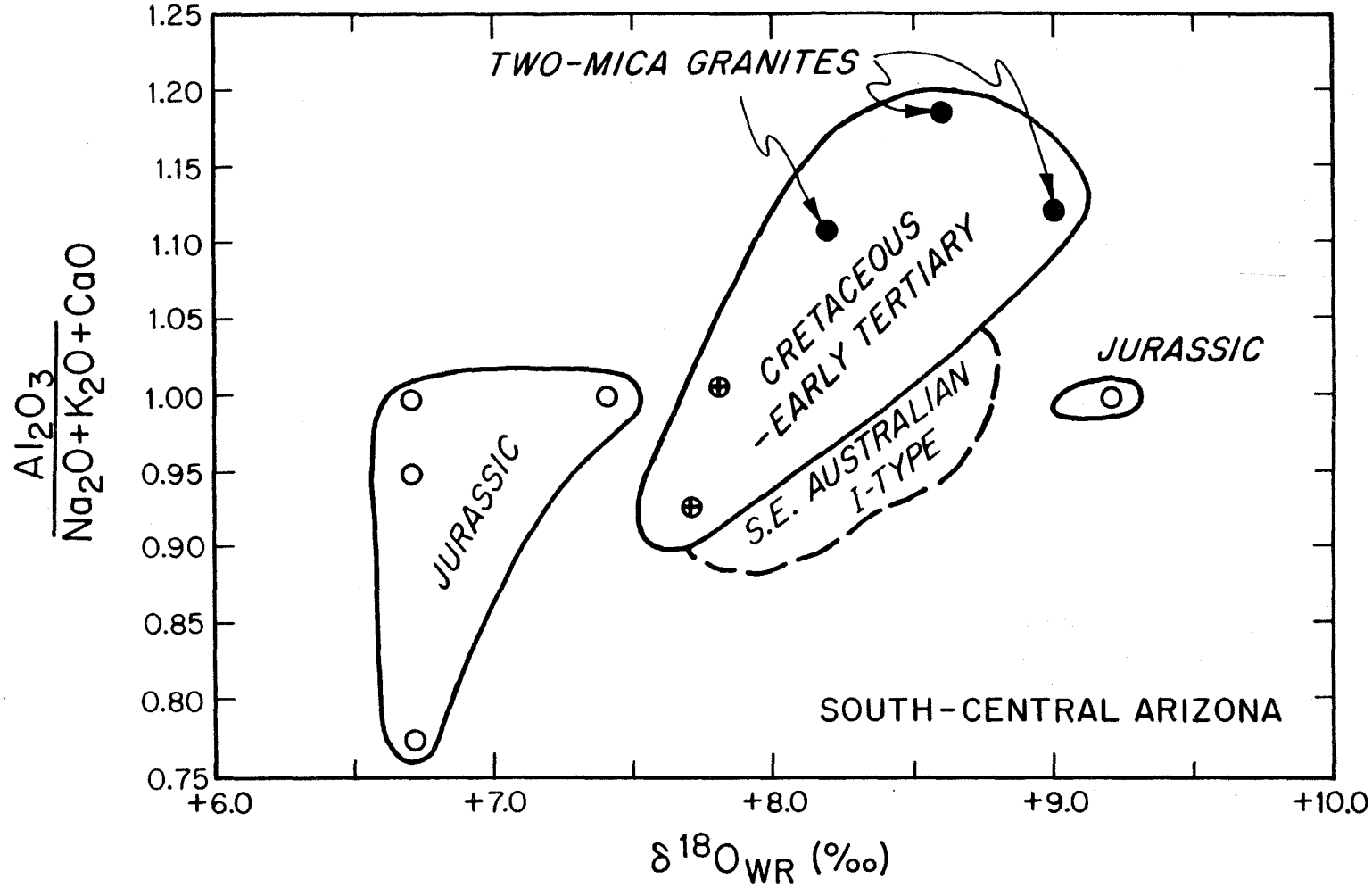
TWO-MICA GRANITES
CRETACEOUS -EARLY TERTIARY
S.E. AUSTRALIAN I-TYPE
JURASSIC
JURASSIC
SOUTH-CENTRAL ARIZONA
1.25
1.20
1.15
1.10
1.05
1.00
0.95
0.90
0.85
0.80
0.75
+6.0
+7.0
+8.0
+9.0
+10.0
$\frac{Al_2O_3}{Na_2O+K_2O+CaO}$
$\delta^{18}O_{WR}$ (‰)

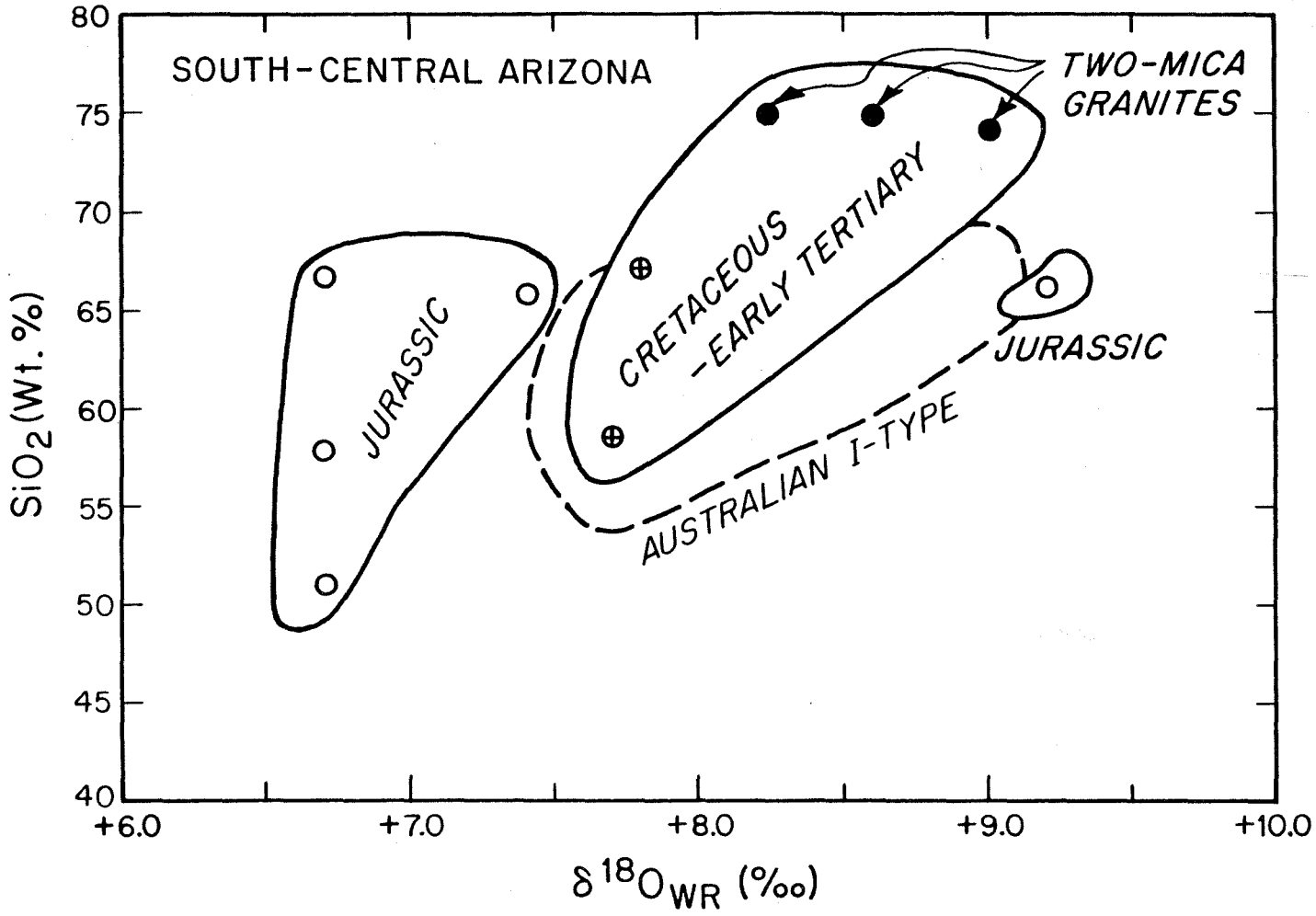
SOUTH-CENTRAL ARIZONA
TWO-MICA GRANITES
CRETACEOUS -EARLY TERTIARY
JURASSIC
JURASSIC
AUSTRALIAN I-TYPE
80
75
70
65
60
55
50
45
40
+6.0
+7.0
+8.0
+9.0
+10.0
SiO2 (Wt. %)
δ 18OWR (‰)

plutons and the ~58 Ma old plutons indirectly argues against differentiation as the scheme to account for the slight increase in $\delta^{18}O$ with increasing SiO_2 content.

Summing up the relationships discussed in this chapter and particularly in Figures 5.6 to 5.11, the suites of Phanerozoic plutons from southern Arizona and from Australia have distinct geochemical and oxygen isotopic signatures. There is no evidence whatsoever for a pelitic, S-type source in southern Arizona. Most of the plutons are alkali-calcic and metaluminous, except for the two-mica granites. The peraluminous two-mica granites from Arizona characteristically have a narrow range of $\delta^{18}O$ from +8.2 to +9.0 per mil, distinctly lower than <u>any</u> of the S-type granites from Australia. The Arizona two-mica granites also all have very high SiO_2 contents (74 to 75 wt. %) and high ratios of ferric to ferrous iron (typically between 0.6 and 0.8) compared to the Australian S-type plutons. The source rocks in Arizona also do not have typical Australian I-type characteristics, even though they are more similar overall to the Australian I-type plutons than to the S-type plutons. For example, the Arizona plutons are mostly more depleted in ^{18}O and more oxidized than the typical I-type plutons in Australia. The Cretaceous suite in Arizona appears to be derived from a <u>slightly</u> more ^{18}O-rich (and slightly less oxidized?) source than the Jurassic suite. The Jurassic suite also is slightly more alkali-rich at a given SiO_2 content (Figure 5.7), but otherwise there are no major geochemical differences between the two plutonic suites.

The early Tertiary two-mica granites, which are intimately associated with the tectonic and metamorphic features of the eastern metamorphic belt, have relatively low $\delta^{18}O$ values of +8 to +9 compared to other musc-

ovite-bearing granites throughout the world. Except for the remote possibility that a pelitic precursor material might have been drastically lowered in ^{18}O by fluid-rock interactions during hydrothermal metamorphism (e.g., involving meteoric waters), it is clear that the source material for the Arizona two-mica granites was not S-type. With this in mind, they are here tentatively classified as related to I-type sources. Based on their high SiO_2 contents and leucocratic characteristics, they are clearly highly fractionated partial melts or late-stage differentiates, and it is this process that appears to be responsible for their peraluminous characteristics. The nature of the source regions for these and other plutons in the Cordillera of the southwestern United States will be discussed further in Chapter 10.

CHAPTER 6. $^{18}O/^{16}O$ COMPOSITIONS OF MESOZOIC AND EARLY TERTIARY PLUTONS IN THE CENTRAL AND EASTERN TRANSVERSE RANGES, CALIFORNIA

6.1 General Statement

The purpose of this chapter is to discuss the $\delta^{18}O$ data from plutons in the Central and Eastern Transverse Ranges of Southern California within the framework of the general geology and geochronology of this region. The $\delta^{18}O$ data are given in Table 1 in the appendix and the major-element geochemistry of granitic plutons in the Transverse Ranges is listed in the appendix in Tables 3a and 3b. In contrast to the south-central Arizona samples discussed above, the major-element data are from different samples than those that were analyzed directly for $\delta^{18}O$.

We note here that the $\delta^{18}O$ data, geology, and geochemistry of Mesozoic plutons lying between the Transverse Ranges and the southern Arizona localities are discussed in Chapter 7, using a similar format to the present chapter. Chapter 8 will then take up a detailed discussion of the geology and geochemistry of the magmatic source regions of all these plutons in both the Central and Eastern Transverse Ranges and in the Mojave Desert region of southeastern California. The new data from these areas will then be integrated into a discussion of the $^{18}O/^{16}O$ patterns previously established for the Peninsular Ranges and Sierra Nevada batholiths.

6.2 Regional Geologic Setting

Figure 6.1 is an index map of the Cordillera of the southwestern United States showing the three sampling regions within the Central and Eastern Transverse Ranges: 1) the San Gabriel Mountains (SGM) area, 2)

Figure 6.1 Map of the southwestern United States and northwestern Mexico showing the location of sampling areas (shown by diagonal shading within heavy boundaries) in the southern Basin and Range (SBR) of southeastern California, and in the Transverse Ranges of southern California. In the Transverse Ranges, these areas are: (1) the San Gabriel Mountains (SGM) Area; (2) the San Bernardino Mountains (SBM) Area and (3) the Little San Bernardino Mountains (LSB) Area. In southeastern California (SECA) they are: (4) the Rodman-Ord Mountains (ROM) Area and (5) the Southeastern Mojave Region (SMR). Also shown are outlines of Mesozoic and early Tertiary batholithic rocks of the southwestern United States Cordillera.

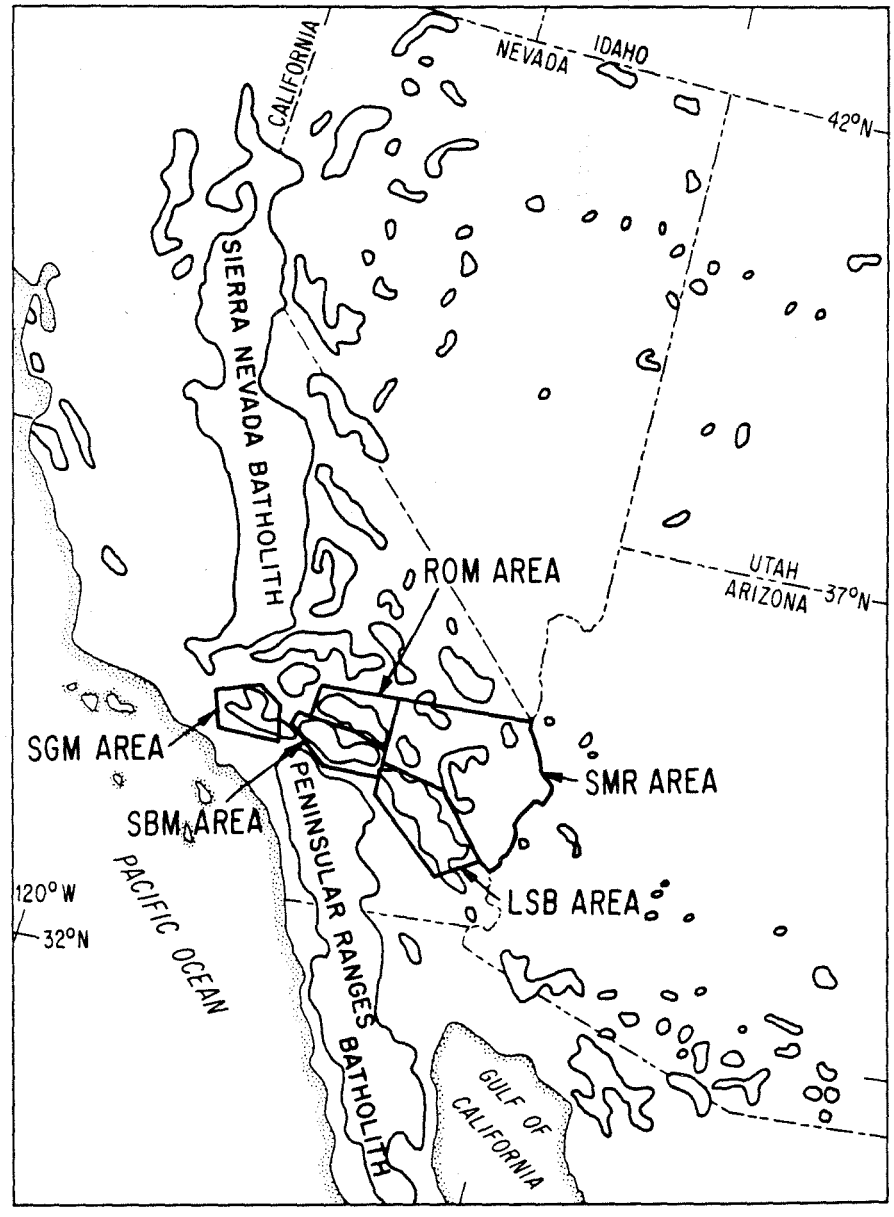
CALIFORNIA
NEVADA
IDAHO
42°N
SIERRA NEVADA BATHOLITH
ROM AREA
UTAH
ARIZONA
37°N
SGM AREA
SBM AREA
SMR AREA
LSB AREA
PENINSULAR RANGES BATHOLITH
120°W
32°N
PACIFIC OCEAN
GULF OF CALIFORNIA

the San Bernardino Mountains (SBM) area, and 3) the Little San Bernardino Mountains (LSB) area. Figure 6.2 is a generalized geologic map of the study area showing the distribution of major pre-mid-Tertiary rock units, as well as the major Mesozoic and Cenozoic structural boundaries.

This region was the site of late Precambrian to Cambrian miogeoclinal sedimentation, which evolved to cratonic sedimentation during the Paleozoic (Burchfiel and Davis, 1981a). The craton is comprised of 1.7 to 1.8 Ga metasedimentary and meta-igneous rocks with locally exposed ~1.2 Ga intrusives. Portions of the older metamorphosed terrane may be tectonically exotic to the North American craton (Powell, 1981; Silver and Anderson, 1974; Silver, 1971), although recent discussions by Powell (1986a; 1986b) indicate continuity between the North American craton and Precambrian units in the western part of the area.

Mesozoic plutons are widespread in the LSB and SBM areas, and they also make up a large part of the SGM area. These plutons are part of a continental magmatic arc that intrudes both the craton and late Precambrian to Paleozoic sedimentary rocks. Throughout the three areas, Mesozoic plutonism is dominated by voluminous late Cretaceous tonalite, granodiorite, and quartz monzonite. Epizonal Jurassic granodiorite and quartz monzonite crop out in the eastern part of the LSB area, and they also may be present as isolated pendants in the north-central part of the SBM area. No Jurassic plutons are presently known in the SGM area. Permo-Triassic monzonites and syenites represent the earliest pulse of Mesozoic plutonism (Ehlig, 1981). The largest plutons of this age are located in the SGM and SBM areas, and smaller isolated outcrops are found in the LSB area.

Figure 6.2 Geologic map of the Central and Eastern Transverse Ranges in Southern California, showing major Cenozoic faults and pre-mid-Tertiary crystalline basement rocks (geology modified after Ehlig, 1982; Powell, 1981; Jennings and Strand, 1969; Silver, 1971; Bortugno and Spittler, 1986). Major Cenozoic faults are: (1) the San Andreas Fault, which extends through the entire region; (2) the San Gabriel Fault (SGF) in the SGM area; (3) the Pinto Mountain Fault, separating the SBM and LSB areas; and (4) thrust faults separating upper-plate crystalline basement from lower-plate Pelona-Orocopia Schist basement in the SGM and LSB areas. The pre-mid-Tertiary rock units are: (1) Tv - mid-Tertiary volcanic rocks; (2) Mesozoic batholithic rocks (stippled pattern on margins of map unit); (3) Jurassic (?) Pelona and Orocopia Schist (diagonal line pattern throughout unit); (4) Paleozoic metasediments (solid black; in the San Gabriel Mountains this unit is of uncertain age but correlated as Paleozoic(?), see text); (5) Precambrian crystalline basement (diagonal line shading along margins of map unit); and (6) gn - gneissic rocks of uncertain age (see text). Also shown is the northeastern portion of the Cretaceous Peninsular Ranges Batholith (south of the San Andreas Fault).

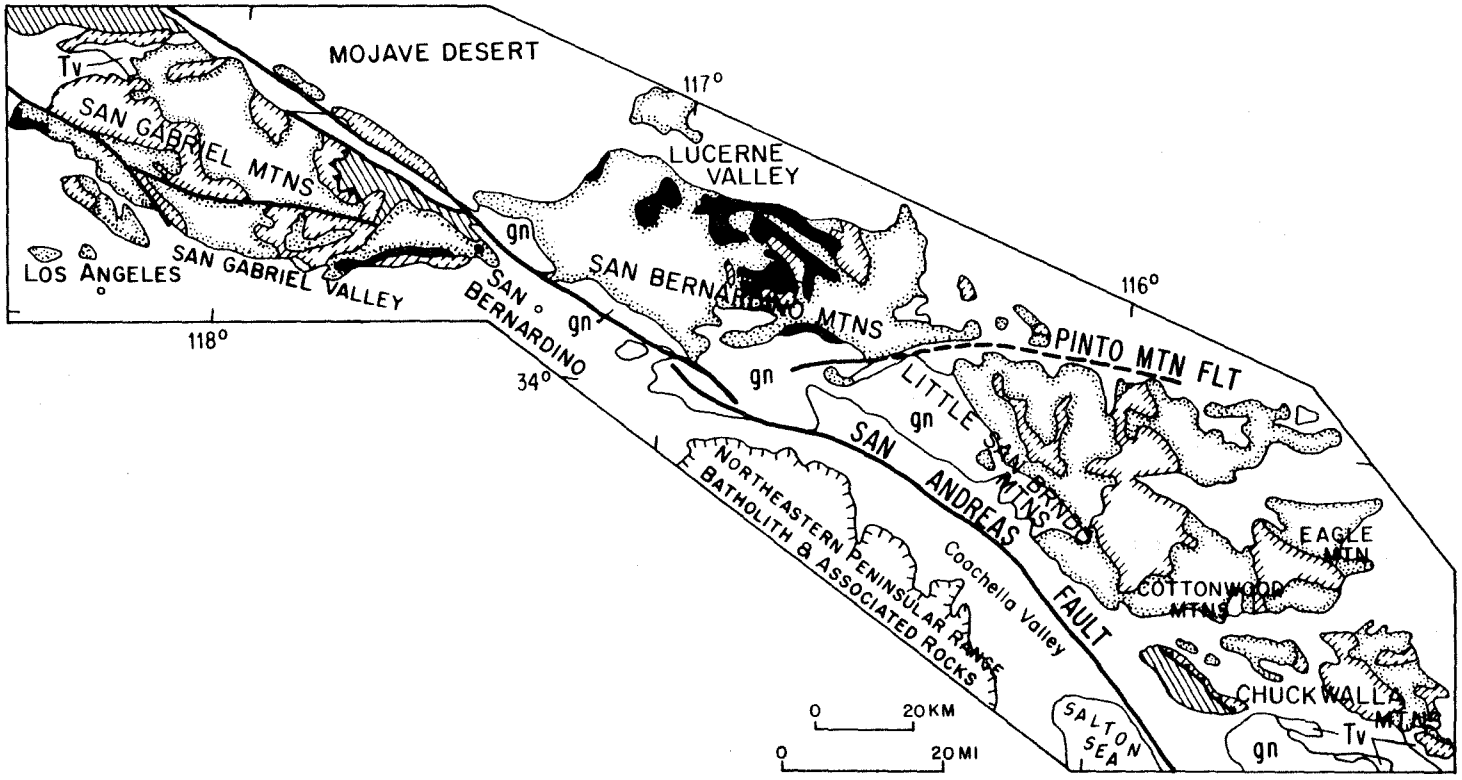
MOJAVE DESERT
Tv
SAN GABRIEL MTNS
LOS ANGELES
SAN GABRIEL VALLEY
118°
SAN BERNARDINO
34°
117°
LUCERNE VALLEY
gn
SAN BERNARDINO MTNS
116°
PINTO MTN FLT
LITTLE SAN BERNDS MTNS
SAN ANDREAS FAULT
NORTHEASTERN PENINSULAR RANGE BATHOLITH & ASSOCIATED ROCKS
Coachella Valley
EAGLE MTN
COTTONWOOD MTNS
CHUCKWALLA MTNS
SALTON SEA
0 20KM
0 20MI

The major structural features of the area are Mesozoic and Cenozoic in age. The Mesozoic features comprise the proposed large-scale, mid-Jurassic, left-lateral shear zone (Mojave-Sonora megashear of Silver and Anderson, 1974), as well as episodes of late Cretaceous to early Tertiary mylonitization and thrusting that occurred during the waning stages of Mesozoic plutonism (Silver, 1982, 1983; Howard, 1986; Hamilton, 1986).

The location of the proposed megashear is not well established, but it must trend through the area, if it follows the northwesterly trend proposed for northern Sonora and southern Arizona (see Dickinson, 1981a). Although its location is controversial, it may juxtapose North American cratonic rocks in the SBM area with exotic basement in the LSB and SGM areas, and it may have separated the Caborca terrane, now in northern Sonora, from the Big Bear Group in the SBM area (Powell, 1981; Cameron, 1982). In that case, it would trend west of Big Bear Lake in the SBM area, although Silver and Anderson (1974) originally proposed that it ran through the eastern Mojave region towards Owens Valley.

Most of the study area was apparently the upper plate of an immense zone of mobility in which Mesozoic batholithic rocks and Precambrian crystalline basement were thrust over the Pelona and Orocopia schists at approximately 60 Ma (Silver, 1982, 1983; Ehlig, 1981). This is in contrast to the southeastern California area (discussed in Chapter 7), which contains abundant mylonitized zones in the upper portions of deep-seated late Cretaceous plutons and which may represent lower-plate rocks that have been internally deformed throughout a very wide area (Howard et al., 1982; Miller et al., 1982).

The lower plate rocks in the Central Transverse Ranges appear as windows of schistose rocks locally exposed through the crystalline base-

ment complexes (Ehlig, 1981). Lower plate rocks have not been identified in the Eastern Transverse Ranges. Late-Cretaceous plutons do not intrude the lower plate schists in the study area. It is interesting to note that, if the study area is indeed a large packet of thrust sheets that are displaced westward, then the original megashear trend of Silver and Anderson (1974) is restored, after the sheets are moved backward to the east.

Much later in time, late Cenozoic right-lateral strike-slip movement along the San Andreas Fault resulted in large-scale displacement of the SGM block relative to the SBM-LSB combined crystalline basement blocks. Prior to the onset of San Andreas movement, the SGM area was adjacent to the southeastern portion of the LSB area (Powell, 1981). Plio-Pleistocene high angle faults and thrust faults, as well as late Cenozoic strike-slip faults of both right- and left-lateral slip, have caused relatively smaller-scale displacements within these crystalline basement complexes.

6.3 San Gabriel Mountains Area (SGM)

6.3.1 Geology and Geochronology

The San Gabriel Mountains area is located in the central Transverse Ranges, and is part of a zone of uplifted crystalline basement along the southwest side of the San Andreas Fault Zone. Figure 6.3 is a geologic map of the SGM area, showing the locations and $\delta^{18}O$ values of the samples listed in Table 1 in the appendix. Uplift began a few million years ago, and is still active. This deformation is related to the convergence of the North American and Pacific plates along the San Andreas Fault (Weldon and Humphreys, 1986).

Ehlig (1981) has reviewed the general geology of the area, and geologic maps have been compiled by Bortugno and Spittler (1986), and

Figure 6.3 Geologic map, $^{18}O/^{16}O$ sample localities and whole-rock $\delta^{18}O$ values for the San Gabriel Mountains (SGM) area. Sample localities are indicated by solid circles, with the whole-rock $\delta^{18}O$ value shown alongside (a complete listing of the $^{18}O/^{16}O$ data is given in Table 1, Appendix). Geology modified after Ehlig (1981); Silver (1971); Jennings and Strand (1969); and Bortugno and Spittler (1986): (1) Tv - mid-Tertiary volcanic rocks; (2) mid-Tertiary intrusive stocks (double hash-mark pattern along margins; located in extreme eastern SGM); (3) late-Cretaceous granitic plutons (stippled pattern on inside margin of map unit); (4) Jurassic(?) Pelona Schist (diagonal line pattern across entire map unit); (5) Triassic Lowe "Granodiorite" (small circles along inside margin of map unit); (6) Paleozoic(?) metasediments (solid black; this includes mylonitized gneissic rocks in the eastern SGM); (7) Precambrian crystalline basement (diagonal line shading along inside margin of map unit); (8) Zone of mylonitization east of the San Antonio fault is shown by "wavy" lines along inside margin of map unit. Thrust fault symbol indicates boundary between upper-plate crystalline basement and lower-plate Pelona Schist. Thick solid lines indicate Cenozoic strike-slip faults discussed in text.

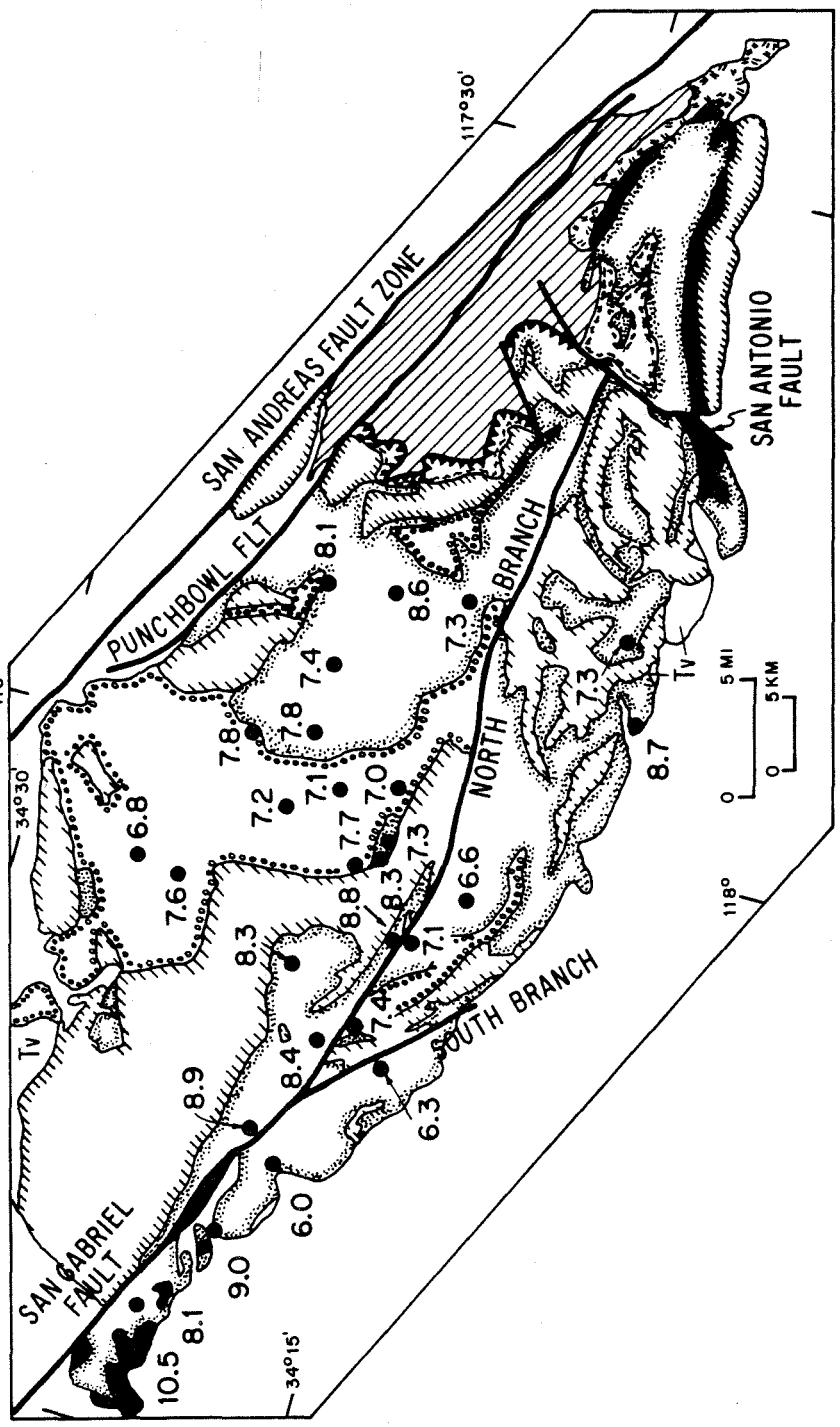
SAN ANDREAS FAULT ZONE
PUNCHBOWL FLT
NORTH BRANCH
SOUTH BRANCH
SAN ANTONIO FAULT
SAN GABRIEL FAULT
Tv
Tv
118°
117°30'
34°30'
34°15'
5 MI
0
5KM
0
8.1
8.6
7.3
7.4
7.8
7.8
7.1
7.0
7.2
7.7
6.8
7.6
8.8
8.3
7.3
6.6
8.3
7.1
7.4
8.4
8.9
6.3
6.0
9.0
8.1
10.5
7.3
8.7

Jennings and Strand (1969). The basement terrane of the main mass of the SGM area was adjacent to the Chocolate and Orocopia Mountains prior to late Cenozoic right-lateral offset by the San Andreas Fault. This reconstruction is accomplished by matching Triassic plutons and Tertiary sedimentary basins on different sides of the fault, which results in approximately 240 km of slip along the San Andreas Fault, and another 60 km of slip along the San Gabriel Fault (Ehlig, 1981; L.T. Silver, pers. comm.).

The crystalline basement within the range is divided into two plates by the Vincent thrust fault (Fig. 6.3). Lower plate rocks are mainly thin-bedded, white mica-quartz-albite schist (Pelona Schist) originally derived from a protolith of arkosic graywacke, siltstone, and shale (Ehlig, 1981). Greenschist associated with thin beds of chert is common in the upper part of the sequence. The depositional age of the Pelona Schist is unknown, but metamorphism has been dated at 58.5 to 59.0 Ma by Rb-Sr mineral isochrons obtained from schist in the Vincent thrust (Conrad and Davis, 1977; Ehlig, 1981). Metamorphism must have been syntectonic because post-thrust whole-rock K-Ar cooling ages have been measured at around 52.5 Ma (Ehlig et al., 1975).

The upper plate contains the SGM crystalline basement complex. A small portion of the range lies to the northeastern side of the San Andreas Fault, and consists of Mesozoic granitic plutons, migmatite, gneiss, marble, and calc-silicate rocks. These rocks have an uncertain relationship to the SGM basement complex because of the Cenozoic displacements on the San Andreas Fault, and thus were not sampled. All of the $\delta^{18}O$ data in the SGM area were collected on samples from upper plate plutons. The basement complex in the SGM proper is divided into fault blocks by the Punchbowl (PB) fault, by the north and south branches of the San Gabriel (SG) fault system, and by the San Antonio (SA) fault.

The main mass of basement crops out between the PB fault and the north branch SG fault, and consists of a Precambrian gneiss-amphibolite-granite terrane intruded by a Precambrian anorthosite-syenite-gabbro complex, all intruded by early Triassic quartz diorite to albite granite and late Cretaceous granitic rocks. The north branch of the SG fault has offset the southern portion of the main mass by 22 km of right slip.

Deformation and metamorphism affected each rock group in the main mass except the latest granites. East of the San Antonio fault, a thick sequence of Paleozoic(?) metasediments occurs with gneiss, migmatite, and late Cretaceous granitic rocks. South of the south branch of the SG fault, basement rocks consist of gneiss, migmatite and late Cretaceous granitic rocks that contain screens of Paleozoic(?) metasediments.

The Precambrian rocks include layered gneiss, amphibolite, migmatite, and granitic rocks that have undergone upper-amphibolite facies metamorphism and intrusion by an anorthosite complex. Zircon U-Pb ages are as follows: augen gneiss of Soledad Basin, 1670 ± 15 Ma (Silver, 1968); foliated quartz monzonite in the central SGM, 1670 ± 20 Ma (Ehlig, 1981); older layered gneiss, 1715 ± 30 Ma (Silver, 1968); anorthositic complex, 1220 ± 30 Ma (Silver et al., 1963; Silver, 1971). Carter and Silver (1972) interpret the anorthosite complex to be an inverted, cone-shaped stratiform intrusion that differentiated by crystal fractionation to yield anorthositic, gabbroic, and syenitic layered rocks.

No reliable dating exists for the Paleozoic(?) metasediments in the SGM area. Ehlig (1981) has tentatively assigned these metasediments a Paleozoic age because in a gross way they resemble the metamorphosed equivalents of sedimentary rock types found in late Precambrian to Cambrian miogeoclinal sections elsewhere in eastern California (e.g., Burchfiel and Davis, 1981a; Cameron, 1982; Stewart, 1980).

South of the SG fault, the Paleozoic(?) lithologies consist of marble, calc-silicates, quartzite, and aluminous and graphitic schists that occur as lenses included within deformed and metamorphosed gneisses, migmatites, and granitic rocks. In the reconstruction of Ehlig (1981) the southern metasedimentary terrane must be moved eastward along the south branch of the SG fault; it would originally have been located directly south of Mount Wilson. The Paleozoic(?) metasedimentary section east of the SA fault is composed of similar lithologies, although it is much thicker. Both Paleozoic(?) terranes in the SGM area were metamorphosed to upper amphibolite facies, and are intimately associated with migmatization in the vicinity of late Cretaceous granitic plutons.

The oldest samples collected for $^{18}O/^{16}O$ study in the SGM area are from a Triassic pluton that intrudes the Precambrian basement complex. This pluton is laccolithic in shape and relatively leucocratic, being characterized by a low average quartz content (~ 60 to 95%). It is popularly known as the Lowe Granodiorite, but this name is not descriptive of its actual composition. From its base upward, it is composed of hornblende diorite and quartz diorite, grading upward to albite-rich granite and syenite. In the middle of the sequence is a distinctive orthoclase-garnet zone with K-feldspar crystals as large as 10 cm across. The pluton underwent upper amphibolite metamorphism adjacent to the Cretaceous Mount Waterman pluton. Silver (1971) determined a U-Pb zircon age of 220 ± 10 Ma for the Lowe Granodiorite, and Joseph et al. (1978) report Rb-Sr whole-rock age of 208 Ma.

Most of the samples collected from the SGM area are from late Cretaceous granitic plutons. The largest of these Cretaceous bodies is known as the Mount Waterman pluton north of the north branch of the SG fault,

and as the Mount Wilson pluton south of the SG fault. The eastern border of this body against gneiss is gradational and extensively migmatized, but to the west the contact is relatively sharp against Lowe Granodiorite. Granitic rocks with relatively sharp contacts against gneiss and anorthosite crop out west of Mount Waterman and Mount Wilson. Locally, Paleozoic(?) metasediments and older gneiss are migmatized adjacent to younger granite. The late Cretaceous plutons are typically composite in nature, ranging from early hornblende quartz diorite to late, leucocratic biotite-quartz monzonite.

Carter and Silver (1971) dated one of the western bodies (Josephine Mountain pluton) at 80 ± 10 Ma using zircon U-Pb methods. For the same pluton, Evernden and Kistler (1970) obtained a K-Ar age of 65.8 Ma on biotite and 70 Ma on hornblende. These are obviously cooling ages. Miller and Morton (1980) found similar K-Ar age relations on other Cretaceous granitic outcrops throughout the SGM area. In addition, several Miocene granitic porphyries occur in the eastern portion of the SGM area, but these have not been sampled for $^{18}O/^{16}O$ work. They have been dated at 14 to 16 Ma by K-Ar (Miller and Morton, 1977).

6.3.2 $^{18}O/^{16}O$ Data

The range of $\delta^{18}O$ values within the Triassic Lowe Granodiorite is relatively narrow, +6.8 to +7.8 per mil. Ehlig (1981) interpreted this body as a layered intrusion, tilted to the northeast such that its base is exposed along the southwest margin and its roof is exposed along the northeast margin. Thus the progression from west to east, from dioritic rocks at the base to granitic rocks at the top, may represent a differentiation sequence. Figure 6.4 is a somewhat more detailed geological and $^{18}O/^{16}O$ map of the Lowe Granodiorite, based on a pre-faulting reconstruc-

Figure 6.4 Generalized geologic map of the Triassic Lowe "Granodiorite" zoned pluton, showing $^{18}O/^{16}O$ sample localities and $\delta^{18}O$ values, and mineral facies discussed in text (geology and facies taken from review by Ehlig, 1981). Mineralogical facies are: H - Hornblende Zone; K - Orthoclase Zone; G - Garnet Zone (shown with stippled pattern); and B - Biotite Zone. In this pre-faulting reconstruction, 22 km of right-slip displacement (Ehlig, 1981) along the north branch of the San Gabriel Fault (see Figure 6.3) has been removed. The present outcrop and $\delta^{18}O$ distribution is shown on Figure 6.3. A complete listing of the $^{18}O/^{16}O$ data is given in Table 1 (Appendix).

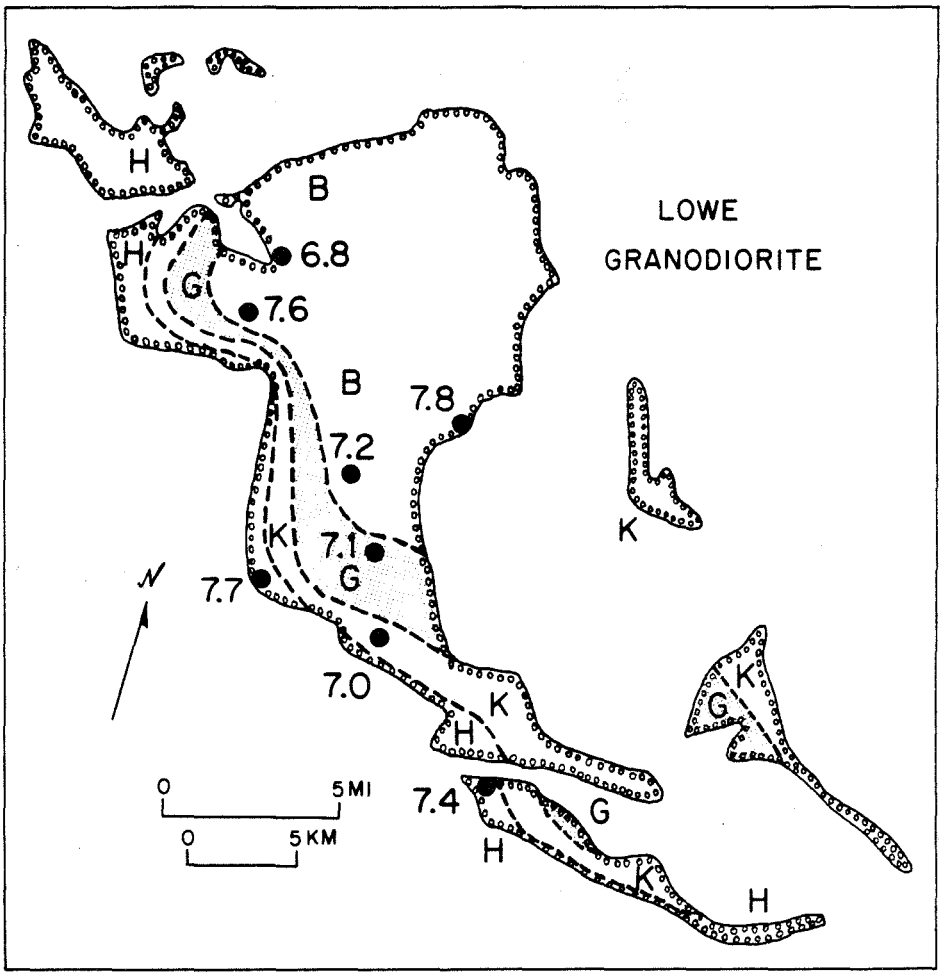
LOWE
GRANODIORITE
H
B
H
G
6.8
7.6
B
7.8
7.2
K
7.1
G
7.7
7.0
K
H
7.4
G
H
K
K
G
K
H
N
0
5MI
0
5KM

tion of the generalized map in Figure 6.3. The entire SGM area is reconstructed in Figure 6.6.

Even though the range of $\delta^{18}O$ in the Lowe Granodiorite is within the limits for a single differentiated magma body that developed as a closed system (see discussion in Chapter 3), the $\delta^{18}O$ variation within the pluton does not exhibit a systematic pattern relative to the sequence of zones mapped by Ehlig (1981). The $\delta^{18}O$ data of Figure 6.4 show a weakly-defined $\delta^{18}O$ minimum in the central part of the body, and this low-^{18}O zone ($\delta^{18}O < 7.3$) cuts across the primary igneous layering. The highest $\delta^{18}O$ values are observed right at the margins of the pluton ($\delta^{18}O > 7.6$). It is concluded here that the minimum $\delta^{18}O$ zone is probably our best indication of the original, primary $\delta^{18}O$ of the Lowe magma, and that there may have been some very limited exchange or modification of the marginal samples by interactions with higher-^{18}O country rocks, analogous to the effects discovered by Turi and Taylor (1971a) in the Peninsular Ranges batholith.

The $\delta^{18}O$ contouring of the SGM Cretaceous plutonic rocks, discussed below, suggests that even though the Lowe Granodiorite is much older, in a geographic sense it fits right in with the $\delta^{18}O$ values of the Cretaceous plutons. There is an ^{18}O-depleted belt that includes the Lowe Granodiorite and trends right through the entire San Gabriel terrane as a unified feature, after allowance is made for the late Cenozoic fault displacements. We must consider the possibility that this zone of lower-^{18}O rocks might be a secondary feature related to hydrothermal alteration, because it appears to be aligned along a zone of Miocene intrusive bodies (Ehlig, 1981). Also, as will be shown in the following discussion of data from the Mojave Desert and the Little San Bernardino Mountains

area, it is clear that ^{18}O-depletion effects of regional scale exist in those areas, and that at least some of these patterns are a result of meteoric-hydrothermal activity at various times from the Jurassic to the mid-Tertiary. However, we do not favor such an explanation for the region-wide, lower-^{18}O zone in the SGM area, because there is no direct evidence for it (see below), and there are no $\delta^{18}O$ values lower than +6, as are generally observed in areas of meteoric-hydrothermal alteration (see Chapter 7).

No quartz $^{18}O/^{16}O$ analyses have been performed, so it is not possible to directly evaluate the extent of possible meteoric-hydrothermal exchange effects that may have produced some of these ^{18}O-depletions. However, note that none of the measured $\delta^{18}O$ values lies outside the plausible range of primary igneous values determined for the Sierra Nevada and Peninsular Ranges batholiths. Also, we do not observe any of the extreme ^{18}O-depletions ($\delta^{18}O < +6$) that are characteristically observed in most terranes affected by meteoric-hydrothermal activity (Taylor, 1977; Criss and Taylor, 1983). In addition, samples from a single, individual pluton typically display fairly uniform and constant $\delta^{18}O$ values, compatible with a primary, igneous origin. Therefore, we tentatively interpret the $\delta^{18}O$ variations in the SGM terrane as primary igneous values, perhaps locally somewhat modified by wall-rock exchange effects or very minor meteoric-hydrothermal activity.

The range of $\delta^{18}O$ values for the SGM Cretaceous plutonic rocks (+10.5 to +6.0) is much larger than that for the Triassic Lowe Granodiorite. Rocks of the Mount Waterman pluton north of the San Gabriel Fault show a range of +8.6 to +7.3, while the rocks of the Mount Wilson facies of this pluton (south of the fault) range between +8.7 and +6.6. Farther

west in the range, the Josephine Mountain pluton is slightly higher in $\delta^{18}O$, +8.9 to +8.3. The plutonic rocks southwest of the south branch of the San Gabriel Fault display the largest variation in $\delta^{18}O$, with values between +10.5 to +6.0; the lowest values in this zone are all within the Mt. Lukens granite (+6.0 to +6.3).

The variation of $\delta^{18}O$ throughout the SGM area is, in general, not related to rock type, although the more mafic, granodioritic phases of the Mount Wilson pluton do have relatively low $\delta^{18}O$ values. The most ^{18}O-rich plutonic sample (+10.5) and the most ^{18}O-depleted sample (+6.0) both come from plutons that are quartz monzonitic in composition. Thus, for plutons lying within a relatively narrow range of silica content (Baird et al., 1979), there is a large primary, magmatic $\delta^{18}O$ variation. As discussed in Chapter 3 and by Taylor (1978), this is indicative of open-system effects or of $\delta^{18}O$ variations in source regions; it cannot be produced by closed-system magmatic differentiation.

Figure 6.5 is a map of whole-rock $\delta^{18}O$ contours for all of the plutons in the San Gabriel Mountains. The map is contoured with each fault-bounded block as a separate entity, and it can be seen that the $\delta^{18}O$ patterns themselves seem to be offset along the faults. For example, immediately south of the north branch of the SG fault are 3 samples with $\delta^{18}O$ = +6.6, +7.1, and +7.4, whereas in the same vicinity just to the north of the fault are 3 samples with $\delta^{18}O$ = +8.4, +8.8, and +8.9. Similarly, in this same area south of the south branch of the SG fault, 2 samples of Mt. Lukens granite have $\delta^{18}O$ = +6.0 and +6.3. Thus, just in this small area where the north and south branches of the SG fault come together (Figure 6.3), there is a +1 per mil $\delta^{18}O$ "step" from the South Block to the Central Block, as well as a +1 to +2 per mil discontinu-

Figure 6.5 Geologic map of the San Gabriel Mountains (SGM) area, showing Mesozoic granitic rocks and whole-rock $\delta^{18}O$ contours within individual fault blocks. Solid circles indicate $^{18}O/^{16}O$ sample localities (see Figure 6.3 and Table 1 in the Appendix). Late Cretaceous plutons have stippled pattern along inside margins of map unit; Triassic Lowe Granodiorite has small circle-pattern along inside margins of map unit. Geology modified after Ehlig (1981); Jennings and Strand (1969); and Bortugno and Spittler (1986).

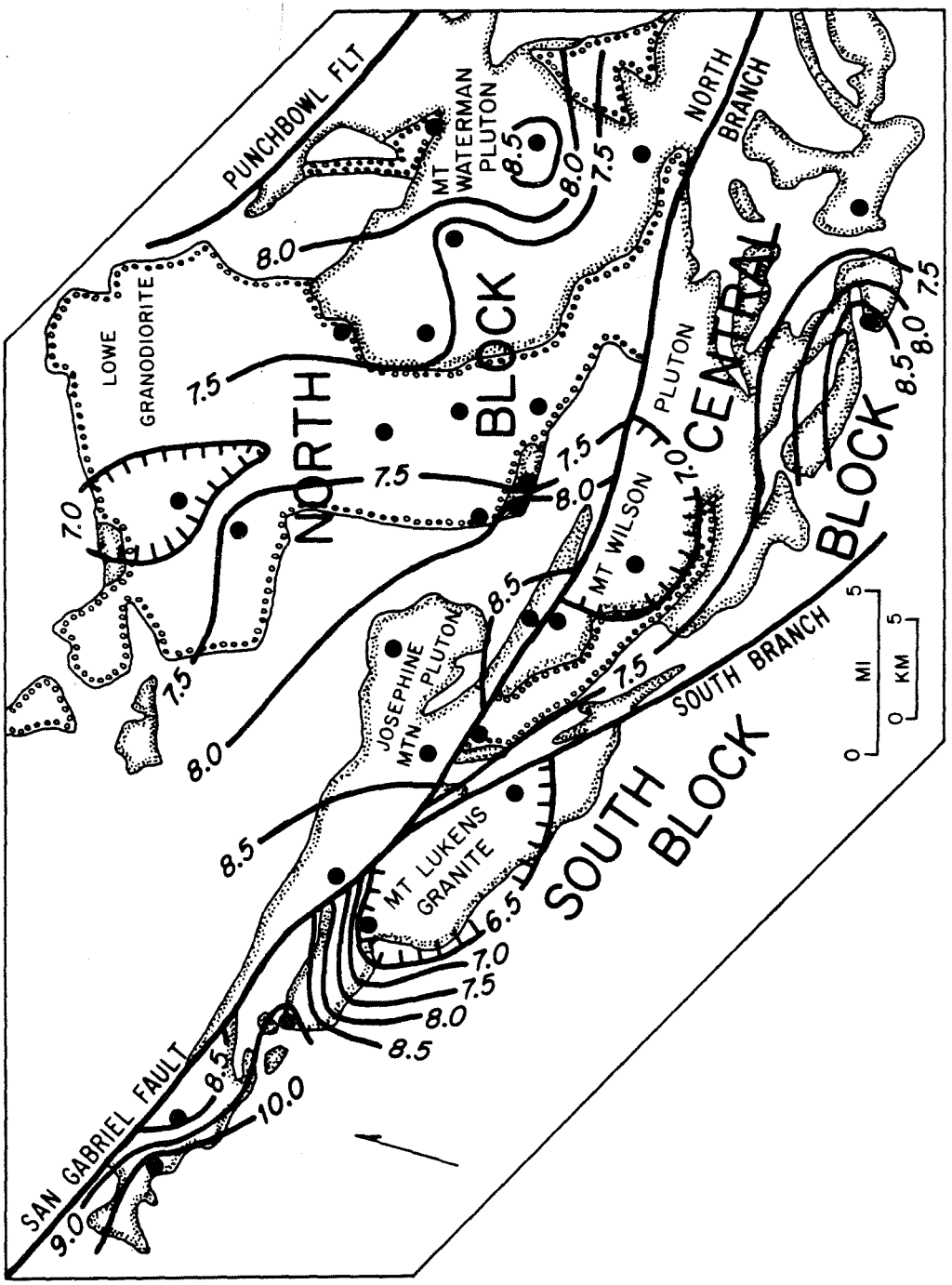
PUNCHBOWL FLT
MT WATERMAN PLUTON
NORTH BRANCH
LOWE GRANODIORITE
NORTH BLOCK
CENTRAL BLOCK
MT WILSON PLUTON
JOSEPHINE MTN. PLUTON
SOUTH BRANCH
MT LUKENS GRANITE
SOUTH BLOCK
SAN GABRIEL FAULT
7.0
7.5
8.0
8.5
9.0
10.0
6.5
1.0
0 MI 5
0 KM 5

ity between the Central Block and the North Block (Figure 6.5). In addition, note that 3 prominent minima in $\delta^{18}O$ exist, centered on the Mt. Lukens and Mt. Wilson plutons and the central part of the Mt. Lowe pluton. Each of these zones where the whole-rock $\delta^{18}O$ values are lower than +7.0 is presently located within a different fault block. It will be shown below that these 3 minima merge into a single low-^{18}O belt after reconstruction of the terranes to remove late Cenozoic fault displacements.

Ehlig (1981) has presented evidence for approximately 22 km of right-slip displacement along the north branch of the San Gabriel Fault zone. Right-slip displacement along the combined north and south branches of that fault totals approximately 60 km. Figure 6.6 is a map of the San Gabriel area that shows the effects of these fault movements removed, and the terrane reconstructed according to the scheme favored by Ehlig (1981). The $\delta^{18}O$ patterns of the SGM plutons contoured after removing the effects of late Cenozoic fault movement are much simpler and more straightforward than in Figure 6.5, and this constitutes independent support for the geological estimates of fault displacement. Two northwest-trending belts of rocks extend all the way across the reconstructed SGM terrane, with $\delta^{18}O < 8.0$ per mil on the northeast and $\delta^{18}O > 8.0$ on the southwest (Fig. 6.6).

Although the data are sparse, there is a suggestion in Figure 6.6 of a more-or-less continuous decrease from $\delta^{18}O > +9$ on the southwest to a zone of strong ^{18}O-depletion with $\delta^{18}O \leq +7$ centered on the Triassic Lowe Granodiorite and the Cretaceous Mt. Wilson and Mt. Lukens plutons. These systematics are interrupted only by a single sample with $\delta^{18}O = +8.7$ between the latter two plutons, and it should be noted that this anomal-

Figure 6.6 Reconstructed geologic map of Mesozoic granitic rocks in the SGM area showing whole-rock $\delta^{18}O$ contours after restoration of strike-slip displacements on the North and South Branches of the San Gabriel Fault. Approximately 22 km of right-slip was first removed along the North Branch, and subsequently, an additional 38 km was removed along the South Branch (see Ehlig, 1981). Figure 6.5 shows the present configuration of the SGM terrane, prior to reconstruction along these late Cenozoic faults. Solid circles indicate $^{18}O/^{16}O$ sample localities (the $^{18}O/^{16}O$ data are listed in Table 1, Appendix, as well as on Figure 6.3). Dot-dash line indicates boundary between terranes characterized by: (1) predominantly 1.2-1.7 Ga Precambrian gneiss, anorthosite and granite; and (2) the presence of Paleozoic(?) metasedimentary rocks (see discussion in text). Late-Cretaceous plutons are indicated by stippled pattern along inside margins of map unit; Triassic Lowe Granodiorite shown by small circle-pattern along inside margins of map unit. The diagonal lined patterns in the vicinity of the eastern margin of the Lowe Granodiorite represent zones where the Mesozoic plutons are peraluminous (Al/(Na+K+Ca/2) > 1.05; data from Table 3a and Baird et al., 1979).

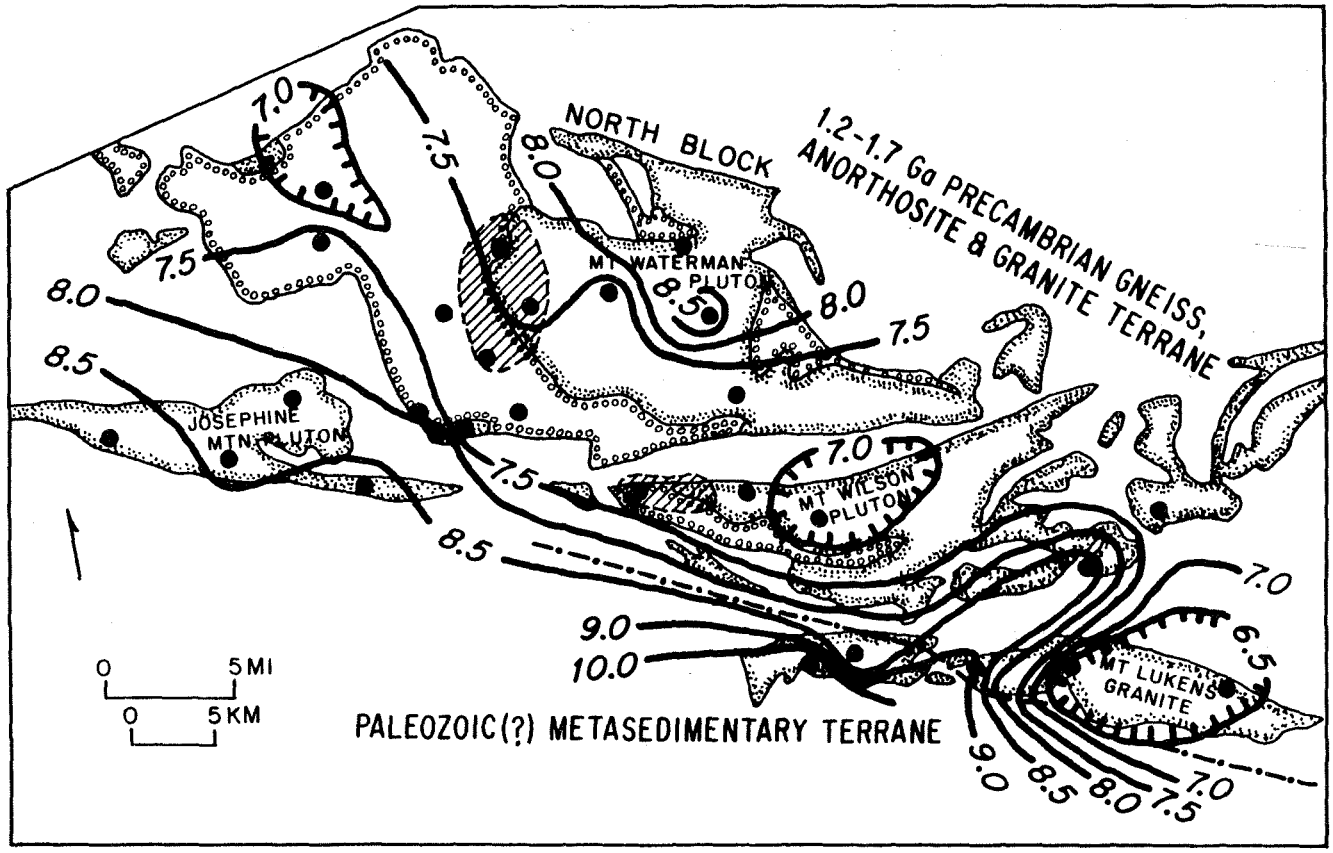
NORTH BLOCK
1.2-1.7 Ga PRECAMBRIAN GNEISS, ANORTHOSITE & GRANITE TERRANE
MT WATERMAN PLUTON
JOSEPHINE MTN. PLUTON
MT WILSON PLUTON
MT LUKENS GRANITE
7.0
7.5
8.0
8.5
9.0
10.0
6.5
0 5MI
0 5KM
PALEOZOIC(?) METASEDIMENTARY TERRANE

ous sample was itself collected fairly close to the margin of a relatively small pluton. There is, however, also an indication of a local $\delta^{18}O$ reversal to the north, as the Mt. Waterman pluton has $\delta^{18}O > +7.3$, extending up to one value as high as +8.6. Except for these local features, the fairly abrupt decrease in $\delta^{18}O$ northward and eastward in the reconstructed SGM terrane fits in well with the broad regional $\delta^{18}O$ patterns that occur in the San Bernardino and Little San Bernardino Mountains (see below), and which are also seen along the east side of the Peninsular Ranges batholith (Taylor and Silver, 1978). Thus, this constitutes further evidence that these regional $\delta^{18}O$ patterns in the SGM are very likely of a primary nature. Because differentiation cannot account for the geographic $\delta^{18}O$ variations within these rocks, these variations must be related to geographic or depth-zone differences in the source regions for these plutons, as discussed more fully in the synthesis presented in Chapter 8.

A very important feature of the SGM $^{18}O/^{16}O$ data is indicated on Figure 6.6. The plutons with $\delta^{18}O > +9$ all lie to the south of the principal outcrops of the basement rocks that are known to have cratonal characteristics, namely the 1.2 to 1.7 Ga Precambrian anorthosite-gneiss complex. A similar phenomenon is observed in the San Bernardino Mountains (Section 6.4.2).

6.4 San Bernardino Mountains Area (SBM)

6.4.1 Geology and Geochronology

The San Bernardino Mountains Area (SBM) is located in the northeastern Transverse Ranges. It is bounded by the San Andreas Fault to the southwest, the Pinto Mountain Fault to the southeast, and by the Mojave Desert region on the north and east. The SBM area is a recently uplifted

crystalline basement terrane dominated by Mesozoic batholithic rocks in its western and eastern portions, and by Precambrian gneiss in its central portion. Late Precambrian and Paleozoic miogeoclinal sediments crop out in the western and central parts of the area. Figure 6.7 is a geological map of the SBM area depicting major rock units and structures, and also showing $^{18}O/^{16}O$ sample localities with $\delta^{18}O$ values for the Mesozoic plutonic rocks.

Dibblee (1964a,b, 1967a,b,c) mapped the area in reconnaissance fashion, and Baird et al. (1979) and Baird and Miesch (1984) determined the major-element chemistry and distribution of igneous rock types in a detailed geochemical study. A geologic map for the area was compiled by Bortugno and Spittler (1986).

The oldest SBM rocks are included in the Baldwin Gneiss (Guillou, 1953), which is exposed to the east and south of Big Bear Lake and east of Cushenberry Grade. Correlative gneisses occur in isolated outcrops along the eastern edge of the SBM. This gneiss complex consists of an older group of paragneiss, schist, and quartzite, intruded by orthogneiss and pegmatite. Silver (1971) reports a U-Pb zircon age of 1750 ± 15 Ma for a younger orthogneiss near Baldwin Lake.

A composite 2.5 km-thick sequence of upper Precambrian to Cambrian miogeoclinal rocks unconformably overlies the Baldwin Gneiss terrane in the Big Bear Lake area. Individual formations within the upper part of the sequence are lithologically correlative with miogeoclinal strata elsewhere in the southern Great Basin. These include the Bonanza King, Carrara, Zabriskie, and Wood Canyon formations, comprised of quartzite, schist, phyllite, conglomeratic quartzite, marble, and calc-silicates.

Figure 6.7 Geologic map of the San Bernardino Mountains (SBM) area, showing $^{18}O/^{16}O$ sample localities and whole-rock $\delta^{18}O$ values of Mesozoic plutons. Sample localities indicated by solid circles; $\delta^{18}O$ shown alongside (a complete listing of the $^{18}O/^{16}O$ data is given in Table 1, Appendix, and includes quartz $\delta^{18}O$ values not shown on this map). Geology modified after Bortugno and Spittler (1986) and described in text: (1) late-Cretaceous granitic plutons (Cactus granite of Vaughn, 1922; Rattlesnake pluton of MacColl, 1964) shown by stippled pattern (biotite monzogranite and muscovite-biotite granite) and by "wavy" pattern (granodiorite) along inside of margins of each map unit; (2) Jurassic granitic plutons shown by cross-pattern along inside margins of map unit; (3) Triassic monzonitic plutons shown by small circle-pattern along inside margins of map unit (Fawnskin Monzonite); (4) P - Paleozoic and late Proterozoic sedimentary rocks; (5) Precambrian Baldwin Gneiss of Silver (1971) shown by diagonal line pattern along inside margins of map unit; (6) M - gneissic and mylonitic rocks of uncertain age. Thrust fault symbol indicates the North Frontal fault system discussed by Meisling and Weldon (1989). Cenozoic strike-slip faults shown by heavy lines.

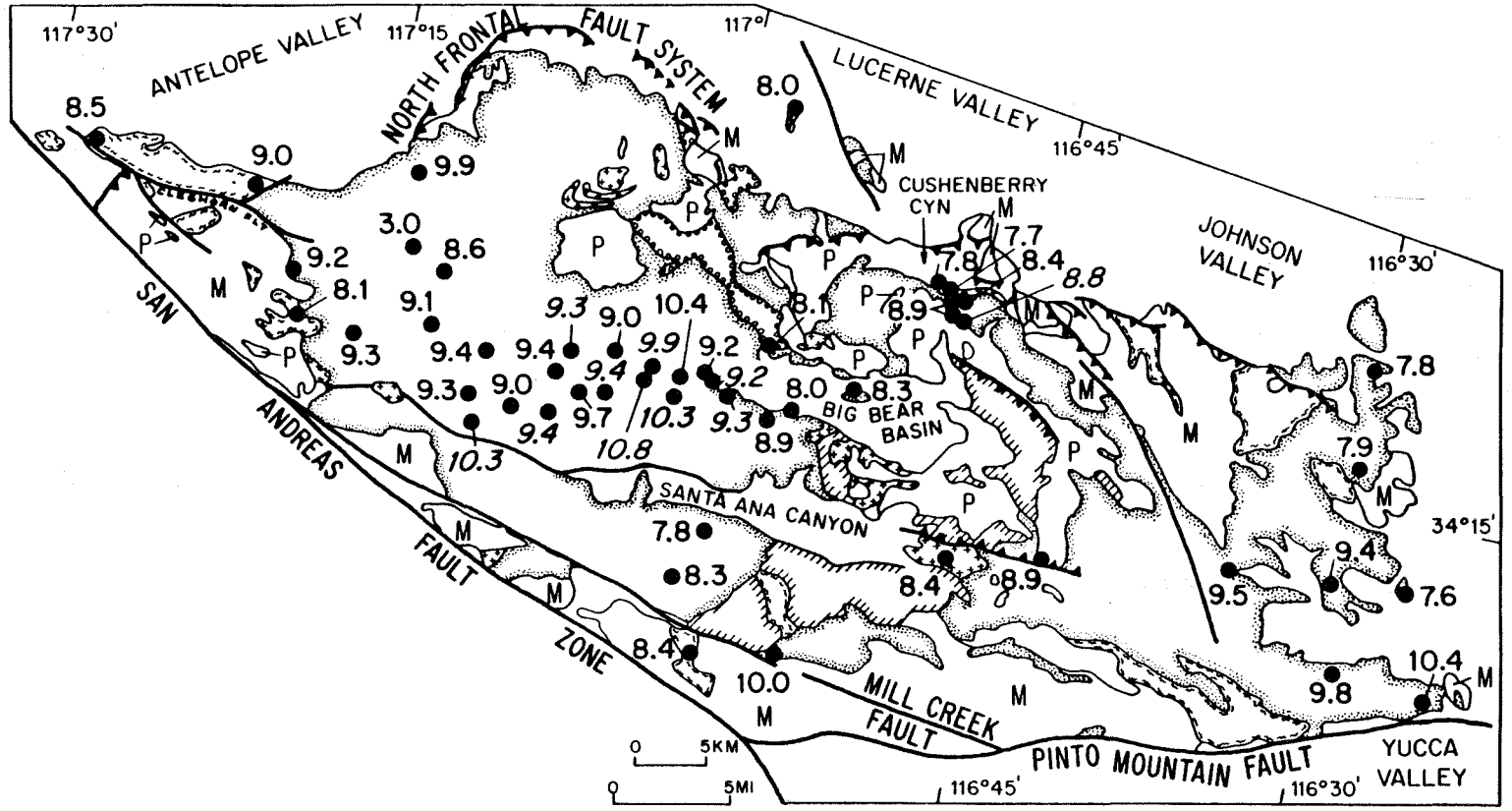
117°30'
117°15'
117°
116°45'
116°30'
34°15'
ANTELOPE VALLEY
NORTH FRONTAL FAULT SYSTEM
LUCERNE VALLEY
CUSHENBERRY CYN
JOHNSON VALLEY
SAN ANDREAS FAULT ZONE
SANTA ANA CANYON
BIG BEAR BASIN
MILL CREEK FAULT
PINTO MOUNTAIN FAULT
YUCCA VALLEY
0 5KM
0 5MI

Cameron (1982) refers to the lower portion of the sequence as the Big Bear Group (quartzite, marble, and metapelite). This sequence is lithologically different from, but stratigraphically correlative with, the Noonday-Johnny-Stirling sequence in the southern Great Basin. Cameron (1982) proposes that the stratigraphically equivalent Caborca carbonate terrane in northern Sonora may have had an original position near the Big Bear Group. If so, then the Mojave-Sonora megashear proposed by Silver and Anderson (1974) must have passed to the west of the Big Bear Group, and the location of the megashear must be obscured by late Cretaceous plutonism and Tertiary to Quaternary tectonic features.

Mesozoic batholithic rocks are the most volumetrically important type of rock in the SBM area. Three lithologically distinct age groups are present. Granitic plutonic rocks with alkalic affinites crop out in the north-central area; these are termed the Fawnskin Monzonite, and they range in composition from low-quartz (<5%) hornblende monzonite to quartz monzonite. Armstrong and Suppe (1973) determined a minimum (K-Ar) age for these rocks of 194 Ma. Miller and Morton (1980) obtained K-Ar ages of 197 and 126 Ma on hornblende and 85 Ma on biotite from a single sample from this monzonite complex. Cameron (1981) obtained $^{40}Ar/^{39}Ar$ ages on hornblende of 214 ± 2.9 Ma. These minimum ages suggest that these alkalic rocks may be part of the widespread Triassic alkalic episode of plutonism (e.g., Lowe Granodiorite event) that occurred in the southern Great Basin and in the SGM area (Miller, 1977a,b).

In the Holcomb Valley area, Dibblee (1964a) mapped a granitic porphyry complex that displays features strikingly similar to epizonal Jurassic plutonic rocks in the Rodman and Ord Mountains discussed in detail in Chapter 7 (also see Dibblee, 1964a,c). The Holcomb Valley

complex consists of fine-grained granitic porphyry that grades into a quartz latite porphyry. Both facies exhibit hydrothermal alteration, including epidotization and sericitization. The intrusive age of the complex is not well known because its contact relations are obscure, and there are no radiometric age dates.

Based on field examinations of lithology and style of alteration, the author tentatively concludes that, like the Rodman-Ord Mtns. complex, these altered SBM rocks are also most likely Jurassic in age. The style of alteration and hypabyssal nature of the rocks are also characteristic of Jurassic plutons in the Pinto Mountains and elsewhere in the Mojave Desert Region (John, 1981; Powell, 1981).

Late Cretaceous granitic rocks comprise the bulk of Mesozoic plutons throughout the SBM area. These rocks are dominantly biotite quartz monzonite (Cactus Granite of Vaughn, 1922; Rattlesnake Pluton of MacColl, 1964), and are lithologically similar to other late Cretaceous biotite quartz monzonites found throughout the Mojave Desert region.

The rocks are generally gray-white equigranular to subporphyritic, medium to coarse-grained, and composed of quartz (>15%) and two feldspars in roughly equal proportions. They rarely contain hornblende, they typically have between 3 to 7% biotite, and they generally contain less than two percent sphene and other accessory minerals. Based on personal field observations, along the southern areas to the north of the Santa Ana River and in the eastern area between Yucca Valley and Rimrock, the potassium feldspars are commonly pinkish to brick-red in color and small quartz-two feldspar pegmatitic pods and segregations are abundant.

Biotite- and hornblende-bearing granodiorites are abundant northeast of Big Bear Lake, in the extreme western area, and south of the Santa Ana

River near Forest Falls, extending to Morongo Valley. Muscovite (± garnet)-bearing granite crops out in the Johnson Grade area of Cushenberry Canyon (Richmond, 1960). The author sampled a distinct leucocratic, fine-grained, muscovite-bearing granite along Highway 18 approximately 5 km west of Big Bear Lake, on the west side of Bear Creek. This unit has not been previously described, and may be a gradational phase of the surrounding biotite quartz monzonite. Pegmatitic segregations are abundant in the area around the leucogranite.

K-Ar age dating of biotites and hornblendes in the SBM area indicates that portions of the SBM underwent prolonged cooling subsequent to the latest Cretaceous plutonism (Miller and Morton, 1980). The K-Ar ages range from 65 to 80 Ma for biotite and from 65 to 75 Ma for hornblende, with several samples as high as 197 Ma. Silver (1971) reports U-Pb zircon dates between 75 and 90 Ma in the area, and these should be close to true emplacement ages (e.g., see Silver et al., 1979).

The southern area, extending from Running Springs eastward to Pioneertown, and the area around Cushenberry Canyon both show unusually young K-Ar biotite dates. As discussed later in this section, these areas are also characterized by relatively high $\delta^{18}O$ values (> 9.0 per mil), they show abundant accumulation of pegmatitic material, and they locally contain muscovite-bearing rocks. In conjunction with the relatively young K-Ar ages, these features are strongly indicative of slow cooling at fairly deep levels in the crust.

Another feature in the SBM area that is associated with fairly deep structural levels is large-scale mylonitization of the batholithic rocks. Paleocene tectonic elements may account for significant transport of the area as an allochthonous thrust sheet (Silver, 1982, 1983) rooted

farther to the east within the Mojave Desert province. There is a major zone in the western and extreme southwestern parts of the SBM area where granodiorites have been cataclasized and mylonitized (Meisling, 1984). The zone is characterized by sub-horizontal foliation. Meisling (1984) was able to trace batholithic rocks continuously to deeper structural levels, and he found that the degree of cataclasis increases with depth, resulting in gneissic rocks. MacColl (1964) also documents cataclastic granitic rocks in the northern part of the SBM near the lower portions of the Rattlesnake pluton. Richmond (1960) describes granite cataclasites in Cushenberry Canyon.

The cataclastic zones described above are suggestive of thrusting, but it is difficult to reconstruct the original position of the SBM area in the Mojave region, because granitic lithologies are ubiquitous within the region. However, in the Johnson Grade area along Highway 18, we note that outcrops of muscovite-garnet-quartz monzonite bear a strong resemblance to rocks in the Cadiz Valley batholith near Iron Mountain and in the central Coxcomb Mountains (Howard et al., 1982). These rocks lie approximately 50 to 60 km to the east of the SBM area (see Section 7.4, Chapter 7). K-Ar biotite cooling ages for these eastern Mojave rocks are very similar to those of the SBM area (Armstrong and Suppe, 1973). The occurrence of ~65 Ma cooling ages at structurally low regions of the SBM area, as well as in the roofs of mylonitized plutons farther to the east, is suggestive of westward tectonic transport of the SBM terrane in the late Cretaceous or early Tertiary.

Late Cenozoic structural features have shaped the present-day topography in the SBM, which may be regarded as a single tectonic block internally deformed by late Cenozoic uplift and faulting. Meisling (1984)

and Sadler (1982) mapped thrust faults and high-angle faults in the northern and northeastern SBM, and these are apparently responsible for the regional uplift during the Pliocene to middle Pleistocene. Meisling and Weldon (1989) describe regional tilting and high-angle faulting that caused uplift in the western portion of the SBM area. The northeast-trending Cleghorn Fault has a left-lateral offset of about 4 km, but the extension of the Helendale Fault, and the thrusts of Sadler (1982) have no documented offsets. Meisling (1984) found no evidence for rotational movement of the northwestern portion of the range since Pliocene time. Thus, late Cenozoic faulting within the SBM block has jumbled the sub-blocks of the range, but not to such a degree that the primary igneous $^{18}O/^{16}O$ patterns would have been disturbed in a significant way, particularly with respect to the density of sampling undertaken in the present study.

6.4.2 $^{18}O/^{16}O$ Data

Figure 6.7 shows the sample locations and whole-rock $\delta^{18}O$ data for the SBM area. The $\delta^{18}O$ values of the granitic rocks range between +10.8 and +3.0, with the majority of samples between +9.5 and +8.5; only one (obviously hydrothermally altered) sample has a value lower than +7.6.

Figure 6.8 is a graph of whole-rock $\delta^{18}O$ plotted versus the $\delta^{18}O$ of coexisting quartz. The graph shows that for virtually all the samples the $^{18}O/^{16}O$ fractionation between quartz and the corresponding whole-rock is between +0.8 and +1.2 per mil. Thus, as discussed in Chapter 3, these rocks exhibit a perfectly "normal" $^{18}O/^{16}O$ fractionation that is characteristic of rocks that have retained their primary, magmatic isotopic compositions.

Figure 6.8 Plot of $\delta^{18}O$ of quartz (qtz) versus whole-rock $\delta^{18}O$ (WR) for late Cretaceous granitic plutons of the San Bernardino Mountains (SBM) area (also see Table 1, Appendix). The two diagonal lines indicate constant quartz-whole-rock fractionations of +0.8 and +1.2 per mil. Comparison of these lines with the $^{18}O/^{16}O$ data points shows that these plutons have not been affected by secondary hydrothermal alteration with low-^{18}O meteoric waters.

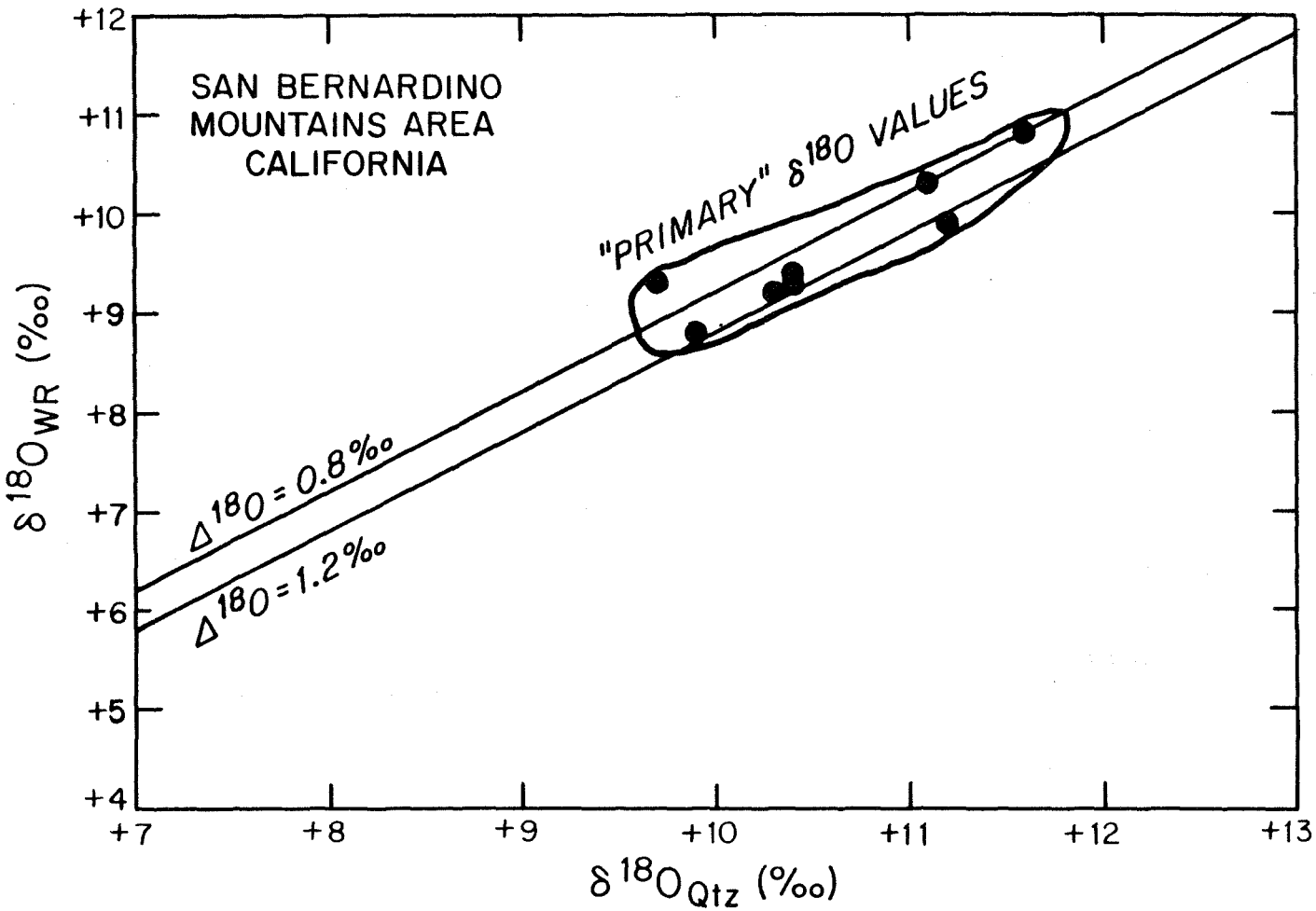
SAN BERNARDINO
MOUNTAINS AREA
CALIFORNIA
"PRIMARY" δ18O VALUES
Δ18O = 0.8‰
Δ18O = 1.2‰
δ18OWR (‰)
δ18OQtz (‰)
+12
+11
+10
+9
+8
+7
+6
+5
+4
+7
+8
+9
+10
+11
+12
+13

Quartz diorite southeast of Big Bear Lake has $\delta^{18}O$ between +8.9 and +8.4. Granodiorites show a range from +8.4 to +7.7 in the Cushenberry Canyon area, and near Forest Falls the granodiorites have $\delta^{18}O$ as high as +10.0. Granodiorite in the Silverwood Lake area in the western part of the range has $\delta^{18}O$ = +8.5 to +9.0. The highest $\delta^{18}O$ value in the SBM is +10.8 in a muscovite granite located immediately west of Big Bear Lake. The biotite-muscovite quartz monzonite exposed along the Johnson Grade in Cushenberry Canyon has $\delta^{18}O$ = +8.8 to +8.9, slightly higher than the nearby granodiorites. Quartz in the muscovite granite is +11.6 per mil, and in the Johnson Grade pluton is +9.9 per mil, so both of these rock types clearly record primary magmatic whole-rock $^{18}O/^{16}O$ compositions.

There appears to be only a minor correlation between rock type and primary whole-rock $\delta^{18}O$ in the SBM area. Both of the relatively aluminous, muscovite-bearing plutons have only slightly higher $\delta^{18}O$ than nearby granitoids that are devoid of primary muscovite. Regional variations in the nature of the sources of the plutons must therefore account for most of the variation in whole-rock $\delta^{18}O$.

Figure 6.9 is a contour map of whole-rock $\delta^{18}O$ values for the late Cretaceous plutons of the SBM area. The contours are drawn without considering the locations of the faults shown in Figure 6.7. As discussed above in Section 6.4.1, the SBM area can basically be considered to be one single tectonic block, with sub-blocks that have been jumbled by faulting, but not in a significant way when considered on a large-scale regional basis. This is in contrast to the fault blocks of the San Gabriel Mountains where relatively large amounts of slip have occurred.

Except for the single altered sample located northwest of Lake Arrowhead that has a low $\delta^{18}O$ value of +3.0, the most prominent feature on

Figure 6.9 Generalized geologic map of the SBM area (after Bortugno and Spittler, 1986), showing whole-rock $\delta^{18}O$ contours for Mesozoic granitic plutons, based on $^{18}O/^{16}O$ data listed in Table 1 (Appendix) and shown on Figure 6.7. Solid circles are $^{18}O/^{16}O$ sample localities. Mesozoic granitic rocks are indicated according to age of emplacement by different symbols along inside margins of map units: (1) late Cretaceous plutons are shown by stippled pattern; (2) Jurassic plutons are indicated by cross-pattern; and (3) Triassic plutons are shown by small circle-pattern. Diagonally-lined patterns enclosed by dashed curves indicate zones where the plutons have Al/(Na+K+Ca/2) > 1.05 (see text; based on data of Baird et al., 1979; data listed in Table 3a, Appendix). Two-mica granites are associated with two of these zones: one east of Holcomb Valley, and another west of the Baldwin Gneiss terrane, where whole-rock $\delta^{18}O$ exceeds +10. The line of open triangles indicates the boundary separating Baldwin Gneiss + Paleozoic shelf sediments on the northeast from a terrane with no Precambrian outcrops on the southwest (see text).

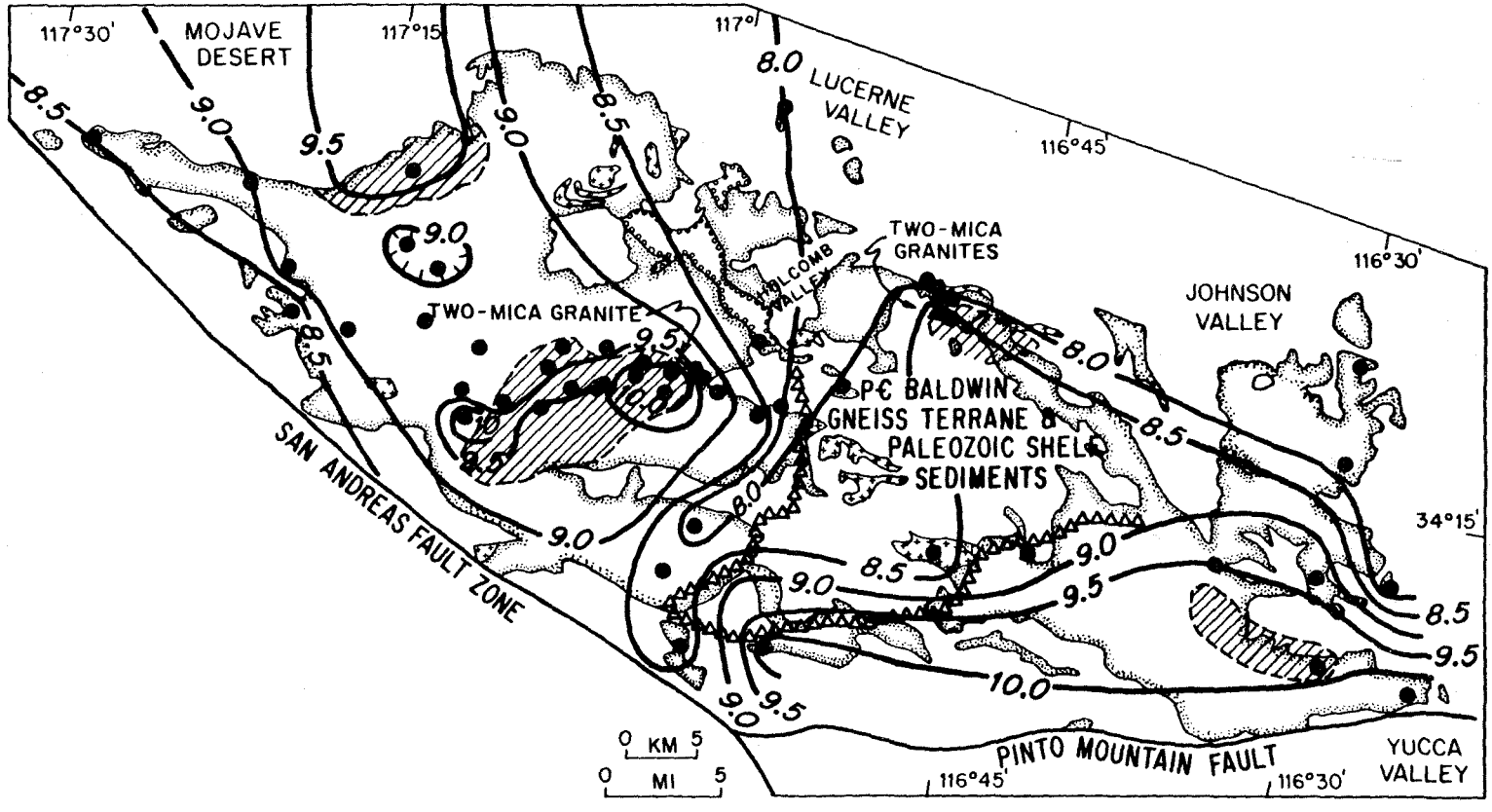
117°30'
MOJAVE DESERT
117°15'
117°
LUCERNE VALLEY
116°45'
116°30'
TWO-MICA GRANITES
TWO-MICA GRANITE
JOHNSON VALLEY
PC BALDWIN GNEISS TERRANE & PALEOZOIC SHELF SEDIMENTS
SAN ANDREAS FAULT ZONE
34°15'
PINTO MOUNTAIN FAULT
YUCCA VALLEY
0 KM 5
0 MI 5
8.0
8.5
9.0
9.5
10.0

the contour map is the zone of plutonic rocks with $\delta^{18}O$ > 9.0 per mil, going up locally to +10.8. This west- to northwest-trending zone extends nearly continuously through the entire length of the SBM area, interrupted only by a minor "reentrant" with $\delta^{18}O$ as low as +7.8 in the Forest Falls area between Santa Ana Canyon and the Mill Creek fault.

Figure 6.9 shows the local relation between the high-^{18}O zone and the transitional geological boundary, as drawn from the data of Cameron (1982) and Silver et al. (1977a) in the San Bernardino Mountains. It can be seen that everywhere in the area, the high-^{18}O zone lies just to the south and west of the mapped outcrops of this basement terrane of the North American craton. Even the area of the "reentrant" can be correlated with a prong of older gneiss that juts toward the southwest and is cut off by the Mill Creek fault. Within the +9.0 per mil contour, several areas have $\delta^{18}O$ as high as +10.0 per mil or greater. It is important to note that, without exception, these high-^{18}O plutons all lie to the west or south of the major cratonal outcrops of the Baldwin gneiss. Miogeoclinal rocks are the predominant pre-batholithic rock type in the vicinity of all of the high-^{18}O zones. North and northeast of the zone of high-^{18}O rocks, the $\delta^{18}O$ values decrease systematically downward to values lower than +8.0 per mil on the northeast side of the SBM. This northeast-trending gradient from > +9.0 to < +8.0 over a short horizontal distance marks a fundamental $\delta^{18}O$ boundary that can be observed throughout the southwestern Cordillera. Geologically, this feature correlates most closely with the transition from a paleogeography of cratonic character on the east to a miogeoclinal and/or eugeoclinal paleogeography on the west. The broader-scale significance of all of these observations is discussed in more detail in Chapters 8, 9 and 10.

6.5 Little San Bernardino Mountains Area (LSB)

6.5.1 Geology and Geochronology

The Little San Bernardino Mountains (LSB) area is a fault-bounded region that encompasses the southeasternmost portion of the Eastern Transverse Ranges. Figure 6.10 is a geologic map of the area showing the relations between geologic units and structures, and the locations of the samples studied in this thesis together with their $\delta^{18}O$ values. As defined here, the LSB area is bounded on the west by the Salton Sea and the San Andreas Fault, on the north by the Pinto Mountain Fault, and on the east and south by Chuckwalla Valley and the southern Chocolate Mountains, along the assumed extensions of the Sheephole and Salton Creek Faults, respectively. It encompasses the whole of Joshua Tree National Monument. The geology of parts of the area were recently mapped by Powell (1981) and Dibblee (1967a,b); the remainder is compiled in reconnaissance fashion by Rogers (1966), Bishop (1963), Jennings (1967), and Bortugno and Spittler (1986).

The LSB area is underlain by a Precambrian crystalline basement terrane (Powell, 1981) that is intruded by two distinct suites of Mesozoic batholithic rocks. The older suite, which mainly crops out on the eastern side of the map area (Fig. 6.10) is composed of Jurassic hypabyssal plutons that exhibit local hydrothermal alteration. The younger suite, made up of latest Cretaceous granodiorites and quartz monzonites with local muscovite-granite facies, mainly crops out on the southwest side.

A latest Cretaceous to early Tertiary cataclastic zone underlies the southwestern escarpment of the area, and is inferred to represent the zone over which the crystalline terranes have been thrust westward over

Figure 6.10 Generalized geologic map of the Little San Bernardino Mountains (LSB) area (geology modified after Powell, 1981; Bortugno and Spittler, 1986; Bishop, 1963; and Jennings, 1967), showing $^{18}O/^{16}O$ sample localities and whole-rock $\delta^{18}O$ values for Mesozoic plutons. Sample localities indicated by solid circles; whole-rock $\delta^{18}O$ shown alongside (Q indicates quartz $\delta^{18}O$). A complete listing of the $^{18}O/^{16}O$ data is given in Table 1, Appendix. Geologic map units are: (1) Tv - mid-Tertiary volcanic rocks; (2) Kg - late Cretaceous granitic plutons shown by stippled pattern along inside margins of map unit; (3) Jurassic granitic plutons shown by cross-pattern along inside margins of map unit; (4) Msch - Orocopia Schist; (5) PG - Precambrian crystalline basement rocks; (6) M - gneisses and mylonitic rocks of uncertain age. Thrust fault symbol indicates boundary between upper-plate crystalline basement and lower-plate Orocopia Schist. Cenozoic strike-slip faults shown by heavy solid and dashed lines.

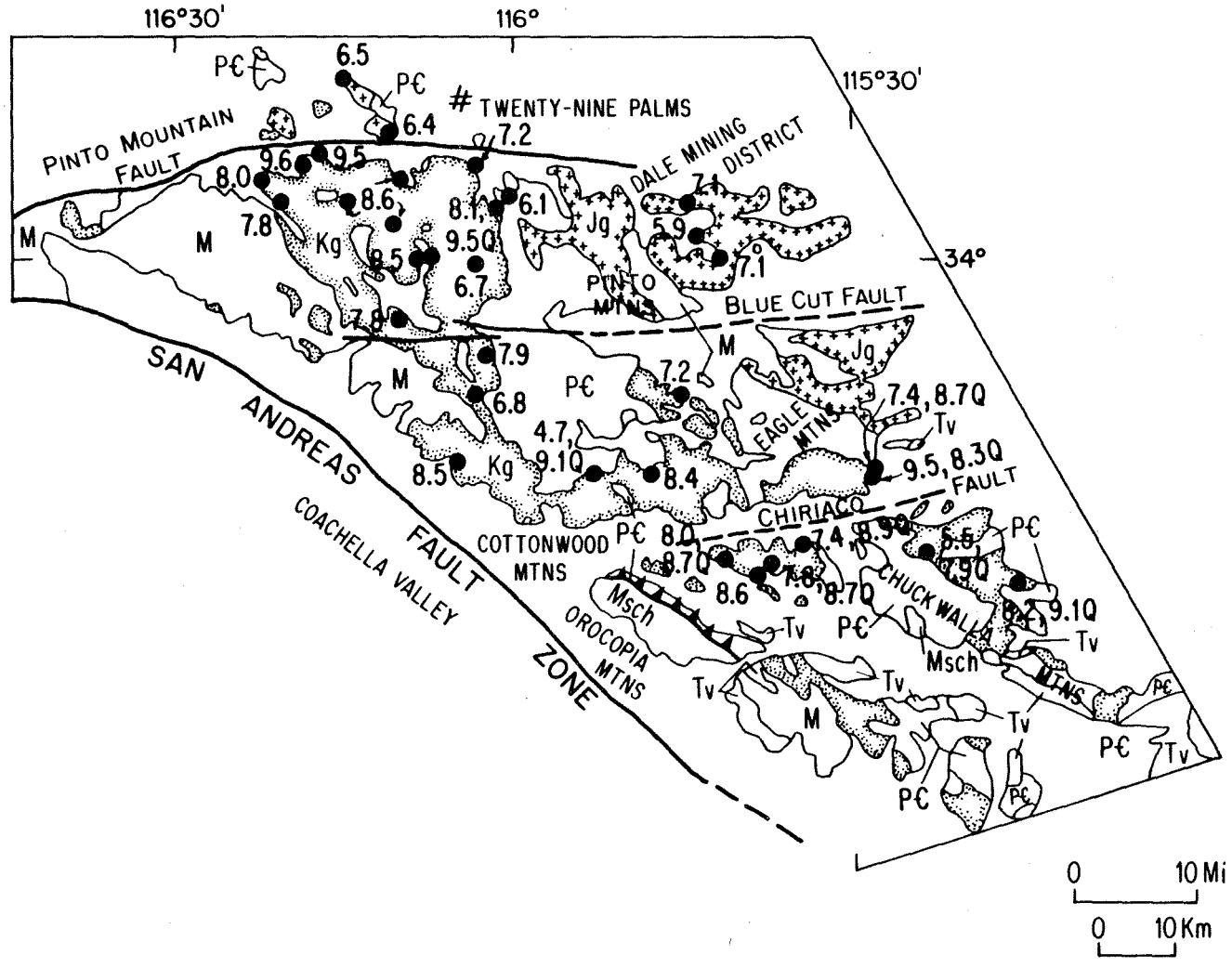
116°30'
116°
115°30'
34°
PC
6.5
PC
TWENTY-NINE PALMS
6.4
7.2
PINTO MOUNTAIN FAULT
9.6
9.5
8.0
8.6
8.1
6.1
DALE MINING DISTRICT
7.1
M
7.8
Kg
9.5
9.5Q
6.7
Jg
5.9
7.1
PINTO MTNS
BLUE CUT FAULT
7.8
7.9
M
Jg
M
6.8
PC
7.2
7.4, 8.7Q
Tv
4.7,
9.1Q
8.5
Kg
8.4
EAGLE MTN
9.5, 8.3Q
FAULT
CHIRIACO
SAN ANDREAS FAULT
COACHELLA VALLEY
ZONE
COTTONWOOD MTNS
PC
8.0
8.7Q
8.6
7.4, 8.9Q
8.7Q
5.6
5.9Q
PC
CHUCK WALLA
9.1Q
Tv
Msch
OROCOPIA MTNS
Tv
PC
Msch
Tv
Tv
M
Tv
PC
PC
PC
Tv
PC
0 10 Mi
0 10 Km

the top of the Orocopia schist. Late Cenozoic strike-slip movements have offset the Mesozoic and older basement rocks along east-trending left-lateral faults, as well as along the right-lateral San Andreas Fault. Prior to the late Cenozoic displacements along the San Andreas Fault, the basement complex of the San Gabriel Mountains was juxtaposed against the extreme south-central portion of the LSB area (Ehlig, 1981; Powell, 1981; L.T. Silver, pers. comm.). The offsets along the left-lateral faults are much smaller, typically less than 15 km (Powell, 1981).

The Precambrian crystalline basement is made up of two lithologically distinct terranes that have been tectonically juxtaposed and complexly deformed (Powell, 1981; 1982). These are referred to by Powell (1981) as the Joshua Tree Terrane (JTT) and the San Gabriel Terrane (SGT). The JTT consists of regionally metamorphosed gneisses that are unconformably overlain by pelitic, quartzitic, and carbonate metasediments.

The SGT is allochthonous over the JTT along the Red Cloud thrust fault. The SGT is made up of an upper amphibolite-facies paragneiss that is intruded by orthogneiss. This unit overlies a granulite-facies suite of tonalitic to granitic rocks that were intruded by a younger syenitic pluton and retrograded to upper amphibolite-facies. Silver (1971) obtained a zircon U-Pb date of 1650 Ma on an augen orthogneiss from the JTT. This unit is correlated with similar rocks in the Soledad Basin to the north of the San Gabriel Mountains (Powell, 1982; Silver, 1971).

Powell (1982) correlates the granulitic rocks with the gneisses found in the San Gabriel Mountains west of the Mount Waterman Pluton. The syenitic rocks are time-correlative with the 1.2 Ma anorthositic rocks of the San Gabriel Mountains (Silver, 1971; Powell, 1982; Carter and Silver, 1972) previously discussed in Section 6.3.1.

Mesozoic batholithic rocks crop out in two northwesterly trending belts of different ages. The older or northeasternmost suite consists of gabbro and monzodiorite to granodiorite crosscut by quartz monzonite. Sphene is an abundant accessory mineral, and the granodiorites contain both biotite and hornblende. Powell (1982) reports that L.T. Silver found mid-Jurassic zircons in quartz monzonite of the Pinto Mountains, and Bishop (1963) reports mid-Jurassic K-Ar dates for the suite. The rocks contain chlorite and epidote in many localities and several areas in the northern Pinto Mountains are hydrothermally altered and contain epithermal ore mineralization (Dale Mining District).

The younger suite consists of hornblende-biotite granodiorite and quartz monzonite, and is texturally distinct from the older suite. Sphene is an abundant accessory mineral in the granodiorite. The granodioritic unit extends from Yucca Valley southeastward to Berdoo Canyon in a well defined trend. The area around Fargo Canyon just to the south is underlain by quartz diorite. On a west to east traverse through Berdoo Canyon, the author noted that plutonic lithologies changed from cataclasized quartz diorite to granodiorite, and finally to quartz monzonite in Joshua Tree National Monument. This general west to east change to more felsic plutons appears to be characteristic of this terrane. In the area between the Cottonwood and Chuckwalla Mountains, however, the trend is not apparent, and the younger rocks are all dominantly felsic. Locally, coarse-grained biotite quartz monzonite is muscovite- and garnet-bearing. A prominent example of this is the White Tank Quartz Monzonite of Rogers (1961).

The geochronology of the younger suite in the LSB area is not well constrained. Joseph and Ehlig (1981) dated a quartz monzonite from Ther-

mal Canyon at 74.1 ± 0.9 Ma by Rb-Sr. This quartz monzonite is known as "the Polkadot Granite" (Ehlert and Ehlig, 1977), and can be correlated with similar plutonic rocks in the La Panza Range north of the San Gabriel Mountains on the west side of the San Andreas Fault. Armstrong and Suppe (1973) obtained K-Ar ages of 67.9 to 74.8 Ma on biotites and hornblendes from a suite of the younger intrusions. The ~73 Ma ages may approach the true emplacement ages of the rocks, but the biotite ages in the ~68 Ma range likely represent only the later cooling history of deeply emplaced plutons.

Powell (1982) points out that the Precambrian crystalline basement in the LSB area could be lithologically and chronologically distinct from the Baldwin gneiss of the SBM area. This would imply that the Jurassic megashear would have to trend to the west of the Big Bear Lake area, but east of the crystalline basement in the LSB area. This is in good agreement with Cameron's (1982) proposal that the Caborca terrane must have once been juxtaposed adjacent to the Big Bear Group. The actual location of the megashear is not well-established, and probably will not be determined until the complex post-batholithic tectonic features of the area, including the Mojave Desert region, are better understood (L.T. Silver, pers. comm.).

The crystalline rocks of the western boundary of the Little San Bernardino Mountains have been pervasively cataclasized by an event that post-dates the younger plutonic suite. Foliation in the zone of deformation dips shallowly to the east, and has been deformed into an antiform in its westernmost exposures (Powell, 1981, 1982, 1986a,b). Farther south in the Orocopia Mountains, the Orocopia-Vincent thrust fault has juxtaposed mylonitized crystalline rocks over the Orocopia Schist. The

age of the thrusting is probably similar to ages found elsewhere in the Transverse Ranges, probably between 57 and 67 Ma. Thrust-related mylonitization is coincident with the waning stages of the late Cretaceous plutonism everywhere in the overall study area.

6.5.2 $^{18}O/^{16}O$ Data

Figure 6.10 shows the locations and $^{18}O/^{16}O$ data for the samples from the LSB area. The late Cretaceous plutonic belt of Powell (1981) was fairly well-sampled within the Joshua Tree National Monument, but it is sampled in only reconnaissance fashion in the area around the Cottonwood, Chuckwalla, and Orocopia Mountains. The Jurassic belt of Powell (1981) is sampled in a reconnaissance fashion in the Dale Mining District of the Pinto Mountains.

The whole-rock $\delta^{18}O$ values of 33 samples from the LSB range from +9.6 to +4.7, with half of the analyses falling in a narrow range between +8.6 and +7.8. The bulk of these samples are quartz monzonites, and the entire range of $\delta^{18}O$ variation from +9.6 to +4.7 can be observed in that lithology. Values above +9 are only observed in the extreme northwest part of the range. Note that these rocks with $\delta^{18}O > +9$ all lie to the west of mapped Precambrian outcrops, just as in the SGM and SBM areas discussed previously. Thus, in terms of both geology and $^{18}O/^{16}O$ geochemistry, most of the LSB area closely corresponds to the northeast side of the SBM area underlain by the Baldwin Gneiss.

The biotite-muscovite facies of the White Tank Quartz Monzonite has a $\delta^{18}O$ value of +8.0. A single quartz diorite sample taken near Fargo Canyon has a $\delta^{18}O = +8.5$, and late Cretaceous(?) granodiorite directly to the southeast of Yucca Valley has $\delta^{18}O = +8.0$ to +7.8. The same granodioritic rock farther to the southeast near Lost Horse Mountain is +7.8 per

mil. Thus, within the late Cretaceous belt, the $\delta^{18}O$ values show no particular correlation with differentiation index. The limited number of Jurassic samples from the Dale Mining District have distinctly lower $\delta^{18}O$ values between +5.9 and +7.1. The latter samples apear to have been locally depleted in ^{18}O by meteoric-hydrothermal activity (see below).

Figure 6.11 is a graph depicting whole-rock $\delta^{18}O$ values plotted versus the $\delta^{18}O$ of coexisting quartz, for randomly selected samples. The majority of these samples show $\Delta^{18}O$ quartz-whole-rock fractionations indicating that the rocks retained primary, magmatic $^{18}O/^{16}O$ compositions. Two samples, however, exhibit fractionations that are much larger than +1.2 per mil, indicating that these samples experienced subsolidus interaction with low-^{18}O fluids under hydrothermal conditions. These low-^{18}O sample localities are discussed below.

Figure 6.12 is a map showing contours of the whole-rock $\delta^{18}O$ values for the LSB area. Five relatively ^{18}O-depleted areas on the map are enclosed within the +7.0 per mil contour; samples in these areas have $\delta^{18}O$ values that range from +4.7 to +6.8 per mil. One of these areas is centered on the Jurassic plutonic rocks of the Dale Mining District. These rocks are characterized by abundant epidote veins and overall pervasive hydrothermal alteration, resulting in a greenish cast that is characteristic of epidotization or chloritization of plagioclase. John (1981) notes that the igneous intrusions in this area show hypabyssal characteristics, and their low $\delta^{18}O$ values undoubtedly are the result of epizonal hydrothermal circulation within a Jurassic volcanic center.

A second low-^{18}O area is located directly north of the Hexie Mountains and south of Twentynine Palms, and is shown on Figure 6.12 as a westward extension of the ^{18}O-depleted zone associated with the Dale

Figure 6.11 Plot of $\delta^{18}O$ of quartz (qtz) versus whole-rock $\delta^{18}O$ (WR) for Cretaceous granitic rocks in the LSB area (also see Table 1, Appendix, and Figure 6.10). The two diagonal lines show constant quartz-whole-rock $^{18}O/^{16}O$ fractionations of +0.8 and +1.2, indicating "equilibrium" conditions for coexisting quartz and whole-rock at magmatic temperatures (see Chapter 3). Most of the data plot near these two lines; however samples from the Cottonwood Mountains and Chuckwalla Mountains exhibit distinctly "altered" whole-rock $\delta^{18}O$ values (discussed in text).

Figure 6.12 Geologic map of the LSB area, showing whole-rock $\delta^{18}O$ contours on Mesozoic granitic rocks, based on $^{18}O/^{16}O$ data from Figure 6.10 and Table 1, Appendix. Solid circles indicate $^{18}O/^{16}O$ sampling localities; geologic nomenclature similar to that for Figure 6.10. Plutons with $\delta^{18}O < +7.0$ per mil indicated by closed +7.0 contour with inward-pointing hash-marks. Note apparent 15 km left-lateral offset of a low-^{18}O zone along Pinto Mountain fault west of Twentynine Palms (see text).

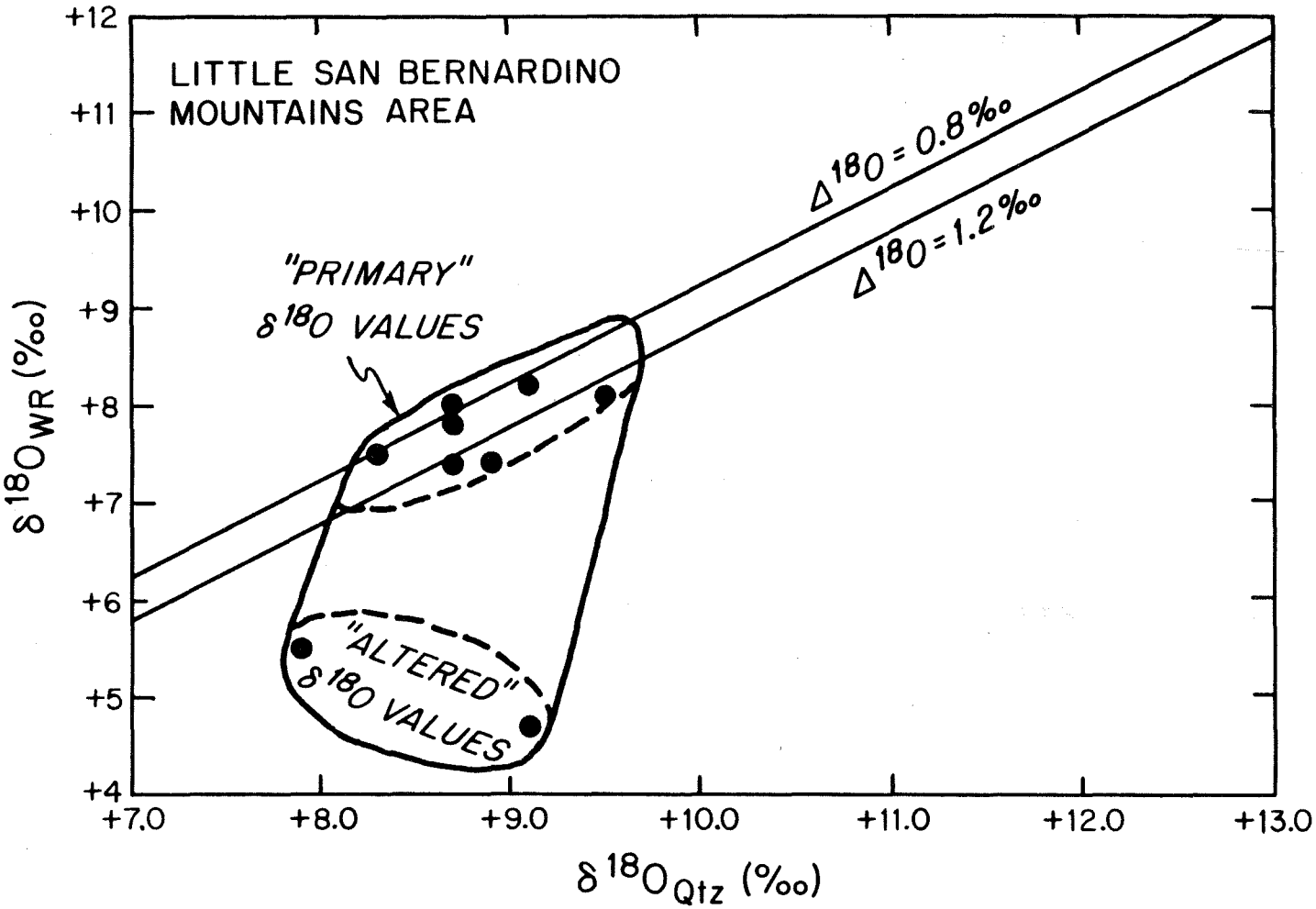
LITTLE SAN BERNARDINO
MOUNTAINS AREA
"PRIMARY"
δ 18O VALUES
"ALTERED"
δ 18O VALUES
Δ 18O = 0.8‰
Δ 18O = 1.2‰
δ 18O WR (‰)
δ 18O Qtz (‰)
+12
+11
+10
+9
+8
+7
+6
+5
+4
+7.0
+8.0
+9.0
+10.0
+11.0
+12.0
+13.0

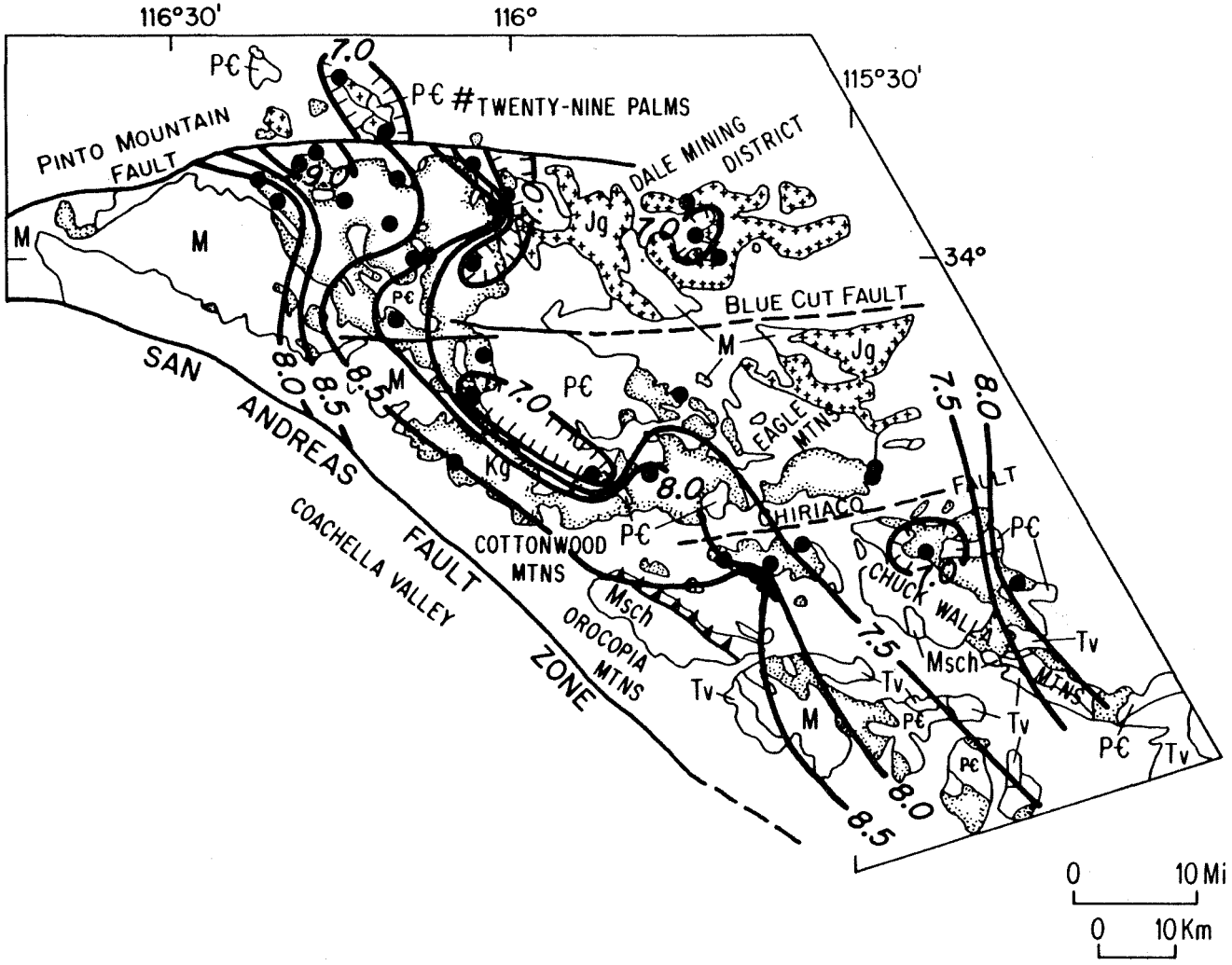
116°30'
116°
115°30'
34°
PC
7.0
TWENTY-NINE PALMS
PINTO MOUNTAIN FAULT
DALE MINING DISTRICT
M
Jg
BLUE CUT FAULT
8.0
8.5
SAN ANDREAS FAULT
COACHELLA VALLEY ZONE
Kg
EAGLE MTNS
CHIRIACO FAULT
COTTONWOOD MTNS
Msch
OROCOPIA MTNS
Tv
CHUCK WALLA MTNS
7.5
0 10 Mi
0 10 Km

Mining District. However, Powell (1981) did not differentiate between Jurassic and late Cretaceous plutons in this area, and it is not clear from the mapping of Dibblee (1967a) what age assignment could be made. On Dibblee's map, these rocks are indicated as "older granitic" rocks; in the surrounding quadrangle this assignment commonly corresponds to rocks that are probably Jurassic in age. Field examination by the author, however, did not allow any more conclusive inferences, and this area is therefore not assigned an age. The low-^{18}O rocks (+6.7 to +6.1) may have experienced hydrothermal $^{18}O/^{16}O$ exchange either during the Jurassic or at a later time. Another low-^{18}O area is located just north of the Pinto Mountain fault, and it is interesting to consider whether this might be the offset extension of the Hexie Mountains low-^{18}O zone; if so, this would suggest an overall left-lateral displacement of at least 10 to 15 km on this fault, which is a plausible offset, as it compares favorably with the ~ 16 km offset suggested by Powell (1981).

The other two ^{18}O-depleted zones are located in the area around Corn Springs Wash in the Chuckwalla Mountains ($\delta^{18}O$ = +5.5), and in the region extending from the Cottonwood Mountains to the head of Berdoo Canyon (+4.7 to +6.8). Whole-rock and quartz $\delta^{18}O$ values for samples from each of these areas are plotted on Figure 6.11. In both cases, the $^{18}O/^{16}O$ fractionations (+2.4 to +4.4 per mil) are much greater than are expected for equilibrium at magmatic temperatures. The reconnaissance nature of sampling in these areas prohibits more detailed discussion of these hydrothermal systems. However, we note below that, after reconstruction of late Cenozoic movement along the San Andreas Fault system, the low-^{18}O zones found in the San Gabriel Mountains are roughly coincident in trend with these LSB low-^{18}O zones (see Chapter 8).

The remaining data in Figure 6.11 indicate that whole-rock $\delta^{18}O$ values of +8.0 to +9.6 in the LSB area all represent primary, magmatic values. There is, however, no well-defined geographic pattern of primary $\delta^{18}O$ values on the contour map in Figure 6.12, except that values higher than +9.0 per mil are restricted to a small area in the northwestern portion of the LSB terrane, and that the east side of the map area is typically lower in ^{18}O (< +8) than the west side. Of all the major batholithic terranes between and including the Sierra Nevada and northern Peninsular Ranges batholiths, the LSB terrane is the only one that lacks a distinct high-^{18}O zone (> 9.0 per mil) of significant areal extent. Also, note that the high-^{18}O zone in the directly adjacent (pre-faulting!) SGM terrane is also very small (Figure 6.6).

Two factors may account for the lack of an extensive high-^{18}O (> +9.0 per mil) zone in the LSB and adjacent SGM: (1) high-^{18}O source regions were actually present at depth during the late Cretaceous magmatism, but major structural events such as fan-folding and thrusting in early Tertiary times (Powell, 1986a,b) or late Cenozoic tectonic movements along the system of San Andreas-related structures disrupted, covered, or obscured the zone of high-^{18}O plutons; or (2) high-^{18}O source regions were simply not present at the depths at which melting occurred during the late Cretaceous magmatic event. The latter possibility might imply either that these LSB and SGM plutons were generated much farther to the east and later thrust westward into their present positions, or that the high-^{18}O sources were tectonically removed prior to generation and emplacement of the plutons. These factors are discussed in more detail in Chapter 8, where regional patterns in $\delta^{18}O$ are synthesized for the Transverse Ranges and southeastern California.

6.6 Comparison of $^{18}O/^{16}O$ and Major-Element Geochemistry in the SGM, SBM, and LSB Areas

Baird et al. (1979) and Baird and Miesch (1984) report whole-rock major element analyses for the late Cretaceous plutons exposed in the Central and Eastern Transverse Ranges. Their data are recalculated in terms of the oxides and listed in the appendix in Tables 3a and 3b. Analyses of the Lowe Granodiorite and the Jurassic suite of plutons in the LSB area (suite M1 of Powell, 1981) are not included in their data base. Their sampling grid is different than the one employed for $^{18}O/^{16}O$ samples in this study, and thus it is not possible to make a one-to-one comparison between their chemical data and the $\delta^{18}O$ data in Table 1 in the appendix.

In light of the geochemical classification scheme of Chappell (1978), Hine et al. (1978), and O'Neil and Chappell (1977) (discussed earlier in Chapter 5), it is instructive to review the salient aspects of the geochemistry of the plutons in the Transverse Ranges, and then to compare the $\delta^{18}O$ contours in the area with the chemical data. Unfortunately, Baird et al. (1979) and Baird and Miesch (1984) have not distinguished between FeO and Fe_2O_3 in their data base; thus it is not possible to compare ferrous/ferric ratios with $\delta^{18}O$, as was done for the Arizona plutons in Figs. 5.8 and 5.9.

Figure 6.13 shows a ternary plot of the C.I.P.W. normative values for An, Ab, and Or (normalized to 100 per cent) for samples from the Transverse Ranges. Also shown is the "Sierra Nevada trend line" of Presnall and Bateman (1973) (line M-N). The data points fall in a cluster to the sodic side of the Sierra Nevada Batholith trend line.

Figure 6.13 Ternary plot of C.I.P.W. normative mineralogy (An-Ab-Or end-members, normalized to 100%) for Mesozoic granitic rocks of the Central and Eastern Transverse Ranges, California (based on data of Baird et al., 1979). This diagram was prepared from chemical data listed in Table 3a (Appendix), and mineralogical data listed in Table 3b (Appendix). Line M-N is the Sierra Nevada Batholith trend-line of Presnell and Bateman (1973). Region labeled "B" is a likely source region composition for calc-alkaline plutons in the SGM, SBM and LSB areas.

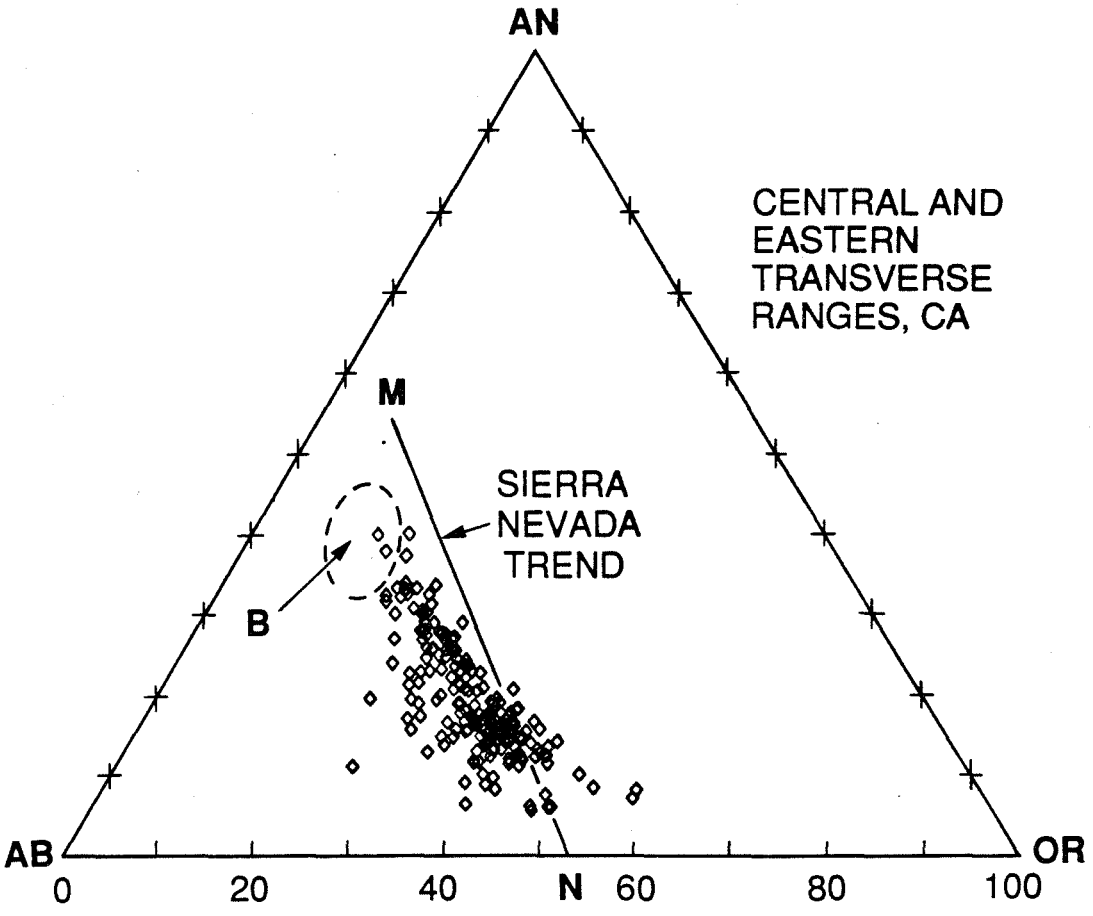
AN
CENTRAL AND
EASTERN
TRANSVERSE
RANGES, CA
M
SIERRA
NEVADA
TREND
B
AB
OR
0
20
40
N
60
80
100

It is likely that the positions and shapes of the SGM, SBM, and LSB data point arrays on the diagram in Figure 6.13 are a result of the same general process that was responsible for the Sierra Nevada line. However, in the case of the Transverse Ranges, the source would have to have a lower Ca/Na ratio than the source(s) for the Sierra Nevada rocks, possibly with a composition in the general vicinity of point B on the diagram. As discussed in Chapter 7, the plutons of southeastern California also show a similar shift compared with the Sierra Nevada trend.

Figure 6.14 is a Peacock diagram that depicts the variation of CaO and (Na_2O + K_2O) versus SiO_2 for the late Cretaceous plutons from the Transverse Ranges. The two trends converge to a more or less common alkali-lime index of approximately 57 to 60 weight percent SiO_2. According to the classification scheme of Peacock (1931), the suite is "calc-alkaline". For comparison, the Sierra Nevada Batholith is also calc-alkaline (Bateman et al., 1963; Kistler 1974; Lockwood, 1975; Bateman and Lockwood, 1976), and the Peninsular Ranges Batholith is calcic (Larsen, 1948; Silver et al., 1979). The regional implications of these classifications are discussed in Chapter 8.

A small number of "anomalous" samples from the Transverse Ranges, labeled group "A" in the plot shown in Figure 6.14, cluster with total alkali values of 8.5 to 9.5 weight percent at SiO_2 values from 59 to 69 weight percent. This cluster is clearly aberrant compared with the rest of the samples, which line up nicely in a typical Peacock array.

Because of the scale at which the data are plotted, it is difficult to translate the localities of Baird and Miesch (1984) in terms of the geology mapped by Dibblee and other investigators mentioned earlier. However, several of these "anomalous" areas display evidence for hydro-

Figure 6.14 Plot of SiO_2 (wt.%) versus Na_2O+K_2O and CaO (wt.%) (Peacock Diagram of Peacock, 1931), showing generalized data fields for more than two hundred samples of Mesozoic granitic rocks of the Central and Eastern Transverse Ranges, California (based on data of Baird et al., 1979; see the major-element chemical data listed in Table 3a (Appendix), and calculated total alkalies listed in Table 3b (Appendix). The intersections of the data envelopes between SiO_2 > 57 wt.% and < 61 wt.% indicates that the plutons in the SBM and LSB areas are calc-alkaline. However, the SGM area exhibits an intersection near 56 wt.%, indicating alkali-calcic affinity (Peacock, 1931). Group A has anomalously high alkali contents relative to the rest of the samples, and may be either hydrothermally altered, or represent Triassic monzonitic rocks (e.g. Fawnskin Monzonite).

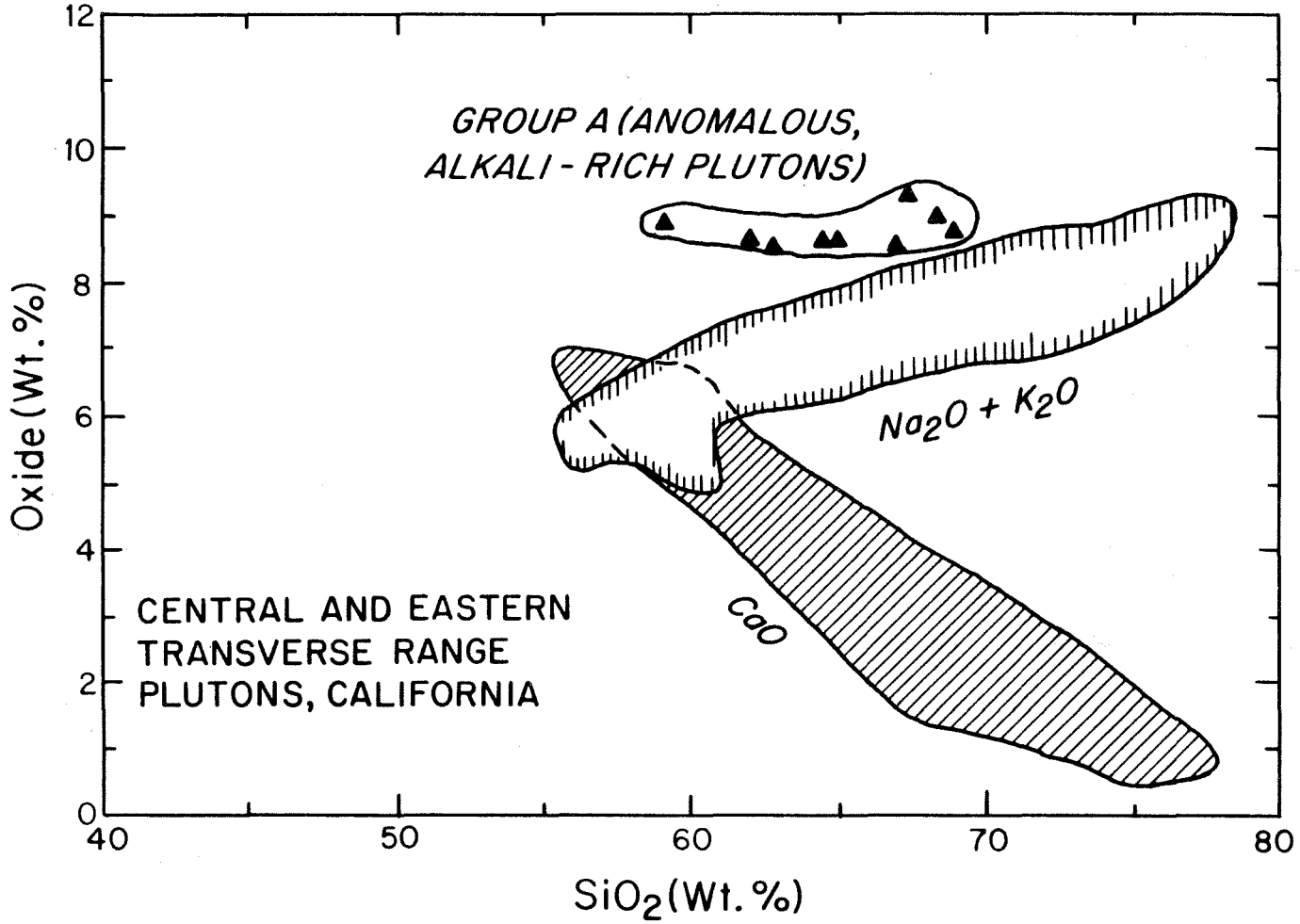
GROUP A (ANOMALOUS,
ALKALI - RICH PLUTONS)
$Na_2O + K_2O$
CaO
CENTRAL AND EASTERN
TRANSVERSE RANGE
PLUTONS, CALIFORNIA
Oxide (Wt. %)
SiO_2 (Wt. %)
0
2
4
6
8
10
12
40
50
60
70
80

thermal alteration, notably those in Holcomb Valley and in Lucerne Valley to the north of the San Bernardino Mountains. The anomalous population in Figure 6.14 therefore may represent an early set of plutons (possibly Jurassic and almost certainly older than late Cretaceous) that have undergone varying degrees of sub-solidus alkali enrichment as a result of hydrothermal alteration.

Figure 6.15 is a histogram showing a frequency plot of the mole ratio Al/(K+Na+Ca/2) for the Transverse Ranges plutons. This parameter is crucial in the I-type and S-type classification scheme, because silicic melts (e.g. quartz monzonites) derived from pelitic sources should be peraluminous (ratio > 1.05); this is because shales and pelitic schists are generally high in alumina due to their high clay and mica content (Chappell, 1978). The diagram in Figure 6.15 shows that the bulk of the plutons in the Transverse Ranges are metaluminous, with approximately one fifth of the samples plotting with values greater than 1.05. Only about 5 per cent of the samples have ratios that are strongly peraluminous (> ~1.10).

"S-type" plutons typically have $\delta^{18}O$ > +10.0 per mil because pelitic rocks are generally ^{18}O-enriched due to interaction with the hydrosphere at low temperature during sedimentation (O'Neil and Chappell, 1977; O'Neil et al., 1977; Taylor, 1978). Thus, even though there is not a one-to-one correspondence between the analyzed SGM, LSB, and SBM samples in the respective $^{18}O/^{16}O$ and geochemical data bases, we can compare these parameters by examining the areal distributions of the $\delta^{18}O$ contours relative to those of the alumina/calcic-alkali ratios.

Figures 6.6, 6.9, and 6.12 show the $\delta^{18}O$ contours for the SGM, SBM and LSB areas, as well as showing the regions where Al/(K+Na+Ca/2) >

Figure 6.15 Histogram showing the frequency of occurrence and range for the mole ratio $Al_2O_3/(Na_2O+K_2O+CaO)$ in Mesozoic granitic rocks from the Central and Eastern Transverse Ranges, California (based on data of Baird et al., 1979). The major-element chemical data that were used to calculate this ratio are listed in Table 3a (Appendix), and the calculated ratios are listed in Table 3b (Appendix).

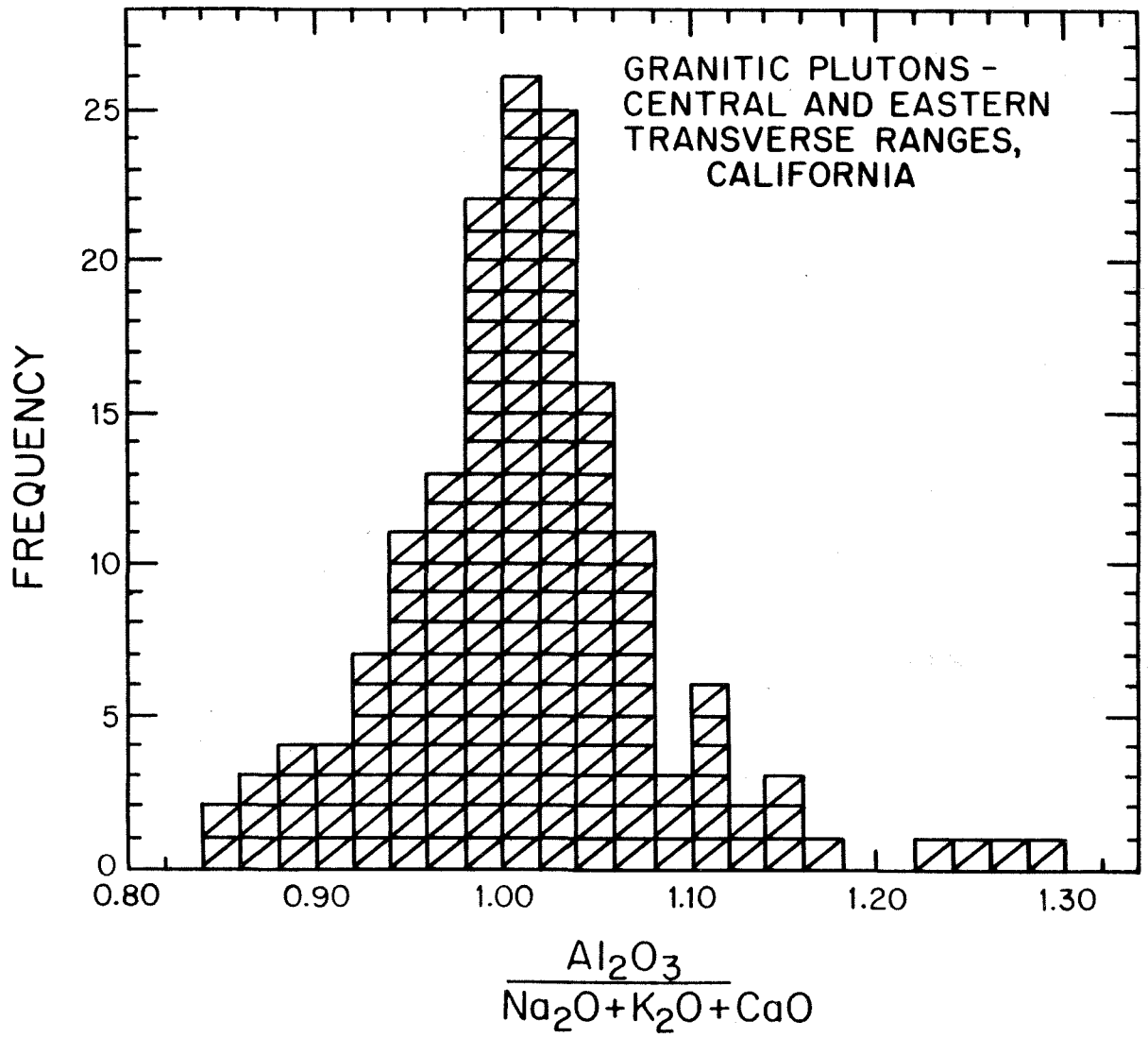
GRANITIC PLUTONS -
CENTRAL AND EASTERN
TRANSVERSE RANGES,
CALIFORNIA
FREQUENCY
0
5
10
15
20
25
0.80
0.90
1.00
1.10
1.20
1.30
$\frac{Al_2O_3}{Na_2O+K_2O+CaO}$

1.05. It can be seen on these maps that for the entire SGM-SBM-LSB region there is no clear-cut one-to-one relationship between peraluminous plutons and the contours where $\delta^{18}O > +10.0$ per mil. Plutons with ratios greater than 1.05 display a very wide range of $\delta^{18}O$ values, ranging from +7.5 to +10.8 per mil.

Nevertheless, at least in the SBM area, there is a clear indication of a geographic correlation between the Al/(K+Na+Ca/2) parameter and $\delta^{18}O$ (Figure 6.9), most notably in 3 areas along the central axis of the mountain range, west of Running Springs, near Forest Falls, and east of Pioneertown. In these three areas the $\delta^{18}O$ values are all greater than +9.5, and in particular, in an elongate zone to the north of Santa Ana Canyon there is a very good geographic correspondence between the largest area of peraluminous plutons in the SBM and the locations of the highest-^{18}O plutons analyzed in this study ($\delta^{18}O$ up to +10.8). According to the definition of O'Neil and Chappell (1977), these also happen to be the only true "S-type" plutons (i.e., those combining both high $\delta^{18}O$ values and peraluminous compositions) in the Transverse Ranges. All other peraluminous plutons in the combined SGM-SBM-LSB region would probably be classified as "I-type" based on their low $\delta^{18}O$ values and their relatively low Al/(K+Na+Ca/2) ratios. For example, this statement applies to the muscovite granites in Cushenberry Canyon in the SBM area and the White Tank Quartz Monzonite of the LSB area, all of which are only mildly peraluminous.

As a generalization, we can draw the following conclusions: (1) The $\delta^{18}O$ values tend to be low (+7.0 to +8.5) in peraluminous plutons from the eastern parts of the Transverse Ranges, where the country rocks are made up of abundant Precambrian cratonal basement. These occurrences are

thus analogous to those in the Mojave Desert area described below in Section 7.4, as well as in the southern Arizona area discussed previously in Section 5.6; all of these "highly differentiated," SiO_2-rich plutons have $\delta^{18}O$ values that are very low, indicating that they are almost certainly not derived from an "S-type" source. (2) On the other hand, the $\delta^{18}O$ values of peraluminous plutons from areas west of the mapped outcrops of Precambrian basement rocks all tend to be high ($+9.5 < \delta^{18}O < +10.8$), and these would indeed fit the O'Neil-Chappell definition of an S-type pluton. At the present time, plutons with this combination of very high $\delta^{18}O$ and peraluminous character are known to occur only in southern California in the San Bernardino Mountains (Figure 6.9) and perhaps very locally in the Peninsular Ranges batholith (Taylor and Silver, 1978; Todd and Shaw, 1985).

CHAPTER 7. $^{18}O/^{16}O$ COMPOSITIONS OF MESOZOIC AND EARLY TERTIARY PLUTONS IN THE MOJAVE DESERT OF SOUTHEASTERN CALIFORNIA

7.1 Introduction

This chapter describes the general geology, geochronology, and oxygen isotope geochemistry of the Mojave Desert region of southeastern California (SECA). Figure 7.1 is an index map that shows the major geographic features of the study area. The area is bounded on the east by the Colorado River, on the south by latitude 33°45'N, on the west by the Transverse Ranges and the other localities discussed in Chapter 6, and on the north by latitude 35°N; it occupies the southern portion of the Mojave Desert.

The Mojave Desert portion of the SECA study area is divided into two major sampling regions (see Figure 6.1): (1) the Rodman-Ord Mountains (ROM) area, and (2) the Southeastern Mojave Region (SMR). Both $^{18}O/^{16}O$ and major-element analyses are discussed for plutons in the SMR region. No major-element data are available for plutons in the ROM region. Later, in Chapter 8, we present a synthesis of the regional aspects of $\delta^{18}O$ in the Mojave Desert plutons, integrating this with data from the Central and Eastern Transverse Ranges, and from the Peninsular Ranges batholith.

7.2 Regional Geologic Setting

Figure 7.1 is a generalized geologic map of the Mojave Desert region, showing the distribution of crystalline basement outcrops. Mesozoic plutonic and volcanic rocks form a northwest-trending continental magmatic arc that intrudes both the craton and a section of late Precambrian to Paleozoic sedimentary and volcanic rocks (Burchfiel and Davis, 1981a;

Figure 7.1 Generalized geologic map of the Mojave Desert region of southeastern California (SECA), showing pre-Cenozoic geology and whole-rock $\delta^{18}O$ contours for late Cretaceous granitic plutons. The $\delta^{18}O$ contours are based on the $^{18}O/^{16}O$ data given in Table 1 (Appendix), and shown on Figures 7.2, 7.3, 7.5, 7.6, and 7.7. Late Cretaceous $^{18}O/^{16}O$ sampling localities (solid circles) in the southeastern Mojave Region (SMR) are shown on this figure; Cretaceous localities in the Rodman-Ord Mountains (ROM) area are shown on Figures 7.2 and 7.3. Geology after Bishop (1963); Bortugno and Spittler (1986); and K. Howard, B. John and C.F. Miller (unpublished mapping of Needles 2° sheet, California): (1) late Cretaceous granitic plutons, shown by stippled pattern along inside margins of map unit; (2) Jurassic granitic plutons, shown by cross-pattern along inside margins of map unit; (3) Triassic monzonitic pluton (located in the southwestern ROM area) shown by small circle-patterns along the inside of the map unit; (4) Mv - early Mesozoic volcanic and sedimentary rocks; (5) P - Paleozoic sedimentary rocks; (6) PGc - Precambrian crystalline basement; and (7) M - gneisses and mylonitic gneisses of uncertain age.

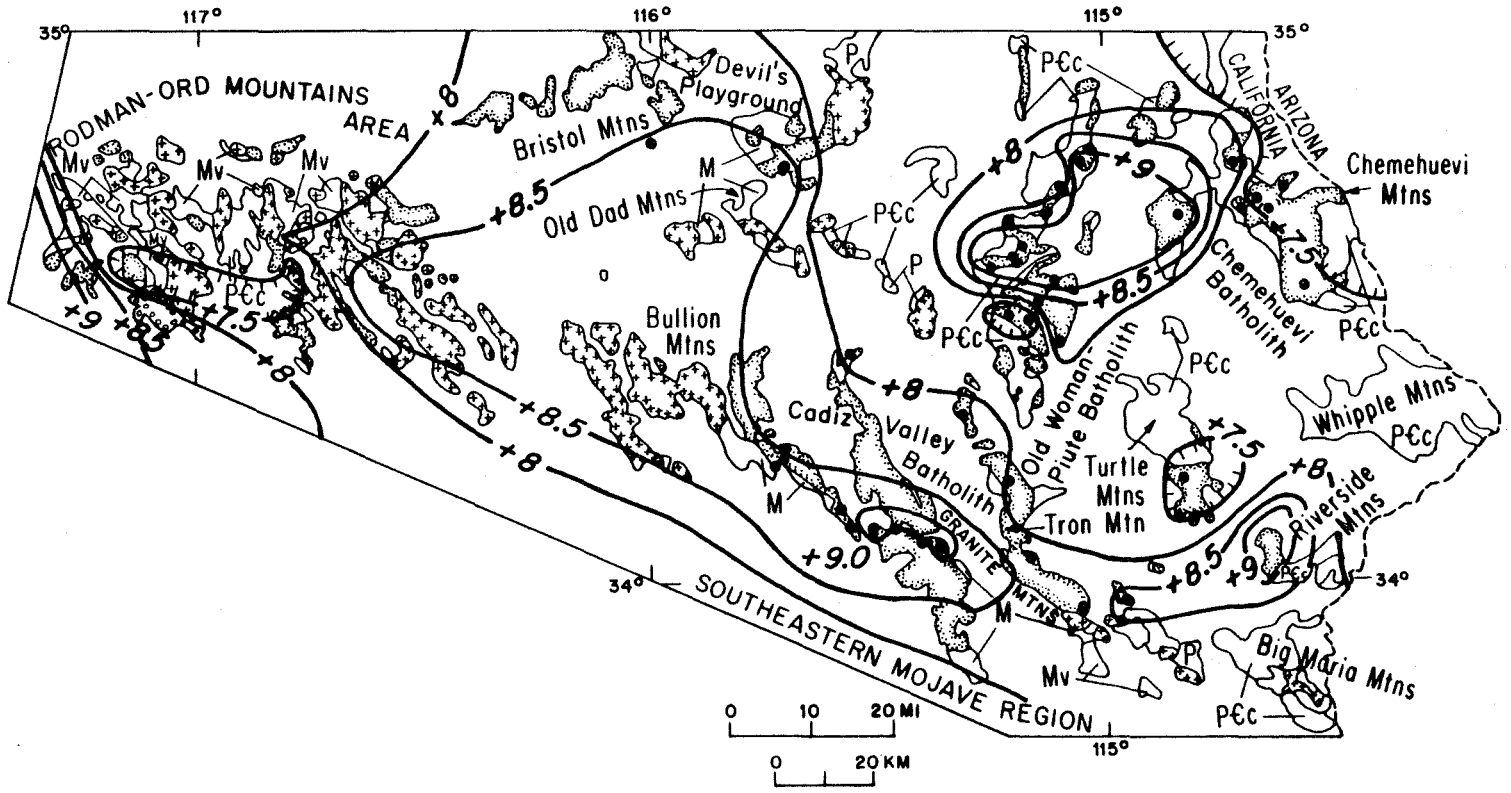
117°
116°
115°
35°
34°
RODMAN-ORD MOUNTAINS AREA
Devil's Playground
Bristol Mtns
Old Dad Mtns
Bullion Mtns
Cadiz Valley Batholith
Old Woman-Piute Batholith
Chemehuevi Batholith
Chemehuevi Mtns
Turtle Mtns
Tron Mtn
Whipple Mtns
Riverside Mtns
Big Maria Mtns
GRANITE MTNS
SOUTHEASTERN MOJAVE REGION
CALIFORNIA
ARIZONA
Mv
M
P
PEc
+7.5
+8
+8.5
+9
+9.0
0 10 20 MI
0 20 KM

Miller, 1978; John, 1981). The volcanic units of the arc interfinger with Mesozoic marine sedimentary units to the west, and interfinger with nonmarine, back-arc sedimentary rocks to the east. Mesozoic plutonism is characterized by at least 3 separate magmatic episodes: (1) sparsely outcropping Permo-Triassic monzonite and granodiorite; (2) epizonal Jurassic granodiorite and quartz monzonite; and (3) widespread late Cretaceous granodiorite and quartz monzonite.

The Jurassic plutons commonly show intense hydrothermal alteration, and in places are mineralized. In particular, the area underlain by Jurassic plutons around the Ord Mountains exhibits the sort of $^{18}O/^{16}O$ relationships that are characteristic of most fossil meteoric-hydrothermal systems throughout the world, such as are found in Tertiary volcanic centers like the Eocene parts of the Idaho Batholith (Taylor, 1978; Criss and Taylor, 1983).

Late Cretaceous plutonism in the Mojave Desert was locally accompanied by emplacement of muscovite-bearing granites, and in places developed pegmatitic facies. No volcanic carapace has been mapped for the Cretaceous episode of magmatism, and in general that plutonic episode appears to have been relatively deep-seated.

Prior to the episode of Mesozoic plutonism and arc-related sedimentation, the region was the site of late Precambrian miogeoclinal sedimentation. This locally evolved to cratonic, shelf-type sedimentation during the Paleozoic (Stewart, 1980; Burchfiel and Davis, 1981a). The platform on which this sedimentation occurred is comprised of 1.7 to 1.8 Ga metasedimentary and meta-igneous rocks with locally exposed ~1.4 Ga and ~1.1 Ga intrusives (Silver et al., 1977a). These latter units are similar to the rocks that lie immediately to the east of the southwestern

edge of the North American Precambrian craton. The edge of the craton is composed of rocks that are similar to the Precambrian crystalline basement discussed in Chapter 6.

The major structural features of the Mojave Desert area are Mesozoic and Cenozoic in age. The Mesozoic features include the proposed mid-Jurassic left-lateral shear zone (Mojave-Sonora megashear of Silver and Anderson, 1974), as well as episodes of late Cretaceous to early Tertiary mylonitization and thrusting that occurred in concert with the waning stages of Mesozoic magmatic activity. The location of the proposed megashear to the north of Yuma, Arizona is not well known, but it trends into the southern portion of the SMR study area (L.T. Silver, pers. comm.). Powell (1982) earlier concluded that the megashear might lie between the Baldwin gneiss of the San Bernardino Mountains and the Joshua Tree Terrane of the Little San Bernardino Mountains, but more recently he questions whether the megashear is present in this region (Powell, 1986a,b).

Late Cretaceous mylonitization and thrusting are well documented in the Cadiz Valley and Old Woman Mountains, and link the SMR portion of the study area to the areas discussed in Chapter 5 of this thesis, namely the Eastern Metamorphic Belt described by Miller and Bradfish (1980) and Haxel et al. (1984).

In contrast with the Central and Eastern Transverse Ranges (discussed in Chapter 6), the lower plate rocks associated with late Cretaceous mylonitization and thrusting in southeastern California are not Mesozoic schists, but are composed of mylonitized roof zones of late Mesozoic plutons that show ductile deformation below the zone of mylonitization (e.g., Howard et al., 1982).

The tectonic processes responsible for the immense mobility of upper plate rocks in latest Cretaceous time eventually culminated in the formation of mid-Tertiary metamorphic core complexes (Coney, 1980). Miocene volcanism and related hypabyssal plutonism occur in the central portion of the study area in a northwest-trending belt that extends throughout the Mojave region. These features post-date the igneous events of concern in this thesis, and are not discussed further. Finally, late Cenozoic strike-slip faulting has resulted in relatively small-scale displacements of the crystalline basement within the study area.

7.3 Rodman-Ord Mountains Area (ROM)

7.3.1 Geology and Geochronology

Figure 7.2 is a geologic map showing $^{18}O/^{16}O$ sampling localities and some of the measured $\delta^{18}O$ values for the Rodman-Ord Mountains (ROM) area in relation to major geologic units and structures. Figure 7.3 shows the geology and $\delta^{18}O$ values of the eastern portion of the area in more detail. This eastern region between the Lenwood and Camp Rock faults was sampled in more detail because an initial reconnaissance revealed a large area of "disturbed" $^{18}O/^{16}O$ ratios in the rocks, indicative of a major Jurassic hydrothermal system. A detailed sampling program was therefore undertaken (1) to define the size and characteristics of this area of altered rocks, because no such $^{18}O/^{16}O$ study of a fossil hydrothermal system had ever been carried out in the Mojave Desert region; and (2) to test the possible usefulness of $\delta^{18}O$ studies in determining offset along late Cenozoic faults in the area, by defining the limits of hydrothermal exchange and plotting any offsets of the regional $\delta^{18}O$ contours.

The ROM study area is bounded on the east by the Fry and Rodman Mountains, on the south by the northern range front of the San Bernardino

Figure 7.2 Geologic map of the ROM area, showing Mesozoic batholithic rocks, pre-batholithic country rocks, late Cenozoic strike-slip faults and whole-rock $\delta^{18}O$ contours on Jurassic intrusive rocks (geology after Bishop, 1963; and Bortugno and Spittler, 1986). The $\delta^{18}O$ contours are based on whole-rock $\delta^{18}O$ values for Jurassic $^{18}O/^{16}O$ sample localities (indicated by solid circles; $\delta^{18}O$ values shown southwest of the Lenwood Fault (LF) on this figure, and shown on Figure 7.3 for rocks northeast of LF; the data are also given in Table 1, Appendix). The late Cretaceous sampling localities are shown on this figure by solid triangles; the Triassic localities are indicated by solid squares. Mesozoic batholithic rocks are indicated according to age of emplacement by different symbols along inside margins of map units: (1) Triassic plutons are shown by small circle patterns; (2) Jurassic plutons are shown by cross patterns; and (3) late Cretaceous plutons are indicated by stippled patterns. Unlabeled outcrops on the map are the pre-batholithic country rocks, and include early Mesozoic silicic pyroclastic units and volcanic flows, Mesozoic sedimentary rocks (discussed in text) and Baldwin Gneiss-equivalent crystalline basement (see Figure 7.1).

Figure 7.3 Geologic map of the northeastern portion of the ROM area, showing Jurassic and Cretaceous granitic plutons, early Mesozoic volcanic units and $^{18}O/^{16}O$ sample localities with whole-rock $\delta^{18}O$ values (geology after Dibblee, 1964c,d; $^{18}O/^{16}O$ data also given in Table 1, Appendix). Geologic map unit and $^{18}O/^{16}O$ sample symbols are the same as those listed above for Figure 7.2; except for (1) Mv - Mesozoic volcanic rocks (described in text); and (2) Mvb - Mesozoic volcanic breccia facies. Late Cenozoic faults are shown by solid heavy lines.

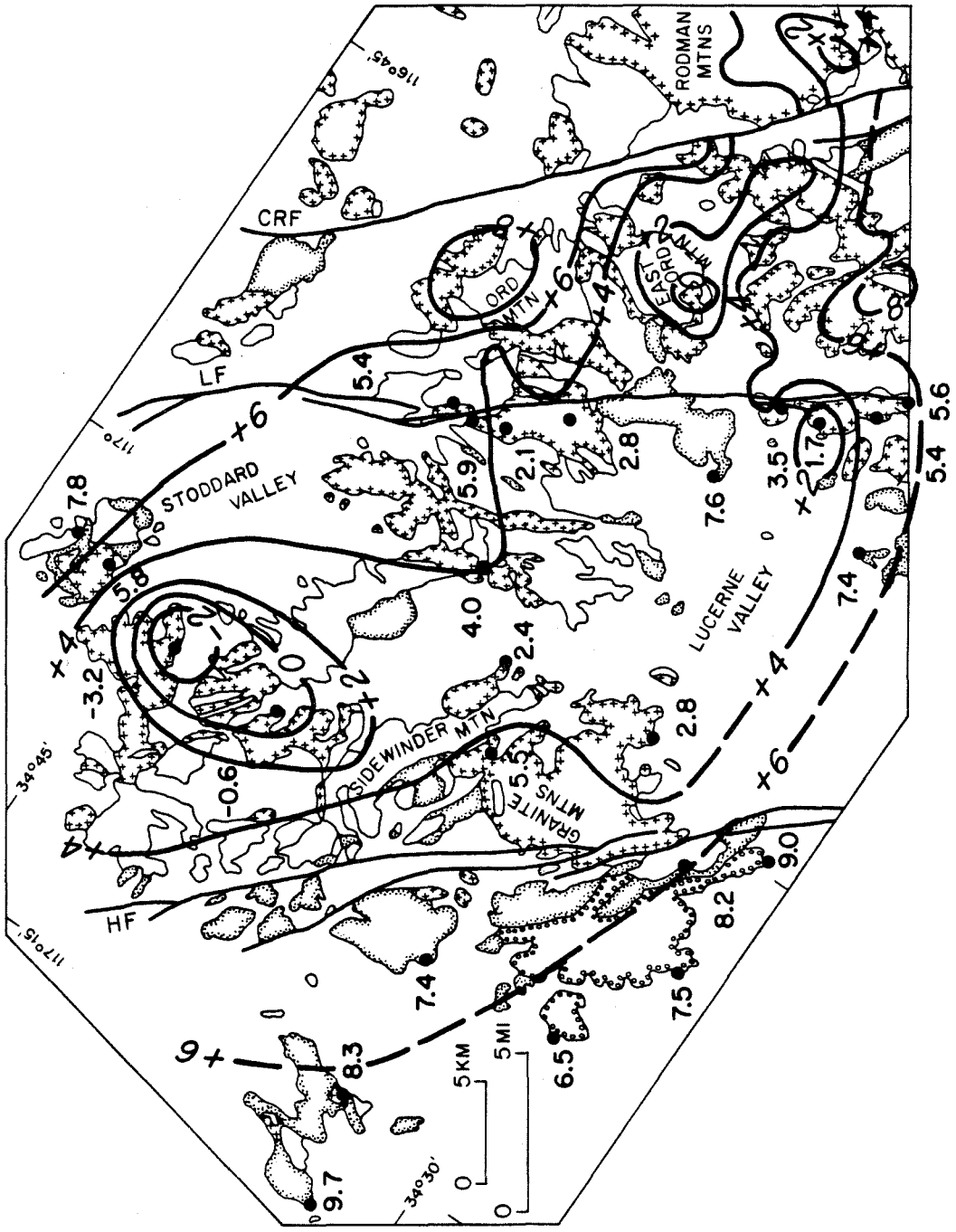
RODMAN MTNS
CRF
ORD MTN
EAST ORD MTN
LF
STODDARD VALLEY
LUCERNE VALLEY
SIDEWINDER MTN
GRANITE MTNS
HF
117°45'
117°
117°15'
34°45'
34°30'
5KM
5MI
0
0
+6
+4
+2
-2
-4
-6
7.8
5.8
5.4
5.9
2.1
2.8
7.6
3.5°
21.7°
5.4
5.6
7.4
4.0
2.4
2.8
-3.2
-0.6
5.5
9.0
8.2
7.4
7.5
6.5
8.3
9.7

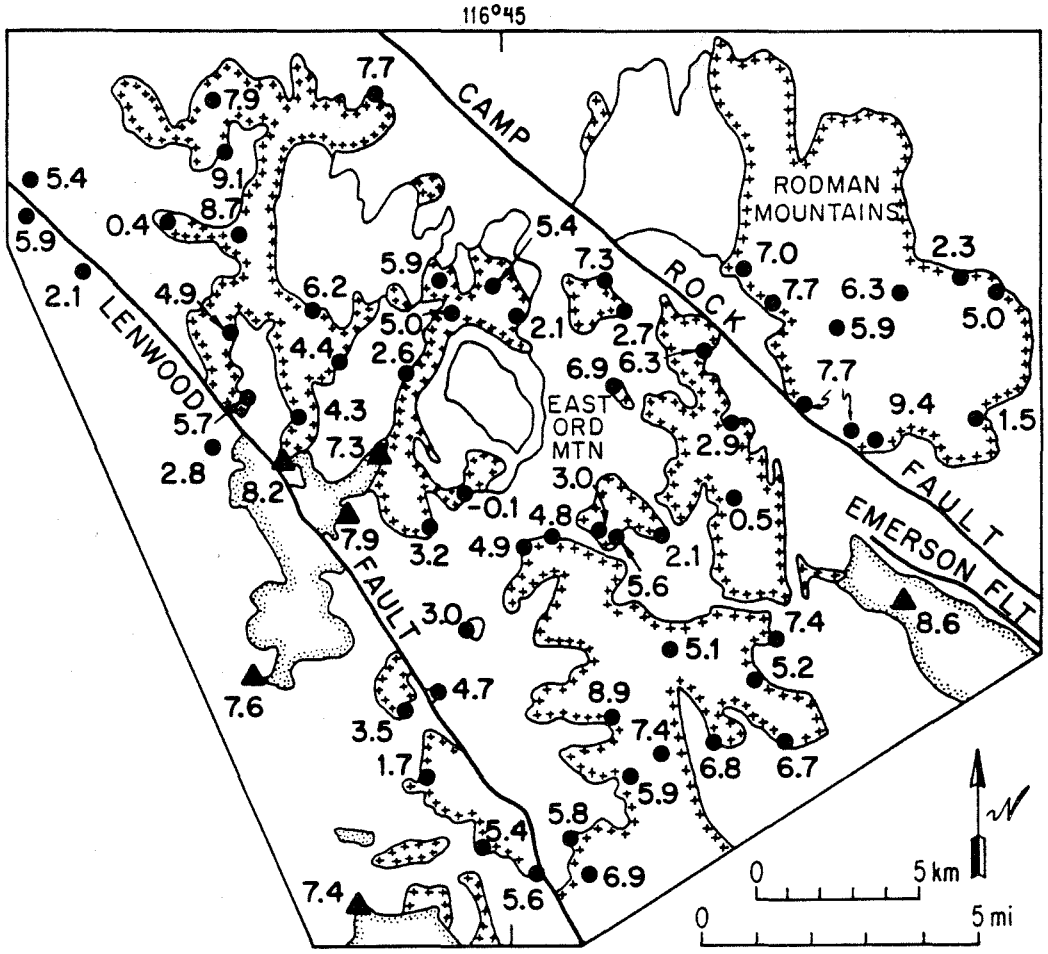
116°45
CAMP ROCK FAULT
LENWOOD FAULT
EMERSON FLT
RODMAN MOUNTAINS
EAST ORD MTN
7.7
7.9
9.1
8.7
0.4
5.4
5.9
2.1
4.9
6.2
5.0
4.4
2.6
5.9
5.4
7.3
2.1
2.7
6.9
6.3
4.3
7.3
5.7
2.8
8.2
7.9
3.2
-0.1
4.8
4.9
3.0
2.1
5.6
0.5
2.9
3.0
7.6
4.7
3.5
1.7
8.9
7.4
5.9
5.8
5.4
6.9
7.4
5.6
7.0
7.7
6.3
2.3
5.0
5.9
7.7
9.4
1.5
8.6
7.4
5.1
5.2
6.8
6.7
0
5 km
0
5 mi

Mountains, on the west by the area immediately around Victorville, and on the north by the Newberry Mountains. The zone of detailed sampling is centered on Ord Mountain, East Ord Mountain, and the Rodman Mountains.

The geology in the ROM area was mapped in reconnaissance by Dibblee (1960a,b,c; 1964c,d; 1967d), Miller (1978), Miller and Carr (1978), and Miller and Cameron (1982). The area is underlain by Mesozoic plutonic rocks that are intrusive into Precambrian crystalline basement, Permo-Triassic(?) volcanic rocks, and Paleozoic and Mesozoic metasediments. The Mesozoic plutonism began in Triassic time with the intrusion of alkalic plutons, but it is dominated by hydrothermally altered Jurassic granodiorites that appear to be associated with a number of propylitized, low-^{18}O ring zones that are aligned along a major northwest-trending lineament. A prominent late-Jurassic(?) latite dike swarm is oriented sub-parallel to this lineament, and cuts the Jurassic plutons and their associated volcanic country rocks.

Late Cretaceous plutons cross-cut the area, but are not affected by either the hydrothermal alteration or by the main group of latite dikes, although several large felsic dike-like bodies may be late Cretaceous in age. Late Cenozoic faults are oriented in a northwest trend, and exhibit right-lateral offsets of local scale (1.5 to 10 km, although possibly as much as 20 km).

The Precambrian crystalline terrane has not been studied in detail. These rocks crop out between Stoddard Ridge and Ord Mountain, and consist of quartz dioritic gneiss, granitic gneiss, and hornblende-biotite schist. Dibblee (1964c) describes these units as being "generally similar to, and presumably correlative with, Precambrian(?) gneissic rocks of the San Bernardino Mountains." Silver et al. (1977a) groups the

gneisses in the ROM area with the North American craton, presumably on the basis that they have similar U-Pb dates as the Baldwin Gneiss (Silver, 1971).

The area was the site of late Precambrian to Paleozoic miogeoclinal sedimentation prior to the intrusion of Mesozoic batholithic rocks. Stewart and Poole (1975) proposed that the Paleozoic section at Quartzite Mountain near Victorville is correlative with strata elsewhere in the southern Great Basin. Miller and Cameron (1982) review the Paleozoic geology, and conclude that the lack of Ordovician through lower Devonian strata in the Sidewinder Mountains suggests that this region may represent the transition from miogeoclinal to cratonal sedimentation.

During early Mesozoic plutonism, the Paleozoic rocks were multiply deformed and metamorphosed. The Triassic(?) alkalic pluton on the east side of Apple Valley in the Granite Mountains was intruded at this time. This pluton is a low-quartz (< 10%), hornblende-bearing monzonite very similar in composition to the alkalic intrusives found in the north-central San Bernardino Mountains. Miller (1977a) reports a U-Pb zircon age of 230 ± 8 Ma for this pluton from a locality near the Granite Mountains, and Miller and Sutter (1981) obtained a ^{40}Ar-^{39}Ar hornblende age of 233 ± 13 Ma on a similar pluton in the Black Mountain area.

Mesozoic sedimentary and volcanic rocks unconformably overlie the Paleozoic section. These consist of shallow marine quartzites interbedded with latite porphyry flows and tuffs. The quartzitic rocks are lithologically correlative with the early Jurassic Aztec Sandstone in the eastern part of the Rodman Mountains area. West of the Granite Mountains, however, these quartzites are older and they are there called the Fairview Valley Formation. These older sedimentary rocks may correlate

with the Triassic Moenkopi Formation and its equivalents in the Mojave region.

The volcanic rocks are known locally as the Sidewinder Volcanics, and consist mainly of latite porphyry and latite porphyry breccia ranging in composition from quartz latite to andesite. Hydrothermal alteration is conspicuous throughout the area, with chlorite and sericite replacing groundmass minerals, and epidote filling fractures and vesicles.

The main episode of Mesozoic plutonism in the ROM area involved the intrusion of Jurassic hypabyssal biotite- and hornblende-bearing granodiorites and less abundant quartz monzonites and granitic stocks. All of these plutons are affected by hydrothermal alteration. The granodiorites are medium to coarse grained and have sphene as an accessory mineral. Chlorite, epidote, and sericite are the common alteration minerals, and in places impart a greenish cast to the rock where feldspar has been pervasively altered. Epidote-filled fractures are common.

On the west flank of Ord Mountain, molybdenum veinlets are locally abundant in intensely altered rocks. Surrounding the flanks of East Ord Mountain is a fine-grained, buff-colored, aplitic quartz monzonite whose outcrop pattern distinctly resembles a "ring structure" about four to five km in diameter (see Figure 7.3). This rock has abundant miarolitic cavities and a myrmekitic texture in thin section, indicating a shallow depth of emplacement.

The final pulse of Mesozoic batholithic activity was the intrusion of late Cretaceous plutons. Medium-grained quartz diorite (not hydrothermally altered on a significant scale) crops out in the area around Bell Mountain near Victorville. Throughout the ROM area, isolated late Cretaceous quartz monzonites intrude the hydrothermally altered Jurassic

rocks, and are not themselves hydrothermally altered except in areas of silicification associated with aplitic-facies rocks.

The late Cretaceous quartz monzonites are medium-grained, mostly equigranular rocks whose main accessory mineral is biotite. These rocks weather in a friable manner by breaking down to separate grains around mounds of outcrop. This serves to distinguish them from the Jurassic plutons, which are generally made up of much tougher rocks that are not readily broken down to friable masses, mainly because of the effects of hydrothermal alteration. An excellent outcrop showing the intrusive contact of a late Cretaceous pluton into Jurassic granodiorite is exposed at the extreme southern tip of Ord Mountain (shown in Figure 7.3).

The exact geochronology of the Jurassic plutons in the ROM area is not well known. For the northern and western portions of the area, minimum K-Ar ages obtained by Miller and Morton (1980) on hornblende are 163 to 186 Ma, and for biotite the ages are between 68 and 134 Ma. Where hornblende and biotite from the same sample are dated, the hornblende shows much older ages than the biotite, with most biotites clustering between 70 and 80 Ma. Clearly, the late Cretaceous thermal event is very important in imprinting biotite K-Ar ages on the Jurassic rocks.

The cluster of biotite ages probably gives a minimum age for the late Cretaceous plutonism, and with dates between 70 and 80 Ma, this event appears to be essentially synchronous with the late Cretaceous plutonism in the San Bernardino Mountains (see Chapter 6). Because the latitic dikes cut the Jurassic granodiorites, the age of dike emplacement must be younger than 163 Ma but earlier than 70 to 80 Ma. The dike swarm may correlate in age with the Independence Dike Swarm of the Owens Valley, which has been dated at around 142 Ma (L.T. Silver, pers. comm.; Chen and Moore, 1982).

Late Cretaceous to early Tertiary mylonitization is not known within the ROM area, which is a unique feature of this area compared with most of the other localities studied in this thesis. It is thus unclear how the area fits into the scheme for southwesterly directed thrusting, as proposed by Silver (1982; 1983). Perhaps the thrust zone is buried. Other than the mid-Tertiary detachment fault in the Newberry Mountains (Dokka and Glazner, 1982), the dominant Cenozoic structural elements in the ROM area are northwest-trending, right-lateral wrench faults, which give rise to the present-day physiography of linear mountain ranges.

The major wrench faults are, from west to east, the Helendale, Lenwood, Johnson Valley, and Camp Rock Faults. The Emerson Fault forms the southeastern extension of the Camp Rock Fault, which dies out near Iron Ridge. These faults are part of the major group of strike-slip faults that have absorbed most of the late Cenozoic deformation in the Mojave Desert block (Dokka, 1983). Dokka (1983) places the timing of movement along the faults as mainly between early Miocene and Pleistocene time.

Figure 7.3 shows the locations of the Camp Rock and Lenwood Faults relative to the detailed $^{18}O/^{16}O$ sampling grid around the Ord and Rodman Mountains. Estimates of offset for the Camp Rock fault range anywhere from 1.5 km to 10 km, and estimates for the Lenwood fault range from 1.5 km to 20 km (Hawkins, 1975; Garfunkel, 1974; Dokka, 1983).

There is a wide disparity between these above estimates, because of the uncertain nature of geologic contacts in the post-Mesozoic volcanic terranes in the region, and because no tightly constrained piercing points have been found in the pre-Tertiary crystalline basement. Knowledge of the actual magnitudes of displacement would be extremely useful in reconstructing the deformation the Mojave Region has experienced.

Values of these displacements, obtained by matching offset $\delta^{18}O$ contours, are discussed below.

7.3.2 $^{18}O/^{16}O$ Data

Figure 7.2 shows the sample locations and $^{18}O/^{16}O$ data for the western part of the ROM area, and Figure 7.3 shows similar data for the more densely sampled eastern part of the area, at a somewhat larger scale. Triassic rocks crop out in the Granite Mountains and at Pitzer Butte; three of these samples have whole-rock $\delta^{18}O$ ranging from +6.5 to +8.0, and one sample from the southern edge of a dike-like extension of the major Granite Mountains pluton has a $\delta^{18}O$ = +9.0. None of these rocks show obvious mineralogic signs of hydrothermal alteration, and it is assumed that these $\delta^{18}O$ values are primary, magmatic values. Note the general similarity of the $\delta^{18}O$ of these Triassic rocks to the values obtained for the Lowe Granodiorite complex (+6.8 to +7.8), a pluton of similar age in the SGM area (Chapter 6).

Late Cretaceous plutons occur as scattered outcrops across the area, but are overshadowed volumetrically by the Jurassic rocks. The Cretaceous rocks do not show any signs of widespread ^{18}O depletion attributable to hydrothermal alteration; except for the most westerly sample near Victorville, which has $\delta^{18}O$ = +9.7, they have whole-rock $\delta^{18}O$ values that range from +7.3 to +8.6. Generalized contours of the whole-rock $\delta^{18}O$ values of these Cretaceous plutons are shown in schematic fashion on Figure 7.1. As in the San Gabriel and San Bernardino Mountains, the pattern of $\delta^{18}O$ contours in the ROM area is characterized in a general way by an eastwardly decreasing $\delta^{18}O$, from +9.7 in the west to values as low as +7.3 and +7.4 in the east. In addition, as was found for the other areas, the higher-^{18}O plutons are generally located adjacent to

outcrops of Paleozoic miogeoclinal sediments, and the eastward decrease in $\delta^{18}O$ corresponds with the appearance of a predominantly cratonic basement around West Ord Mountain.

The most voluminous plutons in the ROM area are Jurassic in age, and they exhibit strong ^{18}O depletions due to hydrothermal alteration. These rocks are associated with volcanic rocks that grade downward into hypabyssal stocks (Dibblee, 1964c,d). Figure 7.2 shows contours of whole-rock $\delta^{18}O$ for these plutons. The zone of ^{18}O-depletion is approximately 60 km in the east-west dimension, and 15 to 30 km in the north-south dimension. The low-^{18}O zone is broadest in the north and west and becomes narrower to the south and east. In detail, the contours define several oval-shaped, "ring-like" patterns within a broad, west-northwest trending zone in which the $\delta^{18}O$ values are all less than +4.0 per mil. Within the elliptical ring zones defined by the +2.0 per mil contours, the rocks are extremely variable in $^{18}O/^{16}O$, and they have $\delta^{18}O$ as low as 0.0 per mil or lower. The lowest value, -3.2 per mil, is obtained just north of Stoddard Ridge in a sericitized dike-like body that intrudes the Sidewinder Volcanics.

The overall size of the ^{18}O-depleted zone and the magnitude of the ^{18}O-depletion are both nearly as large as those discovered by Taylor and Magaritz (1978) and Criss and Taylor (1983) surrounding Eocene batholiths emplaced into the Cretaceous Idaho Batholith. The $^{18}O/^{16}O$ effects in the ROM area are much larger than those reported by Taylor (1971), Larson and Taylor (1986), or Forester and Taylor (1978) around Tertiary hypabyssal stocks in the Western Cascade Range in Oregon or in the San Juan volcanic field of southwestern Colorado. The $\delta^{18}O$ contour patterns in these other areas have been proven to be the result of sub-solidus interaction

between the plutons and low-^{18}O, heated meteoric waters within a hydrothermal circulation system. Therefore, a similar model undoubtedly also applies to the ROM area.

All of these meteoric-hydrothermal systems characteristically require that extremely large quantities of water must flow through highly fractured, permeable rocks, fed from surface recharge in a convection pattern around the plutonic heat source (e.g., see Criss and Taylor, 1986). The low-^{18}O fluids exchange oxygen isotopes with the rocks, producing higher-^{18}O fluid, and by material-balance, an $\delta^{18}O$-depleted rock. The actual magnitude of the effect depends on the initial $\delta^{18}O$ of the water, the $^{18}O/^{16}O$ fractionation factors between minerals and the fluids (which are a function of temperature), and on the overall mass of water that flowed through the system at temperatures where reaction kinetics promote exchange.

Cretaceous plutons in the area cross-cut the altered Jurassic plutons, and the Cretaceous rocks do not exhibit ^{18}O-depletions; therefore, it is clear that the hydrothermal systems responsible for ^{18}O-depletion in the ROM area must have been older than the late Cretaceous plutonism, but either younger or synchronous with the Jurassic plutonism. If this is true, then these rocks represent some of the oldest documented low-^{18}O hydrothermal systems in the Cordillera of North America.

The ROM low-^{18}O zone is coincident with, and subparallel to, a major late Jurassic dike swarm. This low-^{18}O zone very likely continues to the northwest of the map area shown in Figure 7.2, because there is no indication that the zone is narrowing in that direction. Indeed, Busby-Spera (1988) has recently suggested that the ROM area is one of a series of mid-Jurassic volcanic centers and calderas that occupied a continuous

graben depression, more than 1,000 km long, that extended from the central Sierra Nevada Batholith at least as far as the Baboquivari Mountains and Cobre Ridge in southern Arizona (see Chapter 5).

It is therefore tempting to speculate that we may be looking at a very large rift-zone feature that may have been responsible for a whole series of overlapping meteoric-hydrothermal systems, and one which might conceivably be traced much farther to the northwest, as well as to the southeast. We know that the most important deep-seated hydrothermal systems on Earth today are all associated with such rift systems, notably Iceland, Yellowstone, and the mid-ocean ridge spreading centers (e.g., see Taylor, 1988). It would be most interesting to extend the $^{18}O/^{16}O$ study area, and try to follow the ROM low-^{18}O zone along strike to the northwest or to the southeast; in particular, it is important to see whether or not these $^{18}O/^{16}O$ effects correlate with the emplacement of the ~142 Ma Independence Dike Swarm in the Sierra Nevada region (Chen and Moore, 1984). The regional implications of these oxygen isotopic results are discussed more thoroughly in Chapter 8.

The existence of such low-^{18}O fossil hydrothermal systems in Jurassic rocks of the Mojave Desert region has interesting paleogeographic implications. Meteoric waters derived from rainfall or snowfall become increasingly ^{18}O-depleted with decreases in the atmospheric temperature, either as a result of increasing elevation or latitude, or both. Thus, in North America there is a general correlation with distance from the Pacific Coast, because oceanic water vapor, which is the ultimate source of the atmospheric meteoric H_2O, becomes steadily depleted in ^{18}O as the air mass moves to the east and north (e.g., see Sheppard, 1986). Because of this fractionation process, inland regions have relatively lower-^{18}O

surface waters (e.g., < -10.0 per mil), particularly the high, mountainous regions that have low atmospheric temperatures (e.g., Sierra Nevada region, Rocky Mountains).

The feldspar-H_2O $^{18}O/^{16}O$ fractionation data of O'Neil and Taylor (1967) allow some simple comparative calculations to be made. Between 300°C and 400°C, which are likely hydrothermal temperatures, the equilibrium fractionation factors for An_{30}-water are estimated at +4.8 (300°C), +3.5 (350°C), and +2.55 (400°C). Even if we conservatively assume an infinite water/rock ratio, the observed $\delta^{18}O$ value of -3.2 in sample 164-80 would require an initial $\delta^{18}O$ at least as low as -8.0 to -5.8 for the hydrothermal fluid. The actual $\delta^{18}O$ values of the surface waters in this region during Jurassic time therefore must be at least this low, and were probably lower than -10.. However, studies of the Mesozoic sedimentary rocks near Fairview Valley suggest that the environment was coastal in nature during the Jurassic (Burchfiel and Davis, 1981a; Miller, 1978; Miller and Carr, 1978). If true, the Jurassic edge of the continent must have been a rather high mountainous region somewhat similar to the present-day geographic environment, in order to produce meteoric waters having $\delta^{18}O$ values as low as -10. To give a more specific comparison, this area could not possibly have had a climate or a topography similar to that in the Gulf Coastal Region of the U.S.A. today. The fossil hydrothermal systems in this area clearly deserve more detailed study than was possible in this reconnaissance $^{18}O/^{16}O$ investigation.

7.3.3 Late Cenozoic Fault Offsets

Late Cenozoic faults cut through and offset the plutons that were affected by the Jurassic hydrothermal circulation systems. Dokka (1983) comments upon the disparate estimates for the magnitudes of offset along

these faults. In order to see if $\delta^{18}O$ contours could be of use in unraveling fault offsets, the area around East Ord Mountain and the Rodman Mountains was studied in somewhat more detail than the rest of the area. It is clear that the primary igneous $\delta^{18}O$ values in the late Cretaceous plutonic rocks do not have a large enough variation to be used for detailed local contouring. However, it was hoped that more closely-spaced sampling of the Jurassic rocks would give sufficient contour resolution to detect any offsets of these fossil hydrothermal circulation centers along the Lenwood and Camp Rock faults.

Figure 7.4 is a map showing a more detailed set of Jurassic $\delta^{18}O$ contours in the vicinity of the Camp Rock and Lenwood faults. These northwest-trending faults are known to exhibit right-lateral offsets (Dokka, 1983). From the contours in Figure 7.4 it is not possible to accurately determine offset along the Lenwood fault, but it is probably very small (<5 km), as there is no obvious offset of the major trend of the regional low-^{18}O zone shown in Figure 7.2. As one crosses over to the east side of the Lenwood fault, this broad zone of low-^{18}O rocks (Figure 7.2) narrows abruptly, but there are simply not enough outcrops of altered Jurassic plutons to establish detailed contouring. The low-^{18}O zone continues to narrow eastward, however, and on Figure 7.4 it can be seen that the Camp Rock fault truncates a much narrower, better-defined, and more prominent low-^{18}O "ring" structure in the $\delta^{18}O$ contours. Surrounding East Ord Mountain, and extending with its long axis in an easterly direction, is an ovoid contour pattern defined by rocks with $\delta^{18}O < 3.0$ per mil. The low-^{18}O ovoid zone abruptly terminates on its eastern end, against the Camp Rock fault, and these low-^{18}O rocks are juxtaposed against a Jurassic pluton where the $\delta^{18}O$ values are all higher than +7.7 (Figures 7.3 and 7.4).

Figure 7.4 Geologic map of the northeastern portion of the ROM area (geology after Dibblee, 1964c,d), showing Jurassic whole-rock $\delta^{18}O$ contours based on $^{18}O/^{16}O$ data in Figure 7.3 (also listed in Table 1, Appendix). The Jurassic $^{18}O/^{16}O$ sample localities are shown with solid circles; late Cretaceous sampling localities are shown with solid triangles. Symbolism for geologic map units is the same as in Figure 7.3. The diagonal line pattern indicates areas where whole-rock $\delta^{18}O$ values are less than +2 per mil. Right lateral offset of $\delta^{18}O$ contours (< +3 per mil) along the Camp Rock Fault is approximately 4 km (see discussion in text).

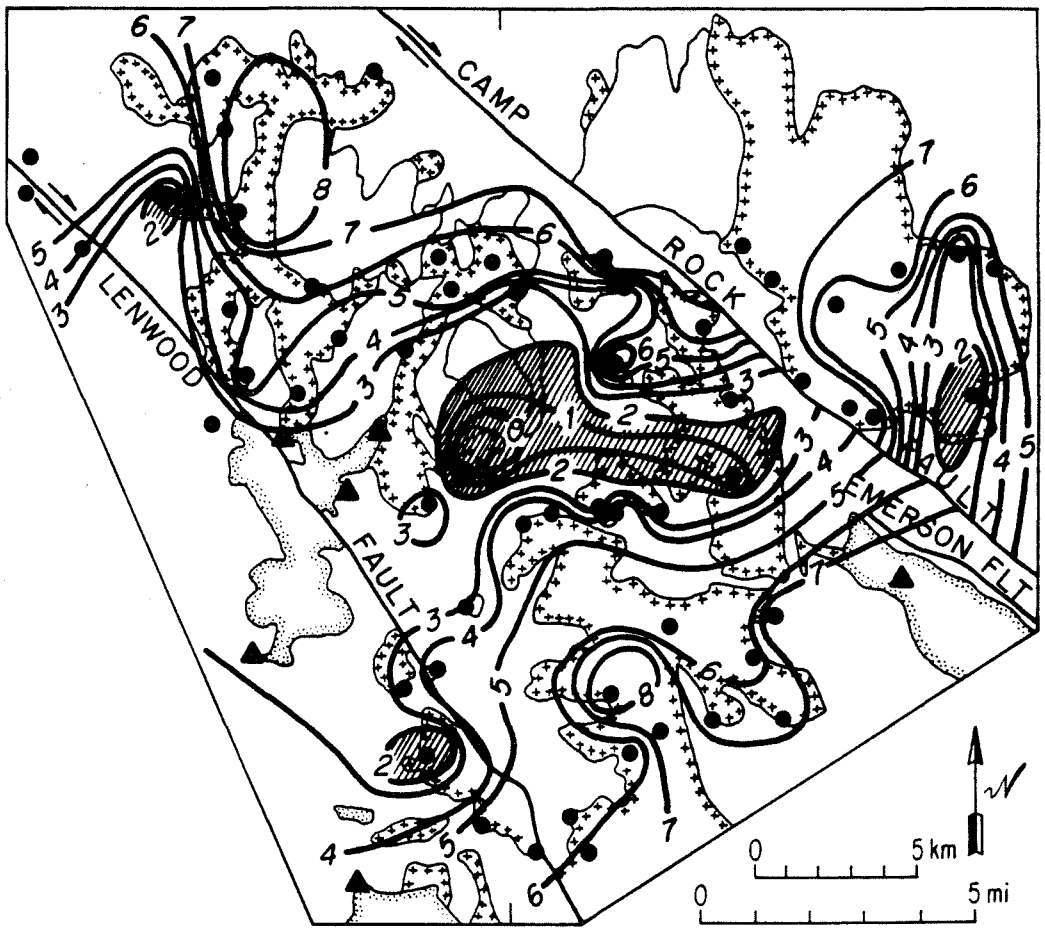
CAMP
ROCK
LENWOOD
FAULT
EMERSON FLT
FAULT
N
0
5 km
0
5 mi

Contouring of $\delta^{18}O$ values in the Rodman Mountains to the east of the fault reveals another zone where $\delta^{18}O$ values are less than 3.0 per mil. If the $\delta^{18}O$ contours that define these two zones are extended to intersect the Camp Rock fault (as shown in Figure 7.4), then the magnitude of apparent right-lateral offset on the combined Emerson and Camp Rock faults is seen to be approximately 5 ± 2 km. Considering the errors involved, this compares well with Dokka's (1983) estimate of 1.6 to 4.0 km, which is based upon offset of an early Miocene structural horizon. We note, however, that our minimum suggested displacement of about 3.0 km seems to be very tightly constrained by 3 closely-spaced samples with $\delta^{18}O$ = +7.7 to +9.4 collected just northeast of the Camp Rock fault. The $^{18}O/^{16}O$ data corroborate, at least on the Camp Rock fault, Dokka's hypothesis that offsets along these strike-slip faults in the ROM area are relatively small, and that large interior translations in this portion of the Mojave Block have not occurred.

7.4 Southeastern Mojave Region (SMR)

7.4.1 Geology and Geochronology

Figure 7.5 is a map of the Southeastern Mojave Region (SMR) showing the generalized geology of the area, our sample localities, and some of the $\delta^{18}O$ analyses. The SMR extends from the eastern edges of the ROM and LSB areas (see Figure 6.1) to the Colorado River at the Arizona border. Dibblee (1967a, 1967b, 1967c) mapped the geology of the extreme western portion of the area in reconnaissance fashion. Farther east, recent geologic studies compiled by Frost and Martin (1982) have vastly improved on the earlier geologic mapping shown in the compilations of Bishop (1963), and Jennings (1967).

Figure 7.5 Generalized geologic map of the southeastern Mojave Region (SMR), showing major mountain ranges, Mesozoic granitic plutons, and $^{18}O/^{16}O$ sampling localities (geology after Bishop, 1963; and unpublished mapping by K. Howard, B. John and C.F. Miller in the area of the Needles 2° California State Map). The $^{18}O/^{16}O$ localities are shown by solid circles. For localities outside of areas outlined by light dashed lines, the whole-rock $\delta^{18}O$ values are listed beside the sample locality, and also given in Table 1 (Appendix). Light dashed lines outline areas of the Cadiz Valley and Old Woman-Piute-Chemehuevi Batholiths, with geology, sample localities, and $\delta^{18}O$ values shown in more detail in Figures 7.6 and 7.7. Mesozoic granitic plutons are indicated according to age of emplacement by different patterns along the inside margins of map units: (1) late Cretaceous granitic rocks (stippled pattern); and (2) Jurassic granitic rocks (cross-pattern).

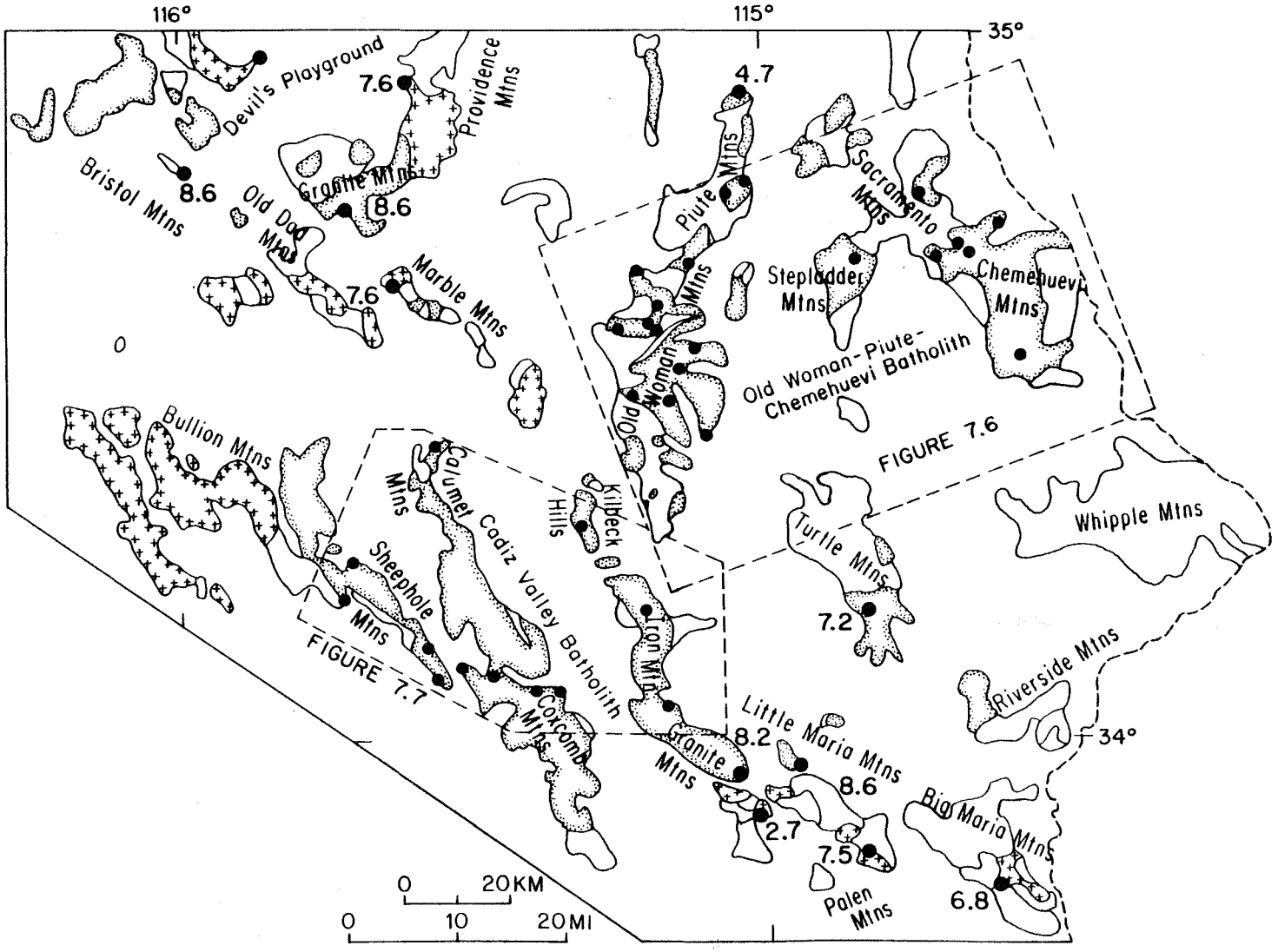
116°
115°
35°
Devil's Playground
7.6
Providence Mtns
Bristol Mtns
8.6
Old Dad Mtns
Granite Mtns
8.6
7.6
Marble Mtns
4.7
Piute Mtns
Sacramento Mtns
Stepladder Mtns
Chemehuevi Mtns
Old Woman Mtns
Old Woman-Piute-Chemehuevi Batholith
FIGURE 7.6
Bullion Mtns
Calumet Mtns
Cadiz Valley Batholith
Kilbeck Hills
Sheephole Mtns
FIGURE 7.7
Iron Mtn
Granite Mtns
8.2
Turtle Mtns
7.2
Whipple Mtns
Riverside Mtns
34°
Little Maria Mtns
8.6
2.7
7.5
Big Maria Mtns
6.8
Palen Mtns
Corcomb Mtns
0 20KM
0 10 20MI

The SMR contains isolated mountain ranges separated by wide (10 to 30 km) alluvium-filled valleys. The area is underlain by crystalline basement ranging in age from early Proterozoic through to late Cretaceous and early Tertiary. The major tectonic and petrologic elements consist of (1) Precambrian metasediments and batholithic rocks that comprise part of the North American craton, and which have a northeast-trending tectonic fabric; (2) late Precambrian to Paleozoic shelf and miogeoclinal sediments; and (3) the northwest-trending Mesozoic continental magmatic arc.

In the SMR, Miocene volcanic rocks locally make up the upper portions of metamorphic core complexes where allochthonous younger rocks are thrust over older autochthonous crystalline basement (e.g., the Whipple Mountains; Coney, 1980; Davis, 1980). These mid-Tertiary core complexes are geologically very interesting, and they merit more detailed $^{18}O/^{16}O$ and D/H studies. However, they are not discussed further in this thesis because the scope of this study centers on the origin of the older Mesozoic plutonic terranes.

The Precambrian terrane consists of 1700-1800 Ma eugeoclinal metavolcanic and metasedimentary rocks that extend from southeastern California northeastward at least as far as the Front Range of Colorado (Silver et al., 1977a). These schists and paragneisses are intruded by granitic plutons that closely post-date the formation of the metasediments. Silver et al. (1977a) dated zircons in paragneiss and orthogneiss at 1730 to 1770 Ma, and 1700 to 1740 Ma, respectively. Burchfiel and Davis (1981a) note that these rocks crop out in the Marble Mountains, and Miller et al. (1982) describe analogous rocks in the Old Woman Mountains.

In the Old Woman-Piute Mountains (Figure 7.6), the Precambrian rocks consist of granodioritic augen gneiss, amphibolite, metagraywacke, meta-

Figure 7.6 Geologic map of the late Cretaceous Old Woman-Piute-Chemehuevi Batholith, showing geographic features, sample localities, and whole-rock $\delta^{18}O$ contours; $\delta^{18}O$ values are shown adjacent to each sample locality, as well as in Table 1 (Appendix). The plutons of the batholith are subdivided according to lithology by different patterns along the inside margins of the map units: (1) older granodiorite (small random-line pattern); and (2) younger muscovite-biotite granite (stippled pattern). Plutons in the Old Woman Mountains are labeled (after Miller et al., 1982): (1) LDP - Lazy Daisy Pluton; (2) SWWP - Sweetwater Wash Pluton; (3) RP - Rattlesnake Pluton; (4) OWP - Old Woman Pluton. Geology is based on Bishop (1963); Miller et al. (1982); and John (1982).

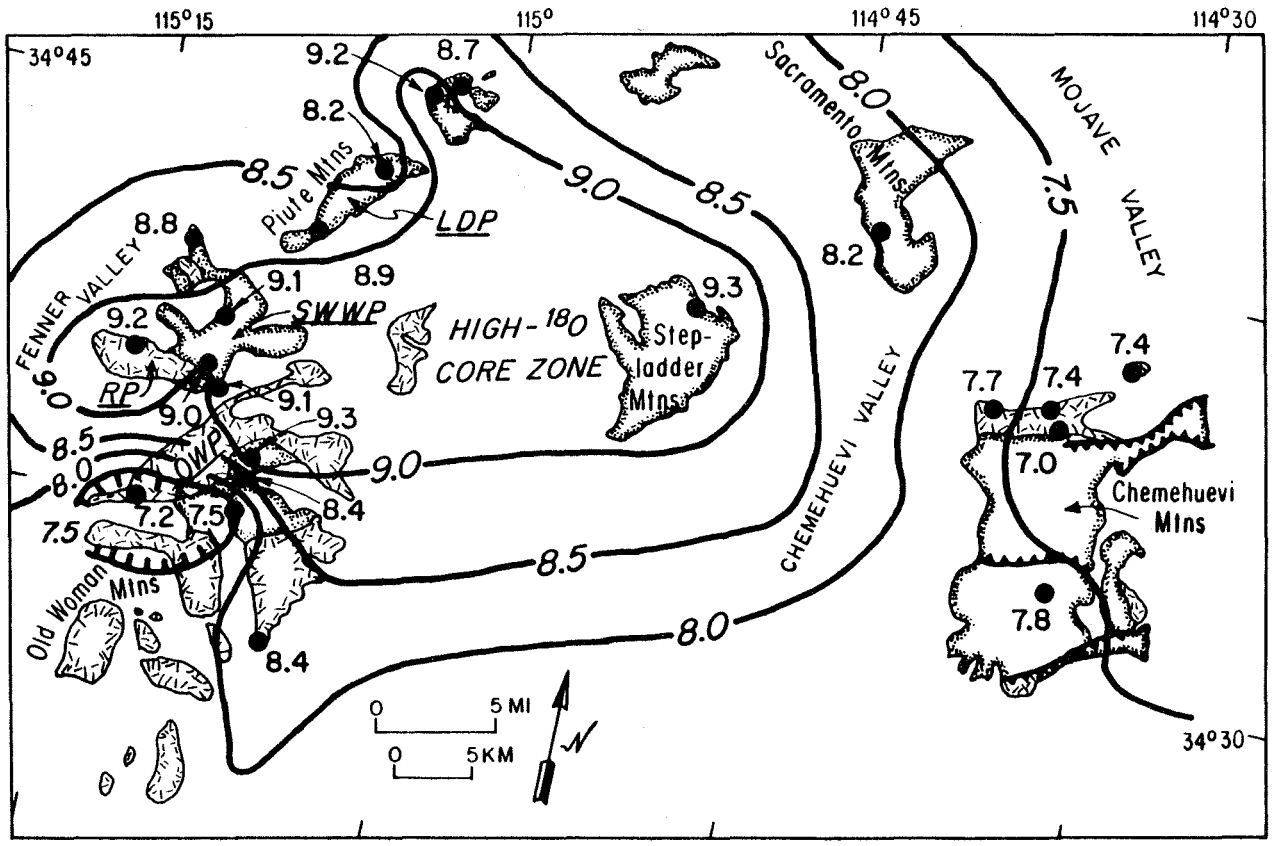
115°15
115°
114°45
114°30
34°45
34°30
9.2
8.7
8.2
8.5
9.0
8.5
8.0
7.5
Piute Mtns
LDP
8.8
9.1
8.9
SWWP
9.2
HIGH-180
CORE ZONE
9.3
Step-
ladder
Mtns
RP
9.1
9.0
9.3
8.5
OWP
9.0
8.0
7.2
7.5
8.4
7.5
8.5
8.0
8.4
Old Woman Mtns
Sacramento Mtns
8.2
MOJAVE
VALLEY
FENNER VALLEY
CHEMEHUEVI VALLEY
7.7
7.4
7.4
7.0
Chemehuevi
Mtns
7.8
0
5 MI
0
5KM
N

pelite, and quartzo-feldspathic paragneiss. Miller et al. (1982) report a Rb/Sr age of 1750 Ma for the orthogneiss, with an initial $^{87}Sr/^{86}Sr$ of 0.7020. The structurally lowest portions of the terrane are characterized by migmatized gneiss with pods and segregations of Mesozoic granite as large as 1 km across (K.A. Howard, pers. comm.; Miller et al., 1982).

Other areas that contain outcrops lithologically similar to the ortho- and paragneiss in the Old Woman Mountains are the Chemehuevi, Whipple, and Turtle Mountains (John, 1982; Davis et al., 1980; Howard et al., 1982). Tosdal (1982) and Hamilton (1982) describe Precambrian gneiss and schist in the Mule Mountains and Big Maria Mountains in the southern and southeastern portion of the SMR. No detailed radiometric ages are published for these units, and it is not certain whether the gneisses of the Big Maria Mountains have affinities with those of the old Woman Mountains.

The older Precambrian gneiss and schist are, in several ranges, intruded by a distinctive suite of anorogenic granitic rocks, which are part of a northeast-trending belt that extends from southeastern California to Labrador. Zircons from these rocks yield U-Pb ages in the narrow interval 1410 ± 25 Ma in both the Marble Mountains and the Big Maria Mountains (Silver et al., 1977b; Lanphere, 1964; Hamilton, 1982). Granitic rocks with similar ages are found throughout southeastern California and in central and southern Arizona, and they are an important part of the upper crust in the southwestern Cordillera (Burchfiel and Davis, 1981a; Silver et al., 1977b; Conway, 1977).

Regionally metamorphosed and deformed Paleozoic strata occur as isolated outcrops in several SMR mountain ranges. These include the Big Maria, Little Maria, Riverside, Palen, and Arica Mountains in the south-

eastern part of the area, and the Old Woman, Piute, Little Piute, Bristol, Ship, Marble, Calumet, and Providence Mountains, as well as the Fenner and Kilbeck Hills, in the north-central portion of the area (Figures 7.5, 7.6, and 7.7). The geology of these areas is discussed by Hamilton (1982), Emerson (1982), Lyle (1982), Baltz (1982), and Miller et al. (1982). Throughout the region, these Paleozoic rocks unconformably overlie Precambrian basement.

The southeastern SMR exposures are the metamorphosed equivalents of the cratonal Paleozoic sequence of the western Grand Canyon, Arizona (Stone et al. (1980). In the north-central part of the SMR, the Paleozoic strata can be directly correlated with the Grand Canyon section, but they have features that are transitional between cratonal and miogeoclinal sedimentation (Burchfiel and Davis, 1981a; Stone et al., 1980). These features include development of upper Precambrian terrigenous units and westward thickening. The Marble Mountains and Kilbeck Hills sections display a cratonal character. The Providence Mountains contain miogeoclinal upper Precambrian units beneath the Cambrian Tapeats Sandstone. However, the boundary between the Cambrian and the middle Devonian Sultan Formation is unconformable in the Providence Mountains; thus the section at that locality shows cratonal affinities. Miogeoclinal sections farther west contain Ordovician rocks below this unconformity.

The Paleozoic section in the Old Woman Mountains has equivalents in the Marble, Ship, and Providence Mountains that indicate the original section was between 1 and 3 km thick. The rocks are now metamorphosed and deformed such that only 5 to 50% of the original thickness remains (Miller et al., 1982). In sequence, the units consist of basal quartzite (Tapeats Sandstone), pelitic schist and minor carbonate (Bright Angel

Figure 7.7 Geologic map of the late Cretaceous Cadiz Valley Batholith, showing geographic features, sample localities, and whole-rock $\delta^{18}O$ contours; $\delta^{18}O$ values are shown adjacent to each sample locality, as well as in Table 1, appendix). The plutons of the batholith are subdivided according to lithology by different patterns along the inside margins of the map units: (1) granodiorite (single random-dash pattern); (2) porphyritic granodiorite (double random-dash pattern); and (3) muscovite-biotite granite (stippled pattern). Geology is based on John (1981) and Howard et al. (1982).

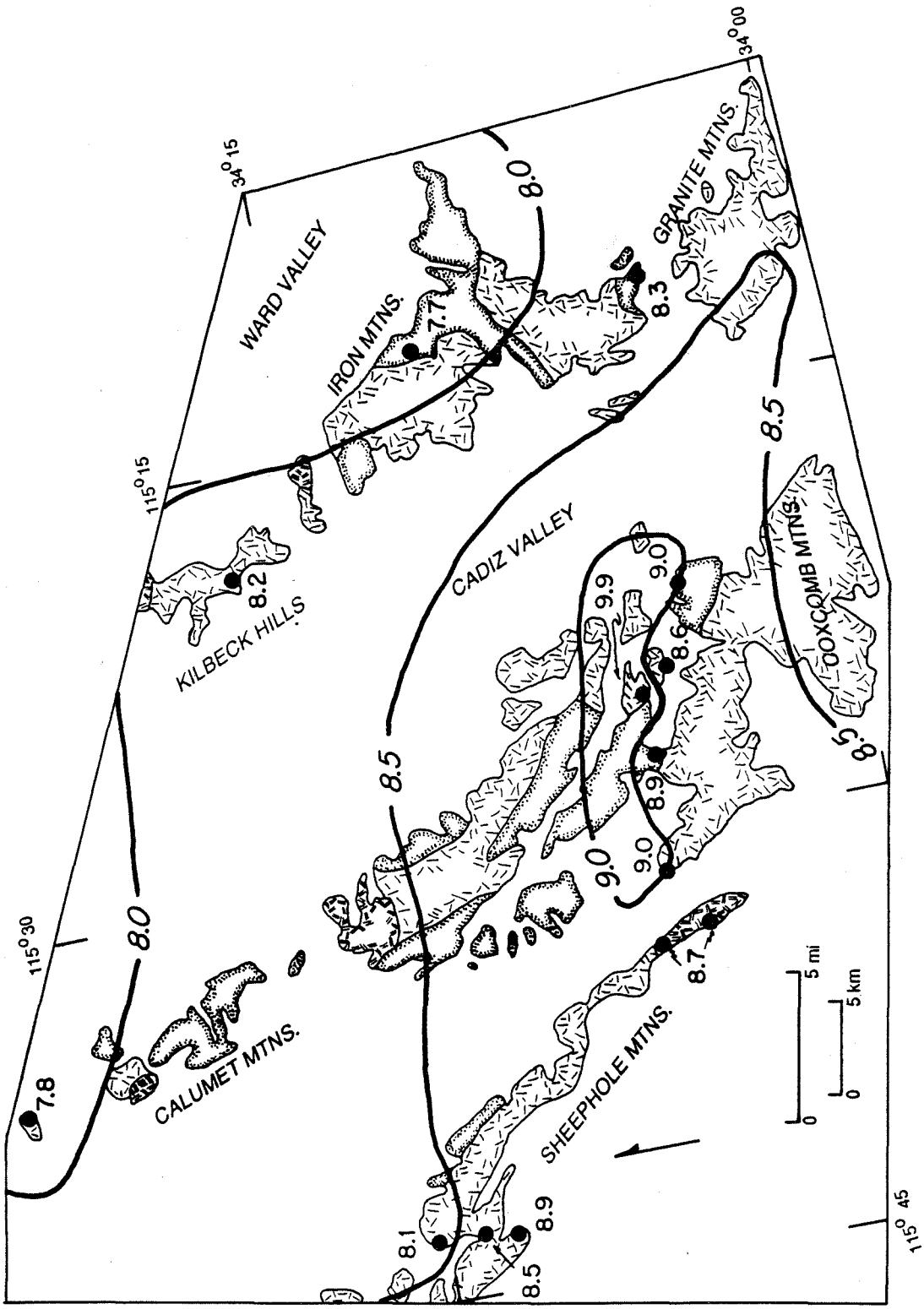
34°00
34°15
115°15
115°30
115°45
WARD VALLEY
IRON MTNS.
GRANITE MTNS.
KILBECK HILLS
CADIZ VALLEY
COXCOMB MTNS.
CALUMET MTNS.
SHEEPHOLE MTNS.
8.0
8.5
9.0
7.7
8.3
8.2
9.9
8.6
8.9
8.7
7.8
8.1
8.9
8.5
0
5 mi
0
5 km

Shale), banded marble (lower Bonanza King Formation), dolomitic marble (upper Bonanza King Formation, Nopah Formation, and Sultan Limestone), and finally a series of limestones and dolomites of Mississipian through Permian age.

The Bright Angel Shale equivalents show well developed regional metamorphic zones in the Old Woman-Piute Mountains (Hoisch et al., 1988; Miller et al., 1982). The highest metamorphic grades occur in the core of the range (sillimanite plus potassium feldspar). Northward, the grade decreases to andalusite- and staurolite-grade. Based upon the intersection of univariant aluminosilicate stability curves and dehydration curves for biotite and muscovite, Miller et al. (1982) estimate that peak metamorphic conditions occurred between 515°C and 685°C, and between 3.3 to 5.0 kbars (with total pressure equal to water pressure). Miller et al. (1982) propose that in the core of the range, development of migmatized banded gneiss occurred essentially synchronously with metamorphism of the Bright Angel shale and intrusion of late Cretaceous plutons.

In the SMR widespread late Cretaceous to early Tertiary mylonitization has affected many of the late Mesozoic batholithic rocks. This deformation predates the mid-Tertiary detachment faulting, and in part appears to have occurred essentially synchronous with pluton emplacement. This represents a fundamentally different tectonic style than the mylonitic zones in the Central and Eastern Transverse Ranges, where cataclasis occurred in the structurally lowest portions of the plutons (see Chapter 6). This difference may have regional importance, given the hypothesis of Silver (1982; 1983) that there has been large-scale southwestward thrusting of the batholithic terranes. However, Howard et al. (1982) conclude that most of the SMR mylonites formed as part of the mechanics of pluton emplacement.

In the Chemehuevi Mountains, mylonitic fabrics are superimposed on xenoliths of Precambrian gneisses embedded within undeformed Cretaceous plutons. John (1982) designates this mylonitization as Precambrian(?) in age, but the fabric could have developed at any time up to intrusion of the Cretaceous granodiorite. Another period of mylonitic deformation is imposed upon the mafic phases of the Chemehuevi Cretaceous intrusive suite. The foliation in the plutons parallels the sub-horizontal foliation of the gneisses, which exhibit this foliation on a regional scale. Thus, foliation cuts across early plutons and country rock and must post-date them. The younger plutons of the suite exhibit only weak foliation. The mid-Tertiary detachment surface cuts sharply across these mylonitic fabrics.

In the Old Woman Mountains, a zone of Mesozoic thrusting is exposed in the central part of the range. Along this zone, Paleozoic units are overturned, ductilely thinned, and foliated. The Jurassic(?) sills in the Paleozoic section are reconstituted into augen gneisses. In general, cataclasis is not predominant during this generation of deformation. The late Cretaceous plutons in the range cut across the thrust faults, and clearly post-date ductile deformation. However, the Old Woman pluton exhibits mylonitization within the southern parts of the range, and is foliated along its roof. The East Piute pluton has weak foliation throughout and shows strong mylonitization at its southern boundary.

The best example of mylonitization at structurally high levels within the late Cretaceous plutons is in the Cadiz Valley batholith (Howard et al., 1982). In the Iron Mountains, where the southeasternmost portion of the batholith is exposed, mylonitic deformation increases in intensity structurally upward. Older intrusive phases in the upper 1.3 km of the

batholith are more deformed than the lower, younger granitic bodies. Howard et al. (1982) proposed that these associations indicate synkinematic to late kinematic cataclastic deformation at the roof of a hot batholithic mass during intrusion of its lower portions by new magma. Other areas of mylonitization in the batholith occur in the northeastern Coxcomb Mountains and southeastern Sheephole Mountains (Howard et al., 1982).

Howard et al. (1982) propose that the mylonites typical of the Iron Mountains may represent the base of a thick zone of mylonite whose top is exposed farther east in the Whipple and Chemehuevi Mountains. The zone is envisioned as the diffuse boundary between a rigid upper plate and a lower zone made up of hotter, more ductile rocks, where batholith-sized bodies of magma are being intruded.

It is intriguing to note that the timing for this eastern deformation in the SMR is coincident with the thrust-related deformation described by Silver (1982, 1983) for plutons much farther to the west in the Central and Eastern Transverse Ranges. It is possible that there is a genetic link between those western occurrences and these more easterly plutons, and that the western plutons actually originated in close proximity with the SMR plutons (L.T. Silver, pers. comm.).

7.4.2 Geology and $^{18}O/^{16}O$ Relationships

The Mesozoic batholithic rocks in the SMR are made up of a northwest-trending Jurassic magmatic arc that is intruded by widespread late Cretaceous to early Cenozoic plutons. No plutons of Permo-Triassic age are known in the area. The Jurassic rocks are characterized by two suites; one is located north and east of the Bristol Mountains, the other to the south (John, 1981).

The northern Jurassic suite is made up of medium- to coarse-grained monzonite and syenite with K-Ar cooling ages between 145 and 158 Ma (John, 1981; Armstrong and Suppe, 1973; Calzia and Morton, 1980). This suite is not well documented at the present time, and it was not analyzed for $^{18}O/^{16}O$ because the outcrops lie to the north of the study area.

The southern Jurassic suite consists of hornblende- and biotite-bearing granodiorite and quartz monzonite lithologically similar to the Jurassic plutons mapped by Powell (1981) in the LSB area (see Chapter 6), as well as to the older granites mapped by Dibblee (1964c, 1964d) in the ROM area. Hamilton (1982) reports a U-Pb zircon age of 160 Ma for a pluton in the Big Maria Mountains, and Martin et al. (1982) report a 159 ± 6 Ma K-Ar age for biotite in a pluton from that range. All six Jurassic samples analyzed in this study come from this southern suite and they have $\delta^{18}O$ = +2.7 to +7.6.

Where late Cretaceous thermal resetting of K-Ar ages is not recorded, the plutons of the southern suite have cooling ages of approximately 165 Ma (John, 1981; Calzia and Morton, 1980). In the Bristol Mountains, the Bullion Mountains, and the Palen Mountains, the southern suite exhibits hydrothermal alteration, and in places apparently intrudes cogenetic volcanic rocks. Very few U-Pb zircon ages have been reported for the area, thus the emplacement ages for these plutons is not well constrained. Age assignments are based upon the reported dates and field mapping by U.S.G.S. personnel (John, 1981; K.A. Howard, pers. comm.).

Calzia (1982) describes the Jurassic Coxcomb granodiorite in the southern Coxcomb Mountains (Figure 7.7) as consisting of three facies: biotite-hornblende granodiorite, porphyritic biotite granodiorite, and quartz monzonite. Calzia (1982) reports a Rb-Sr age of 145 Ma for the

granodiorite, and K-Ar ages on biotite from this unit are between 54.1 ± 1.5 Ma and 70.8 ± 1 Ma (Armstrong and Suppe, 1973; Calzia and Morton, 1980). The biotite-hornblende granodiorite phase was not analyzed for $^{18}O/^{16}O$.

The northern part of the Coxcomb Mountains (Figure 7.7) contains a muscovite-quartz monzonite with a biotite K-Ar age of 65.1 ± 2 Ma. This phase of the "Coxcomb Granodiorite" has $\delta^{18}O$ = +8.9 to +9.0 (2 samples), and actually may be related to the Cretaceous Cadiz Valley batholith, even though it is assigned a Jurassic(?) age by Calzia (1982). In addition the porphyritic granodiorite phase ($\delta^{18}O$ = +8.6) is locally mapped as part of the Cadiz Valley batholith by John (1981) and Howard et al. (1982).

Late Cretaceous plutonism in the SMR produced a large, composite batholith (1700 km^2 in area) in the Cadiz Valley region (Figure 7.7), as well as many discrete quartz monzonite, granodiorite and muscovite granite plutons in the Old Woman, western Sacramento, Turtle, and Chemehuevi Mountains regions (John, 1981; Calzia, 1982; Miller et al., 1982; John, 1982; Howard et al., 1982). Sheet-like bodies of late Cretaceous to early Tertiary foliated muscovite granite occur in the Whipple Mountains (Davis et al., 1980). These latter bodies were not analyzed for $^{18}O/^{16}O$ because it was not possible to obtain samples farther than several hundred feet from their contacts with country rock (see Chapter 3 for sampling constraints). The oldest pluton in the Cadiz Valley batholith is a sphene-bearing porphyritic biotite granodiorite ($\delta^{18}O$ = +8.7, two samples) containing abundant mafic and Jurassic plutonic xenoliths. This unit is intruded by a pluton containing fewer xenoliths that ranges in composition from granodiorite to quartz monzonite, and which locally

contains muscovite. A monzodiorite from this phase has $\delta^{18}O$ = +7.8, and 6 samples of the quartz monzonite have $\delta^{18}O$ = 8.1 to 9.0. The central part of the batholith contains the youngest unit, which is a biotite (± muscovite ± garnet) quartz monzonite that forms a gradational contact with the second unit. Four samples of this unit have $\delta^{18}O$ = 7.7, 8.3, 8.9, and 9.0. Garnet- and muscovite-bearing aplites and pegmatites commonly intrude the granodiorite along the margins of the batholith. The total range of $\delta^{18}O$ in the 13 samples from the Cadiz Valley batholith is only 1.2 per mil, from +7.8 to +9.0. There is no correlation between $\delta^{18}O$ and age or $\delta^{18}O$ and lithology.

There are no reported U-Pb zircon ages from the Cadiz Valley batholith, but John (1981) estimates its emplacement age at between 75 and 85 Ma based on assumed cooling rates and K-Ar dates on biotites (Calzia and Morton, 1980; Calzia, 1982). K.A. Howard (pers. comm.) believes that the batholith probably formed at about the same time as the late Cretaceous granodiorite and muscovite granite plutons in the Old Woman Mountains, which have U-Pb zircon ages of about 72 Ma (Miller et al., 1989; unpublished data of J.E. Wright). The Miller (1977) report of a Rb-Sr age of 95 Ma for the granodiorite is no longer considered valid (C.F. Miller, pers. comm.).

The total areal extent of the numerous Cretaceous plutons in the Old Woman-Piute-Chemehuevi area (Figure 7.6) is approximately 400 km^2, and is divided roughly equally between a younger suite and an older suite. The younger suite of five muscovite granite plutons has $\delta^{18}O$ values as follows: Painted Rock (3 samples, 7.5, 8.4, 9.3); Sweetwater Wash (4 samples, 8.8, 9.0, 9.1, 9.1); Lazy Daisy (8.2, 8.9); North Piute (no analyzed samples); East Piute (8.7, 9.2). The older suite of three granodiorite

plutons is made up of the Old Woman (+7.2, +8.4), Rattlesnake or Florence (+9.2), and Goffs (+4.7; altered, possibly Jurassic, see Fig. 7.5) plutons. The younger suite is made up of felsic, biotite-muscovite (± garnet) rocks. The older granodiorites typically contain biotite, sphene, and hornblende. Miller et al. (1982) describe a few deformed sills of granitic gneiss in the Paleozoic section; they tentatively assign a Jurassic(?) age to these rocks, because they resemble Jurassic plutonic rocks farther to the west.

The late Cretaceous granodioritic rocks are medium grained and typically equigranular, although locally the rocks contain phenocrysts of potassium feldspar > 1 cm in size. Xenoliths and roof pendants of Precambrian gneiss are also present locally, and range in size from centimeters to nearly 5 km^2. Near the roof of the Old Woman pluton, the granodiorite is strongly foliated parallel to contacts, and contains abundant flattened mafic inclusions ranging in size from < 10 cm across to > 10 m across.

The Sweetwater Wash pluton (Figure 7.6) is a muscovite-biotite granite with local garnet-bearing facies, and is the best-studied muscovite granite in the area (Miller et al., 1982). The southern portion of the pluton contains abundant xenoliths of Precambrian crystalline basement ranging up to several hundred meters in size. The adjacent country rocks, as well as many of the xenoliths, show injection by the muscovite granite. No significant difference in $\delta^{18}O$ is observed between the northern part ($\delta^{18}O$ = +8.8) and the southern part (+9.0 to +9.1). The Sweetwater Wash pluton clearly crosscuts the granodiorite of the Old Woman pluton.

The other felsic plutons are similar in composition and nature to the Sweetwater Wash pluton, except for the East and North Piute plutons (Figure 7.6). These two bodies are more heterogeneous, and include a distinctive biotite granodiorite that doesn't contain sphene, has less biotite, and occasionally contains small amounts of muscovite. The East Piute pluton contains xenoliths of intermediate igneous composition that range in size between 5 and 20 cm across. Intense mylonitic lineations are developed along the southern part of this pluton.

The Chemehuevi Mountains (Figure 7.6) contain late Cretaceous plutons exposed in the lower plate of an Oligocene(?) to Miocene-age detachment fault that encircles the range (John, 1982). All of the samples collected for this study are from the autochthonous rocks of the core complex, but, as seen in Figure 7.6, these autochthonous rocks are divided into two plates by the Mojave Wash Fault of John (1982). The Chemehuevi detachment fault separates the two plates of the autochthonous section from rocks that belong to the upper plate of the detachment zone, in the sense of Davis et al. (1980) and Coney (1980).

The Mesozoic plutonic suite in the Chemehuevi Mountains intrudes autochthonous Precambrian crystalline rocks, and underlies most of the central and southern portion of the mountain range. The suite consists of five intrusive phases ranging in composition from hornblende- and sphene-rich quartz diorite, through granodiorite, to leucocratic biotite-muscovite (± garnet) granite.

John (1982) mapped the suite as a cogenetic, crudely concentric series with the younger and more felsic rocks in the interior. The older, more mafic rocks have a foliation parallel to that of the Precambrian rocks they intrude, and the hornblende-bearing granodioritic rocks ($\delta^{18}O$

= +7.0 and +7.4) contain wallrock xenoliths and quartz diorite inclusions. Two samples of related quartz monzonite facies have $\delta^{18}O$ = +7.4 and +7.7.

The volumetrically most important rock type in the suite is the biotite granodiorite-quartz monzonite. This unit has typically gradational, locally intrusive contacts with the older plutons. A muscovite-bearing facies ($\delta^{18}O$ = +7.8) is the youngest phase of the suite, and locally it contains blocks of the earlier biotite granodiorite. The most felsic rocks of the suite are small bodies of leucocratic garnet-bearing muscovite granite that are generally less than 2 km across; these bodies have gradational contacts with the muscovite-biotite quartz monzonite of the preceding unit, but they clearly crosscut the still earlier biotite granodiorite. The total variation in $\delta^{18}O$ in the Chemehuevi suite is +7.0 to +7.8, and there is only a very slight increase in $^{18}O/^{16}O$ in the sequence: granodiorite-quartz monzonite-muscovite granite.

Based upon limited geochronologic data, and experience with dated rocks of similar lithology elsewhere in the SMR, John (1981, 1982) suggests that the Chemehuevi Mountains plutonic suite is Cretaceous. John (1982) reports a minimum K-Ar age of 64.1 ± 2.2 Ma for biotite from the muscovite-biotite quartz monzonite. The lithologic similarities of the plutonic rocks in the Cadiz Valley batholith and Old Woman Mountains to the intermediate and felsic members of the Chemehuevi suite argue for a late Cretaceous emplacement age for the latter.

7.4.3 Regional $^{18}O/^{16}O$ Patterns

The locations and $^{18}O/^{16}O$ data for all of the SMR samples are shown in Figures 7.1, 7.5, 7.6, and 7.7. The $\delta^{18}O$ values range from +2.7 to +9.3, with a median value around +8.6. The weakly sampled Jurassic plut-

onic suite (only 6 samples) ranges from +2.7 to +7.6, with no systematic variation within the granodiorite and quartz monzonite rock types. The Cretaceous suite varies from +4.7 to +9.3, again with no significant correlation between $\delta^{18}O$ and rock type. The muscovite-bearing plutons have $\delta^{18}O$ between +7.7 and +9.3, while granodioritic rocks vary from +7.2 to +9.2.

An older subgroup of probable mid- to early-Cretaceous samples, made up of only 13 out of the total of 40 Cretaceous samples, ranges from +7.2 to +8.6, except for a single anomalous sample with $\delta^{18}O$ = +4.7 (hydrothermally altered, possibly Jurassic?). The dominant subgroup of probable late Cretaceous samples ranges from +7.0 to +9.3, with two thirds of the samples (18 out of 27) falling between +8.5 and +9.3. Figure 7.5 is a map showing $\delta^{18}O$ contours for the Cretaceous suite over the entire SMR area. This should be compared with analogous data in Figure 7.1 and in Chapter 6. Note the general eastward and northward decrease in $\delta^{18}O$ from values above +9.0 in the San Bernardino Mountains (SBM) to values below +7.5 near the Colorado River. The pattern is interrupted in a significant way only by the ^{18}O-rich zone centered on the intense metamorphism and migmatization of country rocks associated with the Old Woman-Piute batholith (Figure 7.5).

As in many of the other sample areas described in this thesis, the Jurassic suite shows evidence for hydrothermal alteration, with correspondingly low-^{18}O values. For example, a low value of +4.2 per mil has been measured for a granodiorite from the northwest part of the Devil's Playground, although the other Jurassic plutons in that general area exhibit essentially "normal" magmatic $\delta^{18}O$ values of about +7.6 (Granite Mountains and Marble Mountains). Farther to the southeast, altered gran-

odiorite associated with volcanic rocks from the Palen Mountains has a very low $\delta^{18}O$ value of +2.7, clearly indicative of meteoric-hydrothermal alteration. In the Big Maria Mountains, however, the relatively low $\delta^{18}O$ of +6.8 in a Jurassic gabbro-diorite could represent the primary, magmatic $^{18}O/^{16}O$ ratio of this pluton, because this is a very plausible value for such a low-SiO_2 (49.8 wt. %), mafic igneous rock.

It is likely that all of these areas, if sampled in more detail, would show systematic $\delta^{18}O$ contours and ^{18}O-depleted zones analogous to those described above for the Jurassic plutons in the ROM area. However, without more detailed sampling we cannot show $\delta^{18}O$ contours for the Jurassic rocks like those shown for the ROM area in Figures 7.2 and 7.4. Nor can we exclude the possibility that some of the low $\delta^{18}O$ values have been caused by hydrothermal events synchronous with the emplacement of the late Cretaceous plutons or Tertiary volcanic rocks, or possibly even during hydrothermal activity on the mid-Tertiary detachment faults. However, arguing against this is the fact that the late Cretaceous rocks do not seem to be depleted in ^{18}O in the regions where the Jurassic rocks are altered. The only Cretaceous(?) sample that appears to have interacted with meteoric-hydrothermal fluids is the +4.7 sample from the Goffs pluton.

The two major late-Cretaceous batholithic terranes in the SMR are the Cadiz Valley batholith (Figure 7.7), and the Old Woman-Piute-Chemehuevi batholith (Figure 7.6). On Figure 7.5, the core zones of these two batholiths show up as oval-shaped zones of strong ^{18}O-enrichment ($\delta^{18}O$ > +8.5) where the rocks locally have $\delta^{18}O$ > +9.0 per mil. In other words, these patterns represent the exact opposite of the Jurassic, ROM-type, meteoric-hydrothermal ring zones described previously. These areas are

characterized by a lack of any indications of hydrothermal activity. There is no evidence of the steep ^{18}O-gradients over small areas that are so characteristic of areas containing hydrothermally altered rocks, as in the Jurassic ROM suite. Thus, the ^{18}O-gradients shown for the late Cretaceous rocks in Figures 7.1 and 7.5 must be ascribed either to effects of magmatic differentiation, to assimilation processes (AFC), or to local variations in the $\delta^{18}O$ of the source regions of the plutons. As described in more detail below, we favor the latter interpretation.

The $\delta^{18}O$ contours for the Cadiz Valley batholith are asymmetrically distributed with respect to the boundaries of the batholith, and also with respect to rock type (Figures 7.5 and 7.7). However, both high and low-$\delta^{18}O$ contours cut through areas underlain by muscovite granite; these muscovite-bearing plutons have $\delta^{18}O$ values showing a fairly wide range from +7.7 to +9.0. Thus, there is no correlation between $\delta^{18}O$ and rock type, strongly favoring some mechanism other than fractional crystallization to explain the $\delta^{18}O$ distribution in these rocks.

The Old Woman-Piute-Chemehuevi batholith also displays $\delta^{18}O$ contours that cut across the "grain" of the rock types, with the lower values (< +8.6 per mil) concentrated within granodiorite and muscovite granite in the southern and eastern outcrops, and higher values (> +8.6 per mil) located in granodiorite and muscovite granite to the northwest. This overlap between the $\delta^{18}O$ values for these two rock types is not a feature that would be expected from any type of magmatic differentiation process operating on a single well-mixed magma chamber encompassing the entire area shown within the northeastern part of Figure 7.5.

As has been established above for the SGM and SBM areas and previously for the PRB by Taylor and Silver (1978), the distribution of $\delta^{18}O$

values for the two late-Cretaceous batholiths described above clearly varies more as a function of geography than as a function of rock type. The geographic variation in $\delta^{18}O$ and lack of any overall correlation between silica content and $\delta^{18}O$ are features that are best explained by geographic $\delta^{18}O$ variations in the source regions for the plutons. It is also interesting that throughout the entire SMR area the whole-rock $\delta^{18}O$ values are generally less than +8.0, except in the core zones of the two areas where Cretaceous magmatism was most intense, namely the Old Woman-Piute batholith and the Cadiz Valley batholith. Thus, it appears that where the lower and middle crust was most intensely melted, some higher-^{18}O magmas were developed even within the craton (where most of the Mesozoic magmas formed with significantly lower $\delta^{18}O$ values). These ideas are elaborated upon and discussed at length in Chapter 8, where Sr isotopic data are presented for a suite of some of the same plutons from the SMR area on which $\delta^{18}O$ analyses were made.

7.4.4 Correlations Between $^{18}O/^{16}O$ Data and Major-Element Geochemistry

Major-element geochemical and, where available, isotopic data for the SMR plutons are listed in Table 7.1. There are no data available for the ROM area. Chappell (1978), Hine et al. (1978), and more recently, Hill (1984), have shown that the chemical compositions of granitic plutons commonly reflect the nature of their source regions. Plutons derived from pelitic metasedimentary sources (S-type) have $Al/(Na + K + Ca/2) > 1.1$ and $Fe^{3+}/(Fe^{3+} + Fe^{2+}) < 0.2$, generally do not contain hornblende, and usually have abundant biotite and (or) muscovite as primary phases.

Plutons derived from igneous-type (I-type) sources often do have hornblende as a primary phase, they are metaluminous, and they have $Fe^{3+}/(Fe^{3+} + Fe^{2+}) > 0.2$. Inasmuch as the plutons in the SMR area have

Table 7.1 Major-element geochemistry, C.I.P.W. normative mineralogy and isotopic data (whole-rock $\delta^{18}O$, ε_{Sr} and ε_{Nd}) for selected plutons in southeastern California (SECA).*

	Sample Identifier[a]								
	CH307	CAL199	KI128	MM232	GR375	LM374	SH33P	IM357	SH33W
Major-Element Geochemistry[b]									
SiO_2	60.41	49.18	68.56	73.89	68.10	68.16	69.88	75.31	65.29
TiO_2	1.01	0.70	0.38	0.34	0.52	0.43	0.43	0.09	0.60
Al_2O_3	16.48	23.69	16.52	13.32	17.08	15.26	15.48	13.98	16.77
Fe_2O_3	2.27	2.05	1.24	1.31	0.95	1.68	1.23	0.53	1.37
FeO	2.86	3.06	1.19	0.16	1.45	1.32	1.12	0.42	2.00
MgO	2.82	3.18	0.79	0.35	0.96	1.13	0.81	0.23	1.29
CaO	4.96	10.71	3.09	0.32	3.28	2.92	2.83	1.32	3.69
Na_2O	4.38	3.82	4.67	3.50	4.97	3.66	4.26	3.66	4.64
K_2O	3.38	1.54	2.92	5.90	2.32	4.90	3.30	4.98	2.80
Total	98.57	97.93	99.36	99.09	99.63	99.46	99.34	100.52	98.45
Trace Element and Isotopic Data[c]									
$\delta^{18}O$	+7.4	+7.8	+8.2	+7.6	+8.2	+7.5	+8.7	+7.7	+8.7
Age, Ma	Kt	Kt	Kt	Jr	Kt	Jr	Kt	Kt	Kt
I(Sr)	--	--	0.7107	--	0.7095	0.7094	0.7097	0.7151	--
ε_{Sr}[d]	--	--	+89	--	+72	--	+75	+152	--
Sr, ppm	956	--	724	--	776	--	780	246	--
C.I.P.W. Normative Mineralogy[e]									
Qtz	8.51	0.00	22.32	30.02	21.47	20.95	25.36	31.54	17.68
Cor	--	--	0.06	0.60	0.43	--	--	0.17	--
Or	20.26	9.29	17.37	35.19	13.76	29.11	19.63	29.28	16.81
Ab	37.60	24.58	39.77	29.89	42.21	31.14	36.29	30.81	39.88
An	15.55	43.85	15.43	1.60	16.33	10.80	13.43	6.51	16.92

* Whole-rock $\delta^{18}O$ and initial $^{87}Sr/^{86}Sr$ from literature sources (shown on Figure 8.1): (1) $\delta^{18}O$=+9, I-Sr=0.7083; sample 14, Masi et al. (1981; and see Table 1.1); (2) +7.5, 0.7070; $\delta^{18}O$ from GCS153 (Table 1, Appendix); I-Sr from Miller (1977a) for monzonitic pluton in Granite Mountains near Victorville; (3) +7.7, 0.7091; $\delta^{18}O$ from pers. comm. V. Frizzell (1984); I-Sr from Frizzell et al. (1986); (4) +8.1, 0.7095; Liebre Mountain Cretaceous pluton; Masi et al. (1981); (5) +8.5, 0.7090; $\delta^{18}O$ from GCS208 (Table 1, Appendix); I-Sr from Joseph and Ehlig, 1981; (6) 0.7095; Bouquet Canyon Cretaceous pluton; Kistler and Peterman, 1978; (7) +7, 0.7040; $\delta^{18}O$ is assumed primary value for Lowe magma (see Chapter 6); I-Sr reported in Ehlig (1982); (8) $\delta^{18}O$ values reported by Lee et al. (1981a; and see Table 1.2), +8.6 (GR167), +9.2 (GR171), and +9.9 (GR175); and (9) initial $^{87}Sr/^{86}Sr$ values reported by Calzia et al. (1986) for Cretaceous granitic rocks in the Coxcomb Mountains, 0.7092, 0.7097, 0.7104 (GR175), and 0.7109 - $\delta^{18}O$=+9 for nearby sample GCS93 (Table 1, Appendix).

Table 7.1 cont'd.

Sample Identifier[a]									
	SA6	CH200	DP220	CH198	PA189	TM486A	LM119	CH305	SH191
Major-Element Geochemistry[b]									
SiO_2	74.30	72.22	77.12	66.18	65.09	69.45	70.97	60.61	68.07
TiO_2	0.06	0.14	0.11	0.54	0.69	0.33	0.27	0.83	0.43
Al_2O_3	14.50	15.10	11.96	15.37	15.60	14.73	14.92	16.68	16.62
Fe_2O_3	0.37	0.77	0.65	1.52	1.64	1.76	0.96	2.36	1.33
FeO	0.33	0.57	0.09	1.42	2.58	1.16	0.57	3.47	1.14
MgO	0.19	0.33	0.13	1.42	1.55	0.93	0.48	2.63	0.82
CaO	1.07	1.91	0.25	2.80	3.02	2.50	2.04	5.28	3.23
Na_2O	4.07	4.34	3.98	4.03	3.74	3.49	3.96	3.64	4.56
K_2O	4.55	3.68	4.62	4.34	4.41	4.72	4.13	2.98	3.10
Total	99.44	99.06	98.91	97.62	98.32	99.07	98.30	98.48	99.30
Trace Element and Isotopic Data[c]									
$\delta^{18}O$	+8.2	+7.8	+4.2	+7.7	+2.7	+7.2	+8.6	+7.0	+8.5
Age, Ma	Kt	Kt	Jr	Kt	Jr	Kt	Kt	Kt	Kt
I(Sr)	0.7153	--	--	--	0.7106	0.7097	--	0.7083	0.7097
ε_{Sr}[d]	+154	--	--	--	+89	+75	--	+55	+75
Sr, ppm	201	514	--	--	--	407	--	547	797
C.I.P.W. Normative Mineralogy[e]									
Qtz	30.72	28.49	35.98	18.87	17.43	24.91	27.51	12.86	21.39
Cor	0.94	0.51	--	--	--	--	0.23	--	--
Or	27.04	21.95	27.60	26.27	26.51	28.15	24.83	17.88	18.45
Ab	34.63	37.07	34.05	34.93	32.19	29.81	34.09	31.28	38.86
An	5.34	9.57	1.14	11.30	12.97	10.69	10.30	20.69	15.84

Table 7.1, cont'd.

	Sample Identifier[a]								
	BM372B	GM365	ST7	BR218	KH78-1	CH208	E6	E8	P76
	Major-Element Geochemistry[b]								
SiO_2	49.81	72.52	71.45	71.37	64.37	65.47	67.90	74.30	71.20
TiO_2	1.18	0.21	0.40	0.30	0.78	0.53	0.38	0.07	0.13
Al_2O_3	19.13	14.75	14.45	14.85	15.29	16.48	14.90	14.50	14.50
Fe_2O_3	3.24	1.45	1.30	1.14	2.90	1.47	2.87	0.56	1.71
FeO	5.45	0.69	1.14	0.62	2.04	1.47	--	--	--
MgO	4.32	0.44	0.70	0.61	1.82	1.34	0.64	0.07	0.32
CaO	8.69	1.99	2.21	2.04	3.20	3.28	2.68	0.60	1.34
Na_2O	4.83	4.07	3.89	4.17	3.60	4.19	3.49	3.91	4.11
K_2O	0.76	4.04	3.48	3.57	4.82	3.87	3.85	4.02	4.03
Total	97.41	100.16	99.02	98.67	98.82	98.10	96.71	98.03	97.34
	Trace Element and Isotopic Data[c]								
$\delta^{18}O$	+6.8	+8.6	+9.3	+8.6	+7.6	+7.4	+8.7	+9.2	+8.2
Age, Ma	Jr	Kt	Kt	Kt	Jr	Kt	70	70	70
I(Sr)	0.7085	0.7103	--	--	--	--	0.7092	0.7100	0.7160
ε_{Sr}[d]	+59	+84	--	--	--	--	+68	+79	+164
Sr, ppm	1081	461	--	--	--	785	487	9	330
	C.I.P.W. Normative Mineralogy[e]								
Qtz	0.00	28.42	29.86	28.55	16.56	17.65	nd	nd	nd
Cor	--	0.06	0.27	0.42	--	--	nd	nd	nd
Or	4.61	23.84	20.77	21.38	28.82	23.31	nd	nd	nd
Ab	36.00	34.38	33.24	35.76	30.83	36.14	nd	nd	nd
An	29.02	9.86	11.07	10.26	11.46	15.02	nd	nd	nd

Table 7.1 cont'd

	Sample Identifier[a]							
	G	W285	W172B	W261	W324	W345	P109	SW8
	Major-Element Geochemistry[b]							
SiO_2	75.10	72.70	73.30	64.30	60.70	62.00	60.90	73.00
TiO_2	0.04	0.08	0.05	0.43	0.91	0.62	0.68	0.10
Al_2O_3	13.30	13.30	13.70	17.00	17.20	15.80	15.70	14.10
Fe_2O_3	1.11	1.35	0.51	2.79	4.64	5.25	5.77	1.63
FeO	--	--	--	--	--	--	--	--
MgO	0.14	0.16	0.14	0.87	1.63	2.13	2.78	0.18
CaO	0.75	1.03	0.94	3.37	4.37	4.17	4.65	1.24
Na_2O	4.24	3.88	4.36	4.98	4.50	3.66	3.47	3.46
K_2O	4.25	4.59	4.45	3.23	2.79	3.44	3.37	4.43
Total	98.93	97.09	97.45	96.97	96.74	97.07	97.32	98.14
	Trace Element and Isotopic Data[c]							
$\delta^{18}O$	+9.1	+8.4	+9.3[f]	+8.4	+7.2[g]	+9.2	+4.7	+9.1[h]
Age, Ma	70	70	70	70	70	70	70	70
I(Sr)	0.7180	--	--	--	0.7100	0.7108	0.7084	0.7170
ε_{Sr}[d]	+193	--	--	--	+79	+91	+57	+179
Sr, ppm	47	65	70	850	830	530	550	218

[a] Sample Identifier linked to "GCS" Sample Number in Table 1 (Appendix).
[b] Unpublished data of K. Howard (pers. comm., 1984); data from Chemehuevi batholith from John (1989); data from Old Woman batholith unpublished data of C. F. Miller (pers. comm., 1984).
[c] Unpublished data of K. Howard and M. Lanphere (pers. comm., 1984); C.F. Miller (Old Woman batholith, pers. comm., 1984); and for Chemehuevi batholith, data is from John (1989).
[d] Calculated using equation in Farmer and DePaolo, 1983, assuming ages of 70 Ma for Kt plutons, and 160 Ma for Jr plutons.
[e] Calculated using Ed Stolper's computer program (1984)
[f] Nearby sample (W236) has ε_{Nd} = -16.0, ε_{Sr} = +177, Sr,ppm = 122 (Miller et al., 1989; Farmer and DePaolo, 1983); another nearby sample (W311) has ε_{Nd} = -16.8, ε_{Sr} = +193, Sr,ppm = 240 (Miller et al, 1989).
[g] ε_{Nd} = -10.3 (Miller et al, 1988; Bennett and DePaolo, 1987)
[h] $\delta^{18}O$ value from nearby sample GCS189 (see Table 1, Appendix), pers. comm. C.F. Miller, 1984.

$\delta^{18}O$ variations, which must reflect geographic variations in their source regions, it is useful to compare the major element chemistry of these plutons with the S- and I-type classification scheme of the Australian workers.

Figure 7.8 shows a ternary plot of the C.I.P.W. normative values for An, Ab, and Or (normalized to 100 percent) from the data in Table 7.1. Also shown is the "Sierra Nevada trend line" of Presnall and Bateman (1973) (line M-N). The samples from the SMR area plot in a cluster falling to the sodic side of the Sierra Nevada trend line.

A detailed interpretation of Figure 7.8 in terms of equilibrium phase relations is not possible without information on P_{water}, T, and the bulk composition of source rocks (Steiner et al., 1977). However, in general terms, Presnall and Bateman (1973) propose that the Sierra Nevada trend (M-N) indicates equilibrium fusion of the quartzofeldspathic source material (indicated in Figure 7.8 by the region near point M), followed by subsequent fractional crystallization of the melts. Whitney (1975) showed in laboratory melting experiments that partial melts of quartzofeldspathic material would follow such a trend, and that the position occupied by the two-mica granites (the region near point N in Figure 7.8) would represent either minimum melts, or extremely differentiated melts in the Qtz-Ab-An-Or system at $P_{water} < 15$ Kbars.

It is likely that the position and shape of the SMR data-point envelope on Figure 7.8 are a result of the same general process responsible for the Sierra Nevada trend line. However, in the SMR case, the source would have to have a somewhat less calcic composition than the source(s) for the Sierra Nevada rocks, possibly with a composition just to the sodic side of point M on the diagram. In this respect, the SMR plutons

Figure 7.8 Ternary plot of C.I.P.W. normative mineralogy (An-Ab-Or end-members, normalized to 100%) for Mesozoic granitic rocks of the SMR area in SECA (based on data given in Table 7.1). The Jurassic samples are indicated by solid circles; late Cretaceous samples by solid triangles. Line M-N is the Sierra Nevada Batholith trend-line of Presnell and Bateman (1973); the data envelope for Jurassic samples (albeit based on a limited number of samples) roughly parallels line M-N; however the late Cretaceous samples show a markedly different trend. Region labelled "B" is a likely source region composition for these late Cretaceous alkali-calcic plutons in the SMR (see Figure 7.9 for alkali-lime index).

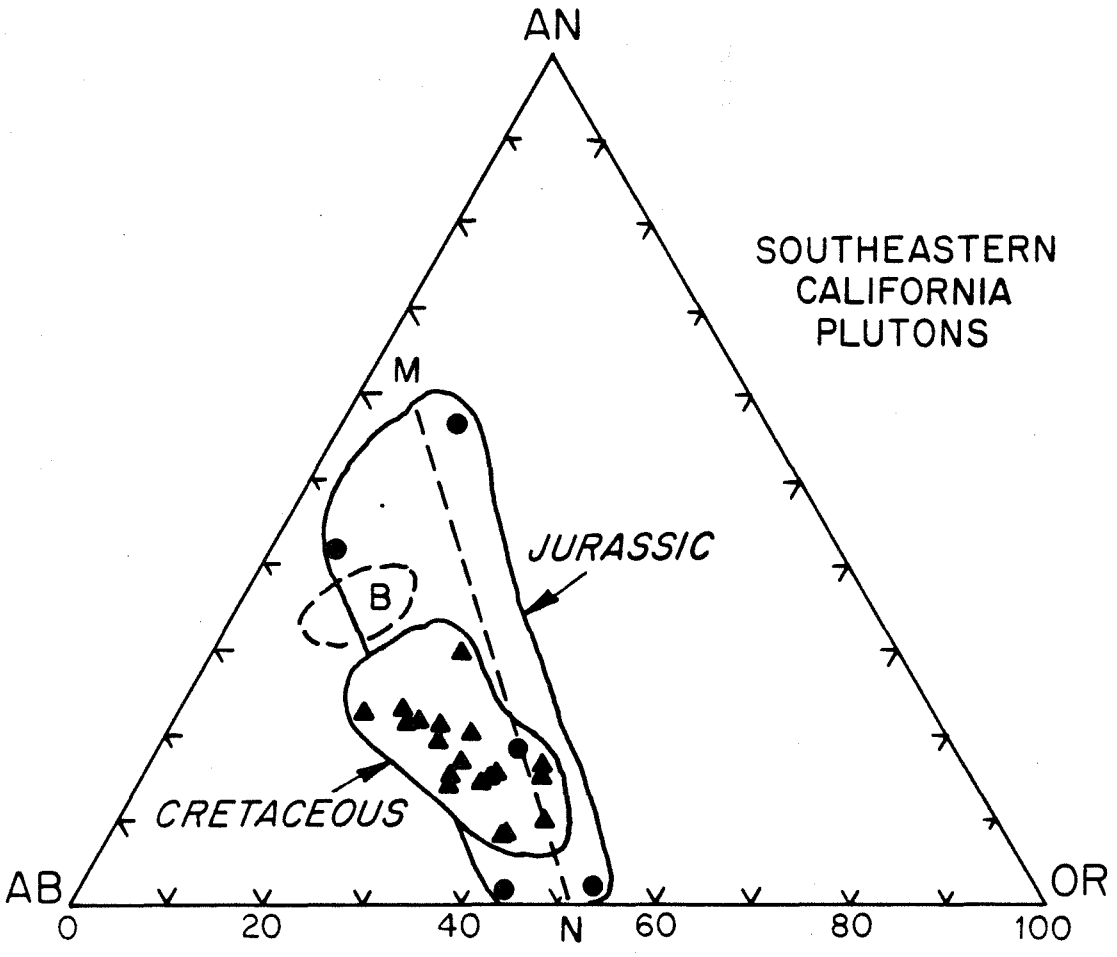
AN
SOUTHEASTERN
CALIFORNIA
PLUTONS
M
JURASSIC
B
CRETACEOUS
AB
OR
0
20
40
N
60
80
100

are chemically similar to those from the LSB and SBM areas (Figure 6.13) and to the Cretaceous plutons from southern Arizona (Figure 5.6).

Figure 7.9 shows a Peacock diagram plotting the variation of CaO and (Na_2O + K_2O) versus SiO_2 for the Jurassic and late Cretaceous plutonic suites from the SMR area. The two trends converge to a more or less common alkali-lime index of approximately 55 to 57 weight percent SiO_2, but the Jurassic suite shows higher alkali content and lower calcic content relative to the younger suite, at a weight percent SiO_2 > 65.0.

According to the classification scheme of Peacock (1931), both suites are "alkali-calcic," verging upon "calc-alkaline." For comparison, the Sierra Nevada Batholith is calc-alkaline (Bateman et al., 1963; Kistler, 1974; Lockwood, 1975; Bateman and Lockwood, 1976), Peninsular Ranges batholith and the western Idaho batholith are calcic (Larsen and Schmidt, 1958; Silver et al., 1979). Plutons in the Great Basin region of Nevada occupy a geographic position similar to those in the SMR study area, but have an alkali-lime index of approximately 60 weight percent SiO_2 (Lee, 1984), which makes them "calc-alkaline". In terms of the Peacock classification, the plutons of the SMR area are thus chemically similar to those of the south-central Arizona region (Chapter 5). Those of the Transverse Ranges of southern California (Chapter 6) have affinities closer to Sierra Nevada batholithic rocks.

Figure 7.10 is a plot of the variations in Fe_2O_3 and FeO for the SMR plutons. The Jurassic suite contains relatively high amounts of both ferric and ferrous iron whereas the Cretaceous suite generally has lower iron contents. Shown for comparison in Figure 7.10 are the values that the Australian I- and S-type plutons exhibit. From Figure 7.10, it is clear that the SMR plutons of both age-suites plot with distinctly higher

Figure 7.9 Plot of SiO_2 (wt.%) versus Na_2O+K_2O and CaO (wt.%) (Peacock Diagram; see Peacock, 1931) for Mesozoic granitic plutons from the southern Mojave Region (SMR), based on data listed in Table 7.1. Circles indicate Jurassic samples (solid = CaO; half-shaded = alkalies); the late Cretaceous samples are shown by solid squares (CaO) and triangles (alkalies).

Figure 7.10 Plot of FeO (wt.%) versus Fe_2O_3 (wt.%) for Mesozoic granitic plutons from the SMR, based on data listed in Table 7.1. Closed circles indicate Jurassic samples; open circles - late Cretaceous granodiorites, monzogranites, and two-mica granites. Fields labeled "S.E. Australian I- and S-type" indicate the generalized data fields for plutons studied by Hine et al. (1978) in the Lachlan Fold Belt of southeastern Australia.

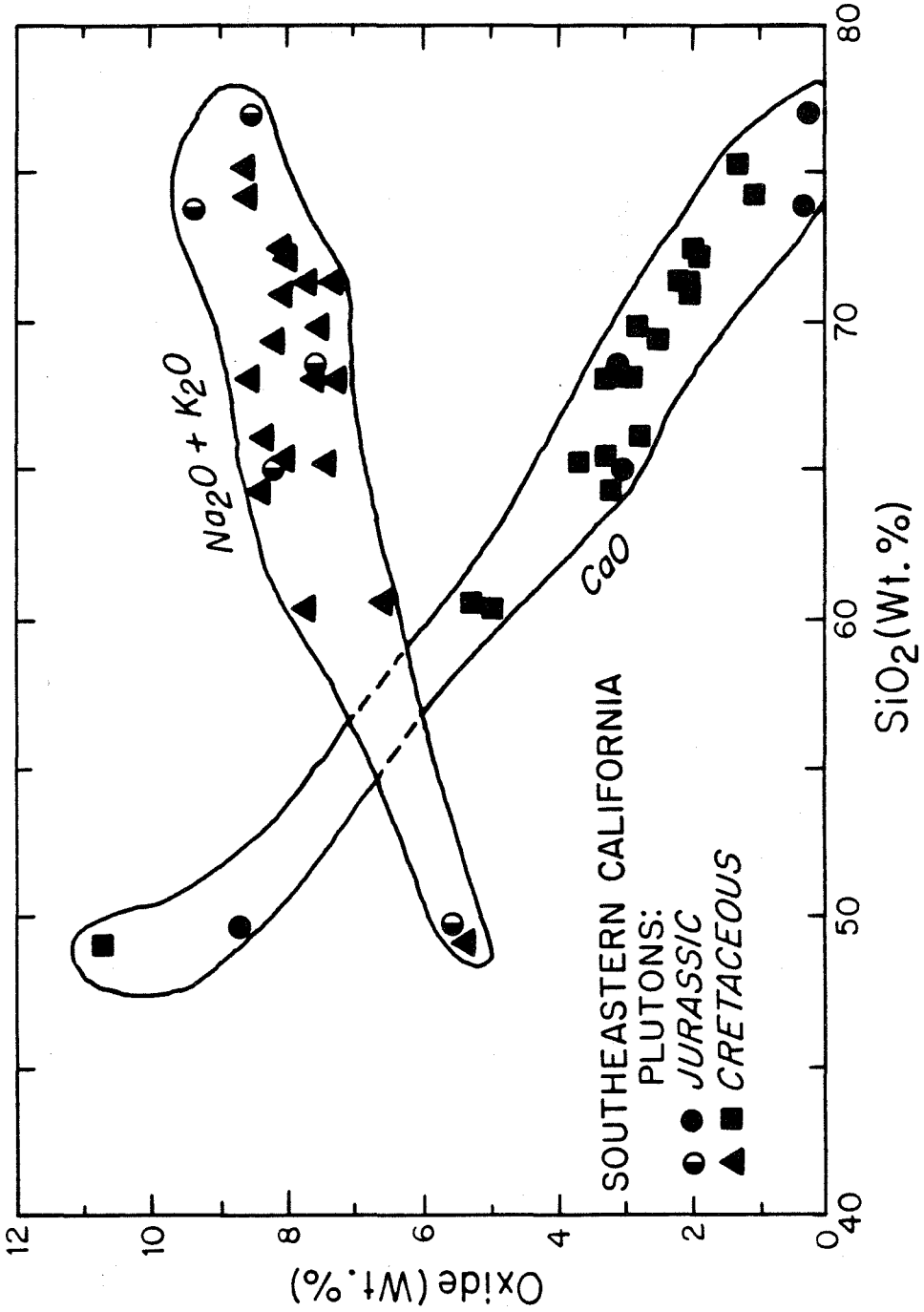
Oxide (Wt.%)
SiO2(Wt.%)
Na2O + K2O
CaO
SOUTHEASTERN CALIFORNIA
PLUTONS:
JURASSIC
CRETACEOUS
0
2
4
6
8
10
12
40
50
60
70
80

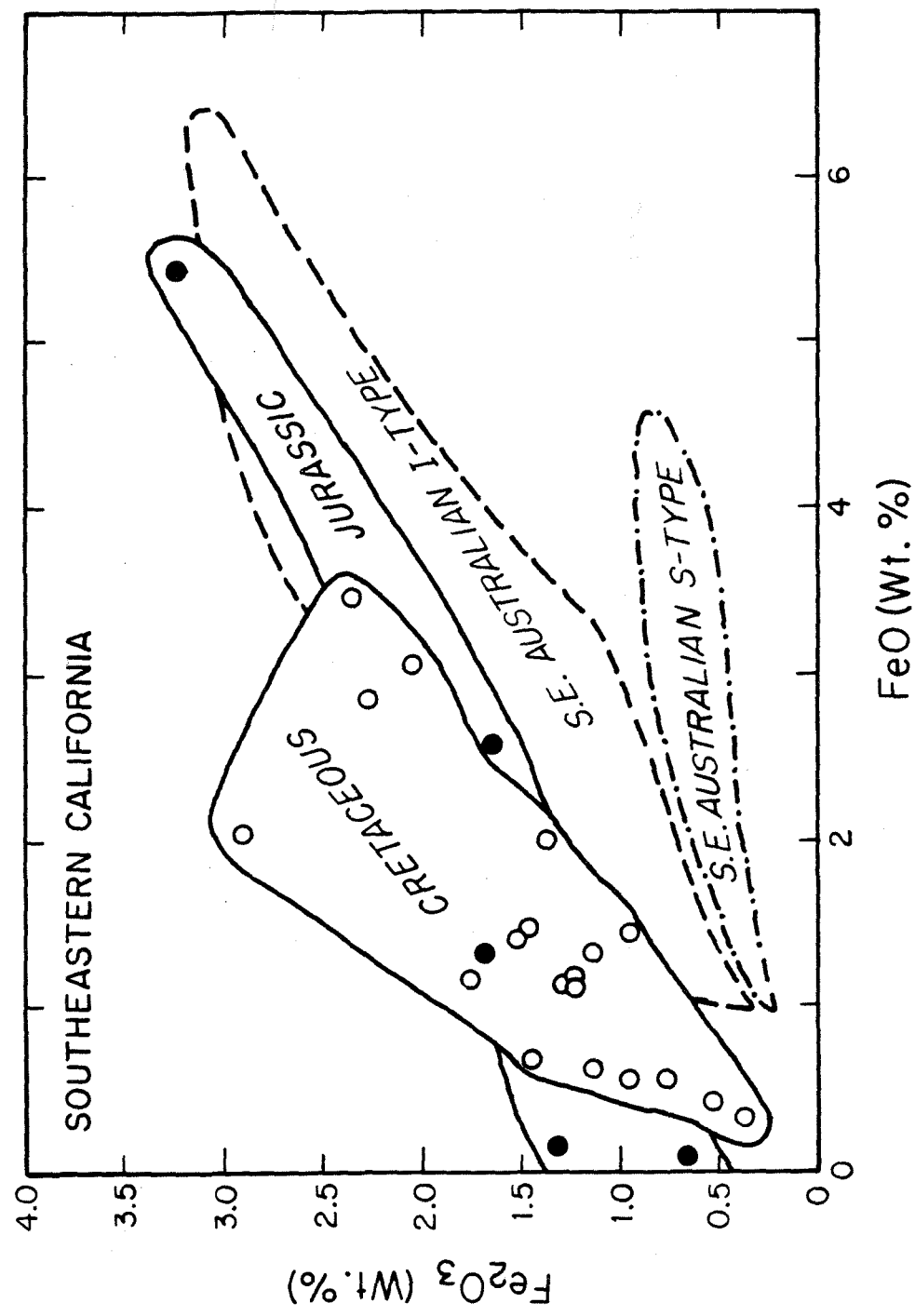
SOUTHEASTERN CALIFORNIA
JURASSIC
CRETACEOUS
S.E. AUSTRALIAN I-TYPE
S.E. AUSTRALIAN S-TYPE
Fe_2O_3 (Wt. %)
FeO (Wt. %)
0
0.5
1.0
1.5
2.0
2.5
3.0
3.5
4.0
2
4
6

ferric iron values than either the typical Australian S-type plutons or the typical Australian I-type plutons. This is significant because this means that the muscovite granites in the SMR suites probably must come from a much more oxidized source than the Australian granites.

Figures 7.11 and 7.12 are plots of whole-rock $\delta^{18}O$ vs. mole percent ferric iron, and of whole-rock $\delta^{18}O$ vs. the ratio of alumina to alkalies plus calcium. Each of these diagrams is crucial to the I-type and S-type classification scheme, because melts derived from pelitic sources should be both peraluminous and high in ferrous iron.

The ferric/total iron ratios of all the SMR samples are between 0.3 and 0.8, with most of the samples bracketed between 0.35 and 0.7 for the entire $\delta^{18}O$ range between +6.8 and +9.3 per mil. There is no overlap whatsoever with the Australian S-type field, both because $\delta^{18}O$ is less than +10.0 per mil for all of the SMR samples, even the muscovite granites, and because the ferric/total iron ratios are also very high. With few exceptions, the SMR samples have even higher ferric/ferrous ratios than the typical I-type plutons from Australia, even though they have similar $\delta^{18}O$ values. Both the ferric/ferrous ratios and the whole-rock $\delta^{18}O$ values for the SMR plutons are very similar to those of plutons from the south-central Arizona region described in Chapter 5.

It can be seen from Figure 7.12 that the Jurassic samples are metaluminous with Al/(Na+K+Ca/2) < 0.93, except for one sample at ~ 1.04. This places them within the "I-type" field, as defined by Chappell (1978) and O'Neil and Chappell (1977). The Cretaceous plutons have aluminum/(alkali + calcium) ratios that range between 0.82 and 1.07, and in general have higher alumina contents than the Jurassic samples.

Figure 7.11 Plot of whole-rock $\delta^{18}O$ versus the mole ratio of Fe^{3+} to total Fe for granitic plutons from the SMR, based on data listed in Table 7.1. Closed circles indicate Jurassic samples; open circles - late Cretaceous granodiorites, monzogranites and two-mica granites. Late Cretaceous samples have been further subdivided into separate data envelopes that correspond with geographic localities discussed in text (and shown in Figure 7.5).

Figure 7.12 Plot of whole-rock $\delta^{18}O$ versus the mole ratio of Al_2O_3 to Na_2O+K_2O+CaO for Mesozoic granitic plutons from the SMR, based on data listed in Table 7.1. Closed circles indicate Jurassic samples; open circles - late Cretaceous granodiorites, monzogranites, and two-mica granites. Late Cretaceous samples have been further subdivided into separate data envelopes that correspond with the geographic localities discussed in text (and shown in Figure 7.5).

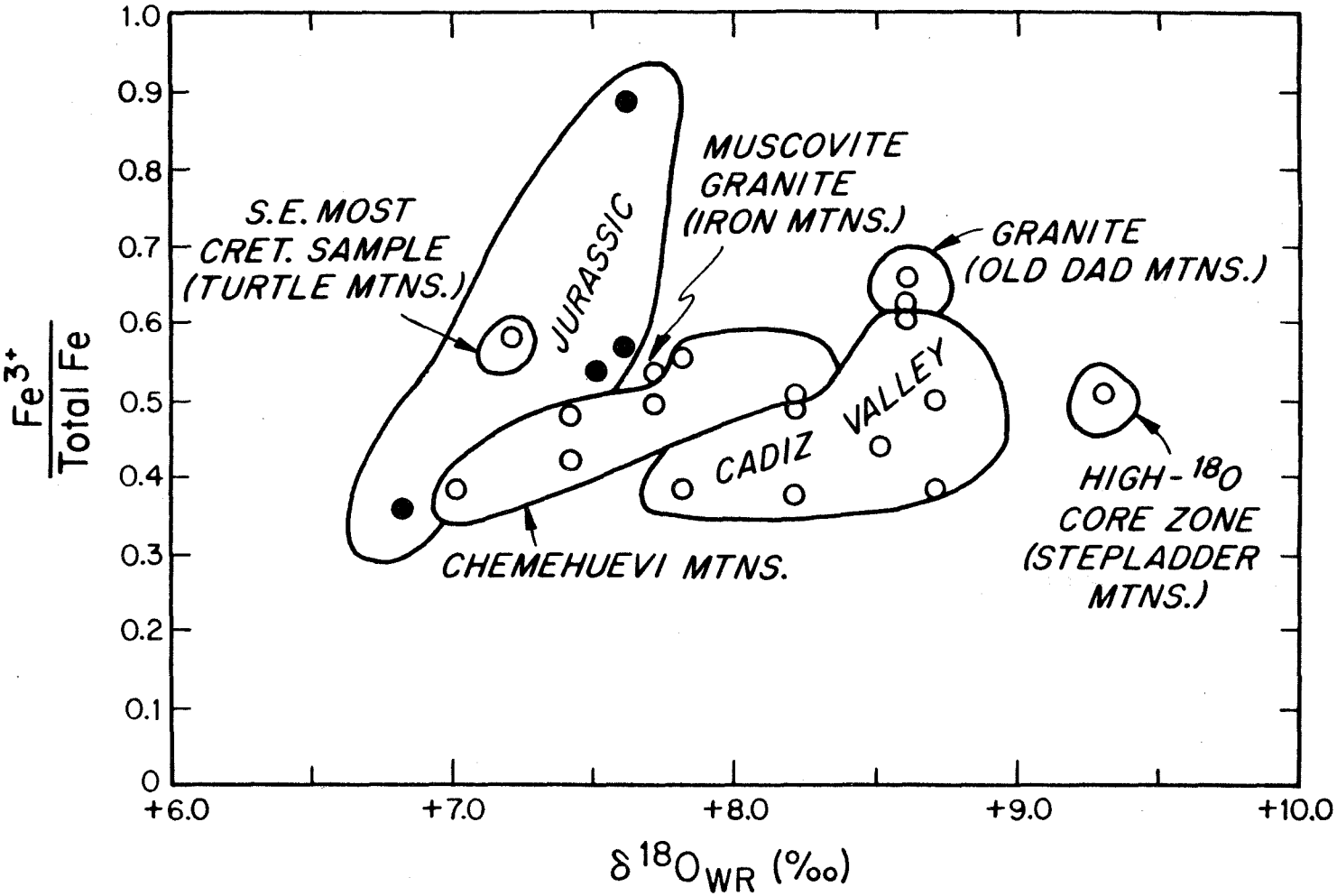
1.0
0.9
0.8
0.7
0.6
0.5
0.4
0.3
0.2
0.1
0
+6.0
+7.0
+8.0
+9.0
+10.0
$\frac{Fe^{3+}}{Total\ Fe}$
$\delta^{18}O_{WR}$ (‰)
S.E. MOST CRET. SAMPLE (TURTLE MTNS.)
JURASSIC
MUSCOVITE GRANITE (IRON MTNS.)
GRANITE (OLD DAD MTNS.)
CADIZ VALLEY
HIGH-^{18}O CORE ZONE (STEPLADDER MTNS.)
CHEMEHUEVI MTNS.

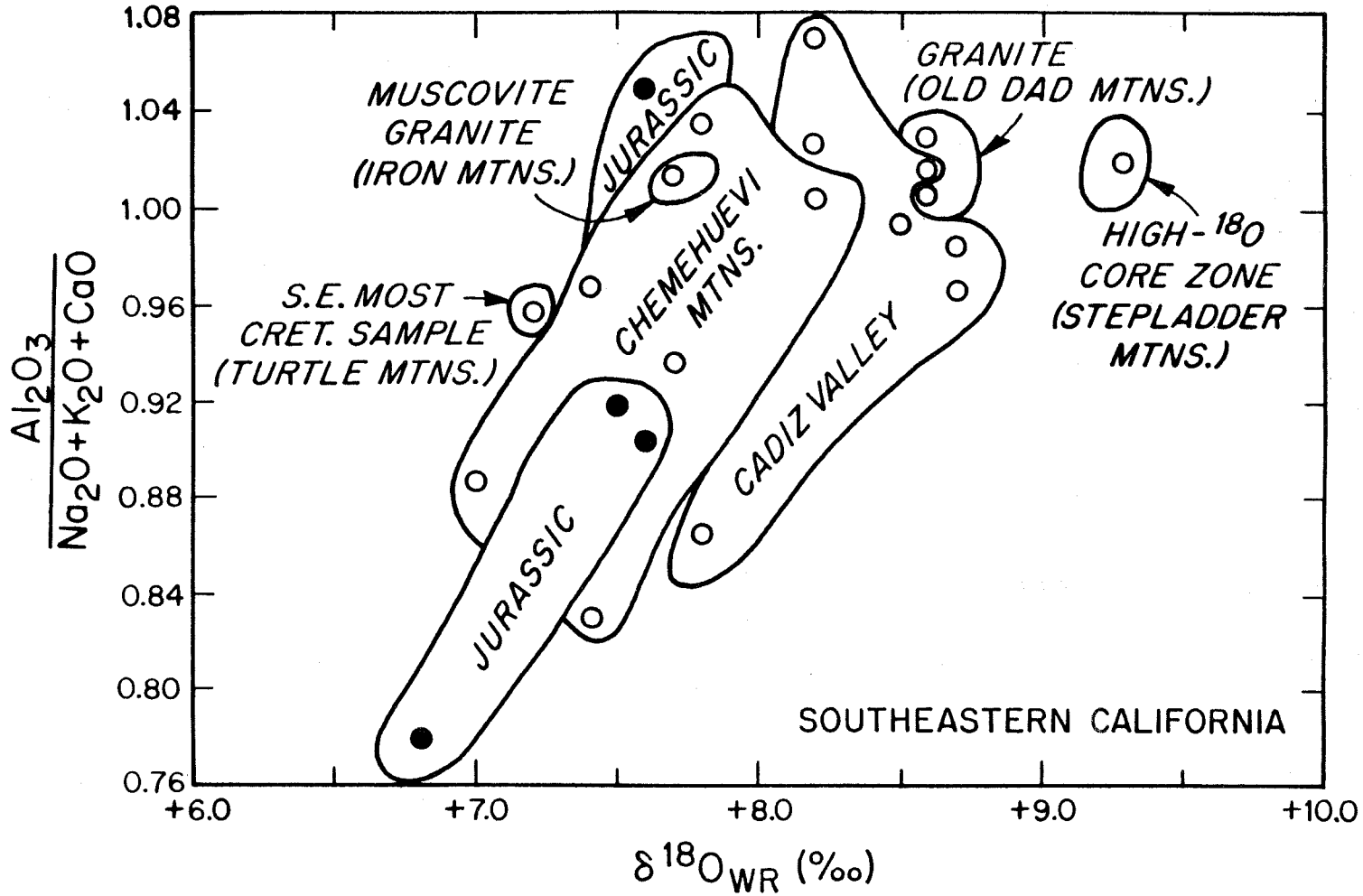
1.08
1.04
1.00
0.96
0.92
0.88
0.84
0.80
0.76
+6.0
+7.0
+8.0
+9.0
+10.0
$\frac{Al_2O_3}{Na_2O+K_2O+CaO}$
$\delta^{18}O_{WR}$ (‰)
MUSCOVITE GRANITE (IRON MTNS.)
JURASSIC
CHEMEHUEVI MTNS.
S.E. MOST CRET. SAMPLE (TURTLE MTNS.)
GRANITE (OLD DAD MTNS.)
HIGH-^{18}O CORE ZONE (STEPLADDER MTNS.)
CADIZ VALLEY
JURASSIC
SOUTHEASTERN CALIFORNIA

The muscovite granites are weakly peraluminous with values around 1.06 to 1.07. This is in strong contrast with Australian "S-type" peraluminous muscovite granites, which generally have values greater than 1.10. It is clear that both the Jurassic and Cretaceous plutons in the SMR area best fit the "I-type" category in relation to both their alumina content and $^{18}O/^{16}O$ composition, and this most definitely applies even to the muscovite-bearing plutons.

Figure 7.13 is a plot of SiO_2 content vs. $\delta^{18}O$ for the SMR samples. SiO_2 contents for both the Jurassic suite and the Cretaceous suite range from around 49 weight percent to as high as nearly 75 weight percent. However, the Jurassic samples are overall lower in $\delta^{18}O$ than the bulk of the Cretaceous plutons. The late Cretaceous granitic rocks with SiO_2 between 60 and 75 weight percent display a $\delta^{18}O$ range of more than 2 per mil. The bulk of the Cretaceous samples contain more than 65 weight percent SiO_2, and this > 2 per mil range in $\delta^{18}O$ is also observed in the entire grouping of samples between 65 and 75 wt. % SiO_2. Thus, for the Cretaceous samples as a whole, there is no correlation whatsoever between SiO_2 and $\delta^{18}O$.

As alluded to above, and as even more clearly indicated on Figure 7.13, it is not possible to derive the whole-rock $\delta^{18}O$ values of all of the SMR plutons from a common parent magma. The individual groupings of plutons on Figure 7.13 are obviously much more a function of age of intrusion or of geographic location than of chemical composition. For example, the Chemehuevi suite is overall distinctly lower in ^{18}O than both the Cadiz Valley suite and the core zone of the nearby Old Woman-Piute suite, even though all three suites have similar ages and span the same general range in major-element chemistry (e.g., SiO_2). The $\delta^{18}O$ values

Figure 7.13 Plot of whole-rock $\delta^{18}O$ versus SiO_2 (wt.%) for Mesozoic granitic plutons from the SMR, based on data listed in Table 7.1. Solid circles indicate Jurassic samples; open circles - late Cretaceous granodiorites, monzogranites, and two-mica granites. Late Cretaceous samples have been further subdivided into data envelopes that correspond with geographic and geologic entities discussed in text and shown in Figure 7.5.

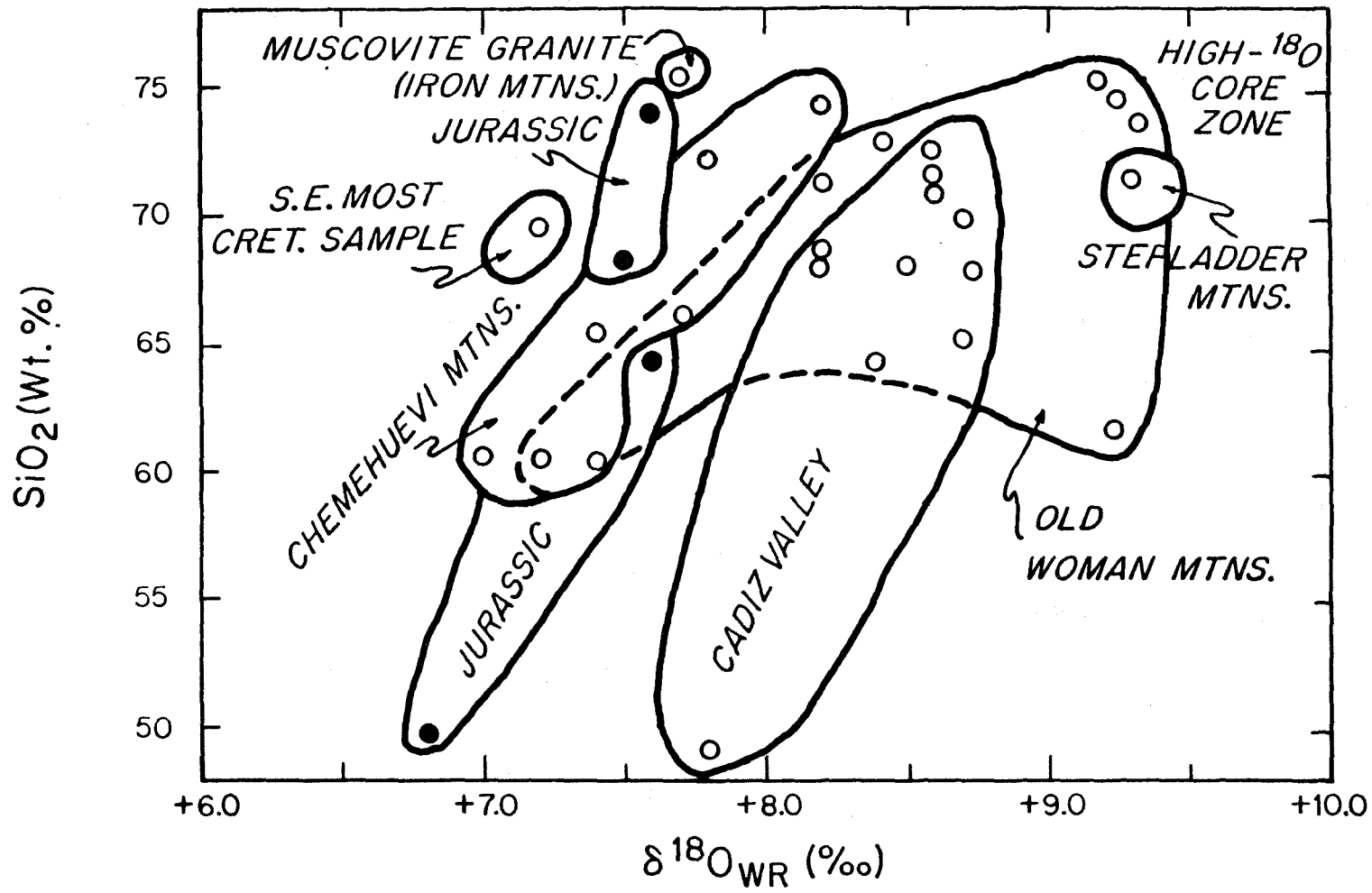
MUSCOVITE GRANITE
(IRON MTNS.)
JURASSIC
S.E. MOST
CRET. SAMPLE
CHEMEHUEVI MTNS.
JURASSIC
CADIZ VALLEY
HIGH-^{18}O
CORE
ZONE
STEPLADDER
MTNS.
OLD
WOMAN MTNS.
75
70
65
60
55
50
+6.0
+7.0
+8.0
+9.0
+10.0
SiO_2 (Wt. %)
$\delta^{18}O_{WR}$ (‰)

within each geographic or age grouping of plutons do, however, tend to increase with increasing SiO_2 content, but typically by only about 1 per mil over a change in SiO_2 from 50 to 75 weight percent. All of the age and geographic groupings in the SMR that have a sufficiently wide range of SiO_2 contents show these steep positive correlations on a $\delta^{18}O$-SiO_2 diagram, namely the Jurassic suite, the Cretaceous Chemehuevi suite, and the Cretaceous Cadiz Valley suite.

It is very important to note on Figure 7.13 that some of the samples with the highest SiO_2 contents are muscovite granites with relatively low $\delta^{18}O$ values. For example, even though the muscovite granite from the Iron Mountains has the highest SiO_2 of any SMR pluton (75.3 wt.%), it also has a $\delta^{18}O$ of only +7.7, lower than all of the other samples from the adjacent Cadiz Valley batholith, and much lower than the typical Australian S-type granite. This again confirms our earlier statements in Chapters 5 and 6 that in areas of abundant Precambrian cratonal basement outcrops, the peraluminous plutons from the southwestern Cordillera of the United States are generally <u>not</u> enriched in ^{18}O.

CHAPTER 8. $^{18}O/^{16}O$ and $^{87}Sr/^{86}Sr$ RELATIONSHIPS IN MESOZOIC PLUTONIC ROCKS OF SOUTHERN CALIFORNIA, WITH IMPLICATIONS FOR THE MAGMA SOURCE REGIONS

8.1 Introduction

This chapter synthesizes the results of our $^{18}O/^{16}O$ survey of the Mesozoic batholithic rocks from southern California. The area studied includes the Central and Eastern Transverse Ranges and the southeastern California desert, and is collectively referred to as the SECA area. In the Mojave Desert portion of SECA, $(^{87}Sr/^{86}Sr)_i$ values from the same $^{18}O/^{16}O$ sampling localities are presented where available, and these are discussed in terms of end-member mixing parameters, in an attempt to define the simplest possible characterization of the source rocks of these plutons. These studies extend our knowledge of the $\delta^{18}O$ and $^{87}Sr/^{86}Sr$ systematics in Cordilleran batholithic rocks eastward from the well-studied Peninsular Ranges Batholith (PRB) of southern and Baja California (Taylor and Silver, 1978; Silver et al., 1979; Hill et al., 1986; Taylor, 1986).

The concepts discussed in this chapter expand upon, and complement, a broader study of the whole-rock $\delta^{18}O$ values in Cordilleran Mesozoic plutonic rocks of the entire southwestern part of the United States (Solomon and Taylor, 1981; Taylor, 1986). These regional relationships are described more fully in Chapter 10.

Combined oxygen and strontium isotopic data on individual samples of plutons from the Transverse Ranges are not available at the present time. Also, only limited $^{87}Sr/^{86}Sr$ data are available for the Mojave Desert region. Nevertheless, even these reconnaissance geochemical stud-

ies can provide powerful constraints on magma genesis and on the nature of the source regions where melting takes place. It was noted in the preceding three chapters that the whole-rock $\delta^{18}O$ values of the Cordilleran granitic plutons are much more a function of geographic position than of rock type. It is also clear that, just as was discovered for the PRB (Taylor and Silver, 1978), the whole-rock $\delta^{18}O$ values of the plutons correlate most closely with large-scale geological features such as distance from the Pacific coast and the nature of the continental crust, rather than with petrography or major-element geochemical parameters (e.g., SiO_2 content or K/Na ratio).

The regional variations in whole-rock $\delta^{18}O$ of the Mesozoic plutons must be reflecting in some way, source-region compositional variations. Therefore, the combination of strontium isotope and oxygen isotope studies is particularly useful, because the variations in these two isotopic ratios in rocks are a result of completely different mechanisms. When these different mechanisms are imprinted upon the same package of possible protoliths of granitic magmas, they produce systematic isotopic variations that often provide characteristic "signatures" of specific source rocks. Thus, geochemical studies of granitic magmas may be one of the few ways to obtain direct information about packages of rocks making up large sections of the Earth's crust or mantle (see Chapters 3 and 4), because these rocks will impart their isotopic characteristics to the derivative melts.

Rocks characteristically become enriched in ^{87}Sr due to the accumulation of radiogenic strontium produced by the decay of ^{87}Rb; thus, in general, older source region terranes will have higher $^{87}Sr/^{86}Sr$ values than will younger terranes (Moorbath and Bell, 1965; Faure, 1977).

Strontium isotopic ratios also depend strongly upon the Rb/Sr contents of the source region, because Rb-enriched material will yield, over time, relatively higher $^{87}Sr/^{86}Sr$ values than will Rb-depleted material of the same age. The major reservoirs for ^{87}Sr-enriched material, then, are the older continental rocks and the sediments that are shed from them (McCulloch and Wasserburg, 1976).

On the other hand, all ^{18}O-enriched igneous rocks ($\delta^{18}O > 10.0$ per mil) essentially must be the result of previous stages of interaction between minerals and water at relatively low temperatures near the Earth's surface (Sheppard et al., 1969; Lawrence and Taylor, 1972; Savin and Epstein, 1970; Taylor, 1974; Taylor and Sheppard, 1986). This is due to the very large fractionation factors associated with oxygen isotope exchange between silicates and water at temperatures below 150°-250°C. Therefore, processes active in the surface- or near-surface environments during sedimentation, diagenesis, or low-temperature hydrothermal alteration create potential magma-forming reservoirs that may have $\delta^{18}O$ values ranging from the original, unaltered composition of the affected rock to values as high as +20 to +40 per mil for cherts and limestones and +10 to +20 for sandstones and shales.

Obviously, the package of source rocks undergoing melting need not be either chemically or isotopically homogeneous. Any mixing between isotopically distinct components within the package of source rocks that occurs prior to, during, or subsequent to anatexis should result in distinct correlations between strontium and oxygen isotopic ratios (Taylor and Silver, 1978; Vollmer, 1976; Taylor, 1980; Taylor and Sheppard, 1986). Indeed, strong correlations between oxygen and strontium isotopic compositions have now been observed in a large number of calc-alkaline

batholithic belts throughout the world (Taylor, 1980; Michard-Vitrac et al., 1980; Hill et al., 1986; Halliday and Harmon, 1981; Taylor and Silver, 1978; Wenner, 1981; Taylor, 1986; Sheppard, 1986).

8.2 The Peninsular Ranges Batholith Model

Taylor and Silver (1978; reviewed by Silver et al., 1979 and Taylor, 1986) discovered a remarkably systematic $\delta^{18}O$ - $^{87}Sr/^{86}Sr$ correlation in the Peninsular Ranges Batholith (PRB) of southern and Baja California. The primary $\delta^{18}O$ values of plutons were found to range from values as low as +6.0 on the west side of the batholith to values higher than +12.0 in the eastern half of the PRB. Also, the $\delta^{18}O$ values were found to increase systematically from west to east across the strike of the batholith along its entire 600 km length. An analogous west-to-east increase in $^{87}Sr/^{86}Sr$ ratios in the plutons of the PRB had previously been found by Early and Silver (1973); the initial $^{87}Sr/^{86}Sr$ ratios increase from 0.7027 on the west to 0.7072 or higher on the eastern side of the batholith. A unique feature of the $^{18}O/^{16}O$ data is the abrupt change in the whole-rock $\delta^{18}O$ values (termed the "^{18}O-step") near the central axis of the PRB. At the "^{18}O-step" the $\delta^{18}O$ values of the plutons change from $< +8.5$ to $> +9.0$ over a very short horizontal distance (typically right at a pluton boundary or on either side of a metamorphic screen or roof pendant between two plutons).

Taylor and Silver (1978) also discovered that all along its western edge, epizonal plutons were emplaced into the roof zone of the batholith. Hydrothermal systems were established in this shallowest part of the PRB during the early Cretaceous (130 - 105 Ma), and these display some interesting along-strike variations. North of the border between the U.S.A. and Mexico, these hydrothermal systems all involved low-^{18}O

meteoric waters, indicating subaerial conditions. However, south of a latitude about halfway between Ensenada and San Diego, these hydrothermal waters changed to much higher $\delta^{18}O$ values characteristic of ocean waters or marine formation waters. Thus, it appears that to the north this Cretaceous volcanic arc was emplaced on land, but that to the south it became submarine (analogous to the transition from the Alaska Peninsula to the Aleutian Island Arc today?). These hydrothermal effects are, however, all confined to the extreme western edge of the PRB and do not complicate the bulk of the batholith.

Taylor and Silver (1978) attributed the primary $^{18}O/^{16}O$ and $^{87}Sr/^{86}Sr$ signatures in the PRB to mixing between two end-members: (1) $\delta^{18}O$ ~ +6.0 per mil and $^{87}Sr/^{86}Sr$ ~ 0.7030; and (2) $\delta^{18}O$ ~ +13.0 per mil, or slightly higher, and $^{87}Sr/^{86}Sr$ ~ 0.7080, or slightly higher. They concluded that possible source materials with these characteristics might be a Rb-depleted upper mantle (MORB-type) source for component (1), and high-^{18}O metasedimentary rocks and/or altered volcanic rocks for component (2). They suggested that component (2) might be similar to Franciscan-type graywacke with intermixed basaltic greenstone (see Chapter 4).

Taylor and Silver (1978) found that this simple west-to-east pattern of a coupled increase in both $\delta^{18}O$ and $^{87}Sr/^{86}Sr$ did not apply to the northeasternmost portion of the PRB. Plutons in this zone, termed the San Jacinto-Santa Rosa Mountain (SJ-SR) block, exhibit high initial $^{87}Sr/^{86}Sr$ ratios, but have eastwardly decreasing $\delta^{18}O$ values. Taylor and Silver (1978) concluded that a third end-member with relatively high $^{87}Sr/^{86}Sr$ (> 0.7090) but relatively low $\delta^{18}O$ (< +9.0) was required in the source rocks of the plutons in this part of the PRB. Hill et al. (1986) followed this up with a detailed study of this portion of the batholith,

and they confirmed this conclusion of Taylor and Silver (1978); Hill et al. (1986) suggested that the third end-member probably had $\delta^{18}O$ ~ +6.0 to +8.0 per mil and $^{87}Sr/^{86}Sr$ ~ 0.7100. This component also becomes apparent at the extreme eastern edge of the main PRB; it appears to be the factor responsible for the decrease in $\delta^{18}O$ that can just barely be discerned along virtually the entire east side of the PRB (Taylor, 1986). However, the only place in the PRB where this component becomes volumetrically important is in the aforementioned San Jacinto-Santa Rosa Mountains (SJ-SR) block, where it has been termed the "model lithosphere component" or MLC by Hill et al. (1986); the source of the MLC is thought to be in the mafic lower crust or upper mantle beneath the North American craton (Taylor and Silver, 1978; Taylor, 1986).

Solomon and Taylor (1981) supplemented their own $\delta^{18}O$ data for Mesozoic and early Cenozoic plutons in southwestern North America with a general compilation of all available data by other workers (e.g., see Taylor, 1986). Solomon and Taylor (1981) recognized three $\delta^{18}O$ belts within the overall broad zone of Cordilleran batholithic rocks. In each of these belts, one or the other of the three components discovered by Taylor and Silver (1978) in the PRB appears to become dominant: (1) a western low-^{18}O zone (< +8.5 per mil) suggested to be dominantly derived from the upper mantle or from subducted oceanic crust; (2) a central high-^{18}O zone (> +9.0 per mil) derived dominantly from geosynclinal sediments or marine volcanic material altered at low temperatures, or both; and (3) an eastern low-^{18}O zone characterized by a zone of mixing between magmas derived from the upper mantle and the lower continental crust of the North American craton. Such a breakdown into only 3 end-member components is obviously too simplistic. Nevertheless, the Taylor and Silver

(1978) model for the PRB is a useful starting point, and in that context we shall in the subsequent discussion refer to these three hypothetical end-members as: (1) The "oceanic island-arc" source region (OIA), a representative example of which is the Marianas Arc (see Chapter 4), and which has many geochemical similarities to MORB-type materials. (2) The "sedimentary-altered volcanic" pile (SAV), a mixed greenstone-graywacke source with eugeoclinal affinities; the most prominent characteristic of this material is its very high $\delta^{18}O$ value ($\geq$ +13) combined with relatively unradiogenic $^{87}Sr/^{86}Sr$ ($\leq$ 0.710). (3) The "model lithosphere component" (MLC), which is a more ancient source region composed of material from either the subcontinental lithospheric mantle (SCLM), lower continental crust of the craton (LCC), or both.

8.3 $^{18}O/^{16}O$ and $^{87}Sr/^{86}Sr$ Contour Maps of SECA

Many of the details of the geology and geochemistry of the Jurassic and Cretaceous plutons in the SECA area (Figure 8.1) have already been discussed in Chapters 5, 6, and 7. Figure 8.1 shows all of the $^{18}O/^{16}O$ sample sites in the SECA area, the available $^{87}Sr/^{86}Sr$ analyses, the generalized geology of the Mesozoic plutons, the generalized age assignments for these plutons (Triassic, Jurassic, or Cretaceous, based on the literature reviews in Chapters 6 and 7), and the westernmost limits of observed Precambrian outcrops (again based on the references discussed in Chapters 6 and 7). Localities where both oxygen and strontium isotopic determinations were made at exactly the same sampling site are also shown on Figure 8.1.

The plutons are grouped into three generalized age categories: (1) ~ 200 Ma monzonites from the San Bernardino Mountains and the adjacent Granite Mountains area east of Victorville, together with the 230 Ma

Figure 8.1 Reconstructed geologic map of southeastern California (SECA), showing Mesozoic batholithic rocks and $^{18}O/^{16}O$ - $^{87}Sr/^{86}Sr$ sample localities. Small circles indicate localities where only $\delta^{18}O$ is available (from this thesis, as discussed in Chapters 6 and 7; $\delta^{18}O$ values given in Table 1, Appendix); large circles show thesis localities where $\delta^{18}O$ and initial $^{87}Sr/^{86}Sr$ are available (data shown in this figure, and also given in Table 7.1); and large triangles show $^{18}O/^{16}O$ and/or $^{87}Sr/^{86}Sr$ data taken from the literature. These latter data are given in Tables 1.1 and 1.2, or in Table 7.1 as footnotes, and shown in this figure: (1) Masi et al. (1981); (2) Miller (1978); (3) Frizzell (1986); pers. comm. (1984); (4) Joseph and Ehlig (1981); (5) Kistler (1979); (6) Ehlig (1982); (7) Lee et al. (1981); and (8) Calzia et al. (1986). The Mesozoic plutons are subdivided according to age into map units with the following patterns: (1) Triassic - diagonal lines; (2) Jurassic - crosses; and (3) late Cretaceous - stipples. Late-Cenozoic strike-slip displacements have been restored as follows: The SGM terrane has been reconstructed by first restoring movement along the north and south branches of the San Gabriel Fault (see Figure 6.8), and then by returning this entire terrane to its position prior to right-lateral movement along the San Andreas Fault using the reconstruction of Powell (1982). Finally, approximately 15 km of left-lateral movement along the Pinto Mountain Fault was removed (Powell, 1982). Sources for geology are listed in Figures 6.6, 6.9, 6.12, and 7.1. Dashed polygonal outlines indicate positions of various larger-scale maps discussed in Chapters 6 and 7 (Figures 6.6, 6.9, 6.12, 7.2, 7.6, and 7.7).

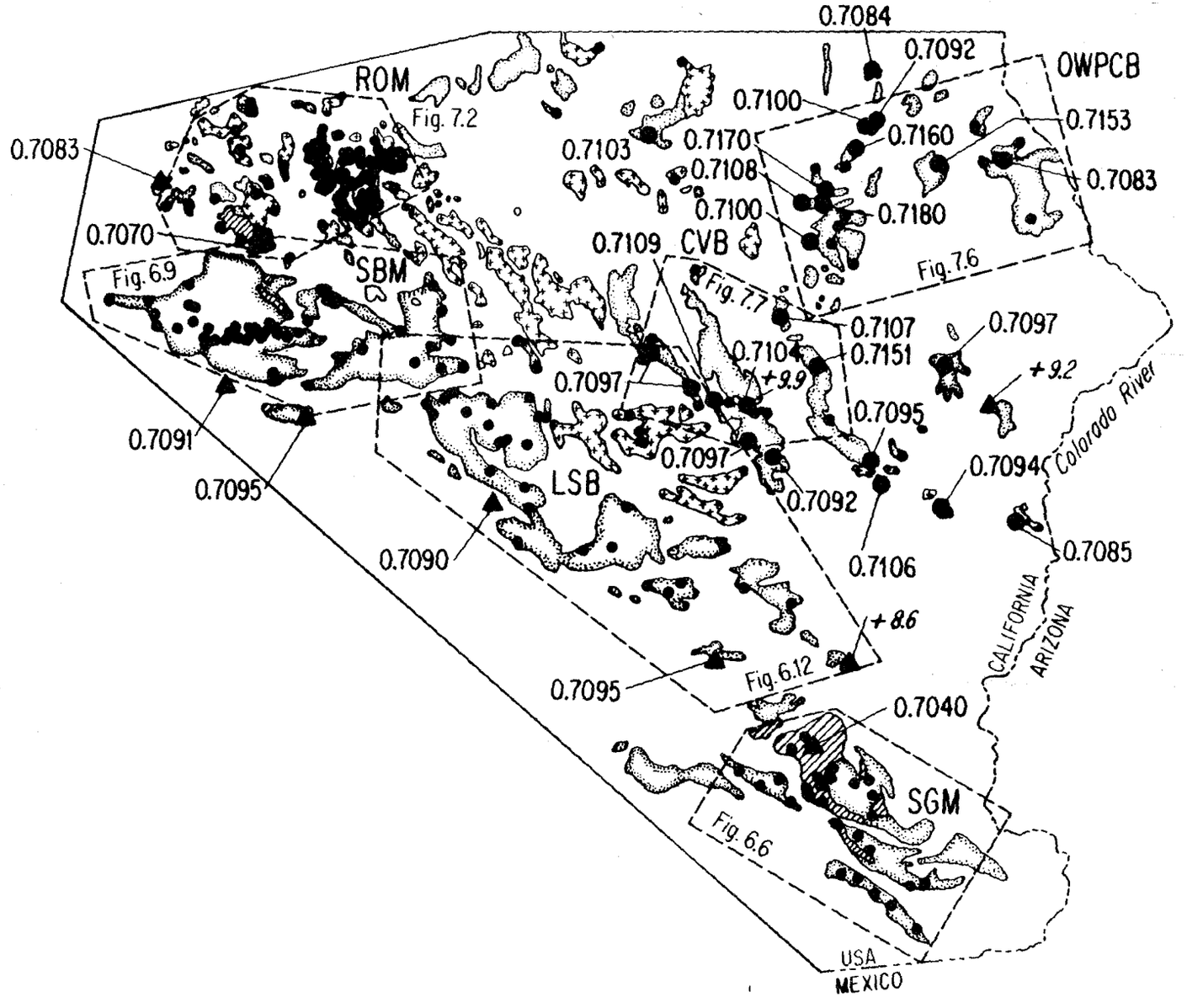
0.7084
0.7092
OWPCB
ROM
Fig. 7.2
0.7100
0.7153
0.7083
0.7103
0.7170
0.7160
0.7108
0.7100
0.7180
0.7070
0.7109
CVB
SBM
Fig. 7.7
Fig. 7.6
Fig. 6.9
0.7107
0.7097
0.7104
0.7151
+9.9
+9.2
0.7097
0.7095
Colorado River
0.7091
0.7097
0.7094
LSB
0.7092
0.7095
0.7106
0.7085
0.7090
+8.6
CALIFORNIA
ARIZONA
Fig. 6.12
0.7095
0.7040
SGM
Fig. 6.6
USA
MEXICO

Mount Lowe granodiorite from the San Gabriel Mountains basement complex; (2) ~ 145 to ~ 170 Ma monzodiorite, granodiorite, quartz monzonite, and syenite exposed in various ranges in the eastern portion of the SECA study area; and (3) the most important intrusive event, the emplacement of voluminous mid- to late-Cretaceous quartz monzonite plutons, together with less-abundant granodiorite and two-mica granite.

8.4 Pre-Cretaceous Igneous Rocks

Figure 8.2 shows initial $^{87}Sr/^{86}Sr$ values and contours of whole-rock $\delta^{18}O$ values for Triassic and Jurassic plutons in the SECA area. Most of these plutons have emplacement ages older than 160 Ma. The $\delta^{18}O$ contours are compiled from the more detailed $\delta^{18}O$ maps previously shown in Figures 6.6, 6.9, 6.12, 7.5, 7.6, and 7.7. This map for the early Mesozoic plutons (Figure 8.2) does not have anywhere near the resolution of the $^{18}O/^{16}O$ map for the Cretaceous plutons (Figure 8.4), both because the extent of outcrop is less for older plutons, and also because there is less areal geochemical coverage for the older plutons. In addition, many of these older rocks have "disturbed" $\delta^{18}O$ values (and $^{87}Sr/^{86}Sr$ ratios?) as a result of hydrothermal alteration. Also note that the $^{87}Sr/^{86}Sr$ results are far less detailed than the $^{18}O/^{16}O$ results. Nonetheless, several interesting observations may be made regarding the older set of plutons.

The initial $^{87}Sr/^{86}Sr$ contours for the older groups of plutons display a minimum value of 0.7040 centered on the Triassic Lowe granodiorite in the southern part of the fault-reconstructed SECA area (Figure 8.2). The values increase northward in the Jurassic plutons of the Big Maria and Little Maria Mountains area to values between 0.7085 and 0.7106 (3 localities). No higher values are known within the present very limited

Figure 8.2 Reconstructed geologic map of SECA, showing Jurassic and Triassic plutons, and the locations of Jurassic hydrothermal centers defined by whole-rock $\delta^{18}O$ contours (based on data given in Table 1, Appendix). Also shown are the sample localities where initial $^{87}Sr/^{86}Sr$ data are available (data shown on Figure and also given in Table 7.1). Restoration of strike-slip displacements along late Cenozoic faults is the same as that used for Figure 8.1. Jurassic plutons have crosses along the inside margins of map unit, and Triassic plutons are indicated by diagonal lines inside map unit. Heavy dashed line indicates the western limit of mapped Precambrian crystalline basement rocks. The SGM terrane has been restored to its position prior to late-Cenozoic displacement along the San Andreas Fault using the reconstruction of Powell (1982). Paleocene horizontal tectonic movements (Silver, 1982, 1983) have not been restored. Jurassic hydrothermal centers (HC) are: (1) ROM - Rodman-Ord Mountains; (2) DP - Devil's Playground; (3) BM - Bristol Mountains; (4) HV - Holcomb Valley; (5) CM - Copper Mountain; (6) DMD - Dale Mining District; (7) PM - Palen Mountains; (8) BMM - Big Maria Mountains. Source of geology is the same as cited for Figure 8.1.

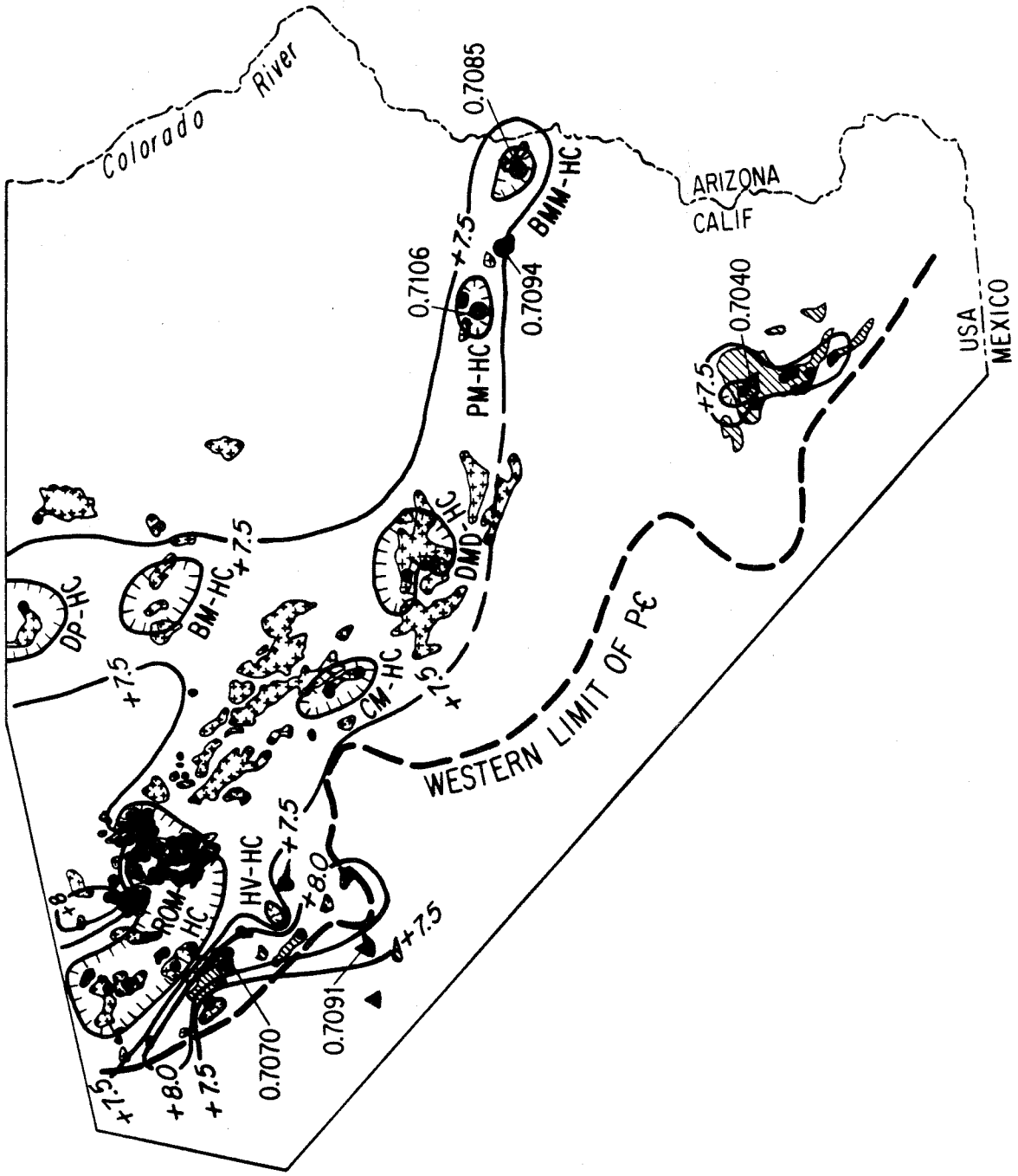
Colorado River
0.7085
BMM-HC
+7.5
0.7106
0.7094
PM-HC
ARIZONA
CALIF
0.7040
+7.5
USA
MEXICO
DMD-HC
DP-HC
BM-HC
+7.5
+7.5
CM-HC
+7.5
WESTERN LIMIT OF PC
HV-HC
+7.5
+8.0
+8.0
ROM HC
+7.5
0.7091
0.7070
+7.5
+8.0
+7.5

data base. In the northwestern portion of the area, only two localities have been studied, and these samples gave 0.7070 in the Triassic Granite Mountains pluton east of Victorville and 0.7091 in the Triassic Mill Creek pluton just to the south of the San Bernardino Mountains.

Discussions of the primary $^{18}O/^{16}O$ ratios in the Triassic-Jurassic plutons are complicated by the effects of widespread hydrothermal alteration by low-^{18}O meteoric waters. However, in the northwestern area, presumably "primary" $\delta^{18}O$ values have $\delta^{18}O > +8.0$, with some indication of a slight decrease to the west to values lower than +7.0, and a very clear indication of a broad decrease to characteristic regional values of about +6.5 to +7.5 in the eastern Mojave Desert. Fox (1988) analyzed K feldspars from the Jurassic plutons in the Bristol Mountains (see Figure 8.2), and found that primary $\delta^{18}O$ values were between +6.5 and +7.4; this indicates that primary whole-rock $\delta^{18}O$ for these rocks is likely to be near +7.8, after one takes into account the fact that $\delta^{18}O$ quartz will add about +0.4 per mil to the whole-rock mixture. The $\delta^{18}O$ contours have a northwesterly strike that roughly parallels the regional strike exhibited by the Jurassic magmatic arc as a whole. However, in the large Rodman-Ord Mountains (ROM) hydrothermal center, the primary $\delta^{18}O$ patterns are almost totally obliterated. This is also true to a lesser extent in the other areas of hydrothermal alteration (see Chapter 7).

When we view $^{18}O/^{16}O$ in Jurassic hydrothermal centers on a regional basis, within the Jurassic arc extending from western Nevada southeast to southern Arizona and Sonora, some remarkable patterns emerge. The Jurassic hydrothermal centers in SECA make up the central portion of the northwest-trending, 1,000 km graben depression proposed by Busby-Spera (1989) for the early Mesozoic continental arc (Figure 8.3). Whole-rock

Figure 8.3 Map of the southwestern United States showing Jurassic tectonic features discussed by Busby-Spera (1989). The 1,000 km graben depression is indicated by lines with perpendicular hash marks along the inside margins of the graben. The depositional environment for quartz arenitic sandstones associated with Jurassic volcanic centers is mapped by dashed lines, and differentiated according to either marine (horizontal lines within map unit), or non-marine deposition (stippled pattern within map unit). Jurassic hydrothermal centers are indicated by open circles and annotated with the following abbreviations: (1) Yn - Yerington District, NV; (2) Mineral King, CA; (3) RM - Rodman Mountains, CA; (4) Ch - Cowhole Mountains, CA; (5) CM - Copper Mountain, CA; (6) DMD - Dale Mining District, CA; (7) DP - Devil's Playground, CA; (8) BM - Bristol Mountains, CA; (9) PM - Palen Mountains, CA; (10) BMM - Big Maria Mountains, CA; (11) DR - Dome Rock Mountains, AZ; (12) CMB - Comobabi Mountains, AZ; (13) CR - Cobre Ridge, AZ; and (14) SR - Santa Rita Mountains, AZ. Line with thrust-fault symbols indicates approximate location of the axis of a Jurassic subduction zone.

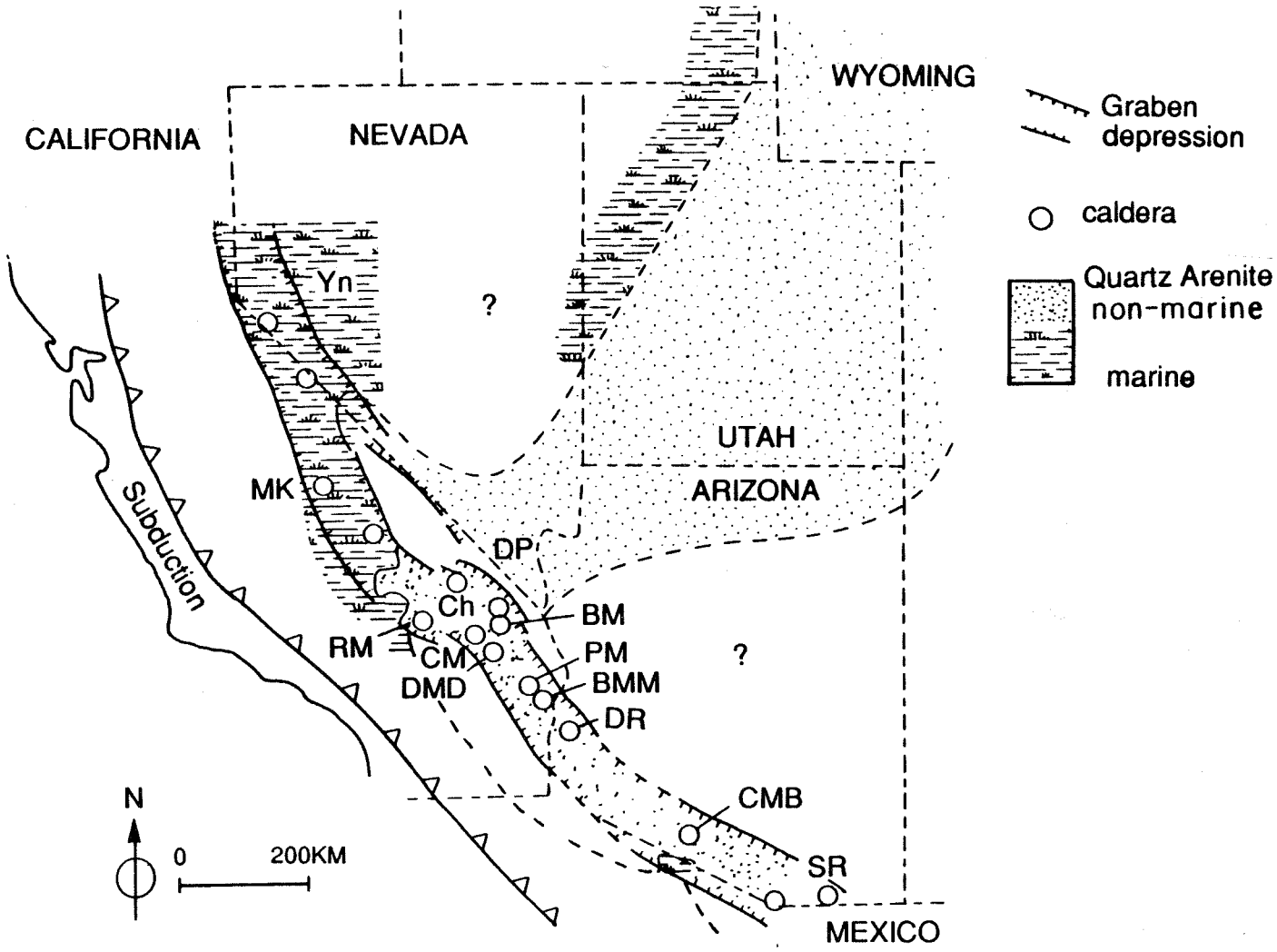
WYOMING
CALIFORNIA
NEVADA
Yn
?
UTAH
ARIZONA
MK
Subduction
DP
Ch
BM
RM
CM
PM
?
DMD
BMM
DR
CMB
SR
MEXICO
N
0
200KM
Graben
depression
caldera
Quartz Arenite
non-marine
marine

$\delta^{18}O$ values are available, at least in reconnaissance fashion, for most of the major Jurassic hydrothermal centers along the strike of the graben. These centers are (with range of whole-rock $\delta^{18}O$; and where available, initial $^{87}Sr/^{86}Sr$), from northwest to southeast: (1) the Yerington District, western Nevada (YN; +5.7 to +7.8; 0.7039 to 0.7045; Dilles et al., 1989, Solomon et al., 1983, and see Table 1, Appendix); (2) the Rodman-Ord Mountains (ROM; -3.2 to +9.0); (3) Devil's Playground (DP; +4.2); (4) Bristol Mountains (BM; ~+1.7 to ~+7.8; Fox, 1988); (5) Copper Mountain and Dale Mining District (CM and DMD; +5.2 to +7.0); (6) Palen Mountains (PM; +2.6; 0.7106); (7) Big Maria Mountains (BMM; +6.7; 0.7085); and (8) Brownell and Comobabi Mountains, south-central Arizona (BM and CM; +6.7 to +9.2; 0.7070).

Busby-Spera (1989) proposes that the major graben structure was occupied by calderas, which in places were flooded by lakes or marine embayments, as evidenced by thick sequences of ignimbrites intercalated with fluvial, lake, or marine sedimentary deposits. Our $^{18}O/^{16}O$ data coincide nicely with Busby-Spera's boundary separating marine-type sedimentary sequences on the northwest from predominantly continental-type strata on the southeast (see Figure 8.3). The centers to the southeast, or continental-side of the boundary, such as ROM, contain Jurassic plutons that were clearly hydrothermally altered by heated, low-^{18}O meteoric waters. In the case of the ROM area, these waters must have initially had $\delta^{18}O$ values as low as -10 per mil (see Section 7.3.2) indicating a relatively high, cool, mountainous terrane capable of fractionating coastal precipitation sufficiently to produce low-^{18}O rain and snow (e.g., see Taylor, 1974). Farther southeast, in Arizona, there is no indication of such ^{18}O-depleted meteoric waters, and thus that region must have lain

in an area with a warmer climate, lower topography, or closer proximity to the coast (or all three).

The only center for which we have $^{18}O/^{16}O$ data northwest of the marine/continental boundary is at Yerington, Nevada, where $\delta^{18}O$ values are relatively high (+5.7 to +7.8). One point worth mentioning is that granitic rocks at the Yerington center with $\delta^{18}O$ = +5.7 are as intensely altered mineralogically as those with $\delta^{18}O$ between -3.4 and +2.0 at the ROM center. Both areas contain granodiorites and quartz monzonites with intense propylitic epidote-chlorite veining, and albitic replacement of K-feldspars. In some cases, hand specimens from both areas look indentical to one another, but as indicated by whole-rock $\delta^{18}O$ values, the type of water involved in the alteration is clearly different between the two areas. At Yerington, Dilles et al. (1989) and Solomon et al. (1983) demonstrated that waters with initial $\delta^{18}O$ of around 0.0 per mil were responsible for propylitic alteration, as compared with much lighter water (-10 per mil) at the ROM area. Thus, the waters at Yerington were either sea water or some type of connate or formation water; either of these types of waters would fit nicely with the inferences made by Busby-Spera (1988) about the distribution of marine and terrestrial environments surrounding the graben depression shown on Figure 8.3.

Another interesting point to make is that the initial $^{87}Sr/^{86}Sr$ values also show the transition from a marine, island arc-type environment on the northwest to a continentally-rooted arc to the southeast. Where the arc sat in an oceanic environment, initial $^{87}Sr/^{86}Sr$ values were ~0.7040 (as at Yerington); and along the strike of the arc, to the southeast, much higher ratios are encountered (0.7085 to 0.7106 in SECA; and 0.7070 in southern Arizona; see Figure 8.2). This type of effect is

very reminiscent of the scenario for the East Japan-Marianas arc discussed in Chapter 4 and by Taylor (1986), where Ito and Stern (1985) showed that $\delta^{18}O$ and initial $^{87}Sr/^{86}Sr$ were elevated at the point where the northern portion of that arc cuts across continental terrane. Clearly, further $^{18}O/^{16}O$ and $^{87}Sr/^{86}Sr$ studies of unsampled portions of the Jurassic plutonic centers within Busby-Spera's regional graben would help refine and elaborate upon our initial, reconnaissance observations, and better map out these kinds of paleogeographic boundaries.

8.5 Cretaceous Igneous Rocks

The $^{87}Sr/^{86}Sr$ contours and $\delta^{18}O$ map patterns for the Cretaceous plutons in Figure 8.4 are compiled from data shown earlier in Figures 6.6, 6.9, 6.12, 7.5, 7.6, and 7.7. The map patterns in Figure 8.4 are based on many more data-points than in Figure 8.2, and they are also much less complicated by hydrothermal alteration effects. Thus, Figure 8.4 displays a much more regular distribution of isotopic contours, and there is a better resolution of regional strontium and oxygen isotope patterns than in Figure 8.2.

Initial strontium isotope contours in the eastern part of the SECA area show a concentric pattern with a split high-^{87}Sr region centered on the Old Woman - Piute batholith and the Cadiz Valley batholith. To the west, the $^{87}Sr/^{86}Sr$ values are as low ~ 0.7085 along the western side of the San Bernardino Mountains. Eastward, they rise to above 0.7100 in the Cadiz Valley batholith, and finally to values above 0.7150 still farther to the east in the Old Woman - Piute batholith. No $^{87}Sr/^{86}Sr$ contours are indicated for the San Gabriel Mountain block (southernmost portion of the map), but values there are reported to range between 0.7080 and 0.7095 (L.T. Silver, pers. comm.).

Figure 8.4 Reconstructed geologic map of SECA late-Cretaceous batholithic terranes, showing initial $^{87}Sr/^{86}Sr$ contours and $\delta^{18}O$ map units. Plutons are indicated by map unit with light stippled pattern along inside margins of map unit. The batholithic terranes are discussed in the text, and have the following abbreviations: (1) SBM - San Bernardino Mountains (Ch. 6); (2) LSB - Little San Bernardino Mountains (Ch. 6); (3) SGM - San Gabriel Mountains (Ch. 6); (4) ROM - Rodman-Ord Mountains (Ch. 7); and (5) SMR - southern Mojave Region (Ch. 7). Reconstruction of the relative position of these terranes by removing late-Cenozoic fault displacements is the same as discussed in Figure 8.1. The initial $^{87}Sr/^{86}Sr$ contours are based on values associated with $^{87}Sr/^{86}Sr$ sample localities, and are shown either as large triangles (data obtained from literature; see Figure 8.1 and footnotes in Table 7.1), or large circles (locations with combined $^{18}O/^{16}O$ and $^{87}Sr/^{86}Sr$ analyses; see Figure 8.1). Small circles indicate $^{18}O/^{16}O$ sample localities discussed in Chapters 6 and 7, with $\delta^{18}O$ values given in Table 1 (Appendix). The batholithic terranes have been subdivided into $\delta^{18}O$ map units, based on whole-rock $\delta^{18}O$ values as follows: (1) $\delta^{18}O \geq +9.5$ - solid pattern; (2) $+9.5 > \delta^{18}O \geq +9$ - diagonal line-pattern; (3) $+9 > \delta^{18}O \geq +8$ - no pattern; and (4) $\delta^{18}O < +8$ - large, random-dash stipple pattern. The western limits of Precambrian crystalline basement are shown by the heavy solid, dashed line (PCBL). Sources for geology are the same as Figure 8.1.

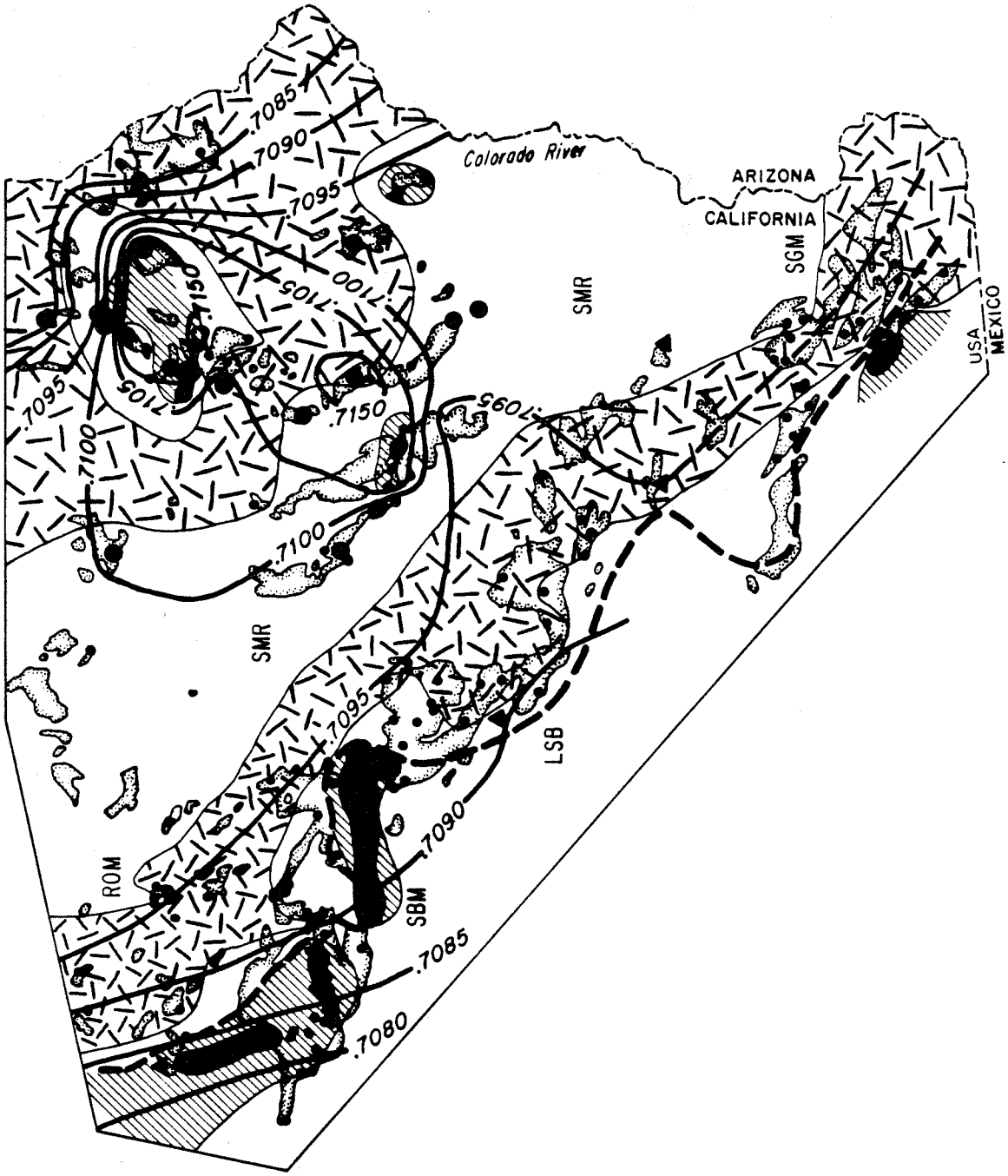
Colorado River
ARIZONA
CALIFORNIA
SGM
SMR
USA
MEXICO
.7085
.7090
.7095
.7100
.7105
.7150
SMR
LSB
ROM
SBM
.7080

A closed 0.7100 contour can be drawn completely around a large area (> 3,000 km^2) in the eastern Mojave Desert, encompassing the central Cadiz Valley batholith and a large portion of the Old Woman batholith extending eastward as far as the Stepladder Mountains. Locally, the values go up to 0.718 within this contour boundary (Figure 8.4). To the east, the $^{87}Sr/^{86}Sr$ values decrease abruptly in the eastern portions of this batholith, and near the Colorado River they go back down to 0.7085 in the Chemehuevi Mountains.

Considering the entire SECA area (discussed in detail in Chapters 6 and 7, and shown by comparison of Figures 8.2 and 8.4), it is clear that plutons with whole-rock $\delta^{18}O$ values greater than +9.5 essentially only occur west of the western limits of known Precambrian outcrops. The exception to this is in the Granite Mountains (Cadiz Valley Batholith; see Figure 7.7) where a sample analyzed by Lee et al. (1981; GR175, see Table 1.2) has $\delta^{18}O$ = +9.9. This sample is clearly anomalous because nearby samples all have $\delta^{18}O \leq +9$. Regardless of this anomaly, the extremely high-^{18}O zones (locally ranging up to $\delta^{18}O$ values as high as +10.8) west of the limit for Precambrian rocks also have $^{87}Sr/^{86}Sr \leq 0.709$, and as far as this thesis work is concerned, are confined to the southern part of the San Bernardino Mountains (and a tiny area in the San Gabriel Mountains). With the above-mentioned single exception, nowhere else in the southeastern California (SECA) area do Mesozoic plutons attain such high $\delta^{18}O$ values. In fact, except for the areas mentioned above and the well-defined high-^{18}O belt that forms the eastern half of the Peninsular Ranges Batholith (Taylor and Silver, 1978), such high-^{18}O plutons are otherwise totally absent from the entire southern California area. In this connection, note that in the pre-fault reconstruction, the

northeast edge of the PRB (San Jacinto-Santa Rosa block) would lie just south of the southernmost (SGM) terrane shown on Figures 8.1, 8.2, and 8.4. Thus, the entire PRB also was emplaced well to the west of any known Precambrian outcrops (Silver et al., 1979).

Another important feature is that, in general, the bulk of the SECA plutons display $\delta^{18}O$ values between +7.5 and +8.5. A low-^{18}O zone with $\delta^{18}O \leq +8.0$ forms a northwest-trending belt lying to the east of the high-^{18}O zone that makes up the central axis of the San Bernardino Mountains (SBM). This low-^{18}O zone lies just to the east of the heavy dashed line on Figures 8.1 to 8.3 that represents the westernmost outcrops of Precambrian craton, and it extends without break all along the east side of the fault-reconstructed terrane now occupied by the Transverse Ranges (Figure 8.4). It represents the western edge of a broader zone with $\delta^{18}O < +9.0$ that extends eastward from the Transverse Ranges across the entire SECA area. This broad low-^{18}O zone is disrupted in only three places where slightly higher $\delta^{18}O$ values (+9.0 to +9.3) occur within the central portions of the Old Woman-Piute and Cadiz Valley batholiths and in one sample collected near the Colorado River. However, it is clear that these areas represent local anomalies around distinctive plutonic centers, because the regional low-^{18}O values are rapidly recovered as one moves to the fringes of each batholith. Also, these areas are nowhere near as ^{18}O-rich as the high-^{18}O belt that occurs farther to the west, and they are also readily distinguishable from that high-^{18}O zone because their initial $^{87}Sr/^{86}Sr$ values are much higher (>0.710).

Primary $^{18}O/^{16}O$ contours show a number of important characteristics that correlate directly with the $^{87}Sr/^{86}Sr$ systematics described above. In the eastern part of the SECA region the only significant area of plut-

ons having $\delta^{18}O > +9.0$ is confined to the zone in the Old Woman batholith that has $^{87}Sr/^{86}Sr > 0.715$. The moderately high-^{18}O values observed in this area and in the other 2 "anomalous" areas correlate very well with the high initial $^{87}Sr/^{86}Sr$ values centered on these same batholiths. We need to emphasize that these local high-^{18}O "centers" in the eastern part of the SECA region contrast sharply with the northwest-trending high-^{18}O zone observed along the western side of the fault-reconstructed Transverse Ranges (Figure 8.4), and which continues farther to the south down the eastern half of the PRB. This linear zone of high-^{18}O plutons exhibits relatively uniform and <u>low</u> initial $^{87}Sr/^{86}Sr$ ratios (0.7070 to 0.7095). The regional patterns and local "anomalies" in both $^{18}O/^{16}O$ and $^{87}Sr/^{86}Sr$ across the SECA area are clearly indicative of isotopic variations in the source regions of the magmas that crystallized to form these batholiths.

Although the narrow belt with $\delta^{18}O \leq +8.0$ that extends along the east side of the reconstructed SGM, SBM, and LSB areas appears to represent a primary $^{18}O/^{16}O$ feature (Figure 8.4), it is likely that <u>some</u> of the low-^{18}O rocks in this belt are a secondary phenomenon attributable to meteoric-hydrothermal alteration (particularly some of the samples with $\delta^{18}O$ lower than +6.0 to +7.0 per mil). These hydrothermal alteration phenomena are, however, nowhere near as important as those associated with the Jurassic hydrothermal events that were prominent throughout the SECA region, particularly the ones in the ROM area. As discussed earlier in this Chapter, as well as in Chapters 6 and 7, the age of the most extensive hydrothermal alteration event(s) is clearly pre-Middle Cretaceous, whereas the regional isotopic variations discussed above apply to plutons emplaced mainly during the Late Cretaceous. Nonetheless, the

existence of outcrops of mid-Tertiary volcanic rocks between the fault-reconstructed SGM terrane and the LSB terrane suggests that there could have been some mid-Tertiary hydrothermal activity.

8.6 Combined Strontium and Oxygen Isotopic Results

The combined $\delta^{18}O$ and initial $^{87}Sr/^{86}Sr$ results from the SECA study area are shown in Figure 8.5, and the data are listed in Table 7.1. Several of the data pairs come from other studies (shown with special symbols in Figure 8.1, and listed as footnotes in Table 7.1), including results from Thermal Canyon in the LSB area (Joseph and Ehlig, 1981); the western ROM area (Masi et al., 1981; Miller, 1978); Mill Creek in the SBM area (Frizzell, 1986; pers. comm., 1984); Liebre Mountain (Masi et al., 1981); and the Cadiz Valley batholith (Calzia et al., 1986). We do not show the data pair for GR175 from Lee et al. (1981; and see Table 1.2) on Figure 8.5 because we feel this sample is anomalously high in $\delta^{18}O$ (+9.9), as explained above. Also shown for comparison are the initial $^{87}Sr/^{86}Sr$ ratios and oxygen isotopic data determined by Taylor and Silver (1978) and Hill et al. (1986) for the main part of the Peninsular Ranges Batholith (PRB) and the San Jacinto-Santa Rosa Mountains (SJ-SR) portion of the PRB.

The array of data-points for the main part of the PRB (Taylor and Silver, 1978) forms a well-defined linear cluster with a steep slope on Figure 8.5. The $^{87}Sr/^{86}Sr$ - $\delta^{18}O$ data for the SECA area, on the other hand, form a more poorly defined linear array with a much shallower slope on Figure 8.5. The Cretaceous SECA data roughly extend from an end-member with $\delta^{18}O$ ~ +7.0 per mil and $^{87}Sr/^{86}Sr$ ~ 0.7080 to one with ~ +9.0 per mil and ~ 0.7180. The SECA sample with highest $^{87}Sr/^{86}Sr$ and $^{18}O/^{16}O$ values is a two-mica ± garnet granite that intrudes upper amphibolite-grade metasediments in the Old Woman Mountains (Miller et al., 1982).

Figure 8.5 Plot of initial $^{87}Sr/^{86}Sr$ versus whole-rock (WR) $\delta^{18}O$ of Mesozoic granitic rocks from SECA and the Peninsular Ranges Batholith (PRB), including the San Jacinto-Santa Rosa (SJ-SR) block of the PRB. Data from the PRB are taken from Taylor and Silver (1978) and Hill et al. (1986). SECA data are shown in Figure 8.1, and also given in Table 7.1. Data are subdivided as follows: (1) Cretaceous PRB - solid circles; (2) Cretaceous SJ-SR block - open squares (single open triangle indicates sample 15, Table 1.1, Western Mojave Desert); (3) SECA Triassic plutons - crosses; (4) SECA Jurassic plutons - solid triangles; (5) SECA Cretaceous granodiorites and quartz monzonites - open circles; and (6) SECA Cretaceous two-mica granites - open circles with dots. MLC = Model Lithospheric Component of Hill et al. (1986).

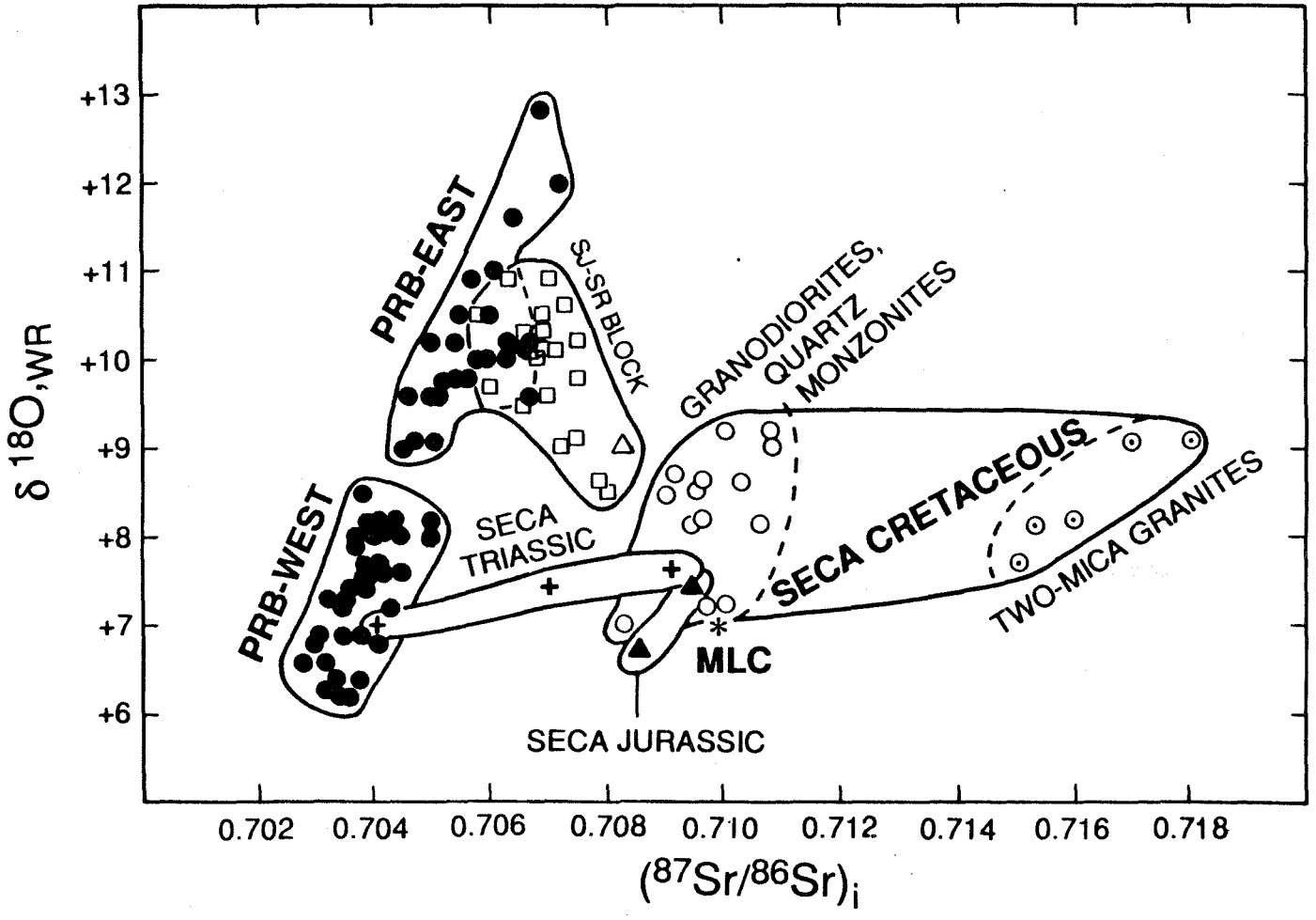
+13
+12
+11
+10
+9
+8
+7
+6
δ 18O,WR
PRB-EAST
SJ-SR BLOCK
GRANODIORITES,
QUARTZ
MONZONITES
SECA CRETACEOUS
TWO-MICA GRANITES
PRB-WEST
SECA
TRIASSIC
MLC
SECA JURASSIC
0.702
0.704
0.706
0.708
0.710
0.712
0.714
0.716
0.718
(87Sr/86Sr)i

The other Cretaceous SECA samples plotted on Figure 8.5 are comprised of monzogranites and granodiorites; one sample is particularly important because it comes from a Cretaceous granodioritic pluton intruded by the aforementioned Cretaceous two-mica granite of the Old Woman Mountains batholith. This granodiorite pluton has $\delta^{18}O$ ranging between +7.5 and +9.1, together with an initial $^{87}Sr/^{86}Sr$ ratio < 0.7110, indicating that the nature of the source regions of these two geographically and temporally associated plutons are clearly different.

The remainder of the SECA samples are a mixture of Cretaceous, Jurassic and Triassic plutons (see discussion in Chapters 6 and 7; and John, 1981; Howard et al., 1982; Miller et al., 1982). The Jurassic samples form a sub-set within the cluster of SECA samples, they have a narrower range of $^{87}Sr/^{86}Sr$ < 0.7110 and $\delta^{18}O$ < +8.4 per mil. Cretaceous plutons overlap the Jurassic range, but also extend to much more evolved values, with $^{87}Sr/^{86}Sr$ > 0.7110 and $\delta^{18}O$ > +8.5 per mil. The Triassic samples are the only ones that form an array that appears to be "rooted" in the main PRB trend; this array extends towards the vicinity of the model lower crust of Hill et al. (1986).

As mentioned earlier, Taylor and Silver (1978) interpreted the main PRB linear array to be the result of simple two-component mixing, with the simplest possible end-members defined by the limits of the array at (~0.703; +6.0 per mil) and (0.708 to 0.710; +13.0 to +16.0 per mil). Hill et al. (1986) interpreted the isotopic array from the Cretaceous SJ-SR area to represent mixing between the higher-^{18}O end of the PRB array and a hypothetical end-member derived from the lower continental crust or the subcontinental lithospheric mantle; the latter was suggested to have $\delta^{18}O$ and $^{87}Sr/^{86}Sr$ of about +7.0 to +8.0 and 0.708 to 0.709, respective-

ly. The SECA Jurassic and Cretaceous samples fall along a broad, slightly curved array with a shallow positive slope (Figure 8.5); one end of this array is rooted on Figure 8.5 in a position very close to the proposed "model lithosphere component" or MLC of Hill et al. (1986).

8.7 $\delta^{18}O$-$^{87}Sr/^{86}Sr$ Mixing Models

Simple two-component mixing of materials with different isotopic ratios has been discussed by many investigators (Vollmer, 1976; Langmuir et al., 1978; DePaolo and Wasserburg, 1976), and mixing along with assimilation during fractional crystallization (AFC) has been discussed by Taylor (1980, 1986) and DePaolo (1981) for $\delta^{18}O$-$^{87}Sr/^{86}Sr$ systems. The study by Taylor (1980) ruled out high-level assimilation processes as an important factor in the production of the major calc-alkaline batholithic magmas in the Peninsular Ranges Batholith, the Caledonian terrane of Scotland, and several others. This is principally because assimilation at high levels in the crust requires large amounts of crystallizing cumulate material to provide the heat necessary for melting, implying a correlation between the extent of assimilation and the stage of fractional crystallization (Taylor, 1980), whereas in fact the $\delta^{18}O$ variations in the intrusive sequences are essentially independent of rock type or of major-element geochemistry (Silver et al., 1979; Gromet and Silver, 1985). The same constraints apply to the SECA plutons studied in this work because the SiO_2-rich plutons span a wide range of $\delta^{18}O$ throughout the eastern portions of the Cordillera (Figure 7.13). SiO_2-rich (74-76 wt. %) "minimum melt"-type plutons can be found with more primitive, relatively low $\delta^{18}O$ values, as well as with higher-^{18}O, crustal $\delta^{18}O$ values.

Additionally, within the zones occupied by high-^{18}O plutons, essentially all of the rock types (granodiorite, tonalite, and quartz monzonite, as well as two mica-granite), have $\delta^{18}O > +9.0$ per mil (e.g., San Bernardino Mountains, see Chapter 6; also, see Solomon and Taylor, 1982). This is not compatible with an AFC process. If assimilation may be ruled out as a major process, then we are left basically with some form of two-component, source-region mixing to explain the strong correlation observed between the two isotopic systems (Figure 8.5). For example, such a two-component mixing system could be composed of two different magmas from distinct source regions having differing isotopic compositions, or it could be characterized by fusion of interlayered rocks dominated by two main components with drastically different isotopic compositions, such as mafic amphibolite and granitic gneiss.

The methods of Vollmer (1976) are employed to evaluate the isotopic data. A two-component mixing system may be described in the most general case by the equation for a hyperbola:

$$Ax - Bxy + Cy + D = 0 \quad (1)$$

where:

$$A = a_2b_1y_2 - a_1b_2y_1 \quad (2)$$

$$B = a_1b_2 - a_2b_1 \quad (3)$$

$$C = a_2b_1x_1 - a_1b_2x_2 \quad (4)$$

$$D = a_2b_1x_2y_1 - a_2b_1x_1y_2 \quad (5)$$

$y = {}^{87}Sr/{}^{86}Sr$ in the mixture (6)

$x = \delta^{18}O$ in the mixture (7)

$y_1 = {}^{87}Sr/{}^{86}Sr$ in component 1 (8)

$y_2 = {}^{87}Sr/{}^{86}Sr$ in component 2 (9)

$x_1 = \delta^{18}O$ in component 1 (10)

$x_2 = \delta^{18}O$ in component 2 (11)

a_1 = ^{86}Sr content of component 1 with the isotopic ratio y_1 (12)

a_2 = ^{86}Sr content in component 2 with the isotopic ratio y_2 (13)

b_1 = ^{16}O content in component 1 with the $\delta^{18}O$ x_1 (14)

b_2 = ^{16}O content in component 2 with the $\delta^{18}O$ x_2 (15)

As discussed by Taylor (1978, 1980, 1986), in general, differences in oxygen content of rocks are not important in these calculations, because the oxygen concentrations are all fairly uniform between about 45 to 50 weight percent for any protoliths that could reasonably be considered sources for granitic magmas. Thus, in order to simplify the solution to equation (1), the assumption may be made that:

$$b_1 = b_2 \tag{16}$$

The solution to equation (1) may be obtained by solving for x and y simultaneously through the use of the simple mass balance of oxygen between the two components:

$$x = X_2(x_2 - x_1) + x_1 \tag{17}$$

where X_2 is the mole fraction (or weight fraction) of oxygen from component 2 in the mixture. The mole fractions and weight fractions are identical in the case of oxygen, because the oxygen contents of the two end-members are assumed to be identical.

Figure 8.6 presents solutions to equation (1) for the combined isotopic systems, which illustrate the mixing between a hypothetical "mantle" or MORB-type component, with $^{87}Sr/^{86}Sr$ = 0.7030 and $\delta^{18}O$ = +5.7 per mil, and a hypothetical sedimentary or "upper continental crust" component, with $^{87}Sr/^{86}Sr$ = 0.7350 and $\delta^{18}O$ = +19.0. Taken as an isolated mixing system, a plot of the weight fraction of one mixing component versus $\delta^{18}O$ would be a simple straight line connecting the end-member compositions, as per equations (16) and (17). The similar plot for iso-

Figure 8.6 Plot of whole-rock $\delta^{18}O$ versus initial $^{87}Sr/^{86}Sr$ showing calculated curves that result from simple two-component mixing of end-members with: (1) $\delta^{18}O$ = +5.7; initial $^{87}Sr/^{86}Sr$ = 0.7030; and (2) $\delta^{18}O$ = +19; initial $^{87}Sr/^{86}Sr$ = 0.7350; and (3) variable strontium (ppm) concentrations in each end-member. The curves plot the solutions to equation (1) in the text, for different weight fractions of the two components, given the key assumption that oxygen concentrations are the same in each component (see equation 16, in the text). The Z-value shown with each curve indicates the ratio of Sr (ppm) for the two end-members (see equation 18, in text).

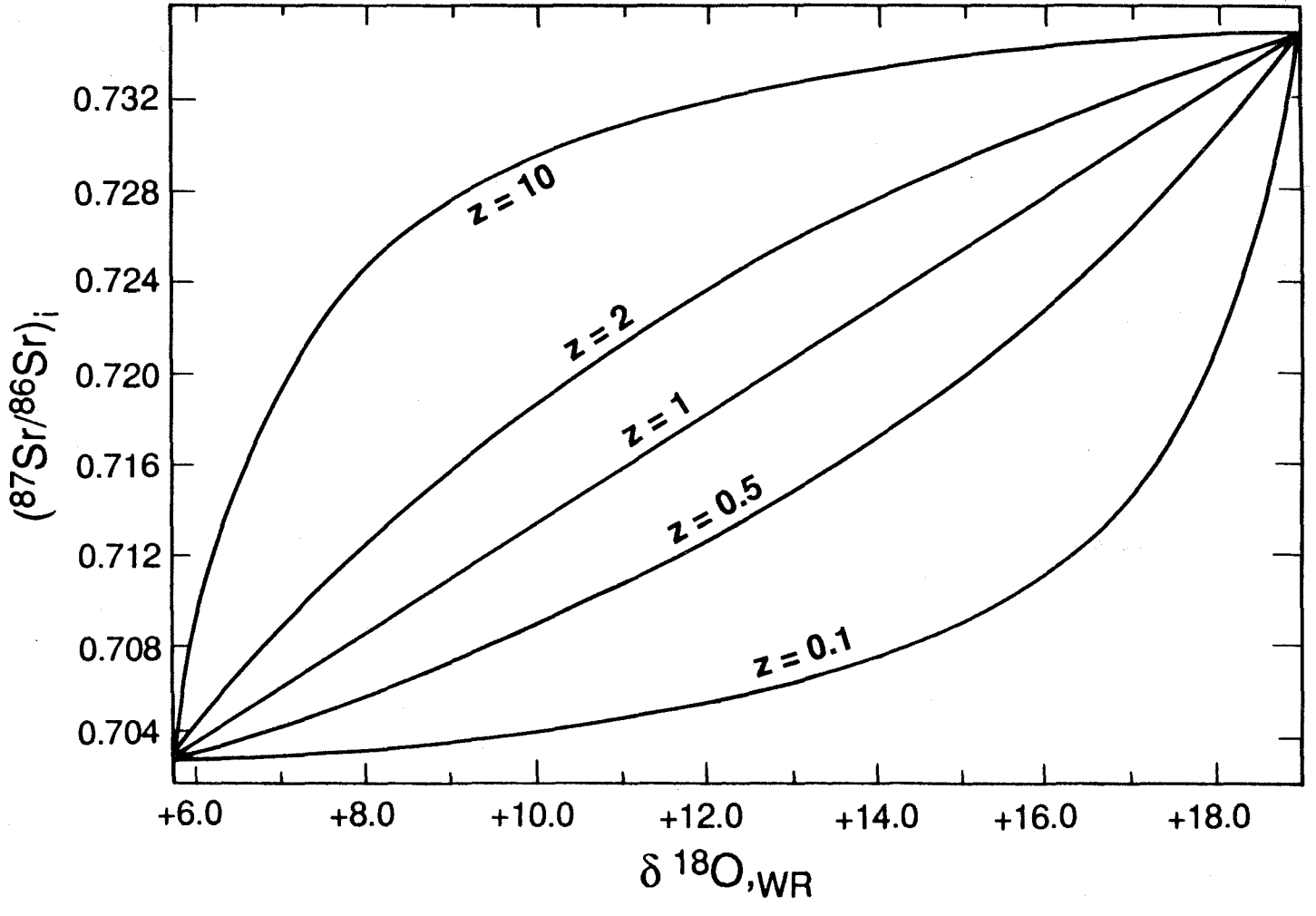
0.732
0.728
0.724
0.720
0.716
0.712
0.708
0.704
$(^{87}Sr/^{86}Sr)_i$
z = 10
z = 2
z = 1
z = 0.5
z = 0.1
+6.0
+8.0
+10.0
+12.0
+14.0
+16.0
+18.0
$\delta\ ^{18}O_{,WR}$

lated mixing of strontium isotopes is more complex, however, and shows the consequences of mixing together various weight fractions of end-members having unequal strontium concentrations (in ppm). For strontium, each solution is a hyperbola whose curvature depends upon the ratio:

$$Z = (Sr_1, \text{ppm})/(Sr_2, \text{ppm}) \quad (18)$$

where, as a first approximation:

$$a_2 = (Sr_2, \text{ppm})/(y_2 + 1), \text{ and} \quad (19)$$

$$a_1 = (Sr_1, \text{ppm})/(y_1 + 1). \quad (20)$$

On Figure 8.6, the large curvatures for the cases where Z is much less than, or much greater than one, are simply a result of dilution of the isotopic composition of one end-member by either a much more strontium-rich or a much more strontium-poor end-member, respectively. An important result of these calculations is that simple two-component mixing need not result in straight line behavior for the strontium-oxygen isotopic system.

Given the wide range in strontium contents (~70 to ~800 ppm) of potential magma sources (Turekian, 1961; Halliday and Harmon, 1981; Hill et al., 1986; Michard-Vitrac et al., 1980), plausible two-component mixing systems may have values for Z between 10 and 0.1. Older felsic continental crust tends to be low in strontium, with values around 100 to 300 ppm (e.g., Kistler et al., 1981) or less (70 ppm Sr in some metasediments from the Peninsular Ranges Batholith; Hill et al., 1986). More mafic amphibolitic material, graywacke sandstones, and mafic intrusives typically have higher values, between 400 and 1000 ppm (Turekian, 1962; Halliday and Harmon, 1981). In general, for magmas derived from the sub-continental lithosphere or asthenosphere, the more primitive and "mantle"-like a material is, the higher its strontium content. Alkalic mafic

magmas tend to be particularly rich in Sr (> 1000 ppm); therefore, as a suite of igneous rocks becomes more alkalic (i.e., K-rich), one can in general also expect it to become more Sr-rich. However, it must be stressed that some tholeiitic mafic rocks (e.g., MORBs) may have very low strontium contents (e.g., ~70 ppm Sr in gabbros in the PRB, L.T. Silver, pers. comm.). In addition, some felsic rocks may be high in strontium (650 ppm Sr in crustal material, Ruby Mountains, Nevada, Kistler et al., 1981), particularly if they contain intermixed limestones and dolomites.

Model solutions for simple two-component mixing have been calculated for the Cretaceous SECA and PRB arrays shown in Figure 8.5. The model calculations are depicted on Figure 8.7. End-member compositions similar to those predicted in Taylor and Silver (1978) were used for the PRB samples, while the simplest possible combination of end-members was utilized for the SECA array. The high-^{18}O end-member was chosen by virtue of the fact that it closely bounds the "minimum melt" type two-mica granite composition, which may itself represent a relatively pure "first melt" of some portion of the continental crust. In addition, the chosen values are similar to values one may expect for the Precambrian basement terrane that underlies much of the SECA area (Silver, 1977). The low-^{18}O end-member was chosen so that the calculated curves would encompass all the points in the array with reasonable values for Z (~10 to 0.1), and also so that its composition would lie as close as possible to the most "primitive" data-points to the left of the array, and still yield a reasonable curve. This hypothetical end-member turns out to be very similar to the MLC or "model lithosphere component" that was suggested to be one of the major components of the plutons in the San Jacinto-Santa Rosa Mountain block by Hill et al. (1986). Obviously, a major part of the scatter in

Figure 8.7 Plot of initial $^{87}Sr/^{86}Sr$ versus whole-rock $\delta^{18}O$ comparing data from Mesozoic granitic plutons in the Peninsular Ranges Batholith (PRB), the San Jacinto-Santa Rosa (SJ-SR) block and SECA with model two-component mixing curves. The data represent a hypothetical west-east traverse, as discussed in the text, and are subdivided into two major trends: (1) the Cretaceous PRB trend (solid circles; Taylor and Silver, 1978); and (2) the SECA trend (Triassic plutons - crosses, Jurassic plutons - open circles, and Cretaceous plutons - solid triangles; see Table 7.1). The SJ-SR transition (Cretaceous SJ-SR plutons - open squares; Taylor and Silver, 1978; Hill et al., 1986; Cretaceous pluton near Victorville, CA - open square with cross; Masi et al., 1981) is the transitional "link" between the PRB and SECA trends, as one goes from west to east along the hypothetical traverse. Using terminology defined in Table 4.1 and discussed in the text, the model mixing curves for the PRB trend are calculated for mixing between OIA ($\delta^{18}O$=+5.7; I-Sr=0.7025) and SAV ($\delta^{18}O$=+13; I-Sr=0.7075); curves for the SECA trend show mixing between SCL, or LCC ($\delta^{18}O$=+7; I-Sr=0.7070) and MCC ($\delta^{18}O$=+9.5; I-Sr=0.7190). The Z-values shown with each mixing curve indicate ratios of Sr concentrations in the two end-members of each trend. The SJ-SR transition clearly shows that the SAV component is lost as one traverses to the inboard side of the craton. Although no $^{87}Sr/^{86}Sr$ data are available for Cretaceous plutons from the SBM area (see Figure 8.1), because of their geographic position, it is likely these high $\delta^{18}O$ rocks would fit in with the SJ-SR grouping (see Chapter 6).

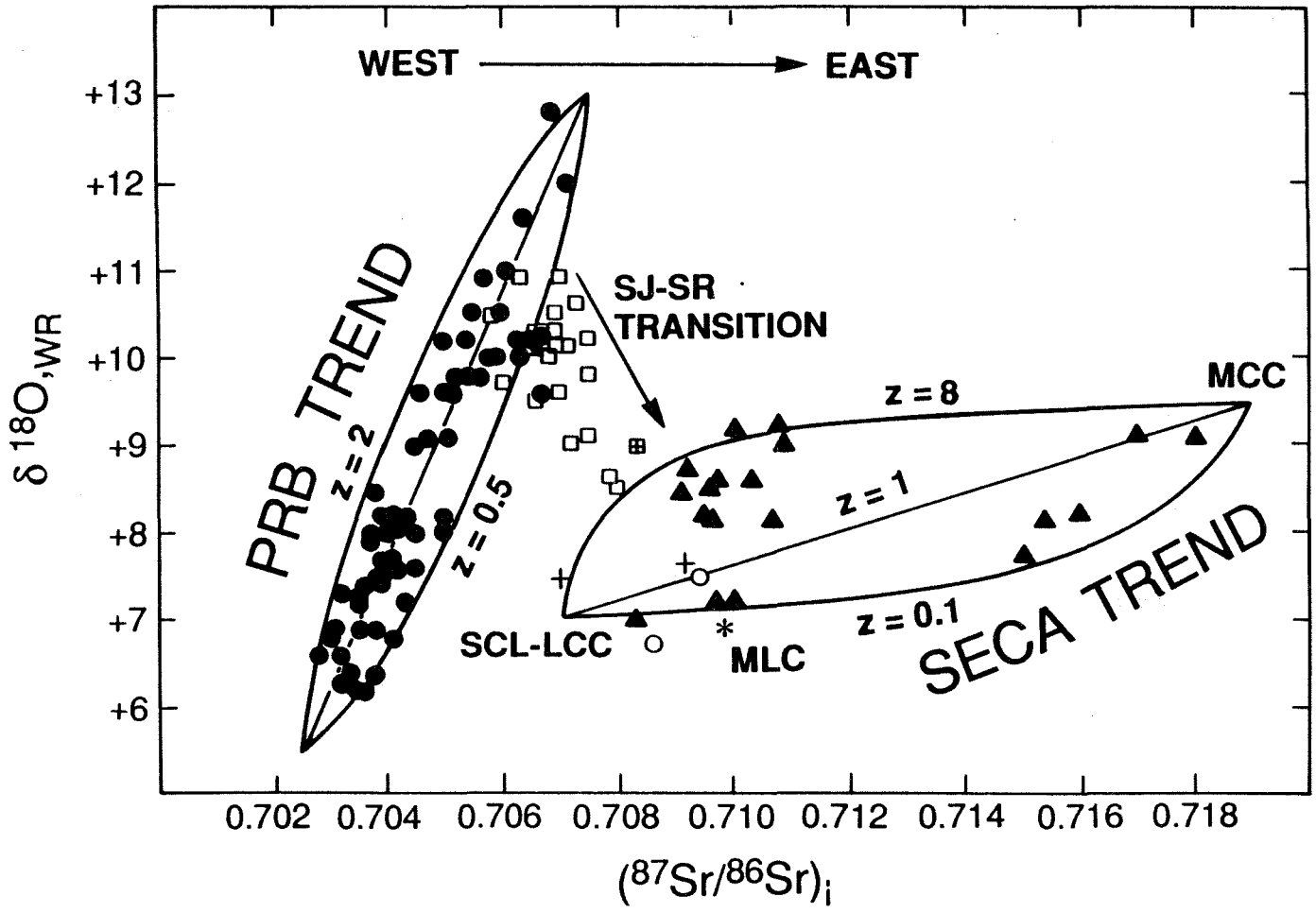
WEST
EAST
+13
+12
+11
+10
+9
+8
+7
+6
δ 18O,WR
PRB TREND
z = 2
z = 0.5
SJ-SR
TRANSITION
z = 8
MCC
z = 1
z = 0.1
SECA TREND
SCL-LCC
MLC
0.702
0.704
0.706
0.708
0.710
0.712
0.714
0.716
0.718
(87Sr/86Sr)i

both the SECA and the PRB data on Figure 8.7 could also be attributed to variations in the isotopic compositions of the two end members, rather than to a variation in the Z values. However, it is not reasonable to illustrate all of the various possibilities, and in any case, each pair of possible end members would define a series of hyperbolas similar to the ones actually shown on Figure 8.7.

8.8 Discussion

Several observations may be made regarding the model calculations depicted in Figure 8.7. All of the data-points in the main PRB array are easily accounted for within the envelopes obtained assuming values of Z = 2 to 0.5, because, as noted by Taylor (1980), the main PRB array is extremely linear. This linearity requires that the two end-members must, within a factor of about two, have a Z-value close to unity, and it lends credence to the idea that the PRB formed through mixing between mantle-derived OIA components and a mixed source composed of sedimentary rocks such as graywackes and altered basalts (SAV), because both such end-members would in general have similar ppm Sr contents. The required similarity in Sr concentrations basically exists because the SAV component in a eugeosynclinal suite is dominantly derived from igneous precursor materials similar to those that make up the volcanic-plutonic island arc itself. Thus, the ppm Sr contents in the SAV and OIA end-members would be similar, even though the SAV end-member would have evolved a much higher $\delta^{18}O$ due to various weathering, hydrothermal, and diagenetic processes that take place in the depositional basins surrounding the various Mesozoic arc terranes.

The SR-SJ array fits in well as a transitional group on Figure 8.7. This array is terminated on one end by a component that lies within

the high-^{18}O portion of the main PRB array and on the other end by a component that appears to have a cratonal isotopic signature. It is clear that the latter end-member became more and more important as the magmatism migrated eastward onto the Cretaceous continent, just as would be predicted for a source material within the lower crust at the edge of the craton. The proposed variability in the MLC of Hill et al. (1986) encompasses the lower-^{18}O portion of the SECA array.

The isotopic variations within the SECA array may be accounted for either by assuming isotopically variable end-members, or by assuming a series of different Z values that vary from perhaps ~8 down to ~0.15, consistent with mixing between a relatively high-Sr MLC and a more felsic "upper" crustal component with lower ppm Sr. At present it is impossible to decide whether the $^{87}Sr/^{86}Sr$-rich component(s) has a higher or a lower ppm Sr content than the $^{87}Sr/^{86}Sr$-poor component(s). These Sr contents could range from about 1200 ppm or more for an alkalic basaltic magmatic component to about 600 ppm for the MLC to perhaps 100 to 200 ppm for the upper crustal component. In a model traverse across the terranes comprising the combined (PRB)-(SJ-SR)-(SECA) Cretaceous magmatic arc, the $^{87}Sr/^{86}Sr$ values change in a reasonably regular fashion practically all the way to the Colorado River, generally increasing to the northeast. For example, this ratio increases steadily from west to east in the main PRB, continues to increase into the SJ-SR block, and finally culminates in an extremely high $^{87}Sr/^{86}Sr$ (0.718) in the eastern part of the SECA area, where both the strontium and the oxygen isotopic patterns start to deviate from the regional northwest-trending strike, and start showing local heterogeneities. Note that this simple eastward monotonic change does not apply to the $\delta^{18}O$ values, which reverse and begin to show an

eastward decrease even within the SJ-SR area, and well before we move into the main part of the SECA area (Figure 8.4). Not until much farther east, in the vicinity of the California-Arizona border, do the $^{87}Sr/^{86}Sr$ ratios show a similar reversal and begin to decrease eastward.

The systematics described above may imply that sedimentary and volcanic processes rather efficiently mixed the high-^{18}O source materials for the PRB, whereas the cratonal zone of the SECA area is dominated by sources that are more heterogeneous in their Sr-O isotopic characteristics (i.e., both vertically and laterally within the crust). Probably the easiest way to characterize the system would be to break it into a lower crustal component and an upper crustal component. However, the model as presented here contains no information on the mechanism of mixing of the SECA components; the hybrid material conceivably could represent mixtures of magmas derived from different levels, mixing of magma from one level with rocks from another level, or perhaps heterogeneous interlayered materials within a single source region that was undergoing melting.

8.9 Conclusions

This reconnaissance study of $\delta^{18}O$ and $^{87}Sr/^{86}Sr$ systematics in Mesozoic plutons from southeastern California mainly provides a good framework for further, more detailed investigations. However, it also has already led to the following fairly firm conclusions:

(1) Plutons with $\delta^{18}O$ greater than +9.5 per mil are confined to a zone that lies west of the western limits of major Precambrian basement outcrops. East of this boundary, only two zones of significant areal extent (Old Woman Mountains; central Coxcomb Mountains) are known to exhibit relatively high $\delta^{18}O$ values, and these range upward only to +8.5 to +9.3 per mil, with one anomalous sample at +9.9. Also, these two

areas locally contain muscovite-bearing granitoids and locally display much higher $^{87}Sr/^{86}Sr$ ratios (>0.715) than the high-^{18}O plutons farther to the west.

(2) Plutons with $\delta^{18}O$ less than +7.5 to +8.0 per mil lie in a belt that extends southeastward through the eastern Transverse Ranges and the fault-restored San Gabriel Mountains. This zone lies just to the east of the aforementioned boundary defined by the western limits of Precambrian basement. Thus, moving east toward the North American craton, the whole-rock $\delta^{18}O$ values of plutons that have penetrated upward through the western edge of the Precambrian basement of the craton exhibit a decrease in ^{18}O, down to $\delta^{18}O$ values that are typically about +6.5 to +8.0. Instead of being positively correlated with $^{87}Sr/^{86}Sr$ as in the main part of the PRB (Taylor and Silver, 1978), this abrupt decrease in $\delta^{18}O$ from west to east is typically accompanied by an <u>increase</u> in $^{87}Sr/^{86}Sr$; thus, these lower-^{18}O SECA plutons can be clearly delineated from Cretaceous plutons emplaced farther to the southwest that make up the entire western half of the PRB; the latter <u>also</u> have $\delta^{18}O$ = +6.0 to +8.0, but they exhibit <u>much</u> lower $^{87}Sr/^{86}Sr$ (< 0.706). The abruptness of the $\delta^{18}O$ shift that occurs along this northwest-trending linear zone may in part be a "telescoping" effect related to Tertiary tectonic events, wherein these terranes underlain by Precambrian basement have been thrust westward considerable distances (Silver, 1982, 1983). Thus the isotopic characteristics of the plutons in these allochthonous SECA terranes may actually have been imprinted on magmas that were formed much farther to the east.

(3) The $\delta^{18}O$ and $^{87}Sr/^{86}Sr$ values for Mesozoic plutons in southeastern California range between +7.0 and +9.3 per mil and 0.707 and

0.718, respectively. On a plot of $\delta^{18}O$ vs. $^{87}Sr/^{86}Sr$, these SECA data form a broad array with a much different slope than the well-defined linear array observed in the PRB. However, like the PRB (Taylor and Silver, 1978), the SECA data are best explained by relatively simple two-component mixing, and not by combined fractional crystallization-assimilation (AFC) processes. The end-member source regions for the SECA plutons may have had widely different bulk Sr contents, or have had less uniform isotopic compositions than in the case of the PRB, accounting for the less well-defined mixing array. Isotopically, the two dominant components in the SECA plutons could be characterized as: Model Lower Crust (MLC) +7.0 per mil, 0.7070, ppm Sr ~ 800 to 900; and Upper Continental Crust (UCC) +9.5 per mil, 0.7190, ppm Sr ~ 60 to 200. In reality, these components are undoubtedly variable in composition from region to region in the melting zones, but the above compositions are sufficient to explain the observed spread in data. Jurassic and Triassic plutons typically have primary isotopic compositions much closer to the model lower crust-upper mantle (MLC) component than do the Cretaceous plutons; this probably requires input of both an upper crustal and a lower crustal cratonal component. None of these older plutons, with the possible exception of the Triassic Mt. Lowe pluton, shows much indication of a deep-seated MORB-type mantle component, indicating they are all sourced within the upper or lower continental crust or just beneath the crust in the subcontinental lithospheric mantle.

(4) Cretaceous plutons in the SECA area appear to have been dominantly sourced within the continental crust, and generally in the lower crust. In the central and eastern parts of the SECA area, there are, however, two major plutonic centers where a component of upper- or mid-

crustal magmatism appears, namely in the Cadiz Valley and Old Woman-Piute-Chemehuevi batholiths. In these two areas of intense granitic magmatism, the lower crustal magmas apparently co-mingled with minimum melt (two-mica granite) type magmas that may represent local involvement of middle crustal rocks in the melting process. Farther to the west in the SJ-SR area, or the so-called "Santa Rosa" transitional zone where $\delta^{18}O$ is typically about +9 to +10 and initial $^{87}Sr/^{86}Sr$ about 0.709 to 0.710, magmatism was just beginning to impinge upon the continental crust of the craton as the magmatic arc swept eastward with time. Thus, moving eastward, it is within this transitional SR-SJ zone that we see the last vestige of the deep-seated SAV geosynclinal source terrane that is dominant in the Cretaceous plutons of the eastern half of the PRB.

(5) The isotopic signatures in the Cretaceous plutons of the SJ-SR area in the northeasternmost portion of the PRB are intermediate between the bulk of the PRB data and the SECA data (Figure 8.7). It is therefore tempting to speculate that the SJ-SR plutons and the SECA plutons have a common end-member with $\delta^{18}O \sim +7.5$ and $^{87}Sr/^{86}Sr \sim 0.708$. This MLC end-member (Hill et al., 1986) probably represents a very abundant type of lower crustal material lying just beneath the western edge of the Mesozoic craton of North America. The other more radiogenic, somewhat higher-^{18}O SECA end-member is probably derived from higher crustal levels comprised of more evolved sialic material. The data are thus all consistent with an evolving Cretaceous magmatic arc that swept eastward from a simatic, oceanic island arc environment (western half of the PRB), through the prograding volcanic-sedimentary pile that had been accumulating to the west of the Precambrian craton (eastern half of the PRB), then through a transitional zone on the edge of the craton (SJ-SR block),

ultimately migrating into and melting parts of the craton and forming the various plutons found throughout the SECA area. The extreme isotopic variations in the easternmost SECA plutons suggest melting at various levels of the lower and mid-cratonal crust, together with a mixing process that involved varying proportions of these two (or more) broadly characterized end-members. Thus, the eastern limits of high-$\delta^{18}O$ (> 10.0 per mil), low-$^{87}Sr/^{86}Sr$ (< 0.7090) plutons probably mark the transition between altered volcanic- and sediment-dominated (SAV) source regions, and source regions embedded within or just beneath the ancient sialic crust of the North American craton.

(6) Apparently, the earliest plutonism in the area (Triassic) tapped sources ranging from the mantle in the southern (SGM) region (Mt. Lowe pluton) to the model lower crust (MLC) along the main portion of the Jurassic arc. As yet there is no evidence for heavy involvement of mid-level or high-level crustal material in the Triassic or Jurassic magmatism. This is consistent with the epizonal nature of most of the Jurassic plutons studied in this research. These may have been derived from relatively deep, dry sources, thus yielding magmas that were capable of ascending much higher in the crust, perhaps to within one to five kilometers of the Earth's surface. This scenario applies for the Jurassic arc where it cuts across SECA; however, the arc appears to be sourced in an oceanic island arc (OIA) setting northwest of SECA in western Nevada. Both settings contain epizonal plutons that host metallic mineralization, and are hydrothermally altered; in the NW portion of the arc, heated seawater was the predominant fluid involved with hydrothermal alteration, and in the continental portion of the arc (ROM-type centers), heated meteoric waters produced propylitic alteration.

(7) A plausible model might be as follows: The earlier was of mantle-derived magma swept through the deepest parts of the lower continental crust (LCC) and the subcontinental lithospheric mantle (SCL) during Jurassic and Triassic time, raising the isotherms and causing melting of appropriate lithologies. The earliest (Triassic) magmas tended to be dominantly from the mantle, whereas during the Jurassic there was greater involvement of the LCC and/or the SCLM source regions. In any case, these materials all tended to be relatively "dry" and low in $\delta^{18}O$ (< +8.0), and together they might be characterized as the "model lithospheric component" (MLC) of Hill et al. (1986). Perhaps combined with a change from a generally extensional regime in the Jurassic to a compressional regime, continued influx of mantle-derived magmas during Cretaceous time produced less and less melting of the MLC, in part because by this time those source rocks probably had become more refractory. Thus, the continued influx of heat energy forced the melting event(s) to impinge upward higher and higher in the crust, melting more ^{18}O-rich, more hydrous lithologies. These more H_2O-rich magmas could not penetrate as high in the crust (e.g., see Burnham, 1979), and thus, in general, they congealed and crystallized at deeper levels than the Jurassic plutons. In addition, the continental crust itself probably would have become thicker during the early Mesozoic events, because of continued eugeoclinal sedimentation and because these epizonal plutons and their associated volcanic rocks would have been continuously piled on top of the crust. Thus, the high-^{18}O, relatively hydrous source rocks would have sunk deeper and would have become much hotter than they were earlier during the Jurassic and Triassic. During the widespread Cretaceous magmatic event these more H_2O-rich lithologies were melted on a large scale, perhaps in

part because they were H_2O-rich, and thus would melt at lower temperatures.

Some of these concepts will be discussed in greater detail below, but first it is useful to turn our attention to the oxygen and radiogenic (Nd, Sr) isotopic systematics in plutons located in the Northern Basin and Range Province of Nevada and Utah, which are discussed in Chapter 9. Following this, we shall present a synthesis of the various isotopic systems applied to the origin of the Cordilleran batholithic rocks of the entire southwestern United States (Chapter 10).

CHAPTER 9. OXYGEN ISOTOPE STUDIES OF MESOZOIC AND TERTIARY GRANITIC ROCKS IN THE NORTHERN BASIN AND RANGE PROVINCE, NEVADA AND UTAH

9.1 Introduction

Farmer and DePaolo (1983) determined the Nd and Sr isotopic compositions of 25 Mesozoic and Tertiary granitic plutons exposed within a 700 km-long and 200 km-wide transect that extends from the Sierra Nevada Batholith (SNB) to central Utah, across the northern Great Basin (Figure 9.1). Farmer and DePaolo combined their Nd and Sr isotopic data with previous isotopic studies and geologic studies of this broad region, in an attempt to better understand the sources of granitic magma as a function of the structure of the continental crust. Most of the same samples analyzed by Farmer and DePaolo (1983) were also analyzed for $^{18}O/^{16}O$ in the present study, and with this additional information, we are able to further constrain the possible parent materials of these magmas.

The framework for this study of the NGB and the previous study by Farmer and DePaolo (1983) was provided by earlier Sr, O, and Pb isotopic studies of the Mesozoic granitic batholiths of the western United States (Kistler and Peterman, 1973; 1978; Zartman, 1974; Taylor and Silver, 1978; Chen and Tilton, 1978; DePaolo, 1980, 1981; Armstrong *et al.*, 1977; Masi *et al.*, 1981; Silver *et al.*, 1979; Solomon and Taylor, 1981; Gromet and Silver, 1986; Taylor, 1986; Silver and Chappell, 1988). In a broad sense, all of these earlier studies have shown that the granitic magmas represent complex mixtures of material derived both from the upper mantle and from the continental crust, with variations in the age, composition, and geologic history of the crust being reflected in variations in the isotopic compositions of the plutons. In particular, Kistler and Peter-

Figure 9.1 Map of the Northern Great Basin (NGB), showing major mountain ranges and other geographic features, the northeastern Sierra Nevada Batholith (SNB) and sample localities studied by Farmer and DePaolo (1983). Sample numbers corresponding to Map Numbers in Table 9.1 are shown next to each locality, along with whole-rock $\delta^{18}O$ and ε_{Nd} (parentheses) values. The geologic boundaries discussed by Farmer and DePaolo (1983) are shown at the top of the map; the Eugeocline region lies west of the dashed line on the western side of the stippled Transition Zone, and the Miogeocline region lies east of the Roberts Mountains Thrust (RMT). Figure 9.2 is a geologic cross-section that shows these boundaries projected onto a transect parallel with latitude 40°N.

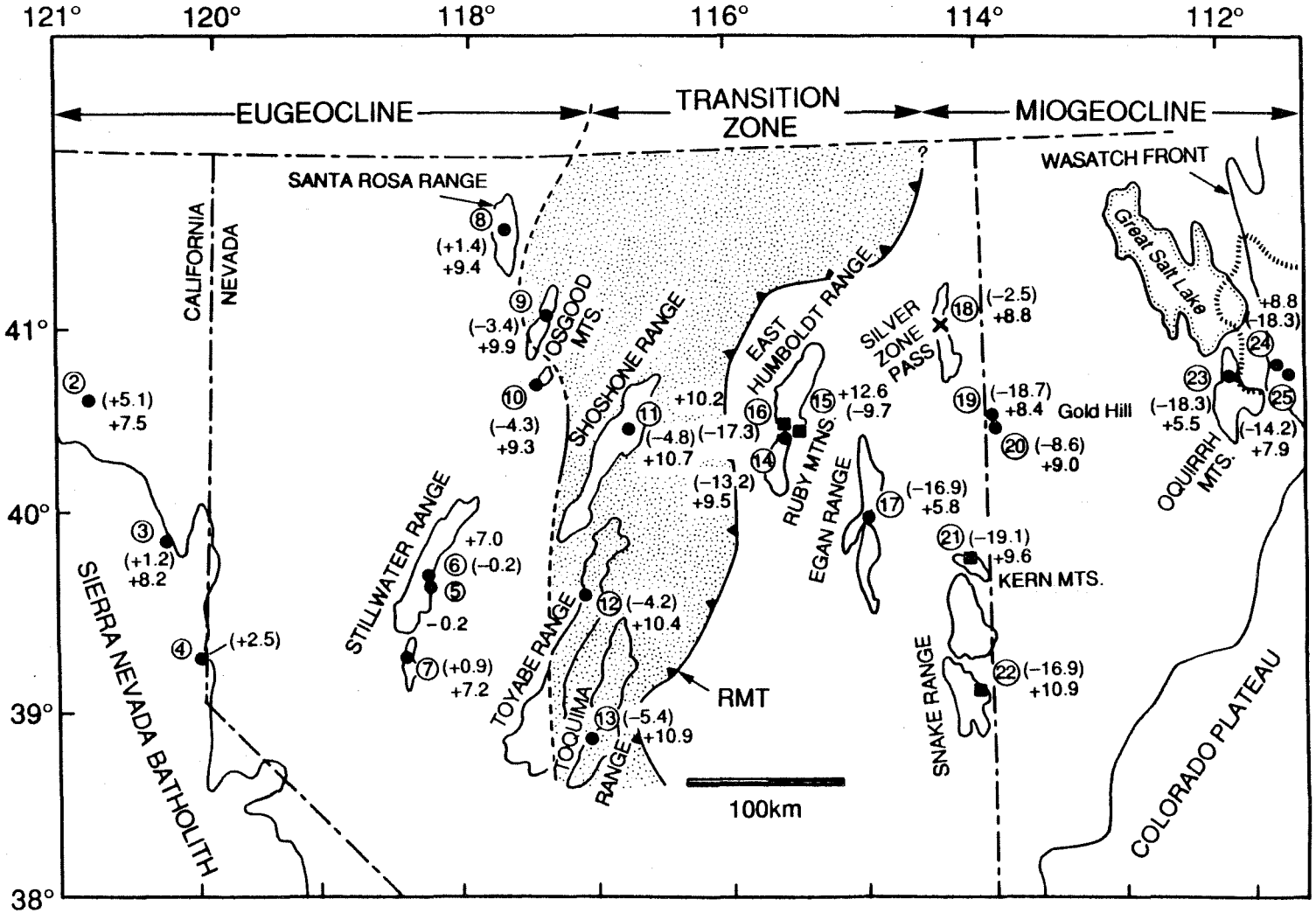
121°
120°
118°
116°
114°
112°
EUGEOCLINE
TRANSITION ZONE
MIOGEOCLINE
41°
40°
39°
38°
CALIFORNIA
NEVADA
SANTA ROSA RANGE
WASATCH FRONT
Great Salt Lake
OSGOOD MTS.
SHOSHONE RANGE
EAST HUMBOLDT RANGE
SILVER ZONE PASS
RUBY MTNS.
EGAN RANGE
STILLWATER RANGE
TOYABE RANGE
TOQUIMA RANGE
SNAKE RANGE
KERN MTS.
OQUIRRH MTS.
Gold Hill
SIERRA NEVADA BATHOLITH
COLORADO PLATEAU
RMT
100km
(+5.1) +7.5
(+1.2) +8.2
(+2.5)
+7.0
(−0.2)
−0.2
(+0.9) +7.2
(+1.4) +9.4
(−3.4) +9.9
(−4.3) +9.3
+10.2
(−4.8) +10.7
(−17.3)
(−13.2) +9.5
(−4.2) +10.4
(−5.4) +10.9
+12.6 (−9.7
(−2.5) +8.8
(−18.7) +8.4
(−8.6) +9.0
(−16.9) +5.8
(−19.1) +9.6
(−16.9) +10.9
+8.8 (−18.3)
(−18.3) +5.5
(−14.2) +7.9

man (1973; 1978) and Farmer and DePaolo (1983) showed that there were systematic variations from west to east in the isotopic compositions of both Nd and Sr. Farmer and DePaolo (1983) outlined some very sharp regional geochemical boundaries and proposed that the crustal components of the granitic magmas changed sequentially from west to east in this sequence: eugeocline, miogeocline, and craton. They also concluded that in the eastern NGB a mantle component was virtually non-existent in these magmas. The detailed models proposed by Farmer and DePaolo (1983) are discussed below in terms of the new oxygen isotope data generated on these same samples.

The $^{18}O/^{16}O$ data are presented in Figure 9.1 and Table 9.1. When combined with previous $^{18}O/^{16}O$ studies of the Basin and Range Province in Nevada and Utah (e.g., Lee et al., 1981; see Figure 1.4 in Chapter 1 of this thesis), these data provide a fairly comprehensive oxygen isotopic data set for the entire Northern Great Basin (NGB). We also include in this data set information on the 168 Ma Yerington batholith of westernmost Nevada (Dilles, 1987; Solomon et al., 1983; and data from the northern Sierra Nevada Batholith (SNB) from Masi et al., 1981). The Nd and Sr isotopic data for these samples are also shown in Table 9.1. In addition to the isotopic data, the whole-rock major-element geochemistry of a large number of these samples is available (Lee, 1984; Farmer and DePaolo, 1983; Kistler et al., 1981).

This data set (O, Nd, Sr, and major-elements) appears to be one of the best now available for directly comparing $\delta^{18}O$ with geochemical trends in Mesozoic plutonic rocks in the Cordillera of the southwestern United States. Only the Peninsular Ranges Batholith (PRB) terrane in southern and Baja California has a comparable data set (i.e., where

Table 9.1 Geochronology, isotopic data ($\delta^{18}O$, ε_{Sr}, ε_{Nd}), Sr(ppm), and selected geochemical parameters for plutons in the northern Basin and Range of Nevada and western Utah.[a]

Map No.[b]	Age, Ma	Whole-rock $\delta^{18}O$[h]	Initial $^{87}Sr/^{86}Sr$[c]	ε_{Sr}	ε_{Nd}	Sr, ppm	Fe^{3+}/total Fe[d]	Al_2O_3/ Na_2O+K_2O+CaO[d]
02[e]	121	+7.5	0.7037	-10	+5.1	620	--	--
03[e]	88	+8.2	0.7048	+6.0	+1.2	726	--	--
04	90	--	0.7043	-1.0	+2.5	332	--	--
05	28	-0.2	0.7050	+8.2	-0.2	547	--	--
06	28	+7.0	0.7050	+8.3	-0.2	769	--	--
07	76	+7.2(3)	0.7047	+3.8	+0.9	736	--	--
08	98	+9.4(2)	0.7049	+7.9	+1.4	528	0.33	1.04
09	90	+9.9	0.7057	+19	-3.4	706	0.40	1.00
10	153	+9.3(2)	0.7059	+22	-4.3	892	0.29	0.89
11	37	+10.7	0.7072	+39	-4.8	436	0.19	1.01
12	142	+10.4(4)	0.7071	+38	-4.2	405	--	--
13	76	+10.9(3)	0.7067	+33	-5.4	648	--	--
14	36	+9.5	0.7110	+93	-13.2	406	0.22	1.06
15	83	+12.6	0.7373	+466	-9.7	86	0.48	1.20
16	160	+10.2	0.7138	+133	-17.3	126	0.24	1.29
17	32	+5.8	0.7137	+131	-16.9	393	--	--
18[f]	124	+8.8	0.7054	+15	-2.5	920	--	--
19	38	+8.4	0.7157	+160	-18.7	316	--	--
20	152	+9.0	0.7099	+78	-8.6	693	0.48	1.03
21	58	+9.6(2)	0.7212	+238	-19.1	355	0.08	1.12
22	79	+10.9	0.7165	+171	-16.9	349	0.70	1.12
23[g]	40	+5.5(2)	0.7073	+41	-18.3	1497	0.49	0.82
24	28	+8.8	0.7083	+55	-18.3	570	0.33	0.97
25	32	+7.9(3)	0.7072	+39	-14.2	1150	0.47	0.91

[a] $\delta^{18}O$ is from this thesis except where noted, other data from Farmer and DePaolo (1983), except where noted.
[b] Map number appears with corresponding GCS sample number in Table 1 (appendix) unless noted.
[c] Calculated from equation given by Farmer and DePaolo (1983) unless noted.
[d] Calculated from data cited in Farmer and DePaolo (1983).
[e] $\delta^{18}O$, initial $^{87}Sr/^{86}Sr$ from Masi et al. (1981); ε_{Nd} from DePaolo (1981).
[f] Whole-rock $\delta^{18}O$ calculated using +1.2 per mil fractionation factor and coexisting quartz with $\delta^{18}O$=+10.0 (see Table 1, appendix).
[g] Nearby sample has $\delta^{18}O$=+6.7 (whole-rock), +7.9 (quartz), see $\delta^{18}O$ analyses of Last Chance stock in Bowman et al. (1987).
[h] Because these are aliquots of the same samples studied by Farmer and DePaolo (1983), we felt it was important to determine their $\delta^{18}O$ values with the highest possible precision; thus selected samples were analyzed for $^{18}O/^{16}O$ numerous times, with a reproducibility of ±0.1 per mil (the numbers in parentheses indicate the number of replicate analyses).

several types of geochemical analyses are available for individual sample localities). This abundance of data on aliquots of the same samples provides more stringent constraints on magmatic source regions in the NGB than is presently possible in southern Arizona and southeastern California.

Comparisons of the isotopic and major-element relationships in granitic plutons throughout this broad region allow us to discern the effects of the changing structure, thickness, and chemical composition of the continental crust on the origin and evolution of the granitic magmas. Note that the intensity of the magmatic activity in the NGB in Nevada and Utah (i.e., the areal density of plutons) is much less than in the Sierra Nevada and Peninsular Ranges Batholiths to the west and south. Also, because the regional geology of the NGB is comparatively well understood (Stewart, 1980), it is easier to correlate the isotopic variations in the NGB plutons with the geology of the surrounding country rocks than is possible in the structurally more complex SNB and PRB. Whereas the SNB and particularly the PRB plutons were emplaced tightly together over a relatively restricted interval of time and along a relatively narrow zone at the Mesozoic continental margin, the plutons in the NGB are more widely dispersed and were emplaced much farther into the continental interior over an extended period of time from the early Jurassic to the late Tertiary.

9.2 Geologic Setting

Farmer and DePaolo (1983) present a schematic pre-Jurassic geologic cross section of the NGB; a slightly modified version of their section is shown in Figure 9.2. The depth to basement and the nature of the basement are both highly speculative. However, the thicknesses and general

Figure 9.2 Schematic geologic cross-section across the Northern Great Basin (NGB) of northern California, northern Nevada and western Utah, parallel to latitude 40°N (see Figure 9.1), modified after a diagram in Farmer and DePaolo (1983). The cross-section begins on the west (point A) at the Pacific Coast of northern California, terminates at the Wasatch Front in western Utah, and shows the major petrotectonic assemblages discussed in Farmer and DePaolo (1983) and in the present work (from west to east, together with the major zones delineated by Farmer and DePaolo for this region (listed along the top of the cross section): (1) Eugeocline consisting of a down-warped, synformal assemblage of intercalated Paleozoic and early Mesozoic arc-type volcanic rocks, terrigenous clastics and greenstone rocks; (2) Transition Zone gradational between (1) and (3); "suture", rift, or thrust-fault contact between the Paleozoic volcanic and volcaniclastic sediments on the west and the late Proterozoic (<1.5 Ga) miogeoclinal terrigenous clastic sediments and metasediments on the east and ancient (>1.5 Ga) crystalline basement rocks of the craton farthr east as shown in the diagram; (3) Miogeocline consisting of Paleozoic terrigenous clastics and shelf carbonates. Farmer and DePaolo (1983) and Kistler and Peterman (1978) place the edge of the >1.5 Ga craton approximately beneath the Transition Zone-Miogeocline Zone boundary. However, the present $^{18}O/^{16}O$ study suggests a slightly different model cross section, in which the aforementioned boundary is some type of strike-slip fault, ancient rift zone, or suture zone.

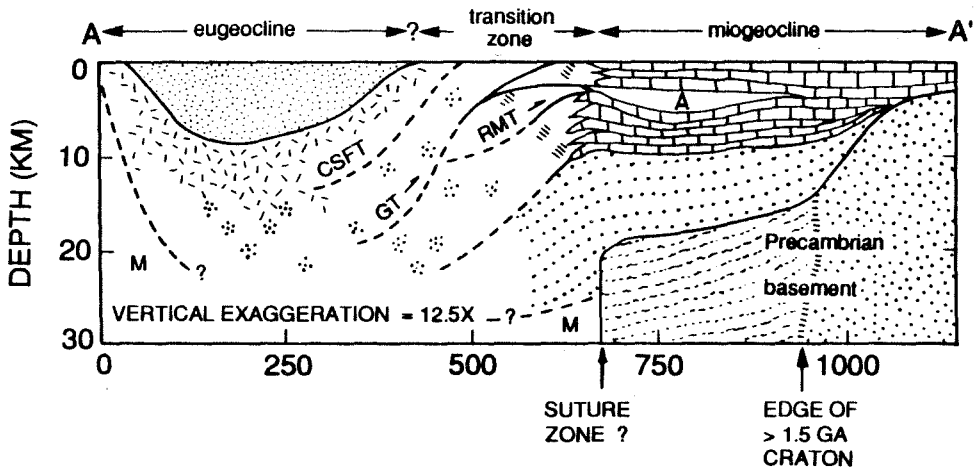

Arc-type volcanic rocks	DEVONIAN TO JURASSIC	
Terrigenous clastics and intermixed arc-type volcanics	CAMBRIAN (?) TO DEVONIAN	
Terrigenous clastics with intermixed ocean-floor type greenstones	CAMBRIAN (?) TO PERMIAN OR YOUNGER	
Terrigenous clastics plus carbonate	CAMBRIAN TO TRIASSIC	
Terrigenous clastics	MAINLY LATE PRECAMBRIAN TO EARLY CAMBRIAN	(Windemere Equivalents) or Mc Coy Creek Formation
Carbonate	CAMBRIAN TO TRIASSIC	
Terrigenous clastics	1.4 TO 1.1 GA METASEDIMENTS	(Belt Series Equivalents) or Uinta Group Equivalents
Sialic crust	> 1.4 GA CRATON PARAGNEISS, ORTHOGNEISS AMPHIBOLITES	

geologic characteristics of the sedimentary rocks shown in the eastern half of Figure 9.2 are constrained by extensive mapping and drilling (Stewart, 1980; Schweickert and Snyder, 1981; Speed and Moores, 1981). Various models have been proposed for the Devonian to Jurassic tectonic history of this region, particularly in the western half of the area shown in Figures 9.1 and 9.2; all of these models are fairly complex (Coney et al., 1980; Dickinson, 1981; Burchfiel and Davis, 1981a; Saleeby, 1981; Saleeby et al., 1987). Nonetheless, the general nature of the sedimentary lithologies and the sedimentary provenances, which are basically very important factors in any $^{18}O/^{16}O$ study, are similar for all of the models (Farmer and DePaolo, 1983).

As shown in Figure 9.2, the NGB generally consists of a western eugeoclinal terrane and an eastern miogeoclinal terrane, with the latter thinning to the east as it laps onto the craton. The western part of the eugeocline (in the SNB area) is composed of Paleozoic and Mesozoic chert, shale, and volcanic rocks, with minor carbonate and quartzite (Irwin, 1981; Stewart, 1980). This region was apparently the site of a volcanic island arc during Devonian to Jurassic time. The lower part of the section is inferred to contain detritus from earlier volcanic arcs, along with fragments of earlier oceanic crust (Speed, 1979; Dickinson, 1981). None of the eugeoclinal sediments are interpreted as having been deposited on old continental crust, even though the sediments are inferred to be largely composed of continentally derived material. This latter conclusion is confirmed by the strongly continental character of the Nd isotopes in two sedimentary composites from the western SNB (DePaolo, 1981).

The eastern portion of the eugeocline in the NGB area consists primarily of lower Paleozoic terrigenous clastics and hemipelagic sediments with some greenstone. The volcanic rocks here are inferred to be fragments of oceanic crust, with little or no arc-type volcanic rocks (Dickinson, 1981). The eastern eugeoclinal sediments are generally considered to represent the distal portions of a thick sedimentary-volcanic sequence that formed to the west of the North American craton from the late Proterozoic to the Mesozoic. Sedimentation was temporarily interrupted during the mid-Paleozoic Antler Orogeny when lower Paleozoic eugeoclinal rocks were thrust eastward about 100 km along the Roberts Mountains Thrust (RMT). The rocks making up the upper plate of the RMT structurally overlie time-equivalent miogeoclinal sedimentary rocks (Stewart, 1980).

Using the Farmer-DePaolo terminology, the transition zone of Figures 9.1 and 9.2 marks the known extent of overlap of eugeoclinal and miogeoclinal sediments, and it also corresponds to the region where the pre-thrusting facies transition from miogeocline to eugeocline is thought to have occurred (Stewart, 1980; Roberts et al., 1958). Eastward thrusting occurred again in the Permo-Triassic Sonoma Orogeny along the Golconda Thrust (GT), as upper Paleozoic eugeoclinal rocks were thrust eastward over the previously emplaced Roberts Mountains allochthon. Cumulative late Proterozoic and Phanerozoic sediment thicknesses reach ~15 km in eastern Nevada, and thin to the east in Utah (Figure 9.2). Local deep sedimentary basins formed in western Utah (e.g. Oquirrh Basin) after the Antler Orogeny. Geosynclinal sedimentation probably began during a mid-continent rifting event in the late Proterozoic (Stewart, 1972; Dickinson, 1981). Miogeoclinal sedimentation ceased during the mid-Mesozoic Sevier Orogeny.

Direct evidence for the position of the rifted edge of the Precambrian basement is unknown in the NGB, although this boundary previously has been placed near the western edge of the miogeoclinal carbonates in central Nevada (Kistler and Peterman, 1973; Farmer and DePaolo, 1983; Snoke and Miller, 1987). However, unequivocal outcrops of Archean basement exist in the Albion Range of southwestern Idaho, and in the Raft River and Grouse Creek Ranges in northwest Utah. Snoke and Lush (1984) and Snoke and Miller (1987) have described Archean orthogneiss, paragneiss and amphibolite in a large recumbant fold in the East Humboldt Range of northeastern Nevada (the so-called "metamorphic suite of Angel Lake"), which are apparently correlative with the Archean Green Creek Complex in the Albion Mountains. Also, Proterozoic (and possibly Archean) basement is exposed in several localities to the east and south (Condie, 1981).

Of special interest is the occurrence of late Proterozoic rocks that accumulated in sedimentary basins along the margins of the rifted continent. These are the Belt- and Windemere-equivalent rocks discussed by Stewart (1972) and Kistler et al. (1981). These rocks represent the initial accumulation of miogeoclinal sediments at the edge of the continent, and they represent a large reservoir of high-^{18}O material that was deeply buried, and thus could have been a potential source material for some of the NGB plutons. For example, the late Proterozoic Uinta Mountain Group was deposited in an elongate east-trending trough that reached thicknesses of up to 8 km. This trough is located east of the Wasatch Front in northern Utah, and the axis of the trough extends toward the area in eastern Nevada occupied by the Ruby-East Humboldt and Snake Ranges. The McCoy Creek Formation is an uppermost Proterozoic unit that

crops out in northeastern Nevada (Miller et al., 1987) near the border with Utah; it possibly has correlative units overlying the Uinta Mountain Group farther east in northern Utah (E.L. Miller, pers. comm., 1988). Farther west, in the Ruby-East Humboldt Ranges, Kistler et al. (1981) have described an assemblage of quartzites, schists and marbles that were strongly metamorphosed between 1450 and 550 Ma, and which could be equivalent to similar late Precambrian miogeoclinal rocks located in Idaho (or possibly, in the Uinta Mountain Group in Utah). The metamorphic grade of these rocks in northern Nevada suggests they were buried to depths of at least 10-15 km.

9.3 Petrology and Age of Northern Great Basin Granites

In a general sense, the locus of igneous activity in the NGB appears to have moved eastward with time, beginning in the early Mesozoic in the SNB, and culminating in Laramide (~60-70 Ma) and mid-Tertiary (20-40 Ma) igneous activity in Utah and Colorado (Snyder et al., 1976; Cross and Pilger, 1978). The majority of granitic rocks in Nevada are Cretaceous in age (Stewart, 1980), and thus fit this generalized concept of an inland sweep of Mesozoic magmatism. However, there exist many local anomalies and "reversals" in the ages of the igneous rocks, particularly during the mid-Tertiary, when magmatism extended across the entire NGB. Also, although much of this magmatism is clearly related in some way to Mesozoic subduction of oceanic crust beneath North America, it is necessary to invoke unusually flat-dipping geometries and structures of the subducted plate to account for the fact that the magmatism extended inland some 1500 km (Lipman et al., 1972; Lipman, 1980).

Using the nomenclature from Streckeisen (1976) that was followed by Farmer and DePaolo (1983), there is a fairly systematic change in

composition from predominantly tonalite in the western SNB to granodiorite in the eastern SNB and western Nevada (Bateman et al., 1963; Johnson, 1977; Willden and Speed, 1974), to monzogranite in the transition zone of west-central Nevada (Stewart and McKee, 1977). This general eastward increase in potassium content toward the edge of the RMT was first recognized by Moore (1959) and is evident in the bulk chemical compositions of the plutons analyzed in this study (Section 9.4.5; also see Lee, 1984, and Table 1 of Farmer and DePaolo, 1983). The compositional trends appear to be largely independent of emplacement age.

To the east of the RMT, granitic plutons become less abundant as we enter the miogeocline of eastern Nevada and western Utah (Stewart, 1980); also the plutons generally have higher SiO_2 (>70%) and K_2O (>3%). However, the most dramatic difference between the eugeoclinal and miogeoclinal granitic rocks is the common occurrence of two-mica monzogranite plutons in the miogeocline, all of which are free of hornblende and strongly peraluminous. Typical examples occur in the Ruby Mountains (Kistler et al., 1981), the Snake Range (Lee and van Loenen, 1971), and the Kern Mountains (Best et al., 1974). A summary of two-mica granite occurrences in northeastern Nevada is given by Lee et al. (1981); these range from Jurassic to early Tertiary in age, and commonly are observed in the so-called "metamorphic core complexes" where miogeoclinal sedimentary rocks have undergone Mesozoic(?) greenschist- to amphibolite-grade metamorphism (Howard, 1980).

Granodiorite predominates in the easternmost NGB in Utah, which is known to be underlain by the Precambrian craton. The sampled plutons in the Oquirrh and Wasatch Mountains intrude Paleozoic miogeoclinal carbonates and Precambrian platform sedimentary rocks. These bodies are Oligo-

cene in age, metaluminous, and contain modal hornblende ± pyroxene (Lanier et al., 1978; James, 1979).

9.4 Discussion of the Oxygen Isotope Results

9.4.1 $^{18}O/^{16}O$-$^{87}Sr/^{86}Sr$ Correlations

On Figure 9.3, the $^{87}Sr/^{86}Sr$ data of Farmer and DePaolo (1983) are plotted against distance, as projected onto a transect line perpendicular to the Pacific Coast of central California (see Figure 9.6 for location of the transect). This figure thus differs somewhat from a similar figure in Farmer and DePaolo (1983), which is based on a projection onto the 40° parallel of latitude. The whole-rock $\delta^{18}O$ data shown in Figure 9.1 are lettered in alongside each sample point on Figure 9.3.

West of the RMT, in the eugeoclinal and transitional terranes, there is a regular west-to-east increase in initial $^{87}Sr/^{86}Sr$ ratios (or in the equivalent ε_{Sr} values). This indicates that the Sr isotopic compositions of these plutons basically depend only on distance from the coast and not on age of emplacement (Farmer and DePaolo, 1983). There is also a corresponding west-to-east increase in $\delta^{18}O$, although the $\delta^{18}O$-distance trend is less systematic than the $^{87}Sr/^{86}Sr$-distance trend (Figure 9.4). The $\delta^{18}O$ change is actually better characterized as being roughly uniform at +6.5 to +8.5 in the westernmost region for a distance of more than 200 km, and then as one moves to the east, increasing abruptly to $\delta^{18}O$ = +9.4 to +10.8 over a distance of less than 50 km (Figure 9.4). This abrupt change in $\delta^{18}O$ in the NGB occurs near the eugeoclinal zone-transitional zone boundary delineated by Farmer and DePaolo (1983), and is very reminiscent of the $\delta^{18}O$ "step" that separates the low-^{18}O western half of the PRB in southern California from the high-^{18}O eastern half. Note that there is also no discontinuity in the $^{87}Sr/^{86}Sr$ trend in the

Figure 9.3 Plot of distance (km) along a transect perpendicular to the Pacific Coast of central California (see Figure 9.6), versus $(^{87}Sr/^{86}Sr)_i$ of Mesozoic to early Tertiary NGB granitic plutons, based on data given in Table 9.1, modified after diagram in Farmer and DePaolo (1983). Whole-rock $\delta^{18}O$ values are shown adjacent to corresponding data-points, and the $(^{87}Sr/^{86}Sr)_i$ - distance trend is subdivided into the geographic $\delta^{18}O$ zones discussed in the text (Section 9.4.2) and shown in Figure 9.6: (1) the Western Zone (WZ) consisting of plutons with whole-rock $\delta^{18}O < +8.5$ per mil; (2) the Central Zone (CZ) with $+9 < \delta^{18}O < +13$; and (3) the Eastern Zone (EZ) with $+7 < \delta^{18}O < +9$. Also shown are the boundaries of the geographic regions discussed by Farmer and DePaolo (1983).

Figure 9.4 Plot of distance (km) along a transect perpendicular to the Pacific Coast of central California (see Figure 9.6), versus whole-rock $\delta^{18}O$ of Mesozoic and early Tertiary NGB granitic plutons, based on the data given in Tables 1.1, 1.2, and 9.1 (see also Figures 1.2, 1.4, and 9.1). The whole-rock $\delta^{18}O$ - distance trend is subdivided into the geographic $\delta^{18}O$ zones discussed for Figure 9.3 and in Section 9.4.2 (WZ - Western Zone; CZ - Central Zone; EZ - Eastern Zone), and the range of $(^{87}Sr/^{86}Sr)_i$ is given for each $\delta^{18}O$ zone. The CZ is further subdivided into two subzones based on the $(^{87}Sr/^{86}Sr)_i$ of CZ plutons: (1) the V-type subzone (shown with stippled pattern) with $0.7049 < I\text{-}Sr < 0.7072$; and (2) the S-type subzone with $0.7110 < I\text{-}Sr < 0.7372$. The solid triangles are the Farmer-DePaolo samples and the open circles are mid-Tertiary ash-flow tuff magmas from the Central Nevada caldera complex studied by Larson and Taylor (1986).

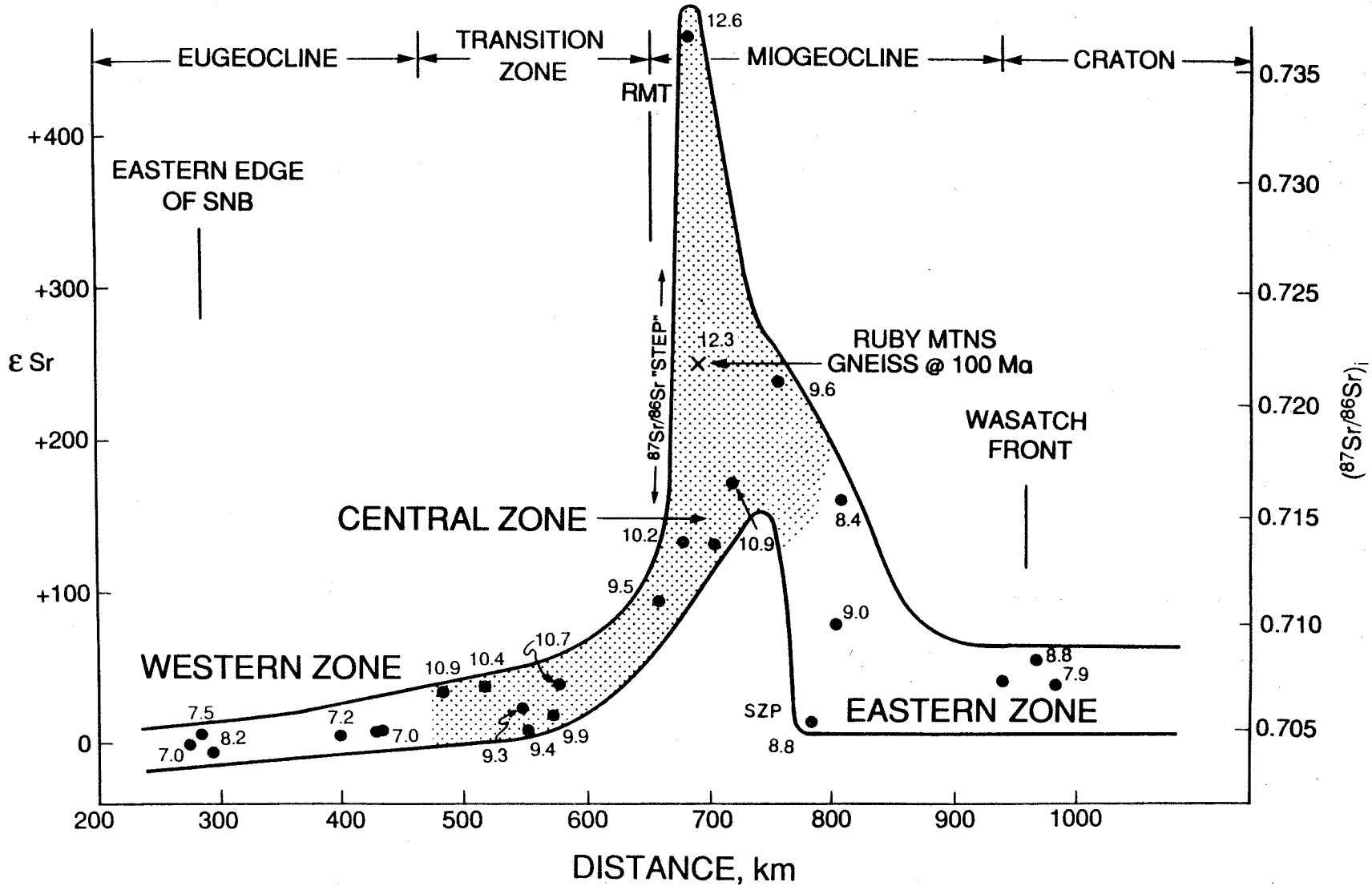
EUGEOCLINE
TRANSITION ZONE
MIOGEOCLINE
CRATON
RMT
EASTERN EDGE OF SNB
+400
+300
+200
+100
0
ε Sr
0.735
0.730
0.725
0.720
0.715
0.710
0.705
$(^{87}Sr/^{86}Sr)_i$
$^{87}Sr/^{86}Sr$ "STEP"
RUBY MTNS GNEISS @ 100 Ma
WASATCH FRONT
CENTRAL ZONE
WESTERN ZONE
EASTERN ZONE
SZP
12.6
12.3
9.6
8.4
10.2
10.9
9.5
9.0
10.7
10.9
10.4
8.8
7.9
7.5
8.2
7.0
7.2
7.0
9.3
9.4
9.9
8.8
200
300
400
500
600
700
800
900
1000
DISTANCE, km

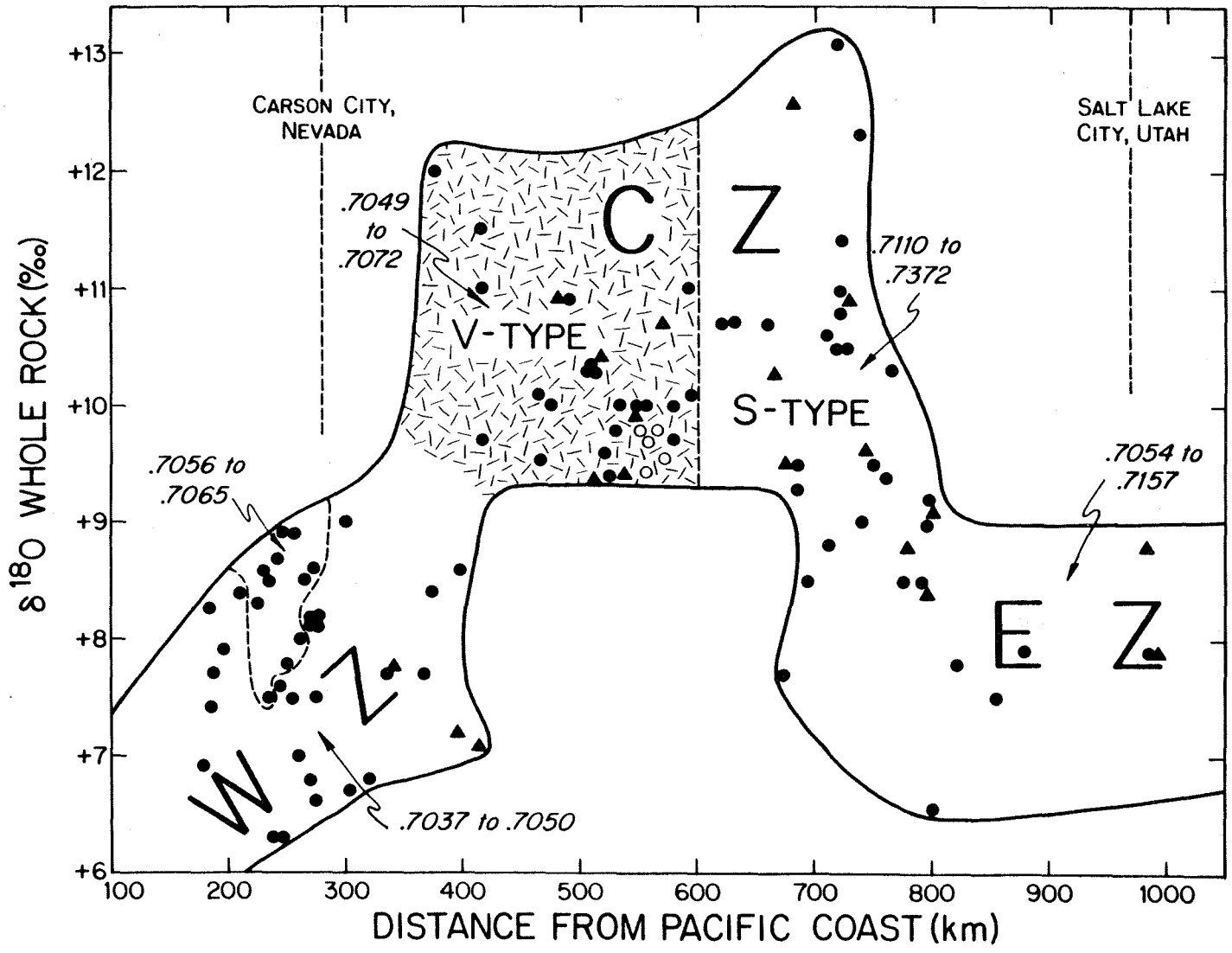
CARSON CITY, NEVADA
SALT LAKE CITY, UTAH
.7049 to .7072
.7110 to .7372
.7056 to .7065
.7054 to .7157
.7037 to .7050
V-TYPE
S-TYPE
CZ
WZ
EZ
δ18O WHOLE ROCK (‰)
DISTANCE FROM PACIFIC COAST (km)
+13
+12
+11
+10
+9
+8
+7
+6
100
200
300
400
500
600
700
800
900
1000

PRB; this parameter changes much more gradually across the axis of the PRB than does the $^{18}O/^{16}O$ (Early and Silver, 1973; Taylor and Silver, 1978).

These similarities between the NGB and the PRB show up very well on Figure 9.5. The overall range of isotopic compositions and the regularity of the west-to-east increase of ε_{Sr} and $\delta^{18}O$ are virtually identical to those found in the granitic plutons of the Peninsular Ranges Batholith, which is entirely Cretaceous in age (Silver et al., 1979; Taylor and Silver, 1978). There is also an $^{18}O/^{16}O$ "gap" in the Nevada data-set between $\delta^{18}O$ = +8.2 and $\delta^{18}O$ = +9.4 that corresponds nicely to the +8.5 to +9.0 per mil "gap" in the PRB (Figure 9.5). The only significant difference is that the complete range of ε_{Sr} (initial $^{87}Sr/^{86}Sr$) values from -20 to +40 (0.7025 to 0.7075) and the complete range of $\delta^{18}O$ values from +6.5 to +11.5 occurs over a horizontal distance of only 100-150 km in the PRB, whereas the effects span at least 400-500 km in the NGB.

The $^{87}Sr/^{86}Sr$ and the $\delta^{18}O$ trends in the NGB are both independent of age, and they are also similar to the isotopic trends defined for volcanic rocks in the Great Basin (Farmer and DePaolo, 1983; Armstrong et al., 1978; Larson and Taylor, 1986b). East of the RMT, within the zone of miogeoclinal rocks, the granitic plutons attain much higher ε_{Sr} than those to the west in the eugeoclinal and transitional terranes. However, the $\delta^{18}O$ values do not change markedly across the RMT at the transitional zone-miogeoclinal zone boundary, remaining at +9.5 to +10.9. Thus the abrupt change or "step" in $^{87}Sr/^{86}Sr$ takes place approximately 100-150 km east of the position where the abrupt $^{18}O/^{16}O$ change occurs. East of this $^{87}Sr/^{86}Sr$ "step," the miogeoclinal granites vary widely in ε_{Sr} from +40 to +250, with one two-mica granite from the Ruby Mountains having an

Figure 9.5 Plot of initial $^{87}Sr/^{86}Sr$ versus whole-rock $\delta^{18}O$ for Mesozoic and early Tertiary NGB granitic plutons, compared with the $^{87}Sr/^{86}Sr$ - $\delta^{18}O$ trend for the Cretaceous Peninsular Ranges Batholith (PRB), based on data given in Table 9.1 (NGB) and Taylor and Silver (1978; PRB). The $^{87}Sr/^{86}Sr$ - $\delta^{18}O$ values from the NGB are subdivided into data-fields based on the geographic $\delta^{18}O$ zones discussed in Section 9.4.2: (1) the Western Zone (WZ) with $\delta^{18}O < 8.5$ and $0.7037 < I\text{-}Sr < 0.7050$; (2) the Central V-type Subzone (CZ-V) with $+8.5 < \delta^{18}O < +11$ and $0.7050 < I\text{-}Sr < 0.7075$; (3) the Central S-type Subzone (CZ-S) with $+9.5 < \delta^{18}O < +13$ and $0.7110 < I\text{-}Sr < 0.7370$; and (4) the Eastern Zone (EZ) with $+7.9 < \delta^{18}O < +9$ and $0.7055 < I\text{-}Sr < 0.7160$. This type of plot presents several important observations regarding O - Sr isotopic compositions of NGB plutons, namely: (1) the WZ is almost entirely analogous to the western half of the PRB; (2) The CZ-V is analogous to the eastern half of the PRB; (3) the CZ-S plutons plot in an entirely unique position relative to the PRB trend, and are not rooted in that trend, suggesting a unique source region for these NGB plutons; and (4) the EZ plutons plot in an envelope that does not overlap with the CZ-S, and which is rooted in the PRB trend, although, for the most part, EZ O - Sr compositions extend away from the PRB trend; thus, the EZ trend appears to be analogous to that of SECA (see Figure 8.7).

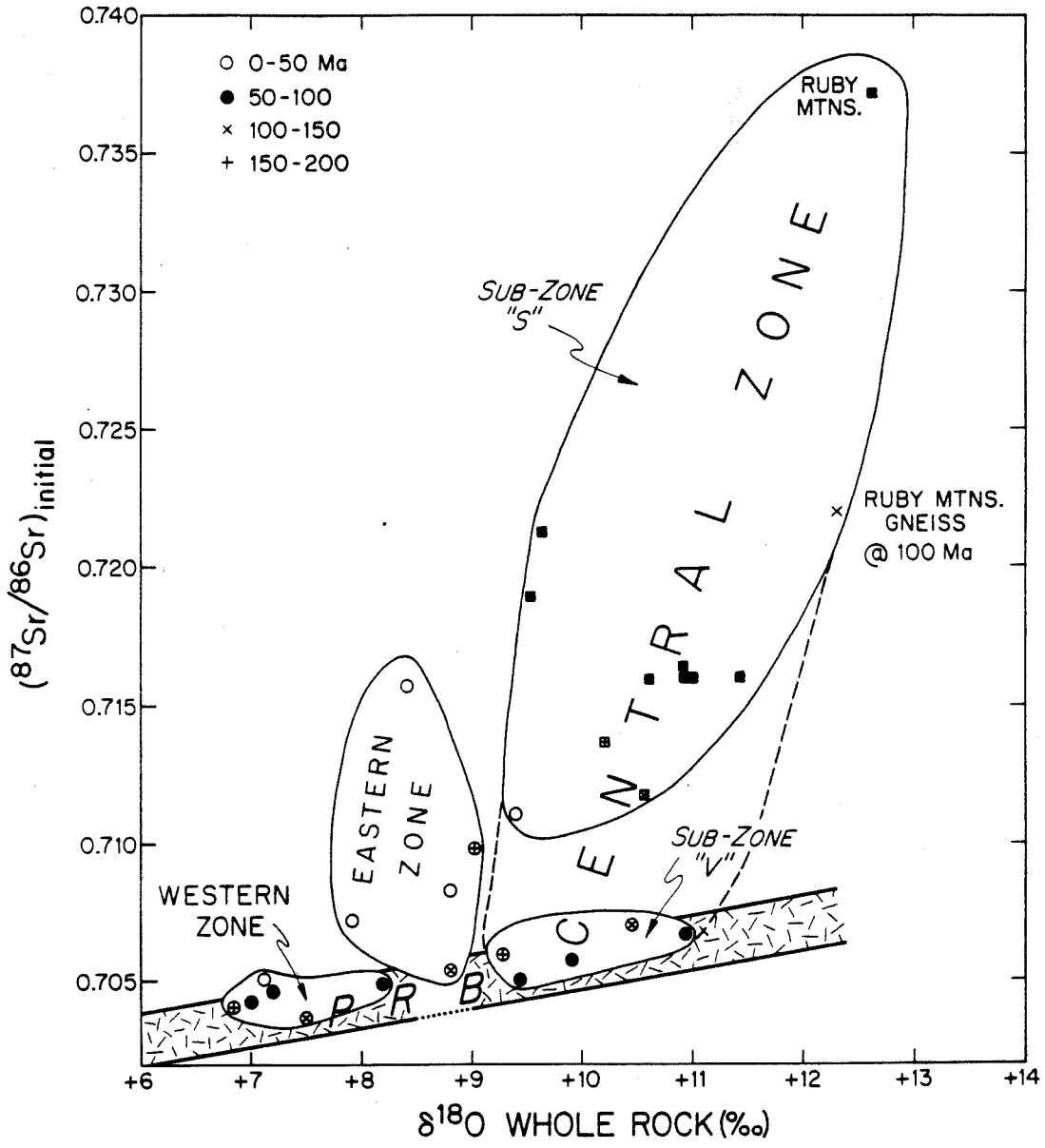
0.740
0.735
0.730
0.725
0.720
0.715
0.710
0.705
$(^{87}Sr/^{86}Sr)_{initial}$
○ 0-50 Ma
● 50-100
× 100-150
+ 150-200
RUBY MTNS.
SUB-ZONE "S"
CENTRAL ZONE
RUBY MTNS. GNEISS @ 100 Ma
EASTERN ZONE
SUB-ZONE "V"
WESTERN ZONE
PRB
+6
+7
+8
+9
+10
+11
+12
+13
+14
$\delta^{18}O$ WHOLE ROCK (‰)

extremely high ε_{Sr} = +466, as well as a particularly high $\delta^{18}O$ = +12.6. Both the ε_{Sr} values and the $\delta^{18}O$ values of the peraluminous granites tend to be somewhat higher than the Tertiary (metaluminous) monzogranites from the same geographic region.

9.4.2 Regional Isotopic Zones

Based mainly on the $\delta^{18}O$ systematics, which define a very clear-cut separation between the NGB granites of central and eastern Nevada ($\delta^{18}O$ = +9.4 to +12.6) and those of either western Nevada and California ($\delta^{18}O$ = +6.4 and +9.0) or of Utah ($\delta^{18}O$ = +7.5 to +8.9), we have delineated three major provinces or zones: Western, Central, and Eastern (shown in Figure 9.6). This very simple geographic classification nicely characterizes the first-order $^{18}O/^{16}O$ differences in all of the NGB plutons. The Western Low-^{18}O Zone includes plutons that characteristically have +6.5 < $\delta^{18}O$ < +8.5. Continuing eastward, the Central High-^{18}O Zone includes plutons with +9 < $\delta^{18}O$ < +13. Still farther to the east in Utah, the Eastern Intermediate-^{18}O Zone includes plutons with +7 < $\delta^{18}O$ < +9 (Figure 9.4).

Our Western Low-^{18}O Zone corresponds almost exactly to the eugeoclinal zone of Farmer and DePaolo (1983). The only difference is that two plutons (samples 8 and 10 in Table 1, Farmer and DePaolo, 1983) that lie just slightly west of their transitional zone-eugeoclinal zone boundary are here included within our Central Zone, because they have very high $\delta^{18}O$ values (+9.4 to +10.2). Based on these new $^{18}O/^{16}O$ data, it seems logical to place these two plutons in the Farmer-DePaolo transitional zone, as well, and we have done this on Figures 9.3 and 9.4.

The boundaries of our Central High-^{18}O Zone, however, differ markedly from the major zonal boundaries defined by Farmer and DePaolo (1983)

Figure 9.6 Map of a portion of the western United States showing the boundaries of $\delta^{18}O$ zones within the NGB of northeastern California, northern Nevada and western Utah, based on $^{18}O/^{16}O$ data from Tables 1.1, 1.2 and 9.1 (also see Figures 1.2, 1.4 and 9.1). The solid circles indicate sample localities of Farmer and DePaolo (1983; and see Figure 9.1, this study; SZP indicates Silver Zone Pass pluton). The $\delta^{18}O$ zones are shown by light, solid lines, and are geographic regions where, from west to east, the Mesozoic and early Tertiary granitic plutons are restricted to the following primary whole-rock $\delta^{18}O$ values: (1) Western Zone (WZ) - <+8.5; (2) Central Zone (CZ) - +8.5 in the western part, to as high as +13, and back down to as low as ~+9.5 near its eastern edge; and (3) Eastern Zone (EZ) - <+9. The CZ is further subdivided into two regions on the basis of initial $^{87}Sr/^{86}Sr$ ratios: (a) Central V-type subzone (CZ-V) - I-Sr < 0.7080; and (b) Central S-type subzone (CZ-S) - I-Sr > 0.7110. Consult Figure 1.2 for the way in which the WZ-CZ and CZ-EZ boundaries extend farther to the south in the vicinity of the Sierra Nevada Batholith (SNB). The V-S subzone boundary within the CZ pinches out in southern Nevada, and is not observed in SECA, or southern Arizona. The location of the $^{18}O/^{16}O$ transect shown in Figure 9.4 is the line drawn across the map from SW to NE, crossing near Carson City (CC), Nevada and Salt Lake City (SLC), Utah. Roman numerals (Ia, Ib, II and III) indicate the Pb-isotopic zones of Zartman (1974), shown on the map by the stippled boundaries. Heavy, solid numbered N-S lines labeled 1 and 2 indicate the isotopic boundaries of Farmer and DePaolo (1983): (1) the Transitional Zone-Miogeoclinal Zone boundary separating plutons with $[^{87}Sr/^{86}Sr]_i$ < 0.708 on the west and those with $[^{87}Sr/^{86}Sr]_i$ > 0.7110 to the east (slightly modified in southern Nevada from the Farmer-DePaolo position), and (2) the Miogeoclinal Zone-Craton Zone boundary. The reasons why Farmer and DePaolo (1983) singled out line 2 as a major boundary are not at all clear to the present author.

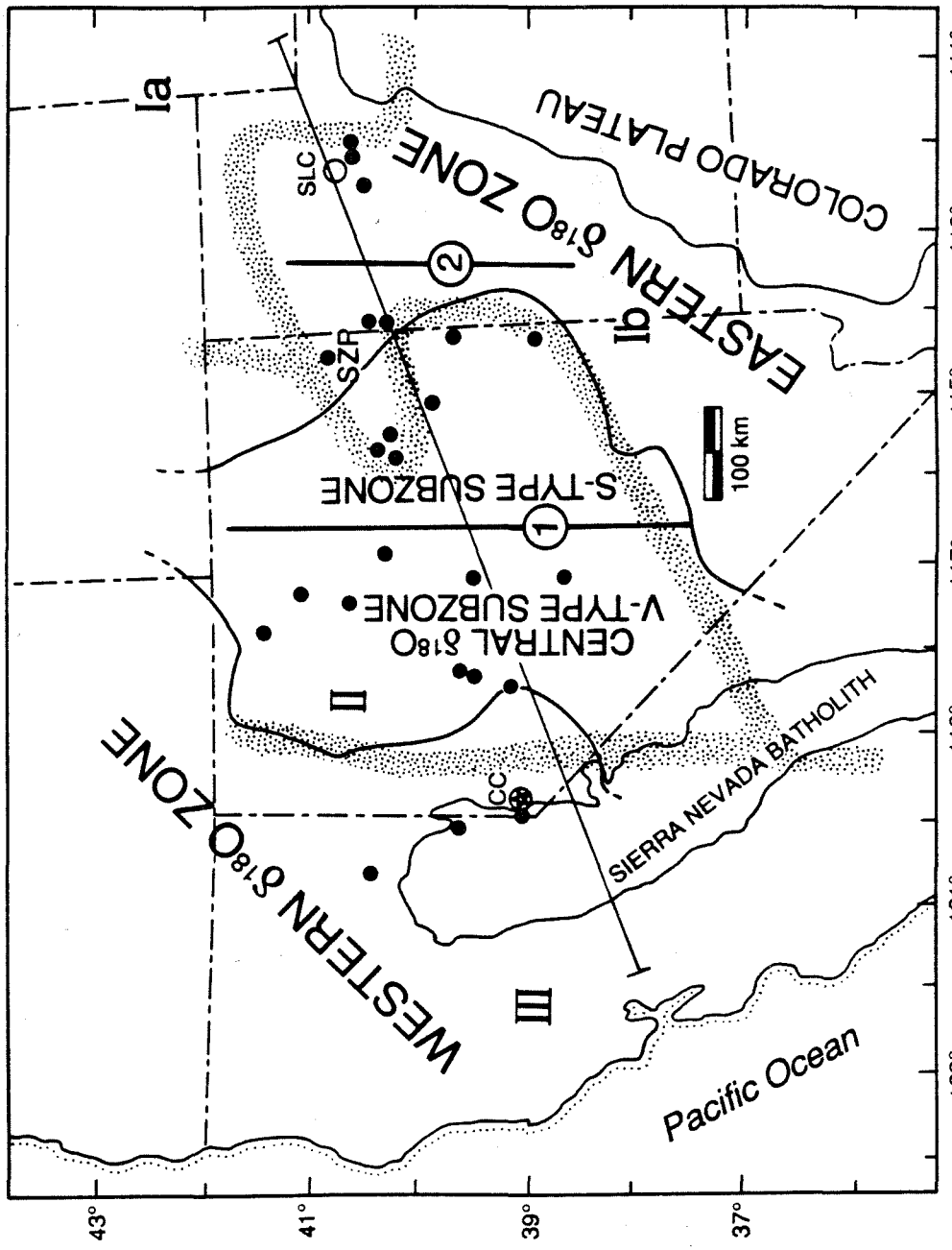
Ia
Ib
II
III
SLC
SZR
CC
EASTERN δ18O ZONE
WESTERN δ18O ZONE
CENTRAL δ18O
V-TYPE SUBZONE
S-TYPE SUBZONE
1
2
100 km
COLORADO PLATEAU
SIERRA NEVADA BATHOLITH
Pacific Ocean
111°
113°
115°
117°
119°
121°
123°
43°
41°
39°
37°

(see Figure 9.6). The western edge of the Central High-^{18}O Zone lies well to the west of the major ε_{Sr} discontinuity observed in the vicinity of the RMT, which constitutes the boundary between the transitional and miogeoclinal zones of Farmer and DePaolo (1983). Also, we place the eastern boundary of our Central Zone right in the middle of their miogeoclinal zone, well to the west of the position of another major ε_{Sr} discontinuity that Farmer and DePaolo (1983) proposed in the eastern NGB (Figure 9.1). Thus our Central High-^{18}O Zone encompasses only the western half of their miogeoclinal zone, but all of their transitional zone, and it straddles the major $^{87}Sr/^{86}Sr$ "step" that they have delineated. Also, whereas our Eastern Intermediate-^{18}O Zone corresponds in large part to their craton zone, this Eastern Zone in addition includes the eastern half of their miogeoclinal zone. Note that with our new rearrangement of zonal boundaries in the NGB, the geochemistry of the Silver Zone Pass pluton (SZP on Figure 9.6) fits in much better with the other plutons of the Eastern Zone, whereas Farmer and DePaolo (1983) considered this magma body to be "anomalous."

Within the Central High-^{18}O Zone, the sharp change in average ε_{Sr} value from about +40 in the transitional region to values in excess of +100 in the miogeocline indicates a dramatic difference in the magma sources between the two regions (Farmer and DePaolo, 1983), in spite of the fact that similarly high $\delta^{18}O$ values are characteristic of both the transitional region and the western half of the miogeoclinal region. It is thus clear from the <u>combined</u> $^{18}O/^{16}O$ and $^{87}Sr/^{86}Sr$ data that the Central High-^{18}O Zone in Nevada <u>must</u> be subdivided into two geographic subzones at this Sr isotope "step" (Figure 9.6).

Inasmuch as many of the high-^{87}Sr granites in the eastern half of the Central High-^{18}O Zone are characteristically peraluminous and muscovite-bearing, they appear to satisfy many of the criteria for S-type granites, using the terminology of Chappell and White (1978). We therefore propose to designate this area east of the ε_{Sr} "step" as the Central (S-type) subzone. We realize that, in the strict sense of the "type" locality for S-type plutons in southeastern Australia, certain "S-type" criteria are not met by some of these NGB plutons (see White et al., 1986). However, the combination of high $\delta^{18}O$ and high initial $^{87}Sr/^{86}Sr$ values in all of these samples demand a sedimentary origin (see below). This is elaborated upon in the following discussion in Section 9.4.5, utilizing major-element geochemistry together with the isotopic systematics.

For the part of the Central High-^{18}O Zone to the west of the ε_{Sr} "step," which is directly analogous to the zone of high-^{18}O plutons that forms the eastern half of the Peninsular Ranges Batholith (Figure 9.5), the source materials of the granitic plutons undoubtedly also include some sedimentary rocks. However, at least in the PRB, these source materials also must include a major proportion of weathered or hydrothermally altered high-^{18}O basalt or basaltic andesite (greenstone) or volcanogenic sediments derived therefrom (Taylor and Silver, 1978; Taylor, 1986). Therefore, we propose to emphasize the volcanic component of this pile of transitional-zone country rocks, and we shall refer to this (western) part of our Central High-^{18}O Zone in Nevada as the Central (V-type) subzone.

Note that the two subzones discussed above might equally well be called MCC-type or High-^{18}O PRB-type, respectively, for their character-

istic appearance elsewhere in the Cordillera, either in metamorphic core complexes or in the eastern half of the Peninsular Ranges Batholith. However, we certainly cannot utilize the MG-type and EG-type designations for miogeoclinal granites and eugeoclinal granites used by Farmer and DePaolo (1983), even though several of our S-type and V-type plutons, respectively, fit their classification; although a number of plutons with those designations also fit our categories, a number also do not. In any case, each of these previous classifications brings with it a set of other characteristic geochemical and petrologic features that may or may not be directly applicable to the $^{18}O/^{16}O$ systematics in the NGB, and thereby might introduce an element of ambiguity or confusion.

Tertiary granodiorites farther east in the craton area have much lower ε_{Sr} (+30 to +50) than most of the miogeoclinal granites (Farmer and DePaolo, 1983). These low ε_{Sr} values of the cratonal granitic rocks of Utah are also similar to those found for Tertiary intrusions still farther east in the Colorado Mineral Belt (Simmons and Hedge, 1978). Thus, there is obviously a marked change in magma source characteristics between the craton and the miogeocline, and Farmer and DePaolo (1983) placed this discontinuity about 50-75 km east of the Nevada-Utah border (Figure 9.1). However, based on the new $^{18}O/^{16}O$ evidence (and the Pb isotope data of Zartman, 1974; see below), we believe that a case can be made that the important regional boundary lies between our Eastern High-^{18}O Zone and our Central High-^{18}O Zone, slightly to the west of the Nevada-Utah border, and about 75-100 km west of the position favored by Farmer and DePaolo (1983). This important regional $\delta^{18}O$-derived boundary is similar in nature to the transitional boundaries observed in southern California that are discussed in Chapter 6 (see Figures 6.6 and 6.9);

this boundary marks the westernmost occurrence of plutons having isotopic signatures that seem to be predominantly from ancient cratonal basement.

The geochemical boundaries described above all trend approximately N-S, although the CZ-EZ boundary near the Utah-Nevada border is clearly arcuate in shape, with a convex "bulge" toward the east (Figure 9.6). These N-S boundaries do not, however, continue undisturbed into the Southern Basin and Range (SBR). In particular, the $^{87}Sr/^{86}Sr$ "step" between the S-type and V-type subzones appears to abruptly terminate along a generally E-W boundary that extends all the way across central Nevada. North of this boundary, the Central High-^{18}O Zone is extremely wide and very well defined (Figure 9.6). South of the E-W boundary, the CZ is much narrower and is displaced much farther to the west, where it reappears in the vicinity of the SNB. The plutons in southern Nevada all appear to have Eastern Zone characteristics, implying that the entire S-type subzone portion of the CZ is truncated at this E-W boundary. These various features have some very interesting and far-reaching implications concerning the geological history of the entire southwestern Cordillera of North America; this discussion is, however, deferred to Chapter 10, where it is taken up in a regional context.

9.4.3 $\delta^{18}O$-ε_{Nd} Correlations

Farmer and DePaolo (1983) showed that there was a strong correlation between ε_{Nd} and ε_{Sr} in the NGB granites (Figure 9.7), as well as a good correlation between ε_{Nd} and distance (Figure 9.8). The range of ε_{Nd} values is extremely large, about half the range measured in all terrestrial rocks; it overlaps the range of mid-ocean ridge basalts at the positive extreme and extends to values typical of Precambrian continental

Figure 9.7 Plot of ε_{Sr} versus ε_{Nd} for Mesozoic and early Tertiary NGB granitic plutons showing ε_{Sr} - ε_{Nd} relations within the context of $\delta^{18}O$ zones, based on the isotopic data given in Table 9.1; modified after diagram in Farmer and DePaolo (1983). The $\delta^{18}O$ zones are discussed in Section 9.4.2 and shown in Figure 9.6. Heavy, solid line labeled OCL is the oceanic correlation line discussed by Farmer and DePaolo (1983). SZP = Silver Zone Pass pluton; Ely = Ely porphyry-Cu pluton (Farmer and DePaolo, 1984).

Figure 9.8 Plot of distance (km) along a transect perpendicular to the Pacific Coast (see Figure 9.6), versus ε_{Nd} of Mesozoic and early Tertiary NGB granitic plutons, based on data given in Table 9.1, modified after diagram in Farmer and DePaolo (1983). Whole-rock $\delta^{18}O$ values are indicated for each data-point. The distance - ε_{Nd} trend is subdivided into the $\delta^{18}O$ zones discussed in Section 9.4.2 (also see Figure 9.6). The geographic regions discussed by Farmer and DePaolo (1983), and shown on the map and geologic cross-section in Figures 9.1 and 9.2, are indicated at the top edge of the diagram. SZP = Silver Zone Pass pluton.

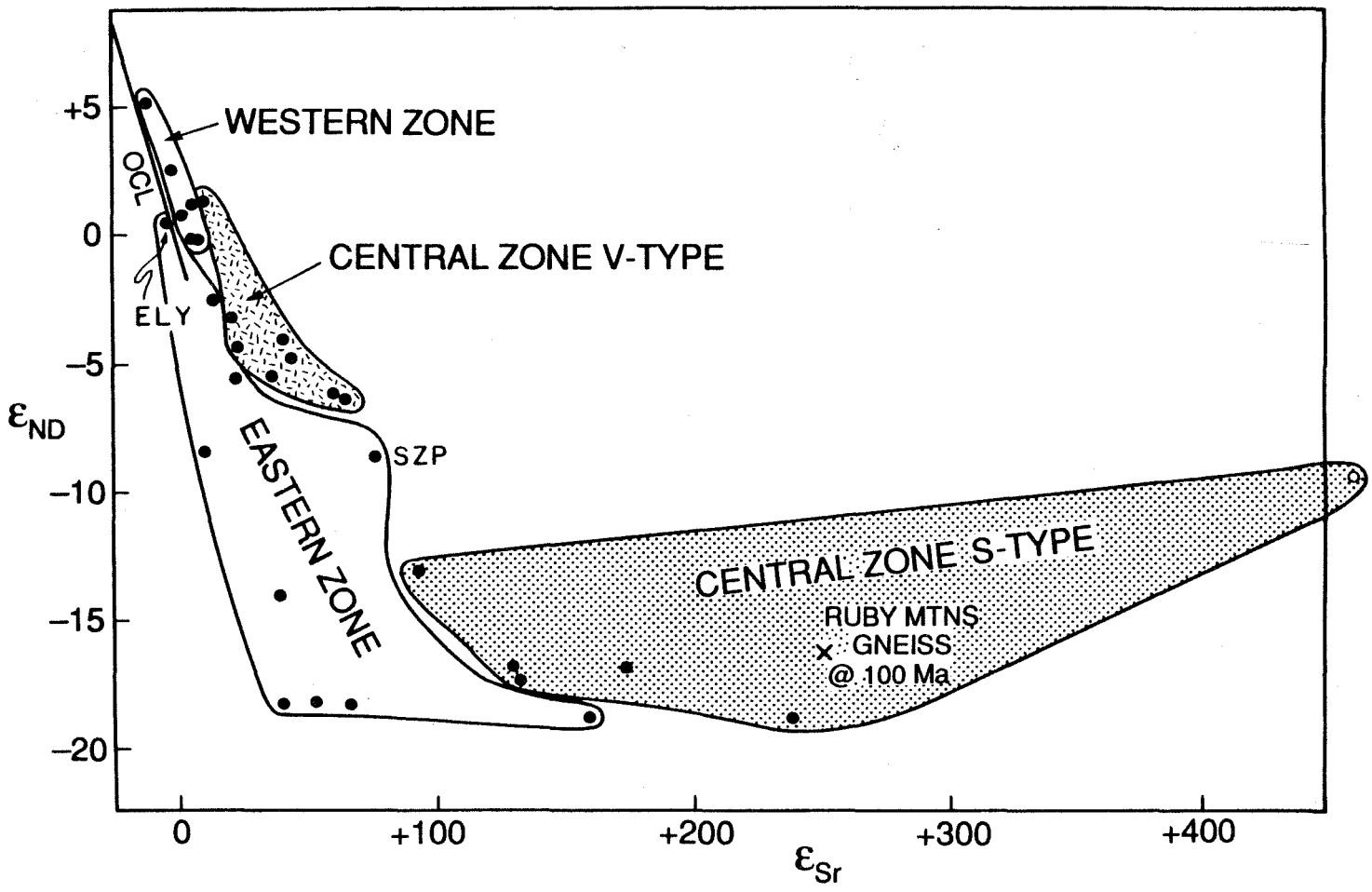
WESTERN ZONE
OCL
ELY
CENTRAL ZONE V-TYPE
SZP
EASTERN ZONE
CENTRAL ZONE S-TYPE
RUBY MTNS
GNEISS
@ 100 Ma
+5
0
−5
−10
−15
−20
ε_{ND}
0
+100
+200
+300
+400
ε_{Sr}

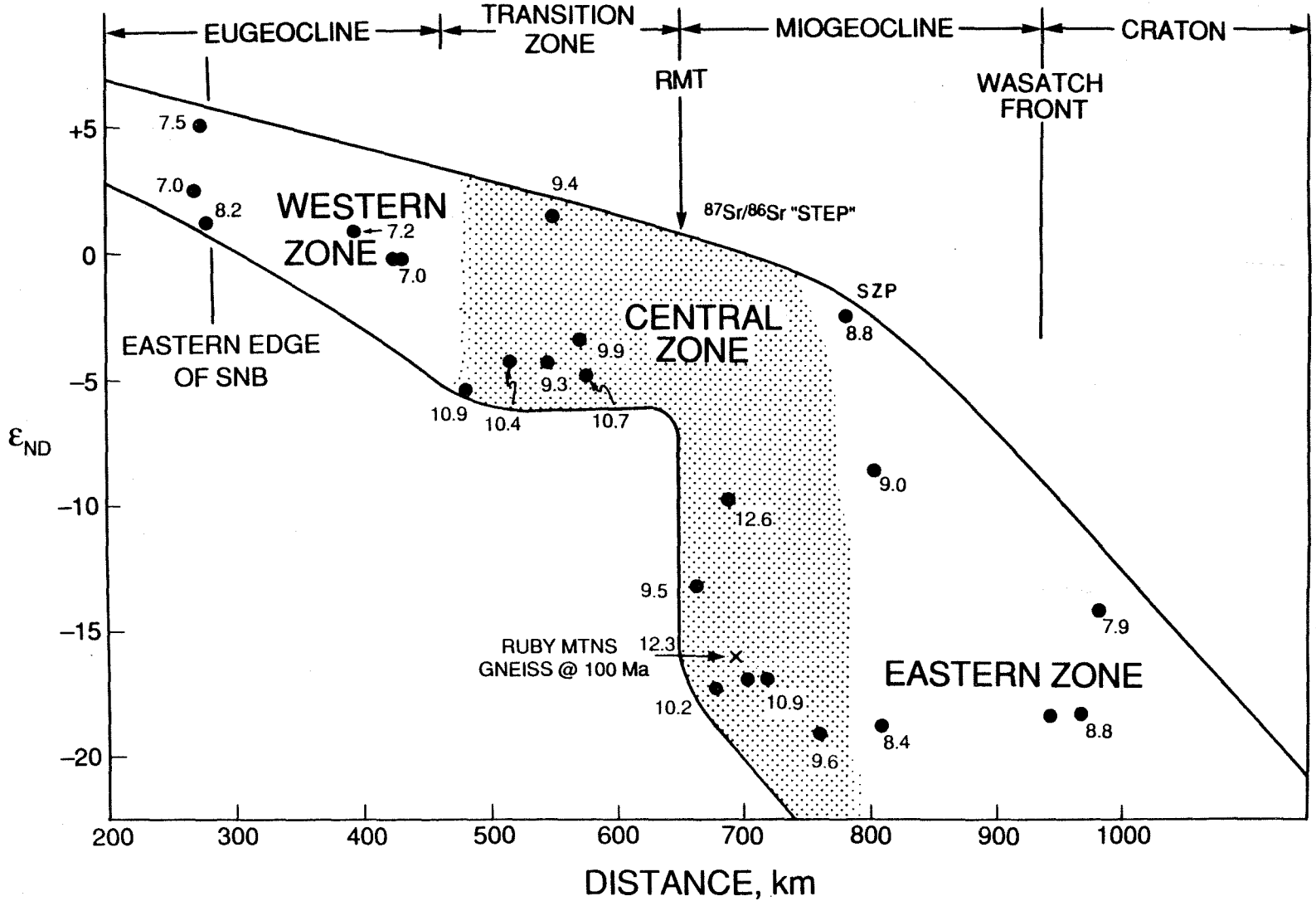
EUGEOCLINE
TRANSITION ZONE
MIOGEOCLINE
CRATON
RMT
WASATCH FRONT
WESTERN ZONE
CENTRAL ZONE
EASTERN ZONE
EASTERN EDGE OF SNB
$^{87}Sr/^{86}Sr$ "STEP"
SZP
RUBY MTNS GNEISS @ 100 Ma
12.3
7.5
7.0
8.2
7.2
7.0
9.4
9.9
9.3
10.9
10.4
10.7
8.8
9.0
12.6
9.5
7.9
10.2
10.9
9.6
8.4
8.8
+5
0
−5
−10
−15
−20
ε_{ND}
200
300
400
500
600
700
800
900
1000
DISTANCE, km

crust at the negative extreme (Farmer and DePaolo, 1983). However, in contrast to the very abrupt isotopic changes and sharp geographic boundaries observed for both $^{87}Sr/^{86}Sr$ and $^{18}O/^{16}O$, Farmer and DePaolo (1983) conclude that the ε_{Nd} values show only gradational changes. Nevertheless, one can interpret the ε_{Nd}-distance trend in terms of an abrupt "drop" from an $\varepsilon_{Nd} \sim -5$ to values of -18 to -20 at the position of the $^{87}Sr/^{86}Sr$ "step" (Figure 9.8).

Starting near the Oceanic Correlation Line (OCL) defined for MORBs and oceanic islands, two well-defined trends show up on Figure 9.7. A continuation of the generally steep OCL gradient leads toward the Eastern Zone granites, whereas a shallower (more ^{87}Sr-rich) trend leads toward the Central Zone granites. Again, using our simple 3-fold $^{18}O/^{16}O$ classification, we obtain a somewhat more straightforward set of correlations than those defined by Farmer and DePaolo (1983), particularly in that the SZP pluton is no longer anomalous, and instead fits right in with the other Eastern Zone granites on Figures 9.7 and 9.8.

The Eastern Zone and Central Zone crustal "end-members" in these plutons appear to have similarly low ε_{Nd} values of about -15 to -20, but they clearly have distinctive ε_{Sr} values of about +40 to +100 and +150 to +500, respectively (Figure 9.7). The $^{87}Sr/^{86}Sr$ differences in these "end-members" go hand-in-hand with the marked $^{18}O/^{16}O$ differences indicated above (Figure 9.5); these two distinct crustal "end-members" also are very distinctive in $^{18}O/^{16}O$, with $\delta^{18}O$ values of approximately +8 to +9 versus +10 to +15, respectively. The lower-^{18}O component is readily identifiable with typical basement rocks of the North American craton (Shieh and Schwarcz, 1976; Turi and Taylor, 1971b), and the higher-^{18}O component fits in nicely with the typical $\delta^{18}O$ values of detrital sedimentary or metasedimentary rocks (shales, sandstones, and mudstones).

There is no overlap whatsoever between the fields of the Central Zone plutons and the Eastern Zone plutons on the $\delta^{18}O$-ε_{Sr} plot of Figure 9.5. In both cases, these fields appear to be "rooted" within the PRB $\delta^{18}O$-$^{87}Sr/^{86}Sr$ data-point envelope, and they extend upward and to the right from that envelope toward more ^{87}Sr-rich compositions. The extrapolated values defined by the two trends may be readily identified with the hypothetical crustal "end-members" discussed above. It is clear that these "end-members" must each have drastically different and distinctive $\delta^{18}O$ and ε_{Sr} values (Figure 9.5).

9.4.4 Assimilation-Fractional Crystallization (AFC) Models

Taylor (1980) and DePaolo (1981) developed the so-called assimilation-fractional crystallization (AFC) model, and showed that in general such AFC processes lead to drastically different isotopic and trace element effects than those that would be predicted by simple mixing of two end-members. Farmer and DePaolo (1983) believe that their ε_{Sr} and ε_{Nd} data strongly support the idea that the NGB granites originated by AFC processes involving interactions between mantle-derived magmas and the continental crust. Although we agree with Farmer and DePaolo (1983) that AFC processes could have been important in Nevada, we disagree with their statements that there is strong evidence in favor of such an origin. The available data set for strontium and neodymium is simply too limited to make such sweeping statements about magmatic evolution over such a broad area of the continental crust. In particular, much more isotopic and trace element data would have to be obtained on the country rocks at various depths throughout the NGB region, in order to constrain the end-member that is being assimilated.

Some of these concerns can be elaborated upon by referring to Figure 9.9, which plots the ε_{Sr} data of Farmer and DePaolo (1983) against the measured concentration of Sr in each rock. Figure 9.9 is analogous to Figures 11a, 11b, and 11c of Farmer and DePaolo (1983), but it is more easily understood than those diagrams because the Sr isotope data are plotted vs. 1/Sr instead of directly against ppm Sr. Plots of isotopic ratios of a certain element versus the inverse concentration of that element produce straight lines, both for simple two-component mixing and for simple AFC processes in which the ratio of cumulates to assimilated rock is held constant (Taylor, 1980; also see Figure 12 in Taylor and Sheppard, 1986, which is repeated here as Figure 9.10). Thus, the strongly curved AFC trajectories on Figures 11a, 11b, and 11c of Farmer and DePaolo (1983) all transform to straight lines on plots like Figures 9.9 and 9.10, and this makes it easier to discern any plausible correlations in a set of data-points.

The Western, Central (V-type), Central (S-type), and Eastern $^{18}O/^{16}O$ zones all separate out nicely on Figure 9.9, and the model crust and model mantle magmas favored by Farmer and DePaolo (1983) are also shown on the diagram. The data envelopes on Figure 9.9 conceivably could be interpreted as radiating upward and to the right (i.e., toward lower ppm Sr and higher $^{87}Sr/^{86}Sr$) from a common type of parent magma that might have the general characteristics of the 168 Ma Yerington batholith of western Nevada (Dilles, 1987). The low ε_{Sr} (-10), low $\delta^{18}O$ (+6.8), and high Sr concentration (1200 ppm) of the Yerington batholith all strongly favor a more-or-less direct mantle origin for this set of plutons, as does the fact that the Yerington area contains a major porphyry copper deposit. Note that the four data-point envelopes referred to above

Figure 9.9 Plot of 1/Sr versus initial $^{87}Sr/^{86}Sr$ for Mesozoic and Cenozoic NGB granitic plutons, based on data taken from Farmer and DePaolo (1983) and Dilles (1987); also see Table 9.1. The data-points have been subdivided into envelopes based on the geographic $\delta^{18}O$ zones discussed in Section 9.4.2 (see Figure 9.6). The stars indicate the model mantle and model crust compositions used by Farmer and DePaolo (1983) to explain their AFC model for NGB plutons. It is clear from this figure that the four $\delta^{18}O$ zones or subzones all separate nicely into different packages on the diagram, and that their trends bear little relationship to the model compositions assumed by Farmer and DePaolo (1983). Rather, the data envelopes for the WZ, CZ-S and EZ appear to be rooted in their low-1/Sr ranges along a "mantle-mixing" zone (see Figure 10.12a). This zone could represent mantle that increasingly acquires a "crustal" signature over large amounts of time (e.g., 1.8 Ga - age of the craton) due to subduction, or some sort of exchange process, as distance from the Pacific Ocean increases. Then, the extension from the roots in this mantle-mixing zone up to high 1/Sr values for each envelope could reflect simple two-component mixing between magmas from "ancient continental mantle" beneath the craton, and a mid-level crustal end-member. Also, the WZ data-envelope could conceivably represent simple closed-system crystallization from a single type of parent magma (see Figure 9.10). CZ-S appears not to be related to either of the previous three zones, but could have formed from simple melting of heterogeneous mid-level crustal materials.

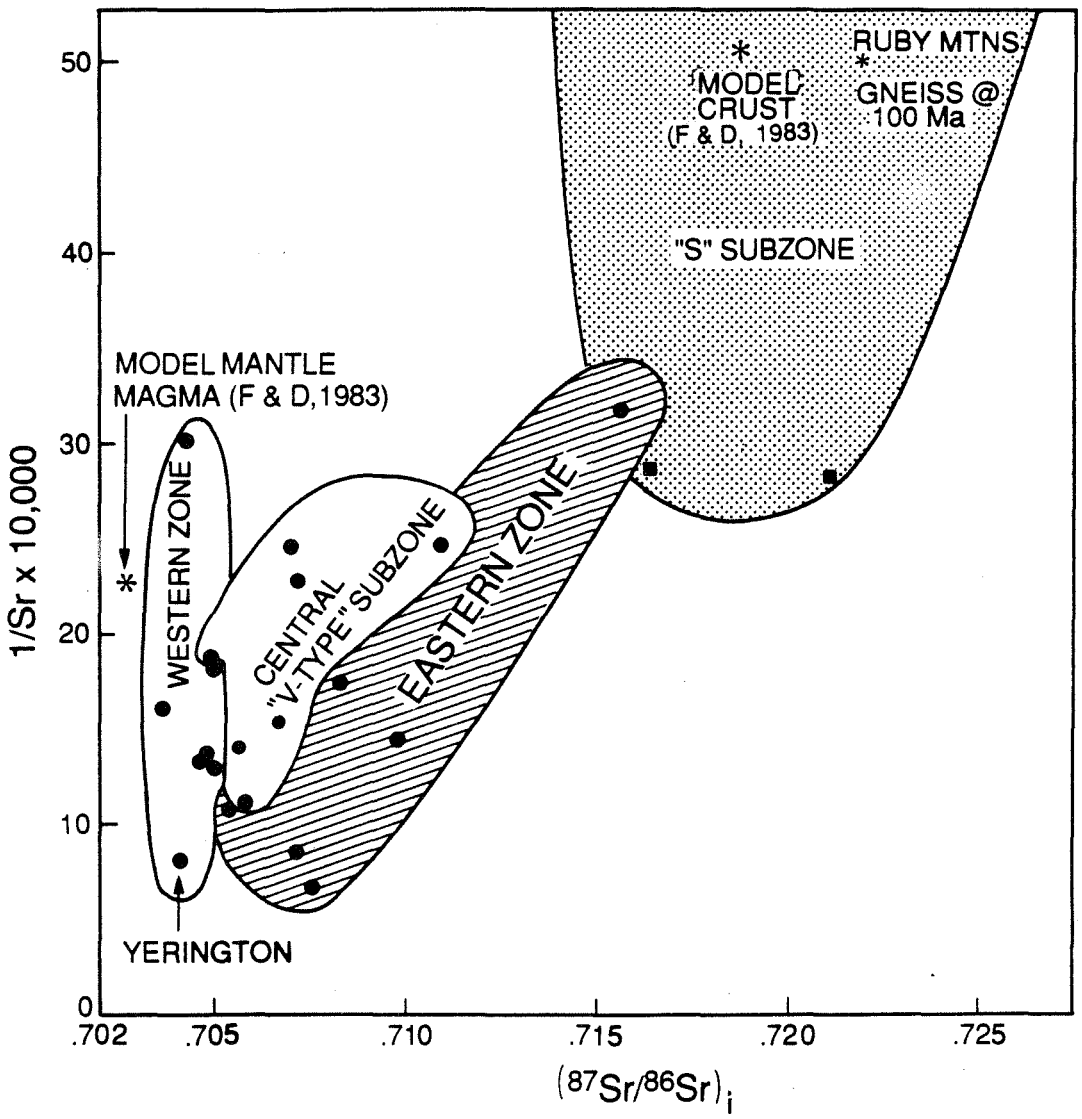
RUBY MTNS.
GNEISS @
100 Ma
MODEL
CRUST
(F & D, 1983)
"S" SUBZONE
MODEL MANTLE
MAGMA (F & D,1983)
WESTERN ZONE
CENTRAL
"V-TYPE" SUBZONE
EASTERN ZONE
YERINGTON
1/Sr x 10,000
50
40
30
20
10
0
.702
.705
.710
.715
.720
.725
$(^{87}Sr/^{86}Sr)_i$

Figure 9.10 Plot of 1/Sr versus normalized $^{87}Sr/^{86}Sr$, showing various AFC paths for a magma starting with 1200 ppm Sr and country rocks that contain 180 ppm Sr, assuming different β values and R values (see Taylor, 1980); after diagram in Taylor and Sheppard (1986). All trajectories are for R = 4 unless otherwise indicated. All AFC paths in this coordinate system are straight lines, but the only path that projects to the correct isotopic composition of the country rock end-member is the Simple Mixing line, which is coincident with the β = 1 AFC line (Taylor, 1980). The opposite-directed vertical arrows at a normalized ε value of 0.0 represent either perfect closed-system crystallization, or AFC processes with $\beta \rightarrow 0$ (downward arrow) or $\beta \rightarrow \infty$ (upward arrow).

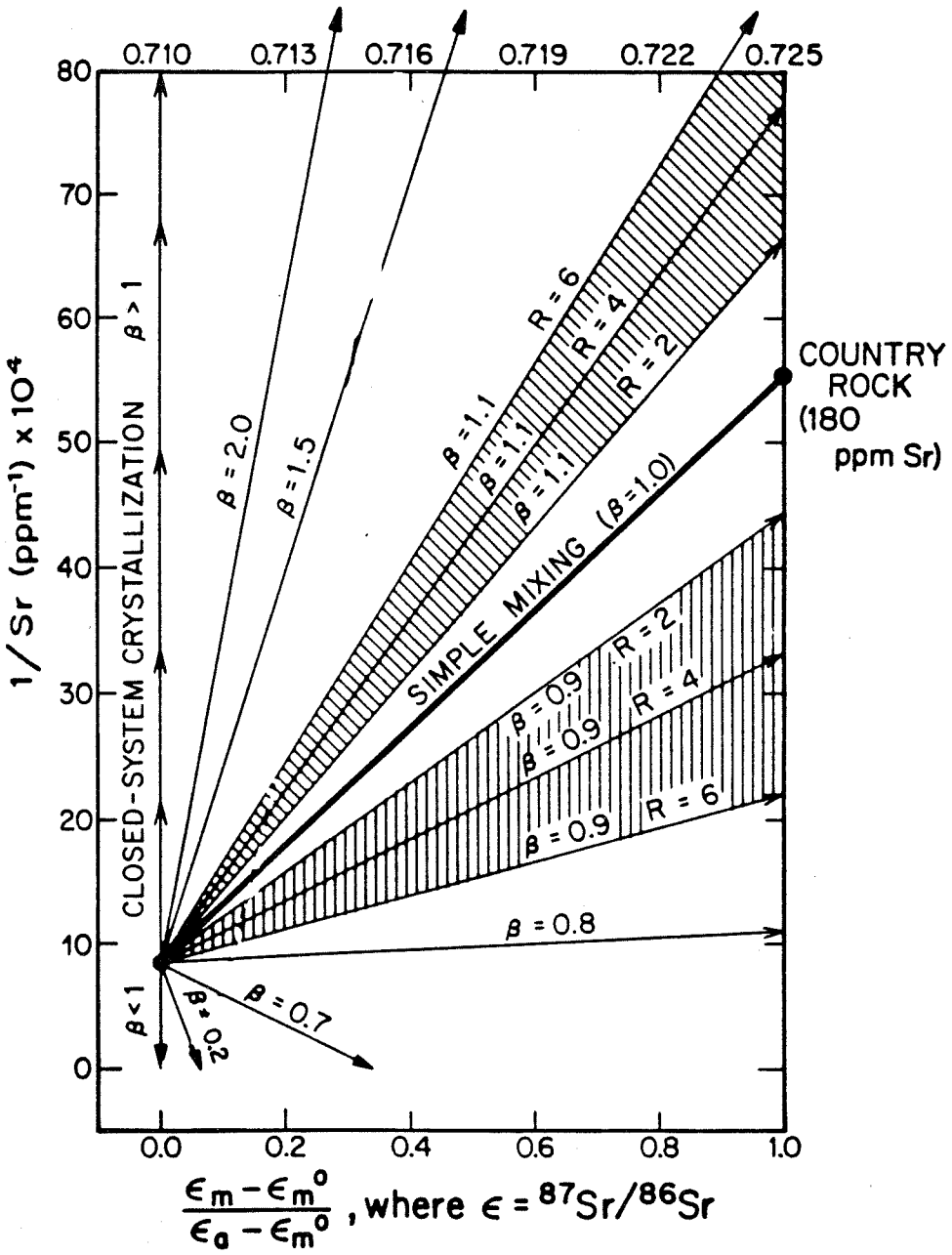
0.710
0.713
0.716
0.719
0.722
0.725
80
70
60
50
40
30
20
10
0
1/Sr (ppm⁻¹) x 10⁴
CLOSED-SYSTEM CRYSTALLIZATION
β > 1
β < 1
β = 2.0
β = 1.5
β = 1.1
R = 6
β = 1.1
R = 4
β = 1.1
R = 2
SIMPLE MIXING (β=1.0)
COUNTRY ROCK (180 ppm Sr)
β = 0.9
R = 2
β = 0.9
R = 4
β = 0.9
R = 6
β = 0.8
β = 0.7
β = 0.2
0.0
0.2
0.4
0.6
0.8
1.0
(εm − εm⁰) / (εa − εm⁰) , where ε = 87Sr/86Sr

project toward the Yerington data-point on the diagram, but there is no indication of any such linear extrapolation toward the values of the model mantle magma favored by Farmer and DePaolo (1983).

Let us consider the trajectories defined by the Western, Central (V-type), and Eastern Zones on Figure 9.9 in more detail. In a general sense, each of these trajectories could represent either simple two-component mixing or a simple AFC process (Figure 9.10). The only difference is that: (1) in the simple mixing case, at least 3 separate crustal end-members would be required, a different one for each zone, with the ε_{Sr} of these crustal components increasing systematically from west-to-east across Nevada; or (2) in the simple AFC case, a single crustal end-member possibly might suffice, but then the bulk distribution coefficients for strontium between the cumulates and the magmas (β_{Sr}), or the ratios of cumulates to assimilated rock (R), or both, must change systematically from west-to-east (see Taylor, 1980; Taylor and Sheppard, 1986). For example, keeping the R-value constant at about 3 to 10 and assuming a uniform crustal end-member plotting somewhere in the Central (S-type) Zone field on Figure 9.8, the β_{Sr} values would have to change from very high values ($\geq$ 2) in the Western Zone to low values (0.6 to 0.8) in the Eastern Zone. On the other hand, for values of $\beta_{Sr} > 1$ this might also be accomplished with a smaller variation in β_{Sr}, if the R-value decreased from > 10 in the Western Zone to values of 1.2 or lower in the Eastern Zone.

It is, of course, unrealistic to propose a single crustal end-member all the way across the NGB from California to Utah; no one in the literature favors such a model and there is nothing whatsoever to recommend it. Therefore, AFC models are really not required to explain the data

shown in Figure 9.9, because we are almost certainly going to require major compositional variations in the crustal end-members (and probably also in the mantle end-members, as well). The only reason an AFC trajectory would be required by the data would be if a linear extrapolation did not pass through a plausible country-rock end-member. However, given the paucity of data on possible country-rock end-members (even those available in outcrop) and given the inaccessibility of much of the lower crust, there is simply not sufficient reason to rule out simple mixing processes in the evolution of the NGB magmas. In fact, although at first glance it may appear contradictory, it is very important to remember that if one is able to sample the latest-stage differentiates in any igneous rock suite, the isotopic and trace-element differences between simple mixing processes and AFC processes are always going to be most profound at the shallowest levels in the crust where the R-values are very large (> 10); these effects will always be less apparent in the earlier-stage differentiates or in the deeper, hotter parts of the crust where the R-values are very low (Taylor, 1980). Because the latter region is clearly a very important one in the genesis of the NGB magmas, it is going to be very difficult to distinguish between the simple mixing and AFC mechanisms in the NGB.

As Taylor (1980) has shown, we can certainly rule out shallow assimilation effects in the California batholiths, and the same statement probably also applies to most of the NGB granites, as long as samples are taken well away from the margins of the plutons. For example, Shieh and Taylor (1969) demonstrated that, except within 200-400 m of the marginal contacts, the $\delta^{18}O$ values of the granodiorite plutons of the Santa Rosa Range in northwestern Nevada are not affected by assimilation or exchange

with the local country rocks. Summing up, at this stage of our knowledge of the evolution of NGB granites, there really is very little reason to call upon AFC processes, both because large variations in the country-rock end-members are required, and because the actual processes at depth will in any case closely mimic simple mixing.

9.4.5 $\delta^{18}O$ and Major-Element Correlations

The major-element geochemical data found in Lee (1984) and Farmer and DePaolo (1983) can be combined with our $\delta^{18}O$ data and the $\delta^{18}O$ data of Lee et al. (1981) to further constrain possible source regions for NGB plutons, especially when viewed within the geographic framework of $\delta^{18}O$ zones established for the NGB. The data from the NGB are particularly useful because, as explained in the previous discussions of the geochemistry of plutons in southern Arizona (Chapter 5) and southern California (Chapters 6 and 7), most of these southern Cordilleran plutons occur in geographic regions comparable to the Eastern Zone as defined for the NGB. Thus, outside of the PRB and possibly the southernmost SNB, only the NGB provides such a diversity of $\delta^{18}O$ zones with which to compare major-element trends. Another minor exception to this rule is found along the westernmost edge of the Central and Eastern Transverse Ranges, where there are a couple of isolated occurrences of plutons with $\delta^{18}O > +10.0$; however, the isotopic patterns in these regions have been strongly disturbed by Cenozoic tectonic events.

It is difficult to subdivide most of the Central Zone plutons in the southwestern United States into the two subzones "V" and "S", as was done above for the NGB. Generally, extremely high-^{18}O, high-$^{87}Sr/^{86}Sr$ plutons characteristic of the NGB S-type subzone have not been recognized farther south in Arizona and southern California (this is clarified in Chapter

10, where we synthesize data for the entire southwestern United States). Therefore, the NGB offers an exciting arena for comparing major-element geochemistry with $\delta^{18}O$ because there is such a large diversity of source-regions and these are spread out in such a systematic geographic fashion, as shown by the existence of all three of our major $\delta^{18}O$ zones (and also including the two subzones of the Central Zone). If major-element geochemistry is going to be at all useful as a fundamental discriminator in plutonic source regions, the NGB plutons should so indicate!

Figures 9.11, 9.12, and 9.13 show the trends and features of several major-element geochemical parameters, namely, K_2O versus Na_2O, SiO_2 versus both total alkalies and CaO (Peacock diagrams), and FeO versus Fe_2O_3. We have shown on each diagram the data-point envelopes for the four-fold $\delta^{18}O$ zonation (Western Zone, V-type and S-type subzones, and Eastern Zone). All zones show a fairly wide range in SiO_2 (Figure 9.12), with the Eastern Zone exhibiting the largest variation, from approximately 58 to 77 weight percent SiO_2. Values range from 61 to 73 percent SiO_2 in the Western Zone, and from 63.5 to 76-78 percent SiO_2 in the two Central Zone subgroups. Because of the wide variations within each group, it is clear that no one $\delta^{18}O$ zonal group can be characterized as either predominantly low- or high-SiO_2. This is consistent with our previous assertions for areas farther to the south (in the PRB and in the areas discussed in Chapters 5 through 8) in which the $\delta^{18}O$ values of the plutons are very uniform within certain specific geographic regions, whereas the SiO_2 contents of the corresponding groups of plutons vary widely, typically from about 60 to 75 percent SiO_2.

Figure 9.11 Plots of K_2O (wt.%) versus Na_2O (wt.%) for Mesozoic and Cenozoic NGB granitic plutons: (1) west of the $^{87}Sr/^{86}Sr$ step, and (2) east of the $^{87}Sr/^{86}Sr$ step; based on data given in Table 1.2 (derived from Lee, 1984) and Farmer and DePaolo (1983). The data-points are subdivided into envelopes according to geographic $\delta^{18}O$ zones discussed in Section 9.4.2 (see Figure 9.6): (1) Western Zone (WZ) - open squares; (2) Central V-type Subzone (CZ-V) - solid squares; (3) Central S-type Subzone (CZ-S) - solid squares; and (4) Eastern Zone (EZ) - open squares.

Figure 9.12 Plots of SiO_2 (wt.%) versus Na_2O+K_2O and CaO (wt.%) (Peacock Diagram; see Peacock, 1931) for the NGB granitic plutons to the west and east of the $^{87}Sr/^{86}Sr$ step; based on data given in Table 1.2 (derived from Lee, 1984; and Farmer and DePaolo, 1983). The data-points are subdivided into envelopes according to the four $\delta^{18}O$ zones discussed above, and have the same symbols for data, except in the case of Na_2O+K_2O, for which open and solid diamonds are used.

Figure 9.13 Plots of FeO (wt.%) versus Fe_2O_3 (wt.%) for the NGB granitic plutons west and east of the $^{87}Sr/^{86}Sr$ step; based on data given in Table 1.2 (derived from Lee, 1984; and Farmer and DePaolo, 1984). The data-points are subdivided into envelopes according to $\delta^{18}O$ zones with the same patterns and symbols used in Figure 9.11. Shown for comparison are the generalized data-envelopes for SE Australian I- and S-type plutons, based on the data of Hine et al. (1978).

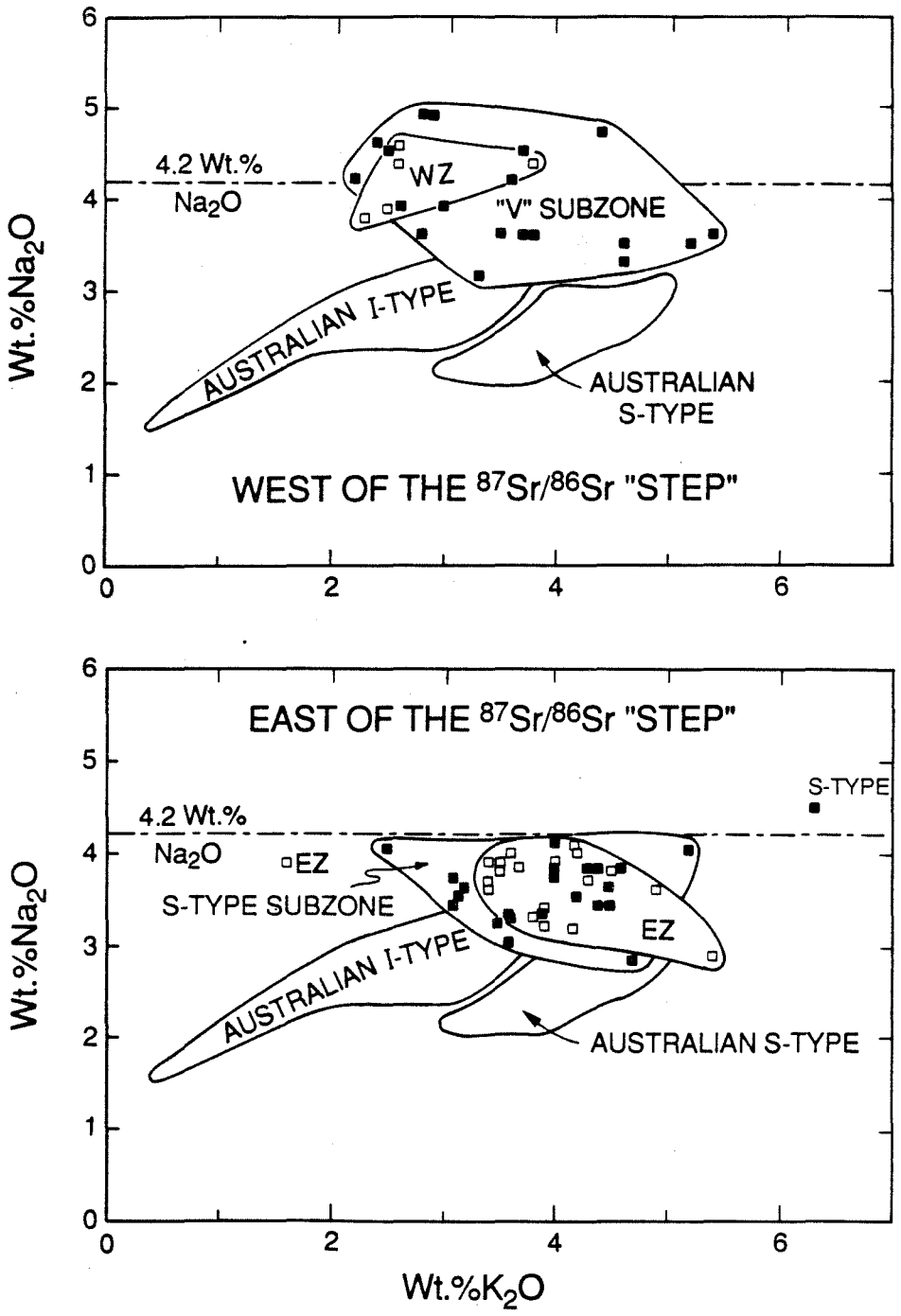
WEST OF THE $^{87}Sr/^{86}Sr$ "STEP"
4.2 Wt.% Na_2O
WZ
"V" SUBZONE
AUSTRALIAN I-TYPE
AUSTRALIAN S-TYPE
EAST OF THE $^{87}Sr/^{86}Sr$ "STEP"
S-TYPE
EZ
S-TYPE SUBZONE
Wt.%Na_2O
Wt.%K_2O

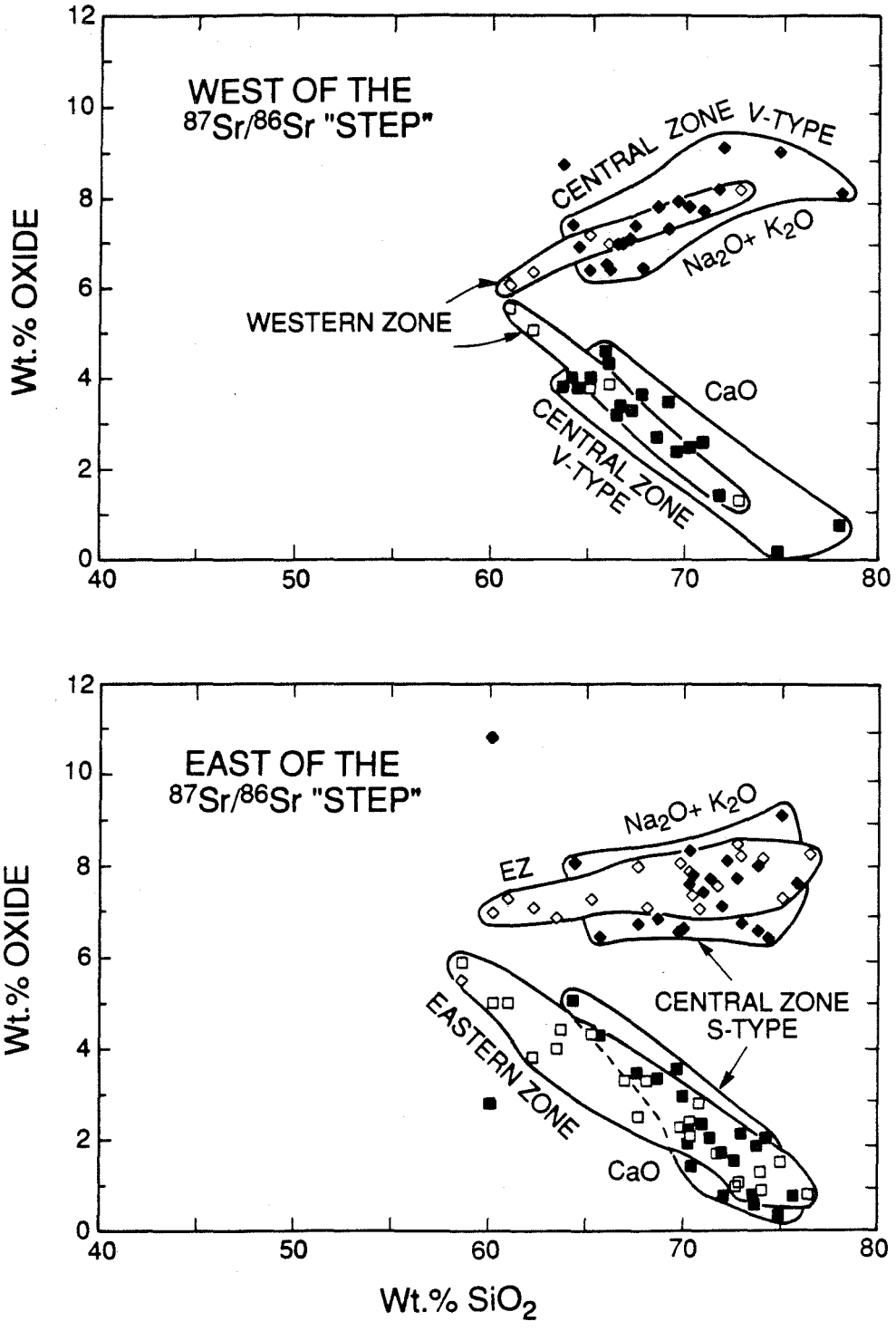
WEST OF THE
87Sr/86Sr "STEP"
CENTRAL ZONE V-TYPE
Na2O+ K2O
WESTERN ZONE
CaO
CENTRAL ZONE V-TYPE
EAST OF THE
87Sr/86Sr "STEP"
Na2O+ K2O
EZ
CENTRAL ZONE S-TYPE
EASTERN ZONE
CaO
Wt.% OXIDE
Wt.% SiO2
0
2
4
6
8
10
12
40
50
60
70
80

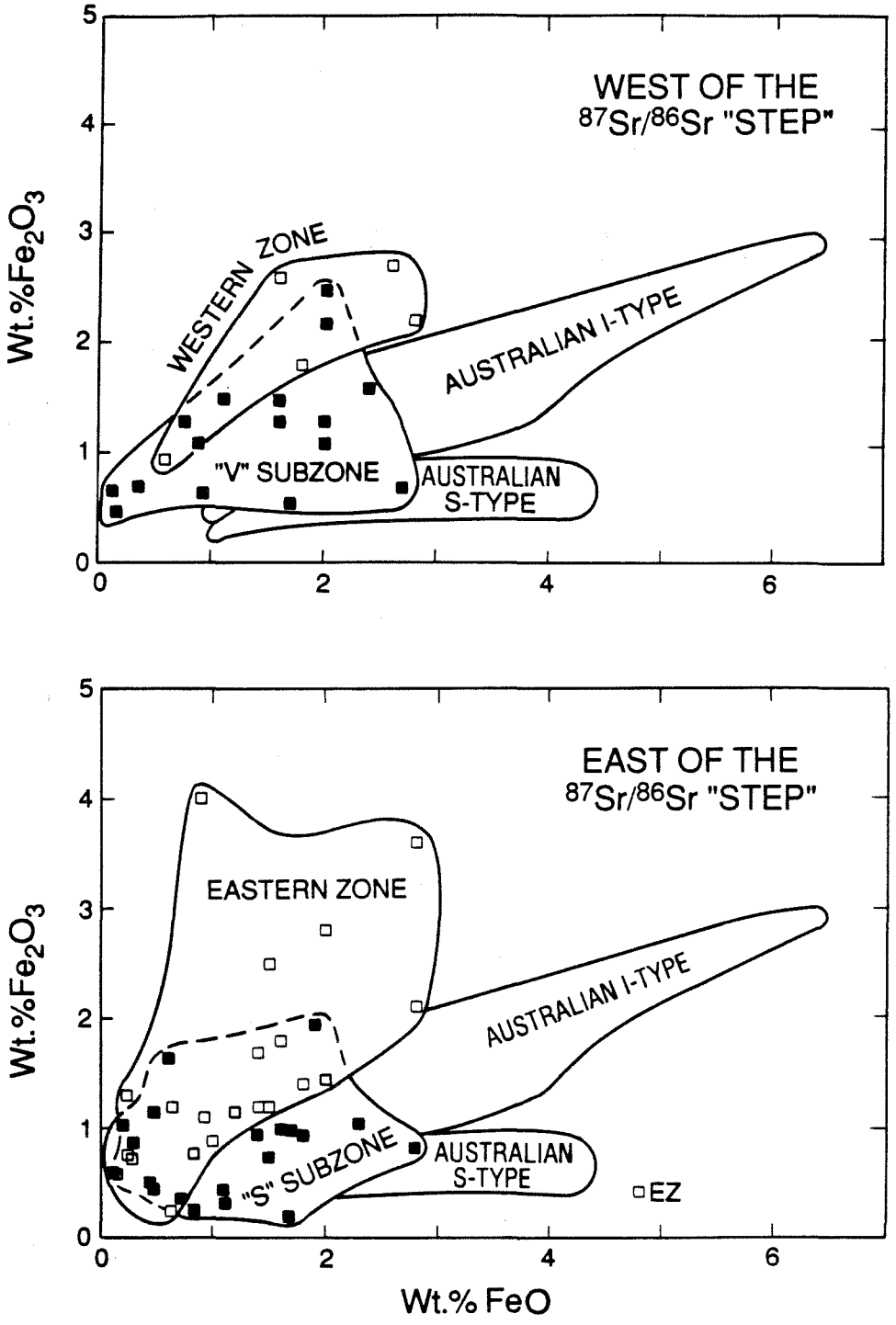
WEST OF THE
87Sr/86Sr "STEP"
WESTERN ZONE
AUSTRALIAN I-TYPE
"V" SUBZONE
AUSTRALIAN
S-TYPE
EAST OF THE
87Sr/86Sr "STEP"
EASTERN ZONE
AUSTRALIAN I-TYPE
"S" SUBZONE
AUSTRALIAN
S-TYPE
EZ
Wt.%Fe2O3
Wt.% FeO
0
1
2
3
4
5
6

With the exception of one extremely K-rich sample referred to below, all samples collected east of the $^{87}Sr/^{86}Sr$ "step" (i.e., all S-type subzone and Eastern Zone samples) have Na_2O less than 4.2 percent (Figure 9.11). Thus, even though there is considerable overlap in Na_2O contents, the average Na_2O contents of both the Western Zone and the V-type subzone are distinctly higher than either of the more easterly zones. Combining these observations with the K_2O systematics discussed below, this means that in a general way the plutons exhibit higher K/Na ratios with increasing distance from the Pacific Coast. We note that these observations in the NGB contrast with the situation in southeastern Australia, where Hine et al. (1978) showed that I- and S-type plutons had major differences in K_2O and Na_2O, with little or no overlap.

Except for the Western Low-^{18}O Zone, all of the zonal groups exhibit a wide variation in K_2O, from about 2 percent to between 5 and 6 weight percent (Figure 9.11). Plutons in the Western Zone exhibit a much smaller variation, between about 2.2 and 4.0 percent K_2O, with most samples less than 3.0; also, the V-type subzone completely overlaps the Western Zone, and if we exclude a single anomalously low-K_2O Eastern Zone sample, it extends to lower K_2O values than either the Eastern Zone or the S-type subzone. We note that the two easternmost zones overlap one another in K_2O, and they also overlap the high end of K_2O found within the Western Zone. In keeping with their relatively wide variation in SiO_2 (Figure 9.12), the Eastern Zone plutons also show a larger variation in K_2O than all of the other zones put together (Figure 9.11). However, this wide range is largely attributable to the "anomalous" sample referred to above (K_2O ~ 1.6%); the other Eastern Zone plutons have more uniform K_2O (3.3 to 5.4%). Thus the general postulate of eastwardly increasing K_2O by

Moore (1959) has some validity, although this only shows up with respect to the average K_2O contents of the plutons across the 3 major $^{18}O/^{16}O$ zones. Obviously, neither the K_2O contents nor any of the other major-element parameters can be used to discriminate between these geographic zones in anywhere near as precise a way as can the various isotopic signatures.

A strongly alkalic sample collected within the S-type subzone (GR125, Lee et al., 1981; Lee, 1984) has K_2O = 6.3 and Na_2O = 4.5. This sample occupies a clearly anomalous position on the Peacock diagrams of Figure 9.12, and it is therefore not included in Figure 9.11 or in any of the following discussions of the origin of the general NGB pluton population.

A consequence of the above relationships is that the alkali-lime index of NGB plutons (Figure 9.12) switches from calc-alkaline (with an index of about 60 percent SiO_2; see Peacock, 1931) to alkali-calcic (with an index at about 56 percent SiO_2) as one moves eastward from the Western Zone into the Eastern Zone. The pluton population west of the $^{87}Sr/^{86}Sr$ "step" plots well into the calc-alkaline field (Figure 9.12). We have also observed this transition from calc-alkaline to alkali-calcic in the plutons of the Central and Eastern Transverse Ranges in southern California, also at about the same general position with respect to eastwardly decreasing $\delta^{18}O$ (see Chapters 6 and 7). In addition, we also note that plutons from southern Arizona have alkali-calcic affinity, in keeping with their location well into the Precambrian craton. In the Transverse Ranges, this geochemical transition marks the first eastward appearance of mapped Precambrian basement of cratonal affinity (ancient crust); thus the change in alkali-lime index is probably an important

indicator of the introduction of a new source-region as magmatism swept eastward in the Cordillera (ancient sialic crust, > 1.4-1.5 Ga? See the Chapter 8 summary). This feature shows up better in the NGB because it is a much wider region and thus has been relatively less affected during late Cenozoic time by structural complexities such as strike-slip faulting and major overthrusting. Thus, the transition in the NGB is very well delineated as compared with the SECA and PRB terranes discussed above. We make note of the fact that this transition would have been very difficult, or impossible, to discern were it not for our ability to use $\delta^{18}O$ to divide the NGB plutons into geographic zones (Figure 9.6).

Figures 9.13 and 9.14 show variations of FeO with respect to Fe_2O_3, and $\delta^{18}O$ with respect to the mole ratio Fe^{3+}/total Fe. The data for the NGB plutons are compared with the typical fields for the southeastern Australia I- and S-type plutons. Hine et al. (1978) note that S-type plutons in southeastern Australia have a fairly wide range in FeO (1.0 to 4.5 weight percent), but a narrow range of Fe_2O_3 values (< 1.0 percent), whereas I-type plutons contain more total iron and also higher Fe_2O_3 (Figure 9.13).

The NGB plutons show a much wider range of Fe_2O_3, and a much smaller range of FeO than the southeastern Australian plutons, although there is considerable overlap among the Australian samples and all of the NGB zones and subzones on Figure 9.13. Nevertheless, assuming that the major-element analytical data for the Australian NGB samples do not contain any systematic errors as a result of the differing analytical procedures utilized, we may make the following comparisons among the various sets of data: (1) For samples east of the $^{87}Sr/^{86}Sr$ step, the Eastern Zone samples are generally somewhat more oxidized than S-type subzone samples;

Figure 9.14 Plots of whole-rock $\delta^{18}O$ versus the mole ratio Fe^{3+}/total Fe for Mesozoic and Cenozoic NGB granitic plutons: (1) west of the $^{87}Sr/^{86}Sr$ step, and (2) east of the $^{87}Sr/^{86}Sr$ step; based on the data given in Table 1.2 (derived from Lee, 1984) and Table 9.1. The data are subdivided into envelopes based on the geographic $\delta^{18}O$ zones discussed in Section 9.2.4 (also see Figure 9.6): (1) WZ - open squares; (2) CZ-V - solid squares; (3) CZ-S - solid squares; and (4) EZ - open squares. Data from SE Australian S-type plutons are shown for comparison (see O'Neil and Chappell, 1977; O'Neil et al., 1977; Chappell, 1984; McCullough and Chappell, 1982; and Shaw and Flood, 1981). The data shown in this figure have been screened so that samples with total iron (as FeO) < 1.5 wt.% have been eliminated. This procedure eliminates samples whose low total iron contents could result in analytical error.

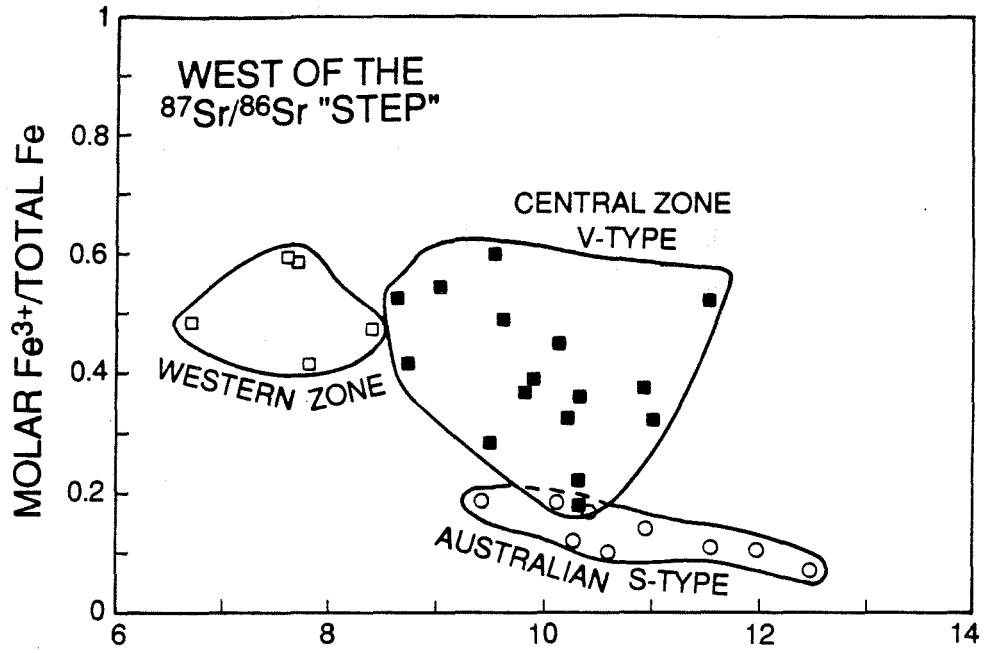
WEST OF THE
87Sr/86Sr "STEP"
CENTRAL ZONE
V-TYPE
WESTERN ZONE
AUSTRALIAN S-TYPE
MOLAR Fe3+/TOTAL Fe
1
0.8
0.6
0.4
0.2
0
6
8
10
12
14

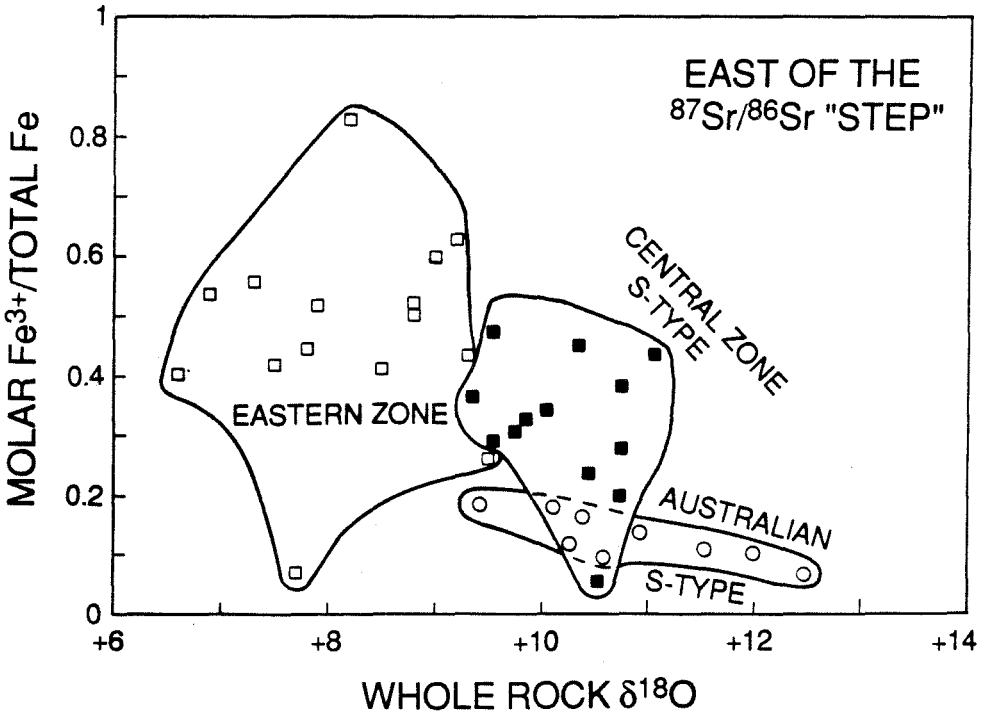
EAST OF THE
87Sr/86Sr "STEP"
CENTRAL ZONE
S-TYPE
EASTERN ZONE
AUSTRALIAN
S-TYPE
MOLAR Fe3+/TOTAL Fe
1
0.8
0.6
0.4
0.2
0
+6
+8
+10
+12
+14
WHOLE ROCK δ18O

(2) West of the $^{87}Sr/^{86}Sr$ step, the Western Zone samples are somewhat more oxidized than the V-type subzone samples; (3) The V-type subzone is, on the average, slightly more oxidized than the S-type subzone; (4) Thus, just from the FeO and Fe_2O_3 analyses and without even looking at the $\delta^{18}O$ data, we might broadly catagorize the plutons in the Western Zone and Eastern Zone as having certain "I-type" tendencies, while the more reduced plutons in both of the Central subzones tend more toward "S-type" characteristics (using the Australian data as a model). We understand that the actual Fe^{3+}/total Fe ratios in the NGB Central Zone are not identical to the southeastern Australian S-type plutons, which are typically restricted to values < 0.2 (Figure 9.13); however, we view this more as a function of the possibility that metasediments (of either volcanic or continental derivation) in the Central Zone source regions were more variable in their reduced carbon content, rather than as negative evidence for a sedimentary protolith for the Central Zone plutons (also see White, et al., 1986).

When the $\delta^{18}O$ data are plotted against the Fe^{3+}/total Fe data (Figure 9.14), it is difficult to observe any systematic correlation. However, there is some suggestion that the Central Zone "S-type" plutons (and the Central Zone "V-type" plutons, as well) attain lower Fe^{3+}/total Fe ratios than do the Western Zone and Eastern Zone plutons. The exception to this is the single Eastern Zone sample that plots with Fe^{3+}/total Fe less than 0.1, however we consider this sample to be anomalously low in Fe^{3+}. The Fe^{3+}/total Fe - $\delta^{18}O$ patterns for plutons in different oxygen isotope zones in the NGB may be analogous to the Australian S-type pattern (O'Neil and Chappell, 1977; McCulloch and Chappell, 1982; Chappell, 1984), in which the $\delta^{18}O$ values of the plutons

increase as the Fe^{3+}/total Fe contents decrease (Figure 9.14). In the NGB data set, one can also discern what appears to be a similar trend toward more reduced conditions for the higher-^{18}O samples within the overall data set (Figure 9.14). These patterns become apparent after screening out samples where total iron (as FeO) is less than 1.5 weight percent. This data screen helps eliminate errors in Fe^{3+}/total Fe due to analytical difficulties with low-Fe samples.

Although we obviously cannot assume simple two-component mixing (see Chapter 8, and discussions below), the data in Figure 9.14 suggest that the NGB magmas may have been hybrids in which varying proportions of relatively more reduced, higher-$\delta^{18}O$ (sedimentary?) material mixed with low-^{18}O, moderately oxidized material in the main part of the Central Zone, or with low-^{18}O, strongly oxidized material in the vicinity of the Central Zone-Eastern Zone boundary. On the other hand, some of these Fe-oxidation phenomena may be a result of post-magmatic hydrothermal activity, and further work is required to sort this out. In comparison with the southeastern Australian S-type plutons, much more highly "reducing" sediments must have been involved in the source regions of those magmas as compared with the NGB magmas (e.g., graphite-rich pelites?).

If we consider a plot of $\delta^{18}O$ versus molar alumina ratio, $Al_2O_3/(Na_2O+K_2O+CaO)$, for NGB plutons (Figure 9.15), we see that the Western Zone and Central V-type subzone plutons are metaluminous throughout their entire range in $\delta^{18}O$. The data-point envelopes for these two isotopic zones are constrained within relatively narrow boundary lines (shown as straight, dashed lines on Figure 9.15). The lower boundary is drawn across Figure 9.15 at a constant ratio of 0.85 for the entire $\delta^{18}O$ range (+6.7 to +12.6), whereas the upper boundary slopes gently from a

Figure 9.15 Plots of whole-rock $\delta^{18}O$ versus the mole ratio Al_2O_3/Na_2O+K_2O+CaO for Mesozoic and Cenozoic NGB plutons: (1) west of the $^{87}Sr/^{86}Sr$ step, and (2) east of the $^{87}Sr/^{86}Sr$ step; based on data given in Tables 1.2 and 9.1. The data points are subdivided into envelopes according to which $\delta^{18}O$ zone they belong (see Section 9.4.2; also see Figure 9.6): (1) WZ - open squares; (2) CZ-V - solid squares; (3) CZ-S - solid squares; and (4) EZ - open squares. Shown for comparison are data from SE Australian S-type plutons, based on work done by O'Neil and Chappell (1977); O'Neil et al. (1977); Chappell (1984); McCullough and Chappell (1982); and Shaw and Flood (1981). Dashed lines indicate the boundaries for the WZ-CVS trend.

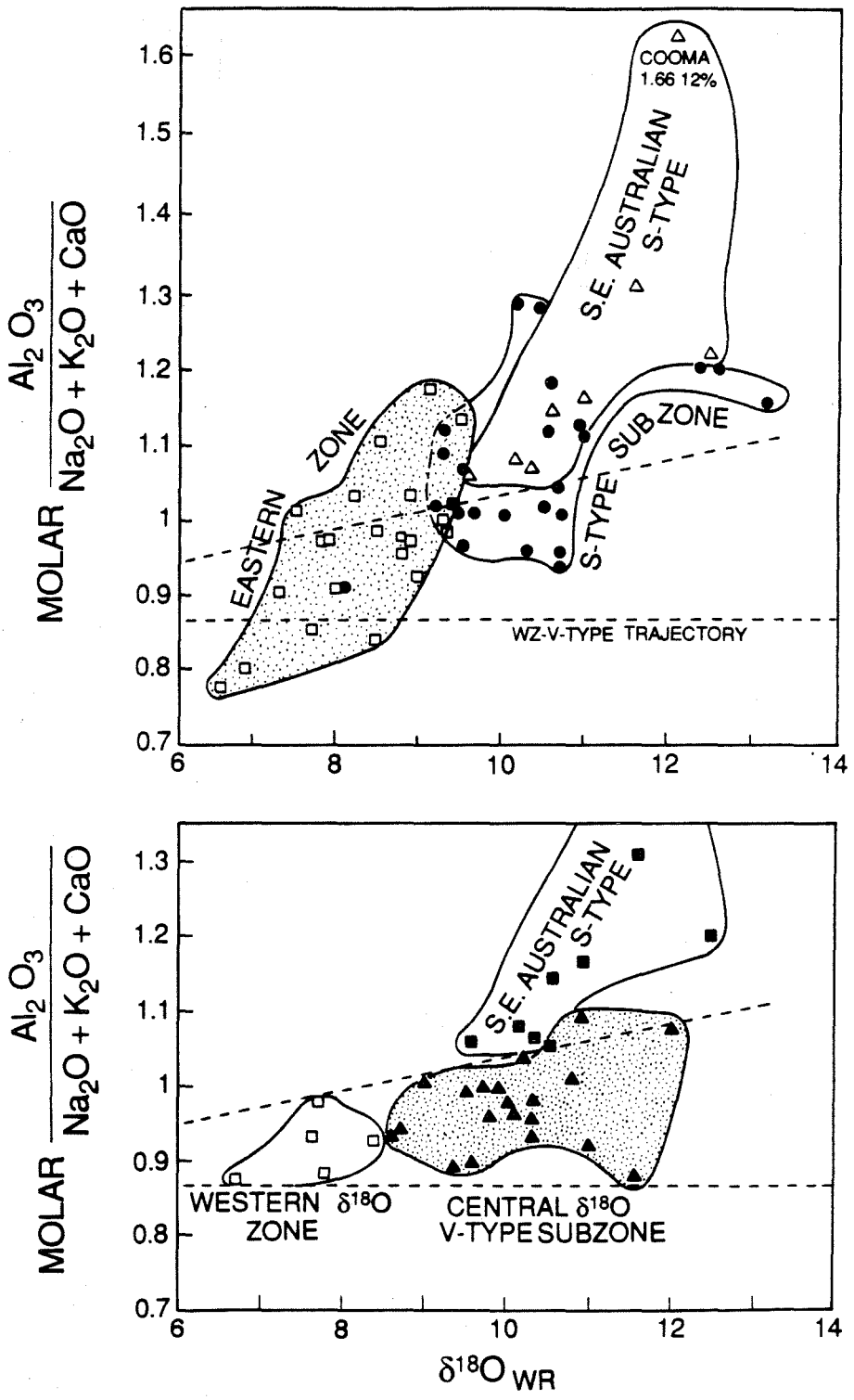
MOLAR Al2O3 / (Na2O + K2O + CaO)
COOMA
1.66 12%
S.E. AUSTRALIAN S-TYPE
S-TYPE SUB ZONE
EASTERN ZONE
WZ-V-TYPE TRAJECTORY
WESTERN δ18O ZONE
CENTRAL δ18O V-TYPE SUBZONE
δ18O WR

molar alumina ratio of about 1.07 for the highest-^{18}O rocks to a value of about 0.95 for the lowest-^{18}O rocks. Included on Figure 9.15 are data from the southeastern Australia S-type plutons that are postulated to have originated by melting of pelitic metasediments. Based on the relative positions of the NGB and Australian data-point envelopes on Figure 9.15, even though they have similar $^{18}O/^{16}O$ ratios, it would be difficult or impossible to derive V-type NGB plutons from the same type of source that melted to form the Australian S-type plutons. However, the plutons from both the NGB Western Zone and the V-type subzone could have a source with similar major-element chemistry (basaltic to andesitic?), but with strikingly differing $\delta^{18}O$ compositions.

The narrowly constrained plots of molar alumina ratio versus $\delta^{18}O$ on Figure 9.15 represent a crucial observation, because the high-^{18}O V-type subzone plutons obviously must have come from high-^{18}O sources, and yet the above discussion apparently eliminates pelitic metasediments from consideration as a source-type. The only alternative might be that very small amounts of pelites were involved, but that these had such high $\delta^{18}O$ contents that only small amounts were required to be mixed with another type of source, sufficient to produce magma with a $\delta^{18}O$ between +10 and +12. This is probably not a realistic option in general, because where pelitic sources are unequivocally demonstrated (e.g., Cooma in southeastern Australia, Chappell, 1984, see Figure 9.15), the $\delta^{18}O$ values of the plutons are usually no higher than about +13 to +14. Rather, we believe, the source region type for the high-^{18}O V-type subzone is more likely a mixture of volcanogenic sediments shed from an island-arc type terrane interbedded with a pile of hydrothermally altered volcanic rocks. Such a volcanogenic protolith would also explain the similarity in molar alumina

ratio for the Western Zone and V-type subzone plutons, because the Western Zone magmas likely represent melting of a "pristine" mafic igneous rock parent in an island-arc environment where the source-protoliths did not previously interact with large amounts of surface waters at low temperatures.

In contrast to the limited range in molar alumina ratio for the V-type subzone plutons, the S-type subzone and Eastern Zone plutons exhibit a much wider variation (Figure 9.15). Eastern Zone plutons have molar alumina ratios ranging from 0.78 on the low-^{18}O end to as high as 1.15 in plutons with $\delta^{18}O$ values of about +9.0. Central Zone S-type plutons range from 0.95 to as high as 1.29. Plutons with $\delta^{18}O$ between +9.0 and +11.0 span the entire range from peraluminous to metaluminous, but those with $\delta^{18}O$ higher than +11.0 are all definitely peraluminous, with ratios between 1.15 and 1.20. Taken as a group, the Eastern Zone and S-type subzone data-point envelopes distinctly cut across the dashed-line boundaries that encompass the Western Zone and V-type subzone plutons.

The overlap of Australian and NGB S-type plutons on Figure 9.15 indicates that high-^{18}O metasediments of generally similar nature could be responsible for both suites. However, based on their Fe^{3+}/total Fe ratios (Figures 9.13 and 9.14) the NGB magmas apparently did not form under oxygen fugacity conditions similar to the Australian magmas. We do not view this as an impediment to labeling the NGB plutons as "S-type" because they simply may have formed from metasediments with lesser amounts of reduced carbon, other things being equal (we also might raise the question of whether there might be systematic errors involved in comparing the two sets of analytical data for Fe_2O_3 and FeO).

The Eastern Zone NGB plutons are generally metaluminous, although they have a large range in alumina ratio (0.78 to 1.15), much larger than the values observed in either the Western Zone or the V-type subzone plutons. Some of the Eastern Zone plutons have relatively high molar alumina ratios, but their low $\delta^{18}O$ values (+6.7 to +9.0) require that if any pelitic rocks were involved in their source regions, such pelitic materials must have been either: (1) older, metamorphosed basement rocks whose $\delta^{18}O$ had evolved to lower values, perhaps because of interaction with deeper crustal materials over time (see Chapter 4, and Longstaffe and Schwarcz, 1977), or (2) pelites that were altered as a result of interactions with meteoric-hydrothermal waters originally derived from the surface (Wickham and Taylor, 1985, 1987; Bickle et al., 1989).

9.5 Summary

The NGB area, along with its western boundary consisting of the Sierra Nevada Batholith, offers the opportunity to test for lateral changes in the deep continental crust by observing geographic variations in major-element, Nd, Sr, and O isotopes in plutons that have formed from, or whose parent magmas have interacted with, such crust. A series of such plutons of Mesozoic to late Cenozoic age crop out across a broad swath of territory from the SNB inland to the Wasatch Front of Utah. This region does not appear to have been modified in Cenozoic time by any major strike-slip faults (although extensional tectonics have been very important). The NGB terrane is known to be underlain by at least three major packages of pre-Jurassic country rocks: (1) western eugeosynclinal assemblages (accreted terranes); (2) central miogeosynclinal assemblages; and (3) an eastern terrane composed of Precambrian cratonal crust. The absence of large-scale late Cenozoic strike-slip faulting means that we

can study the changes in chemistry of the plutons along transects perpendicular to the Pacific Coast, without having to resort to the kinds of complex palinspastic reconstructions that are necessary in southern California. However, we do have to consider a major widening of the entire NGB area by as much as 100 to 200 percent as a result of Basin-and-Range extension.

Our study of the geochemistry and isotopic systematics of the NGB plutons suggests that a minimum of four source protoliths must be involved in the formation of plutons in the NGB. These are discussed in more detail below, but briefly, they must consist of: (1) a deep-seated mafic igneous oceanic island-arc component (Western Zone); (2) an ^{18}O-modified mafic igneous source material such as altered island-arc volcanic rocks or volcanogenic sediments (Central V-type subzone); (3) high-$\delta^{18}O$ metasedimentary rocks that are relatively aluminous (Central S-type subzone); and (4) a heterogeneous, older crystalline basement with both lower and mid-crustal characteristics depending on depth of melting and local geological relationships (Eastern Zone). We may briefly summarize the evidence for the four source protoliths as follows:

(1) Three major $\delta^{18}O$ zones are readily recognized in the plutons of the NGB, namely a Western Low-^{18}O Zone (WZ) with $\delta^{18}O$ = +6.5 to +8.5; a Central High-^{18}O Zone (CZ) with $\delta^{18}O$ = +9 to +13; and an Eastern Intermediate Zone (EZ) with $\delta^{18}O$ = +7 to +9. The WZ-CZ boundary is very sharp, and is analogous to the $\delta^{18}O$ "step" in the Peninsular Ranges Batholith (PRB). A similarly abrupt initial $^{87}Sr/^{86}Sr$ "step" (<0.708 to the west and >0.710 to the east) defined by Farmer and DePaolo (1983) lies 150-200 km east of the WZ-CZ "step" defined by the $^{18}O/^{16}O$ data, requiring that the Central High-^{18}O Zone be divided into two subzones: a west-

ern region with "V-type" plutons, corresponding to the eastern half of the PRB (but much wider because of Cenozoic extension), and an eastern region with "S-type" plutons, which has no major counterpart in southern California, and which is associated with intense metamorphism of a thick section of late Precambrian sedimentary rocks.

(2) Simple mixing relationships involving a minimum of four source-region end-members can account for most of the major-element and isotopic variations observed in the NGB plutons. The suggested end-members are: a) an oceanic island-arc (OIA) type ($\delta^{18}O$ = +6 to +8; ε_{Nd} = 0 to +6; initial $^{87}Sr/^{86}Sr$ = 0.702 to 0.704); b) sedimentary or altered volcanic (SAV) assemblage, primarily derived from OIA-type materials but likely to contain some continental material near its eastern limits ($\delta^{18}O$ = +10 to +13.5; ε_{Nd} = +2 to -6; initial $^{87}Sr/^{86}Sr$ = 0.705 to 0.707); c) miogeoclinal sediments, in large part of late Precambrian (Proterozoic) age, and derived primarily from the craton ($\delta^{18}O$ = +9 to +13; ε_{Nd} = -12 to -20; initial $^{87}Sr/^{86}Sr$ > 0.710); and d) ancient sialic craton comprised of both lower continental crust (LCC) and middle continental crust (MCC) ($\delta^{18}O$ = +7 to +9; ε_{Nd} = -2 to -20; initial $^{87}Sr/^{86}Sr$ > 0.705).

(3) In terms of major element chemistry, OIA has a molar alumina ratio between 0.85 and 0.95, Fe^{3+}/total Fe = 0.35 to 0.55, and is relatively sodium enriched (>4.2 wt.% Na_2O). SAV is similar, except that Fe^{3+}/total Fe generally tends to be less than 0.3 (similar to graywackes; Pettijohn, 1972). The miogeoclinal-sediment source has relatively high alumina ratios (0.95 to 1.30), is relatively low in sodium (<4.2 wt%) and would seem to have Fe^{3+}/total Fe < 0.2. The cratonal end-member is fairly heterogeneous with alumina ratio between 0.75 and 1.15 indicating it could be a mix of metagabbros, granulitic and amphibolitic gneiss,

and anorthosites in its lower portions (LCC with A1 ratios between 0.75 and 1.06; Heier and Thoresen, 1971; McGetchin and Silver, 1972), and metasediments and gneisses in middle crustal levels (MCC with ratios 0.93 to 1.15). The high-Fe^{3+} rocks in the EZ may indicate contributions from MCC sources (e.g., the Pinal Schist in southern Arizona has Fe^{3+}/total Fe between 0.57 and 0.75; Silver and Anderson, 1964).

The source-protolith end-members defined above, together with the discussions in Chapters 5 through 8, explain the broad, regional isotopic patterns that exist in the Phanerozoic plutons of the entire southwestern North American Cordillera, and make some generalizations concerning the geologic history of this area and the geographic distribution of source regions. It will be seen that the original PRB model of Taylor and Silver (1978), combined with the new systematics gleaned from the NGB, allows us to construct a plausible model for the intervening areas, where strike-slip and horizontal tectonics have disrupted the fundamental regional patterns.

CHAPTER 10. REGIONAL SYNTHESIS OF OXYGEN, STRONTIUM, NEODYMIUM, AND LEAD ISOTOPE GEOCHEMISTRY

10.1 General Statement

This chapter summarizes the results of this thesis, and it also incorporates all of our new oxygen isotope data from Arizona, southern California, and Nevada in a regional synthesis with previously existing data obtained on plutons throughout the Mesozoic and early Tertiary batholithic terranes of the southwestern United States. The latter are compiled from various literature sources, most of which represent work done in the last decade. This regional synthesis represents a new data base never before evaluated in its entirety, and such a discussion is extremely germane to the concepts presented on a more local basis in Chapters 5 through 9. Included in this synthesis is a discussion of the correlations between the $^{18}O/^{16}O$ data and previous $^{87}Sr/^{86}Sr$, $^{144}Nd/^{143}Nd$, and Pb isotope data obtained on the granitic plutons of the Cordillera by other workers (see Chapters 8 and 9).

Figure 10.1 is a histogram showing the variation in whole-rock $\delta^{18}O$ for Mesozoic and early Cenozoic plutons in the southwestern U.S.A., taken from a combination of the present work (see Table 1, Appendix) and all available literature sources (cited in Chapters 1 and 2). Although most of the analyses plot between +7.0 and +10.0, the data cover a very wide range, almost 14 per mil. However, the spread in primary $\delta^{18}O$ for these rocks is only from about +5.5 to +13.5 per mil, because the samples with $\delta^{18}O < +5.5$ can either be <u>proven</u> to have been subjected to sub-solidus meteoric-hydrothermal alteration, or they can be readily inferred to have been so affected.

Figure 10.1 Histogram showing the range and frequency of occurrence of whole-rock $\delta^{18}O$ values in Mesozoic and Cenozoic granitic plutons from the western United States. Data are from sources discussed in Chapters 1 and 2 for samples from the Idaho Batholith, the Northern Great Basin, the Sierra Nevada Batholith, the western Mojave Desert, the Peninsular Ranges Batholith, and the Southern Basin and Range Province of southeastern California and southern Arizona. Sample localities are shown on maps found in Chapters 1, 5, 6, 7, and 9. The frequency bars on the diagram are pattern-coded according to the $^{18}O/^{16}O$ groups discussed in text (from left to right on the diagram): Hydrothermally Altered Group ($\delta^{18}O < +5.5$); Group 1 ($+5.5 \leq \delta^{18}O < +7$); Group 2 ($+7 \leq \delta^{18}O < +8.5$); Group 3 ("$^{18}O$-step", $+8.5 \leq \delta^{18}O < +9$); Group 4 ($+9 \leq \delta^{18}O < +10$); and Group 5 ($\delta^{18}O \geq +10$). Interestingly, these are more or less the same groupings Taylor (1968) assigned to granitic rocks in his initial worldwide reconnaissance study, which was of course based on a far smaller data-set.

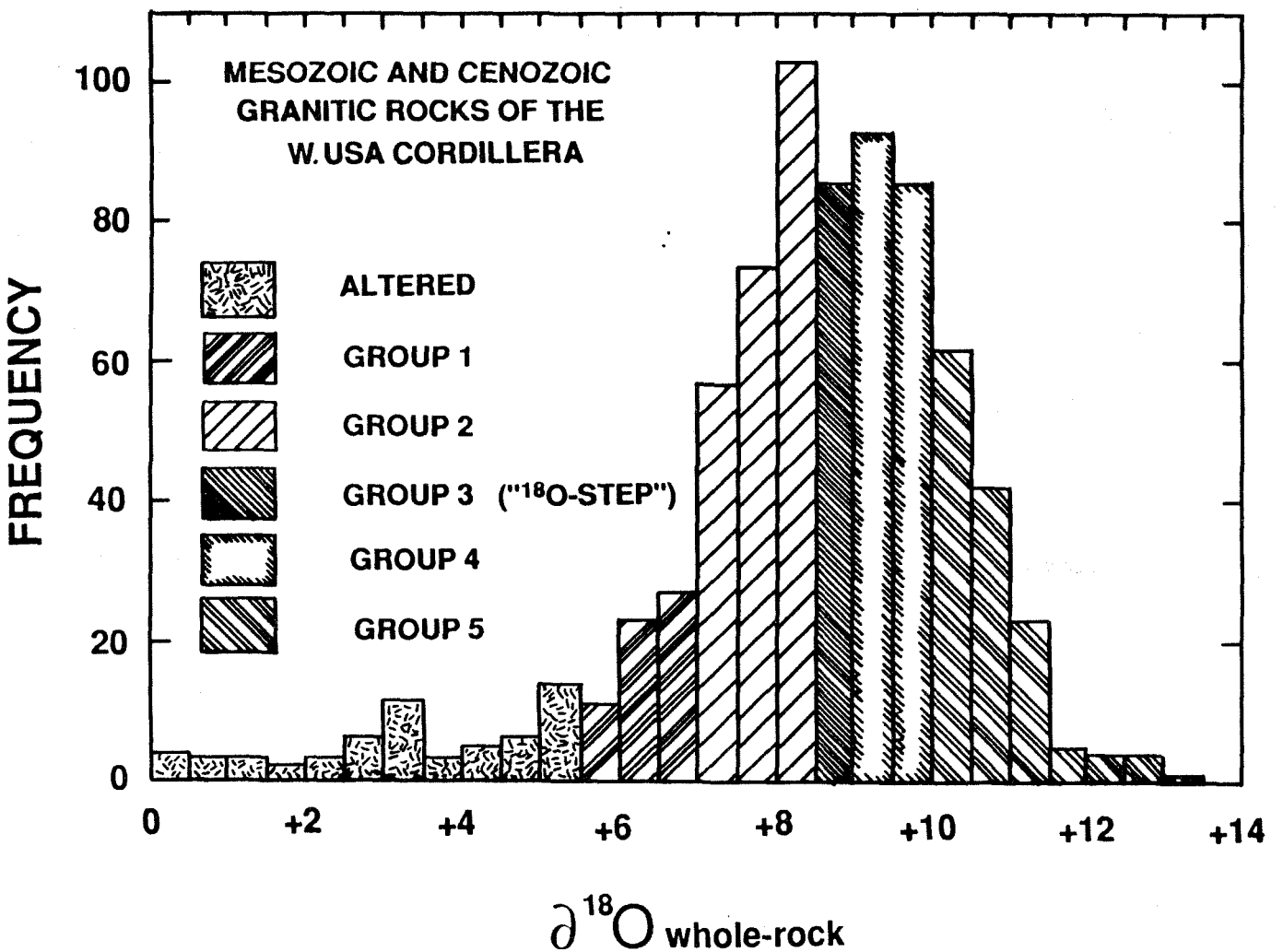
MESOZOIC AND CENOZOIC
GRANITIC ROCKS OF THE
W. USA CORDILLERA
ALTERED
GROUP 1
GROUP 2
GROUP 3 ("18O-STEP")
GROUP 4
GROUP 5
FREQUENCY
100
80
60
40
20
0
0
+2
+4
+6
+8
+10
+12
+14
∂ 18O whole-rock

The 8 per mil primary $^{18}O/^{16}O$ range far overshadows changes expected during either differentiation or partial fusion; such processes are expected to produce effects < 0.5 per mil, except possibly in rare cases involving extreme degrees of fractional crystallization (Taylor and Epstein, 1962b; Taylor, 1968; Kyser et al., 1982; Garlick, 1966; Matsuhisa et al., 1973; Taylor and Sheppard, 1986).

Because only very limited $^{18}O/^{16}O$ changes can occur during closed-system magmatic differentiation, the 8 per mil spread in primary whole-rock $\delta^{18}O$ values in the Mesozoic plutons must indicate a combination of any one or several of the following: (1) simple partial melting of diverse source $^{18}O/^{16}O$ compositions, (2) mixing of deep-seated, mantle-derived magmas with partial melts from one or more relatively high-^{18}O crustal sources; (3) assimilation of country rocks by magmas, either during upward rise or at the site of final emplacement; (4) exchange between melts (or solid plutons) and country rocks, during or after emplacement; and (5) hybridization (mixing) between melts formed during separate fusion events from crustal sources having diverse $^{18}O/^{16}O$ compositions (Taylor, 1968, 1977, 1978, 1980, 1986; Solomon and Taylor, 1981; Taylor and Silver, 1978; Taylor and Sheppard, 1986).

Although this thesis concentrates on $^{18}O/^{16}O$ variations in the granitic plutons, it is difficult to thoroughly evaluate the various factors outlined above with just this parameter alone. Mixing models involving trace elements or other isotopic tracers such as $^{207}Pb/^{204}Pb$, $(^{87}Sr/^{86}Sr)_i$, or ε_{Nd} are usually necessary to definitely distinguish between the various possibilities (Taylor, 1980, 1986; De Paolo, 1981b; Hill et al., 1986; also see Chapters 8 and 9).

10.2 Summary of $\delta^{18}O$ Variations and Possible Models for Source Regions

$^{18}O/^{16}O$ variations in plutons are directly related to $\delta^{18}O$ variations in their source regions, but they are also indirectly related to the factors that focus magmatism at various geographic localities and at various levels in the Earth's crust and mantle. Such parameters would be the availability of H_2O, the bulk chemical composition of the source, and the local geothermal gradient operating on the source. On a large scale, the crust and upper mantle appear to be "stratified" with respect to $\delta^{18}O$ compositions (Longstaffe and Schwarcz, 1977); thus factors that affect the depth of magma generation should also affect the $\delta^{18}O$ characteristics of plutons.

In general, magmas generated at depths greater than 25 to 30 km in the crust (or mantle) are thought to be relatively "dry"; hence they have compositions characteristic of high-temperature (>900° to 1100°C) melts (Presnall and Bateman, 1973). Such magmas tend to rise to high levels in the crust where they are emplaced as epizonal to transitional-mesozonal intrusives (Burnham, 1979; Strong, 1980; Buddington, 1959; Hamilton, 1981). Calc-alkaline melts formed at intermediate crustal levels (between 15 and 30 km) may have more H_2O available to them; therefore, such materials become molten at a lower temperature, and the magmas will be relatively more water-rich than melts derived from deeper levels. As a consequence of their higher H_2O contents, these melts can solidify isothermally if the pressure is reduced and P_{H_2O} is lowered; therefore, such magmas cannot rise to shallow levels in the crust (less than 10 to 15 km; e.g., Kistler, et al., 1981; Miller et al., 1982), because they begin to exsolve H_2O and crystallize at a deeper level than do drier melts

(Hyndman, 1979; Burnham, 1981; Tuttle and Bowen, 1958). It follows that these two broad types of melting scenarios, in addition to lateral regional variations in heat flow and in source isotopic compositions, could affect pluton $\delta^{18}O$ compositions.

To tie in this depth-related variation in the source regions of the plutons with the $^{18}O/^{16}O$ ratios of plausible protoliths, it is necessary to model the petrologic and isotopic characteristics of the continental crust and upper mantle in the western United States, based on observed geological relations. Summarizing Chapter 4, rocks characteristic of the middle continental crust (MCC) are, in general, comprised of complexly intermingled older metasediments, metavolcanics, gneisses, and granitoids associated with various proportions of migmatite. Metamorphic grades up to upper-amphibolite facies are common in these MCC rocks. Complexes in the northern part of the United States Cordillera (Idaho and Nevada) may also be associated with thick sections (8 to 10 km or more) of late Precambrian to early Paleozoic miogeoclinal sediments and metasediments (Stewart, 1980; Burchfiel and Davis, 1981a).

Lower continental crust (LCC) and subcontinental lithospheric mantle (SCL) are more difficult to characterize in the western United States because outcrop abundances of rocks thought to be representative of these great depths is very low. Models based on exposures in other localities on Earth may apply, however. As noted by Hamilton (1981) and Fyfe et al. (1979), based on observations made in crustal sections exposed in the Grenville basement of the Canadian Shield and elsewhere on Earth, the MCC becomes less hydrated downward as the transition from upper-amphibolite facies to lower granulite facies occurs. In this deeper LCC environment, metasediments that record metamorphic events typical for depths of 25 to

40 km are intercalated with igneous rocks comprised of gabbro, anorthosite, and quartz-poor granitic rocks containing pyroxene and mesoperthitic feldspar. The metasediments include refractory assemblages such as quartzite, marble, and aluminous metapelites that have been depleted of their granitic components.

Integrating these geological models with a literature search to characterize the measured $\delta^{18}O$ values of this panoply of rock types (see Table 4.1 in Chapter 4), we conclude that the potential source regions for Cordilleran plutons have, on the average, the following $\delta^{18}O$ compositions: (1) Oceanic upper mantle (MORB), +5.5 to +6.5 per mil; (2) Subducted oceanic crust, +6.0 to +7.0, with around 20% of the bulk between +7.0 and +15.0 per mil (i.e., pelagic sediments, pillow lavas, and sheeted dikes); (3) Upper mantle beneath the continental crust (SCL), +6.0 to +7.5 per mil; (4) Lower continental crust (LCC, > middle-granulite facies), typically ranges from about +6.5 to +8.0 per mil, except for minor, interlayered refractory metasedimentary material with $\delta^{18}O$ > +10.0 (this material is, however, not likely to produce any substantial amount of granitic melt); (5) Middle continental crust (MCC), ~+7.5 to +9.0, with a range from +5.0 to > +12.0 per mil, depending upon rock type, age, and metamorphic grade; (6) Archean and early Proterozoic granitic plutons, basement gneiss, and their associated metavolcanic country rocks (greenstone belts) are also potential source rocks, and these typically average about +7.5 to +9.0 and range from about +6.0 to +12.0 per mil; (7) Middle Proterozoic to Phanerozoic eugeosynclinal metasediments and metavolcanics (excluding cherts and carbonates), termed SAV, commonly range from +8.0 to +15.0 per mil, with an average $\delta^{18}O$ ~ +12.0; and (8) Late Proterozoic to early Phanerozoic miogeosynclinal

sediments (excluding limestone and dolomite), termed MCM, commonly have $\delta^{18}O$ = +10.0 to +18.0 per mil, with the sandstones having an average $\delta^{18}O$ ~ +11.0 and the shales an average $\delta^{18}O$ ~ +15.0.

10.3 Distribution of $\delta^{18}O$ in Cordilleran Plutons

From our discussions in Chapter 9, it is clear that mapping primary $\delta^{18}O$ values of granitic plutons on a regional basis (e.g., for the NGB) is an extremely useful tool for delineating source regions. We continue our discussion by expanding the data base to include most of the southwestern USA in the form of two primary, whole-rock $\delta^{18}O$ maps: (1) a map of Triassic and Jurassic age plutons (> 135 Ma, Figure 10.2); and (2) a map of Cretaceous and early Cenozoic plutons (< 135 Ma, Figure 10.3). We constructed these maps by compiling our own $^{18}O/^{16}O$ data (Tables 5.1, 7.1, 9.1 and Table 1, Appendix), together with literature-derived $^{18}O/^{16}O$ data for the following terranes: (1) the Northern Great Basin (NGB) of Nevada and western Utah (Figure 1.4; Table 1.2); (2) the Sierra Nevada Batholith (SNB) and western Mojave Desert of California (Figure 1.2; Table 1.1); (3) the Central and Eastern Transverse Ranges of California (Figures 6.3, 6.7, 6.10); (4) the southern Mojave Desert in southeastern California (SECA; Figures 1.4, 7.2, 7.3, 7.5, 7.6, 7.7; Table 1.2); (5) the Peninsular Ranges Batholith (PRB) of southern California and Baja California (Figure 1.6); and (6) southern Arizona (Figures 1.4, 5.3, 5.4, 5.5; Table 1.2).

For clarity in comparing the original $\delta^{18}O$ trends displayed by these various batholithic terranes, late Cenozoic movement along the San Andreas Fault zone has been restored by ~300 km (Ehlig, 1981); this places the Peninsular Ranges Batholith below the present-day United States-Mexico border in the position of the northern Gulf of California

Figure 10.2 Map of the southwestern United States and northwestern Mexico showing the distribution of primary whole-rock $\delta^{18}O$ values for Triassic and Jurassic (>135 Ma) granitic plutons, based on data given in Tables 1.1, 1.2, 9.1, Table 1 in the Appendix, and other sources listed in Chapter 1. The black dots indicate all Mesozoic and Cenozoic sample localities for both this figure and Figure 10.3, except that in much of southern and Baja California the dots are generalized, and are far fewer than the actual number of sites; the actual sampling density in the PRB, SGM, SBM, ROM, and LSB terranes cannot be shown with any clarity at the scale of this map. The $\delta^{18}O$ zones are mapped according to the scheme in Figure 10.1 and in the text: Groups 1 and 2 (light blue) - $+5.5 \leq \delta^{18}O < +8.5$; Group 3 ("$^{18}O$-step"; yellow) - $+8.5 \leq \delta^{18}O < +9$; Group 4 (orange) - $+9 \leq \delta^{18}O < +10$; and Group 5 (dark red) - $\delta^{18}O \geq +10$. The Group 5 zone is based on a limited number of samples (<5), and should be regarded as only a preliminary result. The Peninsular Ranges Batholith of southern California has been restored to its original position by removing about 300 km of right-lateral slip along the San Andreas Fault (see Chapter 6). The San Gabriel Mountains and the plutons of the Coast Ranges (Masi et al., 1981) have also been placed in their pre-San Andreas Fault configuration (see Ross, 1984; Powell, 1981).

Figure 10.3 Map of the southwestern United States and northwestern Mexico showing the distribution of primary whole-rock $\delta^{18}O$ values for Cretaceous and Cenozoic granitic plutons, based on data given in Tables 1.1, 1.2, 9.1, Table 1 in the Appendix, and other sources listed in Chapter 1. The $\delta^{18}O$ values are mapped using the same scheme discussed for Figure 10.2, and all other features are as described in the caption to Figure 10.2.

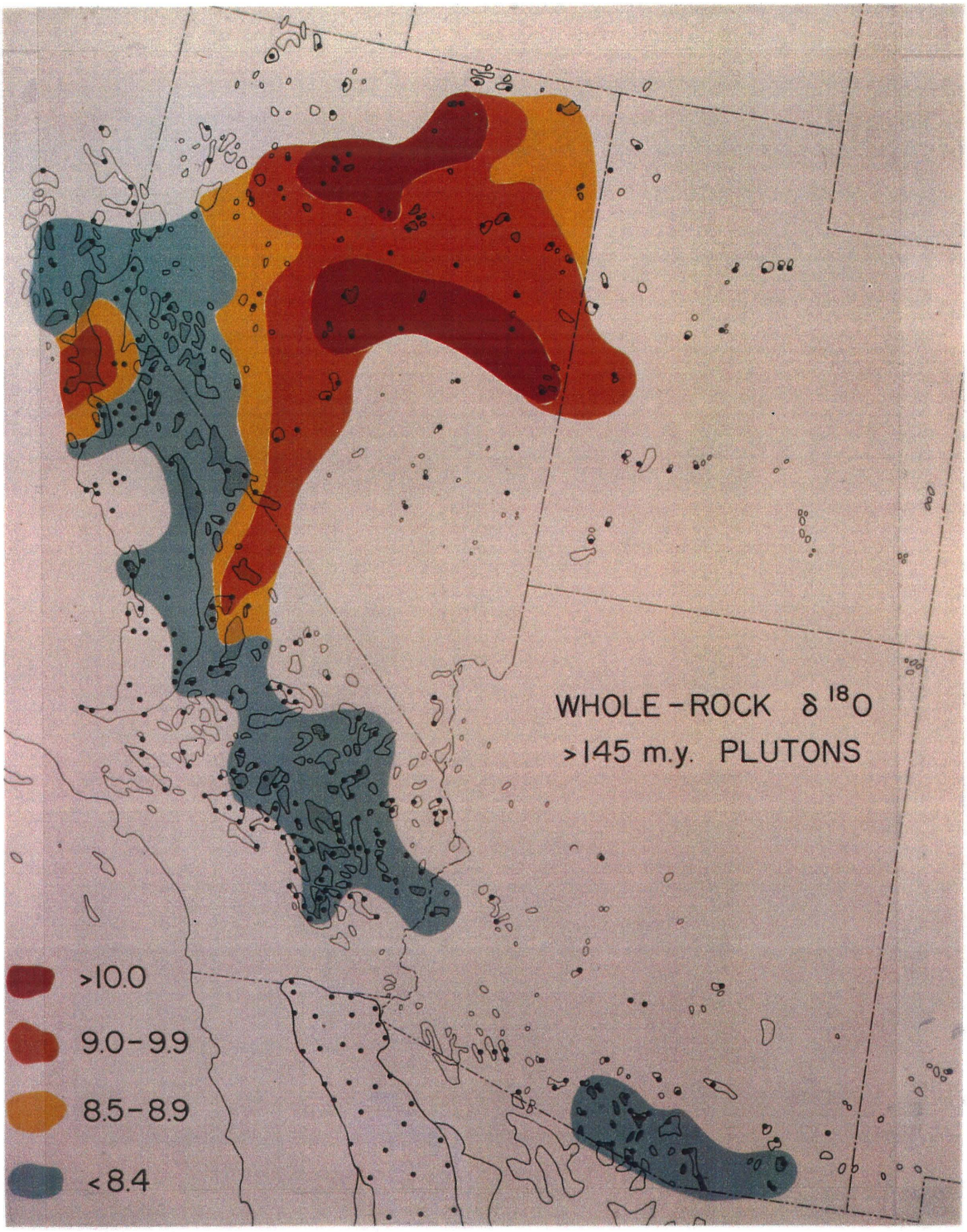
WHOLE-ROCK δ 18O
>145 m.y. PLUTONS
>10.0
9.0-9.9
8.5-8.9
<8.4

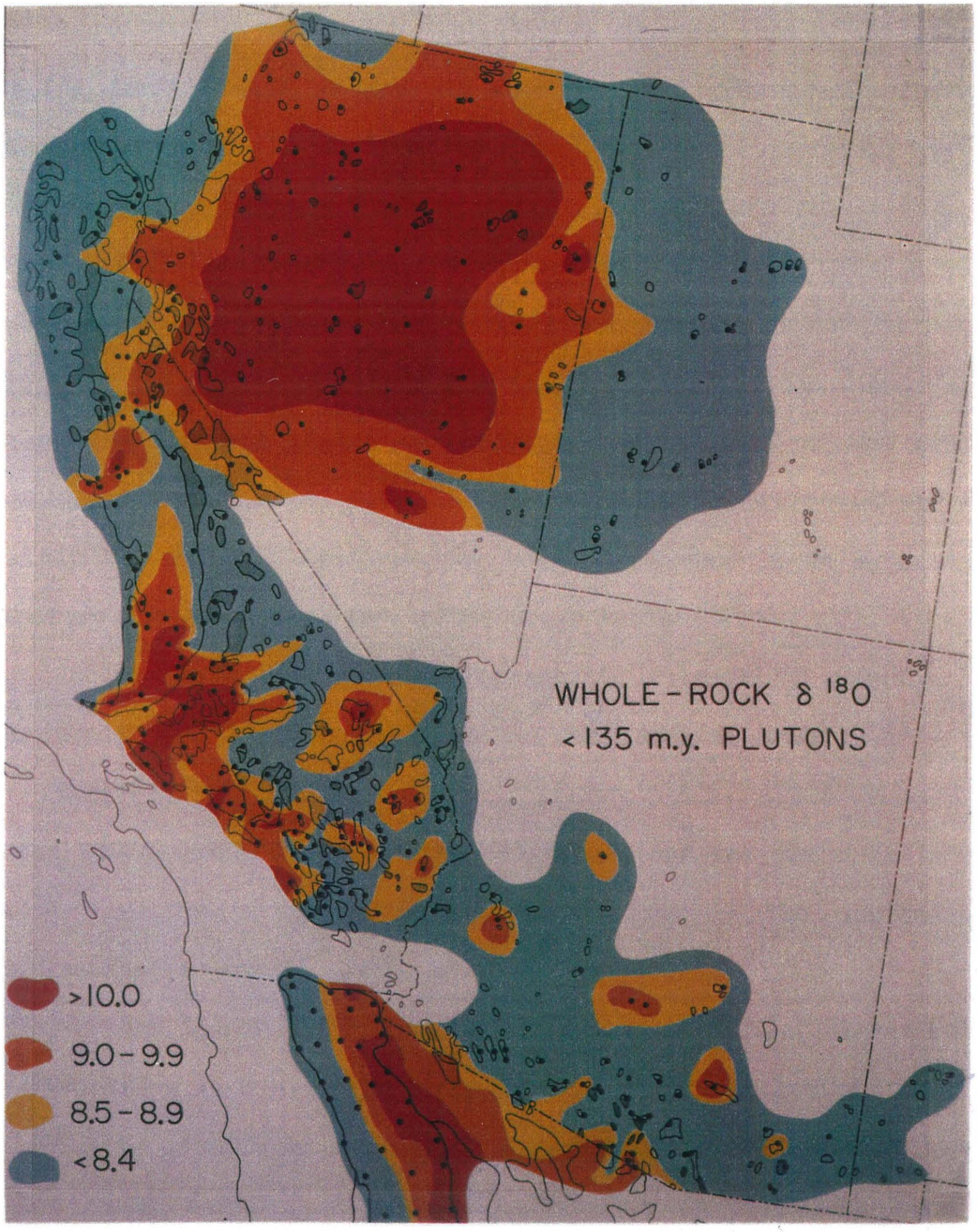
WHOLE-ROCK δ 18O
< 135 m.y. PLUTONS
>10.0
9.0-9.9
8.5-8.9
<8.4

(which is closed by the above palinspastication). In addition, about 25 km of offset has been restored along the San Jacinto fault, which separates the San Jacinto-Santa Rosa Mountain block from the main part of the PRB. Approximately 40 km of right-lateral movement was also restored along the north branch of the San Gabriel fault ("proto-San Andreas" fault) with another ~20 km restored along the south branch of the San Gabriel fault (see Chapter 6).

In a simplified manner, allowing for the ~300 km offset along the San Andreas fault zone and the other minor offsets described above, portions of the Salinian terrane are restored to a position immediately south of the southern Sierra Nevada Batholith and west of the western Mojave Desert region (Ross, 1984). In the northern portion of the map, note that we have not restored the very large amounts of extensional deformation that have occurred in the Great Basin (Eaton, 1982; Stewart, 1971, 1980). Additionally, complex tectonic disruptions (mainly low-angle thrust faults) that occurred in the terranes underlain by the Mojave Desert and Transverse Ranges (Silver, 1982, 1983; Silver and Anderson, 1974, 1983) have not been restored, nor has the left-lateral Cenozoic faulting along the Garlock fault or in the southeastern Transverse Ranges (Powell, 1981, 1982).

Taylor and Silver (1978) noted that for the Peninsular Ranges Batholith (PRB) there is a distinct break in whole-rock $\delta^{18}O$ between +8.5 and +9.0 per mil. The break is evident as a "$\delta^{18}O$ step" along the central axis of the PRB for its entire ~600 km length. On this basis, and because we are using the well-studied PRB as a general model for the rest of the Cordilleran plutons, the primary whole-rock $\delta^{18}O$ zoning pattern for the southern Cordillera is based on the following 5 groupings, with

two groups on each side of the PRB "$\delta^{18}O$ step": (1) +5.5 to +6.9 per mil; (2) +7.0 to +8.4 per mil; (3) +8.5 to +8.9 per mil; (4) +9.0 to +9.9 per mil, and (5) $\geq$ +10.0 per mil. An effect that is readily apparent in the PRB data (Taylor, 1986), and which is also suggested in the histogram of Figure 10.1, is a bimodal distribution of whole-rock $\delta^{18}O$, with one group lying mainly between +7.0 and +8.5 (Group 2) and the other between +9.0 and +10.5 (predominantly within Group 4). Each of the above-designated groups spans an $^{18}O/^{16}O$ range of 1 to 2 per mil, which is well outside the limits of plausible $^{18}O/^{16}O$ changes that could be brought about by magmatic differentiation and fusion-related processes; the latter should be no more than $\pm$ 0.5 per mil for a given batch of magma (Taylor, 1968; Kyser et al., 1982; Garlick, 1966; Matsuhisa et al., 1973; Taylor and Sheppard, 1986).

The whole-rock $\delta^{18}O$ values shown by the patterns in Figures 10.2 and 10.3 include only the analyses that we believe represent primary $\delta^{18}O$ values; samples with $\delta^{18}O$ < +5.5 per mil are not included, as they have been affected by secondary hydrothermal processes. Some other "low" $\delta^{18}O$ values ($\leq$ +6.9) are also not included, if such samples are in the proximity of a hydrothermal center, and if in our judgment such relatively low $\delta^{18}O$ values are likely to be the result of hydrothermal alteration. The $\delta^{18}O$ contour patterns on the two maps (Figures 10.2 and 10.3) are remarkably systematic, showing well-defined, geographically delineated zones where plutons uniquely fit into the groupings (1) through (5). These $\delta^{18}O$ contour patterns were drawn using a simple, linear interpolation between two-dimensional map coordinates for the various sample localities.

The older (> 135 Ma) plutons, in general, display a much narrower range of $\delta^{18}O$ than do the younger (< 135 Ma) plutons. As discussed in Chapters 5 and 8, this is probably attributable to two factors: (1) Except for a number of occurrences in Nevada and northern California, most of the Jurassic and Triassic plutons were emplaced to the east of the western limit of exposed Precambrian basement of the North American craton. In other words, in the southern half of the region shown in Figure 10.2, the > 135 Ma plutons would all belong to the Eastern Intermediate-^{18}O Zone, as defined below for the Cretaceous plutons. (2) The >135 Ma plutons in general appear to have been derived from deeper parts of the continental crust or subcontinental lithosphere than were most of the Cretaceous and early Tertiary plutons; thus they were probably formed from source materials that were, on average, lower in ^{18}O than some of the middle crustal materials that were melted to form the voluminous Cretaceous magmatic arc. Also, the Cretaceous and early Tertiary plutons show more definitive regional isotopic patterns than do the Jurassic and Triassic samples, mainly because the density of sampling sites and the geographic coverage are both far greater for the Cretaceous batholiths. For example, note that the PRB, which is in a sense our "model batholith", is entirely Cretaceous in age; there are no older plutons in that particular segment of the Cordilleran batholithic complex.

For the above reasons, the regional $^{18}O/^{16}O$ systematics in the Cordilleran plutons are more readily discussed for the Cretaceous "event" than for the Jurassic "event." In general, the Cretaceous plutons show an increase in primary whole-rock $\delta^{18}O$ from west to east, throughout the entire map area (Figure 10.3); however, at some place along every traverse there is a "reversal" in $\delta^{18}O$ and the values begin to decrease to

the east. These gradients in $\delta^{18}O$ define 3 major north- to northwest-trending belts of plutons, here termed the Western Low-^{18}O Zone, the Central High-^{18}O Zone, and the Eastern Intermediate-^{18}O Zone. Note that within the broad Eastern Zone there are local areas of ^{18}O enrichment.

The $\delta^{18}O$ values increase from $\delta^{18}O \leq +6.0$ per mil at the western edge of the Western Zone, to $+9.0 \leq \delta^{18}O \leq +13.5$ in the Central Zone. The latter rocks with $\delta^{18}O > 9.0$ per mil form a more-or-less continuous north-trending belt of high-^{18}O plutons from the Northern Great Basin (NGB) of Nevada practically all the way to the southern end of the PRB in Baja California. Remnants of this High-^{18}O Central Belt are also evident along the extreme western margin of the Transverse Ranges in the SECA region, but there, probably because of Cenozoic fault offsets, there is no known corresponding low-^{18}O zone to the west. The Low-^{18}O Western Zone in those areas has very likely been "shaved off" by the northwest-trending late Cenozoic San Andreas fault system, with displacement of the pre-existing Western Zone plutons off to the northwest.

East of the Central High-^{18}O Belt, the pluton $\delta^{18}O$ values decrease to a set of characteristic regional values within the range +7.0 to +9.0. This eastward decrease in $\delta^{18}O$ takes place very abruptly, particularly in southern California, where there has been some "telescoping" as a result of westward thrusting of the SECA terranes (L.T. Silver, pers. comm.). The $\delta^{18}O$ values then remain fairly uniform at about +7.5 to +8.5 as one moves farther east, except for a prominent, albeit discontinuous, zone trending from eastern California to southern Arizona where plutons with $+8.5 \leq \delta^{18}O \leq +10.0$ form a series of localized centers (one very ^{18}O-rich SECA sample, GR145 in Table 1.2 near Halloran Springs, has $\delta^{18}O = +12.9$). This belt of high-^{18}O plutonic centers (Figure 10.4) lies

wholly within the Eastern ^{18}O Zone; many of these are associated with the so-called metamorphic core complexes of the southern Basin and Range Province, discussed in more detail below. These higher-^{18}O plutonic centers are readily distinguished from the High-^{18}O Central Zone farther to the west by their local geological features, and particularly by their much higher $^{87}Sr/^{86}Sr$ ratios (see DeWitt et al., 1984), as well as by the fact that they do not form a continuous zone. Also, this discontinuous belt is commonly separated from the Central Zone by a 50 to 100 km-wide terrane where the $\delta^{18}O$ values are typically lower than +8.5 per mil.

An important observation for the Cordilleran plutons is that their whole-rock $\delta^{18}O$ values within any particular geographic region are essentially independent of rock type (for detailed discussion of lithologies and $\delta^{18}O$ values see Chapters 5 through 9, and Baird et al., 1979; Moore, 1959; Bateman et al., 1963; Taylor and Silver, 1978; John, 1981, 1989; Silver et al., 1979; Taylor, 1986; Miller et al., 1989). In any given geographic zone, the tonalites, granodiorites, and quartz monzonites, as well as most of the two-mica granites, all tend to have similar $\delta^{18}O$ values; thus the most important criterion that is most easily related to $\delta^{18}O$ is simply the geographic location of a pluton relative to the mapped boundaries of the 3 zones defined above. For example, Figure 10.4 shows that for plutons with $\delta^{18}O < +10$, the entire spectrum of lithologies from 58 to 76 weight percent SiO_2 encompasses most of the $\delta^{18}O$ range between +6.5 and +10.

Locally, a few very high-SiO_2, two-mica granites show considerably higher $\delta^{18}O$ values (+12 to +13) than the geographically and temporally associated granodiorites and quartz monzonites, indicating that some of these peraluminous plutons were derived from unique source materials

(more ^{18}O-rich pelitic sediments?). Also, Ague and Brimhall (1987) have recently described a belt of plutons that are true granites (sensu stricto) in an elongate region in the central Sierra Nevada Batholith; this belt of granite plutons displays a set of common chemical characteristics similar to those of many S-type granites; these SNB plutons also all have very high $\delta^{18}O$ values (> +9; H.P. Taylor, pers. comm.). However, such relationships are much less common in the Cordilleran batholiths than the occurrences where all of the various kinds of pluton lithologies from tonalite to granite in a given geographic zone appear to have been derived from essentially similar source materials with a restricted range of $\delta^{18}O$ values.

10.4 $\delta^{18}O$ Zones and Source Region Distribution

Following the terminology we already established for NGB granitic plutons (see Figure 9.6), the three major $\delta^{18}O$ zones (or belts) delineated above for the Cretaceous and early Tertiary plutons in the southwestern United States are here simply referred to as the Western Low-^{18}O Zone (WZ), the Central High-^{18}O Zone (CZ), and the Eastern Intermediate-^{18}O Zone (EZ). For the time being, we defer discussion of the Sr-isotopic "fine-structure" associated with the Central Zone (e.g., the Central V- and S-type subzones) to Section 10.6. It is readily apparent from Figure 10.5 that the three $\delta^{18}O$-zones correlate directly with several prominent geological features, including: (1) the eastern limit of the predominant occurrence of quartz diorite or tonalite (i.e., the quartz diorite line); (2) the western limit of outcropping Precambrian basement rocks; and (3) isopachs of late Precambrian-early Paleozoic geosynclinal sediments.

Figure 10.4 Plot of whole-rock $\delta^{18}O$ versus SiO_2 (wt.%) for granitic plutons from the Northern Great Basin (NGB) and the Southern Basin and Range (SBR) Province of the southwestern USA Cordillera, based on data given in Tables 1.2, 5.1, and 7.1. The data-points are subdivided according to geographic location (NGB - circles; SBR - squares) and age (> 135 Ma - half-filled symbols, < 135 Ma - solid symbols). The NGB and SBR samples are separated into two data-envelopes; the shaded regions of these envelopes highlight the Jurassic samples.

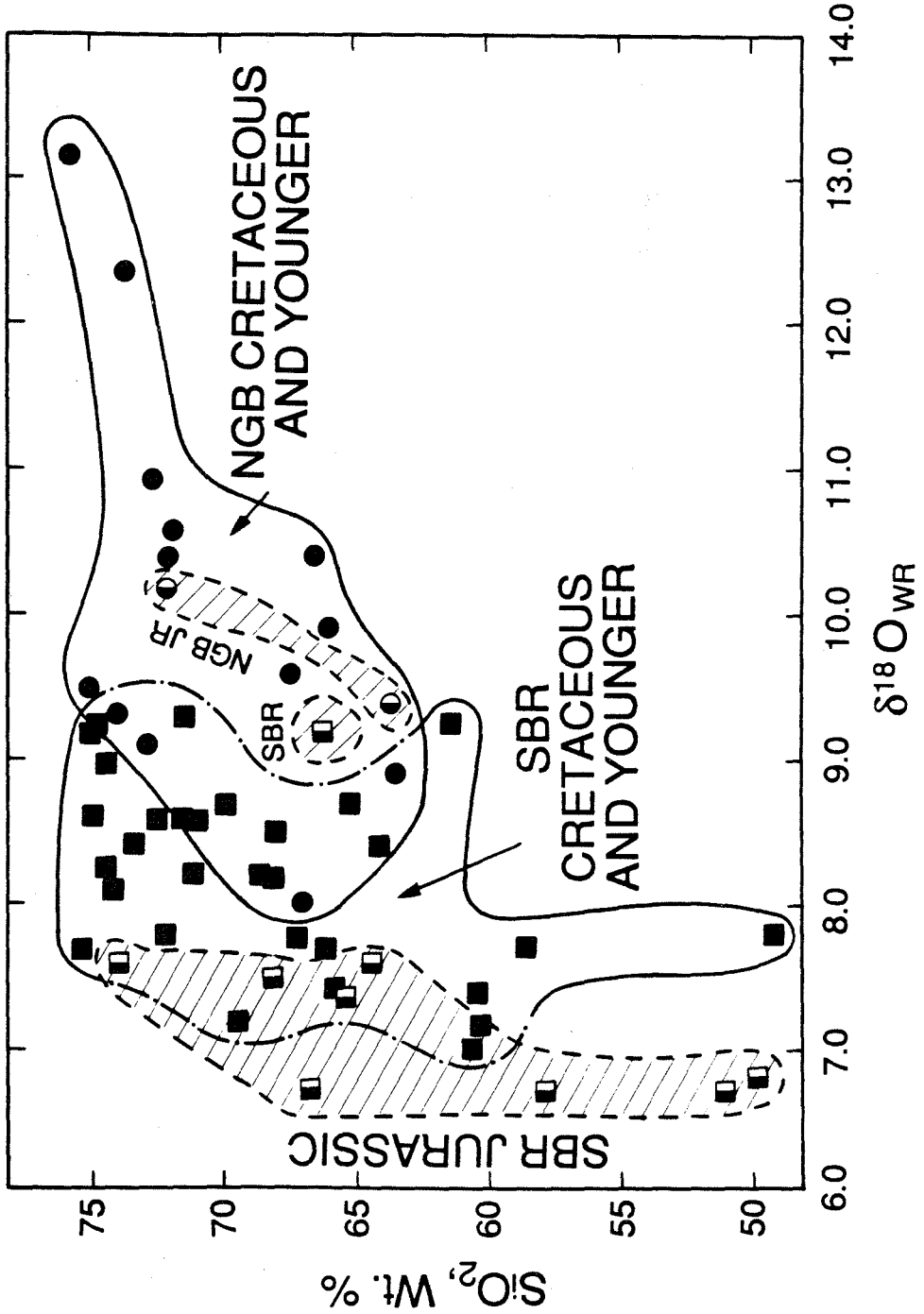
NGB CRETACEOUS AND YOUNGER
NGB JR
SBR
SBR CRETACEOUS AND YOUNGER
SBR JURASSIC
SiO2, Wt. %
75
70
65
60
55
50
6.0
7.0
8.0
9.0
10.0
11.0
12.0
13.0
14.0
δ18OWR

Figure 10.5 Map of the southwestern United States and northwestern Mexico showing the boundaries of the three major $\delta^{18}O$ zones defined in the text in relation to the quartz diorite line (QDL) of Moore (1959), the miogeosynclinal 5000-foot isopach contour, and the western limits of mapped Precambrian outcrops (PCBL; see King, 1977; Stewart, 1972, 1980; Silver et al., 1977a). The Western Low-^{18}O Zone (WZ) lies to the west of the Central High-^{18}O Zone (CZ), which is shown by the cross-hatch pattern. The Eastern Intermediate-^{18}O Zone (EZ) lies to the east of the cross-hatched Central Zone.

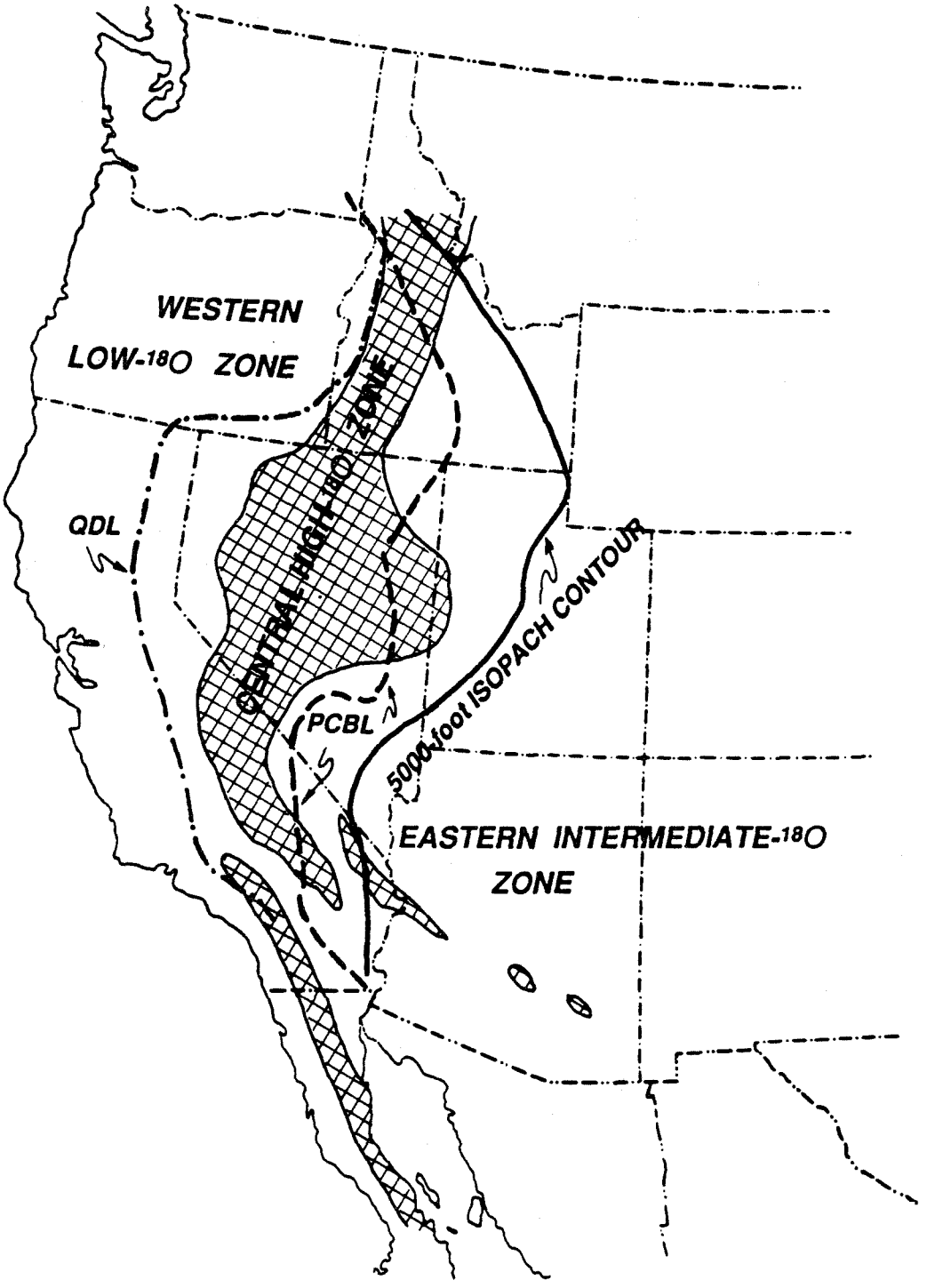
WESTERN
LOW-18O ZONE
CENTRAL HIGH-18O ZONE
QDL
PCBL
5000-foot ISOPACH CONTOUR
EASTERN INTERMEDIATE-18O
ZONE

Moore (1959) evaluated the distribution of rock types among Mesozoic batholithic rocks in the North American Cordillera. He noted that tonalitic plutons predominantly occur west of the boundary shown in Figure 10.5, and he termed this the quartz diorite line (QDL); tonalitic plutons occur only sporadically east of this boundary. West of the QDL, plutons with a wide range of SiO_2 contents may occur in association with the tonalites, so that the entire range from granite through mafic tonalite (and quartz gabbro) is commonly present. However, east of the QDL, plutons are predominantly granodioritic and quartz monzonitic, and the more mafic types are largely absent. Figure 10.5 shows that, in general, the quartz diorite line is parallel with our mapped $\delta^{18}O$ boundary between the Western Low-^{18}O Zone plutons and those of the Central High-^{18}O Zone. Although there is some ambiguity within the PRB itself, because the eastern half of the PRB is dominantly tonalitic (Silver et al., 1979), throughout the rest of the Cordillera the high-^{18}O plutons of the Central Zone are, in general, located east of the QDL, as defined by Moore (1959).

Figure 10.5 also shows the westward limit of outcropping Precambrian basement rocks, as taken from King (1977). These rocks include middle and upper Proterozoic supracrustal sedimentary rocks, as well as outcrops of crystalline basement with ages greater than middle Proterozoic. No Precambrian rocks are known, either in outcrop or in the subsurface, to the west of this line (Figure 10.5), which is here termed the Precambrian Basement Line or PCBL. The rocks immediately to the west of the PCBL are made up of a thick section of miogeosynclinal sediments, which farther to the west grade into a thick section of Paleozoic and early Mesozoic eugeosynclinal sediments and volcanics.

The Central High-^{18}O Zone occurs almost entirely to the west of the PCBL and, in general, mimics its shape and trend. One exception is in east-central Nevada, where the high-^{18}O zone overlaps the western limit of Precambrian rocks by a significant degree. It must be noted, however, that the Precambrian rocks in that area are themselves dominantly made up of mid-Proterozoic geosynclinal metasediments and gneissoid rocks (Kistler et al., 1981); such rocks bear some similarities to rocks of the Salmon River Arch in Idaho (Armstrong, 1975). As discussed below, in Section 10.6, the position of these rocks in the NGB accounts for the $^{87}Sr/^{86}Sr$-related "fine-structure" we see in the NGB Central High-^{18}O Zone.

The rocks of the Salmon River Arch are intercalated with metasediments of the late Precambrian Belt Series, and may owe their existence to sedimentary basins west of a rifted North American craton. Most of the crystalline basement rocks east of the PCBL shown in Figure 10.5 are definitely older, and are clearly associated directly with the craton. Thus, thick sections of supracrustal sedimentary material, together with local fragments of crystalline basement younger than ~1.5 Ga, appear to be strongly associated with the Central High-^{18}O Zone. North of the area considered in Figure 10.5, a similar relationship appears to hold for the Mesozoic plutons and basement rocks in the Idaho Batholith region (Solomon and Taylor, 1981; Criss and Fleck, 1987). Salmon River Arch basement occurs well within the high-^{18}O zone of the Idaho Batholith, whereas farther east in the vicinity of the lower-^{18}O Boulder Batholith of Montana is a package of deeper-seated country rocks from a much older crystalline terrane. In our terminology, the high-^{18}O zone of the (Cretaceous) Idaho Batholith would correspond to our Central High-^{18}O

Zone, and the (Laramide) Boulder Batholith would correspond to our Eastern Intermediate-^{18}O Zone (see Taylor, 1986; Criss and Fleck, 1987; Sheppard and Taylor, 1974).

The third fundamental geologic parameter that bears a relationship to the regional $\delta^{18}O$ zones is the isopach thickness of late Precambrian through early Paleozoic sedimentary rocks that comprise the geosynclinal assemblages of the southwestern Cordillera. Stewart and Poole (1974) and Burchfiel and Davis (1981a) have traced the locations of these miogeoclinal-type sediments through Nevada, Utah, and southeastern California, and the corresponding 5000-foot isopach is shown along with the $\delta^{18}O$ zonation in Figure 10.5.

West of the 5000-foot (1.5 km) isopach, thicknesses of sedimentary rocks up to 30,000 feet (9 km) or more are present, comprising the prism of sediments shed in a westerly direction from the craton during the period 1500 to 300 Ma. Figure 9.2 shows a composite cross section illustrating the relationship between older crystalline basement, possible Belt Series-type sedimentation, and the younger miogeoclinal sedimentary wedge (King, 1977). It is clear that as much as a 10 to 20 km-thick section of miogeoclinal sediments may have existed to the west of cratonal basement, and that locally the deeper parts of these sections are late Precambrian in age.

The Central High-^{18}O Zone occupies the area of the Cordillera where the isopachs show that the sedimentary wedge reached its thickest extent, most notably throughout the central portions of the Great Basin region of Nevada. An obvious facet of the regional distribution of high-^{18}O plutons is that the Central Zone is "sandwiched" between the above-mentioned three geologic features, with the largest proportion of high-^{18}O plutons

occurring east of the quartz diorite line and west of both the 5000-foot isopach and the Precambrian cratonal outcrops, and centered on the thickest portion of geosynclinal sedimentary and volcanic rocks.

10.5 Structural Features

Even after restoration of the movement that has occurred along the northwest-trending, late-Cenozoic, San Andreas system of right-lateral strike-slip faults, there are some further curvatures of the $\delta^{18}O$ contours in Figure 10.3 that do not appear to represent inherent characteristics of the Cretaceous magmatic arc. The most obvious of these features is the major crustal extension that took place during Cenozoic time in the Great Basin region of Nevada. For most of its length in southern and Baja California, the Central High-^{18}O Zone has a width of about 50 to 100 km. However, in the Basin and Range Province in Nevada, this high-^{18}O zone blossoms out to cover virtually the entire state. If the difference in width between the Central High-^{18}O Zone in Nevada and that in California is entirely attributed to crustal extension, this would imply at least 70% extension, and possibly as much as 200% extension or more. Similar amounts of Cenozoic extension have in fact been suggested by some workers (e.g., see Stewart, 1971, 1980; Eaton, 1982; Zoback and Thompson, 1978).

Two other structural features show up well on the $\delta^{18}O$ map. The first is the series of left-lateral strike-slip faults located between the southern Sierra Nevada Batholith and the northern part of the Peninsular Ranges Batholith. The most prominent of these, with approximately 48 to 64 km of slip, is the Garlock fault, immediately south of the Sierra Nevada Batholith (Davis and Burchfiel, 1973; Smith, 1962; Smith and Kettner, 1970). The Garlock fault causes extreme apparent bending in the

Figure 10.6 Map of the southwestern United States and northwestern Mexico comparing the $\delta^{18}O$ patterns described in Figure 10.3 with various Cenozoic tectonic features. The $\delta^{18}O$ zones have the same terminology and colors defined for Figure 10.3. Right-lateral strike-slip displacements along the San Andreas and San Gabriel Faults have been restored, as discussed in the text (also see Chapter 6). The Cenozoic tectonic features shown on this map are: (1) the bulge in the Central High-^{18}O Zone in the NGB, which is due in part to extension (note, however, that the east-trending CZ-EZ boundary in southern Nevada cuts across the grain of regional NGB extension, and therefore part of the CZ "bulge" must be primary in origin; see Chapter 9); (2) GF - Garlock Fault with approximately 40 km of left-lateral strike-slip displacement; (3) WDT - Westward Displacement Terrane, an oval-shaped region that shows somewhat schematically the area that is postulated to be a series of early Cenozoic allochthons that have been transported 50-100 km to the west from their original positions in eastern California (Silver, 1982, 1983; Yeats, 1981; James, 1989); and (4) MT - Mylonitic Terrane, a region outlined by a dashed line, approximately indicating the areas underlain by a zone of mylonitization that has affected the upper portions of Cretaceous plutons in southeastern California (Howard et al., 1982; Hamilton, 1986).

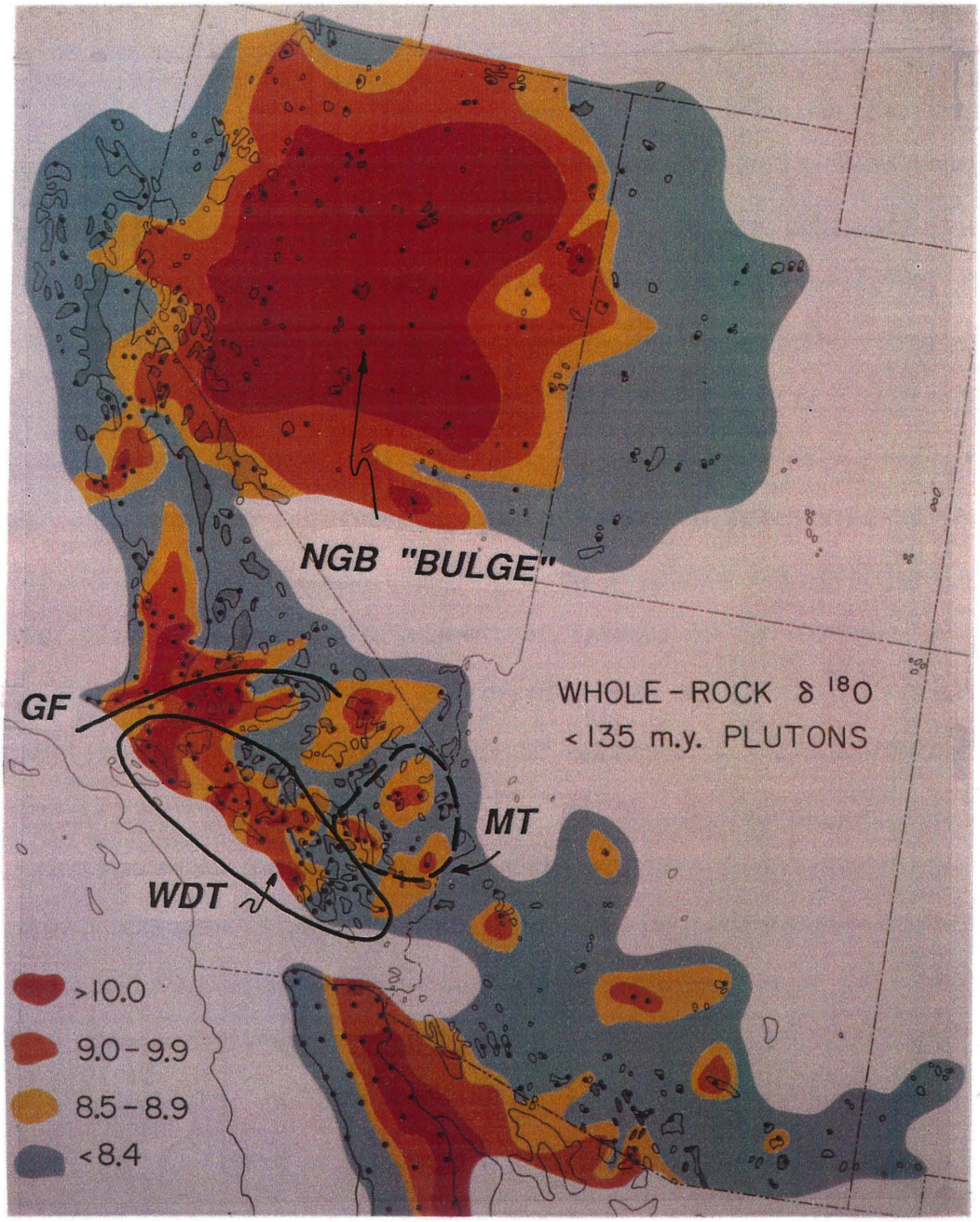
NGB "BULGE"
GF
WHOLE-ROCK δ 18O
<135 m.y. PLUTONS
MT
WDT
>10.0
9.0-9.9
8.5-8.9
<8.4

trend of the High-^{18}O Central Zone, as shown in Figure 10.3. Restoration of the 48 to 64 km of left-lateral displacement would straighten out most of the "bending" (Masi et al., 1981).

The second large-scale structural feature occurs within the Mojave block, immediately south of the Garlock fault. Allowing for restoration of movement along the Garlock fault, the northwest-trending high-^{18}O zone in the Sierra Nevada Batholith abruptly bends to the southwest in the vicinity of the western Mojave Desert (Figure 10.6). Silver (1982, 1983) and Yeats (1981) have suggested that during Paleocene times there was large-scale overthrusting of batholithic terranes comprising portions of the western Mojave Desert and Transverse Ranges. A series of these terranes (approximately outlined in Figure 10.6) are postulated by Silver (1982, 1983) to have moved westward along proposed east-dipping thrust faults, with a westward displacement of perhaps 50 to 100 km. If this hypothesized tectonic movement is correct, then the southwest flexure in the western Mojave high-^{18}O zone may be restored to yield a "corrected" northwest-trending configuration.

Farther south in the central and southeastern Transverse Ranges are the Pinto Mountain, Blue Cut, and Chiriaco faults, the former with around 16 km of slip and the latter two each having several km of slip (Powell, 1981). These left-lateral faults have much smaller displacements than the Garlock fault, and their $\delta^{18}O$ effects do not show up well on the regional map in Figure 10.3. However, on larger-scale maps these offsets are evident (see Chapter 6).

Another $\delta^{18}O$ feature, which could possibly be related to the westward thrusting, is located in the Mojave Desert of southeastern California. It is comprised of the zones where plutons with $\delta^{18}O > 8.5$

per mil (see Figure 10.6) are overprinted by late Cretaceous to early Tertiary mylonitization (Howard et al., 1982). The mylonites occur in the upper portions of these batholiths, and they exhibit northeast-trending lineations; they are interpreted by Howard et al., (1982) to have formed regionally below a rigid roof and above a more fluid floor of crystalline rocks affected by late Cretaceous diapirism. This zone of deformation may extend southeastward along the discontinuous, high-^{18}O belt of plutonic centers ($\delta^{18}O > +8.5$) mentioned earlier, which exists within the Eastern Intermediate-^{18}O Zone. This belt represents a zone where local mid-crustal melting and relatively deep emplacement of peraluminous, two-mica plutons occurred along a path of elevated geotherms (see Chapter 8). Thus the zone could indeed have served as the platform for crustal sliding along a transitional layer between ductile, heated rocks and a brittle cover.

It is possible that the "more rigid roof" could be made up of the (now westwardly displaced) batholithic terranes described by Silver (1982, 1983). The mylonitized zone and the arcuate anomalous $\delta^{18}O$ zone presently lie 50 to 100 km east of the displaced terranes, and they also share the "transitional" $\delta^{18}O$ signature that characterizes the eastern portions of the Transverse Ranges. (The transitional signature is the decrease in $\delta^{18}O$ from the relatively high-^{18}O values of the Central Zone to the lower values of the Eastern Zone).

10.6 $\delta^{18}O$ Zones in Relation to Other Isotopic Systems

Figure 10.7 shows the location of the three $\delta^{18}O$ zones with respect to the regional isotopic provinces established for lead. Following up on a classic study by Doe (1967), Zartman (1974) defined three discrete lead isotopic provinces within the Mesozoic and Cenozoic igneous rocks in the

Figure 10.7 Map of the southwestern United States and northwestern Mexico showing the three $\delta^{18}O$ zones in relation to the lead isotope boundaries defined by Zartman (1974). The Western Low-^{18}O Zone (WZ) is shown by horizontal lines, the Central High-^{18}O Zone (CZ) by cross-hatch, and the Eastern Intermediate-^{18}O Zone (EZ) by random-dash stipple. The heavy, solid lines indicate the boundaries between Pb-isotope zones Ia, Ib, II, and III (see text). The Pb-isotope zones have been extended into southern and Baja California based on new data by L.T. Silver (quoted in Silver and Chappell, 1988). This new data shows that the eastern half of the Peninsular Ranges Batholith exhibits very high $^{206}Pb/^{204}Pb$ values of 18.9 to 19.5 (similar to Zone II Pb and distinctly higher than the values in Zones Ia, Ib and III).

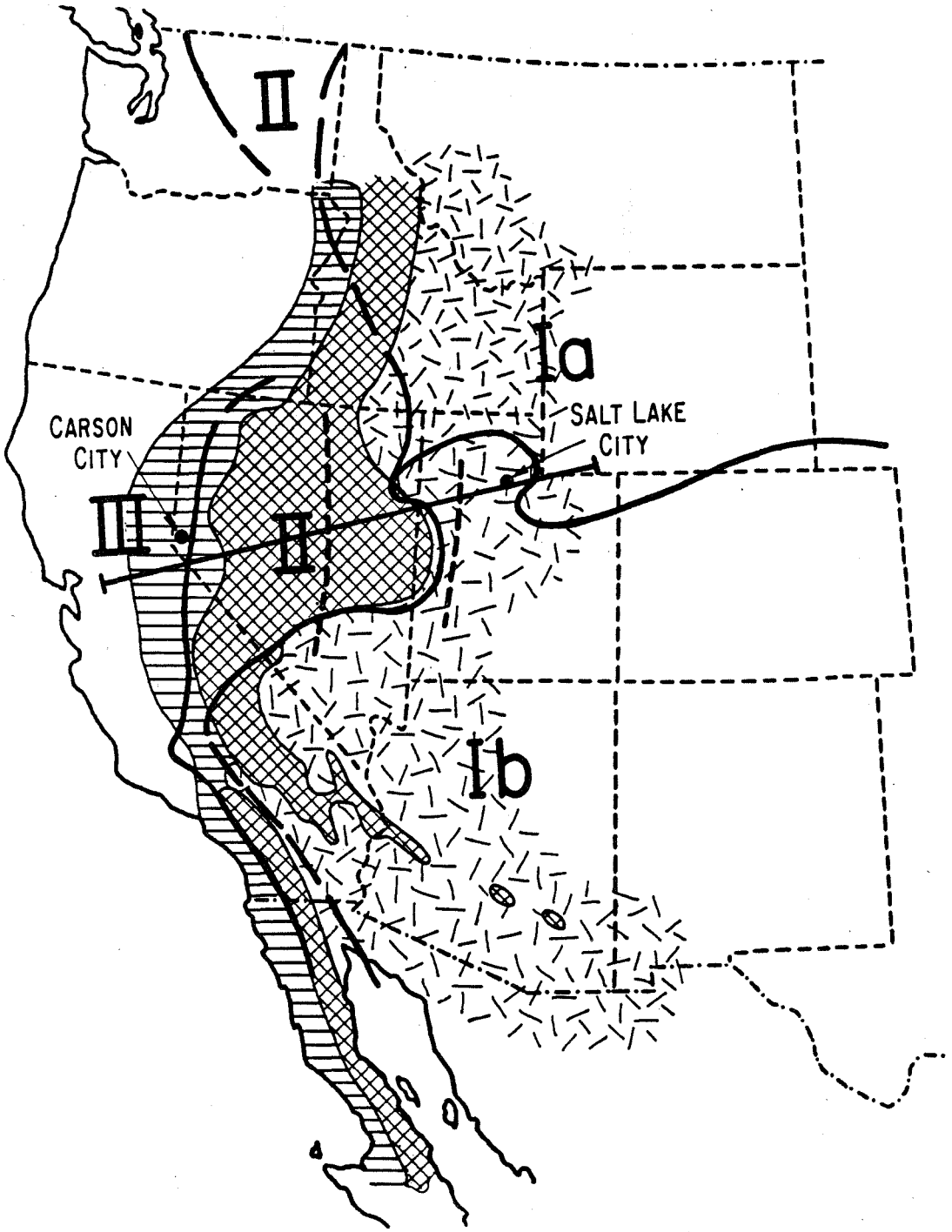
II
Ia
SALT LAKE CITY
CARSON CITY
III
II
Ib

western United States. Pb-Zone I contains relatively unradiogenic lead with $^{206}Pb/^{204}Pb$ ~16.2 to 18.8 and $^{208}Pb/^{204}Pb$ ~36.5 to 39.9, which Zartman ascribed to ancient lower continental crust or upper mantle. Pb-Zone II is much more radiogenic, with relatively homogeneous isotopic compositions ranging from $^{206}Pb/^{204}Pb$ ~19.1 to 19.7 and $^{208}Pb/^{204}Pb$ ~38.9 to 40.3. Plutons displaying this restricted range of Pb isotopic compositions are geographically associated with the great thicknesses of miogeoclinal sediments, and Zartman suggested that those igneous rocks inherited their Pb isotope ratios from sediments derived from well-mixed detrital materials that were eroded off of, and transported westward from, the Precambrian craton. Zone III has Pb isotopic compositions that are intermediate between Zones I and II, which contrasts sharply with the relative geographic positions of the three zones (i.e., Zone II, with the highest $^{206}Pb/^{204}Pb$ values, occupies a central geographic location between Zones I and III; see Figure 10.7). The Pb isotopic compositions of the Zone III igneous rocks are ascribed by Zartman (1974) to an association with, or a derivation from, source materials analogous to mafic oceanic crust or to eugeosynclinal sediments and volcanics.

In the area of the Great Basin of Nevada, our Central High-^{18}O Zone corresponds almost perfectly with Zartman's Pb isotope Zone II, and our Eastern Intermediate-^{18}O Zone plutons occur almost entirely within his Pb isotope Zone I. For the most part, the Western Low-^{18}O Zone coincides with Pb isotope Zone III, although the Pb isotope data are very scanty in this region, which also exhibits considerable structural complexity. There is, then, almost a perfect one-to-one correlation between the positions of the three oxygen isotopic zones defined in this work and the provinces established solely from the lead isotope studies. Note that

the Eastern Zone, which has intermediate $\delta^{18}O$ values, also has intermediate Pb isotopic compositions, and that the highest $\delta^{18}O$ values and the highest $^{206}Pb/^{204}Pb$ values both occur together within the Central Zone (Figure 10.7). The above correlations cannot as yet be evaluated in detail farther to the south within the Cordillera, because very little detailed lead isotope data have been published for this region. However, the Pb isotope data from the PRB generally fit this overall picture (L.T. Silver, pers. comm.).

Kistler and Peterman (1973, 1978), Early and Silver (1973), and Farmer and DePaolo (1983, 1984) are mainly responsible for establishing the regional strontium isotopic systematics for the Mesozoic plutons of the southwestern Cordillera. With the exception of the western Mojave Desert region, where recent tectonic factors complicate some of the relationships (see above), the initial $^{87}Sr/^{86}Sr$ values of the plutons generally increase from west to east along a gradient that is sub-perpendicular to the trends of the Mesozoic batholith belts. This pattern is particularly well-defined for the Cretaceous PRB, where the $^{87}Sr/^{86}Sr$ values range from around 0.7025 to around 0.7080 going from west to east. Contours of $^{87}Sr/^{86}Sr$ parallel the trend of the Cretaceous magmatic arc (Early and Silver, 1973), and they are also subparallel to the $\delta^{18}O$ contours (Taylor and Silver, 1978; Silver et al., 1979). The position of the 0.7050-0.7060 zone in the PRB closely corresponds with the location of the "$\delta^{18}O$ step," across which there are profound changes in the abundances of various rock types, $\delta^{18}O$ chemistry, and trace-element geochemistry (Taylor and Silver, 1978; Silver et al., 1979).

The $^{87}Sr/^{86}Sr$ values in the Sierra Nevada Batholith are similar to those established for the PRB, but the 0.7060 contour line becomes less

regularly behaved in the central portions of the SNB, where it veers off to the east (see Kistler and Peterman, 1973). Nevertheless, as in the PRB, the position of the 0.7060 line in western Nevada coincides in a general way with the western boundary of the Central High-^{18}O Zone, such that rocks with $^{87}Sr/^{86}Sr > 0.7060$ also usually have $\delta^{18}O > +8.5$ to +9.0. A systematic, positive correlation exists between $\delta^{18}O$ and $^{87}Sr/^{86}Sr$ eastward through the Cordillera, at least as far as the boundary between the Central High-^{18}O Zone and the Eastern Intermediate-^{18}O Zone.

Thus, in the southern half of the Cordillera of the southwestern United States (PRB, southern SNB, western Mojave; SECA; southern Arizona); the Sr-O isotopic relationships are consistent with the general source region model developed for the PRB (see Chapters 8 and 9, and Taylor and Silver, 1978). This model uses a minimum of three sources: (1) a simatic, oceanic island arc (OIA) low-^{18}O and low-$^{87}Sr/^{86}Sr$ source in the Western Zone (WZ); (2) a sedimentary or altered volcanic (SAV), high-^{18}O and moderate-$^{87}Sr/^{86}Sr$ source in the Central Zone (CZ); and (3) an intermediate-^{18}O and moderate- to high-$^{87}Sr/^{86}Sr$ source in the Eastern Zone (EZ), lying in the sub-continental lithospheric upper mantle (SCL) and/or the lower continental crust of the craton (LCC). Within the EZ, localized areas are observed where a middle continental crust (MCC) source region appears (e.g., in SECA and southern Arizona; see Chapter 8).

In the northern half of the Cordillera of the southwestern USA (see Chapter 9), we observe the same three-fold division of $\delta^{18}O$ zones mentioned above, but, based upon Sr-O isotopic results, we must add a fourth zone. In the NGB, the WZ-CZ boundary is very sharp, and is

entirely analogous to the $\delta^{18}O$ "step" in the PRB; in other words, we can readily delineate the WZ from the CZ in the western portion of the NGB based entirely on $^{18}O/^{16}O$, and initial $^{87}Sr/^{86}Sr$ ratios across this boundary correspond almost perfectly to the PRB model. However, proceeding farther east in the NGB, there is an abrupt initial $^{87}Sr/^{86}Sr$ "step" that has no counterpart in the PRB. This $^{87}Sr/^{86}Sr$ "step" (< 0.7080 to the west and > 0.7100 to the east) lies 150-200 km east of the WZ-CZ $^{18}O/^{16}O$ "step" (see Figures 9.6 and 10.10), requiring that the CZ be divided into two subzones: (1) The western part (V-type) corresponds to the eastern half of the PRB, but is much wider due to Cenozoic extension; this zone fits in well with the PRB model, and appears to be related to SAV-type sources. (2) The eastern part (S-type) has no equivalent with such great areal extent anywhere in the Cordillera of the southwestern USA; this latter zone is associated with major Mesozoic and Cenozoic metamorphic events that have affected a thick sequence of late Precambrian and Paleozoic miogeoclinal sedimentary rocks (see Section 10.4). This source-type, and the source regions postulated for the other three zones are discussed further in Section 10.8.

Farmer and DePaolo (1983, 1984) and DePaolo (1981a) analyzed the $^{143}Nd/^{144}Nd$ ratios of Mesozoic and Cenozoic plutons from the Great Basin area of Nevada and from southeastern California and Arizona; we have discussed their work in the NGB in detail in Chapter 9. The ε_{Nd} values also vary systematically from west to east elsewhere in the Cordillera; the ε_{Nd} = +6.0 contour lies within the Western Low-^{18}O Zone, and in the Great Basin the ε_{Nd} = -14 contour closely follows the eastern edge of the Central High-^{18}O Zone. In southern Arizona, ε_{Nd} does not get quite this negative, generally lying between -10.0 and -12.0, but there is never-

Figure 10.8 Map of the southwestern United States and northwestern Mexico showing the boundaries of the three major $\delta^{18}O$ zones in relation to the distribution of some important W-skarn and porphyry-Cu ore deposits (see Newberry and Einaudi, 1981 and Titley, 1981). The terminology and symbols for the $\delta^{18}O$ zones are the same as in Figure 10.5 (Central Zone shown by cross-hatch pattern). Solid triangles indicate W-skarn deposits, and solid circles indicate porphyry-Cu deposits. The following porphyry-Cu deposits are indicated on the map: (1) Cananea, Sonora, Mexico; (2) Bisbee, AZ; (3) Santa Rita, NM; (4) Silver Bell, AZ; (5) Pima-Mission, AZ; (6) Morenci, AZ; (7) Ajo, AZ; (8) Ely, NV; (9) Battle Mountain-Copper Canyon, NV; (10) Bingham, UT; and (11) Butte, MT. Individual W-skarn deposits shown are: (12) Yellow Pine, ID; (13) Osgood Mountains, NV; (14) Mill City, NV; (15) Black Rock, CA; (16) Pine Creek, CA; and (17) Tungsten Hills, CA. The only major porphyry-Cu deposits that lie well outside the Eastern Zone are the Battle Mountain-Copper Canyon, NV deposit in the Central High-^{18}O Zone, and the Yerington, NV deposit in the Western Zone (see Figure 8.3). Also, although the Ely, NV porphyry-Cu deposit appears to lie within the Central S-type subzone, this locality actually lies within a small anomalous area having distinctly Eastern Zone $^{18}O/^{16}O$ characteristics ($\delta^{18}O \sim +8.5$). All of the W-skarn deposits lie within or adjacent to the High-^{18}O Central Zone, including several minor deposits not indicated on the map (e.g., Brown's Lake, ID, and Lost Creek, ID).

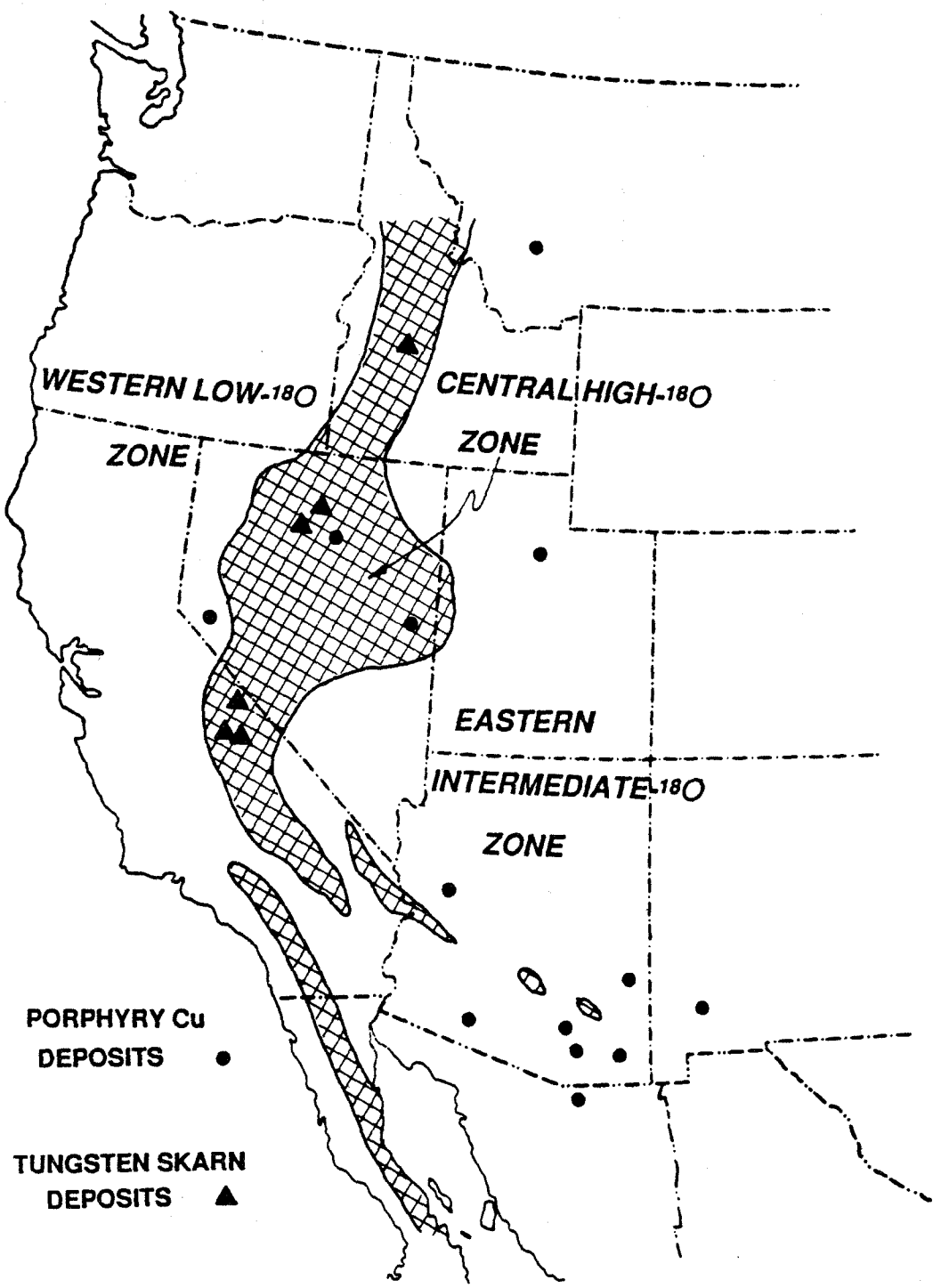
WESTERN LOW-18O ZONE
CENTRAL HIGH-18O ZONE
EASTERN INTERMEDIATE-18O ZONE
PORPHYRY Cu DEPOSITS
TUNGSTEN SKARN DEPOSITS

theless a general parallelism between the $\delta^{18}O$ zones and the ε_{Nd} contours. This disparity in ε_{Nd} between the northern and southern portions of the Eastern Intermediate-^{18}O Zone is likely due to differences in ages (and lithologies?) of the basement rocks in these two regions.

In summary, all of the isotopic systems investigated so far in the Mesozoic plutons of the North American Cordillera show systematic west-to-east variations, together with some north-south fine structure. Isotopic contours or isopleths can be drawn for all these systems, and they are characteristically subparallel to one another. Although in detail each of the isotopic parameters exhibits its own "fine structure," and although each is providing somewhat different constraints on source regions and magma genesis, it is clear that all of these isotopic systems are basically identifying the major source rocks or protoliths of the granitic magmas, and they are indicating that these protoliths tend to be fairly homogeneous within north- to northwest-trending zones parallel to the main Mesozoic structures. However, the isotopic ratios (and thus the nature of the protoliths) clearly change in a dramatic and sometimes an abrupt fashion from west to east across the strike of the magmatic arcs. In addition, an apparent late-Proterozoic rift basin in the east-central half of the NGB has resulted in a unique isotopic province for the Mesozoic plutons in that region (see below).

10.7 Mineral Deposits

The distribution of tungsten skarn deposits (Kerr, 1946; Newberry and Einaudi, 1981) and of Cretaceous or younger porphyry copper deposits (Lowell, 1974; Titley, 1981) in the southwestern United States closely coincides with the boundaries defined by the $\delta^{18}O$ zones. Figure 10.8 shows the location of major ore deposits in these two categories with

respect to the Eastern Intermediate-^{18}O Zone and the Central High-^{18}O Zone. The porphyry Cu deposits are essentially totally absent from the Central Zone. With two exceptions (the Yerington and Copper Canyon porphyry Cu deposits; Dilles, 1988; Batchelder, 1977), the major Cretaceous and Tertiary ore deposits of this type occur either well within the Eastern $\delta^{18}O$ Zone, or at the transition between the Central Zone and the Eastern Zone.

Tungsten skarn deposits, on the other hand, are virtually entirely restricted to the Central High-^{18}O Zone, and they conform to its trend. Newberry and Einaudi (1981) ascribed the localization of tungsten skarn deposits to the relatively deep levels of emplacement of the host plutons compared with the more "epizonal" nature of plutons hosting the major copper deposits. They attribute this to solubility and mass transport factors, which vary as a function of depth, as well as differences in the manner in which magmatic fluids evolve as a function of pressure. However, it is also obvious from the isotopic studies discussed above that there are major changes in the source protoliths of the magmas associated with these two types of ore deposits; it is thus logical to infer that the characteristics of the ore deposits might be even more directly related to compositional factors such as the variations in metal concentrations and metal/sulfur ratios in these magmas.

The plutons within the Central High-^{18}O Zone in general have features characteristic of depths of emplacement much greater than 2 to 3 km, whereas in the Eastern Intermediate-^{18}O Zone a large proportion of the plutons appear to be epizonal in nature. Many plutons in the Central Zone have intruded regionally metamorphosed rocks that have mineral assemblages characteristic of depths as great as 10 to 12 km or more

(Kistler et al., 1981; Hill, 1984; Sharry, 1981; Silver et al., 1979). Also, major pegmatitic zones are commonly associated with plutons within the Central Zone, as well as at the transition between the Central and Eastern Zones (Jahns, 1954; Dibblee, 1967c; Larsen, 1948). This indicates a difference in behavior between deep-seated exsolution of magmatic volatiles (forming pegmatites) and more shallow, epizonal exsolution (leading to vein-dominated porphyry hydrothermal systems; e.g., see Strong, 1980; Burnham, 1979). The porphyry copper deposits are a manifestation of the epizonal environment, while the tungsten skarn deposits are a manifestation of the deeper environments.

10.8 Characterization of Source Regions for the Various $\delta^{18}O$ Zones

The close association of so many geologic and isotopic features with the 3 major $\delta^{18}O$ zones that we have established in the southwestern United States provides some profound constraints on the nature of source regions for the Mesozoic plutons. It also gives some clues as to the distribution of these sources both laterally and with depth. The region may be viewed as a group of pre-existing "petrotectonic" rock assemblages, which have been intersected by zones of high heat flow related either to subsidence and burial, or to influx of mantle-derived magmas. These focused energy sources essentially "sample" the surrounding rock assemblages, mainly by melting the rocks, or as a result of mixing between the mantle-derived magmas and the anatectic magmas (perhaps by assimilating and exchanging with such rocks at depth?). The overall zoning with respect to oxygen isotopes, then, reflects gross lateral and vertical changes in the distribution of the petrotectonic assemblages (sources) within the continental crust.

Figure 10.9 (a) Plot of $[^{87}Sr/^{86}Sr]_i$ versus whole-rock $\delta^{18}O$ for granitic plutons in the Northern Great Basin (NGB) and Southern Basin and Range (SBR) Province; (b) Plot of ε_{Nd} versus whole-rock $\delta^{18}O$ for granitic plutons in the NGB; and (c) Plot of ε_{Nd} versus whole-rock $\delta^{18}O$ for granitic plutons in the SBR, all based on data given in Tables 1.1, 1.2, 5.1, 7.1, and 10.1. Boxes indicate the range of estimated isotopic compositions of source-region end-members discussed in the text (also, see Table 4.1 and Figure 10.11): OIA - Oceanic Island Arc/MORB-type source; SAV - eugeosynclinal sediment and altered volcanic-type source; MCM - metamorphosed cratonal-miogeosynclinal continental margin sediments (largely of Precambrian age in the NGB); SCL/LCC - Sub-continental lithospheric mantle/Lower Continental Crust-type source (assumed to be isotopically different in the NGB and the SBR; see text); MCC - Mid-level Continental Crust-type source. The data points are assigned to different envelopes based upon the 4 geographic $^{18}O/^{16}O$ zones and subzones defined in the test: Western Zone (WZ); Central V-type subzone (CZ-V); Central S-type subzone (CZ-S); and Eastern Zone (EZ).

A.

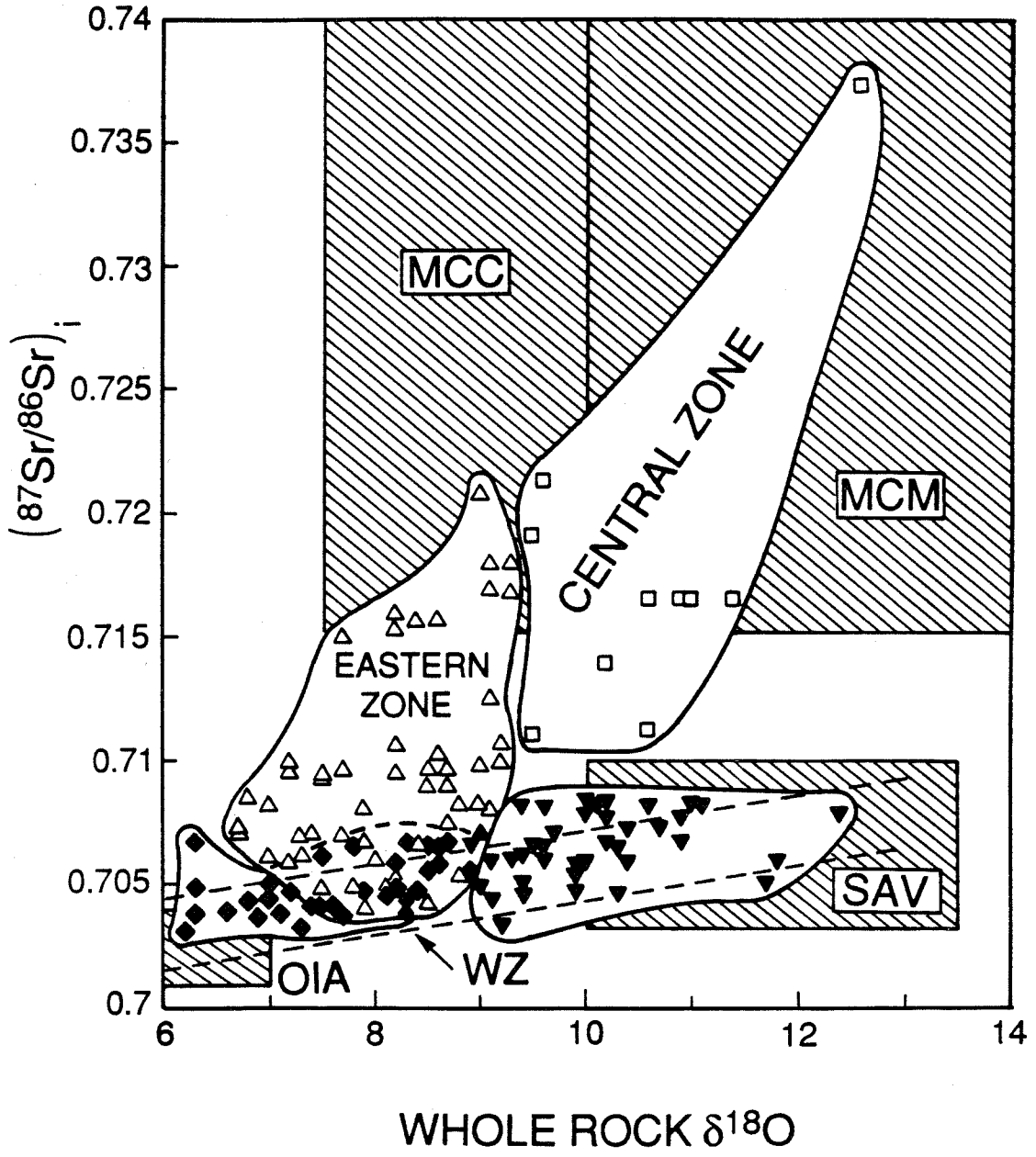
0.74
0.735
0.73
0.725
0.72
0.715
0.71
0.705
0.7
$(^{87}Sr/^{86}Sr)_i$
6
8
10
12
14
WHOLE ROCK $\delta^{18}O$
MCC
CENTRAL ZONE
MCM
EASTERN ZONE
SAV
OIA
WZ

B.

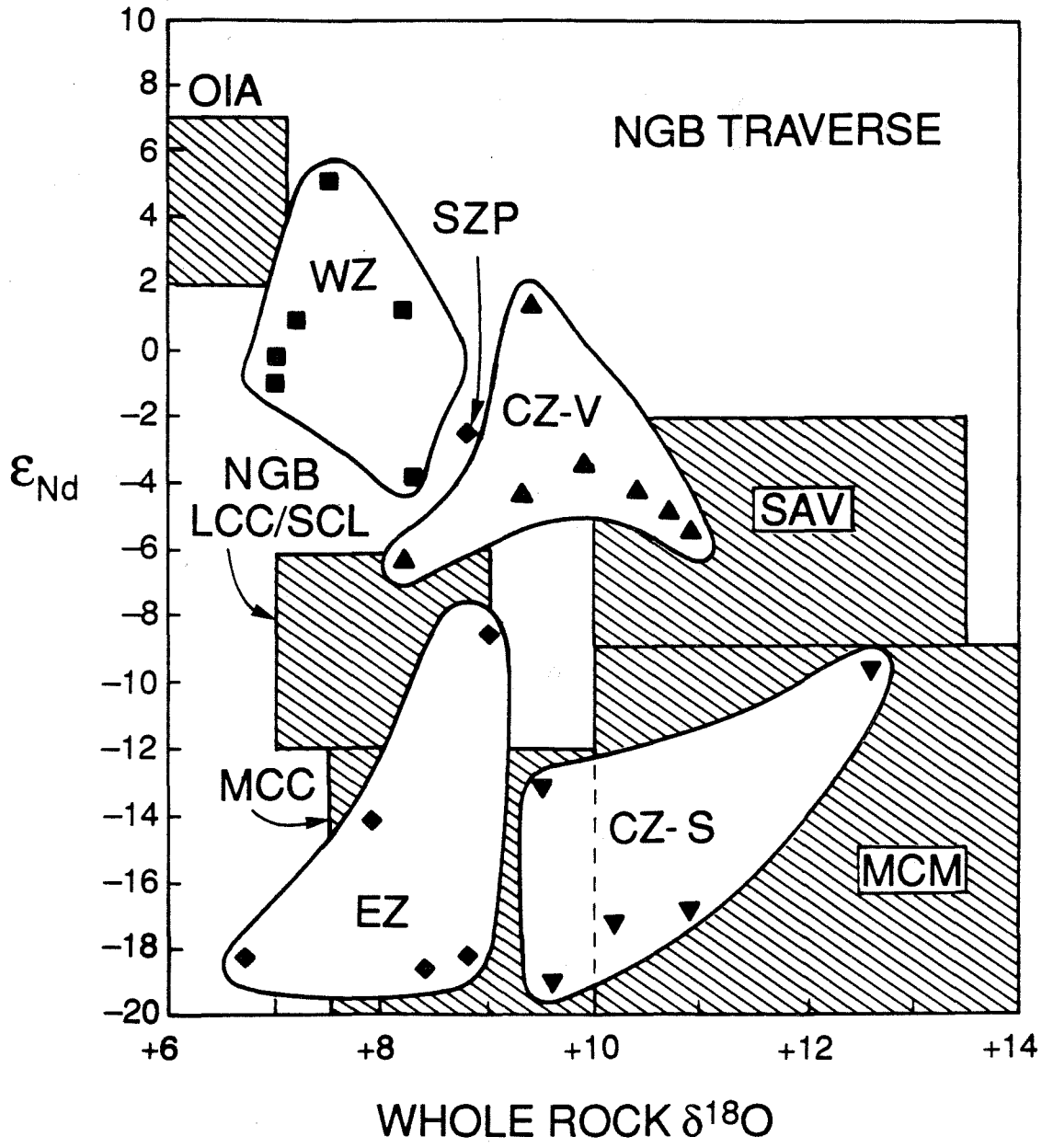
10
8
6
4
2
0
−2
−4
−6
−8
−10
−12
−14
−16
−18
−20
ε_{Nd}
OIA
NGB TRAVERSE
SZP
WZ
CZ-V
NGB
LCC/SCL
SAV
MCC
CZ- S
MCM
EZ
+6
+8
+10
+12
+14
WHOLE ROCK $\delta^{18}O$

c.

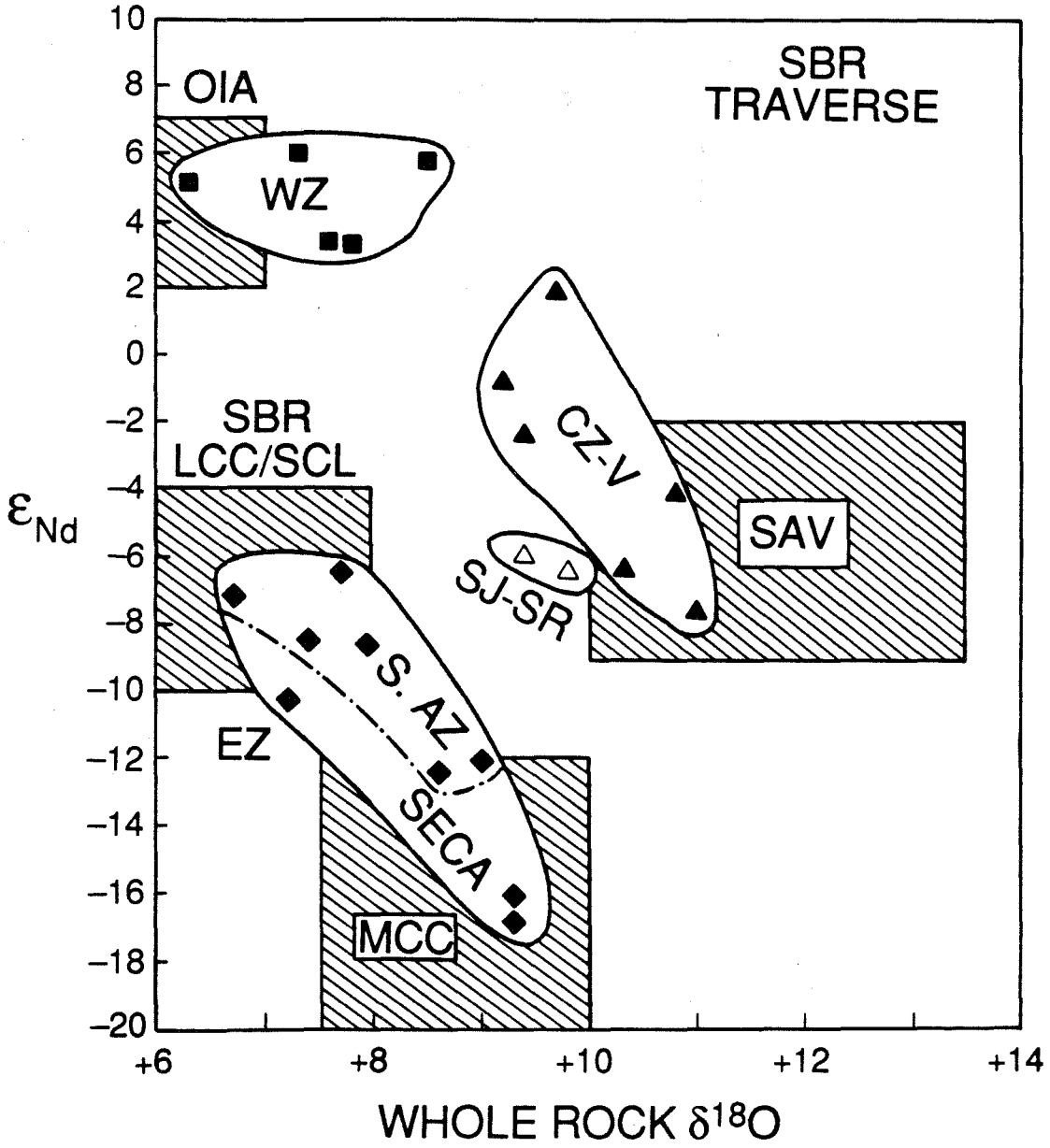
SBR
TRAVERSE
OIA
WZ
SBR
LCC/SCL
CZ-V
SAV
SJ-SR
S. AZ
SECA
EZ
MCC
ε_{Nd}
WHOLE ROCK $\delta^{18}O$
10
8
6
4
2
0
−2
−4
−6
−8
−10
−12
−14
−16
−18
−20
+6
+8
+10
+12
+14

In a general way, the existence of three major $^{18}O/^{16}O$ zones (one of which is readily divided into two separate subzones on the basis of $^{87}Sr/^{86}Sr$ values) implies that at least four major source components (shown in Figure 10.9) were important in the development of the batholiths. Given the enormous west-to-east changes that are known to have taken place in the geologic environments, where mafic and ultramafic rocks of the oceanic crust and mantle give way to an immensely thick sedimentary sequence, which in turn laps onto the crystalline basement of the craton, it is logical to assume that the major end-member components responsible for the $^{18}O/^{16}O$ zonation are:

(1) In the Western Low-^{18}O Zone, a source analogous to that which elsewhere throughout the circumpacific region has formed oceanic island-arc (OIA) magmas of calcic to calc-alkaline chemistry. Such magmas are forming today in the Aleutian, Marianas, and Japan arcs (see Taylor, 1986), and they clearly involve melting either of "fertile" upper mantle material or the subducted oceanic crust, or both, producing magmas with $\delta^{18}O$ around +6.0 to +7.0, but no higher than +7.5 per mil.

(2) In the Central High-^{18}O Zone, two distinct end members are required, both of which have to be derived from some combination of altered volcanic rocks and/or sedimentary rocks, as these are the only known rock types that are sufficiently abundant and also sufficiently high in ^{18}O to constitute viable source materials. It is therefore a distinct "plus" that the Central Zone also happens to geographically coincide with the great prism of high-^{18}O eugeosynclinal and miogeosynclinal sediments and volcanics that lies just to the west of the North American craton (Figure 10.5). Each of these two distinct end-members must be abundant enough to produce the voluminous Cretaceous-age magmas

that formed large portions of the major Cordilleran batholiths (e.g., the entire central Idaho Batholith, the entire eastern Peninsular Ranges Batholith, and much of the eastern part of the southern Sierra Nevada Batholith, as well as virtually all of the Mesozoic and Cenozoic plutons from the Northern Great Basin of central and eastern Nevada). On this basis, eugeosynclinal sedimentary and volcanic sections (SAV) provide a very reasonable source protolith for plutons of the Central Zone in the southern SNB, the eastern PRB, and the western NGB. This end-member component must have had a very high $\delta^{18}O$, at least from +10.0 to +13.0 per mil (and perhaps as high as +16.0), possibly averaging about +12.0; it must also have had a very narrowly circumscribed $^{87}Sr/^{86}Sr$ ratio of about 0.706 to 0.710 (i.e., not as low as MORB or OIA and nowhere near as high as Precambrian granitic rocks of the craton). Obviously, some relatively fresh, unaltered volcanic rocks could also exist locally in such a petrotectonic package, so in rare instances the $\delta^{18}O$ and $^{87}Sr/^{86}Sr$ values might approach pristine MORB-type values.

Note that a source material that is explicitly of basaltic to andesitic composition is required to the south where the Central High-^{18}O Zone occurs within the PRB, because in this area the plutons are dominantly tonalite (Silver et al., 1979; Taylor, 1986; Gromet and Silver, 1987). This constraint is relaxed farther to the north in the Great Basin of Nevada where the dominant lithologies are granodiorite to quartz monzonite; in that region, altered andesitic volcanic rocks and volcanogenic sediments would be permissible protoliths. Thus, SAV-type sources must be dominant in the western part of the CZ in the NGB and in the other parts of the CZ in California and Mexico, but a late-Precambrian sedimentary protolith (MCM, see Table 4.1) with much higher

$^{87}Sr/^{86}Sr$ and much lower ε_{Nd} must be the dominant source in the eastern portion of the CZ in the NGB and also in most of the CZ in the Idaho Batholith (see below). This $^{87}Sr/^{86}Sr$-rich protolith does not appear important as a source of granitic magmas for the major Cordilleran batholiths south of latitude 37°N, although high-$^{87}Sr/^{86}Sr$, high-^{18}O Mesozoic plutons are locally associated with the Cordilleran metamorphic core complexes. Also, note that granitic plutons with $\delta^{18}O \sim +12.9$ in the Halloran Springs area of eastern California seem to be directly associated with high-^{18}O sedimentary rocks of late Proterozoic age (Amargosa Aulacogen).

(3) In the Eastern Intermediate-^{18}O Zone the importance of the high-^{18}O CZ components is greatly diminished, and also an isotopically much more heterogeneous fourth "end-member" is required. This fourth "end-member" cannot be a single type of source-rock material. Locally it may be dominantly from the low-^{18}O lower continental crust (LCC), from the subcontinental upper mantle (SCL), from the middle continental crust (MCC), or from some combination of all these. This "end member" also must include the source material referred to as the "model lithospheric component" (MLC) by Hill et al., (1986).

Further comparison of the $\delta^{18}O$ zones with other isotopic parameters confirms the general conclusions listed above, specifically that the sources can be generalized as being made up of broadly defined end-member components. However, the additional isotopic data indicate a greater degree of "fine structure" and thus allow several subcomponents to be defined, as well. Figure 10.9 shows $\delta^{18}O$ plotted against both initial $^{87}Sr/^{86}Sr$ ratios (Figure 10.9a) and ε_{Nd} (Figures 10.9b and 10.9c) for all available data on Mesozoic plutons in the southwestern United States

Figure 10.10 Map of the western United States and northwestern Mexico showing the three $\delta^{18}O$ zones defined for Cretaceous and Cenozoic plutonic granitic rocks: Western Low-^{18}O Zone (WZ, horizontal-lined); Central High-^{18}O Zone (CZ, cross-hatch); and Eastern Intermediate-^{18}O Zone (EZ, random dash-stipple). Note that the CZ is divided into two subzones (see text): V-type on the west (dominantly in western Nevada and southern and Baja California) and S-type on the east (mainly in NE Nevada and Idaho). CC and SLC indicate Carson City, Nevada and Salt Lake City, Utah, respectively. Several major N-trending features are shown: the heavy dashed line near the California-Arizona border is a late Precambrian shear zone (slightly modified to better fit existing data) proposed by Bennett and DePaolo (1987). The heavy solid line in central Nevada is our hypothetical suture-zone (see text); this coincides with the $^{87}Sr/^{86}Sr$ "step" between the "transitional" and "miogeoclinal" zones of Farmer and DePaolo (1983). The dotted line in Utah is their proposed "miogeoclinal"-"craton" boundary. Also shown are the outcrops (solid black) and boundaries of several late Precambrian sedimentary basins (after Stewart, 1972, 1980): BSG = Belt Super Group; UMG = Uinta Mountain Group; AA = Amargosa Aulacogen of Kistler and Peterman (1978). Mojavia is the older (>2.0 Ga) terrane proposed by Bennett and DePaolo (1987) to have been transported southward along their proposed late Precambrian shear (see text). The heavy brackets define the NGB $^{18}O/^{16}O$ transect discussed in the text (see Chapter 9).

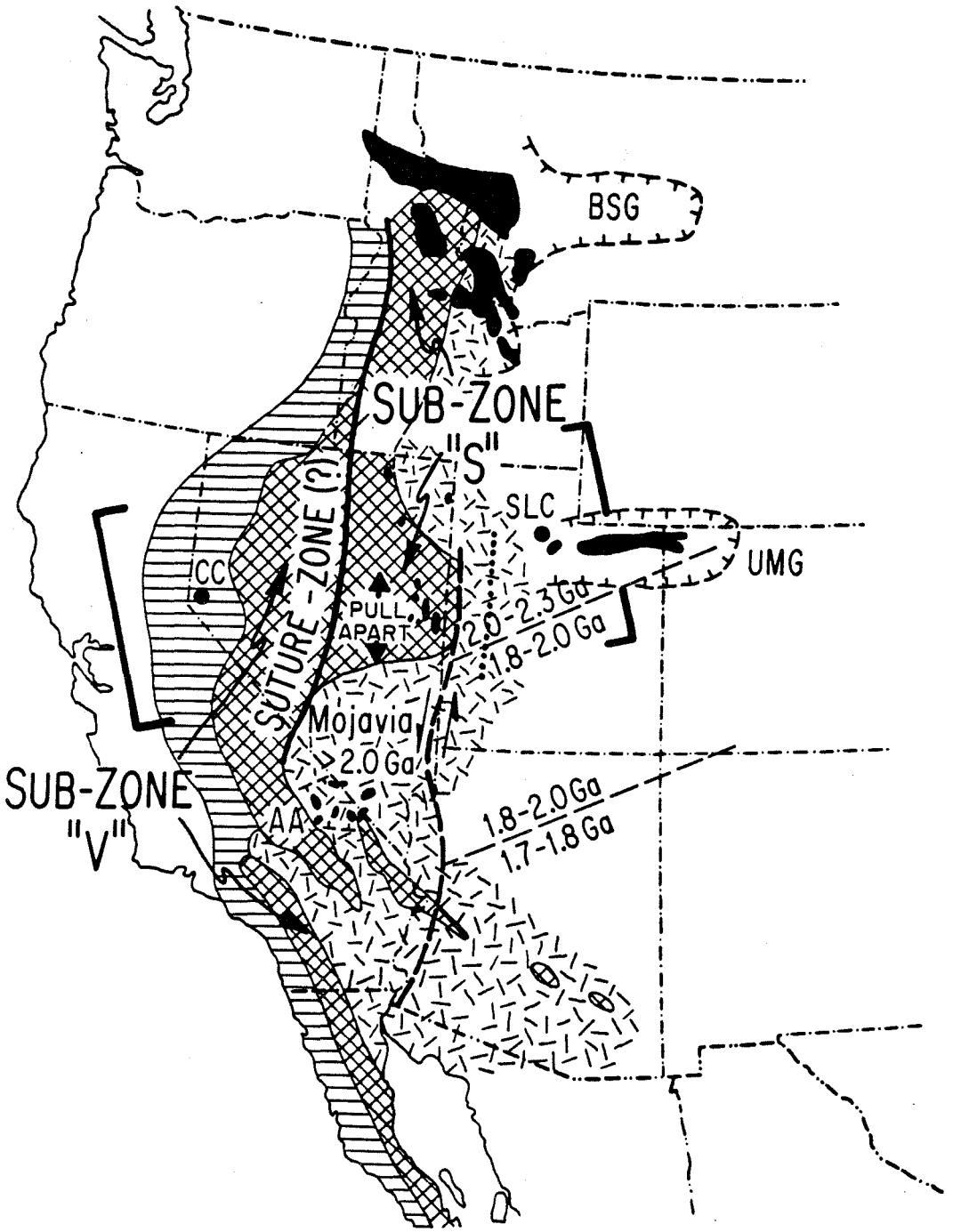
BSG
SUB-ZONE
"S"
SLC
UMG
CC
SUTURE-ZONE (?)
PULL-APART
2.0-2.3 Ga
1.8-2.0 Ga
Mojavia
2.0 Ga
SUB-ZONE
"V"
AA
1.8-2.0 Ga
1.7-1.8 Ga

(Masi et al., 1981; Lee et al., 1981a; Kistler et al., 1981; Taylor and Silver, 1978; Hill et al., 1986; Farmer and DePaolo, 1983, 1984; DePaolo, 1981a; see Tables 1.1, 1.2, 5.1, 7.1, and 9.1). The data in the figures are arranged geographically, according to location of the plutons in one or the other of the 3 major $\delta^{18}O$ zones: Western, Central, or Eastern. Also shown are likely compositions of rocks from the four overall source components listed above, including their subcomponents. These geologic end members may be compared with the map shown in Figure 10.10, and with the model cross-section shown in Figure 10.11 (modified from Figure 4.1), to obtain a feeling for the nature of the vertical and lateral variations in the possible source regions of the Cordilleran plutons.

As shown in Figure 10.9a, the plutons from the Western Low-^{18}O Zone and the V-type subzone of the Central High-^{18}O Zone (see Chapter 9 and Figure 10.10) display characteristics compatible with simple mixing between a component with $\delta^{18}O \sim +6.0$ per mil and $^{87}Sr/^{86}Sr \sim 0.7025$ and one with $\delta^{18}O \sim +13.0$ per mil (or slightly higher) and $^{87}Sr/^{86}Sr \sim 0.7080$. The only appropriate candidates would be an OIA or MORB-type "mantle" source for the former, and a "eugeosynclinal" SAV-type source material dominated by altered basalts and graywacke sandstones and mudstones for the latter (Taylor and Silver, 1978; Harmon and Halliday, 1980). This SAV component extends along the entire length of the Cordillera of the southwestern USA (see Figure 10.10), and it may also be locally present farther north in Idaho and Washington. A very important constraint on this end-member is that it cannot have had a $^{87}Sr/^{86}Sr$ ratio any higher than about 0.710, because an extrapolation of the trends shown in Figure 10.9 to such high $^{87}Sr/^{86}Sr$ values would require that this end-member have $\delta^{18}O > +18$, and there is no plausible source-rock

reservoir of sufficient size with such a high $^{18}O/^{16}O$ ratio known anywhere on Earth. It is worth pointing out that the extreme upper parts of the oceanic basaltic crust (upper 2 to 3 km) have exactly appropriate $\delta^{18}O$ values (Gregory and Taylor, 1981) and $^{87}Sr/^{86}Sr$ ratios (McCulloch et al., , 1980, 1981) for this protolith; thus, if large amounts of such basaltic material could somehow be tectonically scraped off a downgoing subducted slab and "plastered" onto the base of the craton, and if such materials could later be remelted, this would be a very appropriate source material, particularly for that part of the Central High-^{18}O Zone in the eastern half of the PRB (where the plutons are dominantly tonalitic). A relatively "straight line" correlation is exhibited by the WZ and CZ-V data point envelopes on Figure 10.9a, which are linearly distributed between the two end-member components discussed above; this suggests that the two end-members had roughly equal concentrations of strontium (ppm), at least within a factor of 2 (Taylor, 1980; Vollmer, 1976; also see Figure 8.7). This constraint is in fact consistent with the two source environments described above.

A subset of samples from the S-type subzone of the Central High-^{18}O Zone (see Chapter 9 and Figure 10.10) forms an array between the OIA-SAV trend and another apparent end-member; this latter component has a relatively high-$\delta^{18}O$ similar to SAV (~ +10.0 to +16.0 per mil), but much higher $^{87}Sr/^{86}Sr$ (~ 0.715 to 0.740). This subset of samples clearly demands a second type of high-^{18}O component, but instead of a dominantly "eugeosynclinal" (i.e., $^{87}Sr/^{86}Sr$ ~ 0.706-0.710) basaltic or andesitic end member, this component requires a much higher proportion of "miogeosynclinal" sediments shed from the craton ($^{87}Sr/^{86}Sr > 0.720$).

Farmer and DePaolo (1983) showed that this transition in $^{87}Sr/^{86}Sr$ values occurs very abruptly, just east of the Roberts Mountain Thrust in the Great Basin of Nevada (the $^{87}Sr/^{86}Sr$ "step", see Chapter 9), and they interpreted this feature as indicating the western edge of >1.5 Ga cratonal basement (as also did several previous workers; e.g., Kistler and Peterman, 1978). However, we believe that this $^{87}Sr/^{86}Sr$ "step" is not indicative of the edge of the craton, but instead represents a sharp structural boundary between immature, graywacke- and volcanic-dominated sediments on the west, and craton-derived miogeoclinal sediments on the east (see below, and Figures 10.10 and 10.11). The exact nature of the lower-^{18}O component in these particular plutons is very obscure in Figure 10.9a, because the data-point envelope for the S-type plutons is not "rooted" within the PRB trend, and thus is not directly represented in the PRB "model." Geographically, the high-^{18}O, high $^{87}Sr/^{86}Sr$ source component is also not recognized in any major way south of about 37°N. North of 37°N latitude, this S-type subzone source may be represented by a series of large sedimentary basins localized along the western rifted edge of the craton during late Precambrian time (e.g., the Belt Series sedimentary basin in Idaho and Montana).

We note that southern Nevada lies wholly within the Eastern Intermediate-^{18}O Zone (Mojavia of Bennett and DePaolo, 1987; see Figure 10.10) and that the CZ-EZ boundary trends east-west across south-central Nevada. This suggests that the distinct eastward bulge of the high-^{18}O Central Zone (and of Pb isotope province II, see Figure 10.7) in eastern Nevada is probably a primary feature that existed prior to Cenozoic Basin and Range extensional faulting; interestingly, this bulge has a trend grossly similar to the axis of the inferred basin of the late

Figure 10.11 Schematic east-west geologic cross section of the NGB, modified after Figure 4.1, and showing the source-region model in relation to the $^{18}O/^{16}O$ boundaries discussed in the text. The geology and source-region abbreviations are the same as in Figure 4.1, and defined in the text (see Table 4.1). The dashed lines above the cross-section indicate the positions of the WZ, CZ-V, CZ-S, and EZ boundaries, as determined by mapping the isotopic compositions of plutons (the dominant pluton-type in each terrane is indicated above the geologic section). The ranges for O, Sr, and Nd-isotopic compositions of the source-region end-members are indicated in the figure, and are based on actual measurements of country rocks by Taylor and Silver (1978), DePaolo (1981a), Farmer and DePaolo (1983; 1984), Kistler et al. (1981), Kistler and Swanson (1981), Lee et al. (1981a,b), Magaritz and Taylor (1976c), Hill et al. (1986), Peterman et al. (1967), Bennett and DePaolo, 1987, Eslinger and Savin, 1973, Sinha and Davis (1970); combined with inferences from our observations regarding isotopic data-arrays from plutons, as shown in Figures 8.7, 9.5, and 10.9. The "wavy" boundary separating the SAV and MCM source regions is the sharp, lithologic boundary within the Central High-^{18}O Zone in the vicinity of the $^{87}Sr/^{86}Sr$-step where plutons west of the boundary have $(^{87}Sr/^{86}Sr)_i < 0.708$, and those east of the boundary have $(^{87}Sr/^{86}Sr)_i > 0.710$. The section for the SBR would be similar, except the MCM component would not occur at depths greater than 10 km, and it would be much thinner and younger, as shown in the region labelled "cratonal platform sediments" (also see discussions for Figures 9.6, 10.9c, and 10.10).

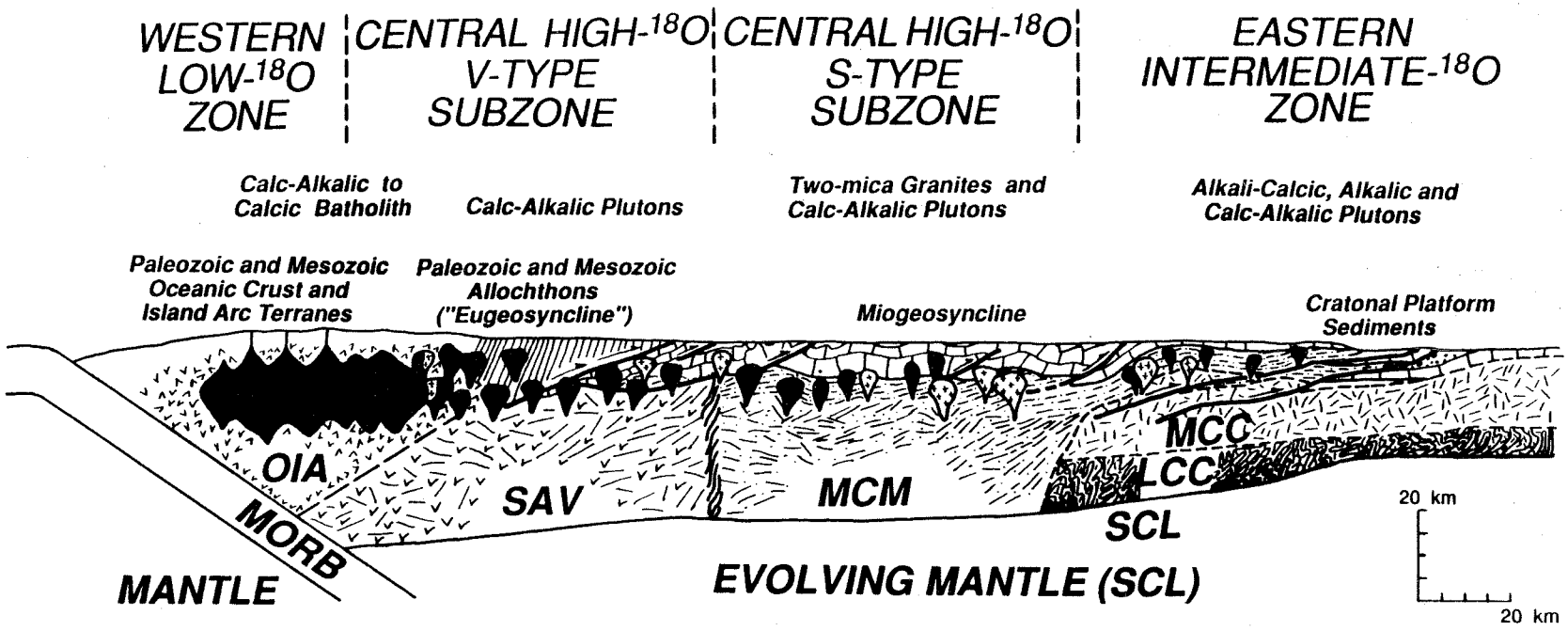

ISOTOPIC COMPOSITIONS (O; Sr; Nd)

	NGB			SBR
OIA-MORB	+6 to +7 ;	.702 to .704;	+2 to +7	Same
SAV	+10 to +13.5;	.703 to .710;	-2 to -9	Same
MCM	>+10;	>.715;	-9 to -20	Absent
MCC	+7.5 to +10;	>.715;	-12 to -20	Same
LCC-SCL	+7 to +9;	.705 to .710;	-6 to -12	+6 to +8; .705 to .710; -4 to -10

Precambrian Uinta Mountain Group (Stewart, 1972; see Figure 10.10). As a tentative hypothesis, we speculate that the S-type subzone in eastern Nevada represents the site of a late Precambrian basin that may have tectonically opened during the southward transport of Mojavia (Bennett and DePaolo, 1987); this would have allowed the deposition of a thick section of sediments in the "pull-apart" basin trailing the northern edge of Mojavia (Figure 10.10). Such rocks would have sufficiently high $\delta^{18}O$ values to be the protolith for the S-type subzone, and they would be comprised of material sufficiently old enough (having been shed from >2.0 Ga craton) to satisfy the ε_{Nd} and ε_{Sr} constraints discussed in Chapter 9, and shown in Figure 10.9. For example, Farmer and DePaolo (1983) emphasize the uniformity of ε_{Nd} values (-9 to -19) of the plutons in the "S" subzone, and we note that sedimentation is a well-recognized large-scale mixing process that could help to explain this kind of uniform isotopic source. It should also be pointed out that the S-type subzone is geographically related to source rocks of this type in Idaho, and although analogous outcrops in eastern Nevada are extremely sparse (McCoy Creek formation; see Miller et al., 1988; Kistler et al., 1981), the correlation may nevertheless be valid. If true, this points out the extreme usefulness of the combined-isotope approach to mapping subcrustal features.

The Eastern Zone array of data points (Figure 10.9; location of EZ shown on map, Figure 10.10) suggests mixing of a component having $\delta^{18}O$ ~ +6.5 to +8.5 and $^{87}Sr/^{86}Sr$ ~ 0.704 to 0.710 with a more heterogeneous end member having $\delta^{18}O$ > +9.0 and $^{87}Sr/^{86}Sr$ > 0.715. The first has characteristics that could apply to older, lower continental crust, or to upper mantle that has interacted with lower crust (Hill et al., 1986; Lee

and Christiansen, 1983; also see Chapters 8 and 9). The second would reflect the composition of an older, quartzofeldspathic to pelitic crystalline basement that resides at higher levels of the continental crust, as indicated by the $\delta^{18}O$ values higher than +9.0. This is graphically depicted in Figure 10.11, and we suggest that Eastern Zone melts may either originate at great depths ("dry") and ascend to form epizonal plutons, or may originate at moderate depths ("wet"), and crystallize as mesozonal plutons at depths near 10 km.

The plot of neodymium isotopic variations versus $\delta^{18}O$ reveals still more fine structure regarding source variations. Figure 10.9b shows data from a traverse across the Sierra Nevada Batholith all the way across the Basin and Range of Nevada and into western Utah (NGB traverse; see Chapter 9). This plot shows the available ε_{Nd} and $\delta^{18}O$ data plotted in relation to the $\delta^{18}O$ zones, and relative to the isotopic characteristics of the several end-member components inferred from Figure 10.9a. The Western Zone ε_{Nd} ranges from ~ +6.0 to as low as ~ -1.0 or lower. The EZ and CZ-V data-point envelopes provide a nice linkage between our OIA and SAV components on Figure 10.9b, confirming the mixing trend shown on Figure 10.9a. East of the $^{87}Sr/^{86}Sr$ "step" in the NGB, the Central Zone ε_{Nd} values become increasingly negative (~ -9.0 to as low as ~ -20.0), indicating mixing with Precambrian continental crustal material (Farmer and DePaolo, 1983); inasmuch as this material also has a very high $\delta^{18}O$ value, it must be largely of sedimentary derivation (MCM). The Eastern Intermediate-^{18}O Zone is characterized by ε_{Nd} between ~ -8.0 and ~ -19.0 and $\delta^{18}O$ between approximately +7.0 and +9.0, characteristics probably inherited from an LCC (or SCL) source.

The data shown on Figure 10.9b for the northern traverse indicate a remarkable anomaly in source composition when compared with the data shown in Figure 10.9c. The data in Figure 10.9c are taken from a traverse across southern Basin and Range (SBR) Province, beginning on the west with the PRB (see DePaolo, 1980), and continuing eastward into southeastern California and southern Arizona (see Tables 5.1 and 7.1). Western Zone and Central Zone plutons in the NGB show isotopic features similar to the analogous zones in the SBR traverse, as shown on Figure 10.9c. However, the "mixing arrays" for cratonal and upper mantle-lower crustal sources (after Hill et al., 1986) are distinctly different in these two broad areas. In the PRB, we observe a distinct transition within San Jacinto-Santa Rosa block, where $\delta^{18}O$ values decrease in the direction of a lower crustal end-member (which itself forms one end-member in an array connected to a cratonal MCC end-member). This effect is not apparent in the NGB traverse. In addition, for the SBR there is an apparent mixing array between an end-member at $\delta^{18}O$ between +7.5 and +10.0 and ε_{Nd} between -12.0 and -20.0 (termed cratonal MCC on the strontium plot in Figure 10.9a), and an end-member with the oxygen isotopic characteristics of the hypothetical upper mantle-lower crust component (LCC/SCL) shown on Figure 10.9a. This latter component appears to have ε_{Nd} between -4.0 and -10.0 and $\delta^{18}O$ between +6.0 and +8.0 per mil. The lower crustal NGB end-member appears to be isotopically distinct from that in the SBR (see discussion below), which indicates that in addition to the abrupt West-East variation (which defines the $^{18}O/^{16}O$ zones), there are some fundamental North-South differences in source regions, as well.

Table 10.1 Whole-rock ε_{Sr}, Sr (ppm), ε_{Nd}, and $\delta^{18}O$ data for Cordilleran granitic plutons from the southwestern U.S.A.

Data Reference[a]	ε_{Sr}[b]	Sr, ppm	1/Sr x 10,000	$\delta^{18}O$[c]	ε_{Nd}[d]
Triassic plutons: 200-210 Ma $\delta^{18}O$ Zones not defined					
KP73-9-CSNB	+13	498	20.08	+8.2	-3.5[e]
KP78-19-SSNB	-2	485	20.62	+7.5	--
KP78-14-SSNB	-4	382	26.18	+8.5	--
KP78-17-SSNB	-2	350	28.57	+7.9	--
KP78-22-WMD	-2	686	14.58	+8.3	--
KP78-25-WMD	+36	592	16.89	+7.3	--
KP78-23-WMD	+36	489	20.45	+7.7	--
KP78-24-WMD	+36	311	32.15	+8.3	--
Jurassic plutons: 145-180 Ma Western $\delta^{18}O$ Zone					
D87-Y767-NGB	-2	1268	7.89	+7.8[f]	--
D87-Y785-NGB	-6	1208	8.28	--	--
D87-Y788-NGB	-6	1179	8.48	--	--
D87-Y800-NGB	-5	1015	9.85	--	--
D87-Y753-NGB	-7	1007	9.93	--	--
D87-Y781-NGB	-7	987	10.13	+7.7[f]	--
D87-Y751-NGB	-7	941	10.63	--	--
D87-Y593-NGB	-7	634	15.77	--	--
D87-Y787-NGB	-10	587	17.04	--	--
V-type Central $\delta^{18}O$ Zone					
KP78-21-WMD	+30	261	38.31	+10.2	--
F&D83-10-NGB	+22	892	11.21	+9.3	-4.3
F&D83-12-NGB	+38	405	24.69	+10.4	-4.2
S-type Central $\delta^{18}O$ Zone					
F&D83-16-NGB	+133	126	79.37	+10.2	-17.3
Eastern $\delta^{18}O$ Zone					
F&D83-20-NGB	+78	693	14.43	+9.0	-8.6
KP78-16-SSNB	+54	731	13.68	+7.9	--
KP73-20-SSNB	+39	673	14.86	--	--
KP78-20-SSNB	+24	664	15.06	+5.6	--

Table 10.1, cont'd.

Data Reference[a]	ε_{Sr}[b]	Sr, ppm	1/Sr x 10,000	$\delta^{18}O$[c]	ε_{Nd}[d]
Jurassic Eastern $\delta^{18}O$ Zone, cont'd.					
KP73-30-SSNB	+71	652	15.34	--	--
KP78-18-SSNB	+24	339	29.50	+7.2	--
HHML-391-SECA	+59	1081	9.25	+6.8	--
F&D84-11-AZ	+40	381	26.25	+7.4	-8.5
F&D84-13-AZ	+40	218	45.87	+6.7	-7.2
F&D84-12-AZ	+46	134	74.63	--	-3.4
Cretaceous and younger plutons: <135 Ma Western $\delta^{18}O$ Zone					
KP73-28-CSNB	-16	482	20.75	+9.2	+6.5[e]
KP73-29-CSNB	0	432	23.15	+7.6	+3.3[e]
F&D83-6-NGB	+8.3	769	13.00	+7.0	-0.2
F&D83-7-NGB	+3.8	736	13.59	+7.2	+0.9
F&D83-3-NGB	+6	726	13.77	+8.2[g]	+1.2[e]
F&D83-2-NGB	-10	620	16.13	+7.5[g]	+5.1[e]
F&D83-5-NGB	+8.2	547	18.28	-0.2	-0.2
F&D83-4-NGB	-1	332	30.12	--	+2.5[e]
KP78-11-SSNB	+20	612	16.34	+8.2	--
SS87-12-SSNB	+9	583	17.15	+7.2	--
KP78-3-SSNB	-16	514	19.46	+7.3	+6.0[e]
SS87-13-SSNB	+9	504	19.84	+8.1	--
SS87-14-SSNB	+9	500	20.00	+7.6	--
KP78-2-SSNB	-1	399	25.06	+9.1	--
KP78-1-SSNB	-8	360	27.78	+8.3	--
SS87-11-SSNB	+8	330	30.30	+5.7	--
SS87-10-SSNB	+24	265	37.74	+7.8	--
V-type Central $\delta^{18}O$ Zone					
KP73-18-CSNB	+38	446	22.42	--	--
KP78-15-WMD	+31	848	11.79	+10.3	-6.3[e]
KP78-10-WMD	+47	609	16.42	+10.0	--
F&D83-9-NGB	+19	706	14.16	+9.9	-3.4
F&D83-13-NGB	+33	648	15.43	+10.9	-5.4
F&D83-8-NGB	+7.9	528	18.94	+9.4	+1.4
F&D83-11-NGB	+39	436	22.94	+10.7	-4.8
F&D84-4-NGB	+65	388	25.77	+9.1[fhi]	-6.4
F&D84-5-NGB	+60	313	31.95	--	-6.3
KP78-7-SSNB	+44	737	13.57	+10.9	--
SS87-15-SSNB	+8	709	14.10	+8.6	--
KP78-8-SSNB	+51	695	14.39	+10.6	--
KP78-9-SSNB	+37	634	15.77	+9.7	--

Table 10.1, cont'd.

Data Reference[a]	ε_{Sr}[b]	Sr, ppm	1/Sr x 10,000	$\delta^{18}O$[c]	ε_{Nd}[d]
Cretaceous and younger V-type Central $\delta^{18}O$ Zone, cont'd.					
SS87-6-SSNB	+38	578	17.30	+10.1	--
SS87-1-SSNB	+41	562	17.79	+11.3	--
KP73-22-SSNB	+34	470	21.28	--	--
KP73-23-SSNB	+28	416	24.04	+9.6	--
SS87-7-SSNB	+22	399	25.06	+8.6	--
KP73-26-SSNB	+7	396	25.25	+7.8	+0.6[e]
SS87-8-SSNB	+28	392	25.51	+9.6	--
SS87-9-SSNB	+34	388	25.77	+9.1	--
SS87-4-SSNB	+21	360	27.78	+10.1	--
KP78-6-SSNB	+20	349	28.65	+10.4	--
KP78-12-SSNB	+8	347	28.82	+11.7	--
KP73-25-SSNB	+54	343	29.15	+11.0	-7.6[e]
KP78-13-SSNB	+16	341	29.33	+8.5	--
SS87-5-SSNB	+19	341	29.33	+9.1	--
KP78-4-SSNB	+25	249	40.16	+9.4	-2.4[e]
KP78-5-SSNB	+13	238	42.02	+9.9	--
KP73-24-SSNB	+53	203	49.26	+9.4	--
KP73-21-SSNB	+37	130	76.92	--	--
S-type Central $\delta^{18}O$ Zone					
F&D83-15-NGB	+466	86	116.28	+12.6	-9.7
F&D83-14-NGB	+93	406	24.63	+9.5	-13.2
F&D83-21-NGB	+238	355	28.17	+9.6	-19.1
F&D83-17-NGB	+131	393	25.45	+5.8	-16.9
F&D83-22-NGB	+171	349	28.65	+10.9	-16.9
Eastern $\delta^{18}O$ Zone					
S&H78-16-CMB	+60	1209	8.27	--	--
F&D84-28-CMB	+24	1087	9.20	--	-5.4
S&H78-11-CMB	+41	1079	9.27	--	--
S&H78-1-CMB	+43	941	10.63	--	--
S&H78-15-CMB	+39	925	10.81	--	--
S&H78-2-CMB	+32	812	12.32	--	--
S&H78-9-CMB	+48	802	12.47	--	--
S&H78-8-CMB	+28	801	12.48	--	--
S&H78-5-CMB	+37	600	16.67	--	--
S&H78-10-CMB	+38	591	16.92	--	--
S&H78-7-CMB	+57	557	17.95	--	--
S&H78-6-CMB	+46	544	18.38	--	--
S&H78-14-CMB	+55	541	18.48	--	--
S&H78-12-CMB	+62	537	18.62	--	--
S&H78-3-CMB	+89	483	20.70	--	--

Table 10.1, cont'd.

Data Reference[a]	ε_{Sr}[b]	Sr, ppm	1/Sr x 10,000	$\delta^{18}O$[c]	ε_{Nd}[d]
Cretaceous and younger Eastern $\delta^{18}O$ Zone, cont'd.					
F&D84-29-CMB	+10	419	23.87	--	-8.4
S&H78-4-CMB	+75	318	31.45	--	--
S&H78-13-CMB	+104	93.1	107.41	--	--
F&D83-23-NGB	+41	1497	6.68	+6.4[fhj]	-18.3
F&D83-25-NGB	+39	1150	8.70	+7.9	-14.2
F&D83-18-NGB	+15	920	10.87	+8.8[f]	-2.5
F&D83-24-NGB	+55	570	17.54	+8.8	-18.3
F&D84-6-NGB	+66	365	27.40	+7.6[fhj]	-18.4
F&D83-19-NGB	+160	316	31.65	+8.4	-18.7
F&D84-7-NGB	-3	263	38.02	--	+0.7
F&D84-2-NRM	+47	978	10.22	--	-14.2
F&D84-3-NRM	+82	396	25.25	--	-29.9
F&D84-1-NRM	+30	119	84.03	--	-6.1
F&D84-26-AZ	+65	644	15.53	--	-8.6
F&D84-15-AZ	+74	628	15.92	+7.7	-6.5
F&D84-14-AZ	+54	615	16.26	--	-7.6
F&D84-23-AZ	+45	593	16.86	+8.2[h]	-8.3
F&D84-27-AZ	+41	540	18.52	--	-6.0
F&D84-22-AZ	+50	535	18.69	+8.0[fhk]	-6.9
F&D84-24-AZ	+80	403	24.81	+6.5[hl]	-8.1
F&D84-20-AZ	+59	388	25.77	--	-6.7
F&D84-9-AZ	+110	365	27.40	--	-11.0
F&D84-25-AZ	+57	360	27.78	+6.7[hl]	-7.7
F&D84-16-AZ	+111	313	31.95	--	-10.0
F&D84-21-AZ	+141	278	35.97	+9.3[fhk]	-5.6
F&D84-18-AZ	+108	197	50.76	--	-9.8
F&D84-17-AZ	+232	163	61.35	+9.0	-12.1
F&D84-8-AZ	+113	120	83.33	+9.5[fhk]	-12.2
F&D84-19-AZ	+162	66	151.52	+8.6	-12.4
CM-504-SECA	+79	830	12.05	+7.2	-10.3[m]
CDN86-03-SECA	+68	805	12.42	--	--
KHML-405-SECA	+75	797	12.55	+8.5	--
KHML-389-SECA	+75	780	12.82	+8.7	--
KHML-396-SECA	+72	776	12.89	+8.2	--
KHML-388-SECA	+89	724	13.81	+8.2	--
CM-497-SECA	+57	550	18.18	+4.7	--
KHML-404-SECA	+55	547	18.28	+7.0	--
CM-494-SECA	+91	530	18.87	+9.2	-12.4[m]
CDN86-16-SECA	+75	515	19.42	--	--
CM-498-SECA	+68	487	20.53	+8.7	--
KHML-397-SECA	+84	461	21.69	+8.6	--
KHML-398-SECA	+75	407	24.57	+7.2	--
CDN86-024-SECA	+92	352	28.41	--	--
CM-491-SECA	+164	330	30.30	+8.2	--

Table 10.1, cont'd.

Data Reference[a]	ε_{Sr}[b]	Sr, ppm	1/Sr x 10,000	$\delta^{18}O$[c]	ε_{Nd}[d]
Cretaceous and younger $\delta^{18}O$, cont'd.					
CDN86-GR175-SECA	+84	323	30.96	+9.9[l]	--
KHML-390-SECA	+152	246	40.65	+7.7	--
F&D83-W311-SECA	+193	240	41.67	+9.3[h]	-16.8
CM-189-SECA	+179	218	45.87	+9.1	--
KHML-392-SECA	+154	201	49.75	+8.2	--
BD87-W236-SECA	+177	122	81.97	+9.3[h]	-16.0[n]
CM-492-SECA	+193	47	212.77	+9.1	--
KP78-29-SSNB	+26	970	10.31	--	--
KP73-19-SSNB	+31	712	14.04	+8.4	--

[a] References are cited as follows: BD87 (Bennett and DePaolo, 1987); CDN86 (Calzia et al., 1986); D87 (Dilles, 1987); F&D83 (Farmer and DePaolo, 1983); F&D84 (Farmer and DePaolo, 1984); KHML (Keith Howard and Marvin Lanphere, unpublished data); CM (Miller, et al., 1989); J89 (John, 1989); KP73 (Kistler and Peterman, 1973); KP78 (Kistler and Peterman, 1978); SH78 (Simmons and Hedge, 1978); SS87 (Saleeby et al., 1987). Geologic regions are: AZ=Arizona; CMB=Colorado Mineral Belt; CSNB, SSNB=Central and Southern Sierra Nevada batholith; NGB=Northern Great Basin; NRM=Northern Rocky Mountains; SECA=Southeastern California; WMD=Western Mojave Desert. Sample numbers are taken from map listings, those with corresponding $\delta^{18}O$ measured in this thesis show the GCS sample number from Table 1, (appendix).
[b] Calculated from equation in Farmer and DePaolo, 1983.
[c] SSNB, CSNB and WMD data from Masi et al., 1981 except samples from Saleeby et al., 1987; NGB, SECA and AZ data from this thesis, except where noted.
[d] ε_{Nd} data from Farmer and DePaolo, 1983, 1984 except where noted.
[e] ε_{Nd} from DePaolo, 1981a.
[f] Whole-rock $\delta^{18}O$ calculated from quartz $\delta^{18}O$ using +1.2 per mil fractionation (see Chapter 3).
[g] Whole-rock $\delta^{18}O$ from Masi et al., 1981.
[h] Whole-rock $\delta^{18}O$ from same pluton, not same sample.
[i] Quartz $\delta^{18}O$ from Batchelder, 1977.
[j] Quartz $\delta^{18}O$ from Bowman et al., 1987.
[k] Quartz $\delta^{18}O$ from Sheppard et al., 1971.
[l] Whole-rock $\delta^{18}O$ from Lee et al., 1981a.
[m] ε_{Nd} reported by Miller et al., 1989.
[n] ε_{Nd} from Bennett and DePaolo, 1987.

Figure 10.12 Plots of ε_{Sr} versus 1/Sr X 10,000 (ppm) for Cretaceous and Cenozoic granitic plutons in: (a) the Northern Great Basin (NGB); and (b) the Southern Basin and Range (SBR) Province, based on data given in Table 10.1. The data are shown in different envelopes based on assignment into one of the $^{18}O/^{16}O$ zones (see text, and Figures 9.6 and 10.10): WZ - Western Low-^{18}O Zone; CZ-V - Central High-^{18}O V-type subzone; CZ-S - Central High-^{18}O S-type subzone; and EZ - Eastern Intermediate-^{18}O Zone. Rectangular boxes show the compositions chosen by Farmer and DePaolo (1983) for model mantle (MM - ε_{Sr} = -22; Sr = 440 ppm) and model crust (MC - ε_{Sr} = +200; Sr = 200 ppm). The heavy solid and heavy dashed lines show the trends of the most "primitive" granitic plutons in each geographic region (NGB versus SBR); these lines are termed "Mantle Mixing Lines", as they probably indicate the evolved nature of Sub-Continental Lithospheric Mantle (SCL) or extreme Lower Continental Crust (LCC) [region B on diagrams], as compared with the compositions of OIA-type sources [region A on diagrams]. Further, there appears to be a distinct difference in this "evolved" end-member between the two geographic regions (NGB vs. SBR; see text).

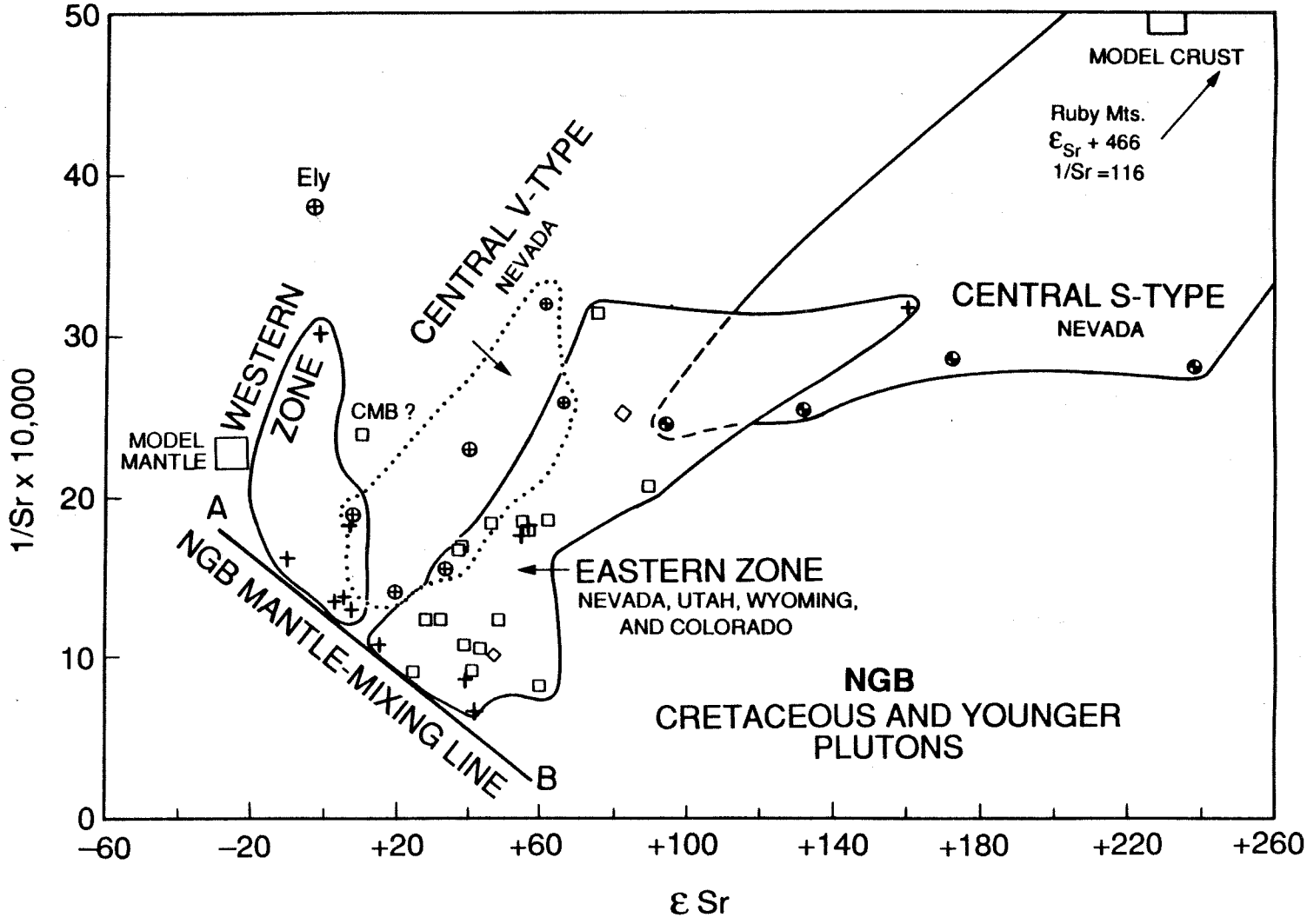
50
40
30
20
10
0
1/Sr x 10,000
–60
–20
+20
+60
+100
+140
+180
+220
+260
ε Sr
MODEL CRUST
Ruby Mts.
ε_{Sr} + 466
1/Sr =116
Ely
CENTRAL V-TYPE
NEVADA
CENTRAL S-TYPE
NEVADA
WESTERN ZONE
CMB ?
MODEL MANTLE
A
B
NGB MANTLE-MIXING LINE
EASTERN ZONE
NEVADA, UTAH, WYOMING,
AND COLORADO
NGB
CRETACEOUS AND YOUNGER
PLUTONS

A.

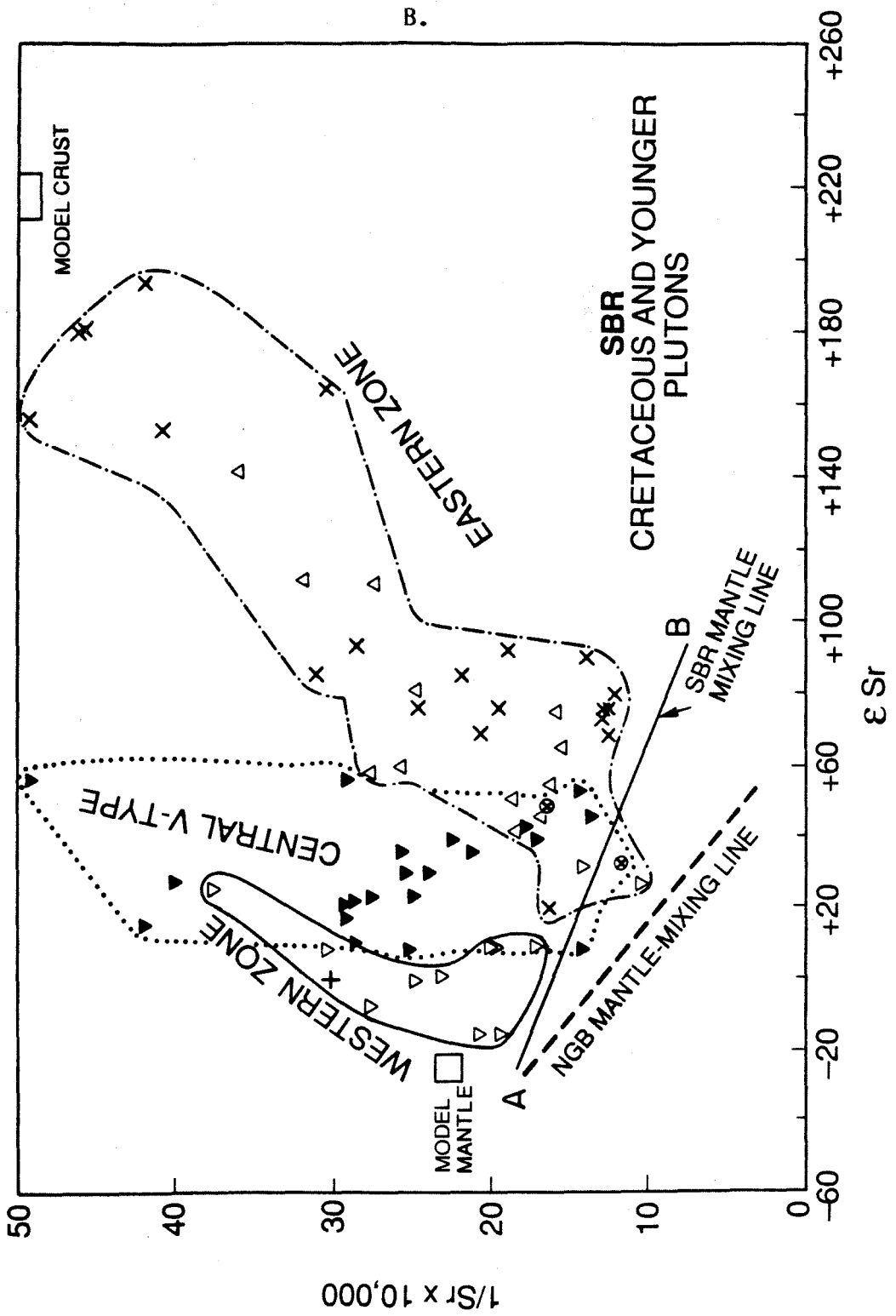
B.
MODEL CRUST
EASTERN ZONE
SBR
CRETACEOUS AND YOUNGER
PLUTONS
SBR MANTLE
MIXING LINE
B
CENTRAL V-TYPE
WESTERN ZONE
MODEL
MANTLE
A
NGB MANTLE-MIXING LINE
1/Sr x 10,000
ε Sr
50
40
30
20
10
0
+260
+220
+180
+140
+100
+60
+20
−20
−60

The evidence for N-S differences in the EZ source regions becomes even more compelling when we look at the ppm strontium - $(^{87}Sr/^{86}Sr)_i$ system (see Table 10.1). Figure 10.12 shows a plot of 1/Sr (ppm) versus ε_{Sr} for Cretaceous and younger granitic plutons in the NGB and SBR traverses, with the data grouped according to our $\delta^{18}O$ zones. The data envelopes for the WZ, CZ (V-type and S-type subzones), and EZ each form distinct groupings on these plots, but these groupings do not appear to be related to any AFC or mixing process between the model crust and mantle components as defined by Farmer and DePaolo (1983; see also discussion in Chapter 9). In both the SBR and the NGB (particularly in the SBR!), the WZ and Central V-type subzone (CZ-V) plutons (on Fig. 10.12) form arrays which, though broad, are oriented nearly vertical at a uniform ε_{Sr} value of about +10 to +40, extending from 1/Sr values of about 12 to 18 to values as high as 35 to 50. In contrast, the EZ plutons in both of these broad areas form arrays with distinctly shallower, positive slopes, extending from relatively low ε_{Sr} values of about +20 to much higher values of +100 to +180. The Central S-type subzone (CZ-S samples) overlap the values of the EZ plutons, but the CZ-S envelope does not define a clear-cut trend projecting toward the heterogeneous "end member" at 1/Sr = 5 to 15 and ε_{Sr} = 0 to +40 that appears to be common to the EZ plutons from both the NGB and SBR. It seems certain from diagrams like Figure 10.12 that several kinds of low-^{18}O, low-$^{87}Sr/^{86}Sr$ "primitive" end members are probably required for plutons in the different $^{18}O/^{16}O$ zones we have defined in the Cordillera. The isotopic differences between these various low-$^{87}Sr/^{86}Sr$ "end members" are, however, nowhere near as large as for the different high-$^{87}Sr/^{86}Sr$ "end members" that we infer for each of the $^{18}O/^{16}O$ zones (Figures 10.9, 10.11, and 10.12).

Some N-S and E-W source differences for these Cordilleran plutons are also suggested when one examines the low 1/Sr region on Figure 10.12. In the NGB, the 1/Sr - ε_{Sr} coordinates of the WZ, CZ-V, and EZ plutons all appear to be rooted along a linear trend, which for purposes of discussion is termed "NGB Mantle Mixing Line." This "line" defines the lower boundary envelope for all of the NGB samples on this diagram; in contrast to the positive trends of the individual data-point envelopes on Figure 10.12, this "line" has a negative slope, such that ε_{Sr} increases as we move from west to east (WZ-CZ-EZ). In other words, the most "primitive" strontium isotopic compositions in each data-point envelope are associated with distinctly higher ppm Sr values as we move east. This suggests that, beneath the EZ, the NGB upper mantle (or lower crust) source region for these plutons is producing magmas that are strikingly enriched in strontium compared with what is occurring beneath the WZ and CZ-V. Overall, the EZ magma source in the NGB also seems to be slightly more Sr-rich than in the SBR, because in the SBR all of these data-point envelopes are rooted along a line with a somewhat shallower negative slope than that defined by the NGB data-point envelopes (Figure 10.12). Thus, there appears to be a distinct difference between the EZ primitive sources in these two broad regions of the southwestern Cordillera of the United States, as evidenced by both the ε_{Nd} - $\delta^{18}O$ and the 1/Sr - ε_{Sr} diagrams. The relatively scattered nature of the data-point arrays from the EZ and CZ-S on Figure 10.12 probably indicates that the strontium (ppm) contents of the high-$^{87}Sr/^{86}Sr$ end-member components were also highly variable.

As a final note, we want to compare the $\delta^{18}O$ and Sr (ppm) differences in the SCL (or LCC) end-members (see Figures 10.9b and 10.12) be-

tween the NGB EZ and the SBR EZ. Because the oxygen isotopic signatures of these various terranes may allow us to distinguish between upper and lower crust, we may tentatively infer a link between the lower crustal source in Arizona and that in southeastern California, one that appears to have a different $\delta^{18}O$ signature from its northern Nevada counterpart (NGB: +7.0 to 9.0; SBR: +6.0 to 8.0). The existence of a common SCL or LCC end-member (at least in terms of $\delta^{18}O$) in southeastern California and southern Arizona implies that the $^{18}O/^{16}O$ composition of this lower crustal component in the SBR was acquired after the tectonic movements proposed by Bennett and DePaolo (1987). This means that: (1) a relatively low-^{18}O source conceivably could have underplated the SBR (including Mojavia) after tectonic emplacement of Mojavia athwart the southern Arizona terrane (as defined by its ε_{Nd} characteristics); or (2) previous fusion events could have modified the SBR deep sources such that $\delta^{18}O$ decreased markedly between 1.5 and 1.0 Ga, compared with their counterparts in the NGB. We tend to favor the latter explanation, simply because there have been two periods of late Precambrian fusion (1.4 Ga and 1.1 Ga; Silver, 1977; L.T. Silver, pers. comm.) in the SBR that do not really have counterparts in the NGB. The 1.4 Ga event produced anorogenic granites with $\delta^{18}O$ = +8 to +10 (Lee et al., 1981) which possibly could have left mafic restite material with sufficiently low $^{18}O/^{16}O$ to account for the $\delta^{18}O$ differences seen during Mesozoic fusion. The 1.1 Ga event produced mafic dike swarms in Arizona, and is responsible for anorthositic rocks in the San Gabriel Mountains, California. We wonder if somehow this latter event didn't fractionally deplete strontium in the SBR crust such that, much later, the Mesozoic SBR granitic plutons would form from a source with a lower Sr content than that associated with the NGB granitic plutons (see Figure 10.12).

Summing up, in addition to considerable "isotopic fine-structure" in the various source regions previously alluded to, consideration of the Nd, Sr, and Pb isotope data within the context of our three major $\delta^{18}O$ zones seemingly allows at least five major end-member components to be distinguished in the Cordillera of the southwestern USA, as enumerated in Figure 10.11 and as follows: (1) An oceanic-type, upper mantle OIA component, which is by far the dominant end member recognized in the Western Low-^{18}O Zone all along the western edge of the batholith belt. (2) A "eugeosynclinal"-type SAV sedimentary and volcanic rock component (probably Paleozoic to Mesozoic in age), which mixes with the OIA component and is dominant in the CZ-V subzone all the way from Baja California at least to the Nevada-Idaho border. (3) A craton-derived, miogeosynclinal sedimentary source (MCM), which dominates the large areas of CZ-S subzone in Idaho and Nevada (this source must be Precambrian in age in most of the NGB and Idaho, so we can locally refer to this as the PC-MCM component). (4) A heterogeneous, lower continental crystalline basement source (LCC) or upper mantle source (SCL) with similar isotopic characteristics; this is the dominant component in the EZ, but there is also a likely input from a more mafic magmatic component from the subcontinental asthenospheric mantle or possibly from a subduction zone that penetrated a considerable distance eastward beneath the continent. (5) A higher-level component from the middle continental crust (MCC) that locally mixes with component (4) throughout the EZ, and which becomes particularly important locally in the metamorphic core complexes. This MCC component locally has some of the same isotopic and chemical characteristics as component (3), and hence it must in some cases include a significant proportion of sedimentary or metasedimentary rocks.

CHAPTER 11. CONCLUSIONS AND IMPLICATIONS FOR FUTURE STUDIES

11.1 Possible Future Studies

The sharp isotopic boundaries observed between different geographic groupings of granitic plutons in the Northern Great Basin (NGB) and Southern Basin and Range (SBR) of western North America clearly demonstrate that combined stable isotope and radiogenic isotope studies can be profitably used as remote-sensing "probes" to provide detailed information on lithologic boundaries at depth in continental crust. This can be done even though we still lack an exact understanding of the processes that produced these geochemical signatures, particularly with regard to the varying effects of source-rock lithology, assimilation-fractional crystallization (AFC), and mixing of magmas (Taylor, 1980; Silver et al., 1979; Farmer and DePaolo, 1983, 1984; Taylor and Sheppard, 1986; Criss and Fleck, 1987). However, because of these complicating factors, in order to gain a full understanding of the genesis of granitic plutons in the North American Cordillera and in other regions of the world, much more isotopic research is required. It is appropriate here to discuss some logical avenues for further research.

Perhaps the most fruitful area of research that could help clarify the above processes would be detailed isotopic studies of the various proposed source-region end-members. For example, to better understand the trends of the data-point envelopes in Figure 10.12, it would be necessary to measure Sr (ppm) and $^{87}Sr/^{86}Sr$ (corrected to the time of magma generation) for the panoply of potential source rocks that exist in each of the $\delta^{18}O$ zones within the Cordillera, and especially in the Great Basin, where all four of the major $\delta^{18}O$ zones and subzones exist. Simi-

larly, Nd, Pb, and oxygen isotope data should also be obtained on the same kinds of country rock samples. Obviously such studies will involve very difficult sampling problems, particularly in order to characterize the petrotectonic assemblages in the lower crust and upper mantle. Careful studies are required of xenolith populations in areas of explosive volcanism and of terranes where erosion has exposed the deep crust (e.g., the metamorphic core complexes). These sorts of studies are locally now underway (e.g., Wickham and Taylor, 1988), and should provide much useful information.

Another line of research, where more detailed work would be very beneficial to our understanding of Cordilleran magmatism, is a much more complete isotopic study of the early Mesozoic granitic rocks. As discussed in Chapter 7, we have identified several prominent low-^{18}O zones within the Jurassic magmatic arc in southeastern California, but outside of the heavily altered Rodman-Ord Mountains area, our sampling density is very low. An interesting study would be to map $\delta^{18}O$ values along the strike of the Jurassic arc from southern Arizona to western Nevada, and to combine the results with $^{87}Sr/^{86}Sr$ analyses. This way, we might be able to trace the impingement of the arc onto the continent by observing where the $\delta^{18}O$ values change as a result of the transition from sea water-related, high-^{18}O hydrothermal fluids to low-^{18}O meteoric-hydrothermal fluids. Analyses of $(^{87}Sr/^{86}Sr)_i$ could also be indicative of this transition onto the craton. Detailed isotopic studies would also help clarify differences in source regions between the Jurassic and the Cretaceous batholiths, and also would provide a better regional $^{18}O/^{16}O$ map for structural studies (e.g., westward tectonic transport of Jurassic terranes in the Mojave Desert, and possible left-lateral displacements on mega-shears; see Chapters 7 and 10).

The present data set for > 135 Ma plutons is simply too scanty at present to come to any firm conclusions about the isotopic differences between these plutons and the < 135 Ma plutons from the same geographic areas. Nevertheless, it certainly appears that the Jurassic (and Triassic) magmas in general had lower $\delta^{18}O$ values than their Cretaceous counterparts, as well as having been "drier" and thus emplaced at shallower depths. We may speculate that the earliest wave of Mesozoic melting in the lower crust caused partial fusion of relatively deep, dry sources. Removal of large fractions of such material from the lower crust/upper mantle would make the residue more refractory. Thus, when the later (Cretaceous) heating event occurred, little melting would occur until the isotherms had been raised to higher levels of the crust; in those regions, more hydrous mineral assemblages in the higher-^{18}O SAV- and MCC-type sources might lead to "wetter," lower-temperature melts (note that, other things being equal, we expect the continental crust to be stratified in terms of $^{18}O/^{16}O$, with higher whole-rock $\delta^{18}O$ values located in the supracrustal sediments and volcanics overlying a lower-^{18}O crystalline basement). These kinds of isotopic differences between early Mesozoic and late Mesozoic plutonism in the western USA deserve much more detailed study.

Another suggestion for further research along the lines conducted in the present $^{18}O/^{16}O$ study is to look at a variety of older batholithic terranes to try to piece together sub-crustal petrotectonic structures further back in time. Specifically, an important terrane that should be studied is the regional Precambrian batholithic belt, which extends in a northeasterly direction from southeastern California and southern Arizona as far as Wisconsin. Barker et al., (1976) and Lee et al., (1981a) have

analyzed some of these rocks for $^{18}O/^{16}O$, but many more analyses would be required to build up the kind of data base we have now collected for Mesozoic plutonic rocks in the present study. Such a larger data base could yield some interesting results regarding the growth of the North American craton between Archean and late Proterozoic time.

Finally, it may be worthwhile to give an example of possible useful linkages between these kinds of geochemical studies of plutons and more direct geophysical studies of the deeper continental crust. Both of these kinds of "remote-sensing probes" complement one another because they give us information about the deep crust. Figure 11.1 shows an aeromagnetic map of Nevada and Utah, upon which we have superimposed some of our $\delta^{18}O$ boundaries. This was done <u>after</u> we had established the $\delta^{18}O$ zones; therefore it is quite remarkable that these $^{18}O/^{16}O$ boundaries so closely coincide with some major linear features on the aeromagmatic map. In particular, the north-trending boundary between our V-type and S-type subzones in the middle of Nevada (heavy solid line) closely coincides with a very sharp gradient in the magnetic contours, defining a boundary between an area of < 2400 gammas on the east and an area of > 2400 gammas on the west. This boundary also truncates an apparent E-W structure (zone between the heavy dashed lines) of < 2400 gammas that can be traced from the (CZ-V) - (CZ-S) subzone boundary all the way to the Uinta Basin in NE Utah; the low magnetic values defined by this feature approximately coincide with the bulge of our High-^{18}O Central Zone in Nevada, where the S-type subzone becomes dominant (Figure 10.10). Our Central Zone-Eastern Zone boundary (heavy dotted line) also approximately coincides with another area where there is a sharp gradient in the magnetic contours. It would be most interesting to examine these

Figure 11.1 Aeromagnetic map of Nevada and Utah, showing the boundary between the V-type and S-type subzones and the Central Zone-Eastern Zone boundary, superimposed on regional magnetic contours, modified after a map in Stewart et al. (1977). The boundary between the CZ-V and CZ-S is shown as a solid, north-trending line which extends across central Nevada. The boundary between the CZ and the EZ is the dotted line extending from northeastern Nevada into western Utah, and southwestward into southern Nevada. The latter boundary does not conform to any obvious magnetic structures, although in southeastern Nevada, it appears to parallel a SW-trending gradient in the magnetic contours. Far more interesting, however, is the fact that the position of the boundary between the V-type and S-type subzones is nearly coincident with a prominent linear trend in magnetic contours separating crust with > 2500 gammas on the west from crust with < 2400 gammas on the east. This aeromagnetic trend diverges slightly from the V/S boundary in central Nevada, but is again coincident with it in southern Nevada. As discussed in the text, we interpret the isotopic V/S subzone boundary as separating a source region composed of altered volcanic rocks, volcanogenic sediments, and oceanic crustal material on the west from a large late-Proterozoic miogeosynclinal sedimentary basin on the east. The agreement between this geophysical technique and our isotopic mapping is very encouraging in terms of the source region interpretations in this thesis. The east-west dashed lines indicate linear trends in a < 2400 gamma magnetic structure that extends from west-central Utah to eastern Nevada, and which fits nicely with the proposed "pull-apart" basin discussed in Figure 10.10.

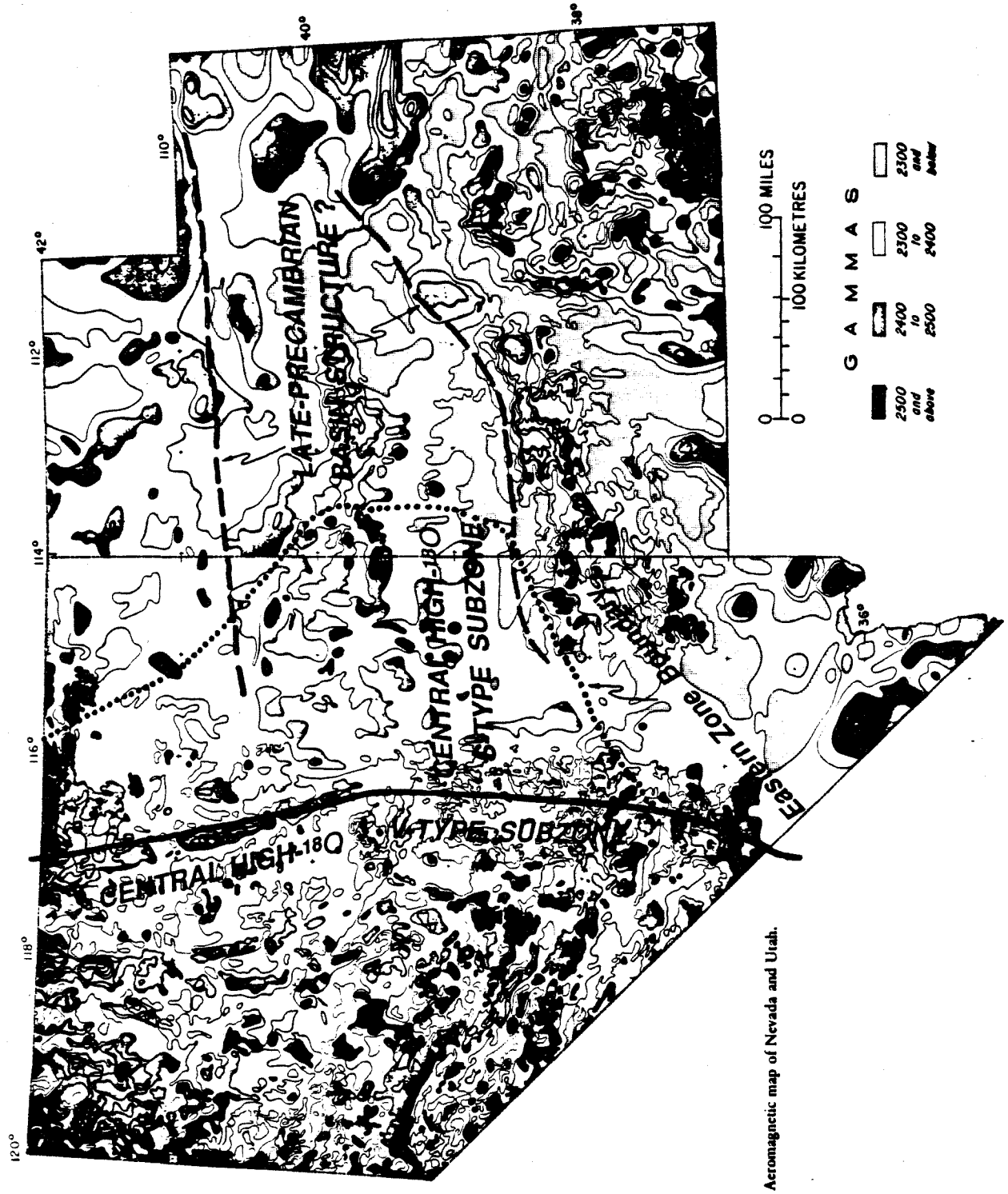

Aeromagnetic map of Nevada and Utah.

possible linkages in more detail by using such geophysical "boundaries" to guide future $^{18}O/^{16}O$ studies.

11.2 Summary of Major Conclusions

This study has provided a framework for viewing the deep crustal and subcrustal petrotectonic packages of rocks in the southwestern United States by mapping regional $^{18}O/^{16}O$ patterns of Mesozoic and younger granitic plutons, and by comparing their $^{18}O/^{16}O$ compositions with other isotopic (Nd, Pb, Sr) signatures. The following major conclusions can be made utilizing the new $^{18}O/^{16}O$ data gathered for this thesis, together with reviews of previous isotopic studies:

(1) The primary, whole-rock $\delta^{18}O$ values of granitic plutons reflect, to within approximately 0.5 per mil, the whole-rock $\delta^{18}O$ values of their source protoliths. We have found that the parent materials of these granitic magmas are almost invariably composed of at least two different end members, and that these various end members vary in a systematic fashion as a function of geographic position in the Cordillera.

(2) The primary, whole-rock $\delta^{18}O$ values for Mesozoic and Cenozoic plutons in the Cordillera of the southwestern USA define three major north-trending belts. These belts are most clearly defined for granitic plutons of Cretaceous age: (a) a Western Zone of low-^{18}O plutons with $\delta^{18}O < +8.5$ per mil; (b) along a very sharp boundary (the "$\delta^{18}O$ step"), this gives way to a Central Zone of high-^{18}O plutons, in which $\delta^{18}O$ gradually increases from west to east from +8.5 to as high as +13 per mil, before beginning to again decrease eastward to values < +9.0 per mil; and (c) an Eastern Zone with variable $\delta^{18}O$, typically lower than +9.0 per mil, but locally exhibiting plutonic centers with $\delta^{18}O > +9.0$. Based on $(^{87}Sr/^{86}Sr)_i$ compositions in the NGB, the Central Zone must be

divided into two geographic and geochemical entities; one lying west of a $(^{87}Sr/^{86}Sr)_i$ "step" (<0.7080 to the west and >0.7100 to the east), and one between this $^{87}Sr/^{86}Sr$ "step" and the western boundary of the Eastern Zone. The westernmost part of the Central Zone is here termed the V-type subzone (CZ-V), and the eastern part is termed the S-type subzone (CZ-S). We find that the CZ-S is not present (except possibly locally and on small scale) south of approximately latitude 37°N. However, the CZ-S subzone is very prominent north of 37°N, where it makes up approximately half of the Central Zone in the NGB, and where it dominates the Cretaceous portion of the Idaho Batholith to the north of the NGB (Criss and Fleck, 1987). In contrast, we find that the CZ-V subzone extends along the entire length of the Cordillera within the United States, although it is very narrow along the western edges of the Idaho Batholith (where it may have been shaved off along a suture zone).

(3) The three geographic $^{18}O/^{16}O$ zones have boundaries coincident with several major geologic features: (a) the Western Zone occurs west of the quartz diorite line (QDL) of Moore (1959); (b) the Central Zone in general lies east of the QDL and west of the western limits of Precambrian (> 1.5 Ga) crystalline basement, and it tends to be centered on the thickest portions of the (300 to 1500 Ma) Cordilleran geosynclinal sedimentary-volcanic section; (c) the CZ-V subzone lies within the area of the geosyncline dominantly characterized by Phanerozoic eugeosynclinal assemblages, whereas the CZ-S subzone seems to be associated with late Proterozoic miogeoclinal metasedimentary rocks; (d) the Eastern Zone plutons are located east of the thick geosynclinal sedimentary section.

(4) Offsets in the regional $\delta^{18}O$ patterns can be recognized at certain structural boundaries that have trends obliquely intersecting the

$\delta^{18}O$ zonation (e.g., Late Cenozoic strike-slip faults or large-scale Basin-and-Range extension in Nevada).

(5) Many plutons in the Central High-^{18}O Zone and those associated with the metamorphic core complexes in the Eastern Zone (particularly those of Cretaceous age) have characteristics that indicate deep emplacement. Many of the Jurassic plutons, as well as a number of the Cretaceous and Cenozoic plutons in the Western and Eastern Zones, are epizonal to mesozonal in nature. Plutons from the western edge of the WZ and throughout the EZ (particularly those of Jurassic age and those of Cenozoic age that are associated with porphyry deposits) have very commonly been hosts to convective hydrothermal systems. The epizonal Eastern Zone plutons tend to be associated with porphyry copper deposits, whereas the deeper-seated Central Zone plutons are more likely to host tungsten skarn deposits.

(6) As graphically depicted in Figure 10.9, the Cordilleran plutons within each of the 3 major geographic $\delta^{18}O$ zones appear to be derived from varying proportions of the following major end-member components: (a) upper mantle and/or subducted oceanic crust (OIA or MORB-type source) with $\delta^{18}O$ = +6.0 to +7.0, $^{87}Sr/^{86}Sr$ ~ 0.7025, and ε_{Nd} ~ +6.0; (b) eugeosynclinal sediments and altered volcanic rocks (SAV-type sources) with $\delta^{18}O$ = +13.0 or slightly higher, $^{87}Sr/^{86}Sr$ ~ 0.7080 or slightly higher, and ε_{Nd} = +6.0 to -2.0, or slightly lower; (c) miogeosynclinal sediments or metasediments with $+10.0 < \delta^{18}O < +19.0$, $^{87}Sr/^{86}Sr > 0.715$, and $\varepsilon_{Nd} < -2.0$ (where these sediments are Proterozoic in age, they would have similar $\delta^{18}O$ values, but ε_{Nd} could be as low as -20 and $^{87}Sr/^{86}Sr$ higher than as 0.730); (d) lower continental crust (LCC) and/or subcontinental upper mantle (SCL) with evolved, crustal isotopic characteristics,

apparently having $\delta^{18}O$ values of about +6.0 to +8.0 in the SBR and +7.0 to +9.0 in the NGB, together with $^{87}Sr/^{86}Sr$ of about 0.705 to 0.715 and ε_{Nd} between -5.0 and -10.0; and (e) mid-level continental crust of the craton (MCC) with $\delta^{18}O$ = +8.0 to +14.0, $^{87}Sr/^{86}Sr > 0.720$, and $\varepsilon_{Nd} < -10.0$. The values for Nd and Sr are strongly dependent on the age of the crust and the values for $\delta^{18}O$ are strongly dependent on the proportion of sedimentary rocks in that part of the crust. The older cratonal materials in the NGB and southeastern California appear to have lower ε_{Nd} values and slightly higher $\delta^{18}O$ values than do those in southern Arizona (see Figures 10.9b and 10.9c, and discussions by Bennett and DePaolo, 1987).

(7) The simplest way to characterize the mixtures of components in the magmas emplaced within each zone appears to be simple two-component mixing between the aforementioned end-member pairs: Western Zone: (a)-(b) mixing with (a) dominant. Central Zone: (a)-(b) or (a)-(c) mixing with (b) dominant in the west and south of 40°N latitude, and (c) dominant in the east and north of 37°N latitude. Eastern Zone: (d)-(e) mixing, with widely varying proportions of the two end-members, probably depending on the level in the crust where melting occurs, and perhaps also including other end-members such as a modified (a)-type component (i.e., one that is older and more LIL-enriched than a Cretaceous OIA or MORB component, and thus one with a relatively high $^{87}Sr/^{86}Sr$ ratio and relatively high Sr ppm). The transition between the Central and Eastern $^{18}O/^{16}O$ Zones may be characterized by (c)-(d) mixtures north of 37°N latitude.

(8) All of the isotopic systems so far investigated (Nd, O, Pb, Sr) are in general agreement with our assessment of the WZ and EZ source

regions (see above); however, there is considerable controversy regarding our placement of the edge of the >1.5 Ga craton at the EZ-CZ boundary. We place this boundary quite a bit east of the position favored by Kistler and Peterman (1978) or Farmer and DePaolo (1983), who respectively place it directly beneath their ~0.706 or ~0.708 $(^{87}Sr/^{86}Sr)_i$ boundaries. In our view, in the NGB the $^{87}Sr/^{86}Sr$ "step" is not the edge of the craton, but instead is probably a structural discontinuity that has juxtaposed an accreted terrane of eugeosynclinal volcanic and volcanogenic sedimentary rocks on the west against a late Precambrian sedimentary terrane on the east. The sharpness of this boundary implies that it must be either the edge of an ancient rift zone (Kister and Peterman, 1978), a strike-slip fault, or (perhaps most likely) some type of suture zone. The conjectured late Precambrian sedimentary terrane appears to be aligned with the trend of the Proterozoic sedimentary basin in which the Uinta Mountain Group was deposited; we therefore suggest that the CZ-S source region itself may be a large sedimentary basin, and we present a tentative model in which southward transport of the "Mojavia" basement terrane of Bennett and DePaolo (1987) produced such a "pull-apart" basin along its trailing edge (Figure 10.10). We need to stress that, outside of possible outcrops in the Ruby Mountains (Kistler et al., 1981), the combination of $^{18}O/^{16}O$ data and radiogenic isotopic data from the Mesozoic and Cenozoic granitic plutons provides the only evidence for this hypothetical "basin" (although the McCoy Creek Formation of eastern Nevada is thought to be possibly correlative with units in the upper portions of the Uinta Mountain Group; Elizabeth Miller, pers. comm.). Note that the McCoy Creek Formation crops out in several localities throughout east-central Nevada (Stewart, 1980; also see Figure 10.10).

References

Ague, J.J., and Brimhall, G.W., 1987, Granites of the batholiths of California; products of local assimilation and regional-scale crustal contamination: Geology, v. 15, p. 63-66.

Anderson, A.T., Jr., Clayton, R.N., and Mayeda, T., 1971, Oxygen isotope thermometry of mafic igneous rocks: Journal of Geology, v. 79, p. 715-729.

Anderson, T.H., and Silver, L.T., 1970, Reconnaissance survey of Precambrian rocks, northwestern Sonora, Mexico: Geological Society of America Abstracts with Program, v. 2, p. 484.

Anderson, T.H., and Silver, L.T., 1971, Preliminary history for Precambrian rocks, Bamori region, Sonora, Mexico: Geological Society of America Abstracts with Program, v. 3, p. 72-73.

Anderson, T.H., and Silver, L.T., 1978, Jurassic magmatism in Sonora, Mexico: Geological Society of America Abstracts with Program, v. 10, p. 359.

Anderson, T.H., and Silver, L.T., 1979, The role of the Mojave-Sonora megashear in the tectonic evolution of the northern Sonora. In Anderson, T.H., and Roldan-Quintana, J. (eds) Geology of Northern Sonora, Guidebook-Field Trip #27, 1979 Annual Meeting of the Geological Society of America: Instituto de Geologia, U.N.A.M., Hermosillo, Sonora, Mexico, and the University of Pittsburgh, Pittsburgh, PA, p. 59-68.

Anderson, T.H., Silver, L.T., and Salas, G.A., 1980, Distribution and U-Pb isotope ages of some lineated plutons, northwestern Sonora, Mexico. In Crittenden, M.D., Jr., Coney, P.J. and Davis, G.H. (eds) Cordilleran Metamorphic Core Complexes: Geological Society of America Memoir 153, p. 269-283.

Armstrong, R.L., 1975, Precambrian (1500 m.y. old) rocks of central Idaho - The Salmon River Arch and its role in Cordilleran sedimentation and tectonics: American Journal of Science, v. 275-A, p. 437-467.

Armstrong, R.L., and Suppe, J., 1973, Potassium-argon geochronometry of Mesozoic igneous rocks in Nevada, Utah, and southern California: Geological Society of America Bulletin, v. 84, p. 1375-1392.

Armstrong, R.L., Taubeneck, W.H., and Hales, P.O., 1977, Rb-Sr and K-Ar geochronometry of Mesozoic granitic rocks and their Sr isotopic composition, Oregon, Washington, and Idaho: Geological Society of America Bulletin, v. 88, p. 397-411.

Atwater, T., 1970, Implications of plate tectonics for the Cenozoic tectonics of western North America: Geological Society of America Bulletin, v. 81, p. 3513-3536.

Baertschi, P., and Silverman, S.R., 1951, The determination of relative abundances of the oxygen isotopes in silicate rocks: Geochimica Cosmochimica Acta, v. 1, p. 317-328.

Bailey, M.C., Jr., Irwin, W.P., and Jones, D.L., 1964, Franciscan and related rocks, and their significance in the geology of western California: California Division of Mines and Geology Bulletin 183, 76 p.

Baird, A.K., and Miesch, A.T., 1984, Batholithic rocks of southern California - A model for the petrochemical nature of their source materials: U.S. Geological Survey Professional Paper 1284, 42 p.

Baird, A.K., Baird, K.W., and Welday, E.E., 1979, Batholithic rocks of the northern Peninsular and Transverse Ranges, southern California. In Abbott, P.L., and Todd, V.R. (eds) Mesozoic Crystalline Rocks. Fieldtrip Guidebook, 1979 Annual Meeting of the Geological Society of America: Department of Geological Science, San Diego State University, San Diego, CA, p. 111-132.

Baltz, R., 1982, Late Mesozoic folding and thrusting and Tertiary extensional faulting in the Arica Mountains, Riverside County, California. In Frost, E.G., and Martin, D.L. (eds) Mesozoic-Cenozoic Tectonic Evolution of the Colorado River Region, California, Arizona, and Nevada. Anderson-Hamilton Volume: Cordilleran Publishers, San Diego, CA, p. 582-596.

Barker, F., Friedman, I., Hunter, D.R., and Gleason, J.D., 1976, Oxygen isotopes of some trondhjemites, siliceous gneisses, and associated mafic rocks: Precambrian Research, v. 3, p. 547-557.

Batchelder, J., 1977, Light stable isotope and fluid inclusion study of the prophyry copper deposit at Copper Canyon, Nevada: Economic Geology, v. 72, p. 60-70.

Bateman, P.C., and Chappell, B.W., 1979, Crystallization, fractionation, and solidification of the Tuolumne Intrusive Series, Yosemite National Park, California: Geological Society of America Bulletin, v. 90, p. 465-482.

Bateman, P.C., and Dodge, F.C.W., 1970, Variations of major chemical constituents across the central Sierra Nevada batholith: Geological Society of America Bulletin, v. 81, p. 409-420.

Bateman, P.C., and Lockwood, J.P., 1976, Shaver Lake quadrangle, central Sierra Nevada, California - Analytical Data: U.S. Geological Survey Professional Paper 774-D, 20 p.

Bateman, P.C., Clark, L.D., Huber, N.K., Moore, J.G., and Rinehart, C.D., 1963, The Sierra Nevada batholith: A synthesis of recent work across the central part: U.S. Geological Survey Professional Paper 414-D, p. 1-46.

Bennett, V.C., and DePaolo, D.J., 1987, Proterozoic crustal history of the western United States as determined by neodymium isotopic mapping: Geological Society of America Bulletin, v. 99, p. 674-685.

Berquist, J.R., Blacet, P.M., and Miller, S.T., 1978, Reconnaissance geologic map of the Santa Rosa Mountains quadrangle, Pima County, Arizona: U.S. Geological Survey Miscellaneous Field Studies Map, MF-935.

Best, M.G., Armstrong, R.L., Graustein, W.C., Embree, G.F., and Ahlborn, R.C., 1974, Mica granites of the Kern Mountains pluton, eastern White Pine County, Nevada: Remobilized basement of the Cordilleran miogeosyncline?: Geological Society of America Bulletin, v. 85, p. 1277-1286.

Bickle, M.J., Wickham, S.M., Chapman, H.J., and Taylor, H.P., Jr., 1988, A strontium, neodymium and oxygen isotope study of hydrothermal metamorphism and crustal anatexis in the Trois Seigneiurs Massif, Pyrenees, France: Contributions to Mineralogy and Petrology, v. 100, p. 399-417.

Bischoff, J.L., and Dickson, F.W., 1975, Seawater-basalt interaction at 200∘C and 500 bars; implications for origin of sea-floor heavy metal deposits and regulation of seawater chemistry: Earth and Planetary Science Letters, v. 25, p. 385-397.

Bishop, C.C. (ed), 1963, Needles sheet: California Division of Mines and Geology, Geologic Atlas of California.

Blacet, P.M., Berquist, J.R., and Miller, S.T., 1978, Reconnaissance geologic map of the Silver Reef Mountains quadrangle, Pinal and Pima Counties, Arizona. U.S. Geological Survey Miscellaneous Field Studies Map, MF-934.

Blake, M.C., Jr., and Jones, D.L., 1974, Origin of the Franciscan melanges in northern California: Society of Economic Paleontology and Mineralogy Special Publication 19, p. 345-357.

Blake, M.C., Jr., and Jones, D.L., 1981, The Franciscan assemblage and related rocks in northern California: A reinterpretation. In Ernst, W.G. (ed) The Geotectonic Development of California, Rubey Volume I, Prentice-Hall, Inc., Englewood Cliffs, NJ, p. 307-328.

Bortugno, E.J., and Spittler, T.E. (eds), 1986, Geologic map of the San Bernardino Quadrangle: California Division of Mines and Geology, Regional Geologic Map Series, Map 3-A (Geology).

Bottinga, Y., and Javoy, M., 1973, Comments on oxygen isotope geothermometry: Earth and Planetary Science Letters, v. 20, p. 251-265.

Bottinga, Y., and Javoy, M., 1975, Oxygen isotope partitioning among the minerals in igneous and metamorphic rocks: Reviews of Geophysics and Space Physics, v. 13, p. 401-418.

Bowen, N.L., 1928, The Evolution of the Igneous Rocks: (reprinted 1956), Dover, New York, NY, 332 p.

Bowman, J.R., Parry, W.T., Kropp, W.P., and Kruer, S.A., 1987, Chemical and isotopic evolution of hydrothermal solutions at Bingham, Utah: Economic Geology, v. 82, p.395-428.

Briskey, J.A., Haxel, G., Peterson, J.A., and Theodore, T.G., 1978, Reconnaissance geologic map of the Gu Achi quadrangle, Pima County, Arizona: U.S. Geological Survey Miscellaneous Field Studies Map, MF-965.

Buddington, A.F., 1959, Granite emplacement with special reference to North America: Geological Society of America Bulletin, v. 70, p. 671-747.

Burchfiel, B.C., and Davis, G.A., 1981a, Mojave Desert and environs. In Ernst, W.G. (ed) The Geotectonic Development of California, Rubey Volume I: Prentice-Hall, Inc., Englewood Cliffs, NJ, p. 218-252.

Burchfiel, B.C., and Davis, G.A., 1981b, Triassic and Jurassic tectonic evolution of the Klamath Mountains-Sierra Nevada geologic terrane. In Ernst, W.G. (ed) The Geotectonic Development of California, Rubey Volume I: Prentice-Hall, Inc., Englewood Cliffs, NJ, p. 50-70.

Burnham, C.W., 1979, Magmas and hydrothermal fluids. In Barnes, H.L. (ed) Geochemistry of Hydrothermal Ore Deposits: John Wiley and Sons, New York, NY, p. 71-136.

Busby-Spera, C.J., 1988, Speculative tectonic model for the early Mesozoic arc of the southwest Cordilleran United States: Geology, v. 16, p. 1121-1125.

Calzia, J.P., 1982, Geology of granodiorite in the Coxcomb Mountains, southeastern California. In Frost, E.G., and Martin, D.L. (eds) Mesozoic-Cenozoic Tectonic Evolution of the Colorado River Region, California, Arizona, and Nevada. Anderson-Hamilton Volume: Cordilleran Publishers, San Diego, CA, p. 173-180.

Calzia, J.P., and Morton, J.L., 1980, Compilation of isotopic ages within the Needles 1° X 2° Quadrangle, California and Arizona: U.S. Geological Survey Open-file Report 80-1303.

Calzia, J.P., DeWitt, E., and Nakata, J.K., 1986, U-Th-Pb age and initial strontium isotopic ratios of the Coxcomb granodiorite, and a K-Ar date of olivine basalt from the Coxcomb Mountains, southern California: Isochron West, v. 47, p. 3-8.

Cameron, C.S., 1981, Geology of the Sugarloaf and Delamar Mountain areas, San Bernardino Mountains, California: Ph.D. thesis, Massachusetts Institute of Technology, Cambridge, MA, 399 p.

Cameron, C.S., 1982, Stratigraphy and significance of the upper Precambrian Big Bear Group. In Cooper, J.D. (ed) Geology of Selected

Areas in the San Bernardino Mountains, Western Mojave Desert and Southern Great Basin, California: Death Valley Publishing Company, Shoshone, CA, p 5-20.

Carter, B., and Silver, L.T., 1971, Post-emplacement structural history of the San Gabriel anorthosite complex: Geological Society of America Abstracts with Program, v. 3, p. 92-93.

Carter, B., and Silver, L.T., 1972, Structure and petrology of the San Gabriel anorthosite-syenite body, California: 24th International Geological Congress, Section 3, p. 303-311.

Chappell, B.W., 1978, Granitoids from the Moonbi District, New England Batholith, eastern Australia: Geological Society of Australia Journal, v. 25, p. 267-283.

Chappell, B.W., 1984, Source rocks of I- and S-type granites in the Lachlan fold belt, southeastern Australia: Philosophical Transactions of the Royal Society of London, Series A, v. 310, p 693-707.

Chappell, B.W., and White, A.J.R., 1974, Two contrasting granite types: Pacific Geology, v. 8, p. 173-174.

Chen, J.H., and Moore, J.G., 1982, Uranium-lead isotopic ages from the Sierra Nevada Batholith, California: Journal of Geophysical Research, v. 87, p. 4761-4784.

Chen, J.H., and Tilton, G.R., 1978, Lead and strontium isotopic studies of the southern Sierra Nevada Batholith: Geological Society of America Abstracts with Program, v. 10, p. 99-100.

Coleman, R.G., 1977, Ophiolites: Springer-Verlag, Berlin, Federal Republic of Germany, 229 p.

Coleman, R.G., and Lanphere, M.A., 1971, Distribution of and age of high-grade blueschist, associated eclogites and amphibolites from Oregon and California: Geological Society of America Bulletin, v. 82, p. 2397-2412.

Coleman, R.G, and Peterman, Z.E., 1975, Oceanic plagiogranites: Journal of Geophysical Research, v. 80, p. 1099-1108.

Condie, K.C., 1981, Precambrian rocks of the southwestern United States and adjacent areas of Mexico: New Mexico Bureau of Mines and Mineral Resources, Resource Map 13.

Coney, P.J., 1978, The plate tectonic setting of southeastern Arizona. In Callender, J.T., Wilt, J.C., and Clemmons, R.E. (eds) Land of Cochise: Guidebook, New Mexico Geological Society 29th Field Conference, p. 285-290.

Coney, P.J., 1980, Cordilleran metamorphic core complexes: An overview. In Crittenden, M.D., Jr., Coney, P.J., and Davis, G.H. (eds) Cordilleran Metamorphic Core Complexes: Geological Society of America Memoir 153, p. 7-34.

Coney, P.J., Jones, D.L., and Monger, J.W.H., 1980, Cordilleran suspect terranes: Nature, v. 288, p. 329-333.

Conrad, R.L., and Davis, T.E., 1977, Rb/Sr geochemistry of cataclastic rocks of the Vicent Thrust, San Gabriel Mountains, southern California: Geological Society of America Abstracts with Program, v. 9, n. 4, p. 403-404.

Conway, C.M., 1977, Petrology, structure, and evolution of a Precambrian volcanic and plutonic complex, Tonto Basin, Gila County, Arizona: Ph.D. Thesis, California Institute of Technology, Pasadena, CA, 523 p.

Cooper, J.R., and Silver, L.T., 1964, Geology and ore deposits of the Dragoon quadrangle, Cochise County, Arizona: U.S. Geological Survey Professional Paper 416, 196 p.

Craig, H., 1957, Isotopic standards for carbon and oxygen and correction factors for mass-spectrometric analysis of carbon dioxide: Geochimica Cosmochimica Acta, v. 12, p. 133-149.

Craig, H., 1961, Standards for reporting concentrations of deuterium and oxygen-18 in natural waters: Science, v. 133, p. 1833-1834.

Criss, R.E., and Fleck, R.J., 1987, Petrogenesis, geochronology, and hydrothermal systems in the northern Idaho batholith and adjacent areas based on $^{18}O/^{16}O$, D/H, $^{87}Sr/^{86}Sr$, K-Ar, and $^{40}Ar/^{39}Ar$ studies: U.S. Geological Survey Professional Paper 1436, Chapter 6, p. 95-137.

Criss, R.E., and Taylor, H.P., Jr., 1983, An $^{18}O/^{16}O$ and D/H study of Tertiary hydrothermal systems in the southern half of the Idaho Batholith: Geological Society of America Bulletin, v. 94, p. 640-663.

Criss, R.E., and Taylor, H.P., Jr., 1986, Meteoric-hydrothermal systems. In Valley, J.W., Taylor, H.P., Jr., and O'Neil, J.R. (eds) Reviews in Mineralogy Volume 16: Stable Isotopes in High Temperature Geological Processes: Mineralogical Society of America, p. 373-424.

Criss, R.E., Lanphere, M.A., and Taylor, H.P., Jr., 1982, Effects of regional uplift, deformation, and meteoric-hydrothermal metamorphism on K-Ar ages of biotites in the southern half of the Idaho Batholith: Journal of Geophysical Research, v. 87, p. 7029-7046.

Cross, T.A., and Pilger, R.H., Jr., 1978, Constraints on absolute motion and plate interaction inferred from Cenozoic igneous activity in the western United States: American Journal of Science, v. 278, p. 865-902.

Davis, G.A., 1980, Problems of intraplate extensional tectonics, western United States. In Continental Tectonics: National Research Council, Washington, D.C., p. 84-95.

Davis, G.A., and Burchfiel, B.C., 1973, Garlock fault: An intra-continental transform structure, southern California: Geological Society of America Bulletin, v. 84, p. 1407-1432.

Davis, G.A., Anderson, J.L., Frost, E.G., and Shackelford, T.J., 1980, Mylonitization and detachment faulting in the Whipple-Rawhide-Buckskin Mountains terrane, southeastern California and western Arizona. In Crittenden, M.D., Jr., Coney, P.J. and Davis, G.H. (eds) Cordilleran Metamorphic Core Complexes: Geological Society of America Memoir 153, p. 79-129.

Davis, G.A., Monger, J.W.H., and Burchfiel, B.C., 1978, Mesozoic construction of the Cordilleran "collage", central British Columbia to central California. In Howell, D.G., and McDougall, K.A. (eds) Mesozoic Paleogeography of the Western United States: Society of Economic Paleontologists and Mineralogists, Pacific Section, Symposium 2, p. 1-32.

DePaolo, D.J., 1980, Sources of continental crust: Neodymium isotope evidence from the Sierra Nevada and Peninsular Ranges: Science, v. 209, p. 684-687.

DePaolo, D.J., 1981a, A neodymium and strontium isotopic study of Mesozoic calc-alkaline granitic batholiths of the Sierra Nevada and Peninsular Ranges, California: Journal of Geophysical Research, v. 86, p. 10,470-10,488.

DePaolo, D.J., 1981b, Trace element and isotopic effects of combined wallrock assimilation and fractional crystallization. Earth and Planetary Science Letters, v. 53, p. 189-202.

DePaolo, D.J., and Wasserburg, G.J., 1976, Nd isotopic variations and petrogenetic models: Geophysical Research Letters, v. 3, p. 249-252.

DePaolo, D.J., and Wasserburg, G.J., 1979, Petrogenetic mixing models and Nd-Sr isotopic patterns: Geochimica Cosmochimica Acta, v. 43, p. 615-627.

DeWitt, E., Armstrong, R.L., Sutter, J.F., and Zartman, R.E., 1984, U-Th-Pb, Rb-Sr, and Ar-Ar mineral and whole-rock isotopic systematics in a metamorphosed granitic terrane, southeastern California: Geological Society of America Bulletin, v. 95, p. 723-739.

Dibblee, T.W., Jr., 1960a, Preliminary geologic map of the Apple Valley quadrangle, California: U.S. Geological Survey Miscellaneous Field Studies Map, MF-232.

Dibblee, T.W., Jr., 1960b, Preliminary geologic map of the Shadow Mountain quadrangle, Los Angeles and San Bernardino Counties, California: U.S. Geological Survey Miscellaneous Field Studies Map, MF-227.

Dibblee, T.W., Jr., 1960c, Preliminary geologic map of the Victorville quadrangle, California: U.S. Geological Survey Miscellaneous Field Studies Map, MF-299.

Dibblee, T.W., Jr., 1964a, Geologic map of the Lucerne Valley quadrangle, San Bernardino County, California: U.S. Geological Survey Miscellaneous Geological Investigations Map, I-426.

Dibblee, T.W., Jr., 1964b, Geologic map of the San Gorgonio Mountain quadrangle, San Bernardino and Riverside Counties, California: U.S. Geological Survey Miscellaneous Geological Investigations Map, I-431.

Dibblee, T.W., Jr., 1964c, Geologic map of the Ord Mountains quadrangle, San Bernardino County, California: U.S. Geological Survey Miscellaneous Geological Investigations Map, I-427.

Dibblee, T.W., Jr., 1964d, Geologic map of the Rodman Mountains quadrangle, San Bernardino County, California: U.S. Geological Survey Miscellaneous Geological Investigations Map, I-430.

Dibblee, T.W., Jr., 1967a, Geologic map of the Joshua Tree quadrangle, San Bernardino and Riverside Counties, California: U.S. Geological Survey Miscellaneous Geological Investigations Map, I-516.

Dibblee, T.W., Jr., 1967b, Geologic map of the Morongo Valley quadrangle, San Bernardino and Riverside Counties, California: U.S. Geological Survey Miscellaneous Geological Investigations Map, I-517.

Dibblee, T.W., Jr., 1967c, Geologic map of the Old Woman Springs quadrangle, San Bernardino County, California: U.S. Geological Survey Miscellaneous Geolical Investigations Map, I-518.

Dibblee, T.W., Jr., 1967d, Areal geology of the western Mojave Desert, California: U.S. Geological Survey Professional Paper 522, 153 p.

Dickinson, W.R., 1975, Potash-depth (K-h) relations in continental margin and intra-oceanic magmatic arcs: Geology, v. 3, p. 53-56.

Dickinson, W.R., 1981a, Plate tectonic evolution of the southern Cordillera. In Dickinson, W.R., and Payne, W.D. (eds) Relations of Tectonics to Ore Deposits in the Southern Cordillera: Arizona Geological Society Digest, v. 14, p. 113-136.

Dickinson, W.R., 1981b, Plate tectonics and the continental margin of California. In Ernst, W.G. (ed) The Geotectonic Development of California, Rubey Volume I: Prentice-Hall, Inc., Englewood Cliffs, NJ, p. 1-28.

Dilles, J.H., 1987, Petrology of the Yerington Batholith, Nevada; evidence for evolution of porphyry copper ore fluids: Economic Geology, v. 82, p. 1750-1789.

Dilles, J.H., Solomon, G.C., Taylor, H.P., Jr., and Criss, R.E., 1989, Oxygen and hydrogen isotopic characteristics of hydrothermal alteration at the Ann-Mason porphyry copper deposit, Yerington, Nevada: manuscript to be submitted to Economic Geology.

Doe, B.R., 1967, The bearing of lead isotopes on the source of granitic magma: Journal of Petrology, v. 8, p. 51-83.

Dokka, R.K., 1983, Displacements on late Cenozoic strike slip faults of the central Mojave Desert, California: Geology, v. 11, p. 305-308.

Dokka, R.K., and Glazner, A.K., 1982, Aspects of early Miocene extension of the central Mojave Desert, California. In Cooper, J.D. (ed) Geological excursions in the California desert: Geological Society of America Cordilleran Section Field Trip Guidebook, p. 31-46.

Early, T.O., and Silver, L.T., 1973, Rb-Sr isotopic systematics in the Peninsular Ranges Batholith of southern and Baja California: Abstract, Transactions of the American Geophysical Union, v. 54, p. 494.

Eaton, G.P., 1982, The Basin and Range Province: Origin and tectonic significance: Annual Review of Earth and Planetary Sciences, v. 10, p. 409-440.

Eberly, L.D., and Stanley, T.B., 1978, Cenozoic stratigraphy and geologic history of southwestern Arizona: Geological Society of America Bulletin, v. 89, p. 921-940.

Ehlert, K.W., and Ehlig, P.L., 1977, The "polka-dot" granite and the rate of displacement on the San Andreas fault in southern California: Geological Society of America Abstracts with Program, v. 9, n. 4, p. 415-416.

Ehlig, P.L., 1981, Origin and tectonic history of the basement terrane of the San Gabriel Mountains, central Transverse Ranges. In Ernst, W.G. (ed) The Geotectonic Development of California, Rubey Volume I: Prentice-Hall, Inc., Englewood Cliffs, NJ, p. 253-283.

Ehlig, P.L., Davis, T.E., and Conrad, R.L., 1975, Tectonic implications of the cooling age of the Pelona Schist: Geological Society of America Abstracts with Program, v. 7, p. 314.

Emerson, W.S., 1982, Geologic development and late Mesozoic deformation of the Little Maria Mountains, Riverside County, California. In Frost, E.G., and Martin, D.L. (eds) Mesozoic-Cenozoic Tectonic Evolution of the Colorado River Region, California, Arizona, and Nevada. Anderson-Hamilton Volume: Cordilleran Publishers, San Diego, CA, p. 245-254.

Ernst, W.G., 1970, Tectonic contact between the Franciscan melange and the Great Valley sequence - crustal expression of a Late Mesozoic Benioff Zone: Journal of Geophysical Research, v. 75, p. 886-901.

Eslinger, E.V., and Savin, S.M., 1973, Oxygen isotope geothermometry of the burial metamorphic rocks of the Precambrian Belt Supergroup, Glacier National Park, Montana: Geological Society of America Bulletin, v. 84, p. 2549-2560.

Evernden, E.V., and Kistler, R.W., 1970, Chronology of emplacement of Mesozoic batholithic complexes in California and western Nevada: U.S. Geological Survey Professional Paper 623, 42 p.

Farmer, G.L., and DePaolo, D.J., 1983, Origin of Mesozoic and Tertiary granite in the western United States, and implications for pre-

Mesozoic crustal structure, 1. Nd and Sr isotope studies in the geocline of the northern Great Basin: Journal of Geophysical Research, v. 88, B4, p. 3379-3401.

Farmer, G.L., and DePaolo, D.J., 1984, Origin of Mesozoic and Tertiary granite in the western United States, and implications for pre-Mesozoic crustal structure, 2. Nd and Sr isotopic studies of unmineralized and Cu- and Mo-mineralized granite in the Precambrian craton: Journal of Geophysical Research, v. 89, B12, p. 10141-10160.

Faure, G., 1977, Principles of Isotope Geology: John Wiley and Sons, New York, NY, 464 p.

Fleck, R.J., and Criss, R.E., 1985, Strontium and oxygen isotopic variations in Mesozoic and Tertiary plutons of central Idaho: Contributions to Mineralogy and Petrology, v. 90, p. 291-308.

Forester, R.W., and Taylor, H.P., Jr., 1972, Oxygen and hydrogen isotope data on the interaction of meteoric ground waters with a gabbrodiorite stock, San Juan Mountains, Colorado: 24th International Geological Congress, v. 10, p. 254-263.

Forester, R.W., and Taylor, H.P., Jr., 1977, $^{18}O/^{16}O$, D/H, and $^{13}C/^{12}C$ studies of the Tertiary igneous complex of Skye, Scotland: American Journal of Science, v. 277, p. 136-177.

Fourcade, S., and Javoy, M., 1973, Rapports $^{18}O/^{16}O$ dans les rockes du vieux socle catazonal d'In Ouzzal (Sahara Algerien): Contributions to Mineralogy and Petrology, v. 42, p. 235-244.

Fox, L.K., 1988, Albitization of K-feldspar during Jurassic hydrothermal sodium metasomatism, Bristol Mountains, east-central Mojave Desert, California: Geological Society of America Abstracts with Program, v 20, n. 7, p. A-225.

Friedman, I., and O'Neil, J.R., 1977, Compilation of stable isotope fractionation factors of geochemical interest: U.S. Geological Survey Professional Paper 440-KK, 12 p.

Friedman, I., Lipman, P.W., Obradovich, J.D., and Gleason, J.D., 1974, Meteoric water in magmas: Science, v. 184, p. 1069-1072.

Frizzell, V.A., Jr., Mattinson, J.M., and Matti, J.C., 1986, Distinctive Triassic megaporphyritic monzogranite: Evidence for only 160 kilometers of offset along the San Andreas Fault, southern California: Journal of Geophysical Research, v. 91, p. 14,080-14,088.

Frost, E.G., and Martin, D.L. (eds), 1982, Mesozoic-Cenozoic Tectonic Evolution of the Colorado River Region, California, Arizona and Nevada: Cordilleran Publishers, San Diego, CA, 608 p.

Fyfe, W.S., Price, N.J., and Thompson, A.B., 1978, Fluids in the Earth's Crust: Their significance in metamorphic, tectonic and chemical transport processes: Elsevier Scientific Publishing Company, New York, NY, 383 p.

Garfunkel, Z., 1974, Model for the late Cenozoic tectonic history of the Mojave desert, California: Geological Society of America Bulletin, v. 85, p. 1931-1944.

Garlick, G.D., 1966, Oxygen isotope fractionation in igneous rocks: Earth and Planetary Science Letters, v. 1, p. 361-368.

Garlick, G.D., MacGregor, I.D., and Vogel, D.E., 1971, Oxygen isotope ratios in eclogites from kimberlites: Science, v. 172, p. 1025-1027.

Gillou, R.B., 1953, Geology of the Johnston Grade area, San Bernardino County, California: California Division of Mines and Geology Special Report 31, 18 p.

Gilluly, J., 1946, The Ajo Mining District, Arizona: U.S. Geological Survey Professional Paper 209, 112 p.

Glazner, A.K., Turner, R.D., and O'Neil, J.R., 1986, Crustal structure of the Mojave Desert: Inferences from $^{87}Sr/^{86}Sr$ and $\delta^{18}O$ in Miocene volcanic rocks: Geological Society of America Abstracts with Program, v. 18, n. 2, p. 109.

Gregory, R.T., and Taylor, H.P., Jr., 1981, An oxygen isotope profile in a section of Cretaceous ocean crust, Samial ophiolite, Oman: Evidence for $\delta^{18}O$-buffering of the oceans by deep (>5 km) seawater-hydrothermal circulation at mid-ocean ridges: Journal of Geophysical Research, v. 86, p. 2737-2755.

Gregory, R.T., and Taylor, H.P., Jr., 1986, Possible non-equilibrium oxygen isotope effects in mantle nodules, an alternative to the Kyser-O'Neil-Carmichael $^{18}O/^{16}O$ geothermometer: Contributions to Mineralogy and Petrology, v. 93, p. 114-119.

Gromet, L.P., and Silver, L.T., 1987, REE variations across the Peninsular Ranges Batholith: Implications for batholithic petrogenesis and crustal growth in magmatic arcs: Journal of Petrology, v. 28, p. 75-126.

Hall, W.E., Friedman, I., and Nash, J.T., 1974, Fluid-inclusion and light-stable-isotope study of the Climax molybdenum deposits, Colorado: Economic Geology, v. 69, p. 884-901.

Halliday, A.N., Stephens, W.E., and Harmon, R.S., 1980, Rb-Sr and O isotopic relationships in 3 zoned Caledonian granitic plutons, Southern Uplands, Scotland: Evidence for varied sources and hybridization of magma: Journal of the Geological Society of London, v. 137, p. 329-349.

Halliday, A.N., Stephens, W.E., and Harmon, R.S., 1981, Isotopic and chemical constraints on the development of peraluminous Caledonian and Acadian granites: Canadian Mineralogist, v. 19, p. 205-216.

Hamilton, W., 1981, Crustal evolution by arc magmatism: Philosophical Transactions of the Royal Society of London, Series A, v. 301, p. 279-291.

Hamilton, W., 1982, Structural evolution of the Big Maria Mountains, northeast Riverside County, southeastern California. In Frost, E.G., and Martin, D.L. (eds) Mesozoic-Cenozoic Tectonic Evolution of the Colorado River Region, California, Arizona, and Nevada. Anderson-Hamilton Volume: Cordilleran Publishers, San Diego, CA, p 1-27.

Hamilton, W., 1986, Crustal evolution of southern California during Cretaceous and Cenozoic time: Geological Society of America Abstracts with Program, v. 18, n. 2, p. 112.

Harmon, R.S., and Halliday, A.N., 1980, Oxygen and strontium isotope relationships in the British Late Caledonian (~400 Ma) granites, Nature, v. 283, p. 21-25.

Hawkins, H.G., 1975, Strike-slip displacement along the Camp Rock-Emerson Fault, central Mojave Desert, San Bernardino County, California: Geological Society of America Abstracts with Program, v. 7, p. 324.

Haxel, G., May, D.J., and Tosdal, R.M., 1981, Reconnaissance geologic map of the Presumido Peak 15' quadrangle, Arizona: U.S. Geological Survey Miscellaneous Field Studies Map, MF-1378.

Haxel, G., May, D.J., Wright, J.E., and Tosdal, R.M., 1980a, Reconnaissance geologic map of the Baboquivari Peak quadrangle, Arizona: U.S. Geological Survey Miscellaneous Field Studies Map, MF-1251.

Haxel, G., Tosdal, R.M., May, D.J., and Wright, J.E., 1984, Latest Cretaceous and early Tertiary orogenesis in south-central Arizona: Thrust faulting, regional metamorphism, and granitic plutonism: Geological Society of America Bulletin, v. 95, p. 631-653.

Haxel, G., Wright, J.E., May D.J., and Tosdal, R.M., 1980b, Reconnaissance geology of the Mesozoic and lower Cenozoic of the southern Papago Indian Reservation, Arizona: A preliminary report. In Jenny, J.P., and Stone, C. (eds) Studies in western Arizona: Arizona Geological Society Digest, v. 12, p. 17-29.

Haxel, G., Briskey, J.A., Rytuba, J.J., Berquist, J.R., Blacet, P.M., and Miller, S.T., 1978, Reconnaissance geologic map of the Comobabi quadrangle, Pima County, Arizona: U.S. Geological Survey Miscellaneous Field Studies Map, MF-964.

Heier, K.S., and Thoresen, K., 1971, Geochemistry of high grade metamorphic rocks, Lofoten-Vesteralen, north Norway: Geochimica Cosmochimica Acta, v. 35, p. 88-99.

Hill, R.I., 1984, Petrology and petrogenesis of batholithic rocks, San Jacinto Mountains, southern California: Ph.D. Thesis, California Institute of Technology, Pasadena, CA, 660 p.

Hill, R.I., Silver, L.T., and Taylor, H.P., Jr., 1986, Coupled Sr-O isotope variations as an indicator of source heterogeneity for the Northern Peninsular Ranges Batholith: Contributions to Mineralogy and Petrology, v. 92, p. 351-361.

Hine, R., Williams, I.S., Chappell, B.W., and White, A.J.R., 1978, Contrasts between I- and S-type granitoids of the Kosciusko Batholith: Geological Society of Australia Journal, v. 25, p. 291-234.

Hoisch, T.D., Miller, C.F., Heizler, M.T., Harrison, T.M., and Stoddard, E.F., 1988, Late Cretaceous regional metamorphism in southeastern California. In Ernst, W.G. (ed) Metamorphism and Crustal Evolution, Western Coterminous United States, Rubey Volume VII: Prentice-Hall, Inc., Englewood Cliffs, NJ, p. 649-682.

Howard, K.A., 1980, Metamorphic infrastructure in the northern Ruby Mountains, Nevada. In Crittenden, M.D., Jr., Coney, P.J. and Davis, G.H. (eds) Cordilleran Metamorphic Core Complexes: Geological Society of America Memoir 153, p. 335-347.

Howard, K.A., 1986, Evolution of crustal layering in southeastern California: Geological Society of America Abstracts with Program, v. 18, n. 2, p. 119.

Howard, K.A., Miller, D.M., and John, B.E., 1982, Regional character of mylonitic gneiss in the Cadiz Valley area, southeastern California. In Frost, E.G., and Martin, D.L. (eds) Mesozoic-Cenozoic Tectonic Evolution of the Colorado River Region, California, Arizona, and Nevada. Anderson-Hamilton Volume: Cordilleran Publishers, San Diego, CA, p. 441-447.

Hyndman, D.W., 1981, Controls on the source and depth of emplacement of granitic magma: Geology, v. 9, p. 244-249.

Irwin, W.P., 1981, Tectonic accretion of the Klamath Mountains. In Ernst, W.G. (ed) The Geotectonic Development of California, Rubey Volume I: Prentice-Hall, Inc., Englewood Cliffs, NJ, p. 29-49.

Ito, E., and Clayton, R.N., 1983, Submarine metamorphism of gabbros from the mid-Cayman Rise; an oxygen isotopic study: Geochimica Cosmochimica Acta, v. 47, p. 535-546.

Ito, E., and Stern, R.J., 1986, Oxygen and strontium-isotopic investigations of subduction zone volcanism; the case of the Volcano Arc and the Marianas Island arc: Earth and Planetary Science Letters, v. 76, p. 312-320.

Ito, E., White, W.M., and Gopel, C., 1987, The O, Sr, Nd and Pb isotope geochemistry of MORB: Chemical Geology, v. 62, p. 157-176.

Jahns, R.H., 1954, Pegmatites of southern California. In Jahns, R.H. (ed) Geology of Southern California: California Division of Mines and Geology Bulletin 170, Chapter 7, p. 37-50.

James, E.W., 1989, Southern extension fo the Independence Dike Swarm of eastern California: Geology, (in press).

James, L.P., 1979, Geology, ore deposits, and history of the Big Cottonwood mining district, Salt Lake County, Utah: Utah Geological and Mineralogical Survey Bulletin 114, 90 p.

Jennings, C.W. (ed), 1967, Salton Sea sheet: California Division of Mines and Geology, Geologic Atlas of California.

Jennings, C.W., and Strand, R.G. (eds), 1969, Los Angeles sheet: California Division of Mines and Geology, Geologic Atlas of California.

John, B.E., 1981, Reconnaissance study of Mesozoic plutonic rocks in the Mojave Desert region. In Howard, K.A., Carr, M.D., and Miller, D.M. (eds) Tectonic Framework of the Mojave and Sonoran Deserts, California and Arizona: U.S. Geological Survey Open-File Report 81-503, p. 48-50.

John, B.E., 1982, Geologic framework of the Chemehuevi Mountains, southeastern California. In Frost, E.G., and Martin, D.L. (eds) Mesozoic-Cenozoic Tectonic Evolution of the Colorado River Region, California, Arizona, and Nevada. Anderson-Hamilton Volume: Cordilleran Publishers, San Diego, CA, p. 317-325.

John, B.E., 1989, Petrology and geochemistry of the plutonic suite of the Chemehuevi Mountains, southeastern California. In Anderson, J.L. (ed) Nature and Origin of Cordilleran Magmatism: Geological Society of America Memoir 174, (in press).

Johnson, M.G., 1977, Geology and mineral deposits of Pershing County, Nevada: Nevada Bureau of Mines and Geology Bulletin 89, 115 p.

Joseph, S.E., and Ehlig, P.L., 1981, Isotopic correlation of La Panza Range granitic rocks in the central and eastern Transverse Ranges: Geological Society of America Abstracts with Program, v. 13, p. 63.

Joseph, S.E., Criscione, J.J., and Davis, T.E., 1978, Rb/Sr geochronology and geochemistry of the Lowe granodiorite, central San Gabriel Mountains, California: Geological Society of America Abstracts with Program, v. 10, n. 3, p. 111.

Kalamarides, R.I., 1984, Kiglapait geochemistry VI: Oxygen isotopes: Geochimica Cosmochimica Acta, v. 48, p. 1827-1836.

Kerr, P.F., 1946, Tungsten mineralization in the United States: Geological Society of America Memoir 15, 241 p.

King, P.B., 1977, The Evolution of North America: Princeton University Press, Princeton, NJ, 197 p.

Kistler, R.W., 1974, Hetch Hetchy Reservoir quadrangle, Yosemite National Park, California - Analytic Data: U.S. Geological Survey Professional Paper 774-B, 15 p.

Kistler, R.W., and Peterman, Z.E., 1973, Variations in Sr, Rb, K, Na and initial $^{87}Sr/^{86}Sr$ in Mesozoic granitic rocks and intruded wall rocks in central California: Geological Society of America Bulletin, v. 84, p. 3489-3512.

Kistler, R.W., and Peterman, Z.E., 1978, Reconstruction of crustal blocks of California on the basis of initial strontium isotopic compositions of Mesozoic granitic rocks: U.S. Geological Survey Professional Paper 1071, 17 p.

Kistler, R.W. and Swanson, S.E., 1981, Petrology and geochronology of metamorphosed volcanic rocks and a middle Cretaceous volcanic neck in the east-central Sierra Nevada, California: Journal of Geophysical Research, v. 86, B11, p. 10,489-10,501.

Kistler, R.W., Ghent, E.D., and O'Neil, J.R., 1981, Petrogenesis of garnet two-mica granites in the Ruby Mountains, Nevada: Journal of Geophysical Research, v. 86, p. 10,591-10,606.

Kyser, T.K., Carmichael, I.S.E., and O'Neil, J.R., 1981, Oxygen isotope thermometry of basic lavas and mantle nodules. Contributions to Mineralogy and Petrology, v. 81, p. 88-102.

Kyser, T.K., O'Neil, J.R., and Carmichael, I.S.E., 1982, Genetic relationships among basic lavas and ultra-mafic nodules: Evidence from oxygen isotope compositions: Contributions to Mineralogy and Petrology, v. 81, p. 88-102.

Langmuir, C.H., Vocke, R.D., Hanson, G.N., and Hart, S.R., 1978, A general mixing equation with applications to Icelandic basalts: Earth and Planetary Science Letters, v. 37, p. 380.

Lanier, G., Raab, W.J., Folsom, R.B., and Cone, S. 1978, Alteration of equigranular monzonite, Bingham mining district, Utah: Economic Geology, v. 73, p. 1270-1286.

Lanphere, M.A., 1964, Geochronologic studies in the eastern Mojave Desert, California: Journal of Geology, v. 72, p. 381-399.

Lanphere, M.A., Blake, M.C., Jr., and Irwin, W.P., 1978, Early Cretaceous metamorphic age of the South Fork Mountain Schist in the northern Coast Ranges of California: American Journal of Science, v. 278, p. 798-815.

Larsen, E.S., 1948, Batholith and associated rocks of the Corona, Elsinore and San Luis Rey quadrangles, southern California: Geological Society of America Memoir 29, 182 p.

Larsen, E.S., and Schmidt, R.G., 1958, A reconnaissance of the Idaho Batholith and comparison with the southern California Batholith: U.S. Geological Survey Bulletin 1070A, 33 p.

Larson, P.B., and Taylor, H.P., Jr., 1986, $^{18}O/^{16}O$ ratios in ash-flow tuffs and lavas erupted from the central Nevada caldera complex and

the central San Juan caldera complex, Colorado: Contributions to Mineralogy and Petrology, v. 92, p. 146-156.

Lawrence, J.R., and Taylor, H.P., Jr., 1972, Hydrogen and oxygen isotope systematics in weathering profiles: Geochimica Cosmochimica Acta, v. 36, p. 1377-1393.

Lee, D.E., 1984, Analytical data for a suite of granitoid rocks from the Basin and Range Province: U.S. Geological Survey Bulletin 1602, 54 p.

Lee, D.E., and Christiansen, E.H., 1983, The granite problem as exposed in the southern Snake Range, Nevada: Contributions to Mineralogy and Petrology, v. 83, p. 99-116.

Lee, D.E., and Van Loenen, R.E., 1971, Hybrid granitoid rocks of the southern Snake Range, Nevada: U.S. Geological Survey Professional Paper 668, 48 p.

Lee, D.E., Friedman, I., and Gleason, J.D., 1981a, Map showing the oxygen isotope composition of granitoid rocks of the Basin-Range Province: U.S. Geological Survey Miscellaneous Field Studies Map, MF-130.

Lee, D.E., Friedman, I., and Gleason, J.D., 1982, The oxygen isotope composition of granitoid and sedimentary rocks of the southern Snake Range, Nevada: Contributions to Mineralogy and Petrology, v. 79, p. 150-158.

Lee, D.E., Kistler, R.W., Friedman, I., and Van Loenen, R.E., 1981b, Two-mica granites of northeastern Nevada: Journal of Geophysical Research, v. 86, p. 10,607-10,616.

Lipman, P.W., 1980, Cenozoic volcanism in the western United States: Implications for continental tectonics. In Continental Tectonics: National Research Council, Washington, D.C., p. 161-174.

Lipman, P.W., Protska, H.J., and Christiansen, R.L., 1972, Cenozoic volcanism and plate-tectonic evolution of the western United States: I. Early and Middle Cenozoic: Philosophical Transactions of the Royal Society of London, v. A271, p. 217-248.

Lockwood, J.P., 1975, Mount Abbot quadrangle, central Sierra Nevada, California - Analytic Data: U.S. Geological Survey Professional Paper 774-C, 18 p.

Longstaffe, F.J., and Schwarcz, H.P., 1977, $^{18}O/^{16}O$ of Archean clastic metasedimentary rocks: a petrogenetic indicator for Archean gneisses: Geochimica Cosmochimica Acta, v. 41, p. 1303-1312.

Loomis, T.P., 1972, Diapiric emplacement of the Rhonda high temperature ultramafic intrusion, southern Spain: Geological Society of America Bulletin, v. 83, p. 2,449-2,473.

Lowell, J.D., 1974, Regional characteristics of porphyry copper deposits of the southwest: Economic Geology, v. 69, p. 601-617.

Lyle, J.H., 1982, Inter-relationship of late Mesozoic thrust faulting and mid-Tertiary detachment faulting in the Riverside Mountains, southeastern California. In Frost, E.G., and Martin, D.L. (eds) Mesozoic-Cenozoic Tectonic Evolution of the Colorado River Region, California, Arizona, and Nevada. Anderson-Hamilton Volume: Cordilleran Publishers, San Diego, CA, p. 470-491.

MacColl, R.S., 1964, Geochemical and structural studies in batholithic rocks of southern California: Part 1, Structural geology of the Rattlesnake Mountain Pluton: Geological Society of America Bulletin, v. 75, p. 805-822.

Magaritz, M., and Taylor, H.P., Jr., 1976a, Isotopic evidence for meteoric-hydrothermal alteration of plutonic igneous rocks in the Yakutat Bay and Skagway areas, Alaska: Earth and Planetary Science Letters, v. 30, p. 179-190.

Magaritz, M., and Taylor, H.P., Jr., 1976b, $^{18}O/^{16}O$ and D/H studies along a 500 km traverse across the Coast Range batholith and its country rocks, central British Columbia: Canadian Journal of Earth Sciences, v. 13, p. 1514-1536.

Magaritz, M., and Taylor, H.P., Jr., 1976c, Oxygen, hydrogen and carbon isotope studies of the Franciscan formation, Coast Ranges, California: Geochimica Cosmochimica Acta, v. 40, p. 215-235.

Magaritz, M., and Taylor, H.P., Jr., 1986, $^{18}O/^{16}O$ and D/H studies of plutonic granitic and metamorphic rocks across the Cordilleran batholiths of southern British Columbia: Journal of Geophysical Research, v. 91, p. 2193-2217.

Martin, D.L., Krummenacher, D. and Frost, E.G., 1982, K/Ar geochronologic record of Mesozoic and Tertiary tectonics of the Big Maria-Little Maria-Riverside Mountains terrane. In Frost, E.G., and Martin, D.L. (eds) Mesozoic-Cenozoic Tectonic Evolution of the Colorado River Region, California, Arizona, and Nevada. Anderson-Hamilton Volume: Cordilleran Publishers, San Diego, CA, p. 518-549.

Masi, U., O'Neil, J.R., and Kistler, R.W., 1981, Stable isotope systematics in Mesozoic granites of central and northern California and southwestern Oregon: Contributions to Mineralogy and Petrology, v. 76, p. 116-126.

Matsuhisa, Y., 1979, Oxygen isotopic compositions of volcanic rocks from the East Japan island arcs and their bearing on petrogenesis: Journal of Volcanology and Geothermal Research, v. 5, p. 271-296.

Matsuhisa, Y., Goldsmith, J.R., and Clayton, R.N., 1981, Oxygen isotopic fractionation in the system quartz-albite-anorthite-water: Geochimica Cosmochimica Acta, v. 43, p. 1131-1140.

Matsuhisa, Y., Matsubaya, O., and Sakai, H., 1973, Oxygen isotope variations in magmatic differentiation processes of the volcanic rocks in Japan: Contributions to Mineralogy and Petrology, v. 39, p. 277-288.

Matthews, A., Goldsmith, J.R., and Clayton, R.N., 1983, Oxygen isotope fractionations involving pyroxenes: The calibration of mineral-pair geothermometers: Geochimica Cosmochimica Acta, v. 47, p. 146-156.

Maxwell, J.C., 1974, Anatomy of an orogen: Geological Society of America Bulletin, v. 85, p. 1195-1204.

May, D.J., and Haxel, G., 1980, Reconnaissance geologic map of the Sells quadrangle, Pima County, Arizona: U.S. Geological Survey Miscellaneous Field Studies Map, MF-1166.

May, D.J., Tosdal, R.M., and Haxel, G., 1981, Imbricate thrust faulting of late Cretaceous or early Tertiary age, Organ Pipe Cactus National Monument, southwestern Arizona: Geological Society of America Abstracts with Program, v. 13, n. 2, p. 95.

McBirney, A.R., and Noyes, R.M., 1979, Crystallization and layering of the Skaergaard intrusion: Journal of Petrology, v. 20, p. 487-554.

McCulloch, M.T., and Chappell, B.W., 1982, Nd isotopic characteristics of S- and I-type granites: Earth and Planetary Science Letters, v. 58, p. 51-64.

McCulloch, M.T., and Wasserburg, G.J., 1978, Sm-Nd and Rb-Sr chronology of continental crust formation: Science, v. 200, p. 1003-1011.

McCulloch, M.T., Gregory, R.T., Wasserburg, G.J., and Taylor, H.P., Jr., 1980, A neodymium, strontium and oxygen isotope study of the Creatceous Samail ophiolite and implications for the petrogenesis and seawater hydrothermal alteration of the oceanic crust: Earth and Planetary Science Letters, v. 46, p. 210-211.

McCulloch, M.T., Gregory, R.T., Wasserburg, G.J., and Taylor, H.P., Jr., 1981, Sm-Nd, Rb-Sr, and 180/160 isotopic systematics in an oceanic crustal section: Evidence from the Samail ophiolite: Journal of Geophysical Research, v. 86, B4, p. 2721-2735.

McDowell, F.W., 1971, K-Ar ages of igneous rocks from the western United States: Isochron/West, v. 2, p. 1-12.

McGetchin, T.R., and Silver, L.T., 1972, A crustal-upper mantle model for the Colorado Plateau based on observations of crystalline rock fragments in the Moses rock dike: Journal of Geophysical Research, v. 77, p. 7022-7037.

Meisling, K.E., 1984, Neotectonics of the north frontal fault system of the San Bernardino Mountains: Cajon Pass to Lucerne Valley, California: Ph.D. Thesis, California Institute of Technology, Pasadena, CA, 394 p.

Meisling, K.E., and Weldon, R.J., 1989, Late Cenozoic tectonics of the northwestern San Bernardino Mountains, southern California: Geological Society of America Bulletin, v. 101, p. 106-128.

Michard-Vitrac, A., Albarede, F., Dupuis, C., and Taylor, H.P., Jr., 1980, The genesis of Variscan (Hercynian) plutonic rocks: Inferences from Sr, Pb, and O studies on the Maladeta Igneous Complex, central Pyrenees (Spain): Contributions to Mineralogy and Petrology, v. 72, p. 57-72.

Miller, C.F., 1977a, Alkali-rich monzonites, California: Origin of near silica saturated alkaline rocks and their significance in a calc-alkaline batholithic belt: Ph.D. Thesis, University of California, Los Angeles, CA, 283 p.

Miller, C.F., 1977b, Early alkalic plutonism in the Calc-alkalic batholithic belt of California: Geology, v. 5, p. 685-688.

Miller, C.F., 1977c, Muscovite granite with high $^{87}Sr/^{86}Sr$, Old Woman Mountains, California: A product of upper crustal anatexis?: Geological Society of America Abstracts with Program, v. 9, p. 466.

Miller, C.F., and Bradfish, L., 1980, An inner Cordilleran muscovite-bearing plutonic belt: Geology, v. 8, p. 412-416.

Miller, C.F., Howard, K.A., and Hoisch, T.D., 1982, Mesozoic thrusting, metamorphism, and plutonism, Old Woman-Piute Range, southeastern California. In Frost, E.G., and Martin, D.L. (eds) Mesozoic-Cenozoic Tectonic Evolution of the Colorado River Region, California, Arizona, and Nevada. Anderson-Hamilton Volume: Cordilleran Publishers, San Diego, CA, p. 561-581.

Miller, C.F., Wooden, J.L., Bennett, V., Wright, J.E., Solomon, G.C., and Hurst, R.W., 1989, Petrogenesis of the composite peraluminous-metaluminous Old Woman-Piute Range Batholith, southeastern California. In Anderson, J.L. (ed) Nature and Origin of Cordilleran Magmatism: Geological Society of America Memoir 174, (in press).

Miller, E.L., 1978, The Fairview Valley Formation: A Mesozoic intraorogenic deposit in the southwestern Mojave desert: In Howell, D.G., and McDougall, K.A. (eds) Mesozoic Paleogeography of the Western United States: Society of Economic Paleontology and Mineralogy, Pacific Section, Pacific Coast Paleography Symposium, v. 2, p. 277-282.

Miller, E.L., and Cameron, C.S., 1982, Late Precambrian to late Cretaceous evolution of the southwestern Mojave Desert, California. In Cooper, J.D. (ed) Geology of Selected Areas in the San Bernardino Mountains, Western Mojave Desert and Southern Great Basin, California: Death Valley Publishing Company, Shoshone, CA, p. 21-34.

Miller, E.L., and Carr, M.P., 1978, Recognition of possible Aztec-equivalent sandstones and associated Mesozoic metasedimentary deposits within the Mesozoic magmatic arc in the southwestern Mojave Desert, California: Society of Economic Paleontologists and Mineralogists, Pacific Section, Mesozoic Paleogeographic Symposium, v. 2, p. 283-290.

Miller, E.L., and Sutter, J.F., 1981, $^{40}Ar/^{39}Ar$ age spectra for biotite and hornblende from plutonic rocks in the Victorville region, California: Geological Society of America Bulletin, v. 92-I, p. 64-69.

Miller, E.L., Gans, P.B., Wright, J.E., and Sutter, J.F., 1988, Metamorphic history of the east central Basin and Range province: Tectonic setting and relationship to magmatism. In Ernst, W.G. (ed) Metamorphism and Crustal Evolution, Western Coterminous United States, Rubey Volume VII: Prentice-Hall, Inc., Englewood Cliffs, NJ., p. 649-682.

Miller, F.K., and Morton, D.M., 1977, Comparison of granitic intrusions in the Pelona and Orocopia schists, southern California: U.S. Geological Survey Journal of Research, v. 5, p. 643-649.

Miller, F.K., and Morton, D.M., 1980, Potassium-argon geochronology of the Eastern Transverse Ranges and southern Mojave Desert, southern California: U.S. Geological Survey Professional Paper 1152, 30 p.

Moorbath, S., and Bewll, J.D., 1965, Strontium isotope abundance studied and rubidium-strontium age determinations on Tertiary igneous rocks fromthe Isle of Skye, northwest Scotland: Journal of Petrology, v. 6, p. 37-66.

Moore, J.G., 1959, Quartz diorite boundary line in the western United States: Journal of Geology, v. 67, p. 198-210.

Morse, S.A, 1969, The Kiglapait layered intrusion, Labrador: Geological Society of America Memoir 112, 146 p.

Muehlenbachs, K., and Clayton, R.N., 1972, Oxygen isotope studies of fresh and weathered submarine basalts: Canadian Journal of Earth Science, v. 9, p. 72-184.

Newberry, R.J., and Einaudi, M.T., 1981, Tectonic and geochemical setting of tungsten skarn mineralization in the Cordillera. In Dickinson, W.R., and Payne, W.D. (eds) Relations of Tectonics to Ore Deposits in the Southern Cordillera: Arizona Geological Society Digest, v. 14, p. 99-112.

Nockolds, S.R., and Allen, R., 1953, Geochemistry of some igneous rock series, I: Geochimica Cosmochimica Acta, v. 4, p. 105-142.

O'Neil, J.R., and Chappell, B.W., 1977, Oxygen and hydrogen isotope relations in the Berridale batholith: Journal of the Geological Society of London, v. 133, p. 559-571.

O'Neil, J.R., and Clayton, R.N., 1964, Oxygen isotope geothermometry. In Craig, H., Miller, S., and Wasserburg, G.J. (eds) Isotopic and Cosmic Chemistry: North-Holland, Amsterdam, Netherlands, p. 157-168.

O'Neil, J.R., and Taylor, H.P., Jr., 1967, The oxygen isotope and cation exchange chemistry of feldspars: American Mineralogist, v. 52, p. 1414-1437.

O'Neil, J.R., Shaw, S.E., and Flood, R.H., 1977, Oxygen and hydrogen isotope compositions as indicators of granite genesis in the New England Batholith: Australia: Contributions to Mineralogy and Petrology, v. 62, p. 313-328.

Peacock, M.A., 1931, Classification of igneous rock series: Journal of Geology, v. 39, p. 54-67.

Peterman, Z.E., Hedge, C.F., Coleman, R.G., and Snavely, P.D., 1967, $^{87}Sr/^{86}Sr$ ratios in some eugeosynclinal sedimentary rocks and their bearing on the origin of granitic magmas in orogenic belts: Earth and Planetary Science Letters, v. 2, p. 433-439.

Pettijohn, F.J., 1963, Chemical composition of sandstones - excluding carbonate and volcanic sands: U.S. Geological Survey Professional Paper 440-S, 21 p.

Pitcher, W.S., 1979, The nature, ascent and emplacement of granitic magmas: Journal of the Geological Society of London, v. 136, p. 627-662.

Powell, R.E., 1981, Geology of the crystalline basement complex, Eastern Transverse Ranges, southern California: Constraints on regional tectonic interpretation: Ph.D. Thesis, California Institute of Technology, Pasadena, CA, 441 p.

Powell, R.E., 1982, Crystalline basement terranes in the southern Eastern Transverse Ranges, California. In Cooper, J.D. (ed) Geologic Excursion in the Transverse Ranges, Southern California, Field Trip: 78th Annual Meeting, Cordilleran Section, Anaheim, CA, Geological Society of America, p. 109-136.

Powell, R.E., 1986a, Palinspastic reconstruction of crystalline-rock assemblages in southern California: San Andreas Fault as part of an evolving system of late Cenozoic conjugate strike-slip faults: Geological Society of America Abstracts with Program, v. 18, n. 2, p. 172.

Powell, R.E., 1986b, Mesozoic and early Cenozoic fan folding in the Transverse Ranges: A window into the evolution of crustal structure in southern California: Geological Society of America Abstracts with Program, v. 18, n.2, p. 172.

Presnall, D.C., 1969, The geometrical analysis of partial fusion: American Journal of Science, v. 267, p. 1178-1194.

Presnall, D.C., and Bateman, P.C., 1973, Fusion relationships in the system $NaAlSi_3O_8$-$CaAl_2Si_2O_8$-$KAlSi_3O_8$-SiO_2-H_2O and generation of granitic magmas in the Sierra Nevada Batholith: Geological Society of America Bulletin, v. 84, p. 3181-3202.

Richmond, J.F., 1960, Geology of the San Bernardino Mountains north of Big Bear Lake, California: California Division of Mines and Geology Special Report 65, 68 p.

Roberts, R.J., Hotz, P.E., Gilluly, J., and Ferguson, H.G., 1958, Paleozoic rocks of north-central Nevada: Bulletin of the American Association of Petroleum Geologists, v. 42, p. 2813-2857.

Rogers, J.J.W., 1961, Igneous and metamorphic rocks of the western part of the Joshua Tree National Monument, Riverside and San Bernardino Counties, California: California Division of Mines and Geology Special Report 68, 26 p.

Rogers, T.H. (ed), 1966, Santa Ana sheet: California Division of Mines and Geology, Geologic Atlas of California.

Ross, D.C., 1984, Possible correlations of basement rocks across the San Andreas, San Gregario-Hosgri, and Rinconada-Reliz-King City Faults, California: U.S. Geological Survey Professional Paper 1317, 37 p.

Rytuba, J.J., Till, A.B., Blair, W., and Haxel, G., 1978, Reconnaissance geologic map of the Quijotoa Mountains quadrangle, Pima County, Arizona: U.S. Geological Survey Miscellaneous Field Studies Map, MF-937.

Sadler, P.M., 1982, Late Cenozoic stratigraphy and structure of the San Bernardino Mountains. In Cooper, J.D. (ed) Geologic Excursions in the Transverse Ranges, Southern California, Field Trip: 78th Annual Meeting, Cordilleran Section, Anaheim, CA, Geological Society of America, p. 55-106.

Saleeby, J.B., 1981, Ocean floor accretion and volcano-plutonic arc evolution of the Mesozoic Sierra Nevada. In Ernst, W.G. (ed) The Geotectonic Development of California: Rubey Volume I: Prentice-Hall, Inc., Englewood Cliffs, NJ, p. 132-181.

Saleeby, J.B., Sams, D.B., and Kistler, R.W., 1987, U/Pb zircon, strontium, and oxygen isotopic and geochronological study of the southernmost Sierra Nevada Batholith, California: Journal of Geophysical Research, v. 92, B10, p. 10,443-10,466.

Saleeby, J.B., et al., 1984, C-2; Central California offshore to Colorado Plateau: Centennial Continent/Ocean Transect, 10, 63 p.

Savin, S.M., and Epstein, S., 1970, The oxygen and hydrogen isotope geochemistry of clay minerals: Geochimica Cosmochimica Acta, v. 34, p. 25-42.

Schweickert, R.A., and Snyder, W.S., 1981, Paleozoic plate tectonics of the Sierra Nevada and adjacent regions. In Ernst, W.G. (ed) The Geotectonic Development of California, Rubey Volume I: Prentice-Hall, Inc., Englewood Cliffs, NJ, p. 182-202.

Shafiqullah, M., Damon, P.E., Lynch, D.J., Reynolds, S.J., Rehrig, W.A., and Raymond, R.H., 1980, K-Ar geochronology and geologic history of southwestern Arizona and adjacent areas. In Jenny, J.P., and Stone, J.C. (eds) Studies in Western Arizona: Arizona Geological Society Digest, v. 12, p. 201-260.

Sharry, J., 1981, Tectonic implications of granulite facies rocks from the western Tehachapi Mountains, California: Transactions of the American Geophysical Union, v. 62, p. 1048.

Shaw S.E., and Flood, R.H., 1981, The New England Batholith, eastern Australia: Geochemical variations in time and space: Journal of Geophysical Research, v. 86, B11, p. 10,530-10,544.

Sheppard, S.M.F., 1977, The Cornubian batholith, SW England: D/H and $^{18}O/^{16}O$ studies of kaolinite and other alteration minerals: Journal of the Geological Society of London, v. 133, p. 573-591.

Sheppard, S.M.F., 1986, Characterization and isotopic variations in natural waters. In Valley, J.W., Taylor, H.P., Jr., and O'Neil, J.R. (eds) Reviews in Mineralogy, Volume 16: Stable Isotopes in High Temperature Geologic Processes: Mineralogical Society of America, p. 165-183.

Sheppard, S.M.F., and Taylor, H.P., Jr., 1974, Hydrogen and oxygen evidence for the origins of water in the Boulder Batholith and the Butte ore deposits, Montana: Economic Geology, v. 69, p. 926-946.

Sheppard, S.M.F., Nielsen, R.L., and Taylor, H.P., Jr., 1969, Oxygen and hydrogen isotope ratios of clay minerals from porphyry copper deposits: Economic Geology, v. 64, p. 755-777.

Sheppard, S.M.F., Nielsen, R.L., and Taylor, H.P., Jr., 1971, Hydrogen and oxygen isotope ratios in minerals from prophyry copper deposits: Economic Geology, v. 66, p. 515-542.

Shieh, Y.N., and Schwarcz, H.P., 1977, An estimate of the oxygen isotope composition of a large segment of the Canadian Shield in northwestern Ontario: Canadian Journal of Earth Sciences, v. 14, p. 927-931.

Shieh, Y.N., and Taylor, H.P., Jr., 1969a, Oxygen and carbon isotope studies of contact metamorphism of carbonate rocks: Journal of Petrology, v. 10, p. 307-331.

Shieh, Y.N., and Taylor, H.P., Jr., 1969b, Oxygen and hydrogen isotope studies of contact metamorphism in the Santa Rosa Range, Nevada, and other areas: Contributions to Mineralogy and Petrology, v. 20, p. 306-356.

Silver, L.T., 1968, Pre-Cretaceous basement rocks and their bearing on large-scale displacements in the San Andreas fault system. In Dickinson, W.R., and Grant, A. (eds) Proceedings of Conference on Geologic Problems in San Andreas Fault System: Stanford University Publications, Geological Sciences, v. 11, p. 279.

Silver, L.T., 1971, Problems of crystalline rocks of the Transverse Ranges: Geological Society of America Abstracts with Program, v. 3, n. 2, p. 193-194.

Silver, L.T., 1978, Precambrian formations and Precambrian history in Cochise County: In Callender, J.T., Wilt, J.C., and Clemmons, R.E., (eds) Land of Cochise: Guidebook, New Mexico Geological Society 29th Field Conference, p. 157-163.

Silver, L.T., 1982, Evidence and a model for west-directed early to mid-Cenozoic basement overthrusting in southern California: Geological Society of America Abstracts with Program, v. 14, p. 617.

Silver, L.T., 1983 Paleogene overthrusting in the tectonic evolution of the Transverse Ranges, Mojave and Salinian regions, California: Geological Society of America Abstracts with Program, v. 15, p. 438.

Silver, L.T., and Anderson, T.H., 1974, Possible left-lateral early to middle Mesozoic disruption of the southwestern North American craton margin: Geological Society of America Abstracts with Program, v. 6, p. 955-956.

Silver, L.T., and Anderson, T.H., 1983, Further evidence and analysis of the role of the Mojave-Sonora Megashear(s) in Mesozoic Cordilleran tectonics: Geological Society of America Abstracts with Program, v. 15, p. 273.

Silver, L.T., and Chappell, B.W., 1988, The Peninsular Ranges Batholith: An insight into the evolution of the Cordilleran batholiths of southwestern North America: Transactions of the Royal Society of Edinburgh, Earth Sciences, v. 79, p. 105-121.

Silver, L.T., Taylor, H.P., Jr., and Chappell, B.W., 1979, Some petrological, geochemical and geochronological observations of the Peninsular Ranges Batholith near the International border of the U.S.A. and Mexico. In Abbott, P.L., and Todd, V.R., (eds) Mesozoic Crystalline Rocks. Fieldtrip Guidebook, 1979 Annual Meeting of the Geological Society of America:, Department of Geological Science, San Diego State University, San Diego, CA, p. 83-110.

Silver, L.T., Anderson, C.A., Crittenden, M.D., Jr., and Robertson J.M., 1977a, Chronostratigraphic elements of the Precambrian rocks of the southwestern and far western United States: Geological Society of America Abstracts with Program, v. 9, p. 1176.

Silver, L.T., McKinney, C.R., Deutsch, S., and Bolinger, J., 1963, Precambrian age determinations in the western San Gabriel Mountains, California: Journal of Geology, v. 71, p. 196-214.

Silver, L.T., Bickford, M.E., Van Schmus, W.R., Anderson, J.L., Anderson, T.H., and Medaris, L.G., 1977b, The 1.4-1.5 b.y. transcontinental anorogenic plutonic perforation of North America: Geological Society of America Abstracts with Program, v. 9, p. 1176-1177.

Silverman, S.R., 1951, The isotope geology of oxygen: Geochimica Cosmochimica Acta, v. 2, p. 26-42.

Simmons, E.C., and Hedge, C.E., 1978, Minor-element and Sr-isotope geochemistry of tertiary stocks, Colorado Mineral Belt: Contributions to Mineralogy and Petrology, v. 67, p. 379-396.

Sinha, A.K., and Davis, T.E., 1970, Geochemistry of Franciscan volcanic and sedimentary rocks from California: Carnegie Institute of Washington Yearbook, v. 69, p. 394-400.

Smith, G.I., 1962, Large lateral displacement on the Garlock fault, California, as measured from offset dike swarm: American Association of Petroleum Geology Bulletin, v. 46, p. 85-104.

Smith, G.I., and Ketner, K.B., 1970, Lateral displacement on the Garlock Fault, southeastern California, suggested by offset section of similar metasedimentary rocks: U.S. Geological Survey Professional Paper 700-D, 9 p.

Snoke, A.W., and Miller, D.M., 1988, Metamorphic and tectonic history of the northeastern Great Basin. In Ernst, W.G. (ed) Metamorphism and Crustal Evolution, Western Coterminous United States, Rubey Volume VII: Prentice-Hall, Inc., Englewood Cliffs, NJ, p. 606-648.

Snyder, W.S., Dickinson, W.R., and Silberman, M.L., 1976, Tectonic implications of space-time patterns of Cenozoic magmatism in the western United States: Earth and Planetary Science Letters, v. 32, p. 91-106.

Solomon, G.C., and Taylor, H.P., Jr., 1981, The geographic distribution of $\delta^{18}O$ values in Mesozoic and early Cenozoic granitic rocks of the southwestern North American Cordillera: Geological Society of America Abstracts with Program, v. 13, p. 558.

Solomon, G.C., and Taylor, H.P., Jr., 1982, Tectonic evolution of oxygen isotope terranes in Mesozoic batholithic rocks of the Transverse Ranges, California: Geological Society of America Abstracts with Program, v. 14, n. 4, p. 235.

Solomon, G.C., Dilles, J.H., Criss, R.E., and Taylor, H.P., Jr., 1983, $^{18}O/^{16}O$ and D/H characteristics of the Ann-Mason porphyry copper deposit, Yerington, Nevada: Geological Society of America Abstracts with Program, v. 15, n. 5, p. 277.

Speed, R.C., 1979, Collided Paleozoic microplate in the western United States: Journal of Geology, v. 87, p. 279-292.

Speed, R.C., and Moores, E.M., 1980, Geologic cross section of the Sierra Nevada and the Great Basin along 40°N Latitude, northeastern California and northern Nevada: Geological Society of America Map Chart Series, MC-28L.

Stakes, D.S., and Taylor, H.P., Jr., 1984, Oxygen isotope and field study of the northern Samail ophiolite, Sultanate of Oman: Geological Society of America Abstracts with Program, v. 16, p. 666.

Steiner, J.C., Jahns, R.H., and Luth, W.C., 1975, Crystallization of alkali feldspar and quartz in the haplogranite system $NaAlSi_3O_8$-$KAlSi_3O_8$-SiO_2-H_2O at 4 Kbar: Geological Society of America Bulletin, v. 86, p. 83-98.

Stewart, J.H., 1971, Basin and Range structure; a system of horsts and grabens produced by deep-seated extension: Geological Society of America Bulletin, v. 82, p. 1019-1044.

Stewart, J.H., 1972, Initial deposits in the Cordilleran geosyncline: Evidence of a late Precambrian (<850 my) continental separation: Geological Society of America Bulletin, v. 83, p. 1345-1360.

Stewart, J.H., 1980, Geology of Nevada: Nevada Bureau of Mines and Geology Special Publication 4, 136 p.

Stewart, J.H., and Poole, F.G., 1974, Lower Paleozoic and uppermost Precambrian Cordilleran miogeosyncline, Great Basin, western United States. In Dickinson, E.R. (ed) Tectonics and Sedimentation: Society of Economic Paleontology and Mineralogy Special Paper 22, p. 28-57.

Stewart, J.H., and Poole, F.G., 1975, Extension of the Cordilleran miogeosynclinal belt to the San Andreas fault, southern California: Geological Society of America Bulletin, v. 86, p. 205-212.

Stewart, J.H., Moore, W.J., and Zietz, I., 1977, East-west patterns of Cenozoic igneous rocks, aeromagnetic anomalies, and mineral deposits, Nevada and Utah: Geological Society of America Bulletin, v. 88, p. 67-77.

Stone, P., Stevens, C.H., and Cavit, C.D., 1980, A regional Early Permian angular unconformity in eastern California: Geological Society of America Abstracts with Program, v. 12, n. 3, p. 154.

Streickesen, A., 1976, To each plutonic rock its proper name: Earth Science Reviews, v. 12, p. 1-33.

Strong, D.F., 1980, Granitoid rocks and associated mineral deposits of eastern Canada and western Europe. In Strangway, D.W. (ed) The Continental Crust and its Mineral Deposits: Geological Association of Canada Special Paper 20, p. 741-769.

Suppe, J., and Armstrong, R.L., 1972, Potassium-argon dating of Franciscan metamorphic rocks: American Journal of Science, v. 272, p. 217-233.

Taylor, B.E., and O'Neil, J.R., 1977, Stable isotope studies of metasomatic Ca-Fe-Al-Si skarns and associated metamorphic and igneous rocks. Osgood Mountains, Nevada: Contributions to Mineralogy and Petrology, v. 63, p. 1-49.

Taylor, H.P., Jr., 1968, The oxygen isotope geochemistry of igneous rocks: Contributions to Mineralogy and Petrology, v. 19, p. 1-71.

Taylor, H.P., Jr., 1970, Oxygen isotope studies of anorthosites, with particular reference to the origin of bodies in the Adirondack Mountains, New York: New York State Museum and Science Service Memoir 18, p. 111-134.

Taylor, H.P., Jr., 1971, Oxygen isotope evidence for large-scale interaction between meteoric ground waters and Tertiary granodiorite intrusions, western Cascade Range, Oregon: Journal of Geophysical Research, v. 76, p. 7855-7874.

Taylor, H.P., Jr., 1974, The application of oxygen and hydrogen isotope studies to problems of hydrothermal alteration and ore deposition: Economic Geology, v. 69, p. 843-883.

Taylor, H.P., Jr., 1977, Water/rock interactions and the origin of H2O in granitic batholiths: Journal of the Geological Society of London, v. 133, p. 509-558.

Taylor, H.P., Jr., 1978, Oxygen and hydrogen isotope studies of plutonic granitic rocks: Earth and Planetary Science Letters, v. 38, p. 177-210.

Taylor, H.P., Jr., 1980, The effects of assimilation of country rocks by magmas on $^{18}O/^{16}O$ and $^{87}Sr/^{86}Sr$ systematics in igneous rocks: Earth and Planetary Science Letters, v. 47, p. 243-254.

Taylor, H.P., Jr., 1986, Igneous rocks: II. Isotopic case studies of circumpacific magmatism. In Valley, J.W., Taylor, H.P., Jr., and O'Neil, J.R. (eds) Reviews in Mineralogy, Volume 16: Stable Isotopes in High Temperature Geologic Processes: Mineralogical Society of America, p. 273-317.

Taylor, H.P., Jr., 1988, Oxygen, hydrogen, and strontium constraints on the origin of granites: Transactions of the Royal Society of Edinburgh, Earth Sciences, v. 79, p. 317-338.

Taylor, H.P., Jr., and Coleman, R.G., 1968, $^{18}O/^{16}O$ ratios of coexisting minerals in glaucophane-bearing metamorphic rocks: Geological Society of America Bulletin, v. 79, p. 1727-1756.

Taylor, H.P., Jr., and Epstein, S., 1962a, Relationship between $^{18}O/^{16}O$ ratios in coexisting minerals of igneous and metamorphic rocks. Part 1. Principles and experimental results: Geological Society of America Bulletin, v. 73, p. 461-480.

Taylor, H.P., Jr., and Epstein, S., 1962b, Relationship between $^{18}O/^{16}O$ ratios in coexisting minerals of igneous and metamorphic rocks. Part 2. Application to petrologic problems: Geological Society of America Bulletin, v. 73, p. 675-694.

Taylor, H.P., Jr., and Epstein, S., 1970, Oxygen and silicon isotope ratios of lunar rock 12013: Earth and Planetary Science Letters, v. 9, p. 208-210.

Taylor, H.P., Jr., and Forester, R.W., 1971, Low-^{18}O igneous rocks from the intrusive complexes of Skye, Mull and Ardnamurchan, Western Scotland: Journal of Petrology, v. 12, p. 465-497.

Taylor, H.P., Jr., and Forester, R.W., 1979, An oxygen and hydrogen isotope study of the Skaergaard intrusion and its country rocks: A description of a 55 m.y. old fossil hydrothermal system: Journal of Petrology, v. 20, p. 355-419.

Taylor, H.P., Jr., and Magaritz, M., 1978, Oxygen and hydrogen isotope studies of the Cordilleran batholiths of western North America. In Robinson, B.W. (ed) Stable Isotopes in the Earth Sciences: New Zealand Department of Science and Industry Research Bulletin 220, Wellington, NZ, p. 151-173.

Taylor, H.P., Jr., and Sheppard, S.M.F., 1986, Igneous rocks: I. Processes of isotopic fractionation and isotope systematics. In Valley, J.W., Taylor, H.P., Jr., and O'Neil, J.R. (eds) Reviews in Mineralogy, Volume 16: Stable Isotopes in High Temperature Geological Processes: Mineralogical Society of America, p. 227-271.

Taylor, H.P., Jr., and Silver, L.T., 1978, Oxygen isotope relationships in plutonic igneous rocks of the Peninsular Ranges Batholith, southern and Baja California. In Zartman, R.E. (ed) Short Papers of the 4th International Conference on Geochronology, Cosmochronology, and Isotope Geology: U.S. Geological Survey Open-File Report 78-701, p. 423-426.

Taylor, H.P., Jr., and Turi, B., 1976, High-^{18}O rocks from the Tuscan magmatic province, Italy: Contributions to Mineralogy and Petrology, v. 55, p. 4-31.

Taylor, H.P., Jr., Gianetti, B., and Turi, B., 1979, Oxygen isotope geochemistry of the potassic igneous rocks from the Roccamonfina Volcano, Roman Comagmatic Region, Italy: Earth and Planetary Science Letters, v. 46, p. 81-106.

Thayer, T.P., 1963, The Canyon Mountain Complex, Oregon, and the alpine mafic magma stem: U.S. Geological Survey Professional Paper 475-C, p. 82-85.

Titley, S.R., 1981, Geologic and geotectonic setting of prophyry copper deposits in the southern Cordillera. In Dickinson, W.R., and Payne, W.D. (eds) Relations of Tectonics to Ore Deposits in the Southern Cordillera: Arizona Geological Society Digest, v. 14, p. 79-98.

Todd, V.R., and Shaw, S.E., 1985, S-type granitoids and an I-S line in the Peninsular Ranges Batholith, southern California: Geology, v. 13, p. 231-233.

Tosdal, R.M., 1982, The Mule Mountains Thrust in the Mule Mountains, California, and its probable extension in the Dome Rock Mountains, Arizona; a preliminary report. In Frost, E.G. and Martin, D.L. (eds) Mesozoic-Cenozoic Tectonic Evolution of the Colorado River Region,

California, Arizona and Nevada: Cordilleran Publishers, San Diego, CA, p. 55-60.

Tosdal, R.M., Peterson, D.W., May, D.J., LeVeque, R.A., and Miller, R.J., (1986) Reconnaissance geologic map of the Mt. Ajo and part of the Pisinimo 15' quadrangle, Pima County, Arizona: U.S. Geological Survey Miscellaneous Field Studies Map, MF-1820.

Turekian, K.K., and Wedepohl, K.H., 1961, Distribution of the elements in some major units of the Earth's crust: Geological Society of America Bulletin, v. 72, p. 175-192.

Turi, B., and Taylor, H.P., Jr., 1971a, An oxygen and hydrogen isotope study of a granodiorite pluton from the Southern California Batholith: Geochimica Cosmochimica Acta, v. 35, p. 383-406.

Turi, B., and Taylor, H.P., Jr., 1971b, $^{18}O/^{16}O$ ratios of the Johnny Lyon granodiorite and Texas Canyon quartz monzonite plutons, Arizona, and their contact aureoles: Contributions to Mineralogy and Petrology, v. 32, p. 138-146.

Tuttle, O.F., and Bowen, N.L., 1958, Origin of granite in the light of experimental studies in the system $NaAlSi_3O_8$-$KAlSi_3O_8$-SiO_2-H_2O: Geological Society of America Memoir, v. 74, 153 p.

Vaughn, F.E., 1922, Geology of San Bernardino Mountains north of San Gorgonio Pass: University of California (Berkeley), Department of Geological Sciences Bulletin 13, p. 319-411.

Vogel, D.E., and Garlick, G.D., 1970, Oxygen-isotope ratios in metamorphic eclogites: Contributions to Mineralogy and Petrology, v. 28, p. 183-191.

Vollmer, R., 1976, Rb-Sr and U-Th-Pb systematics of alkaline rocks: The alkaline rocks from Italy: Geochimica Cosmochimica Acta, v. 40, p. 283-295.

Wager, L.R., and Deer, W., 1939, Geological investigations in East Greenland. Part III. The petrology of the Skaergaard intrusion, Kamgerlugsuaq: Medd. Gronland, v. 105, n. 4, p. 1-353.

Weldon, R.J., and Humphreys, E., 1986, A kinematic model of southern California: Tectonics, v. 5, p. 33-48.

Wenner, D.B., 1981, Oxygen isotopic compositions of the late orogenic granites in the Southern Piedmont of the Appalachian mountains, U.S.A., and their relationship to subcrustal structures and lithologies: Earth and Planetary Science Letters, v. 54, p. 186-199.

White, A.J.R., and Chappell, B.W., 1977, Ultrametamorphism and granitoid genesis: Tectonophysics, v. 43, p. 7-22.

White, A.J.R., Clemmons, J.D., Holloway, J.R., Silver, L.T., Chappell, B.W., and Wall, V.J., 1986, S-type granites and their probable absence in southwestern North America: Geology, v. 14, p. 115-118.

Whitney, J.A., 1975, The effects of pressure, temperature and H_2O on phase assemblage in four synthetic rock compositions: Journal of Geology, v. 83, p. 1-31.

Wickham, S.M., and Taylor, H.P., Jr., 1985, Stable isotopic evidence for large-scale seawater infiltration in a regional metamorphic terrane; the Trois Seigneurs Massif, Pyrenees, France: Contribution to Mineralogy and Petrology, v. 91, p. 122-137.

Wickham, S.M., and Taylor, H.P., Jr., 1987, Stable isotopic constraints on the origin and depth of penetration of hydrothermal fluids associated with Hercynian low-pressure regional metamorphism and crustal anatexis in the Pyrenees: Contributions to Mineralogy and Petrology, v. 95, p. 255-268.

Wickham, S.M., and Taylor, H.P., Jr., 1988, Fluid-rock interaction and circulation mechanisms of surface-derived fluids in ductile shear zones, Pyrenees: Geological Society of America Abstracts with Program, v. 20, n. 7, p. A-330.

Willden, R., and Speed, R.C., 1974, Geology and mineral deposits of Churchill County, Nevada: Nevada Bureau of Mines and Geology Bulletin 83, 95 p.

Wilson, A.F., Green, D.C., and Davidson, L.R., 1970, The use of oxygen isotope geothermometry on the granulites and related intrusives, Musgrave Ranges, Central Australia: Contributions to Mineralogy and Petrology, v. 27, p. 166-178.

Wilson, E.D., Moore, R.T., and Cooper, J.R., 1969, Geologic Map of Arizona: Arizona Bureau of Mines and U.S. Geological Survey, University of Arizona, Tucson, AZ.

Wright, J.E., and Haxel, G., 1983, A garnet-two-mica granite, Coyote Mountains, southern Arizona: Geologic setting, uiranium-lead isotopic systematics of zircons, and nature of the granite source region: Geological Society of America Bulletin, v. 93, p. 1176-1188.

Wright, J.E., Haxel, G., and May, D.J., 1981, Early Jurassic uranium-lead isotopic ages for Mesozoic supracrustal sequences, Papago Indian Reservation, southern Arizona: Geological Society of America Abstracts with Program, v. 13, p. 115.

Wyllie, P.J., 1977, Crustal anatexis: An experimental review: Tectonophysics, v. 43, p. 41-71.

Wyllie, P.J., 1978, Water and magma generation at subduction zones: Bulletin of Volcanology, v. 41-4, p. 360-377.

Wyllie, P.J., 1981a, Magma sources in Cordilleran settings. In Dickinson, W.R., and Payne, W.D., (eds) Relations of Tectonics to Ore Deposits in the Southern Cordillera: Arizona Geological Society Digest, v. 14, p. 39-48.

Yeats, R.S., 1981, Quaternary flake tectonics of the California Transverse Ranges: Geology, v. 9, p. 16-20.

Zartman, R.E., 1974, Lead isotopic provinces in the Cordillera of the western United States and their geologic significance: Economic Geology, v. 69, p. 792-805.

Zoback, M., and Thompson, G., 1978, Basin and Range rifting in northern Nevada: Clues from a mid-Miocene rift and its subsequent offsets: Geology, v. 6, p. 111-116.

Table 1 New $^{18}O/^{16}O$ data obtained in this work for Mesozoic and Cenozoic plutons in Nevada, western Utah, southern California and south-central Arizona.*

GCS#	Sample Description	Age, Ma	$\delta^{18}O$	Remarks	Location
	I. Southern Basin and Range $^{18}O/^{16}O$ Traverse				
	A. South-Central Arizona Segment (see Chapter 5)				
	Presumido Peak-Coyote Mountains (PPCM) Area (see Figure 5.3)				
001	Leucocratic garnet-muscovite granite	58[1]	7.1, 9.2Q 7.2, 9.2Q	Pan Tak Granite, Coyote Mtns, PUP14 (Haxel), approx. 1.3 km SE of Pan Tak	32° 00.30' 111° 03.13'
002	" "		6.8	Approx. 15 m west of 001	
003	Biotite monzogranite		8.9, 10.1Q	Pan Tak Granite, Quinlan Mtns, PUP15 (Haxel), in Sells Wash approx. 4.5 km SE of AZ Hwy 86	31° 57.67' 111° 40.31'
004	" "		8.4	Pan Tak Granite, Quinlan Mtns, in Sells Wash approx. 3.0 km SE of AZ Hwy 86	31° 58.15' 111° 41.36'
005	" "		9.9Q	Approx. 1 m from 004	
006	Leucocratic garnet-muscovite granite	58[1]	9.0, 9.8Q 9.3, 9.3Q	Presumido Peak Granite, Baboquivari Mtns, PUP32 (Haxel), in Los Encinos Wash approx. 2.0 km WSW of Los Encinos Ranch	31° 36.08' 111° 37.18'
008	Biotite monzogranite		7.7, 7.2Q	Presumido Peak Granite, at head of Presumido Cyn, approx. 0.6 km SSW of Presumido Ranch	31° 32.28' 111° 36.07'
009	" "		10.2Q	Presumido Peak Granite, hilltop approx. 0.6 km S of Sasabe	31° 28.96' 111° 32.45'
023	Quartz syenite	150[2]	6.7	Ko Vaya Granite, North Comobabi Mtns, PUP4 (Haxel), approx. 1.1 km SSW of Mt Devine, coll. by Haxel	32° 07.33' 111° 48.48'
026	Hornblende-biotite granodiorite	165[2]	7.4, 8.5Q	Kitt Peak Granodiorite, Quinlan Mtns, PUP11 (Haxel), approx. 1.0 km SW of Kitt Peak, coll. by Haxel	31° 57.41' 111° 36.36'
238	Biotite-hornblende monzodiorite	>145	6.7	Jurassic plutonic complex, Morena Mtn, SP701 (Haxel), approx. 0.6 km NNE of Horse Peak, coll. by Haxel	31° 01.01' 111° 52.43'
241	Biotite-muscovite granite	<135	9.4	Granite correlative with Pan Tak-granite type plutonism, Morena Mtn, SP686 (Haxel), approx. 0.3 km SSW of San Augustin Ranch, coll. by Haxel	31° 31.95' 111° 53.68'
	Gunsight Hills-Sierra Blanca (GHSB) Area (see Figure 5.4)				
011	Leucocratic garnet-muscovite granite	58[3]	8.6, 9.8Q	Sierra Blanca Granite, Sierra Blanca, PUP6 (Haxel), approx. 1.9 km SSE of Rabia (along ridge axis)	32° 11.77' 112° 14.24'

GCS#	Sample Description	Age, Ma	$\delta^{18}O$	Remarks	Location
017	Hornblende-biotite monzogranite	67[1]	8.3, 10.1Q	Gunsight Hills Stock, Gunsight Hills, PUP36 (Haxel), approx. 8 km SSE of AZ Hwy 86 on road to Gu Vo	32° 09.39' 112° 39.14'
018	Hornblende-biotite monzodiorite, alt. (ep, chl)	68[2]	7.7	Cimar Stock, Cimarron Mtns, PUP9 (Haxel), approx. 15 m SE of the Montazona Mine	32° 26.81' 112° 06.41'
019	" " alt. (ep, chl)		8.2, 9.9Q	Cimar Stock, Cimarron Mtns, approx. 1.1 km NW of the Montazona Mine	32° 27.24' 112° 06.92'
020	Hornblende-biotite monzogranite	<135	7.7	Granitic pluton assoc. w/the Cimar Stock, Cimarron Mtns, approx. 0.9 km ESE of the Montazona Mine at S toe of small ridge	32° 26.64' 112° 06.06'
021	" "		8.3, 10.4Q	Granitic pluton assoc. w/the Cimar Stock, Cimarron Mtns, approx. 1.0 km E of the Montazona Mine	32° 26.81' 112° 05.76'
022	" "		7.7, 11.0Q	Granitic pluton assoc. w/the Cimar Stock, Cimarron Mtns, approx. 1.1 km E of the Montazona Mine	32° 26.81' 112° 05.71'
030	Leucocratic granite	67[1]	7.4, 8.0Q	Gunsight Hills Stock, Gunsight Hills, PUP37 (Haxel), approx. 2.0 km SE of Ninemile Peak, coll. by Haxel	32° 11.12' 112° 01.11'
230	Hornblende-biotite granodiorite	165[2]	9.2	Brownell Mtns. Plutonic Complex, Brownell Mtns., B48 (Haxel), approx. 0.7 km SE of Brownell Peak, coll. by Haxel	32° 12.02' 112° 08.63'
231	Hornblende-biotite monzodiorite		6.7	Brownell Mtns. Plutonic Complex, Brownell Mtns., B33 (Haxel), approx. 3.0 km ESE of Brownell Peak, coll. by Haxel	32° 11.69' 112° 07.10'
			Western Area (see Figure 5.5)		
012A	Muscovite-biotite granite	<135	8.0, 9.1Q	Sierra Pinta Granite, Bryan Mtns, PUP31 (Haxel), approx. 4.6 km ENE of BM 851 along Papago Well Dirt Road, coll. by Haxel	32° 16.94' 113° 21.72'
013	Biotite-hornblende monzogranite, alt., (ep., chl., ab)	<135	9.8Q	New Cornelia Stock, Little Ajo Mtns., approx. 0.6 km S of the NE corner of section 17, R6W, T12S	32° 28.02' 112° 53.94'
014A	Muscovite-biotite granite	<135	8.0, 9.1Q	Sierra Pinta Granite, Sierra Pinta, #3 (Silver), approx. 1.9 km N of Pinta Peak, coll. by L.T. Silver	32° 16.77' 113° 32.52'
015	Biotite-hornblende monzogranite, alt., (ep., chl., ab)	<135	8.2, 7.9Q	New Cornelia Stock, Little Ajo Mtns., approx. 10 m SE of GCS013	32° 28.02' 112° 53.94'
215	biotite monzogranite	<135	7.8	Bandeja Well Granite, Quitobaquito Hills, PUP50 (Haxel), approx. 3.0 km W of Cipriano Pass, coll. by Haxel	31° 59.15' 113° 02.88'

GCS#	Sample Description	Age, Ma	$\delta^{18}O$	Remarks	Location
232	Biotite granite	<135	7.4	Sierra Pinta Granite, Granite Mtns., DC22 (Haxel), approx. 1.7 km WSW of Cristobal Peak, coll. by Haxel	32° 20.81' 113° 18.13'
233	" "		7.7	Sierra Pinta Granite, Granite Mtns., DC18 (Haxel), approx. 1.5 km NNW of Granite Pass Tank, coll. by Haxel	32° 19.78' 113° 15.66'
235	" "		7.7	Sierra Pinta Granite, Granite Mtns., DC17 (Haxel), approx. 1.0 km S of Granite Pass Tank, coll. by Haxel	32° 18.49' 113° 15.48'
239	Biotite monzogranite	<135	8.0	Aguajita Wash Granite, Quitobaquito Hills, OP784a (Haxel), approx. 0.6 km NNW of Aguajita Spring, Coll. by Haxel	31° 56.66' 113° 00.78'
240	" "	<135	7.6	Cerro Blanco Granite, Cerro Blanco, OP724 (Haxel), approx. 1.2 km ESE of Corner Well, about 10 m into Mexico from marker "1025", coll. by Haxel	31° 57.41' 113° 04.39'
505	Biotite granite	<135	7.5	Sierra Pinta Granite, Granite Mtns., DC29 (Haxel), approx., 2.1 km NW of Granite Peak, coll. by Haxel	32° 26.42' 113° 19.44'
			Miscellaneous Arizona Localities		
035	Biotite-hornblende monzodiorite	>145	7.7, 9.1Q	Bisbee Intrusive, BiF (Tim Benjamin) Bisbee, AZ	31° 30.49' 109° 58.39'
	B. Central and Eastern Transverse Ranges, California Segment (see Chapter 6)				
	San Gabriel Mountains (SGM) Area (see Figure 6.3)				
113	Biotite monzogranite	71[4]	8.1	Granite of Pacoima Creek, western SGM, roadcut on fire service road, approx. 4.8 km W of Dillon Ranch	34° 21.03' 118° 24.44'
114	" "		10.5	Granite of Pacoima Creek, western SGM, roadcut approx. 2.5 km W of GCS113	34° 21.27' 118° 26.05'
115	" "	71[4]	9.0	Granite of Cold Creek, western SGM, roadcut on Cold Creek road, approx. 2 km N of Middle Ranch	34° 18.96' 118° 20.39'
116	Biotite granodiorite	71[4]	6.0	Granite of Tujunga Canyon, western SGM, roadcut along Big Tunjunga Wash, approx. 3.0 km NE of Sunland	34° 17.76' 118° 16.85'
117	Biotite monzogranite	80[5] 66[4]	8.9	Josephine Mtn. Pluton, western SGM, roadcut on Cold Creek road, approx. 5.0 km ESE of Mendenhall Peak	34° 18.79' 118° 15.52'
118	" "		8.4	Josephine Mtn. Pluton, western SGM, roadcut, approx. 3.0 km SW of junction between Big Tujunga Wash and Palmdale Hwy	34° 17.34' 118° 11.09'

GCS#	Sample Description	Age, Ma	$\delta^{18}O$	Remarks	Location
119	Biotite monzogranite	80[5] 66[4] 75H[4]	8.3	Josephine Mtn. Pluton, western SGM, roadcut, approx. 0.5 km N of bridge over Tujunga Ck. along Palmdale Hwy	34° 18.93' 118° 08.23'
120	Leucocratic syenite	220[6] 74[4]	7.6	Lowe Granodiorite, central SGM, roadcut on Mt. Gleason Rd, approx. 2.0 km WNW of junction with Palmdale Hwy	34° 23.89' 118° 05.97'
121	" "	65[4]	6.8	Lowe Granodiorite, central SGM, roadcut on Palmdale Hwy, approx. 1.5 km N of junction with Aliso Canyon Rd	34° 25.45' 118° 05.55'
122	Biotite monzogranite	65[4]	7.1	Mt. Wilson Pluton, central SGM, roadcut on Red Box Rd, approx. 1.0 km SE of Angeles Crest Hwy	34° 15.00' 118° 05.92'
123	Biotite-hornblende granodiorite		6.6	Mt. Wilson Pluton, central SGM, outcrop, Mt. Wilson tower center	34° 13.45' 118° 03.49'
124	Leucocratic syenite	220[6] 65[4]	7.4	Lowe Granodiorite, central SGM, roadcut on Angeles Crest Hwy, apprx. 1.2 km W of junction with Palmdale Hwy	34° 16.21' 118° 10.06'
125	Biotite monzogranite	70[4]	6.3	Granite of La Canada, central SGM, roadcut on Angeles Crest Hwy, apprx. 1.8 km NW of La Canada Ranger Station	34° 14.83' 118° 11.62'
137	" "	80[5] 65[4]	8.8	Josephine Mtn. Pluton, central SGM, roadcut on Angeles Crest Hwy, apprx. 0.3 km NE of junction with Red Box Rd	34° 15.59' 118° 06.09'
138	Leucocratic syenite	220[6] 65[4]	7.0	Lowe Granodiorite, central SGM, roadcut on Angeles Crest Hwy, apprx. 0.2 km S of Chileo Flats	34° 17.07' 117° 59.67'
139	" "	65[4]	7.1	Lowe Granodiorite, central SGM, roadcut on Angeles Crest Hwy at Maintenance Station N of Chileo Flats	34° 19.21' 118° 00.29'
140	" "	65[4]	7.2	Lowe Granodiorite, central SGM, roadcut on dirt road, approx. 3.7 km NNW of Maintenance Station	34° 20.86' 118° 01.77'
141	" "		7.8	Lowe Granodiorite, central SGM, outcrop on dirt road, approx. 5.0 km NE of GCS 140	34° 22.49' 117° 58.89'
142	Biotite monzogranite	65[4]	7.8	Waterman Mtn. Pluton, central SGM, roadcut on Angeles Crest Hwy, apprx. 3.5 km W of Waterman Mtn.	34° 20.41' 117° 58.15'
143	" "		7.4	Waterman Mtn. Pluton, central SGM, roadcut on Angeles Crest Hwy, apprx. 1.0 km E of Waterman Mtn.	34° 20.41' 117° 55.06'
144	" "		8.1	Waterman Mtn. Pluton, central SGM, roadcut on Angeles Crest Hwy, apprx. 1.0 km W of junction with Hwy 39	34° 21.62' 117° 51.77'

GCS#	Sample Description	Age, Ma	$\delta^{18}O$	Remarks	Location
145	Biotite monzogranite	65[4]	7.3	Josephine Mtn. Pluton (outlier), central SGM, roadcut, road along Tujunga Ck., approx. 2.0 km S of Vetter Mtn.	34° 16.62' 118° 01.87'
146	Leucocratic syenite	220[6] 65[4]	7.7	Lowe Granodiorite, central SGM, roadcut, road along Tujunga Ck., approx. 2.5 km W of Vetter Mtn.	34° 17.76' 118° 03.49'
147	Biotite monzogranite	65[4]	8.3	Josephine Mtn. Pluton (outlier), roadcut, road along Tujunga Ck., approx. 1.0 km W of GCS145	34° 16.89' 118° 02.88'
300	Biotite-hornblende granodiorite	72[4]	8.7	Granite of Silver Mtn., central SGM roadcut on Hwy 39, approx. 3.0 km SW of SW end of Morris Reservoir	34° 09.43' 117° 54.05'
301	" "	72[4]	8.6	Waterman Mtn. Pluton, central SGM, roadcut on Hwy 39, approx. 1.0 km W of Crystal Lake	34° 19.28' 117° 51.21
302	" "	72[4]	7.3	Waterman Mtn. Pluton, central SGM, roadcut on Hwy 39, approx. 2.0 km SSW of Coldbrook Guard Station	34° 16.50' 117° 50.69'
303	" "	72[4]	7.3	Granite of Silver Mtn., central SGM, roadcut on Glendora Rd, approx. 2.0 km E of Morris Dam	34° 10.50' 117° 50.68'
	San Bernardino Mountains (SBM) Area (Figure 6.7)				
043	Biotite monzogranite	66[4]	10.3, 11.1Q	Cactus Granite (Vaughn), central SBM, roadcut on Hwy 30, approx. 2.6 km NNE of Harrison Mtn.	34° 11.16' 117° 08.79'
044	Biotite-hornblende monzogranite	68[4]	8.3	Cactus Granite (Vaughn), central SBM, weathered outcrop, approx. 0.4 km E of junction between Hwy 18 and Stanfield Cutoff	34° 15.38' 116° 52.64'
047	Biotite-muscovite granite (+ dup.)	65[4]	8.8, 9.9Q 8.7	Cactus Granite (Vaughn), central SBM, outcrop, approx. 0.25 km NW of Cactus Spring near Hwy 18	34° 18.96' 116° 48.53'
048	" "	65[4]	8.9	Cactus Granite (Vaughn), central SBM, outcrop, approx. 0.55 km WNW of GCS047, on Hwy 18	34° 19.06' 116° 48.87'
049	Biotite monzogranite	68[4]	8.9	Cactus Granite (Vaughn), central SBM, outcrop, approx. 1.3 km ENE of Hwy 18 on Grapevine Ck. jeep trail	34° 19.62' 116° 48.33'
050	" "	68[4]	8.4	Cactus Granite (Vaughn), central SBM, outcrop, approx. 0.5 km NE of Hwy 18 on Grapevine Ck. jeep trail	34° 19.55' 116° 48.87'
051	Biotite-hornblende granodiorite	71[4] >145?	7.7	Cushenberry Grade Pluton, central SBM, roadcut on Hwy 18, approx. 0.4 km SE of Whiskey Springs	34° 19.93' 116° 49.68'

GCS#	Sample Description	Age, Ma	$\delta^{18}O$	Remarks	Location
052	Biotite-hornblende granodiorite	71[4] >145?	7.8	Cushenberry Grade Pluton, central SBM, roadcut on Hwy 18, approx. 0.1 km ESE of Whiskey Springs	34° 20.05' 116° 49.82'
053	Biotite monzogranite	68[4]	8.0	Cactus Granite (Vaughn), central SBM, weathered outcrop, approx. 1.2 km S of Big Bear Lake at end of Pine Knot Blvd.	34° 14.00' 116° 54.70'
054	" "	68[4]	8.9	Cactus Granite (Vaughn), central SBM, weathered outcrop on jeep trail approx. 0.3 km NW of Elsie Caves	34° 13.66' 116° 55.91'
055	" " Dup.	71[4]	9.3, 9.7Q 9.1	Cactus Granite (Vaughn), central SBM, weathered outcrop on Hwy 18, approx. 0.3 km NW of Kidd Ck.	34° 14.45' 116° 58.35'
056	Monzonite	220Q[7] 71[4]	8.1	Fawnskin Monzonite, central SBM, weathered outcrop on Coxey Rd., approx. 0.6 km NW of junction with Hwy 38	34° 16.39' 116° 56.98'
057	Biotite-hornblende monzogranite	71[4]	9.2, 10.3Q	Cactus Granite (Vaughn), central SBM, roadcut on Hwy 18, approx. 0.3 km WNW of junction with Hwy 38	34° 14.29' 116° 58.81'
058	Biotite monzogranite	71[4]	9.2	Cactus Granite (Vaughn), central SBM, roadcut on Hwy 18, approx. 1.4 km WNW of GCS057	34° 14.97' 116° 59.62'
059	" "	72[4]	10.3	Cactus Granite (Vaughn), central SBM, outcrop on Glory Ridge Rd., lookout point, approx. 1.8 km S of Hwy 18	34° 13.87' 117° 00.24'
060	" "	72[4]	10.4	Cactus Granite (Vaughn), central SBM, outcrop on Glory Ridge Rd., approx. 0.5 SSW of Hwy 18	34° 14.60' 117° 00.29'
061	" "	73[4]	9.9, 11.2Q	Cactus Granite (Vaughn), central SBM, roadcut on Hwy 18, approx. 1.4 km N of Lake View Point	34° 14.77' 117° 01.43'
062	Leucocratic muscovite granite	73[4]	10.8, 11.6Q	Cactus Granite (Vaughn), central SBM, roadcut on Hwy 18, at Lake View Point	34° 14.01' 117° 01.59'
063	Biotite monzogranite	70[4]	9.4, 10.4Q	Cactus Granite (Vaughn), central SBM, outcrop on Hwy 18, approx. 2.0 km W of Snow Valley Ski Area	34° 13.31' 117° 03.37'
064	Biotite granite	71[4]	9.7	Cactus Granite (Vaughn), central SBM, outcrop at Green Valley Lake turnoff from Hwy 18	34° 13.16' 117° 04.26'
065	Biotite monzogranite	71[4]	9.4	Cactus Granite (Vaughn), central SBM, outcrop on Green Valley Rd., approx. 0.5 km N of Camp Awahanee	34° 13.77' 117° 05.65'

GCS#	Sample Description	Age, Ma	$\delta^{18}O$	Remarks	Location
066	Biotite monzogranite	70[4]	9.0	Cactus Granite (Vaughn), central SBM, outcrop at end of dirt road near Crab Creek, approx. 0.6 km NE of Green Valley Campground	34° 14.91' 117° 04.35'
067	" "	70[4]	9.3, 10.4Q	Cactus Granite (Vaughn), central SBM, outcrop on dirt road, approx. 1.2 km NW of Green Valley Lake	34° 14.82' 117° 05.42'
068	" "	70[4]	9.4, 10.4Q	Cactus Granite (Vaughn), central SBM, outcrop on Hwy 18, approx. 0.3 km E of Running Springs Station	34° 12.18' 117° 05.57'
069	" "	70[4]	9.3	Cactus Granite (Vaughn), central SBM, roadcut on Hwy 30, approx. 1.8 km WNW of Fredalba	34° 12.45' 117° 08.95'
070	" "	70[4]	9.0	Cactus Granite (Vaughn), central SBM, roadcut on Hwy 30, approx. 1.6 km W of junction with Hwy 18	34° 12.23' 117° 07.44'
071	Biotite granite	70[4]	9.4	Cactus Granite (Vaughn), central SBM, roadcut on Hwy 18, approx. 0.5 km SW of Heaps Peak	34° 11.77' 117° 08.69'
104	Biotite monzogranite	68[4]	10.4	Cactus Granite (Vaughn), eastern SBM, roadcut on Johnson Valley Rd., approx. 4.0 km NE of Yucca Valley	34° 08.79' 116° 24.88'
105	" "	71[4]	7.6	Granite of Pipe's Wash, eastern SBM, outcrop on Johnson Valley Rd., approx. 2.0 km NNW of Pipe's Wash	34° 12.48' 116° 26.71'
106	Biotite granodiorite	>145?	7.8	SE Johnson Valley Pluton, northeast SBM, outcrop on Johnson Valley Rd., approx. 7.0 km S of Means Lake	34° 20.24' 116° 30.12'
107	" "	>145?	7.9	Pluton at SE portion of Big Horn Mtns., northeast SBM, outcrop on dirt road, approx. 8.0 km W of Landers	34° 16.38' 116° 29.92'
108	Biotite monzogranite	70[4]	9.4	Cactus Granite (Vaughn), eastern SBM, outcrop on Rimrock Rd., approx. 4.5 km E of Rimrock	34° 12.03' 116° 30.00'
109	" "	70[4]	9.5	Cactus Granite (Vaughn), eastern SBM, outcrop on Pipe's Canyon Rd., approx. 2.5 km W of Rimrock	34° 11.65' 116° 34.44'
110	" "	68[4]	9.8	Cactus Granite (Vaughn), eastern SBM, outcrop on Pioneertown Rd., approx. 1.6 km SE of Pioneertown	34° 09.07' 116° 29.01'
126	" "	70[4]	10.0	Cactus Granite (Vaughn), central SBM, outcrop on N side of Mill Ck., approx. 6 km WSW of San Gorgonio Mtn.	34° 05.31' 116° 53.64'
127	Monzonite	200[8]	8.4	Mill Creek Pluton, central SBM, outcrop on S side of Mill Ck., approx. 2.2 km E of Hwy 38	34° 05.31' 116° 56.58'

GCS#	Sample Description	Age, Ma	$\delta^{18}O$	Remarks	Location
128	Biotite granodiorite	72[4]	8.3	Cactus Granite (Vaughn), central SBM, roadcut on Hwy 38, approx. 4.7 km NW of Mill Ck. bend in Hwy	34° 07.24' 116° 58.76'
129	Biotite monzogranite	72[4]	7.8	Cactus Granite (Vaughn), central SBM, roadcut on Hwy 38, approx. 4.0 km NE of GCS128	34° 09.48' 11° 57.74'
130	Biotite-hornblende granodiorite	>145	8.4	Cienaga Seca Pluton, central SBM, outcrop on Hwy 38, approx. 4.5 km SE of Sugarloaf Mtn.	34° 10.24' 116° 47.06'
131	Biotite monzogranite	70[4]	8.9	Cactus Granite (Vaughn), central SBM, roadcut on Hwy 38, approx. 6.5 km ENE of GCS130, near bend in Hwy	34° 10.62' 116° 42.82'
132	" "	67[4]	9.3	Cactus Granite (Vaughn), western SBM, roadcut on Hwy 18, approx. 2.0 km SE of Crestline	34° 09.48' 117° 14.79'
133	" "	70[4]	9.1	Cactus Granite (Vaughn), western SBM, outcrop at Blue Jay	34° 14.65' 117° 11.50'
134	" "	70[4]	8.6	Cactus Granite (Vaughn), western SBM, outcrop on road, approx. 1.0 km N of Lake Arrowhead	34° 16.65' 117° 11.50'
135	" "	70[4]	3.0	Cactus Granite (Vaughn), western SBM, weathered outcrop on dirt road, approx. 3.0 km NW of Lake Arrowhead	34° 17.24' 117° 13.15'
136	" "	68[4]	8.1	Cactus Granite (Vaughn), western SBM, roadcut on Crestline turnoff, approx. 0.3 km NW of Hwy 18	34° 13.79' 117° 17.30'
148	" "	70[4]	8.5	Granite of Cajon Pass, western SBM, weathered outcrop on Frontage Rd., approx. 0.3 km SE of Hwy 138 offramp from Interstate 15	34° 18.45' 117° 27.94'
149	Biotite-hornblende granodiorite	70[4]	9.2	Bighorn Mtn. Pluton, western SBM, roadcut on road to Cedar Pines, approx. 4.0 km NW of Crestline	34° 15.45' 117° 18.37'
150	" "	71[4]	9.0	Bighorn Mtn. Pluton, western SBM, roadcut at entrance to Silverwood Lake Recreation area, approx. 1.7 km SW of Hwy 138	34° 18.10' 117° 20.47'
151	Biotite monzogranite, alt., (ep.)	69[4]	9.9	Cactus Granite (Vaughn), western SBM, roadcut on dirt road above Deep Ck., approx. 0.9 km E of Hwy 138	34° 20.00' 117° 13.68'
	Little San Bernardino (LSB) Mountains Area (Figure 6.10)				
072	Biotite monzogranite	75[9]	7.4, 8.9Q	Orocopia Mtns. Pluton, southern LSB, Cal-Riv Orocop 75p (Powell), approx. 13 km E of Chiriaco Summit, coll. by Powell	33° 38.96' 115° 35.16'

GCS#	Sample Description	Age, Ma	$\delta^{18}O$	Remarks	Location
073	Biotite monzogranite	71[9]	4.7, 9.1Q	Cottonwood Mtns. Pluton, southern LSB, Cal-Riv Cot 5p (Powell), apprx. 8.0 km W of Cottonwood Spring, coll. by Powell	33° 44.65' 115° 53.41'
074	" "	71[9]	8.2, 9.1Q	Chuckwalla Mtns. Pluton, southern LSB, Cal-Riv Chuck 134p (Powell), approx. 4.0 km ESE of Corn Spring, coll. by Powell	33° 36.21' 115° 17.06'
075	" "	<135[10]	7.4, 8.7Q	Cretaceous Eagle Mtns. Pluton, southern LSB, Cal-Riv Eagle 216p (Powell), approx. 9.0 km WNW of Desert Center, coll. by Powell	33° 44.55' 115° 29.18'
076	" "	<135[10]	7.5, 8.3Q	Cretaceous Eagle Mtns. Pluton (dike) southern LSB, Cal-Riv Eagle 86p (Powell), approx. 20 m from GCS075, coll. by Powell	33° 44.83' 115° 28.97'
077	" "	75[9]	7.8, 8.7Q	Orocopia Mtns. Pluton, southern LSB, Cal-Riv Orocop 56p (Powell), approx. 12 km ESE of Chiriaco Summit, coll. by Powell	33° 38.00' 115° 38.23'
078	" "	88[9]	5.5, 7.9Q	Chuckwalla Mtns. Pluton, southern LSB, Cal-Riv Chuck 344p (Powell), approx. 5.0 km W of Corn Spring, coll. by Powell	33° 38.45' 115° 25.06'
079	" "	75[9]	8.6	Orocopia Mtns. Pluton, southern LSB, Cal-Riv Orocop 22p (Powell), approx. 5.0 km SE of Chiriaco Summit, coll. by Powell	33° 37.24' 115° 39.67'
080	" "	75[9]	8.0, 8.7Q	Orocopia Mtns. Pluton, southern LSB, Cal-Riv Orocop 46p (Powell), approx. 0.3 km S of Chiriaco Summit, coll. by Powell	33° 38.10' 115° 41.89'
095	" "	68[9]	9.5	Indian Cove Pluton, northern LSB, outcrop on Twenty-nine Palms Hwy, approx. 3.0 km E of town of Joshua Tree	34° 07.93' 116° 16.97'
096	" "	68[9]	8.6	Indian Cove Pluton, northern LSB, outcrop on Indian Cove Rd., approx. 5.0 km S of Twenty-nine Palms Hwy	34° 05.52' 116° 09.59'
097	" "	71[9]	8.1, 9.5Q	White Tank Pluton, northern LSB, outcrop on Joshua Tree Natl. Mon. Rd., approx. 8.0 km S of Joshua Tree National Monument Headquarters	34° 03.62' 116° 01.77'
098	Biotite granodiorite	>145	6.7	Older Granite (Dibblee), northern LSB, outcrop on Joshua Tree Natl. Mon. Rd., approx. 5.0 km SW of fork in road S of headquarters	33° 59.89' 116° 03.70'

GCS#	Sample Description	Age, Ma	$\delta^{18}O$	Remarks	Location
099	Muscovite-garnet granite	71[9]	8.0	White Tank Pluton, northern LSB, outcrop on Joshua Tree Natl. Mon. Rd., approx. 6 km W of GCS098	34° 00.34' 116° 07.94'
100	" "	71[9]	8.5	White Tank Pluton, northern LSB, outcrop on Joshua Tree Natl. Mon. Rd., approx. 1 km SW of GCS099	33° 59.93' 116° 08.44'
101	Biotite monzogranite	71[9]	8.6	White Tank Pluton, northern LSB, outcrop on Joshua Tree Natl. Mon. Rd. ,approx. 6 km S of GCS096	34° 02.41' 116° 10.69'
102	" "	71[9]	8.6	White Tank Pluton, northern LSB, outcrop on Joshua Tree Natl. Mon. Rd., approx. 9.5 km SE of town of Joshua Tree	34° 04.38' 116° 14.40'
103	" "	68[9]	9.6	Granite of Joshua Tree, northern LSB, outcrop on Joshua Tree Natl. Mon. Rd., approx. 2.0 km S of town of Joshua Tree	34° 07.00' 116° 18.52'
171	" "	71[9]	8.4	Cottonwood Mtns. Pluton, southern LSB, outcrop at Cottonwood Spring Oasis	33° 44.14' 115° 48.49'
173	" "	71[9]	7.2	Smoketree Wash Pluton, southern LSB, outcrop on dirt road in Smoketree Wash, approx. 0.8 km NW of three forks in road	33° 49.93' 115° 45.69'
176	" "	69[9]	7.8	Lost Horse Mtn. Pluton, central LSB, outcrop at end of road leading to vista overlook, approx. 4 km W of Lost Horse Mtn.	33° 55.52' 116° 10.31'
177	Biotite granodiorite	67[9]	7.8	LSB Pluton, northern LSB, outcrop on dirt road, approx. 10 km SE of Yucca Valley Airport	34° 04.07' 116° 20.47'
178	" "	67[9]	8.0	LSB Pluton, northern LSB, outcrop on dirt road, approx. 5.0 km SE of Yucca Valley Airport	34° 06.17' 116° 22.20'
179	Biotite monzogranite alt., (ep.)	69[9]	6.8	Lost Horse Mtn. Pluton, central LSB, outcrop on dirt road at head of Berdoo Canyon	33° 50.17' 116° 03.83'
180	Biotite monzogranite	69[9]	7.9	White Tank Pluton, central LSB, outcrop on dirt road across Pleasant Valley, approx. 6.0 km NE of Lost Horse Mtn.	33° 52.41' 116° 03.00'
194	" "	>145?	7.2	Older Granite (Dibblee), northern LSB, outcrop, approx. 2.0 km SW of Joshua Tree Natl. Mon. Headquarters	34° 06.83' 116° 03.29'
198	" "	>145?	6.1	Older Granite (Dibblee), northern LSB, outcrop, approx. 2.0 km NE of GCS097	34° 04.07' 116° 00.62'

GCS#	Sample Description	Age, Ma	$\delta^{18}O$	Remarks	Location
199	Hornblende-biotite granodiorite, alt., (ep., chl.)	>145[11]	6.5	Copper Mtn. Pluton, northern LSB, outcrop at extreme NW end of Copper Mtn.	34° 13.03' 116° 15.00'
201	" "		6.4	Copper Mtn. Pluton, northern LSB, outcrop in southern Copper Mtn., approx. 12 km W of Twentynine Palms	34° 08.76' 116° 11.13'
202	Hornblende-biotite granodiorite, alt., (ep., chl.)	>145 91[9]	7.1	Dale District Pluton, northern LSB, outcrop on dirt road through Dale Mining District, approx. 7.0 km SE of Twentynine Palms Hwy	34° 04.07' 115° 45.25'
205	Hornblende-biotite granodiorite, alt., (ep., chl.)		5.9	Dale District Pluton, northern LSB, outcrop on dirt road through Dale Mining District, approx. 6.0 km WNW of the Goldenrod Mine	34° 01.83' 115° 44.59'
206	Hornblende-biotite granodiorite, alt., (ep., chl.)		7.1	Dale District Pluton, northern LSB, outcrop on dirt road through Dale Mining District, approx. 2.0 km W of the Goldenrod Mine	34° 00.07' 115° 42.20'
208	Tonalite	74[12] 71[9] 73H[4]	8.5	Fargo Canyon Pluton, central LSB, outcrop on Fargo Canyon Rd., approx. 11 km NE of Hwy 111	33° 45.38' 116° 05.35'
	C. Southeastern California (SECA) Segment (see Chapter 7)				
	Rodman-Ord Mountains Area (Figures 7.2 and 7.3)				
111	Biotite monzogranite	72[4]	9.7	Granite of Mojave River Wash, western ROM, roadcut on Hwy 18, approx. 30 m from bridge over Wash	34° 32.34' 117° 17.18'
112	Leucocratic syenite	230[7]	9.0	Granite Mtns. Pluton, western ROM, outcrop near Hwy 18, approx. 2.0 km E of Rabbit Dry Lake	34° 27.24' 116° 59.59'
152	Tonalite	83[4] 169H[4]	8.3	Bell Mtn. Pluton, western ROM, roadcut, approx. 6.0 km NE of GCS111	34° 33.24' 117° 13.56'
153	Biotite monzogranite	74[4]	7.4	Fairview Valley Pluton, western ROM, outcrop, approx. 7.0 km E of GCS152	34° 33.55' 117° 08.62'
154	Hornblende monzonite	230[7] 74[4]	6.5	Granite Mtns. Pluton, western ROM, outcrop on Hwy 18, approx. 7.0 km E of Apple Valley	34° 29.31' 117° 08.25'
155	" "	230[7] 74[4]	7.5	Granite Mtns. Pluton, western ROM, outcrop on Hwy 18, approx. 4.5 km W of Rabbit Dry Lake	34° 27.48' 117° 04.03'
156	" "	230[7] 71[4]	8.0	Pitzer Butte Pluton, western ROM, outcrop at N end of Pitzer Butte	34° 25.34' 116° 57.94'
157	Biotite monzogranite	74[4]	8.2	Cretaceous Granite Mtns. Pluton, western ROM, outcrop, approx. 4.0 km NW of GCS 112	34° 29.24' 117° 01.11'

GCS#	Sample Description	Age, Ma	$\delta^{18}O$	Remarks	Location
158	Biotite granodiorite	>145 74[4]	2.8	Jurassic Granite Mtns. Pluton, central ROM, roadcut along powerline road, approx. 3.0 km SW of Barstow Rd.	34° 31.89' 116° 58.27'
159	Biotite-hornblende granodiorite, alt., (ep., chl.)	>145 96H[4]	5.5	Sidewinder Mtn. Pluton, central ROM, outcrop on dirt road on S side of Sidewinder Mtn., approx. 6.5 km WNW of Barstow Rd.	34° 35.34' 117° 01.65'
160	Biotite-hornblende monzogranite, alt., (ep., chl.)	>145 96H[4]	2.4	Sidewinder Mtn. Pluton, central ROM, outcrop on Barstow Rd. at junction with dirt road to Stoddard Ridge	34° 36.21' 116° 58.76'
161	Biotite monzogranite, alt., (ep., chl.)	>145 78[4]	4.0	Barstow Rd. Pluton, central ROM, outcrop on Barstow Rd. approx. 5.0 km NE of GCS160	34° 38.27' 116° 56.75'
162	Biotite monzogranite	75[4]	7.8	Cretaceous Stoddard Valley Pluton, northern ROM, outcrop on Stoddard Wells Rd., approx. 4.2 km SSW of junction with Barstow Rd.	34° 48.07' 117° 03.33'
163	Biotite-hornblende granodiorite, alt., (ep., chl.)	>145 106[4] 186H[4]	5.8	Jurassic Stoddard Valley Pluton, northern ROM, outcrop on Stoddard Wells Rd., approx. 2.3 km S of GCS162	34° 46.62' 117° 03.49'
164	Granite porphyry, alt., (ep., ser.)	>145 87[4]	-3.2	Stoddard Well Pluton, northern ROM, outcrop on Stoddard Well Rd., apprx. 2.5 km NE of Stoddard Well	34° 43.96' 117° 04.53'
165	Granite porphyry, alt., (ep., ser.)	>145 87[4]	-0.6	Stoddard Well Pluton, northern ROM, outcrop on Stoddard Ridge Rd., approx. 2.4 km SE of junction with Stoddard Well Rd.	34° 40.69' 117° 04.40'
166	Biotite monzogranite	74[4]	7.6	Cretaceous Ord Mtns. Pluton, central ROM, outcrop on powerline road, approx. 10 km SW of Camp Rock Rd.	34° 34.62' 116° 50.06'
167	Miarolytic granite	>145 149[4]	2.7	East Ord Mtn. Pluton, eastern ROM, outcrop approx. 1.0 km SW of the junction between Camp Rock and Daggett Roads	34° 40.17' 116° 33.06'
168	Biotite-hornblende granodiorite, alt., (ep., chl.)	>145 80[4] 163H[4]	4.9	Jurassic Fry Mtns. Pluton, eastern ROM, outcrop at junction between powerline road and Camp Rock Rd.	34° 36.14' 116° 44.83'
268	" ", alt., (ep., chl.)	>145 80[4]	5.4	Jurassic Eastern Lucerne Valley Pluton, outcrop on W side of Lenwood Fault, approx. 3.5 km SSE of Camp Rock Rd.	34° 32.02' 116° 45.89'
269	Biotite monzogranite	76[4]	7.4	Cretaceous Eastern Lucerne Valley Pluton, outcrop on powerline road, approx. 1.8 km N of Texas Rock Quarry	34° 30.01' 116° 49.48'
272	Biotite-hornblende granodiorite	>145 80[4]	5.6	Jurassic Eastern Lucerne Valley Pluton, outcrop on powerline road, approx. 50 m SW of Lenwood Fault	34° 31.39' 116° 44.69'

GCS#	Sample Description	Age, Ma	$\delta^{18}O$	Remarks	Location
274	Biotite-hornblende granodiorite, alt., (ep., chl.)	>145 [80]	5.8	Jurassic Fry Mtns. Pluton, central ROM, outcrop on powerline road, approx. 1.0 km NE of Lenwood Fault	34° 31.55' 116° 43.99'
275	" ", alt., (ep., chl.)	>145 [80]	5.9	Jurassic Fry Mtns. Pluton, central ROM, outcrop on powerline road, approx. 3 km NE of GCS274	34° 32.59' 116° 42.59'
276	Biotite-hornblende granodiorite	>145 [80]	7.4	Jurassic Fry Mtns. Pluton, central ROM, outcrop on powerline road, approx. 1.0 km SE of Jean Peak	34° 32.89' 116° 41.86'
277	" ", alt., (ep., ab)	>145 [80]	6.8	Jurassic Fry Mtns. Pluton, eastern ROM, outcrop on powerline road, approx. 1.2 km NE of GCS276	34° 33.34' 116° 41.24'
278	" ", alt., (ep., chl.)	>145 [80]	5.2	Jurassic Fry Mtns. Pluton, eastern ROM, outcrop on powerline road, approx. 4.1 km SSW of Red Hill	34° 33.98' 116° 40.43'
279	Biotite monzogranite	76 [4]	8.6	Cret. Fry Mtns. Pluton, eastern ROM, outcrop approx. 3 km SE of Red Hill	34° 35.11' 116° 37.02'
280	Biotite monzogranite, alt., (ep., ser.)	>145 [80]	0.5	Jurassic Fry Mtns. Pluton, eastern ROM, outcrop on powerline road, approx. 3.2 km NW of Red Hill	34° 36.88' 116° 40.72'
281	" " alt., (ep, ser.)	>145 [80]	2.1	Jurassic Fry Mtns. Pluton, eastern ROM, outcrop on powerline road, approx. 3.8 km E of Camp Rock Rd.	34° 36.39' 116° 42.47'
282	Biotite-hornblende granodiorite, alt., (ep., chl.)	>145 [80]	5.6	Jurassic Fry Mtns. Pluton, eastern ROM, outcrop on powerline road, approx. 2.6 km E of Camp Rock Rd.	34° 36.43' 116° 43.21'
283	Biotite monzogranite, alt., (ep., ser.)	>145 [80]	3.0	Jurassic Fry Mtns. Pluton, eastern ROM, outcrop on powerline road, approx., 300 m W of GCS 282	34° 36.43' 116° 43.33'
284	Biotite-hornblende granodiorite, alt., (ep., chl.)	>145 [80] 163H [4]	4.8	Jurassic Fry Mtns. Pluton, eastern ROM, outcrop on powerline road, approx. 1.0 km E of Camp Rock Rd.	34° 36.32' 116° 44.26'
285	" ", alt., (ep., chl.)	>145 [80]	3.0	Jurassic Fry Mtns. Pluton, eastern ROM, outcrop on Camp Rock Rd., approx. 3.0 km NE of Lenwood Fault	34° 35.09' 116° 45.83'
287	" ", alt., (ep., chl.)	>145 [80]	1.7	Jurassic Eastern Lucerne Valley Pluton, outcrop approx. 200 m SW of Lenwood Fault, approx. 1.0 km SE of Camp Rock Rd.	34° 33.15' 116° 47.68'
288	" ", alt., (ep., chl.)	>145 [80]	3.5	Jurassic Eastern Lucerne Valley Pluton, outcrop approx. 100 m SW of Lenwood Fault, approx. 0.5 km NW of Camp Rock Rd.	34° 34.17' 116° 47.14'
289	" ", alt., (ep., chl.)	>145 [80]	4.7	Jurassic Fry Mtns. Pluton, eastern ROM, outcrop on Camp Rock Rd., approx. 200 m NE of Lenwood Fault	34° 34.06' 116° 46.62'

GCS#	Sample Description	Age, Ma	$\delta^{18}O$	Remarks	Location
290	Biotite monzogranite	71[4]	7.9	Cretaceous Ord Mtns. Pluton, eastern ROM, outcrop on Ord Valley Rd., approx. 5.5 NW of Camp Rock Rd.	34° 36.39' 116° 48.33'
292	Biotite-hornblende granodiorite, alt., (ep., chl.)	>145 78[4] 185H[4]	5.7	Ord Mtn. Pluton, eastern ROM, outcrop on Tyler Valley Rd., approx. 4.0 km SSW of Ord Mtn.	34° 38.65' 116° 50.08'
293	" ", alt., (ep., chl.)	>145 78[4]	4.9	Ord Mtn. Pluton, eastern ROM, outcrop on Tyler Valley Rd., approx. 3.0 km SW of Ord Mtn.	34° 39.74' 116° 50.27'
294	" ", alt., (ep., chl.)	>145 78[4]	4.3	Ord Mtn. Pluton, eastern ROM, outcrop at base S ridge of Ord Mtn., Mtn., approx. 3.5 km S of Ord Mtn.	34° 38.77' 116° 49.28'
295	Biotite monzogranite	71[4]	8.2	Cretaceous Ord Mtns. Pluton, eastern ROM, outcrop at base of S ridge of Ord Mtn., approx. 4.8 km S of Ord Mtn.	34° 37.85' 116° 49.37'
296	Biotite granite porphyry, alt., (ep., chl.)	>145 78[4]	5.9	Ord Mtn. Pluton, eastern ROM, outcrop on Ord Valley Rd., approx. 3.5 km E of Ord Mtn.	34° 40.25' 116° 46.50'
325	Biotite-hornblende granodiorite, alt., (ep., chl.)	>145 149[4]	3.2	East Ord Mtn. Pluton, eastern ROM, outcrop at base of S ridge of East Ord Mtn., approx. 3.5 km SSW of peak	34° 36.58' 116° 46.51'
326	Biotite monzogranite	<135	7.3	Cretaceous Ord Mtns. Pluton, eastern ROM, outcrop at base of W flank of East Ord Mtn., approx. 2.0 km W of peak	34° 37.69' 116° 47.25'
328	Granite porphyry, alt., (ep., chl.)	>145 149[4]	-0.1	East Ord Mtn. Pluton, eastern ROM, outcrop near mine, base of S ridge of East Ord Mtn., approx. 2.5 km S of peak	34° 37.24' 116° 45.66'
329	Biotite monzogranite, alt., (bi., ac., ep.)	>145 149[4]	6.9	Jurassic Fry Mtns. Pluton, eastern ROM, outcrop near Camp Rock Rd., approx. 3.1 km SW of junction with Daggett Rd.	34° 38.58' 116° 43.03'
331	" ", alt., (bi., ep.)	>145 149[4]	6.3	Jurassic Fry Mtns. Pluton, eastern ROM, outcrop on dirt road leading SW from Daggett Rd., approx. 3.0 km SE of junction with Camp Rock Rd.	34° 39.29' 116° 41.21'
332	" ", alt., (bi, k, Cu)	>145 149[4]	2.9	Jurassic Fry Mtns. Pluton, eastern ROM, outcrop on dirt road leading SW from Daggett Rd., approx. 5 km SE of junction with Camp Rock Rd.	34° 37.97' 116° 40.76'
333	Miarolytic granite, alt., (ser.)	>145 149[4]	7.3	East Ord Mtn. Pluton, eastern ROM, outcrop approx. 100 m SW of Daggett Rd., approx. 1.5 km NW of junction with Camp Rock Rd.	34° 40.43' 116° 43.04'
334	Biotite granodiorite, alt., (ep., chl.)	>145 149[4]	2.1	East Ord Mtn. Pluton, eastern ROM, outcrop on dirt road, approx. 3.9 km WSW of Camp Rock Rd. junction	34° 39.76' 116° 44.76'

GCS#	Sample Description	Age, Ma	$\delta^{18}O$	Remarks	Location
335	Biotite-hornblende granodiorite, alt., (ep., chl.)	>145 149[4]	5.4	East Ord Mtn. Pluton, eastern ROM, outcrop on dirt road to Ord Valley, approx. 2.2 km SW of Daggett Rd.	34° 40.36' 116° 45.25'
336	Biotite-hornblende granodiorite, alt., (ep., chl.)	>145 149[4]	5.0	East Ord Mtn. Pluton, eastern ROM, outcrop on dirt road to Ord Valley, approx. 1.0 km SW of GCS 296	34° 39.95' 116° 46.16'
337	Granite porphyry, alt., (ep., ser.)	>145 149[4]	2.6	East Ord Mtn. Pluton, eastern ROM, outcrop on dirt road at base of W flank of East Ord Mtn., approx. 1.7 km NW of peak	34° 38.92' 116° 45.66'
338	Biotite-hornblende granodiorite, alt., (ep., bi., Mo)	>145 149[4]	6.2	Ord Mtn. Pluton, eastern ROM, outcrop approx. 0.9 km W of Ord Mtn.	34° 40.21' 116° 49.14'
340	" ", alt., (ep., chl.)	>145 80[4] 163H[4]	4.4	Ord Mtn. Pluton, eastern ROM, outcrop approx. 2.5 km W of GCS337	34° 39.01' 116° 48.72'
342	" ", alt., (ep., chl.)	>145 80[4]	6.9	Jurassic Fry Mtns. Pluton, eastern ROM, outcrop on dirt road approx. 1.0 km SSE of GCS274	34° 31.04' 116° 43.94'
347	Biotite-hornblende granodiorite	>145 80[4]	7.4	Jurassic Fry Mtns. Pluton, eastern ROM, outcrop approx. 500 m NW of powerline road, approx. 1.5 km NE of GCS278	34° 34.62' 116° 40.08'
348	Biotite monzogranite, alt., (ab)	>145 80[4]	6.7	Jurassic Fry Mtns. Pluton, eastern ROM, outcrop approx. 2.0 km ESE of GCS277	34° 33.16' 116° 40.23'
349	Biotite-hornblende granodiorite	>145 80[4]	8.9	Jurassic Fry Mtns. Pluton, eastern ROM, outcrop approx. 2.2 km NW of GCS275	34° 33.46' 116° 43.33'
350	Granite, alt., (ep., chl., ser.)	>145 134[4]	2.8	Jurassic Ord Mtns. Pluton, central ROM, outcrop on dirt road, approx. 1.0 km W of Lenwood Fault, approx. 2.0 km W of GCS292	34° 38.52' 116° 51.26'
351	Biotite-hornblende granodiorite, alt., (ep., chl.)	>145 134[4]	2.1	Jurassic Ord Mtns. Pluton, central ROM, outcrop on dirt road, approx. 3.5 km NW of GCS350	34° 39.65' 116° 52.52'
352	" ", alt., (ep., chl.)	>145 100[4] 167H[4]	5.9	Jurassic Ord Mtns. Pluton, central ROM, outcrop on dirt road, approx. 2.0 km W of GCS351, W side of Lenwood Fault	34° 40.56' 116° 53.04'
353	" ", alt., (ep., chl.)	>145 100[4] 167H[4]	5.4	Ord Mtn. Pluton, central ROM, outcrop on dirt road, approx. 1.3 km N of GCS 352, NE side of Lenwood Fault	34° 41.07' 116° 52.87'
354	" ", alt., (ep., chl.)	>145 100[4] 167H[4]	0.4	Ord Mtn. Pluton, central ROM, outcrop on dirt road, approx. 1.2 km E of GCS 353	34° 41.47' 116° 51.26'

GCS#	Sample Description	Age, Ma	$\delta^{18}O$	Remarks	Location
355	Biotite-hornblende granodiorite, alt., (tr. ep.)	>145 [4] 100 [4] 167H [4]	8.7	Ord Mtn. Pluton, eastern ROM, outcrop on W flank of Ord Mtn., approx. 2.4 km NW of Ord Mtn.	34° 41.12' 116° 39.89'
356	" ", alt., (tr. ep.)	>145 [4] 100 [4] 167H [4]	9.1	Ord Mtn. Pluton, eastern ROM, outcrop on Tyler Valley Rd., approx. 4.7 km NW of Ord Mtn.	34° 42.58' 116° 50.30'
357	" ", alt., (tr. ep., chl.)	>145 [4] 100 [4] 167H [4]	7.9	Ord Mtn. Pluton, eastern ROM, outcrop approx. 2.0 km NW of Tyler Valley Rd. approx. 2.7 km SW of junction with Daggett Rd.	34° 43.62' 116° 50.57'
359	" ", alt., (ep., chl.)	>145 [4] 100 [4] 167H [4]	7.7	Ord Mtn. Pluton, eastern ROM, outcrop approx. 3.1 km SE of junction between Tyler Valley and Daggett Rds.	34° 43.39' 116° 47.58'
506	Biotite-hornblende granodiorite, alt., (ep., chl.)	>145 [4] 74 [4]	5.1	Jurassic Fry Mtns. Pluton, eastern ROM, outcrop approx. 2.9 km S of GCS281	34° 34.89' 116° 42.01'
507	Biotite-hornblende granodiorite	>145 [4] 74 [4]	7.7	Rodman Mtns. Pluton, eastern ROM, outcrop approx. 1.5 km SW of Nellie Bly Peak.	34° 37.79' 116° 38.51'
508	" "	>145 [4] 74 [4]	9.4	Rodman Mtns. Pluton, eastern ROM, outcrop approx. 1.6 km S of Nellie Bly Peak.	34° 37.69' 116° 38.12
509	Biotite-hornblende granodiorite, alt., (ep., chl.)	>145 [4] 74 [4]	1.5	Rodman Mtns. Pluton, eastern ROM, outcrop apprx. 2.6 km ESE of Rod Peak	34° 38.06' 116° 36.04'
510	" ", alt., (ep., chl.)	>145 [4] 74 [4]	5.0	Rodman Mtns. Pluton, eastern ROM, outcrop on dirt road, approx. 0.5 km S of Indian Petroglyphs	34° 40.00' 116° 35.71'
511	Biotite monzogranite, alt., (ep., ser.)	>145 [4] 74 [4]	2.3	Rodman Mtns. Pluton, eastern ROM, outcrop on dirt road, approx. 1.2 km W of Indian Petroglyphs	34° 40.38' 116° 36.43'
512	" " alt., (ep., chl.)	>145 [4] 149 [4]	6.3	Rodman Mtns. Pluton, eastern ROM, outcrop on dirt road, approx. 2.5 km N of Rod Peak	34° 39.84' 116° 37.53'
513	Biotite-hornblende granodiorite, alt., (ep., chl.)	>145 [4] 149 [4]	5.9	Rodman Mtns. Pluton, eastern ROM, outcrop on dirt road, approx. 2.5 km NW of Rod Peak	34° 39.57' 116° 38.70'
514	Biotite monzogranite	>145 [4] 149 [4]	7.7	Rodman Mtns. Pluton, eastern ROM, outcrop approx. 0.4 km E of Camp Rock Mine	34° 40.00' 116° 40.00'
515	Biotite monzogranite, alt., (ep.)	>145 [4] 149 [4]	7.0	Rodman Mtns. Pluton, eastern ROM, outcrop approx. 1.1 km NW of Camp Rock Mine	34° 40.64' 116° 40.29'
516	Biotite monzogranite	>145 [4] 149 [4]	7.7	Rodman Mtns. Pluton, eastern ROM, outcrop approx. 1.9 km W of Nellie Bly Peak	34° 38.33' 116° 39.28'

GCS#	Sample Description	Age, Ma	$\delta^{18}O$	Remarks	Location
		Southeastern Mojave Region (Figures 7.1, 7.5, 7.6 and 7.7)			
088	Muscovite granite	65[9]	8.3	Cadiz Valley Batholith, Iron Mtns, outcrop on Hwy from Desert Center, approx. 5.0 km NE of junction with Twentynine Palms Hwy	34° 04.65' 115° 10.76'
090	Muscovite-garnet granite	68[9]	9.0	Cadiz Valley Batholith, Coxcomb Mtns., outcrop S of Twentynine Palms Hwy, approx. 14 km WNW of Desert Center Hwy junction	34° 05.17' 115° 21.79'
091	Biotite monzogranite	68[9]	8.6	Cadiz Valley Batholith, Coxcomb Mtns., outcrop N of Twentynine Palms Hwy, approx. 4.7 km WNW of GCS090	34° 05.79' 115° 24.79'
092	Muscovite-garnet granite	68[9]	8.9	Cadiz Valley Batholith, Coxcomb Mtns., outcrop on Twentynine Palms Hwy, approx. 5.0 km WNW of GCS091	34° 06.55' 115° 27.55'
093	Biotite monzogranite	68[9]	9.0	Cadiz Valley Batholith, Coxcomb Mtns., outcrop on Twentynine Palms Hwy, approx. 5.0 km NNE of Clark's Pass	34° 06.89' 115° 31.67'
184	" "	69[9]	8.9	Cadiz Valley Batholith, Sheephole Mtns., roadcut on Amboy Rd., approx. 2.8 km S of Sheephole Mine	34° 12.93' 115° 43.23'
185	" "	69[9]	8.1	Cadiz Valley Batholith, Sheephole Mtns., outcrop E of Amboy Rd., approx. 1.8 km N of Sheephole Mine	34° 15.10' 115° 43.02'
188	Muscovite granite	72[13] 73[9]	9.0	Sweetwater Wash Pluton, Old Woman Mtns., outcrop on jeep road, approx. 1.0 km N of Old Ranch Spring	34° 35.69' 115° 10.88'
189	" "	72[13] 73[9]	9.1	Sweetwater Wash Pluton, Old Woman Mtns., outcrop on jeep road, approx. 1.5 km WNW of Honeymoon Spring	34° 37.65' 115° 10.68'
190	Muscovite-garnet granite	72[13] 73[9]	8.9	Lazy Daisy Pluton, Piute Mtns., outcrop on pipeline road, approx. 4.0 km S of Lazy Daisy Ranch	34° 41.03' 115° 07.47'
193	Muscovite granite	72[13] 73[9]	8.8	Sweetwater Wash Pluton, Old Woman Mtns., roadcut on pipeline road, approx. 3.0 km WSW of valve house	34° 40.00' 115° 12.65'
387	Biotite granodiorite	64[14]	7.4	Chemehuevi Batholith, Whale Mtn., BJ80Ch208 (Howard), coll. by Howard	34° 42.53' 114° 21.28'
388	Biotite monzogranite	75[15]	8.2	Cadiz Valley Batholith, Kilbeck Hills, H80Ki128 (Howard), coll. by Howard	34° 17.62' 115° 18.48'
389	Biotite granodiorite	68[9]	8.7	Cadiz Valley Batholith, southern Sheephole Mtns., H80Sh33 (Howard), coll. by Howard	34° 07.12' 115° 34.05'

GCS#	Sample Description	Age, Ma	$\delta^{18}O$	Remarks	Location
390	Muscovite granite	66[9]	7.7	Cadiz Valley Batholith, Iron Mtns., H80IM357 (Howard), coll. by Howard	34° 11.07' 115° 12.08'
391	Biotite-hornblende monzodiorite, tr. alt	145[15]	6.8	Big Maria Mtns. Hydrothermal Center, Big Maria Mtns., H80BM372b (Howard), coll. by Howard	34° 48.95' 114° 37.40'
392	Muscovite granite	<135	8.2	Sacramento Mtns. Pluton, Sacramento Mtns., H80Sa6 (Howard), coll. by Howard	34° 45.13' 114° 43.60'
393	Biotite granodiorite	64[14]	7.7	Chemehuevi Batholith, Chemehuevi Mtns., BJ80Ch198 (Howard), coll. by Howard	34° 39.75' 114° 36.32'
394	Biotite-hornblende granodiorite	159[16]	7.5	Jurassic Little Maria Pluton, Little Maria Mtns., H80LM374 (Howard), coll. by Howard	33° 51.03' 114° 52.07'
395	Biotite monzogranite	160[17]	7.6	Marble Mtns. Pluton, Marble Mtns., H80MM232 (Howard), coll. by Howard	34° 58.90' 115° 36.88'
396	Biotite granodiorite	<135	8.2	Southern Granite Mtns. Pluton, Granite Mtns., H80GR375 (Howard), coll. by Howard	33° 58.13' 115° 04.23'
397	Biotite granite	<135	8.6	Northern Granite Mtns. Pluton, Granite Mtns., H80GM365 (Howard), coll. by Howard	34° 45.90' 115° 42.55'
398	Biotite monzogranite	101[18]	7.2	Turtle Mtns. Pluton, southern Turtle Mtns., H79TM486a (Howard), coll. by Howard	34° 11.33' 114° 49.92'
399	Monzogranite	72[18]	9.3	"Piute Batholith", Stepladder Mtns., H80St7 (Howard), coll. by Howard	34° 41.03' 114° 49.98'
400	Diorite	<135	7.8	Cadiz Valley Batholith, northern Calumet Mtns., H80CAL199 (Howard), coll. by Howard	34° 26.30' 115° 35.83'
401	Biotite monzogranite	<135	8.6	"Old Dad Mtns." Pluton, northern Bristol Mtns., H80BR218 (Howard), coll. by Howard	34° 48.95' 115° 59.12'
402	Biotite-hornblende granodiorite, alt., (ep., chl.)	>145	2.7	Palen Mtns. Hydrothermal Center, Palen Mtns., H80Pal89 (Howard), coll. by Howard	33° 55.17' 115° 02.25'
403	Biotite monzogranite, alt., (ep., chl.)	>145	4.2	Devil's Playground Hydrothermal Center, H80DP220 (Howard), coll. by Howard	34° 58.57' 115° 51.17'
404	Biotite-hornblende quartz monzodiorite	67[14]	7.0	Chemehuevi Batholith, Chemehuevi Mtns., BJ80Ch305 (Howard), coll. by Howard	34° 39.07' 114° 34.20'
405	Biotite monzogranite	66[9]	8.5	Cadiz Valley Batholith, Sheephole Mtns., H80SH191 (Howard), coll. by Howard	34° 13.58' 115° 42.93'

GCS#	Sample Description	Age, Ma	$\delta^{18}O$	Remarks	Location
406	Biotite-hornblende quartz monzodiorite	67[14]	7.4	Chemehuevi Batholith, Chemehuevi Mtn H80Ch307 (Howard), coll. by Howard	34° 40.07' 114° 34.20'
407	Biotite granodiorite	80[15]	8.7	Cadiz Valley Batholith, southeastern Sheephole Mtns., BJ80Sh33 (Howard), coll. by Howard	34° 05.73' 115° 33.62'
408	Muscovite granite	67[15]	7.8	Chemehuevi Batholith, southern Chemehuevi Mtns., BJ80Ch200 (Howard) coll. by Howard	34° 33.12' 114° 32.60'
409	Biotite-hornblende granodiorite	>145	7.6	Devil's Playground area, Providence Mtns., KH78-1 (Howard), coll. by Howard	34° 55.65' 115° 36.13'
410	Biotite monzogranite	<135	8.6	Cret. Little Maria Pluton, Little Maria Mtns. BJ80LM119 (Howard), coll. by Howard	33° 55.35' 114° 39.65'
491	Muscovite granite	72[13]	8.2	Lazy Daisy Pluton, Piute Mtns., P76 (Miller), outcrop at head of wash, approx. 2.7 km SSW of Piute Peak, coll. by Miller	34° 43.71' 115° 04.80'
492	" "	72[13]	9.1	Sweetwater Wash Pluton, Old Woman Mtns., G (Miller), outcrop near jeep trail, approx. 1.5 km NE of Sweetwater Spring, coll. by Miller	34° 34.54' 115° 10.29'
494	Biotite granodiorite	72[13]	9.2	Rattlesnake Pluton, Old Woman Mtns., W345 (Miller), outcrop < 50 m from Florence Mine, coll. by Miller	34° 35.38' 115° 14.09'
495	Muscovite granite	72[13]	9.3	Painted Rock Pluton, Old Woman Mtns., W172 (Miller), outcrop in Azalea Wash, approx. 3.6 km SE of Paramount Spring, coll. by Miller	34° 32.36' 115° 08.25'
496	" "	72[13]	8.4	Painted Rock Pluton, Old Woman Mtns., W285 (Miller), outcrop approx. 2.2 km E of Old Woman Statue, coll. by Miller	34° 31.34' 115° 08.38'
497	Biotite-hornblende granodiorite, alt., (ep., chl.)	72[13]	4.7	Goffs Pluton, nothern Piute Range, P109 (Miller), outcrop approx. 3.8 km E of Goffs, S of National Old Trails Road, coll. by Miller	34° 54.84' 115° 01.23'
498	Biotite monzogranite	72[13]	8.7	East Piute Pluton, Piute Range, E6 (Miller), outcrop approx. 4.6 km NE of Piute Peak, coll. by Miller	34° 47.26' 115° 02.86'
499	Muscovite granite	72[13]	9.2	East Piute Pluton, Piute Range, E8 (Miller), outcrop approx. 3.2 km NNE of Piute Peak, coll. by Miller	34° 46.83' 115° 03.83'
500	" "	72[13]	7.5	Painted Rock Pluton, Old Woman Mtns., W256 (Miller), outcrop approx. 2.9 km SE of Old Woman Statue, coll. by Miller	34° 30.11' 115° 08.51'

GCS#	Sample Description	Age, Ma	$\delta^{18}O$	Remarks	Location
501	Biotite granodiorite	72[13]	8.4	Old Woman Pluton, Old Woman Mtns., W261 (Miller), outcrop approx. 5.3 km ENE of Old Woman Statue, coll. by Miller	34° 25.64' 115° 06.23'
504	" "	72[13]	7.2	Old Woman Pluton, Old Woman Mtns., W324 (Miller), outcrop approx. 5.1 km WSW of Old Woman Statue, coll. by Miller	34° 29.89' 115° 12.66'
	II. Northern Great Basin $^{18}O/^{16}O$ Traverse				
	A. Nevada Segment (see Chapter 9 and Figure 9.1)				
386	Biotite-hornblende granodiorite	28[19]	-0.2	IXL Canyon Pluton, Stillwater Range, NV-73-28 (Farmer), coll. by Hibbard	Map No. 5 Figure 9.1
384	" "	28[19]	7.0	IXL Canyon Pluton, Stillwater Range, NV73-25 (Farmer), coll. by Hibbard	Map No. 6 Figure 9.1
365	Biotite monzogranite	76[19]	7.2	Granitic Pluton, Sand Spring Range, NV63-1 (Farmer), core sample at 1034 feet, borehole ECH.D, coll. by Hibbard	Map No. 7 Figure 9.1
362	Biotite-hornblende granodiorite	98[19]	9.4	Andorno Stock, Santa Rosa Mtns., MV76-42 (Farmer), southern part of range, coll. by Hibbard	Map No. 8 Figure 9.1
360	" "	90[19]	9.9	Osgood Mtns. Stock, Osgood Mtns., NV76-18 (Farmer), north lobe of stock near Getchell, coll. by M. Hibbard	Map No. 9 Figure 9.1
361	Biotite monzogranite	153[19]	9.3	Buffalo Mtn. Stock, Buffalo Mtn., NV76-35 (Farmer), S of Golconda, coll. by Hibbard	Map No. 10 Figure 9.1
372	Biotite-hornblende granodiorite	37[19]	10.7	Granite Mtn. Pluton, Shoshone Range, NV76-27 (Farmer), coll. by Hibbard	Map No. 11 Figure 9.1
367	" "	142[19]	10.4	Austin Pluton, Toiyabe Range, NV72-26 (Farmer), near Austin Summit, coll. by Hibbard	Map No. 12 Figure 9.1
368	Biotite monzogranite	76[19]	10.9	Round Mountain Pluton, Toquima Range, NV72-38 (Farmer), coll. by Hibbard	Map No. 13 Figure 9.1
371	" "	36[19]	9.5, 10.9Q	Harrison Pass Pluton, Ruby Mtns., HP-2 (Farmer), approx. 1.6 km E of Harrison Pass (roadcut), coll. by Farmer	Map No. 14 Figure 9.1
383	Biotite-muscovite granite	83[19]	12.6	Cretaceous granite, Ruby Mtns., RM17-66#2 (Farmer), coll. by Kistler	Map No. 15 Figure 9.1
363	" "	160[20]	10.2	Jurassic Granite, Ruby Mtns., RM47-66 (Farmer), coll. by Kistler	Map No. 16 Figure 9.1

GCS#	Sample Description	Age, Ma	$\delta^{18}O$	Remarks	Location
376	Biotite monzogranite	32[19]	5.8	Cherry Creek Stock, Egan Range, NV-CC-1 (Farmer), mine dump approx. 1.6 km W of town of Cherry Creek, coll. by Farmer	Map No. 17 Figure 9.1
375	Biotite granodiorite alt., (ep, chl)	124[19]	5.5, 10.0Q	Silver Zone Pass Pluton, Silver Zone Pass, NV-SZ-2 (Farmer), roadcut in Interstate 80 at pass, coll. by Farmer	Map No. 18 Figure 9.1
369	Biotite-muscovite granite	58[19]	9.6	Tungstonia Granite, Kern Mtns., NV77-10 (Farmer), Tungstonia Mine Dump, coll. by Hibbard	Map No. 21 Figure 9.1
364	" "	79[20]	10.9	Pole Canyon-Can Young Canyon Pluton, southern Snake Range, SN-95, (Farmer), coll. by Kistler	Map No. 22 Figure 9.1
	B. Western Utah Segment (see Chapter 9 and Figure 9.1)				
370	Biotite monzogranite	38[19]	8.4, 9.5Q	Northern stock, Gold Hills, GH-1 (Farmer), coll. by Farmer	Map No. 19 Figure 9.1
379	Biotite-hornblende monzogranite	152[19]	9.0	Southern stock, Gold Hills, UT-GH-2 (Farmer), coll. by Farmer	Map No. 20 Figure 9.1
377	Hornblende monzonite	40[19]	5.5	Last Chance Stock, Oquirrh Mtns., UT-LTCH-1 (Farmer), coll. by Lanier	Map No. 23 Figure 9.1
380	Biotite-hornblende monzogranite	28[19]	8.8	Little Cottonwood Stock, Wasatch Mtns., UT-LC-1 (Farmer), roadcut opposite Snowbird Lodge, Alta, coll. by Farmer	Map No. 24 Figure 9.1
378	Biotite-hornblende granodiorite	32[19]	7.9	Alta Stock, Wasatch Mtns., UT-AS-1 (Farmer), 1.2 km S of Alta on Sugarloaf Mtn. Road, coll. by Farmer	Map No. 25 Figure 9.1
	Miscellaneous Localities, California and Nevada				
381	Tonalite	142[19]	10.0, 11.0Q	Gold Hill Pluton, Klamath Mtns., KM-5 (Farmer), coll. by Kistler	See Farmer and DePaolo (1983)
385	Paragneiss	PC[20]	12.2	Northern Ruby Mountains Gneiss, LAN-CAN7#2 (Farmer), coll. by Kistler	" "

* $\delta^{18}O$ refers to whole-rock values, except when followed by Q, which indicates Quartz $\delta^{18}O$. Locations are given in degrees (latitude, N; longitude, W) and minutes (to the nearest hundreth of a minute). When a K-Ar age is given, it is for a biotite determination, except if followed by H, which indicates hornblende. References for age determinations are numbered as superscripts to the ages, and are keyed to the numbers in Table 2 of this appendix.

Table 2 Geochronology references cited in Table 1 of this appendix.

TEXT#	REFERENCE	GEOLOGIC SUB-PROVINCE	METHOD
(1)	Haxel and Wright, 1983	Southern Arizona	U-Pb (zircon)
(2)	Haxel et al., 1980	" "	" "
(3)	Farmer and DePaolo, 1984	" "	" "
(4)	Morton and Miller, 1980	Transverse Ranges, CA; Rodman-Ord Mtns., CA	K-Ar biotite & hornblende)
(5)	Carter and Silver, 1971	Central Transverse Range, CA	U-Pb (zircon)
(6)	Silver, 1971	Central Transverse Range, CA	U-Pb (zircon)
(7)	Miller, 1977a	Granite Mountains, CA	Rb-Sr (w.r.)
(8)	Frizzell, et al., 1986	Central Transverse	U-Pb (zircon)
(9)	Armstrong and Suppe, 1973	Southern Transverse Ranges, CA; Southeastern CA desert	K-Ar (biotite & hornblende)
(10)	Powell, 1981	Southern Transverse Ranges, CA	Field mapping
(11)	Hope, 1966	Pinto Mountains, CA	K-Ar (biotite & hornblende)
(12)	Joseph and Ehlig, 1981	Southern Transverse Ranges, CA	Rb-Sr (w.r.)
(13)	Miller, et al., 1989	Old Woman Mountains, CA	Rb-Sr (w.r.)
(14)	John, 1982	Chemehuevi Mountains, southeastern CA	K-Ar (biotite)
(15)	John, 1981	Southeastern CA desert	Compilation of K-Ar dates
(16)	Martin, et al., 1982	Southeastern CA desert	K-Ar (biotite)
(17)	Silver, 1971	Marble Mountains, CA	U-Pb (zircon)
(18)	Howard, et al., 1982	Southeastern CA desert	K-Ar (biotite)
(19)	Farmer and DePaulo, 1983	Northern Great Basin, Nevada and Utah	Rb-Sr (w.r.)
(20)	Kistler, et al., 1981	Northern Great Basin, Nevada and Utah	Rb-Sr (w.r.)

Table 3a. Major-element geochemistry of plutons in the Central and Eastern Transverse Ranges, California[a]

Sample #	SiO_2	TiO_2	Al_2O_3	FeO	MgO	CaO	Na_2O	K_2O	Total
San Gabriel Mountains (Central V-type $\delta^{18}O$ zone)									
B 34	67.66	0.53	15.81	3.60	1.52	3.18	3.61	3.40	99.31
B 37	61.80	0.82	16.82	5.63	2.40	4.31	3.84	3.13	98.75
B 38	56.75	0.80	18.06	6.66	3.40	6.58	3.53	1.94	97.72
San Gabriel Mountains (Eastern $\delta^{18}O$ zone)									
B 27	63.19	0.62	18.33	4.63	1.51	3.99	4.50	2.63	99.40
B 28	68.26	0.42	16.82	2.57	0.94	2.46	3.83	4.15	99.45
B 30	66.89	0.70	15.97	4.23	1.49	3.12	4.08	2.97	99.45
B 31	68.99	0.42	16.00	2.35	0.66	2.06	4.18	4.60	99.26
B 32	64.26	0.53	16.59	4.44	1.54	4.20	4.03	2.85	98.44
B 33	59.98	0.67	18.52	6.24	2.47	5.40	3.80	2.14	99.22
B 35	72.73	0.22	14.74	1.67	0.56	1.82	3.75	4.08	99.57
B 36	66.46	0.48	15.79	3.72	1.56	3.37	3.67	3.52	98.57
B 39	57.37	0.83	17.76	6.92	3.25	5.75	4.08	2.19	98.15
B 40	63.10	0.65	16.44	5.25	2.47	4.45	3.92	2.83	99.11
B 41	55.98	1.05	19.05	6.98	3.30	6.73	4.08	1.90	99.07
B 42	59.90	0.78	17.17	5.89	3.05	5.11	4.11	2.83	98.84
B 43	66.70	0.77	16.42	3.86	1.38	3.93	3.77	2.63	99.46
B 44	62.96	0.73	17.74	4.69	1.49	3.99	4.06	3.34	99.00
San Bernardino Mountains (Central V-type $\delta^{18}O$ zone)									
B 54	72.07	0.37	15.30	0.73	0.26	2.41	3.93	3.93	99.00
B 55	70.38	0.60	15.42	2.46	0.88	3.33	3.61	3.54	100.22
B 56	64.62	0.93	17.02	4.01	1.56	4.39	4.27	3.16	99.96
B 57	62.53	0.87	17.16	3.96	2.12	4.25	3.92	2.91	97.72
B 58	65.14	0.90	17.00	4.13	1.62	4.25	4.12	3.29	100.45
B 59	65.12	0.88	17.12	3.90	1.57	4.34	4.16	3.16	100.25
B 60	67.62	0.72	16.32	3.31	1.11	3.65	3.92	3.73	100.38
B 61	62.46	0.97	17.25	5.52	2.52	5.34	3.93	2.66	100.65
B 62	64.26	0.97	17.14	4.19	1.61	4.48	4.20	3.08	99.93
B 63	70.10	0.55	15.49	2.13	0.79	3.02	3.71	4.17	99.96
B 64	72.84	0.33	14.42	0.80	0.16	1.90	3.67	4.76	98.88
B 65	73.82	0.37	14.38	1.41	0.25	1.94	3.65	4.40	100.22
B 66	66.68	0.73	16.12	3.47	1.46	3.79	3.71	3.82	99.78
B 67	66.23	0.65	17.16	2.89	1.61	3.40	3.80	3.17	98.91
B 68	72.69	0.37	14.53	1.18	0.26	2.11	3.44	4.59	99.17

Table 3a, cont'd.

Sample #	SiO_2	TiO_2	Al_2O_3	FeO	MgO	CaO	Na_2O	K_2O	Total
San Bernardino Mountains (Central V-type $\delta^{18}O$ zone), cont'd.									
B 69	69.65	0.67	15.51	2.40	0.84	3.27	3.93	3.53	99.80
B 70	64.13	0.93	16.68	4.46	1.99	4.62	3.88	3.35	100.04
B 71	68.49	0.68	15.95	3.27	1.11	3.59	3.96	3.47	100.52
B127	71.75	0.47	14.96	1.36	0.36	1.94	3.58	4.44	98.86
B128	63.90	0.77	16.95	4.51	2.07	4.90	3.81	3.29	100.20
B129	73.65	0.40	14.47	1.22	0.33	1.89	3.37	5.03	100.36
B130	71.92	0.43	15.06	1.29	0.48	1.76	3.44	4.37	98.75
B131	73.87	0.37	16.64	1.04	0.25	2.14	3.60	4.46	102.37
B132	73.50	0.40	15.02	1.26	0.30	2.25	3.64	4.05	100.42
B134	73.26	0.33	14.51	0.89	0.18	1.83	3.76	4.31	99.07
B135	72.45	0.33	15.76	0.65	0.20	2.21	4.04	4.44	100.08
B136	71.30	0.52	15.12	1.50	0.55	2.50	3.79	4.15	99.43
B137	71.85	0.52	15.29	1.76	0.60	2.44	3.72	4.15	100.33
B148	71.19	0.48	15.13	1.39	0.50	2.48	3.77	4.12	99.06
B149	72.41	0.43	14.79	1.07	0.35	2.21	3.76	4.40	99.42
B150	71.75	0.47	15.12	1.35	0.41	2.36	3.76	4.32	99.54
B152	66.14	0.70	16.42	3.91	1.67	4.32	3.80	3.34	100.30
B153	67.58	0.53	16.57	3.16	0.98	3.30	4.10	3.91	100.13
B158	61.16	0.93	17.95	5.92	2.42	5.32	4.07	2.84	100.61
B163	73.37	0.72	14.93	0.85	0.21	1.80	3.74	2.75	98.37
B165	74.38	0.32	14.42	0.86	0.20	2.18	3.65	3.85	99.86
B166	59.23	1.00	17.76	6.39	3.35	6.39	3.96	2.26	100.34
B170	69.01	0.45	16.08	1.49	0.48	3.12	4.23	2.88	97.74
B171	68.65	0.55	16.14	2.39	0.94	3.26	3.99	3.28	99.20
B172	60.90	0.93	16.82	5.99	2.78	5.69	4.10	2.29	99.50
B184	74.81	0.40	13.70	0.90	0.18	1.05	2.52	5.68	99.24
B187	71.28	0.43	15.57	1.31	0.56	2.59	3.77	4.24	99.75
B188	70.74	0.48	15.15	1.92	0.71	2.56	3.50	4.43	99.49
B189	74.89	0.28	14.76	0.20	0.07	1.58	3.75	4.64	100.17
B190	72.71	0.38	15.12	0.49	0.20	2.24	3.77	4.23	99.14
B191	73.25	0.32	15.23	0.59	0.12	2.20	3.71	4.89	100.31
B192	70.98	0.35	15.21	0.99	0.40	2.24	3.68	4.09	97.94
B193	73.54	0.35	15.15	0.64	0.20	1.96	3.83	4.26	99.93
B194	68.95	0.53	15.98	2.28	0.94	3.06	3.96	3.67	99.37
B195	74.46	0.32	14.59	0.26	0.15	1.97	3.64	4.46	99.85
B196	67.51	0.60	16.21	2.61	1.06	3.20	3.92	4.00	99.11
B197	74.31	0.33	15.00	0.41	0.21	2.06	3.57	4.65	100.54

Table 3a, cont'd.

Sample #	SiO_2	TiO_2	Al_2O_3	FeO	MgO	CaO	Na_2O	K_2O	Total
San Bernardino Mountains (Eastern $\delta^{18}O$ zone)									
B 74	63.55	0.97	16.57	5.10	2.65	4.90	3.96	2.77	100.47
B 75	73.89	0.37	14.53	0.78	0.30	2.24	3.79	4.11	100.01
B 78	70.06	0.55	15.89	2.49	0.83	1.59	3.96	4.14	99.51
B 79	70.46	0.58	15.34	2.28	0.78	2.43	4.42	3.87	100.16
B 80	65.67	0.83	16.23	3.46	2.06	3.80	3.81	2.70	98.56
B 81	69.63	0.65	14.98	2.37	0.96	2.11	3.98	3.72	98.40
B 85	68.65	0.68	15.51	2.89	0.96	2.94	3.71	4.52	99.86
B 86	76.28	0.27	12.75	0.15	0.00	1.27	3.62	5.01	99.35
B 94	71.32	0.52	15.17	1.49	0.40	2.22	3.67	5.03	99.82
B 95	72.11	0.47	14.60	1.02	0.30	2.01	3.61	5.06	99.18
B 96	73.61	0.37	14.59	0.89	0.35	2.22	3.80	3.93	99.76
B 97	63.00	0.83	16.95	4.60	2.32	4.83	3.98	3.55	100.06
B 98	67.41	0.73	15.91	2.93	1.18	2.83	4.55	4.76	100.30
B 99	65.03	0.82	15.91	3.42	1.57	4.10	3.62	5.02	99.49
B100	72.95	0.27	15.47	0.13	0.10	2.43	4.02	4.14	99.51
B101	68.95	0.63	15.59	2.58	1.11	3.22	3.96	4.15	100.19
B102	67.75	0.68	16.17	2.78	1.23	3.46	4.06	4.13	100.26
B103	70.21	0.57	15.55	2.15	0.84	2.76	3.75	4.38	100.21
B104	68.24	0.55	16.21	2.49	1.03	3.05	4.18	3.94	99.69
B105	75.51	0.37	13.36	0.76	0.20	1.50	3.93	4.38	100.01
B106	71.73	0.50	14.76	1.63	0.60	2.42	3.80	4.24	99.68
B107	71.26	0.53	15.25	1.74	0.71	2.57	3.84	4.26	100.16
B109	74.85	0.33	13.24	1.94	0.31	1.03	2.72	5.00	99.42
B110	75.28	0.35	12.73	1.04	0.20	1.45	2.95	5.09	99.09
B111	76.18	0.32	13.02	0.14	0.08	1.34	2.78	6.13	99.99
B112	75.19	0.38	12.28	1.38	0.35	1.69	3.25	4.78	99.30
B115	73.52	0.32	15.34	0.40	0.20	1.80	4.00	4.23	99.81
B117	71.19	0.43	16.12	1.54	0.56	2.85	4.19	3.52	100.40
B118	73.91	0.38	14.70	1.11	0.31	2.24	3.49	4.30	100.44
B120	72.18	0.52	14.51	2.17	0.56	2.04	3.48	5.14	100.60
B121	68.15	0.77	15.34	3.00	1.24	2.59	3.79	4.20	99.08
B122	62.10	0.77	14.70	6.20	2.93	5.18	3.88	4.79	100.55
B124	72.62	0.45	14.36	1.67	0.55	2.39	3.60	4.32	99.96
B125	72.84	0.47	14.61	1.12	0.36	2.07	3.79	4.29	99.55
B138	72.88	0.47	15.06	1.47	0.40	2.28	3.72	4.37	100.65
B139	72.80	0.45	14.87	1.29	0.38	2.18	3.68	4.28	99.93
B140	73.22	0.45	15.15	1.44	0.38	2.27	3.62	4.55	101.08
B141	70.64	0.52	15.34	1.76	0.56	2.57	3.87	4.34	99.60

Table 3a, cont'd.

Sample #	SiO_2	TiO_2	Al_2O_3	FeO	MgO	CaO	Na_2O	K_2O	Total
San Bernardino Mountains (Eastern $\delta^{18}O$ zone), cont'd.									
B142	71.79	0.48	15.15	1.54	0.51	2.34	3.62	4.54	99.97
B143	71.43	0.45	14.96	1.40	0.45	2.42	3.69	4.47	99.27
B144	72.39	0.48	14.78	1.70	0.51	2.36	3.64	4.50	100.36
B145	71.92	0.50	14.95	1.40	0.50	2.35	3.68	4.44	99.74
B146	73.22	0.42	14.64	1.22	0.33	2.07	3.71	4.26	99.87
B147	71.21	0.50	15.12	1.45	0.50	2.48	3.75	4.41	99.42
B155	62.87	0.85	17.16	5.18	2.45	5.26	3.80	4.71	102.28
B156	64.54	0.32	17.10	4.41	1.61	4.69	4.02	4.59	101.28
B157	71.58	0.42	15.25	1.32	0.33	2.14	3.96	4.59	99.59
B159	65.14	0.75	16.74	4.63	2.27	4.81	3.58	3.19	101.11
B160	65.16	0.70	16.46	4.22	1.96	4.60	3.79	2.96	99.85
B161	67.43	0.67	16.17	3.81	1.64	1.82	3.69	3.43	98.66
B162	69.01	0.52	15.74	3.02	0.81	2.95	3.88	3.78	99.71
B168	60.26	0.98	17.53	6.42	3.17	6.17	3.80	2.63	100.96
B169	60.11	1.05	17.59	6.77	3.32	6.58	3.87	2.42	101.71
B173	73.31	0.35	14.74	0.44	0.20	1.89	3.56	5.12	99.61
B174	71.77	0.45	14.91	1.56	0.56	2.50	3.42	4.37	99.54
B175	70.87	0.45	15.04	1.58	0.61	2.62	3.54	4.36	99.07
B176	70.70	0.45	16.04	1.39	0.53	3.15	4.00	3.07	99.33
B177	72.07	0.35	14.81	0.78	0.21	1.93	3.79	4.96	98.90
B178	74.33	0.28	14.34	0.20	0.08	1.58	3.40	5.05	99.26
B179	64.22	0.77	17.74	4.80	1.79	4.77	4.29	2.18	100.56
B180	71.98	0.42	15.21	0.91	0.51	2.32	4.10	4.09	99.54
B181	74.05	0.32	14.87	0.62	0.21	2.00	3.73	4.24	100.04
B182	72.39	0.45	14.44	1.44	0.53	2.36	3.30	4.71	99.62
B183	71.28	0.62	14.91	2.26	0.93	2.46	3.34	3.87	99.67
B185	69.10	0.65	15.83	2.47	0.99	3.11	3.81	4.20	100.16
B186	70.89	0.50	15.63	1.72	0.84	2.21	3.81	3.71	99.31
Little San Bernardino Mountains (Central V-type $\delta^{18}O$ zone)									
B199	71.66	0.23	14.89	1.77	0.45	1.78	3.76	4.32	98.86
Little San Bernardino Mountains (Eastern $\delta^{18}O$ zone)									
B198	67.26	0.32	14.74	1.05	0.46	1.71	3.52	4.19	93.25
B200	68.41	0.18	16.25	1.74	0.50	2.42	4.74	4.24	98.48
B201	70.93	0.42	16.02	2.35	0.76	2.35	3.91	3.97	100.71
B202	73.91	0.18	16.57	1.25	0.43	1.59	3.41	4.35	101.69
B203	71.34	0.15	16.40	1.16	0.28	1.26	3.69	4.26	98.54

Table 3a, cont'd.

Sample #	SiO_2	TiO_2	Al_2O_3	FeO	MgO	CaO	Na_2O	K_2O	Total
Little San Bernardino Mountains (Eastern $\delta^{18}O$ zone), cont'd.									
B204	73.01	0.22	14.36	1.48	0.55	1.86	3.67	4.09	99.24
B205	71.51	0.43	15.04	2.16	0.70	2.03	3.34	5.21	100.42
B206	77.31	0.23	14.11	1.65	0.23	0.87	3.64	5.42	103.46
B207	74.16	0.20	15.19	1.26	0.43	1.59	3.95	4.22	101.00
B208	73.54	0.35	13.77	2.01	0.48	1.20	4.04	4.09	99.48
B209	69.61	0.38	14.78	2.83	3.05	3.19	3.50	3.69	101.03
B210	66.89	0.50	16.48	3.70	1.49	3.69	3.88	3.23	99.86
B211	72.22	0.32	16.25	1.98	0.61	2.55	4.20	3.13	101.26
B212	69.87	0.37	15.97	2.31	0.78	2.91	4.11	3.00	99.32
B213	62.42	0.77	17.23	5.66	2.24	4.81	3.60	2.58	99.31
B214	60.85	0.88	16.57	5.92	3.07	5.79	3.85	2.17	99.10
B215	75.43	0.08	14.23	0.99	0.25	1.10	3.84	4.48	100.40
B216	64.28	0.62	16.21	1.41	2.24	4.48	3.72	2.96	95.92
B217	71.13	0.27	14.51	2.16	0.30	1.55	3.71	4.82	98.45
B218	67.02	0.62	16.83	3.68	2.20	2.99	4.99	3.56	101.89
B219	68.71	0.52	16.23	3.22	1.82	2.50	4.04	3.83	100.87
B220	70.91	0.25	15.30	1.88	0.63	1.94	3.84	4.28	99.03
B221	64.17	0.63	16.21	4.76	2.65	3.39	3.89	3.46	99.16
B222	63.21	0.78	15.34	5.30	2.15	4.66	3.54	3.09	98.07

[a] Sample locations are plotted on map in Baird and Meisch, 1984; weight per cent oxides in this table were calculated from weight per cent elemental data in Baird et al., 1979. Note, the oxide values used here do not correspond exactly to those found in Baird and Meisch, 1984 because the latter have been recalculated data on an anhydrous basis. Samples have been classified according to the geographic $\delta^{18}O$ zone in which they occur. In some cases, these boundaries are approximate for this data set because localities of Baird and Meisch, 1984, cannot be exactly matched with $\delta^{18}O$ sampling localities in Figures 6.3, 6.7 and 6.9.

Table 3b. C.I.P.W. normative mineralogy and selected geochemical parameters for plutons in the Central and Eastern Transverse Ranges, California[a]

Sample #	Qtz	Cor	Or	Ab	An	Na_2O+K_2O	Al_2O_3/Na_2O+K_2O+CaO
San Gabriel Mountains (Central V-type $\delta^{18}O$ zone)							
B 34	22.11	0.41	20.23	30.76	15.89	7.01	1.03
B 37	11.15	--	18.73	32.90	19.66	6.97	0.96
B 38	5.86	--	11.73	30.57	28.35	5.47	0.91
San Gabriel Mountains (Eastern $\delta^{18}O$ zone)							
B 27	12.82	0.83	15.64	38.31	19.91	7.13	1.05
B 28	21.71	1.56	24.66	32.59	12.27	7.98	1.10
B 30	19.98	0.37	17.65	34.71	15.56	7.05	1.02
B 31	20.17	0.40	27.39	35.63	10.30	8.78	1.03
B 32	16.00	--	17.11	34.64	19.06	6.88	0.96
B 33	9.80	0.14	12.75	32.41	27.00	5.94	1.01
B 35	29.46	0.85	24.21	31.87	9.07	7.83	1.06
B 36	19.74	--	21.10	31.51	16.45	7.19	0.99
B 39	4.05	--	13.19	35.17	24.12	6.27	0.91
B 40	13.15	--	16.87	33.47	19.07	6.75	0.93
B 41	1.76	--	11.33	34.85	28.32	5.98	0.91
B 42	6.55	--	16.92	35.19	20.28	6.94	0.90
B 43	21.70	0.23	15.63	32.07	19.60	6.40	1.01
B 44	12.54	0.19	19.94	34.70	19.99	7.40	1.01
San Bernardino Mountains (Central V-type $\delta^{18}O$ zone)							
B 54	28.57	0.20	23.46	33.59	12.08	7.86	1.01
B 55	25.96	--	20.87	30.48	15.38	7.15	0.97
B 56	14.14	--	18.68	36.15	17.95	7.43	0.92
B 57	14.09	--	17.60	33.94	21.11	6.83	0.99
B 58	14.85	--	19.35	34.71	18.09	7.41	0.94
B 59	15.16	--	18.63	35.11	18.66	7.32	0.94
B 60	19.24	--	21.96	33.04	15.86	7.65	0.95
B 61	11.32	--	15.62	33.04	21.43	6.59	0.91
B 62	14.01	--	18.21	35.56	18.83	7.28	0.93
B 63	23.92	--	24.65	31.41	13.30	7.88	0.96
B 64	29.00	--	28.45	31.41	8.91	8.43	0.98
B 65	30.25	0.09	25.95	30.82	9.60	8.05	1.01
B 66	18.47	--	22.62	31.46	16.09	7.53	0.94
B 67	20.61	1.31	18.94	32.51	17.05	6.97	1.08
B 68	29.74	0.07	27.35	29.35	10.56	8.03	1.00

Table 3b, cont'd.

Sample #	Qtz	Cor	Or	Ab	An	Na_2O+K_2O	Al_2O_3/Na_2O+K_2O+CaO
San Bernardino Mountains (Central V-type $\delta^{18}O$ zone), cont'd.							
B 69	23.99	--	20.90	33.32	14.28	7.46	0.96
B 70	13.86	--	19.79	32.82	18.20	7.23	0.91
B 71	21.00	--	20.40	33.34	15.42	7.43	0.95
B127	28.79	0.75	26.54	30.64	9.74	8.02	1.05
B128	13.40	--	19.40	32.17	19.39	7.10	0.90
B129	29.43	0.05	29.62	28.41	9.34	8.40	1.00
B130	30.32	1.49	26.15	29.48	8.84	7.81	1.11
B131	29.61	1.95	25.75	29.76	10.37	8.06	1.14
B132	30.68	0.56	23.83	30.67	11.12	7.69	1.04
B134	30.49	0.34	25.71	32.11	9.16	8.07	1.02
B135	26.61	0.29	26.22	34.16	10.95	8.48	1.02
B136	26.57	--	24.66	32.25	12.06	7.94	0.99
B137	27.04	0.24	24.44	31.37	12.06	7.87	1.02
B148	26.91	--	24.58	32.20	12.31	7.89	1.00
B149	28.14	--	26.15	32.00	10.54	8.16	0.99
B150	27.05	--	25.65	31.96	11.67	8.08	1.00
B152	17.48	--	19.68	32.06	17.83	7.14	0.93
B153	18.21	--	23.08	34.65	15.24	8.01	0.98
B158	8.19	--	16.68	34.24	22.19	6.91	0.92
B163	37.36	2.57	16.52	32.17	9.08	6.49	1.20
B165	33.01	0.29	22.78	30.93	10.83	7.50	1.02
B166	5.91	--	13.31	33.39	23.93	6.22	0.86
B170	25.65	0.34	17.41	36.62	15.84	7.11	1.02
B171	23.10	0.10	19.54	34.03	16.30	7.27	1.01
B172	9.31	--	13.60	34.87	20.83	6.39	0.86
B184	35.72	1.51	33.82	21.49	5.25	8.20	1.12
B187	26.03	0.07	25.12	31.98	12.88	8.01	1.00
B188	25.80	--	26.31	29.77	12.61	7.93	1.00
B189	31.78	0.69	27.37	31.68	7.83	8.39	1.05
B190	29.63	0.27	25.21	32.18	11.21	8.00	1.02
B191	27.82	--	28.81	31.30	10.43	8.60	0.99
B192	28.55	0.67	24.68	31.79	11.35	7.77	1.05
B193	30.21	0.68	25.19	32.43	9.73	8.09	1.05
B194	22.59	--	21.82	33.72	15.08	7.63	1.00
B195	31.82	0.19	26.40	30.85	9.79	8.10	1.01
B196	19.63	--	23.85	33.47	14.95	7.92	0.98
B197	30.76	0.35	27.33	30.05	10.16	8.22	1.02

Table 3b, cont'd.

Sample #	Qtz	Cor	Or	Ab	An	Na_2O+K_2O	Al_2O_3/Na_2O+K_2O+CaO
San Bernardino Mountains (Eastern $\delta^{18}O$ zone)							
B 74	12.96	--	16.29	33.35	19.17	6.73	0.90
B 75	30.63	--	24.28	32.07	10.49	7.90	0.98
B 78	24.99	2.01	24.58	33.67	7.93	8.10	1.14
B 79	22.38	--	22.83	37.34	10.57	8.29	0.97
B 80	19.98	0.13	16.19	32.71	19.13	6.51	1.01
B 81	25.20	0.58	22.34	34.23	10.64	7.70	1.04
B 85	20.65	--	26.75	31.44	12.34	8.23	0.95
B 86	34.10	--	29.80	30.83	3.77	8.63	0.93
B 94	24.76	--	29.78	31.11	10.08	8.70	0.98
B 95	26.99	--	30.15	30.80	8.76	8.67	0.97
B 96	30.80	0.05	23.28	32.23	11.04	7.73	1.00
B 97	10.54	--	20.97	33.66	17.89	7.53	0.88
B 98	14.06	--	28.04	38.39	8.90	9.31	0.89
B 99	13.19	--	29.82	30.79	12.40	8.64	0.84
B100	28.53	--	24.58	34.18	12.00	8.16	1.00
B101	20.51	--	24.48	33.44	12.48	8.11	0.92
B102	17.97	--	24.34	34.27	13.66	8.19	0.93
B103	23.27	--	25.83	31.67	12.63	8.13	0.98
B104	19.45	--	23.36	35.48	13.87	8.12	0.97
B105	32.35	--	25.88	33.25	5.88	8.31	0.96
B106	26.70	--	25.14	32.26	10.73	8.04	0.97
B107	25.17	--	25.13	32.44	11.77	8.10	0.98
B109	36.06	1.49	29.72	23.15	5.14	7.72	1.13
B110	35.11	--	30.35	25.19	6.52	8.04	0.98
B111	33.93	--	36.23	23.53	4.94	8.91	0.95
B112	33.99	--	28.45	27.69	4.84	8.03	0.90
B115	29.87	0.91	25.04	33.91	8.95	8.23	1.06
B117	25.34	0.23	20.72	35.31	14.08	7.71	1.01
B118	31.11	0.23	25.30	29.40	11.06	7.79	1.02
B120	25.77	--	30.19	29.27	8.74	8.62	0.97
B121	20.98	--	20.98	32.37	12.56	7.99	0.99
B122	4.80	--	28.15	32.65	8.50	8.67	0.70
B124	28.50	--	25.54	30.47	10.27	7.92	0.96
B125	28.97	--	25.47	32.21	10.23	8.08	1.00
B138	27.98	0.06	25.66	31.27	11.24	8.09	1.00
B139	29.06	0.22	25.31	31.16	10.82	7.96	1.02
B140	28.15	0.14	26.60	30.30	11.14	8.17	1.01
B141	24.43	--	25.75	32.88	11.71	8.21	0.97

Table 3b, cont'd.

Sample #	Qtz	Cor	Or	Ab	An	Na_2O+K_2O	Al_2O_3/Na_2O+K_2O+CaO
San Bernardino Mountains (Eastern $\delta^{18}O$ zone), cont'd.							
B142	26.67	0.03	26.84	30.64	11.61	8.16	1.00
B143	26.57	--	26.61	31.45	11.14	8.16	0.98
B144	27.24	--	26.50	30.69	10.66	8.14	0.98
B145	27.13	--	26.31	31.22	11.19	8.12	0.99
B146	29.74	0.16	25.21	31.43	10.28	7.97	1.01
B147	25.97	--	26.21	31.92	11.47	8.16	0.98
B155	6.20	--	27.21	31.44	15.50	8.51	0.82
B156	9.35	--	26.78	33.59	14.87	8.61	0.85
B157	25.29	--	27.24	33.65	10.32	8.55	0.99
B159	15.73	--	18.64	29.96	19.96	6.77	0.93
B160	16.82	--	17.52	32.12	19.19	6.75	0.92
B161	24.14	3.12	20.54	31.65	9.15	7.12	1.24
B162	22.43	--	22.40	32.93	14.41	7.66	0.99
B168	7.09	--	15.39	31.85	22.79	6.43	0.86
B169	6.29	--	14.06	32.20	23.08	6.29	0.84
B173	28.72	--	30.37	30.24	9.15	8.68	0.99
B174	28.12	0.01	25.94	29.07	12.46	7.79	1.00
B175	26.49	--	26.01	30.24	12.39	7.90	0.98
B176	27.50	0.41	18.26	34.08	15.73	7.07	1.03
B177	26.68	--	29.64	32.43	8.85	8.75	0.98
B178	31.96	0.41	30.06	28.98	7.90	8.45	1.03
B179	14.72	--	12.81	36.10	22.58	6.47	0.98
B180	26.53	--	24.28	34.85	11.07	8.19	0.99
B181	31.24	0.51	25.05	31.55	9.92	7.97	1.04
B182	28.79	--	27.94	28.03	10.72	8.01	0.97
B183	29.06	0.76	22.94	28.36	12.24	7.21	1.05
B185	21.49	--	24.78	32.19	13.67	8.01	0.96
B186	27.67	1.34	22.08	32.46	11.04	7.52	1.09
Little San Bernardino Mountains (Central V-type $\delta^{18}O$ zone)							
B199	27.78	0.80	25.82	32.18	8.93	8.08	1.06
Little San Bernardino Mountains (Eastern $\delta^{18}O$ zone)							
B198	27.63	1.40	26.55	31.94	9.10	7.71	1.10
B200	17.95	--	25.44	40.73	10.70	8.98	0.97
B201	25.00	1.01	23.29	32.85	11.58	7.88	1.07
B202	31.93	3.31	25.28	28.37	7.76	7.76	1.25
B203	30.04	3.48	25.55	31.69	6.34	7.95	1.26

Table 3b, cont'd.

Sample #	Qtz	Cor	Or	Ab	An	Na_2O+K_2O	Al_2O_3/Na_2O+K_2O+CaO
Little San Bernardino Mountains (Eastern $\delta^{18}O$ zone), cont'd.							
B204	30.36	0.52	24.35	31.29	9.30	7.76	1.04
B205	25.16	0.21	30.66	28.14	10.03	8.55	1.01
B206	30.91	0.65	30.96	29.77	4.17	9.06	1.05
B207	29.79	1.22	24.69	33.09	7.81	8.17	1.09
B208	29.84	0.52	24.30	34.36	5.98	8.13	1.04
B209	21.90	--	21.58	29.31	13.58	7.19	0.95
B210	19.20	--	19.11	32.88	18.04	7.11	0.99
B211	27.67	1.30	18.27	35.10	12.49	7.33	1.09
B212	25.60	0.68	17.85	35.02	14.54	7.11	1.04
B213	14.04	--	15.35	30.67	23.40	6.18	0.99
B214	10.35	--	12.97	32.94	21.76	6.02	0.86
B215	32.32	1.06	26.37	32.36	5.44	8.32	1.08
B216	19.19	--	18.24	32.82	19.59	6.68	0.93
B217	26.14	0.38	28.93	31.89	7.81	8.53	1.03
B218	12.24	--	20.65	41.44	12.77	8.55	0.96
B219	20.01	0.89	22.44	33.89	12.30	7.87	1.06
B220	25.97	0.83	25.54	32.81	9.72	8.12	1.06
B221	13.75	--	20.62	33.19	16.69	7.35	0.99
B222	15.41	--	18.62	30.54	17.17	6.63	0.87

[a] C.I.P.W. normative mineralogy calculated using Ed Stolper's program; geochemical parameters calculated using data from Table 3a. See Table 3a for footnotes regarding sample locations and data sources.

Table 4. Complete listing of upper-case abbreviations and acronyms which appear in this thesis.

Abbreviation	Description
AA	Amargosa Aulocogen of Kistler and Peterman (1978)
AB	Albite
AFC	Assimilation-Fractional Crystallization
AN	Anorthite
AZ	Arizona
B	Biotite facies of the Lowe Granodiorite, San Gabriel Mountains, California, after Ehlig, 1981
BM-HC	Bristol Mountains Hydrothermal Center, California
BMM-HC	Big Maria Mountains Hydrothermal Center, California
BSG	Belt Supergroup, Montana and Idaho
CA	California
CC	Carson City, Nevada
CMB	Comobabi Mountains, Arizona (or Colorado Mineral Belt - Table 10.1)
CM-HC	Copper Mountain Hydrothermal Center, California
CRF	Camp Rock Fault, Rodman-Ord Mountains area, California
CSNB	Central Sierra Nevada Batholith, California
CVB	Cadiz Valley Batholith, California
CZ	Central Zone
CZ-S	Central S-type Subzone
CZ-V	Central V-type Subzone
DMD-HC	Dale Mining District Hydrothermal Center, California
DP-HC	Devil's Playground Hydrothermal Center, California
EG	Eugeosyncline - Northern Great Basin, Nevada
EZ	Eastern Zone
FLT	Fault
G	Garnet facies of the Lowe Granodiorite, San Gabriel Mountains, California, after Ehlig, 1981
GF	Garlock Fault, California
GHSB	Gunsight Hills-Sierra Blanca, Arizona
H	Hornblende facies of the Lowe Granodiorite, San Gabriel Mountians, California, after Ehlig, 1981
HF	Helendale Fault, Rodman-Ord Mountains area, California
HKS	High-K (potassium) Series, Italy (Taylor, 1980)
HV-HC	Holcomb Valley Hydrothermal Center, San Bernardino Mountains, California
I	Distinguishes igneous source region for granitic plutons
ID	Idaho
K	K-feldspar facies of the Lowe Granodiorite, San Gabriel Mountains, California, after Ehlig, 1981
LCC	Lower continental crust of the craton
LDP	Lazy Daisy Pluton, Old Woman Mountains, California
LF	Lenwood Fault, Rodman-Ord Mountains area, California
LKS	Low-K (potassium) Series, Italy (Taylor, 1980)
LSB	Little San Bernardino Mountains, California
MCC	Middle continental crust of the craton
MCM	Miogeosynclinal Continental Margin
MG	Miogeosyncline - Northern Great Basin, Nevada and Utah

Table 4, cont'd.

Abbreviation	Description
MLC	Model Lower Crust of Hill et al., 1986
MK	Mineral King, California
M-N	End-points of the Sierra Nevada Trend of Presnall and Bateman (1973) for the ternary system AN-AB-OR
MORB	Mid-ocean Ridge Basalt
MT	Mylonitized Terrane, southeastern California
NGB	Northern Great Basin
NRM	Northern Rocky Mountains
NV	Nevada
OC	Oceanic Crust
OCL	Oceanic Correlation Line (DePaolo, 1981a)
OIA	Oceanic Island Arc
OR	Orthoclase
OWP	Old Woman Pluton, Old Woman Mountains, California
OWPCB	Old Woman-Piute-Chemehuevi Batholith, California
PCBL	Precambrian Basement Line, western limits of Precambrian outcrops, not necessarily >1.5 Ga
PM-HC	Palen Mountains Hydrothermal Center, California
PPCM	Presumido Peak-Coyote Mountains, Arizona
PRB	Peninsular Ranges Batholith, California
Q	Quartz
RMT	Roberts Mountain Thrust, Northern Great Basin, Nevada
RP	Rattlesnake Pluton, Old Woman Mountains, California
ROM	Rodman-Ord Mountains, California
ROM-HC	Rodman-Ord Mountains Hydrothermal Center, California
S	Distinguishes sedimentary source region for granitic plutons
SAF	San Andreas Fault
SAV	Sedimentary and altered volcanic rocks
SBM	San Bernardino Mountains, California
SBR	Southern Basin and Range Province
SCL	Sub-continental lithospheric upper mantle
SECA	Southeastern California
SGM	San Gabriel Mountains, California
SI	Differentiation index of Matsuhisa et al., 1973
SJ-SR	San Jacinto-Santa Rosa Block of Taylor and Silver, 1978
SLC	Salt Lake City, Utah
SMOW	Standard Mean Ocean Water
SMR	Southern Mojave Region, California
SNB	Sierra Nevada Batholith, California
SOL	Sub-oceanic Lithospheric upper mantle
SR	Santa Rita, Arizona
SSNB	Southern Sierra Nevada Batholith, California
SWWP	Sweet Water Wash Pluton, Old Woman Mountains, California
SZP	Silver Zone Pass Pluton, Northeastern Nevada
UMG	Uinta Mountain Group
USA	United States of America
V	Distinguishes altered volcanic and volcanogenic sedimentary source region for granitic plutons

Table 4, cont'd.

Abbreviation	Description
WDT	Westward Displaced Terrane, Mojave Desert, California
WMD	Western Mojave Desert, California
WR	Whole-rock
Z	Ratio of Sr (ppm) in component 1 over Sr (ppm) in component 2 for case of simple two-component mixing